



Systematic Mathematical Modeling for Agile Development of Model Based Medical Control Systems

Reenberg, Asbjørn Thode

Publication date:
2023

Document Version
Publisher's PDF, also known as Version of record

[Link back to DTU Orbit](#)

Citation (APA):
Reenberg, A. T. (2023). *Systematic Mathematical Modeling for Agile Development of Model Based Medical Control Systems*. Technical University of Denmark.

General rights

Copyright and moral rights for the publications made accessible in the public portal are retained by the authors and/or other copyright owners and it is a condition of accessing publications that users recognise and abide by the legal requirements associated with these rights.

- Users may download and print one copy of any publication from the public portal for the purpose of private study or research.
- You may not further distribute the material or use it for any profit-making activity or commercial gain
- You may freely distribute the URL identifying the publication in the public portal

If you believe that this document breaches copyright please contact us providing details, and we will remove access to the work immediately and investigate your claim.

Ph.D. Thesis
Philosophiae Doctor

 **DTU Compute**
Department of Applied Mathematics and Computer Science

Systematic Mathematical Modeling for Agile Development of Model Based Medical Control Systems

Asbjørn Thode Reenberg

Kongens Lyngby 2023



DTU Compute
Department of Applied Mathematics and Computer Science
Technical University of Denmark

Matematiktorvet
Building 303B
2800 Kongens Lyngby, Denmark
Phone +45 4525 3031
compute@compute.dtu.dk
www.compute.dtu.dk

Preface

This PhD thesis was prepared at the Department of Applied Mathematics and Computer Science (DTU Compute) at the Technical University of Denmark.

The work presented in this thesis was carried out between December 1st 2019 and April 1st 2020 and between July 1st 2020 and March 1st 2023 with Professor John Bagterp Jørgensen as the main supervisor and Associate Professor Per Bækgaard, (former) Associate Professor Dimitri Boiroux, and Professor Kirsten Nørgaard as co-supervisors.

Kongens Lyngby, March, 2023

A handwritten signature in brown ink, reading "A. Reenberg". The signature is written in a cursive style with a large, looping 'R' and a long, sweeping underline.

Asbjørn Thode Reenberg

Acknowledgements

I would like to thank my supervisor John Bagterp Jørgensen for his advice and support throughout the project as well as my co-supervisors Dimitri Boiroux, Per Bækgaard, and Kirsten Nørgaard. Furthermore, I would like to thank the medical doctors at Steno Diabetes Center Copenhagen for our collaborations and their involvement in the project and Maria Sejersen for the contribution to the DiaCon mobile application. I would also like to thank Jorge Bondia and his research group for welcoming me during my external research stay at UPV and Andrea Burattin and Bernd Dammann for the special courses. I would then like to thank Tobias K. S. Ritscel, my colleagues at Scientific Computing, and my office mates as well as all the graduate and undergraduate students that have been a part of this project. Finally, I would like to thank Anna, my friends, and my family for their continued support.

Summary (English)

Today, many people live with diseases that require constant treatment. An example is diabetes. Diabetes is a growing world-wide problem. In 2021, 537 million adults (20-79 years) were living with diabetes with a total cost of at least USD 966 billion.

Studies have shown that automatic treatment by a closed-loop system (artificial pancreas) based on feedback control can both improve glycemic control and lessen the burden of living with diabetes. The first hybrid closed-loop system became commercially available in 2016. Hybrid closed-loop systems are not fully automatic and require the user to manually announce, e.g., meals or exercise. Furthermore, the currently available systems are only able to administer insulin which lowers the glucose concentration. Consequently, they are unable to actively prevent hypoglycemia by, e.g., administration of glucagon. Severe hypoglycemia can have acute consequences, such as loss of consciousness and seizures. Therefore, there is still a significant interest in developing artificial pancreases (APs). Clinical trials are crucial to ensuring a high level of safety and efficacy, but are also very expensive and time-consuming which makes the development of medical devices (including APs) long and cumbersome. Here, virtual clinical trials (in-silico studies) are beneficial to evaluate the performance and identify potential risks before a real clinical trial.

In this thesis, we 1) develop a parallelized high-performance Monte Carlo simulation toolbox to perform large-scale long-term virtual clinical trials, 2) develop the DiaCon dual-hormone (insulin and glucagon) AP and test it in a clinical trial with 11 adolescents, 3) describe the mathematical models applied in the virtual clinical trials and in the DiaCon AP as well as the models that were developed during the thesis, and 4) develop a web application to visualize and analyze diabetes data from, e.g., an AP or a virtual clinical trial.

The Monte Carlo simulation toolbox is connected to a PostgreSQL database of virtual participants (represented by mathematical models) and protocols. The database makes it straightforward to reuse or add more participants and protocols. We show examples of a virtual clinical trial where two different closed-loop algorithms are compared in 1 mio. virtual participants over 1 year. Using high-performance computing, the virtual clinical trial is conducted in 82 min.

The DiaCon AP is based on nonlinear model predictive control where we use an extension of the Medtronic virtual patient model for predictions. We estimate the model parameters with a prediction error method based on the continuous-discrete extended Kalman filter that is also used for state estimation. The DiaCon AP consists of the control algorithm (implemented in an Android smartphone), a Dexcom G6 continuous

glucose monitor, and two Dana-RS pumps. The clinical trial displayed that it is feasible to use NMPC for APs and the DiaCon AP improved the time in range compared to the baseline, but identifying a model individualized to each participant is a challenging and very time-consuming process. Furthermore, we experienced several technical difficulties during the trial, such as, pressure induced sensor attenuations and loss of connection to the pumps.

The web application allows users to login and view representations of the data depending on the permissions of the users. Individuals can view different representations of their own data from selected periods whereas, e.g., doctors can select between all their patients. The web application is build using a Vue.js frontend application, a Java Spring Boot backend application, and a PostgreSQL database. The web application is a prototype hosted on the localhost and currently only shows virtual people and simulated data.

This thesis consists of a summary report and a collection of thirteen research papers and three technical reports.

Summary (Danish)

I dag lever mange mennesker med sygdomme, som kræver konstant behandling. Et eksempel er diabetes. Diabetes er et stigende verdensomspændende problem. I 2021 levede 537 millioner voksne (20-79 år) med diabetes med en total omkostning på mindst 966 milliarder USD.

Studier har vist, at automatisk behandling med et lukket-sløjfe-system (kunstig pancreas) baseret på feedback-kontrol både kan øge glykæmisk kontrol og mindske byrden af at leve med diabetes. Det første hybride lukket-sløjfe-system blev kommercielt tilgængeligt i 2016. Hybride lukket-sløjfe-systemer er ikke fuldt automatiske og kræver at brugeren manuelt annoncerer eksempelvis måltider eller fysisk aktivitet. Derudover kan de nuværende tilgængelige systemer kun administrere insulin og er ikke i stand til aktivt at forhindre hypoglykæmi. Alvorlig hypoglykæmi kan have akutte konsekvenser såsom tab af bevidsthed og anfald. Derfor er der stadig en stor interesse i at videreudvikle kunstige pancreas (AP). Kliniske forsøg er afgørende for at sikre et højt niveau af sikkerhed og effektivitet, men er også meget dyre og tidskrævende, hvilket gør udviklingen af medicinske enheder (APer inkluderet) lang og omstændig. Her er virtuelle kliniske forsøg (in-silico simuleringer) gavnlige til at evaluere ydeevne og identificere potentielle risici før et rigtigt klinisk forsøg.

I denne afhandling 1) udvikler vi et parallelliseret høj-ydeevne Monte Carlo simuleringsværktøj til at udføre storskala langsigtede virtuelle kliniske forsøg, 2) udvikler vi DiaCon dual-hormon APen og tester den i et klinisk forsøg med 11 eunge (13-18 år), 3) beskriver vi de matematiske modeller, der bruges i de virtuelle kliniske forsøg samt i DiaCon APen såvel som de modeller, der blev udviklet i løbet af afhandlingen, 4) udvikler vi en webapplikation til at visualisere og analysere diabetesdata fra f.eks. en AP eller virtuelle kliniske forsøg.

Monte Carlo simuleringsværktøjet er forbundet til en PostgreSQL database med virtuelle deltagere (repræsenteret af matematiske modeller) og protokoller, som gør det muligt at genbruge eksisterende deltagere og protokoller og tilføje flere. Vi viser eksempler på et virtuelt klinisk forsøg, hvor to forskellige lukket-sløjfe-algoritmer sammenlignes i 1 mio. virtuelle deltagere over 1 år. Ved at benytte høj-ydeevne computerberegninger tager det virtuelle kliniske forsøg 82 min.

DiaCon APen er baseret på ikke-lineær model prædiktiv regulering (NMPC), hvor vi bruger en udvidelse af Medtronic virtual patient modellen til prædiktioner. Modelparametrene er estimeret med en prædiktions-fejl-metode baseret på det kontinuert-diskrete udvidede Kalman filter, som også bruges til tilstandsestimering. DiaCon APen består af kontrolalgoritmen (implementeret i en Android smartphone), en Dexcom G6

kontinuerlig glukosemåler og to Dana-RS pumper. Det kliniske forsøg viste, at det er muligt at benytte NMPC til APer, og DiaCon APen øgede tid-i-område sammenlignet med deltagernes normale tid-i-område, men det er udfordrene og meget tidskrævende at identificere parametre individualiseret til hver enkelt deltager. Derudover oplevede vi også flere tekniske problemer i løbet af forsøget såsom trykinducerede sensor dæmpninger og tab af forbindelsen til pumperne.

Webapplikationen tillader brugere at logge ind og se forskellige repræsentationer af data afhængig af deres rettigheder. Enkelte brugere kan se forskellige repræsentationer af deres egne data fra udvalgte perioder, hvorimod f.eks. læger kan vælge imellem alle deres patienter. Web applikationen er bygget af en Vue.js frontend applikation, en Java Spring Boot backend applikation. Data er gemt i en PostgreSQL database. Web applikationen er en prototype hosted på localhost og som på nuværende tidspunkt kun viser virtuelle mennesker og simuleret data.

Denne afhandling består af en sammenfattende rapport og en samling af tretten forskningsartikler samt tre tekniske rapporter.

Contents

Preface	i
Acknowledgements	iii
Summary (English)	v
Summary (Danish)	vii
Contents	ix
I Summary report	1
1 Introduction	3
1.1 Motivation	3
1.2 Diabetes treatment	3
1.3 Clinical trials and virtual clinical trials	8
1.4 Objectives and contributions	9
1.5 Outline of the thesis	10
1.6 List of publications	12
2 Models	17
2.1 General form	17
2.2 Insulin models	18
2.3 Glucagon models	20
2.4 Meal models	22
2.5 Physical activity models	26
2.6 CGM models	27
2.7 Glucose models	28
2.8 Whole-body models	31
2.9 Models for T2D and the ICU	31
2.10 Summary	33
3 Large scale virtual clinical trials	35
3.1 Monte Carlo simulation	35
3.2 Protocols	36

3.3	Virtual Participants	37
3.4	Examples	38
3.5	High-performance computing	39
3.6	Summary	40
4	Artificial pancreas technology	43
4.1	Artificial pancreas systems	43
4.2	DiaCon artificial pancreas system	44
4.3	Nonlinear model predictive control	44
4.4	Clinical trial	58
4.5	Summary	60
5	User interfaces	63
5.1	Artificial pancreas mobile application	63
5.2	Web application	64
5.3	Summary and future perspectives	66
6	Conclusions	73
6.1	Suggestions for future work	74
	Bibliography	77
II	Appendices	89
A	Conference Paper - FOSBE 2022	91
	A whole-body multi-scale mathematical model for dynamic simulation of the metabolism in man	91
B	Conference Paper - Mathmod 2022	99
	Assessment of a new model of glucagon action with glucagon receptor dynamics	99
C	Journal Paper - Computers in Biology and Medicine	107
	Modeling the effect of glucagon on endogenous glucose production in type 1 diabetes: on the role of glucagon receptor dynamics	107
D	Journal Paper - In preparation	119
	Mathematical meal models for simulation of human metabolism	119
E	Conference Paper - CDC 2021	139
	A High-Performance Monte Carlo Simulation Toolbox for Uncertainty Quan- tification of Closed-loop systems	139
F	Conference Paper - ACC 2022	149
	High-performance Uncertainty Quantification in Large-scale Virtual Clinical Trials of Closed-loop Diabetes Treatment	149

G	Conference Paper - FOSBE 2022	157
	Large-scale Virtual Clinical Trials of Closed-loop Treatments for People with Type 1 Diabetes	157
H	Technical Report	165
	Protocols and virtual participants for large-scale long-term virtual clinical trials of closed-loop diabetes treatment	165
I	Conference Paper - DYCOPS 2022	199
	Nonlinear Model Predictive Control and System Identification for a Dual-hormone Artificial Pancreas	199
J	Journal Paper - In preparation	209
	A Dual- and Single-Hormone Artificial Pancreas based on Nonlinear Model Predictive Control in a Clinical Trial with Adolescents	209
K	Journal Paper - Frontiers in Endocrinology	225
	Performance of a Dual-Hormone Closed-Loop System Versus Insulin-Only Closed-loop System in Adolescents with Type 1 Diabetes. A Single-Blind, Randomized, Controlled Crossover Trial	225
L	Technical Report	237
	DiaCon: Clinical trials of a dual- and single-hormone artificial pancreas for adolescents	237
M	Conference Paper - ECC 2023	319
	A <i>one-size-fits-all</i> artificial pancreas for people with type 1 diabetes based on physiological insight and feedback control	319
N	Conference Paper - BMS 2021	327
	Initial titration for people with type 1 diabetes using an artificial pancreas . . .	327
O	Conference Paper - CDC 2019	335
	Model Predictive Control of the Blood Glucose Concentration for Critically Ill Patients in Intensive Care Units	335
P	Technical Report	345
	User interfaces for diabetes applications	345

Part I

Summary report

CHAPTER 1

Introduction

The subject of this thesis is the development of model based medical control systems. Specifically, we consider a dual-hormone (DH) artificial pancreas (AP) based on non-linear model predictive control (NMPC) for treatment of type 1 diabetes (T1D) and a simulation framework for development and pre-clinical evaluations (virtual clinical trials) of closed-loop diabetes treatments (i.e. APs). The AP was tested in a clinical trial with adolescents. The purpose of an AP is to automatically administer a suitable amount of insulin (decided by a control algorithm) based on measurements from a continuous glucose monitor (CGM). AP systems that only administer insulin are referred to as single-hormone (SH) APs, whereas systems that can administer both insulin and glucagon are referred to as DH APs. The NMPC algorithm and the simulation framework both require a physiological model and in this work, we primarily focus on models for T1D. Furthermore, we present a mobile application that functions as a graphical user interface (GUI) for the AP and a web application for visualizing and analyzing diabetes data.

1.1 Motivation

Diabetes is a growing world-wide problem [1]. In 2021, 537 million adults (20-79 years) were living with diabetes and that number is predicted to increase to 643 million by 2030 and 783 million by 2045. T1D accounts for 5-10%. Diabetes was responsible for 6.7% of deaths in 2021 and accounted for 9% of the global health expenditure with a total cost of at least USD 966 billion. Despite the advances in technology and treatments, only around 50% of adults in the United States in 2018 met the glycemic control target of an hemoglobin A1c (HbA1c) below 7% [2]. Omission of insulin treatment (e.g. due to fear of hypoglycemia or interference with daily activities) is one of potential causes of the poor glycemic outcomes [3]. Insulin treatment is also beneficial in critically ill patients where intensive insulin therapy reduced mortality during intensive care from 8.0% compared to 4.6% with conventional treatment [4].

1.2 Diabetes treatment

Diabetes describes a group of metabolic disorders characterized by elevated blood glucose concentrations (hyperglycemia) in the absence of treatment [5]. In healthy people,

normoglycemia is achieved by 1) insulin secretion from the β -cells in the pancreas to lower the blood glucose and 2) glucagon secretion from the α -cells in the pancreas to increase the blood glucose. Insulin lowers the blood glucose concentration by converting glucose to glycogen in the liver and stimulating glucose uptake in the tissue (such as, muscles and kidney) and glucagon increases the concentration by converting glycogen to glucose in the liver (see Figure 1.1). Insulin secretion from the pancreas can also happen preemptively, e.g., in relation to consumption of carbohydrates [6].

T1D is an autoimmune disease, where the immune system attacks the insulin-producing pancreatic β -cells and prevents insulin production. Therefore, people with T1D require life-long treatment with daily injections of insulin to avoid hyperglycemia. Extended periods of hyperglycemia lead to a range of health complications, e.g., cardiovascular disease, chronic kidney disease, and damage to the nerves and eyes. Too much insulin can cause low blood glucose concentrations (hypoglycemia). Hypoglycemia can cause a variety of acute complications including loss of consciousness, seizures, and, in severe cases, even death. Therefore, it is crucial to administer an appropriate amount of insulin.

Type 2 diabetes (T2D) accounts for the majority (over 90%) of diabetes worldwide and includes various degrees of β -cell dysfunction and insulin resistance [1, 5]. In general, symptoms of T2D are less dramatic and it is expected that between 33% and 50% of people living with T2D are undiagnosed. However, extended lack of treatment causes complications of prolonged hyperglycemia [8]. The cause of T2D is not completely understood, but overweight, age, and genetics seem to be critical factors. The treatment of T2D typically begins with a promotion for life-style change. If life-style changes are not sufficient, treatment with non-insulin drugs (e.g, metformin, glucagon-like peptide 1 (GLP-1), dipeptidyl peptidase 4 (DPP-4) inhibitors) is initiated and eventually insulin treatment may be necessary.

This thesis primarily concerns T1D. Conventional treatment of T1D consists of multiple daily injections with syringes, pens, or with an insulin pump and a self monitoring blood glucose (SMBG) device to measure the glucose concentration. Therefore, people living with T1D have to manually adjust the insulin dose based on the glucose measurement and meal consumption, as shown in Figure 1.2. The first CGM was commercialized in 1999 [9] and allowed for, so called, sensor-augmented insulin-pump therapy, where the subject can continuously monitor and adjust the insulin infusion rate based on the CGM measurements. Sensor-augmented pump therapy resulted in improved glycemic control [10]. However, the person living with T1D is still required to manually adjust the insulin rate. Therefore there has been a significant interest in developing systems that can automatically adjust the insulin infusion rate. Such systems are referred to as closed-loop systems or artificial pancreases.

1.2.1 Closed-loop diabetes treatment

The progress towards fully automatic closed-loop systems has been accelerating since the commercialization of glucose sensors and insulin delivery systems in the mid-2000s [11]. Figure 1.3 shows a sketch of a closed-loop system that consists of a CGM, a con-

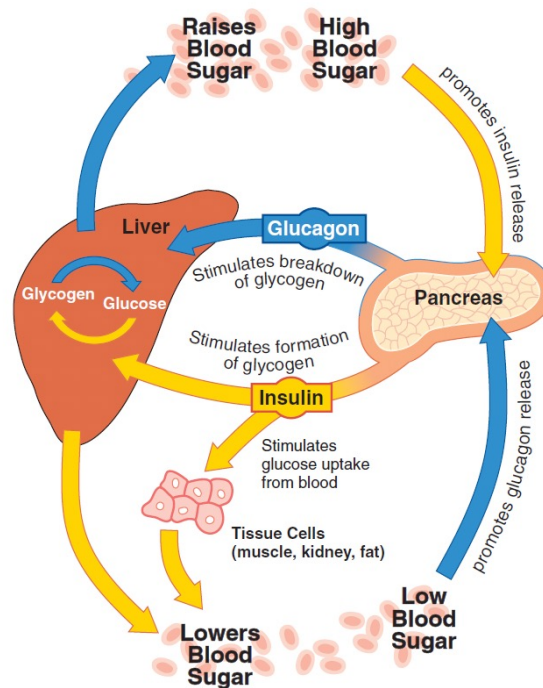


Figure 1.1: Glucose homeostasis in healthy people: 1) insulin secretion from the β -cells in the pancreas converts glucose to glycogen in the liver and stimulates glucose uptake from the blood to lower the blood glucose and 2) glucagon secretion from the α -cells in the pancreas converts glycogen to glucose in the liver to increase the blood glucose [7].

trol algorithm that computes the infusion rate (e.g., in a smartphone), and an insulin pump. Several control algorithm types have been suggested [12], including fuzzy logic [13], proportional-integral-derivative (PID) control [14, 15], linear model predictive control (LMPC) [16, 17], NMPC [18–20], generalized predictive control (GPC) [21], H - ∞ control [22], and algorithms based on multiple control modules [23]. Clinical trials have indicated that closed-loop systems may improve glycemic control [24–29] and in a consensus report Phillip et al. [30] concludes that closed-loop systems should be considered in all populations. The first hybrid closed-loop system became commercially available in 2016, where the Medtronic 670G received approval by the U.S. Food and Drug Administration (FDA). Since then five more closed-loop systems have become available for commercial use in the EU or the US 1) Medtronic 780G, 2) Control-IQ, 3) CamAPS FX, 4) Diabeloop, and 5) Omnipod 5 [30]. These are all categorized as single-hormone hybrid closed-loop systems, where only insulin can be administered and the user is required to manually provide information about, e.g., meals or exercise. Consequently, they are unable to actively increase the glucose concentration in case of hypoglycemia. Therefore, researchers investigate both fully automatic closed-loop systems that does not require manual announcements and systems that can actively prevent hypoglycemia

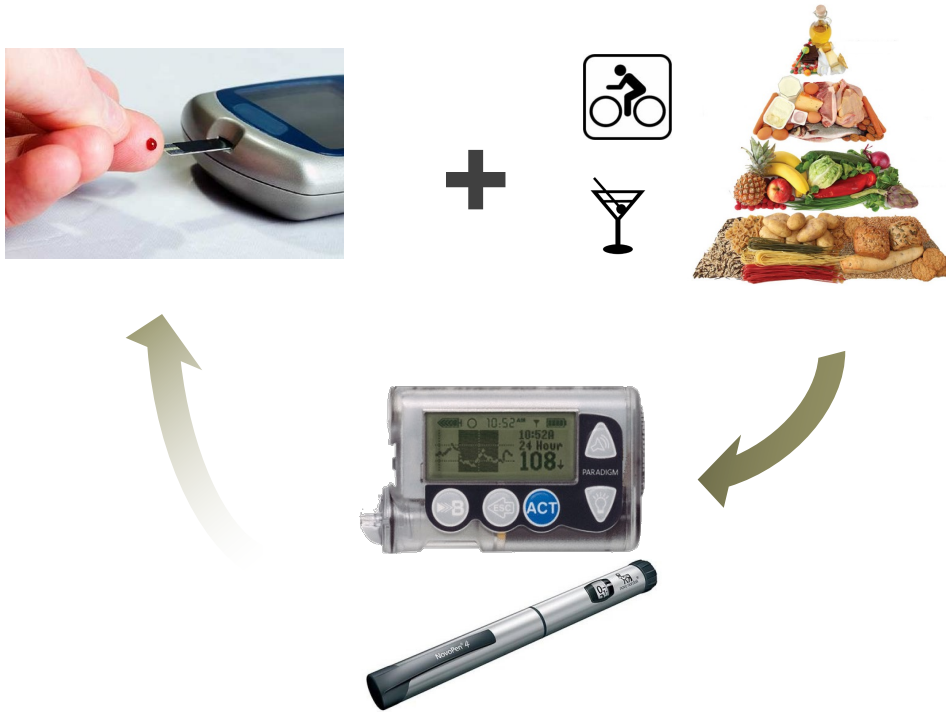


Figure 1.2: Conventional treatment of T1D, where the person measures the glucose concentration with an SMBG and manually administers insulin with a pen or updates the pump settings based on the glucose measurement and meals or exercise.

by, e.g., suggesting carbohydrates [31] or administer glucagon [32–35]. The only commercially available fully automatic closed-loop system is the STG-22 and its successor, the STG-55, that are both only available in Japan and are bedside devices that use intravenous access for glucose measurements and insulin delivery [11]. Initially, clinical evaluations of DH APs did not demonstrate the expected improved performance compared to SH APs [36, 37], but recent studies have displayed improved outcomes for DH systems [32–34]. In addition to the commercially available closed-loop system, there are three systems that received regulatory approval or are under regulatory review, but are not yet commercially available. The Tidepool Loop system [38] has received FDA approval and the Inreda DH system [34] received a CE mark. Furthermore, the iLet insulin only bionic pancreas is under regulatory review. The iLet pancreas also comes in a DH configuration [32]. The success of closed-loop systems and development thus far is promising, but there are still open questions in the capability of adapting to complex scenarios such as exercise, sleep disruption, and variable meal times and sizes [11].

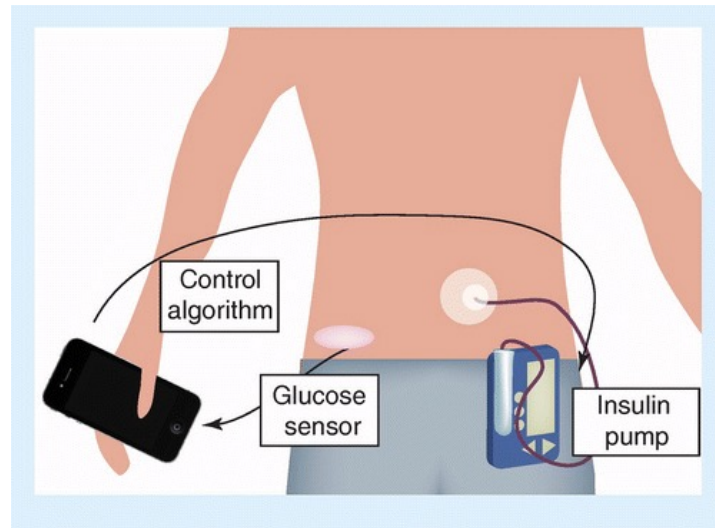


Figure 1.3: Closed-loop system. The insulin administration is automatically updated by the control algorithm based on the measurement received from a CGM [39].

1.2.2 Glycemic targets

In 2019, Battelino et al. [40] formulated recommendations for clinical targets on time in range (TIR) for CGM data. These targets are used to evaluate the glycemic control. Table 1.1 shows the glycemic ranges and the color code used to represent each range in this thesis. Table 1.2 shows the target values for average glucose, glucose management index (GMI), glucose variability (GV), and how much time the CGM should be active as well as targets for time spent in each range. The average glucose and GMI are directly related to HbA1c and GV is an indicator for variations in the glucose concentration. It is recommended that the computed values are based on 14 days of CGM data, which is not always available in this thesis.

Table 1.1: The five glycemic ranges described by Battelino et al. [40].

Category	Range [mmol/L]	Color
Level 2 hyperglycemia	$]13.9, \infty[$	Orange
Level 1 hyperglycemia	$]10.0, 13.9]$	Yellow
Normoglycemia	$[3.9, 10.0]$	Green
Level 1 hypoglycemia	$[3.0, 3.9[$	Light red
Level 2 hypoglycemia	$[0.0, 3.0[$	Red

Table 1.2: The glycemic targets described by Battelino et al. [40].

Quantity	Target
Average glucose	< 8.55 mmol/L
Glucose management index	$< 7\%$
Glucose variability	$\leq 36\%$
Active CGM	100%
Level 2 hyperglycemia	$< 5\%$
Level 1 and 2 hyperglycemia	$< 25\%$
Normoglycemia	$> 70\%$
Level 1 and 2 hypoglycemia	$< 4\%$
Level 2 hypoglycemia	$< 1\%$

1.3 Clinical trials and virtual clinical trials

The development of complex medical devices (e.g. closed-loop systems) is very expensive and time-consuming. In an economic analysis, the mean development cost of bringing a novel therapeutic complex medical device to the US market was estimated to \$54 million. The estimate was \$522 million when accounting for the cost of failed trials and cost of capital [41]. Clinical trials were a key factor associated with the cost. Clinical trials are necessary to ensure the safety and efficacy of medical treatments, but they might result in an undesired outcome. Therefore, it is important to 1) evaluate the potential performance, 2) identify faults and risks, and 3) assess the competitive advantages of the treatment or medical device before the actual clinical trial. This is the purpose of virtual clinical trials. Virtual clinical trials involve virtual participants represented by mathematical models and can be performed with computer simulations. Virtual clinical trials are cheaper and less time-consuming, causes no risk for the participants, and by using high-performance computing, they can involve large populations of virtual participants and long-term protocols. Various T1D simulators have been developed for this purpose. The two most famous simulators are the UVA/Padova simulator [42] and the Cambridge simulator [43]. The UVA/Padova simulator was FDA approved in 2008 as an alternative to animal studies and pre-clinical trials for a single meal scenario only and includes 300 virtual participants (300 sets of model parameters). A new version was published in 2014 [44] and in 2018 another version was published that extended the scenario from a single meal to a single day [45]. The Cambridge simulator was published in 2010 with 18 virtual participants based on the model by Hovorka et al. [46]. These simulators offer limited virtual participants with limited variations. Therefore, several methods to generate larger cohorts of virtual participants with more variability have been developed [47–50]. To utilize *very* large cohorts of virtual participants, the virtual clinical trials must be based on high-performance computing techniques.

1.4 Objectives and contributions

In this work, we aim to develop a DH AP for treatment of T1D and a simulation toolbox for performing large-scale virtual clinical trials of closed-loop diabetes treatment. Furthermore, we develop a web application to visualize the large amounts of diabetes data that has become available with modern technology. Digital package solutions combining mobile communication, smart devices, cloud solutions, and advanced analytics are projected to transform the health care industry in the future and the transformation has already started [51, 52]. Here, we attempt to build a package solution consisting of the AP, the simulation toolbox, and the web application. Figure 1.4 shows the concept. The DH AP continuously uploads data to the database and enables remote monitoring from the web application. Furthermore, the web application enables, e.g., doctors or researchers to analyze data from the AP. The simulator can be used for educational purposes or for tests and development of new closed-loop systems. The web application functions as a high level interface to the simulation toolbox and can visualize the results. In this work, we have developed the individual components, but the full setup, where the web application can start simulations and remotely monitor the AP, is future work. The main contributions are as follows.

Dual-hormone artificial pancreas. We develop the DiaCon DH AP based on NMPC and test it in a clinical trial with 11 adolescents. We use an extended version of the Medtronic Virtual patient (MVP) model for predictions and estimate the parameters using a maximum likelihood (ML) based prediction error method (PEM). We use the continuous-discrete extended Kalman filter (CD-EKF) in both the PEM and for state estimation in the AP. Furthermore, we use heuristics to switch between administering insulin and glucagon (insulin and glucagon cannot be administered simultaneously) and additional safety measures.

Virtual clinical trials. We develop a high-performance Monte Carlo simulation toolbox for uncertainty quantification in closed-loop systems. We apply the toolbox to perform large-scale long-term virtual clinical trials of closed-loop diabetes treatment. The populations of virtual participants are represented by a combination of mathematical models formulated as stochastic differential equations to incorporate the uncertainty in the physiology. The protocols are designed from a set of basis days that we combine to form weeks, months and years. The virtual participants and protocols are stored in a PostgreSQL database to make it straightforward to reuse and sort existing participants and protocols or add more. We demonstrate the utility of the toolbox by 1) comparing two different AP algorithms in a 52 week virtual clinical trial with 1 mio. virtual participants, and 2) comparing the performance of an AP algorithm in a 52 week virtual clinical trial with two different virtual populations of each 1 mio. participants.

Web application and user interfaces. We design and develop a web application to visualize and analyze diabetes data. The web application is build with a Vue.js

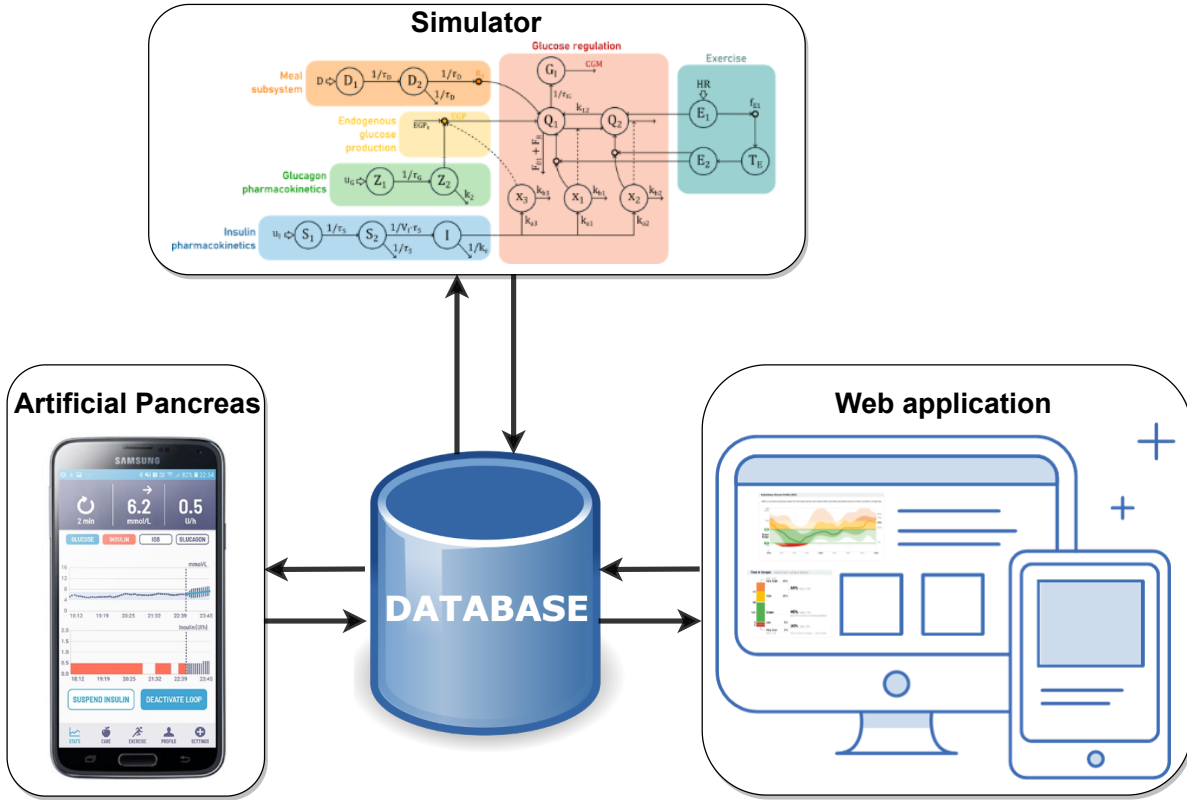


Figure 1.4: Objective of the thesis and concept for a connected solution for diabetes treatment, education, and development of new closed-loop systems.

frontend application, a Java Spring Boot backend application, an application programming interface (API), and a PostgreSQL database. The web application allows patients, doctors, or researchers to inspect different representations of the data based on their permissions through a login page. In this work, we assume that the data already exist in the database and it is not possible to start virtual clinical trials directly from the web application or automatically receive data from the DiaCon AP (due to General Data Protection Regulation (GDPR)).

1.5 Outline of the thesis

Chapter 2 describes the physiological models used in the DiaCon AP, the models used to represent virtual participants in the virtual clinical trials, five meal models, and a glucagon model developed during the thesis. Furthermore, we present the concept of a whole-body model developed during the thesis and discuss T2D and intensive care unit (ICU) models. The physiological models are central to all of the work in this thesis, but the following Appendices are directly related to modeling: Appendix A describes the whole body model, Appendix B and C presents the glucagon model, and Appendix D

collects and compares five meal models.

Chapter 3 presents the Monte Carlo simulation toolbox and the large-scale virtual clinical trials used to prepare and evaluate the performance of closed-loop systems for diabetes treatment before real clinical trials. We describe the virtual participants represented by a combination of the models presented in Chapter 2 and a 1 year (52 weeks) protocol that the participants follow during the trials. Furthermore, we describe how the virtual participants and protocols are stored in a database. Finally, we describe how high-performance computing is used for computational feasibility of the large-scale trials and show an example virtual clinical trial. This chapter is based on Appendices E, F, G, and H.

Chapter 4 presents the DiaCon AP and compares the system to closed-loop systems that are commercially available, received regulatory approval, or are under regulatory review. We show the hardware used to build the DiaCon AP and describe the NMPC algorithm and heuristics used to compute the insulin or glucagon administration. Furthermore, we describe how we identify individualized parameters for each participant in the clinical trial. Finally, we summarize and discuss the results from the clinical trial of the DiaCon AP with 11 adolescents. This chapter is based on Appendices I, J, K, L, M, N, and O.

Chapter 5 presents the GUI of the DiaCon app and describes the web application used to visualize and analyze diabetes data. We demonstrate how the DiaCon app allows the user to connect devices, announce meals and exercise, view time-series of glucose, insulin and glucagon data, and see selected stats. Next, we show the tools applied to build the web application and describe the different roles with individual permissions in the web application. Finally, we show a demonstration of the web application. The web application is described in Appendix P.

Chapter 6 provides conclusions, summarizes the main contributions, and discusses possible improvements and future work.

1.6 List of publications

This section lists the papers, technical reports, and presentations (invited or abstract-only) conducted in collaboration with co-authors.

1.6.1 Journal papers

1. Asbjørn Thode Reenberg, Tobias K. S. Ritschel, Dimitri Boiroux, Maria Sejersen, Emilie B. Lindkvist, Christian Laugesen, Jannet Svensson, Ajenthen G. Ranjan, Kirsten Nørgaard, John Bagterp Jørgensen. A Dual- and Single-Hormone Artificial Pancreas based on Nonlinear Model Predictive Control in a Clinical Trial with Adolescents. 2023. In preparation.
2. Tobias K. S. Ritschel, Asbjørn Thode Reenberg, Peter Emil Carstensen, Jacob Bendsen, John Bagterp Jørgensen. Mathematical meal models for simulation of human metabolism. 2023. In preparation.
3. Emilie B. Lindkvist, Christian Laugesen, Asbjørn Thode Reenberg, Tobias K. S. Ritschel, Jannet Svensson, John Bagterp Jørgensen, Kirsten Nørgaard, Ajenthen G. Ranjan. Performance of a Dual-hormone Closed-loop System Versus Insulin-Only Closed-loop System in Adolescents with Type 1 Diabetes. A Single-Blind, Randomized, Controlled Crossover Trial. *Frontiers in Endocrinology*. 14:1073388, 2023.
4. Clara Furió-Novejarque, Ricardo Sanz, Tobias K.S. Ritschel, Asbjørn Thode Reenberg, Ajenthen G. Ranjan, Kirsten Nørgaard, José-Luis Díez, John Bagterp Jørgensen, Jorge Bondia. Modeling the effect of glucagon on endogenous glucose production in type 1 diabetes: On the role of glucagon receptor dynamics. *Computers in Biology and Medicine*, 106605, 2023.

1.6.2 Peer-reviewed conference papers

1. Tobias K. S. Ritschel, Asbjørn Thode Reenberg, Emilie B. Lindkvist, Christian Laugesen, Jannet Svensson, Ajenthen G. Ranjan, Kirsten Nørgaard, Bernd Dammann, John Bagterp Jørgensen. A *one-size-fits-all* artificial pancreas for people with type 1 diabetes based on physiological insight and feedback control. 2023. Accepted: 2023 European Control Conference (ECC).
2. Tobias K. S. Ritschel, Asbjørn Thode Reenberg, John Bagterp Jørgensen. Large-scale Virtual Clinical Trials of Closed-loop Treatments for People with Type 1 Diabetes. *IFAC-PapersOnLine*, 55–23, 169–174, 2022.
3. Peter Emil Carstensen, Jacob Bendsen, Asbjørn Thode Reenberg, Tobias K. S. Ritschel, John Bagterp Jørgensen. A whole-body multi-scale mathematical model

- for dynamic simulation of the metabolism in man. IFAC-PapersOnLine, 55–23, 58–63, 2022.
4. Asbjørn Thode Reenberg, Tobias K. S. Ritschel, Emilie B. Lindkvist, Christian Laugesen, Jannet Svensson, Ajenthen G. Ranjan, Kirsten Nørgaard, John Bagterp Jørgensen. Nonlinear Model Predictive Control and System Identification for a Dual-hormone Artificial Pancreas. IFAC-PapersOnLine, vol. 55, no. 7, pp. 915–921, 2022.
 5. Clara Furió-Novejarque, Ricardo Sanz, Asbjørn Thode Reenberg, Tobias K. S. Ritschel, Ajenthen G. Ranjan, Kirsten Nørgaard, José-Luis Díez, John Bagterp Jørgensen, Jorge Bondia. Assessment of a new model of glucagon action with glucagon receptor dynamics. IFAC-PapersOnLine, vol. 55, no. 22, pp. 647–652, 2022.
 6. Asbjørn Thode Reenberg, Tobias K. S. Ritschel, Bernd Dammann, John Bagterp Jørgensen. High-performance Uncertainty Quantification in Large-scale Virtual Clinical Trials of Closed-loop Diabetes Treatment. In proceedings: 2022 American Control Conference (ACC), pp. 1367–1372, 2022, Atlanta, Georgia, USA.
 7. Morten Ryberg Wahlgreen, Asbjørn Thode Reenberg, Marcus Krogh Nielsen, Anton Rydahl, Tobias K. S. Ritschel, Bernd Dammann, John Bagterp Jørgensen. A High-Performance Monte Carlo Simulation Toolbox for Uncertainty Quantification of Closed-loop systems. In proceedings: 2021 IEEE 60th Conference on Decision and Control (CDC), pp. 3762–3769, 2021, Austin, Texas, USA.
 8. Maria Sejersen, Dimitri Boiroux, Sarah Ellinor Engell, Tobias K. S. Ritschel, Asbjørn Thode Reenberg, John Bagterp Jørgensen. Initial titration for people with type 1 diabetes using an artificial pancreas. IFAC-PapersOnLine, vol. 54, no. 15, pp. 484–489, 2021.
 9. Asbjørn Thode Reenberg, Dimitri Boiroux, Tobias Kasper Skovborg Ritschel, John Bagterp Jørgensen. Model Predictive Control of the Blood Glucose Concentration for Critically Ill Patients in Intensive Care Units. In proceedings: 2019 IEEE 58th Conference on Decision and Control (CDC), pp. 3762–3769, Nice, France, 2019.

1.6.3 Technical reports

1. Asbjørn Thode Reenberg, Tobias K. S. Ritschel, Emilie B. Lindkvist, Christian Laugesen, Jannet Svensson, Ajenthen G. Ranjan, Kirsten Nørgaard, John Bagterp Jørgensen. DiaCon: Clinical trials of a dual- and single-hormone artificial pancreas for adolescents. Submitted to arXiv, 2023.
2. Asbjørn Thode Reenberg, Tobias K. S. Ritschel, John Bagterp Jørgensen. User interfaces for diabetes applications. Submitted to arXiv, 2023.

3. Asbjørn Thode Reenberg, Tobias K. S. Ritschel, John Bagterp Jørgensen. Protocols and virtual participants for large-scale long-term virtual clinical trials of closed-loop diabetes treatment. Submitted to arXiv, 2023.

1.6.4 Additional presentations (invited or with abstract-only)

1. Asbjørn Thode Reenberg, Tobias K. S. Ritschel, Emilie B. Lindkvist, Christian Laugesen, Jannet Svensson, Ajenthen G. Ranjan, John Bagterp Jørgensen. Large-Scale Long-term Virtual Clinical Trials of Closed-loop Systems for Diabetes Treatment. Advanced Technologies & Treatments for Diabetes (ATTD), February 2023 (Poster).
2. Emilie B. Lindkvist, Christian Laugesen, Tobias K. S. Ritschel, Asbjørn Thode Reenberg, Jannet Svensson, John Bagterp Jørgensen, Kirsten Nørgaard, Ajenthen G. Ranjan. Performance of a Dual-hormone Closep-loop System versus Insulin-only Closed-loop in Adolescents with Type 1 Diabetes. A Single-blind, Randomized, Controlled, Cross-over Trial. Advanced Technologies & Treatments for Diabetes (ATTD), February 2023.
3. M. Eichenlaub, G. Freckmann, T. Schrills, A. Thode Reenberg, T. Ritschel, J. Jørgensen, H.-J. Lüddecke, S. Hohm, I. Seidler, J. Schmitzer, H. Berz, R. Blechschmidt, H. Perscher. A numerical comparison of the UVA/Padova Type 1 Diabetes Simulator and the Open-Source simulator LT1. Advanced Technologies & Treatments for Diabetes (ATTD), February 2023 (Poster).
4. Asbjørn Thode Reenberg, Tobias K. S. Ritschel, Emilie B. Lindkvist, Christian Laugesen, Jannet Svensson, Ajenthen G. Ranjan, John Bagterp Jørgensen. A Dual-Hormone Artificial Pancreas in a Pre-trial Virtual Clinical Trial. Advanced Technologies & Treatments for Diabetes (ATTD), April 2022.
5. Clara Furió-Novejarque, Ricardo Sanz, Asbjørn Thode Reenberg, Tobias K. S. Ritschel, Ajenthen G. Ranjan, José-Luis Díez, John Bagterp Jørgensen, Jorge Bondia. Validation of a novel model of glucagon effect including glucagon receptor dynamics. Advanced Technologies & Treatments for Diabetes (ATTD), April 2022.
6. Asbjørn Thode Reenberg, Tobias K. S. Ritschel, Emilie B. Lindkvist, Christian Laugesen, Ajenthen G. Ranjan, Jannet Svensson, Kirsten Nørgaard, John Bagterp Jørgensen. A Dual-hormone Artificial Pancreas based on Nonlinear Model Predictive Control and Maximum Likelihood Estimation. Nordic Process Control Workshop (NPCW), March 2022 (Poster).
7. Asbjørn Thode Reenberg, Tobias K. S. Ritschel, John Bagterp Jørgensen. NMPC and MLE for a Dual-Hormone Artificial Pancreas. DTU Diabetes Symposium, November 2021 (Invited).

8. Asbjørn Thode Reenberg, Tobias K. S. Ritschel, John Bagterp Jørgensen. Large-scale Virtual Clinical Trials of Closed-loop Diabetes Treatment. Danish Diabetes Academy (DDA) annual meeting, December 2021 (Pitch and poster).
9. Ajenthen G. Ranjan, Christian Laugesen, Dimitri Boiroux, Signe Schmidt, Asbjørn Thode Reenberg, John Bagterp Jørgensen, Kirsten Nørgaard. Performance of a Dual Hormone Closed-Loop System vs. an Insulin-Only Closed-Loop System during Challenging Inpatient Conditions: A Single-Blinded Randomized Controlled Crossover Trial. *Diabetes* 2021;70;215-OR.
10. Ajenthen G. Ranjan, Christian Laugesen, Dimitri Boiroux, Signe Schmidt, Asbjørn Thode Reenberg, John Bagterp Jørgensen, Kirsten Nørgaard. Glucose Sensor Accuracy During Subcutaneous Glucagon Infusion Near Sensor Site. *Advanced Technologies & Treatments for Diabetes (ATTD)*, June 2021.

CHAPTER 2

Models

In this chapter, we describe and list the models used or developed during the thesis. The different models have been a central component during all of the thesis and range from relatively simple models suitable for control to whole-body models. There exist many models in the literature to describe the dynamics in people with both T1D and T2D and for people in ICU, but here we only list the models that were directly used or developed during the thesis. We divide the descriptions of the models into descriptions of the submodels where Section 2.2 describes insulin models, Section 2.3 describes glucagon models, Section 2.4 describes meal models, Section 2.5 describes exercise models, Section 2.6 describes CGM models, Section 2.7 describes glucose models, Section 2.8 describes whole-body models, and Section 2.9 discusses the differences in T2D and ICU models compared to T1D models. Appendices A-C are directly related to modeling and describe a whole-body model and a glucagon model developed during the thesis. Appendix D collects multiple meal models for simulation of the human metabolism. Appendices F-I and M describe the models used to represent virtual participants for virtual clinical trials and Appendix I and J describe the control model used in the DiaCon AP. Finally, Appendix O includes three different models to simulate people in the ICU extended with a simple representation of stress. The model parameters used in the clinical trial of the DiaCon AP are listed in Appendix L and the model parameters used in the virtual clinical trials are listed in Appendix H. Appendix D lists parameters for the meal models and Appendix C lists parameters for the UPV glucagon model.

2.1 General form

The models described in this section can be written (and implemented) as a continuous-discrete stochastic system in the form

$$x(t_0) = x_0, \tag{2.1a}$$

$$dx(t) = f(t, x(t), u(t), d(t), \theta)dt + \sigma(t, x(t), u(t), d(t), \theta)d\omega(t), \tag{2.1b}$$

$$z(t) = h(t, x(t), \theta) \tag{2.1c}$$

$$y(t_k) = g(t_k, x(t_k), \theta) + v(t_k). \tag{2.1d}$$

Here, t is time, t_0 is the initial time, x are the states, x_0 are the initial states, u are manipulated inputs (e.g., insulin and glucagon administration), d are disturbances (e.g., meals and exercise), and θ are parameters. The first term in (2.1b) is the deterministic

(drift) term, and the second term is the stochastic (diffusion) term. y are the measurements (e.g, from a CGM) with measurement noise, v . z , are the outputs and are used in, e.g., the control algorithm. Additionally, $\omega(t)$ is a standard Wiener process, and $v(t_k)$ is normally distributed measurement noise at discrete time, i.e.,

$$d\omega(t) \sim N_{iid}(0, Idt), \quad (2.2a)$$

$$v(t_k) \sim N_{iid}(0, R). \quad (2.2b)$$

2.2 Insulin models

In this section, we present the insulin models used in the thesis. The insulin models include compartments for the plasma insulin concentration and the insulin effect. Furthermore, the models include compartments for subcutaneous insulin absorption to describe insulin delivery from, e.g., a pump or a pen. We describe the insulin subsystem from the 1) Hovorka model [18, 46], 2) UVA/Padova model [53, 54], and 3) MVP model [55].

2.2.1 Hovorka model

The Hovorka model describes the absorption of fast acting insulin (both bolus and basal) as a two-compartment chain, S_1 and S_2 [mU], by

$$\dot{S}_1(t) = u_I(t) - \frac{S_1(t)}{\tau_S}, \quad (2.3a)$$

$$\dot{S}_2(t) = \frac{S_1(t)}{\tau_S} - \frac{S_2(t)}{\tau_S}, \quad (2.3b)$$

$$(2.3c)$$

where u_I [mU/min] is the insulin administration rate and τ_s [min] is a time constant for maximum insulin absorption. The appearance of insulin in the plasma is the amount that leaves S_2 [mU], i.e., $\frac{S_2(t)}{\tau_S}$ distributed in the volume, V_i [L]. The plasma insulin concentration, $I(t)$ [mU/L], is

$$\dot{I}(t) = \frac{1}{V_I} \frac{S_2(t)}{\tau_S} - k_e I(t), \quad (2.4)$$

where k_e [1/min] is the fractional elimination rate. Finally, the three compartments for insulin action on the glucose kinetics are

$$\dot{x}_1(t) = k_{b1}I(t) - k_{a1}x_1(t), \quad (2.5a)$$

$$\dot{x}_2(t) = k_{b2}I(t) - k_{a2}x_2(t), \quad (2.5b)$$

$$\dot{x}_3(t) = k_{b3}I(t) - k_{a3}x_3(t). \quad (2.5c)$$

Here, x_1 [1/min] represents the insulin effect on glucose distribution, x_2 [1/min] represents the insulin effect on glucose disposal, and x_3 [1/min] represents the insulin effect on endogenous glucose production. k_{ai} and k_{bi} [1/min], $i = 1, \dots, 3$, are activation and deactivation rates.

2.2.2 UVA/Padova model

In the UVA/Padova model, the insulin absorption of subcutaneously administered insulin is described by

$$\dot{I}_{sc1}(t) = -(k_d + k_{a1})I_{sc1}(t) + \frac{u_I(t)}{BW}, \quad (2.6a)$$

$$\dot{I}_{sc2}(t) = k_d I_{sc1}(t) - k_{a2} I_{sc2}(t), \quad (2.6b)$$

where I_{sc1} and I_{sc2} [pmol/kg] are insulin in a non-monomeric and monomeric state. k_d , k_{a1} , and k_{a2} [1/min] are rate parameters where $k_{a2} > k_{a1}$ to represent that insulin absorption is faster in the monomeric state. u_I [pmol/min] is the subcutaneous insulin infusion rate. The appearance rate of insulin in the plasma, Ra_{Isc} [pmol/kg/min], is described by the combined absorption from the non-monomeric and monomeric state, i.e.

$$Ra_{Isc}(t) = k_{a1} I_{sc1}(t) + k_{a2} I_{sc2}(t). \quad (2.7)$$

The insulin mass in the liver, I_ℓ , and plasma, I_p [pmol/kg], are described by

$$\dot{I}_\ell(t) = -(m_1 + m_3)I_\ell(t) + m_2 I_p(t), \quad (2.8a)$$

$$\dot{I}_p(t) = -(m_2 + m_4)I_p(t) + m_1 I_\ell(t) + Ra_{Isc}(t), \quad (2.8b)$$

where m_1 and m_2 [1/min] are rate parameters to describe the transport between the liver and plasma and m_3 and m_4 [1/min] are rate parameters for degradation computed by

$$m_2 = \frac{3CL}{5HE_b V_i BW}, \quad (2.9a)$$

$$m_3 = \frac{HE_b m_1}{1 - HE_b}, \quad (2.9b)$$

$$m_4 = \frac{2CL}{5V_i BW}. \quad (2.9c)$$

CL [L/min] is the insulin clearance, HE_b [-] is the basal hepatic insulin extraction, and BW [kg] is the body weight. The plasma insulin concentration, I [pmol/L], is

$$I(t) = \frac{I_p(t)}{V_i}, \quad (2.10)$$

where V_i [L/kg] is the insulin distribution volume. In the UVA/Padova model, insulin affects the glucose utilization and the endogenous glucose production (EGP). The insulin concentration in the interstitial fluid, X [pmol/L], affects the glucose utilization

described in Section 2.7 and is described by

$$\dot{X}(t) = -p_{2U}X(t) + p_{2U}(I(t) - I_b). \quad (2.11)$$

Here, p_{2U} [1/min] is the rate of the insulin action on the peripheral glucose utilization and I_b [pmol/L] is the basal insulin plasma concentration. Furthermore, a delayed insulin signal represented by a two-compartment chain, I_d and I_1 [pmol/L], affects the EGP described in Section 2.7. The delayed insulin signal is described by

$$\dot{I}_d(t) = -k_i(I_d(t) - I_1(t)), \quad (2.12a)$$

$$\dot{I}_1(t) = -k_i(I_1(t) - I(t)), \quad (2.12b)$$

where k_i [1/min] is a rate parameter to describe the delay between the insulin signal and the insulin action on EGP.

2.2.3 Medtronic virtual patient model

The final insulin subsystem is from the MVP model and describes the insulin concentration in the subcutaneous tissue, I_{SC} [mU/L], and the plasma, I_P [mU/L], by

$$dI_{SC}(t) = k_1 \left(\frac{u_I(t)}{C_I} - I_{SC}(t) \right) dt, \quad (2.13a)$$

$$dI_P(t) = k_2 (I_{SC}(t) - I_P(t)) dt, \quad (2.13b)$$

where u_I [mU/min] is the subcutaneous insulin administration rate, $k_2 = k_1$ [1/min] is the inverse insulin absorption time constant, and C_I [L/min] is the insulin clearance rate. We set $k_2 = k_1$ for identifiability [56]. The insulin effect, I_{EFF} [1/min], is described by

$$dI_{EFF}(t) = p_2 (S_I(t)I_P(t) - I_{EFF}(t)) dt, \quad (2.14a)$$

$$d \log(S_I(t)) = \sigma_{S_I} dw_{S_I}(t). \quad (2.14b)$$

$p_2 = k_1$ [1/min] is a time constant, $GEZI$ [1/min] is the glucose effectiveness, EGP [(mmol/L)/min] is the EGP. The insulin sensitivity, S_I [(L/mU)/min], is adaptive and is estimated with the CD-EKF described in Section 4.3.1. Furthermore, σ_{S_I} is the insulin sensitivity diffusion coefficient, and w_G and w_{S_I} are standard wiener processes.

2.3 Glucagon models

In this section, we present the glucagon models used during the thesis. We present 1) the Haider model [57], and 2) the UVP model (Appendix B and C). As the UPV model was developed towards the end of the thesis, we only used the Haider model in the virtual clinical trials and the DiaCon AP.

2.3.1 Haidar model

The Haidar model describes the glucagon absorption as a two-compartment chain, Q_1^G and Q_2^G [μg], by

$$\dot{Q}_1^G(t) = u_G(t) - \frac{Q_1^G(t)}{\tau_{Glu}}, \quad (2.15a)$$

$$\dot{Q}_2^G(t) = \frac{Q_1^G(t)}{\tau_{Glu}} - \frac{Q_2^G(t)}{\tau_{Glu}}, \quad (2.15b)$$

where u_G [$\mu\text{g}/\text{min}$] is the subcutaneous glucagon infusion rate and τ_{Glu} [min] is the glucagon absorption time constant. We describe how the model is included in the Hovorka model and the MVP model in Section 2.7.

2.3.2 UPV model

The UPV model also describes the absorption of glucagon as a two-compartment chain, Q_1^G and Q_2^G [pg], by

$$\dot{Q}_1^G(t) = u_G(t) - k_1 Q_1^G(t), \quad (2.16a)$$

$$\dot{Q}_2^G(t) = k_1 Q_1^G(t) - k_2 Q_2^G(t), \quad (2.16b)$$

where k_1 and k_2 are rate parameters and the glucagon concentration, C [pg/mL], is

$$C(t) = \frac{k_2 Q_2^G(t)}{BW \cdot Cl_{F,C}} + C_b. \quad (2.17)$$

BW [kg] is the body weight, $Cl_{F,C}$ [$\text{ml}/\text{kg}/\text{min}$] is the apparent glucagon clearance, and C_b [pg/mL] is the basal glucagon concentration. In addition to the Haidar glucagon model, the UPV model also includes glucagon receptor dynamics [58]. The receptors are described in three different states 1) available, r , 2) bonded to glucagon, r_c , and 3) internalized, r_i [unitless]. The receptors become unavailable in the internalized state. By assuming that the number of receptors is constant, one state can be eliminated, and we can express the internalized receptors by

$$r_i(t) = 1 - r(t) - r_c(t). \quad (2.18)$$

The available and bonded receptors are described by

$$\dot{r}(t) = -k_{on} V_h C(t) r(t) + k_{off} r_c(t) + k_{rec} r_i(t), \quad (2.19a)$$

$$\dot{r}_c(t) = k_{on} V_h C(t) r(t) - k_{off} r_c(t) - k_{in} r_c(t). \quad (2.19b)$$

k_{on} [$(\text{pg}/\text{min})^{-1}$] is the association rate of glucagon to the receptor, V_h [ml] is the volume of the hepatic interstitial space, k_{off} [$1/\text{min}$] is the dissociation rate, k_{rec} [$1/\text{min}$] is the recycling rate, and k_{in} [$1/\text{min}$] is the internalization rate of the glucagon-bonded receptor.

F_{hgp} [$\mu\text{mol/kg/min}$] is the hepatic glucose production and is dependent on the glucagon receptors by the Michaelis-Menten relation

$$F_{hgp}(t) = \frac{V_r r_c(t)}{K_r + r_c(t)}, \quad (2.20)$$

where V_r [$\mu\text{mol/kg/min}$] is the maximum glucagon-dependent hepatic glucose production rate and K_r [unitless] is the apparent dissociation constant. In the UPV model, the expression for the EGP (described in Section 2.7), the hepatic glucose production is added to the effect of insulin on the glucose production in the liver.

2.4 Meal models

In this section, we present the meal models used in the thesis. The meal models are primarily described in Appendix D. We present the 1) Hovorka model [18, 46], 2) UVA/-Padova model [59], 3) SIMO model [60], 4) Alskär model [61], and 5) CSTR-PFR model based on Moxon et al. [62]. The models introduced here consider only the carbohydrate content of meals and not the nutritional content or, e.g., amount of calories, which also affects the digestion of food and appearance of glucose in the plasma [63]. The DiaCon AP and the virtual participants in the large scale virtual clinical trials are based on Hovorka's meal model.

2.4.1 Hovorka model

The meal absorption subsystem in the Hovorka model is described as a two-compartment chain, D_1 and D_2 [mmol],

$$\dot{D}_1(t) = A_G D(t) - \frac{D_1(t)}{\tau_D}, \quad (2.21a)$$

$$\dot{D}_2(t) = \frac{D_1(t)}{\tau_D} - \frac{D_2(t)}{\tau_D}. \quad (2.21b)$$

Here, D [mmol/min] is the amount of carbohydrates in the meals, A_G [unitless] is the carbohydrate bioavailability, and τ_D [min] is the meal absorption time constant. The amount of carbohydrates in the meal, $D(t)$ [mmol/min], can be converted to $d(t)$ [g CHO/min] by

$$D(t) = \frac{1000}{M_{wG}} d(t), \quad (2.22)$$

where $M_{wG} = 180.1577$ [g/mol] is the molecular weight of glucose. The rate of appearance, RA [mmol/min], is

$$RA = f \frac{D_2(t)}{\tau_D}, \quad (2.23)$$

where f [unitless] is the fraction of the consumed carbohydrates that appears in the blood.

2.4.2 UVA/Padova model

In the UVA/Padova model, meals are consumed by updating the initial condition of the states and it is a single meal model (the UVA/Padova has been extended to a single day [45]). The meal absorption is described by three compartments that represent 1) the solid phase of the stomach, Q_{sto1} [mg], 2) the liquid phase of the stomach, Q_{sto2} [mg], and 3) the glucose mass in the intestine, Q_{gut} [mg]. The solid and liquid phases are described by

$$\dot{Q}_{sto1} = -k_{gri}Q_{sto1}, \quad Q_{sto1}(t_0) = D, \quad (2.24a)$$

$$\dot{Q}_{sto2} = -k_{empt}Q_{sto2} + k_{gri}Q_{sto1}, \quad Q_{sto2}(t_0) = 0. \quad (2.24b)$$

Here, k_{gri} [1/min] is the grinding rate and D [mg] is the total amount of carbohydrates in the meal. The total amount of glucose in the stomach is

$$Q_{sto} = Q_{sto1} + Q_{sto2}, \quad (2.25)$$

where k_{empt} [1/min] is the emptying rate that depends on the amount in the stomach and is described by

$$k_{empt} = k_{min} + \frac{k_{max} - k_{min}}{2} \left(\tanh(\alpha(Q_{sto} - bD)) - \tanh(\beta(Q_{sto} - cD)) + 2 \right), \quad (2.26a)$$

$$\alpha = \frac{5}{2D(1 - b)}, \quad (2.26b)$$

$$\beta = \frac{5}{2Dc}. \quad (2.26c)$$

k_{max} [1/min] is the maximum emptying rate that decreases with a rate α [1/mg] to the minimum emptying rate k_{min} [1/min] until it recovers back to the maximum by a rate β [1/mg]. b and c [unitless] relate to the shape of the curve that the emptying rate decreases and increases with. Finally, the glucose mass in the intestine, Q_{gut} , and the rate of appearance, RA [mg/kg/min], is

$$\dot{Q}_{gut} = -k_{abs}Q_{gut} + k_{empt}Q_{sto2}, \quad Q_{gut}(t_0) = 0, \quad (2.27a)$$

$$RA = \frac{fk_{abs}Q_{gut}}{BW}, \quad (2.27b)$$

where, k_{abs} [1/min] is the absorption rate, BW [kg] is the body weight, and f [unitless] is the fraction of the consumed carbohydrates that appear in the blood.

2.4.3 SIMO model

The SIMO model also describes the absorption of meals with compartments for the stomach and intestine, but the SIMO model describes the transport through the intestine

by modeling 1) the jejunum, J [mmol], 2) a delay compartment, R [mmol], and 3) the ileum, L [mmol]. The stomach, S [mmol], is described by

$$\dot{S} = -k_{js}S, \quad S(t_0) = D, \quad (2.28)$$

where k_{js} [1/min] is glucose transfer rate from the stomach to the jejunum and D [mmol] is the glucose in the stomach (meal) at the initial time. The glucose in the jejunum is described by

$$\dot{J} = k_{js}S - k_{gj}J - k_{rj}J, \quad J(t_0) = 0. \quad (2.29)$$

k_{gj} [1/min] is the transfer rate from the jejunum to the plasma and k_{rj} [1/min] is the transfer rate from the jejunum to the delay compartment. The delay compartment is

$$\dot{R} = -k_{lr}R + k_{rj}J, \quad R(t_0) = 0, \quad (2.30)$$

where k_{lr} [1/min] is the transfer rate from the delay compartment to the ileum. Finally, the ileum is described by

$$\dot{L} = k_{lr}R - k_{gl}L, \quad L(t_0) = 0. \quad (2.31)$$

Here, k_{gl} [1/min] is the transport rate from the ileum to the plasma. The rate of appearance, RA [mmol/L/min], is the combined contribution from the jejunum and the ileum

$$RA = \frac{f(k_{gj}J + k_{gl}L)}{V \cdot BW}, \quad (2.32)$$

where f [unitless] is the fraction of glucose that appear in the plasma, V [L/kg] is the distribution volume and the BW [kg] is the body weight.

2.4.4 Alskär model

The Alskär model includes a compartment for the duodenum instead of the delay compartment in the SIMO model. The Stomach, G_S [mg], duodenum, G_D [mg], G_J [mg], and ileum, G_I [mg] are represented by

$$\dot{G}_S = -k_{SD}\tau G_S, \quad G_S(t_0) = D, \quad (2.33a)$$

$$\dot{G}_D = k_{SD}\tau G_S - k_{DJ}G_D - RA_D, \quad G_D(t_0) = 0, \quad (2.33b)$$

$$\dot{G}_J = k_{DJ}G_D - k_{JI}G_J - RA_J, \quad G_J(t_0) = 0, \quad (2.33c)$$

$$\dot{G}_I = k_{JI}G_J - RA_I, \quad G_I(t_0) = 0, \quad (2.33d)$$

where D [mg] is the glucose in the stomach (meal) at the initial time and the flow rates between the compartments are

$$k_{SD} = k_w \left(1 - \frac{G_D^\gamma}{IG_{D50}^\gamma + G_D^\gamma} \right), \quad (2.34a)$$

$$k_{DJ} = \frac{1}{L_D T}, \quad (2.34b)$$

$$k_{JI} = \frac{1}{L_J T}, \quad (2.34c)$$

$$\tau = \frac{1}{1 + \exp(-\sigma(t - t_{50}))}. \quad (2.34d)$$

k_{SD} [1/min] is the emptying rate of the stomach described as a hill function with the hill factor γ [unitless] and amount of glucose corresponding to a 50% reduction of the gastric emptying rate, IG_{D50} [mg]. k_w [1/min] is the emptying rate for a noncaloric liquid. The hill function represents the pylorus sphincter that can control gastric emptying. K_{DJ} and K_{JI} [1/min] are the transport rates from duodenum to the jejunum and from the jejunum to the ileum. L_D and L_J [unitless] are fractions of the total length of the intestine and T [min] is the transit time. τ [unitless] is a lag coefficient to represent a delay, where σ [1/min] defines the steepness, and t_{50} [min] is the time for which $\tau = 0.5$. The rate of appearance, RA [mg/min/kg], is described as the combined contribution from each compartment in the intestine and is described with Michaelis-Menten relations to represent saturation of the glucose transporters, i.e.

$$RA = F_P \frac{RA_D + RA_J + RA_I}{BW}, \quad (2.35a)$$

$$RA_D = \frac{RA_{maxD} G_D}{K_{mG} + G_D}, \quad (2.35b)$$

$$RA_J = \frac{RA_{maxJ} G_J}{K_{mG} + G_J}, \quad (2.35c)$$

$$RA_I = \frac{RA_{maxI} G_I}{K_{mG} + G_I}, \quad (2.35d)$$

where, K_{mG} [mg] is the amount of glucose corresponding to a 50% reduction of the absorption rate, RA_{max_i} [mg/min] for $i = D, J, I$ is the maximum absorption rate from the duodenum, jejunum, and ileum, F_P [unitless] is the fraction of glucose that appears in the plasma, and BW [kg] is the body weight.

2.4.5 CSTR-PFR model

The CSTR-PFR model describes the stomach as a continuous stirred-tank reactor (CSTR) and the small intestine as a plug flow reactor (PFR). It is based on the second model presented by Moxon et al. [62]. Contrary to the previous models, the CSTR-PFR model also contains partial differential equations (PDEs).

The stomach, m_s [mg], is represented by

$$\dot{m}_s = F_m - F_{sd}, \quad (2.36a)$$

$$F_{sd} = k_{sd}m_s, \quad (2.36b)$$

where $F_m = d$ [mg/min] is the carbohydrates in meals and F_{sd} [mg/min] is the flow rate from the stomach to the duodenum. k_{sd} [1/min] is an inverse time constant and represents the pylorus sphincter. k_{sd} is assumed to be either 1) constant, 2) a function of the glucose rate of appearance in the plasma [64], or 3) a function of the amount of glucose in the duodenum [61]. The glucose concentration, c_{si} [mg/m²], in the small intestine is described by the PDE

$$\partial_t c_{si} = -\partial_z N_p - Q_a, \quad z \in [z_0, z_f]. \quad (2.37)$$

where, z [m] is the spatial coordinate along the small intestine, and the positions z_0 and z_f [m] are the boundaries. The peristaltic movement in the small intestine is described by the flux, N_p [mg/m/min], and it consists of an advection term, N_{ap} [mg/m/min], and a diffusion term, N_{dp} [mg/m/min], i.e.

$$N_p = N_{ap} + N_{dp}, \quad (2.38a)$$

$$N_{ap} = v_p c_{si}, \quad (2.38b)$$

$$N_{dp} = -D_p \partial_z c_{si}. \quad (2.38c)$$

v_p [m/min] is the constant velocity and D_p [m²/min] is the constant diffusion coefficient. The glucose absorption, Q_a [mg/m²/min], is described by

$$Q_a = \frac{2f}{r_{si}} q_a, \quad (2.39a)$$

$$q_a = v_a c_{si}, \quad (2.39b)$$

where r_{si} [m] is the radius of the small intestine, f [unitless] is a factor that describes how much of the glucose that is absorbed, and v_a [m/min] is the glucose absorption rate. The boundary condition between the stomach and the duodenum is

$$A_{si} N_p|_{z=z_0} = F_{sd}, \quad (2.40)$$

which means that the flux at the beginning of the small intestine times the cross-sectional area, A_{si} [m²] must be equal to the glucose flow rate, F_{sd} .

Finally, the glucose rate of appearance, R_A [mg/min], is

$$R_A = A_{si} \int_{z_0}^{z_f} Q_a dz. \quad (2.41)$$

2.5 Physical activity models

During the thesis, we only applied the model by Rashid et al. [65], but more models of physical activity exist in the literature, e.g., the model by Resalat et al. [50] or by

Breton [66]. Some models use heart rate to measure exercise intensity (e.g. the Rashid model), but exercise intensity measured by heart rate can be converted to heart rate reserve by

$$HR = HR_R(HR_{max} - HR_{rest}) + HR_{rest}, \quad (2.42)$$

where HR [BPM] is the heart rate that corresponds to the heart rate reserve, HR_R [%], HR_{max} [BPM] is the maximum heart rate and HR_{rest} [BPM] is the resting heart rate. We use the following simple approximation of the maximum heart rate:

$$HR_{max} = 220 - age. \quad (2.43)$$

2.5.1 Rashid model

The Rashid model includes both the short-term effects of exercise, E_1 [BPM], and the long-term effects of exercise, E_2 [min]. The model is described by

$$\dot{E}_1(t) = \frac{HR(t) - HR_0 - E_1(t)}{\tau_{HR}}, \quad (2.44a)$$

$$\dot{T}_E(t) = \frac{c_1 f_{E1}(t) + c_2 - T_E(t)}{\tau_{ex}}, \quad (2.44b)$$

$$\dot{E}_2(t) = - \left(\frac{f_{E1}(t)}{\tau_{in}} + \frac{1}{T_E(t)} \right) E_2(t) + \frac{f_{E1}(t) T_E(t)}{c_1 + c_2}, \quad (2.44c)$$

$$f_{E1}(t) = \frac{\left(\frac{E_1(t)}{a \cdot HR_0} \right)^n}{1 + \left(\frac{E_1(t)}{a \cdot HR_0} \right)^n}. \quad (2.44d)$$

Here, T_E [min] is the characteristic time for the long-term effects of exercise, where c_1 [min] and c_2 [min] define the steady state value and τ_{ex} [min] is the time constant for how fast the steady state is reached, HR [BPM] is the heart rate, HR_0 [BPM] is the resting heart rate and τ_{HR} [min] is a time constant. a [unitless], n [unitless], and τ_{in} [min] specify the intensity and time constant of the long-term effect exercise on the insulin action. We describe how the exercise subsystem is included in the Hovorka model in section 2.7.

2.6 CGM models

In the thesis, we used the CGM model developed by Facchinetti et al. [67] in a simplified version, where the measurement noise is assumed to be normally distributed. CGM models represent that CGMs measure from the subcutaneous interstitial tissue with some sensor noise.

2.6.1 Fachinetti model

The Fachinetti model describes the glucose transport from the plasma to the interstitial tissues and a non-Gaussian sensor noise. The non-Gaussian sensor noise represents the additional lags and delays caused by the CGM. The interstitial glucose concentration, G_{SC} [mg/dL], is described by

$$\dot{G}_{SC} = \frac{1}{\tau_{G,SC}} (G(t) - G_{SC}(t)). \quad (2.45)$$

The time constant, $\tau_{G,SC}$, is 6.7 min. The non-Gaussian sensor noise is represented by the sum of the two autoregressive processes

$$cc_k = 1.23cc_{k-1} - 0.3995cc_{k-2} + w_{cc,k}, \quad (2.46a)$$

$$\hat{v}_k = 1.013\hat{v}_{k-1} - 0.2135\hat{v}_{k-2} + w_k, \quad (2.46b)$$

where $w_{cc,k} \sim N(0, 11.3 \text{ mg}^2/\text{dL}^2)$ and $w_k \sim N(0, 14.45 \text{ mg}^2/\text{dL}^2)$. The discrete time measurements from the CGM are described by

$$y_k = G_{SC}(t_k) + cc_k + \hat{v}_k. \quad (2.47)$$

During the thesis, we assume that the sensor noise is normally distributed as in (2.1) and neglect the non-Gaussian sensor noise described by this model.

2.7 Glucose models

We applied three different glucose models during the thesis 1) the Hovorka model [18, 46], 2) the UVA/Padova model [53, 54], and 3) MVP model [55]. The glucose models describe the plasma glucose concentration and include different representations of the physiological phenomena that affect both the glucose consumption and glucose production.

2.7.1 Hovorka model

The Hovorka model describes the glucose subsystem by the accessible, Q_1 [mmol], and non-accessible, Q_2 [mmol], glucose compartments

$$\dot{Q}_1(t) = RA(t) - F_{01,c}(t) - F_R(t) - x_1(t)Q_1(t) + k_{12}Q_2(t) + EGP, \quad (2.48a)$$

$$\dot{Q}_2(t) = x_1(t)Q_1(t) - k_{12}Q_2(t) - x_2Q_2(t). \quad (2.48b)$$

Here, RA [mmol/min] is the rate of appearance of meal carbohydrates, k_{12} [1/min] is a transfer rate between the compartments, EGP [mmol/min] is the EGP, and x_i , $i = 1 \dots 3$, is the insulin action (2.5). Furthermore, the corrected total non-insulin dependent

glucose flux, $F_{01,c}$ [mmol/min], and the renal glucose clearance, F_R [mmol/min], are described by

$$F_{01,c}(t) = \begin{cases} F_{01} & G(t) \geq 4.5 \text{ mmol/L}, \\ F_{01}G(t)/4.5 & \text{otherwise,} \end{cases} \quad (2.49a)$$

$$F_R(t) = \begin{cases} 0.003(G(t) - 9)V_G & G(t) \geq 9 \text{ mmol/L}, \\ 0 & \text{otherwise,} \end{cases} \quad (2.49b)$$

where F_{01} [mmol/min] is the nominal total non-insulin dependent glucose flux. The plasma glucose concentration, G [mmol/L], is the glucose in the accessible compartment divided by the distribution volume, V_G [L], i.e.

$$G(t) = \frac{Q_1(t)}{V_G}. \quad (2.50)$$

In the nominal case, the EGP is

$$EGP = EGP_0(1 - x_3(t)), \quad (2.51)$$

where EGP_0 [mmol] is the EGP extrapolated to zero insulin concentration, but the UPV glucagon model modifies the EGP to represent the effect of glucagon on the hepatic glucose production (2.20), i.e.

$$EGP(t) = F_{hgp}(t) + EGP_0(1 - S_{I,h}x_3(t)). \quad (2.52)$$

Here, $S_{I,h}$ [(mU/L)⁻¹] is the hepatic insulin sensitivity. The Haider glucagon model instead adds $K_{Glu}V_GQ_2^G(t)$ to (2.48a), where K_{Glu} [(mmol/L)/μg/min] is the glucagon gain. The Rashid exercise model can be included by subtracting

$$Q_{E21}(t) = \alpha E_2(t)^2 x_1(t) Q_1(t), \quad (2.53)$$

from (2.48a) and adding it to (2.48b). Furthermore,

$$Q_{E22}(t) = \alpha E_2(t)^2 x_2(t) Q_2(t), \quad (2.54)$$

and

$$Q_{E1}(t) = \beta \frac{E_1(t)}{HR_0}, \quad (2.55)$$

are subtracted from (2.48b).

2.7.2 UVA/Padova model

In this thesis, we only used the UVA/Padova model without including glucagon or exercise. In the UVA/Padova model, the glucose subsystem includes compartments for

the glucose mass in the plasma and equilibrating tissues, rapidly equilibrating, G_p [mg], and slowly equilibrating G_t [mg]. It is described by

$$\dot{G}_p(t) = EGP(t) + RA(t) - U_{ii}(t) - E(t) - k_1 G_p(t) + k_2 G_t(t), \quad (2.56a)$$

$$\dot{G}_t(t) = -U_{id}(t) + k_1 G_p(t) - k_2 G_t(t). \quad (2.56b)$$

Here, RA [mg/kg/min] is the rate of appearance of carbohydrates from the meals, and k_1 [1/min] and k_2 [1/min] are rate parameters, E [mg/kg/min] is the renal excretion, and U_{ii} and U_{id} [mg/kg/min] are the insulin-independent and insulin-dependent glucose utilizations given by

$$U_{ii}(t) = F_{cns}, \quad (2.57a)$$

$$U_{id}(t) = \frac{(V_{m0} + V_{mx}X(t))G_t(t)}{K_{m0} + G_t(t)}. \quad (2.57b)$$

F_{cns} [(mg/kg)/min] is the glucose uptake of the erythrocytes and the brain, V_{mx} [mg L/(kg pmol min)] and K_{m0} [mg/kg] are parameters, X [pmol/L] is the insulin concentration in the interstitial fluid (2.11), p_{2U} [1/min] is the rate of the insulin action on the peripheral glucose utilization, I_b [pmol/L] is the basal insulin plasma concentration, and V_{m0} [(mg/kg)/min] is

$$V_{m0} = \frac{(EGP_b - F_{cns})(K_{m0} + G_{tb})}{G_{tb}}, \quad (2.58)$$

with

$$G_{tb} = \frac{F_{cns} - EGP_b + k_1 G_{pb}}{k_2}. \quad (2.59)$$

EGP_b [mg/kg/min] is the basal EGP, and G_{tb} and G_{pb} [mg/kg] are the basal glucose masses. Next, the EGP is

$$EGP(t) = \max\{0, EGP_b - k_{p2}(G_p(t) - G_{pb}) - k_{p3}(I_d(t) - I_b)\}, \quad (2.60)$$

where k_{p2} [1/min] and k_{p3} [mg L/(kg pmol min)] are the liver glucose effectiveness and the amplitude of the insulin action of the liver. I_d is the delayed insulin signal (2.12a), and I_b [pmol/L] is the basal plasma insulin concentration. Finally, the renal excretion, E , is

$$E(t) = \max\{0, k_{e1}(G_p(t) - k_{e2})\}, \quad (2.61)$$

where k_{e1} [1/min] and k_{e2} [mg/kg] are the glomerular filtration rate and the renal glucose threshold. The plasma glucose concentration is computed by dividing the glucose mass in the plasma, G_p , by the distribution volume, V_g [dL/kg], i.e.

$$G(t) = \frac{G_p(t)}{V_g}. \quad (2.62)$$

2.7.3 Medtronic virtual patient model

The MVP model describes the glucose subsystem by a single compartment representing the glucose concentration, G [mmol/L]. We only use the MVP model in the DiaCon AP. We describe the MVP model as a stochastic differential equation (SDE) and include glucagon from Haidar's glucagon model

$$dG(t) = [-(GEZI + I_{EFF}(t))G(t) + EGP + RA(t) + K_{Glu}Q_2^G(t)]dt + \sigma_G dw_G(t). \quad (2.63)$$

Here, I_{EFF} [1/min] is the insulin effect (2.14a), $GEZI$ [1/min] is the glucose effectiveness, EGP [(mmol/L)/min] is the endogenous glucose production, RA [mmol/min/L] is the rate of appearance of meals (we use Hovorka's meal model in the DiaCon AP), K_{Glu} [(mmol/L)/ μ g/min] is the glucagon gain, Q_2^G [μ g] is the second compartment in the Haidar glucagon model (2.15b) (this term should be removed if glucagon is not included in the model), σ_G is the glucose diffusion coefficient, and w_G is a standard wiener processes.

2.8 Whole-body models

Whole-body models describe much more detailed representations of the human physiology, but include many more states and parameters that can be hard, if not impossible to estimate. In 1985, Sorensen presented a whole-body model that includes insulin, glucagon, and glucose dynamics [68]. Since then, more models have been proposed as discussed in Appendix A. During this thesis, we presented a whole-body model that includes 7 organs, 16 metabolites, and 31 enzymatic reactions, and includes digestion of meals (carbohydrates, protein, and lipids) and external administration of glucagon and insulin. Here, we briefly introduce the methodology, but leave out the full system of equations and instead refer to appendix A. Figure 2.1 shows a diagram of the model and the dynamics of each compartment is described in the form

$$V \frac{dC}{dt} = M(Q_{in}C_{in} - Q_{out}C) + RV, \quad (2.64)$$

where V is the volume, C is the concentration of the metabolites, M represents the external and internal component ordering, Q_{in} are the inflow rates, C_{in} is the concentration of the metabolites that flow in, and Q_{out} are the outflow rates. The production rate, R , is defined as

$$R = (TS)'Tr, \quad (2.65)$$

where r are the reaction rates, S is the stoichiometric matrix, T is a matrix to define the reactions that occur in each compartment.

2.9 Models for T2D and the ICU

We mainly focused on modeling T1D during the thesis, but some of the models described here, also exist in versions to represent people in the ICU or people with T2D, such as, the

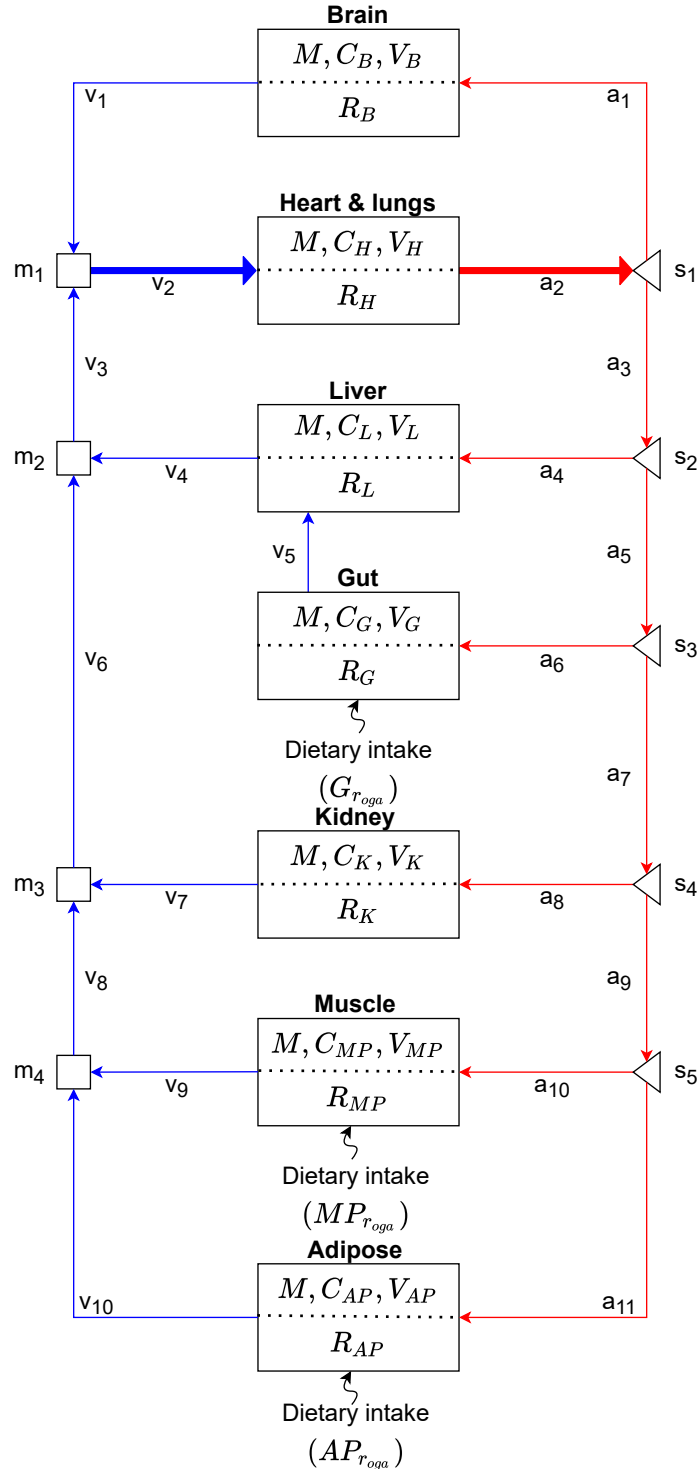


Figure 2.1: Schematic representation of the whole-body model. Solid arrows represent blood circulation, where the right side is the arteries and the left side is the veins. Thick arrows, a_2 and v_2 , represents joining of flows from other organs. M , C_k , and V_k represents the blood tissue exchange and R_k represents the reactions inside the cell. The dotted lines in the compartments suggest free diffusion as cell-permeability is not included.

ICU model by Hovorka et al. [69] or the UVA/Padova simulator for T2D [70]. The major difference between models for T1D and T2D or the ICU is the modeling of the pancreas in the insulin subsystem. People with T1D do not produce any insulin and therefore the pancreas is not included in the insulin subsystem, whereas models describing people in the ICU or with T2D include the insulin production from the pancreas. In Appendix O, we list three different models for the ICU and extend them by a simple representation of stress modeled as an unknown disturbance that directly enters the plasma glucose.

2.10 Summary

In this chapter, we described the models that we used or developed during the thesis. We only described the models that were directly used during the thesis, but more models exist in the literature. Here, we divided the descriptions of the models into descriptions of each subsystem and included models for dynamics of insulin, glucagon, meals, exercise, CGM, and glucose. Finally, we also briefly discussed whole-body models and models for the ICU and people with T2D. We use different combinations and versions of the models described here in the remainder of the thesis, where the large scale virtual clinical trials are based on extensions of Hovorka's model and the UVA/Padova model and the DiaCon AP is based on the MVP model extended with Hovorka's meal model, Haidar's glucagon model and a simplified version of Fachinetti's CGM model. The parameters for the models are listed in the appendix.

CHAPTER 3

Large scale virtual clinical trials

In this chapter, we describe how we use Monte Carlo simulation to evaluate the performance of closed-loop diabetes treatments in large scale virtual clinical trials. The virtual clinical trials include a population of virtual participants represented by a combination of the models described in Chapter 2 and a protocol that describes the events that happen during the trial (i.e. a sequence of model disturbances). We use high-performance computing to make it computationally feasible to perform the large amount of closed-loop simulations. This chapter refers to Appendices E, F, G, and H. Appendix E introduces the Monte Carlo simulation toolbox used to perform the virtual clinical trials. In Appendix F, we extend the Monte Carlo simulation toolbox with a low-memory version and show an example virtual clinical trial, where we compare the performance of two different closed-loop systems in a population of 1 mio. virtual participants over 1 year. Appendix G shows an example, where we instead compare the performance of an AP in two different virtual populations. Finally, Appendix H describes how the protocols and virtual participants for the virtual clinical trials are generated (lists the model parameters) and describes how they are stored in a database.

3.1 Monte Carlo simulation

We use Monte Carlo simulation to conduct the large scale virtual clinical trials. Monte Carlo simulations are used to quantify the uncertainty of certain performance measures (e.g. the TIR for a person with diabetes) for different values of the uncertain quantities. The Monte Carlo simulation toolbox works for systems in the general form (2.1), where we can perform Monte Carlo simulations for different 1) model parameters (i.e. virtual participants), 2) disturbances (i.e. different lifestyles or protocols), 3) realizations of the process noise (i.e. model uncertainty), 4) initial conditions, and 5) realizations of the measurement noise (e.g. measurements from a CGMs). Furthermore, we consider closed-loop feedback control strategies written in a general form

$$x_{k+1}^c = \kappa_k(x_k^c, y_{k+1}, \bar{u}_k, \bar{y}_{k+1}, \hat{d}_k, p_\kappa), \quad (3.1a)$$

$$u_k = \lambda_k(x_k^c, y_k, \bar{u}_k, \bar{y}_k, \hat{d}_k, p_\mu), \quad (3.1b)$$

where x_k^c are the control states estimated by some κ , and u_k are the manipulated inputs computed from some control strategy λ . The general form (3.1) enables simulation of different announced disturbances, \hat{d} , (e.g. misestimated or mistimed meals), hyperparameters in the controller, p_μ , or state estimator, p_κ , and setpoints, \bar{y}_k and \bar{u}_k . This form describes multiple types of closed-loop control strategies including controllers based on heuristics and physiological insight, PID-based controllers, and MPCs. We solve the optimal control problem (OCP) in MPC algorithms with IPOPT [71] and we solve the system of non-stiff SDEs with the Euler-Maruyama method [72]

$$t_{k,n+1} = t_{k,n} + \delta t, \quad (3.2a)$$

$$x_{k,n+1} = x_{k,n} + f(t_{k,n}, x_{k,n}, u_k, d_k, p_f)\delta t + \sigma(t_{k,n}, x_{k,n}, u_k, d_k, p_\sigma)\delta\omega_{k,n}, \quad (3.2b)$$

where $t_{k,0} = t_k$, $x_{k,0} = x_k$, and $\delta\omega_{k,n} \sim N_{iid}(0, I\delta t)$. The internal steps in the SDE solver are not required to have the same sampling time as in the closed-loop system. We let N_k denote the number of steps of size δt in the interval $[t_k, t_{k+1}]$ i.e. $N_k\delta t = \Delta t$. Then

$$t_{k+1} = t_{k,N_k}, \quad (3.3a)$$

$$x_{k+1} = x_{k,N_k}. \quad (3.3b)$$

We use internal steps of 30 seconds.

3.2 Protocols

The protocols describe the activities or events that happen during a clinical trial. Here, the protocols are represented as the model disturbances, d , in (2.1). The protocols can also include, e.g., meals that are not estimated correctly. In that case \hat{d} and d are different. The protocols can include any disturbance described by the model used for simulation. In this thesis, we design protocols that include the meal carbohydrate contents and exercise. We design a set of four season dependent basis days and combine the basis days to form different weeks, months and years. Figure 3.1 shows the basis days during winter and autumn that consist of the 1) standard day, 2) active day, 3) movie night, and 4) late night. During summer and spring, the dinner as a medium meal and the snack is before lunch. Table 3.1 shows the meal sizes. Here, we assume that the all the disturbances are correctly announced, i.e. $d = \hat{d}$. Table 3.2 shows the composition of the basis days in the standard week, the active week, and the vacation week. We attempt to represent a northern European lifestyle with eight vacation weeks (including public holidays) and Table 3.3 shows how the weeks are combined to form seasons that together forms a year. The protocols are stored in a PostgreSQL database which makes it straightforward to reuse the existing protocols, combine them in new combinations, and add new protocols to the framework.

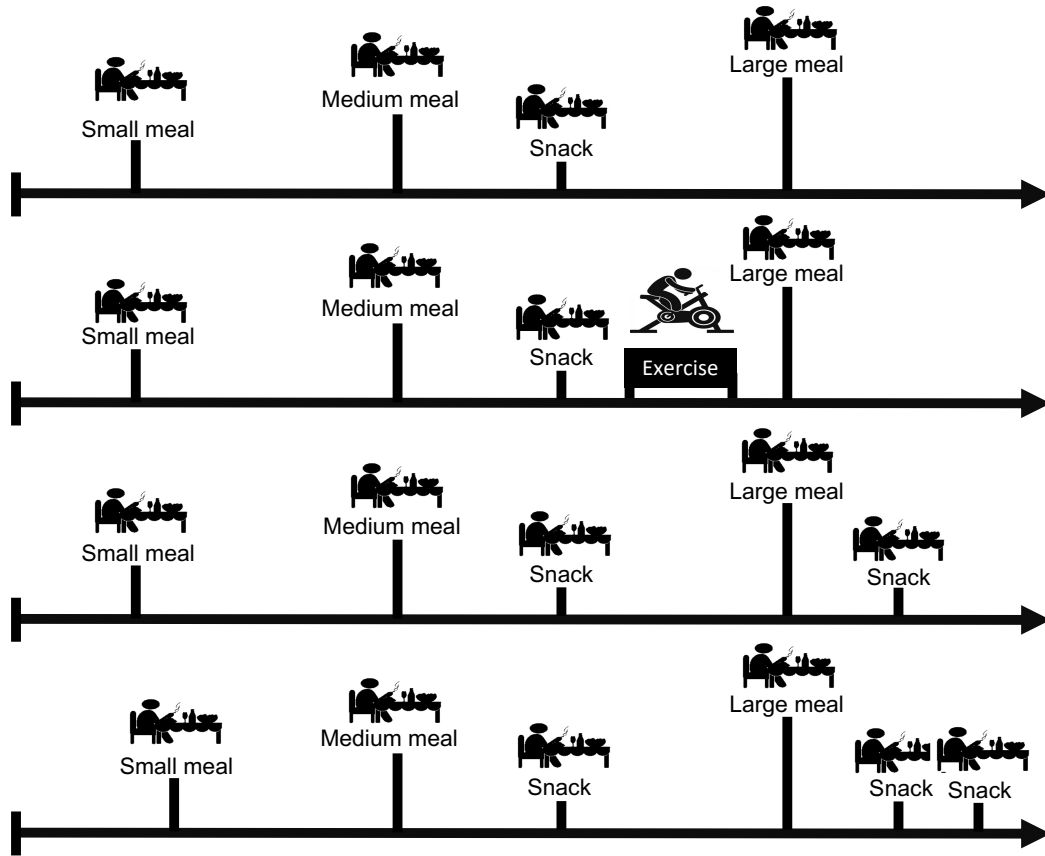


Figure 3.1: From the top: 1) the standard day, 2) the active day, 3) the movie night, and 4) the late night.

Table 3.1: Body weight-dependent meal carbohydrate contents.

Meal size	Amount of carbohydrates	For a 70 kg person
Large meal	1.29 g CHO/kg	90 g CHO
Medium meal	0.86 g CHO/kg	60 g CHO
Small meal	0.57 g CHO/kg	40 g CHO
Snack	0.29 g CHO/kg	20 g CHO

3.3 Virtual Participants

The virtual participants are represented by a mathematical model or a combination of the models described in Chapter 2. Each virtual participant is associated with a unique set of model parameters, and we consider all the virtual participants represented by the same model, a population. Furthermore, we generate personal information for the virtual participants, e.g., name, date of birth, height, body weight etc. to 1) emulate real data and 2) compute, e.g., heart rate related parameters that are dependent on age. Figure 3.2 shows the approximations of age, body weight and resting heart rate in the virtual

Table 3.2: Compositions of the weeks.

Type	Standard days	Active days	Movie nights	Late nights
Standard	4	1	1	1
Active	3	3	1	0
Vacation	5	0	0	2

Table 3.3: Compositions of the seasons.

Season	Standard weeks	Active weeks	Vacation weeks
Winter	6	4	3
Spring	6	6	1
Summer	7	3	3
Autumn	9	3	1

population. In this work, we generate 1 mio. parameter sets for the Hovorka model and extend with Rashid’s exercise model, Haidar’s glucagon model, and Facchinetti’s CGM model and 1 mio. parameter sets for the UVA/Padova model, i.e. we have generated two virtual populations with 1. mio virtual participants in each population. The parameters in the Hovorka model are sampled from the distributions presented by Boiroux et al. [19] and the distributions in the UVA/Padova model are based on the values provided by Colmegna et al. [54] and Kovatchev et al. [73]. Furthermore, we require that 1) the generated parameters are within one standard deviation of the mean, 2) the generated time constants are within one order of magnitude of the mean, 3) the basal rate is above $0.4 U/h$, and 4) the steady state is physical, i.e. non-negative and we discard parameters sets that lead to a steady state glucose concentration above 44 [mmol/L] when no insulin is administered. Clearly, the amount of data used to construct the distributions and sample the parameters is limited, but with more data becoming available, it should become possible to construct more representative distributions in the future. The participants are saved in a PostgreSQL database as described in appendix H that also lists the exact distributions of the model parameters. The database allows the participants to be reused and makes it possible to add more virtual participants to the framework.

3.4 Examples

We demonstrate the utility of the Monte Carlo simulation toolbox with the example large-scale virtual clinical trial from Appendix F. Here, we compare the performance of two different closed-loop systems in a population of 1 mio. virtual participants represented by an extended version of the Hovorka model during a 1 year (52 weeks) virtual clinical trial. In both trials, the participants are treated with a model-free DH AP that makes microadjustments of the basal rate, estimates the insulin-to-carb ratio (ICR) over time to administer meal insulin boli and can administer glucagon boluses at the beginning of exercise or if the participant reaches hypoglycemia. In trial A, the nominal basal rate is

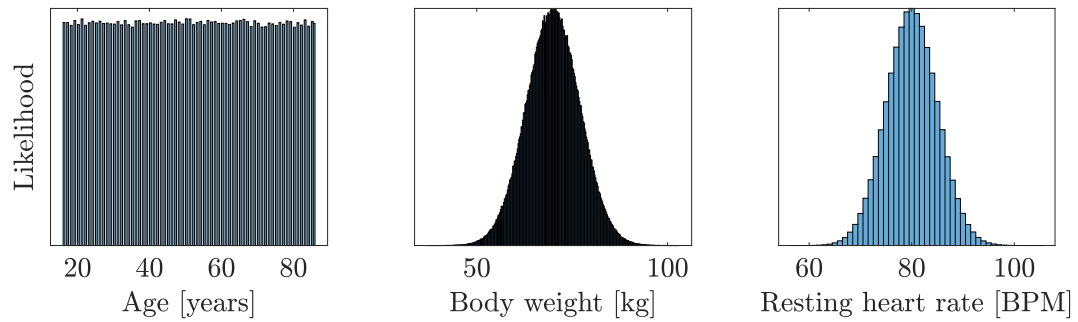


Figure 3.2: Distributions of the personal parameters that affect the simulation models. From the left: 1) The age of the participants with a mean of 51 years, 2) the body weight of the participants with a mean of 70 kg, and 3) the resting heart rate of the participants with a mean of 80 BPM.

correctly estimated and in trial B, the nominal basal rate is underestimated by 50%. The large-scale virtual clinical trials allow us to evaluate the outcomes based on distributions of the KPIs instead of individual values. Figure 3.3 shows the mean and worst-case TIRs for trial A and trial B. We define the worst-case trial as the trial where the participant reaches the lowest glucose concentration. As expected, the TIR in trial A, where the basal rate is correctly estimated, is higher, but surprisingly the worst-case participant spends more time in severe hypoglycemia in trial A compared to trial B. Figure 3.4 shows a cumulative distribution of the glucose concentration for the participants in the two trials, where we can, e.g., inspect the tails of the distribution and see that some participants reach both very low and very high glucose levels. Furthermore, we can also see the span of the all the participants. Figure 3.5 shows a boxplot with the distribution of the time in ranges for all the participants. The boxplot shows that some participants spend almost all the time in hyperglycemia and 0% time in range in trial A which is not the case in trial B. However, on average the participants spend less time in range in trial B. The boxplot also displays that some participants have 100% TIR. Finally, Figure 3.6 shows the distribution of the manipulated inputs during the trials. Since the basal rate is underestimated in trial B, we can see that the AP administers less basal insulin and more bolus insulin in trial B compared to trial A. Furthermore, it also shows that more glucagon is administered in trial B, which is most likely due to the larger insulin boli. Another example of a large-scale virtual clinical trial is shown in Appendix M, where the performance of a closed-loop system is evaluated in two different virtual populations.

3.5 High-performance computing

Virtual clinical trials with millions of virtual participants are not computationally feasible unless high-performance techniques are applied. The Monte Carlo simulation toolbox is implemented in C and uses OpenMP [74] to parallelize the simulations for shared

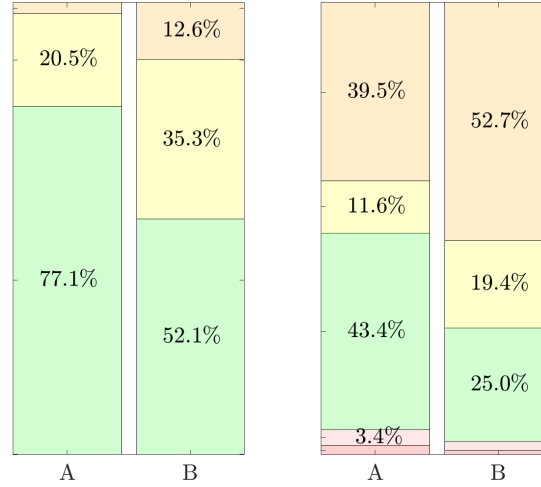


Figure 3.3: Time in ranges for the two different treatments. Left: mean time in ranges for treatment A and treatment B. Right: time in ranges for the worst-case participant (the participant that reaches the lowest blood glucose concentration) for treatment A and treatment B.

memory architectures. The Monte Carlo simulations are straightforward to parallelize as each worker can be assigned to a distinct closed-loop simulation. It requires significant amounts of storage to save the results from the large number of long-term simulations. Therefore, we extend the toolbox presented in Appendix E with a low-memory version in Appendix F and G, where only selected KPIs are stored and not the full simulations for each participant. Whenever the simulation for each participant is completed, we compute its contribution to the selected KPIs such as TIR as well as mean, minimum, and maximum glucose concentration. Consequently, the simulation is only stored if it was worse or better than the previous simulations based on the criterion of the KPIs. We use the DTU HPC system [75], where Table 3.4 shows the computation times of the virtual clinical trial. The computation time of the trial with 1 mio. participants over 1 year is 82 minutes with 64 cores. Rome and Epyc refers to two different CPU types available at DTU. The table shows that the computation time scales almost linearly with the number of cores, which means that the computation time can be further reduced with more cores. Furthermore, it also indicates that the performance could be improved by modifying the toolbox to work for distributed memory architectures (e.g. using MPI [76]) where multiple computers can be used.

3.6 Summary

In this chapter, we described the Monte Carlo simulation framework used to perform large-scale virtual clinical trials of closed-loop diabetes treatment. The virtual participants are represented by a combination of the mathematical models presented in Chapter

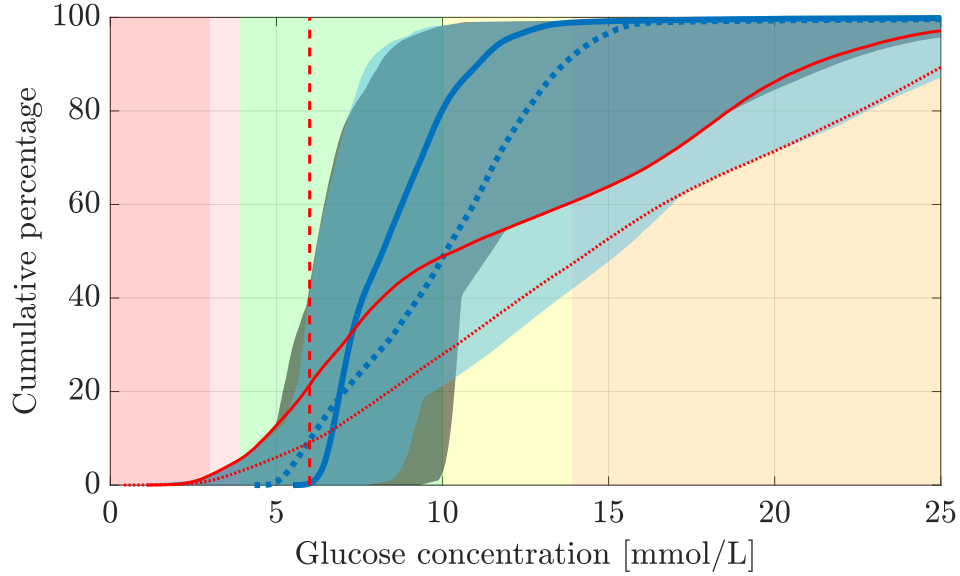


Figure 3.4: Cumulative distribution of the glucose concentration in the two virtual clinical trials with 1 mio. virtual participants over 52 weeks. Blue solid line: the mean glucose concentration in trial A. Blue dotted line: the mean glucose concentration in trial B. Red solid line: the participant that reaches the lowest glucose concentration in trial A. Red dotted line: the participant that reaches the lowest glucose concentration in trial B. Red dashed line: the setpoint. Grey shaded area: the span of all the participants in trial A. Light blue shaded area: the span of all the participants in trial B.

Table 3.4: Computation times of one virtual clinical trial with 1 mio. virtual participants over 52 weeks.

Cores	Epyc	Rome
64	113 min	82 min
32	220 min	158 min
24	287 min	204 min

2, where each participant is associated with a unique set of parameters, and we design the protocols from a set of basis days based on a northern European lifestyle. Both the participants and the protocols are stored in a PostgreSQL database, which allows the user to reuse, modify and add new participants and protocols to the framework. We use a general formulation of the models, control algorithm, and state estimator in the toolbox, which makes it possible to test different control algorithms and represent the participants by different mathematical models. The general formulation also enables Monte Carlo simulation of, e.g., different protocols, realizations of the sensor noise or process noise, or different controller hyperparameters.

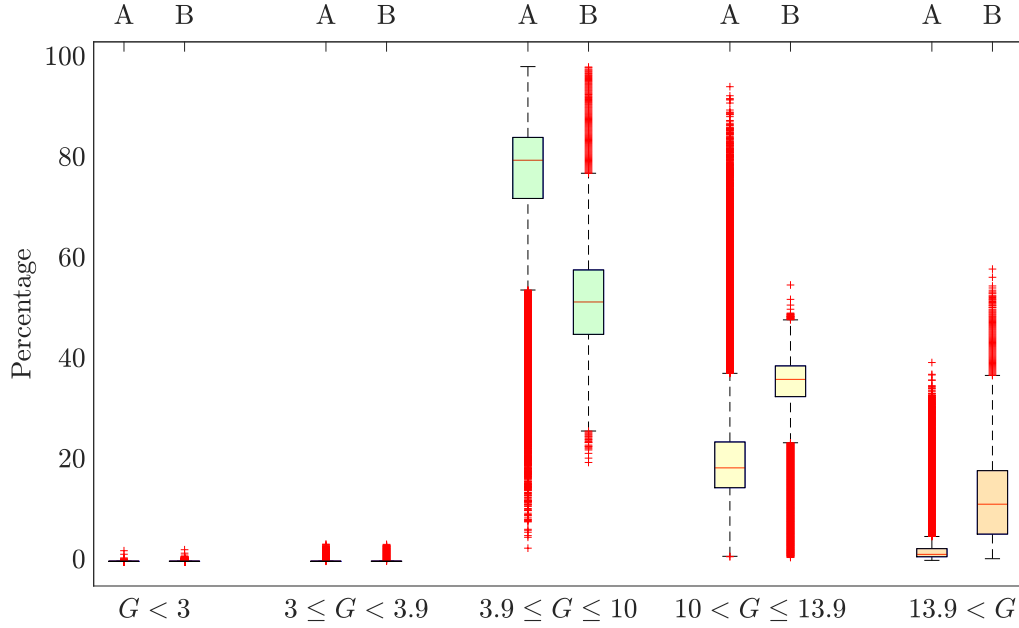


Figure 3.5: Box plot of the time in each range during the two virtual clinical trials with 1 mio. virtual participants over 52 weeks.

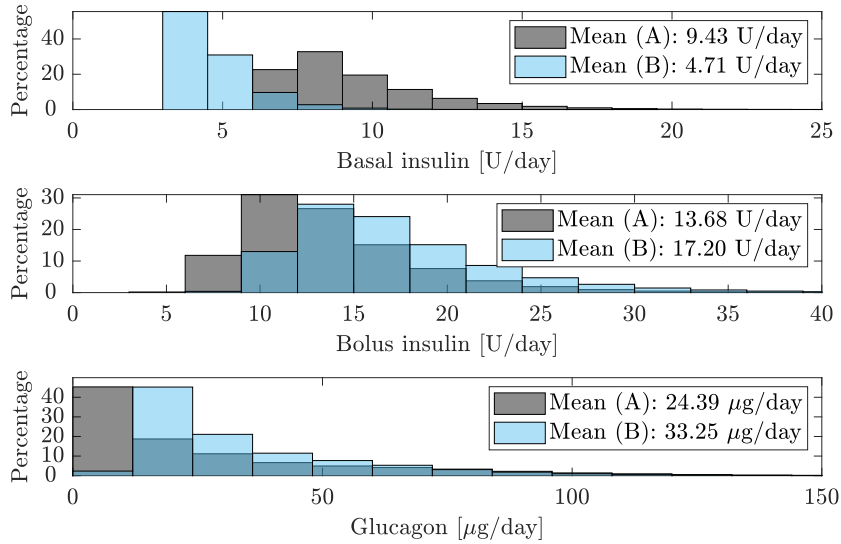


Figure 3.6: Distributions of manipulated inputs during the two virtual clinical trials with 1 mio. virtual participants over 52 weeks.

CHAPTER 4

Artificial pancreas technology

In this chapter, we describe the DiaCon AP and summarize the results from a clinical trial with adolescents ($n = 11$). We provide an overview of the closed-loop systems that are either commercially available, in regulatory review, or received approval and compare with the DiaCon AP. The DiaCon AP consists of a Dexcom G6 CGM, two Dana RS pumps, and the control algorithm is implemented in an Android smartphone. The control algorithm is an NMPC algorithm, where we use a stochastic version of the MVP model extended by Hovorka’s meal model, Haidar’s glucagon model, and Fachinetti’s CGM model described in Chapter 2 for predictions. We use a ML based PEM to estimate the parameters. The CD-EKF is used for state estimation and in the PEM. This chapter is based on Appendices I, J, K, L, M, N, and O. Appendix I introduces the DH AP system and algorithm and shows the results from a pre-clinical virtual clinical trial with 50 participants represented by an extended version of Hovorka’s model. Appendix J provides a full description of the control algorithm used in the AP, discusses the technical challenges, and summarizes the results from the clinical trial. Appendix K describes the clinical trial and trial outcomes in detail. Appendix J and K are the primary resources for this chapter. Appendix L lists and discusses the individual parameter estimates and outcomes for each participant in the clinical trial. Appendix M proposes a model-free *one-size-fits-all* AP for people with T1D that does not require parameter estimation and is in some ways an extension of the titration algorithm proposed Appendix N. Finally, Appendix O proposes a linear MPC algorithm for control of the blood glucose concentration in the ICU.

4.1 Artificial pancreas systems

As also discussed in Chapter 1, there are currently five closed-loop systems commercially available in the EU or the US. Figure 4.1 shows selected specifications of the systems as well as the DiaCon AP for comparison. The licenses differ between each system, and they are not all available in both the EU and the US. Each system have unique features. The DiaCon AP, the CamAPS FX, and the Omnipod 5 all implement the control algorithm in Android smartphones, but the Omnipod 5 uses the Omnipod patch pump which is tubeless instead of the Dana RS pump. The Medtronic systems, Control-IQ, and

Diabeloop implements the control algorithm in pump or a in dedicated device. The Medtronic 780G includes automatic corrections and is an upgraded version of the 670G. Common to all of the commercially available systems is that they require announcements of meals or exercise. Compared to the commercially available systems, the DH feature of the DiaCon AP is unique, but if we compare to other AP systems in development (see Figure 4.2), both the Inreda and Ilet bihormonal systems are able to administer glucagon. Both the Inreda and iLet bihormonal systems have special pumps that contain chambers for both insulin and glucagon, i.e., they do not require two different pumps like the DiaCon AP, but currently, just the insulin only version of the iLet system is in regulatory review. Furthermore, the Inreda system does not require announcements of meals or exercise whereas the iLet system still requires announcements although not specific amounts of carbohydrates. The Inreda system is the only system that uses two CGMs. Finally, the Tidepool loop system is an Iphone app that is compatible with multiple sensors and pumps and also integrates with the Apple watch. As these systems are still in development, the exact features are unknown and some of the details might change.

4.2 DiaCon artificial pancreas system

The DiaCon AP is categorized as a hybrid DH closed-loop system as it can administer both insulin and glucagon and requires the user to announce both meal intake and exercise. The system consists of two Dana Diabecare RS pumps (one for insulin and one for glucagon), a Dexcom G6 sensor, and a Samsung galaxy A5 2017 smartphone. Figure 4.3 shows a picture of the DiaCon AP. The DiaCon app is a Java Android application that also provides a GUI for the user. All computations in the control algorithm are performed with the smartphone. Figure 4.4 shows a flowchart of the closed-loop system as well as the pre-trial preparations. We describe the details of both the pre-trial parameter estimation and the control algorithm in Section 4.3.

4.3 Nonlinear model predictive control

In this section, we describe the NMPC algorithm used to compute the insulin and glucagon administration in the AP, and how we estimate the parameters in the prediction model. NMPC algorithms compute a closed-loop feedback control strategy using the moving horizon principle, where a new open-loop strategy is computed with some sampling time when new measurements are available. NMPC allows to include the non-linear effect of the insulin action on glucose. The NMPC algorithm is combined with a number of heuristics to switch between insulin and glucagon and to provide additional safety constraints.

	DiaCon Single	DiaCon Dual	Medtronic 670G	Medtronic 780G	Control-IQ	CamAPS FX	Diabeloop	Omnipod 5
System appearance								
Continuous glucose monitor	Dexcom G6	Dexcom G6	Guardian Sensor	Guardian Sensor 3 or 4	Dexcom G6	Dexcom G6	Dexcom G6	Dexcom G6
Pump	Dana RS	Dana RS	MiniMed 670G	MiniMed 780G	t:slim X2	Dana RS Dana i	Kaleido	Omnipod
Algorithm configuration	App on Android phone	App on Android phone	On pump	On pump	On pump	App on Android phone	On dedicated device (DBLG1)	App on Android phone
Licensing	-	-	≥7 years (not pregnancy)	≥7 years (not pregnancy)	≥6 years (not pregnancy)	≥1 year incl. pregnancy	≥18 years (not pregnancy)	≥2 years (not pregnancy)
Algorithm target	Treat to target 6.0 mmol/L and range > 4.5 mmol/L	Treat to target 6.0 mmol/L and range > 4.5 mmol/L	Treat to target 6.7 mmol/L	Treat to target 5.6, 6.2 or 6.7 mmol/L	Treat to range 6.2–8.9 mmol/L	Treat to target 5.8 mmol/L but customisable (4.4–11.0 mmol/L)	Treat to target 5.8 mmol/L but customisable (5.6–7.2 mmol/L)	Treat to target 5.6, 6.2, 6.7, 7.2, 7.8 or 8.3 mmol/L
Insulin compatibility	Rapid acting (not ultra-rapid acting insulin)	Rapid acting (not ultra-rapid acting insulin)	Rapid acting (not ultra-rapid acting insulin)	Rapid acting (not ultra-rapid acting insulin)	Rapid acting (not ultra-rapid acting insulin)	Rapid acting or ultra-rapid acting insulin	Rapid acting (not ultra-rapid acting insulin)	Rapid acting (not ultra-rapid acting insulin)
Data review	-	-	Carelink	Carelink	Glooko+Clarity (EU), t:connect (US)	Glooko	Glooko	Glooko
Initialization	Historic CGM, pump, and meal data, IC ratio, insulin sensitivity factor	Historic CGM, pump, and meal data, IC ratio, insulin sensitivity factor	IC ratio, active insulin time, 48 hours run-in	IC ratio, active insulin time, 48 hours run-in	Basal insulin rate, TDI, IC ratio, insulin sensitivity factor, body weight	TDI, body weight	Body weight, TDI, amount of carbs in typical meals	Basal insulin rate, TDI, amount of carbs in typical meals
Additional features	Automatic corrections. Exercise mode with temporary target	Dual hormone. Automatic corrections. Exercise mode with temporary target	Temporary target 8.3mmol/L	Temporary target 8.3mmol/L. Automatic corrections	Sleep mode. Exercise mode. Automatic corrections.	Boost – more aggressive. Ease Off – raise target and less aggressive. Automatic corrections	Automatic corrections. Learning algorithm. Privacy mode possible.	Tubeless

Figure 4.1: Comparison between the DiaCon AP system (SH and DH configuration) with the closed-loop systems commercially available in the EU or the US. From the left: DiaCon SH, DiaCon DH, Medtronic 670G, Medtronic 780G, Control-IQ, CamAPS FX, Diabeloop, and Omnipod 5.







	DiaCon Single	DiaCon Dual	Tidepool Loop	iLet insulin only	iLet bihormonal	Inreda
System appearance						
Continuous glucose monitor	Dexcom G6	Dexcom G6	Dexcom G6 Guardian Sensor	Dexcom G6	Dexcom G6	Medtronic
Pump	Dana RS	Dana RS	Omnipod MiniMed	iLet pump	iLet pump	Inreda pump
Algorithm configuration	App on Android phone	App on Android phone	App on Iphone	On pump	On pump	On pump
Regulatory status	-	-	FDA approved	Pending 510(k)	-	CE mark
Features	Automatic corrections. Exercise mode with temporary target	Dual hormone. Automatic corrections. Exercise mode with temporary target	Compatible with multiple diabetes devices. Automatic corrections. Exercise mode	Automatic corrections. Does not require carb counting	Dual hormone. Automatic corrections. Does not require carb counting	Dual hormone. No announcements required

Figure 4.2: Comparison between the DiaCon AP system (SH and DH configuration) and the closed-loop systems that are in development and either received approval or are in regulatory review (with the exception of the iLet bihormonal system). From the left: DiaCon SH, DiaCon DH, Tidepool Loop, iLet insulin only, iLet bihormonal, and Inreda AP.

4.3.1 Continuous-discrete extended Kalman filter

We use the CD-EKF [77] to estimate the states and the insulin sensitivity from the received CGM measurement every 5 minutes. Furthermore, we use the CD-EKF in the PEM to estimate the model parameters.

Filtering Given the previous one-step prediction of the states, $\hat{x}_{k|k-1}$, its covariance, $P_{k|k-1}$, and a measurement, y_k , the CD-EKF computes the filtered state, $\hat{x}_{k|k}$, and its covariance, $P_{k|k}$. We compute the one-step prediction of the measurement and its derivative by

$$\hat{y}_{k|k-1} = g(t_k, \hat{x}_{k|k-1}, \theta), \quad (4.1a)$$

$$C_k = \frac{\partial g}{\partial x}(t_k, \hat{x}_{k|k-1}, \theta). \quad (4.1b)$$

We use the one-step prediction of the measurements to compute the innovation, e_k , and its covariance, $R_{e,k}$, by

$$e_k = y_k - \hat{y}_{k|k-1}, \quad (4.2a)$$

$$R_{e,k} = C_k P_{k|k-1} C_k^T + R. \quad (4.2b)$$

We then compute the Kalman gain as

$$K_{fx,k} = P_{k|k-1} C_k^T R_{e,k}^{-1}, \quad (4.3)$$



Figure 4.3: The DiaCon AP system. The system consists of 1) an Android smart-phone, 2) a Dexcom G6 sensor, 3) a Dana Diabecare RS pump for insulin administration, and 4) another Dana Diabecare RS pump for glucagon administration.

and obtain the filtered state and its covariance by

$$\hat{x}_{k|k} = \hat{x}_{k|k-1} + K_{fx,k}e_k, \quad (4.4a)$$

$$P_{k|k} = P_{k|k-1} - K_{fx,k}R_{e,k}K_{fx,k}^T. \quad (4.4b)$$

Positive definiteness of the filtered state covariance, $P_{k|k}$, can be ensured by the Joseph stabilized form [78]

$$P_{k|k} = (I - K_{fx,k}C_k)P_{k|k-1}(I - K_{fx,k}C_k)^T + K_{fx,k}RK_{fx,k}^T. \quad (4.5)$$

Prediction From the filtered state-covariance pair (4.4), we compute the one-step prediction

$$\hat{x}_{k+1|k} = \hat{x}_k(t_{k+1}), \quad (4.6a)$$

$$P_{k+1|k} = P_k(t_{k+1}), \quad (4.6b)$$

by solving

$$\frac{d}{dt}\hat{x}_k(t) = f(t, \hat{x}_k(t), u_k, d_k, \theta), \quad (4.7a)$$

$$\begin{aligned} \frac{d}{dt}P_k(t) &= A_k(t)P_k(t) + P_k(t)A_k(t)^T \\ &\quad + \sigma_k(t)\sigma_k(t)^T, \end{aligned} \quad (4.7b)$$

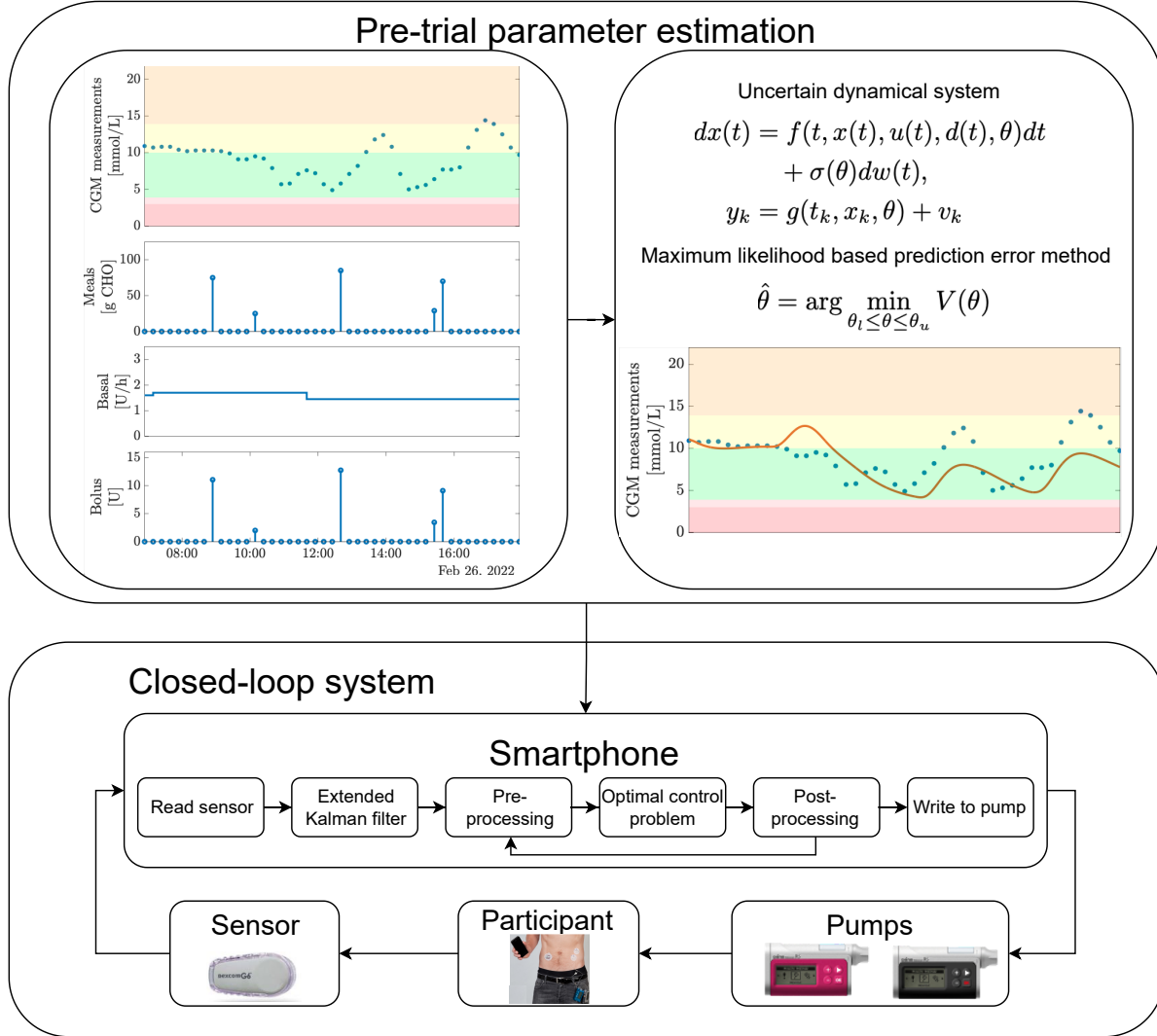


Figure 4.4: A flowchart of the pre-trial preparations and the DiaCon AP as a closed-loop system. Top left: Example of CGM, meal, and insulin data received before the studies. Top right: Parameter estimation using the data provided by the participants. Bottom: We enter the model parameters in the smartphone that is connected to the sensor and pumps. The smartphone reads the sensor and estimates the states using the CD-EKF based on the measurement. We then update the constraints, select either insulin or glucagon administration, and solve the OCP. The post-processing routine evaluates the solution, checks the predictions, and rounds the input to the pump resolution before writing the instructions to the pump.

for $t_k \leq t \leq t_{k+1}$, where

$$A_k(t) = \frac{\partial f}{\partial x}(t, \hat{x}_k(t), u_k, d_k, \theta), \quad (4.8a)$$

$$\sigma_k(t) = \sigma(t, \hat{x}_k(t), u_k, d_k, \theta), \quad (4.8b)$$

with the initial condition

$$\hat{x}_k(t_k) = \hat{x}_{k|k}, \quad (4.9a)$$

$$P_k(t_k) = P_{k|k}. \quad (4.9b)$$

Remark Different versions of the Kalman filter can also be applied for fault-detection [79, 80].

4.3.2 System identification

We estimate the parameters in the extended MVP with a PEM based on the CD-EKF [56] from CGM, meal, and insulin data. In the clinical trial, we received around two weeks of data from the participants prior to the trials and in the pre-clinical virtual clinical trials (Appendix I), we generate data with the simulation model and estimate the parameters from the simulated data to represent a real clinical trial.

4.3.2.1 Maximum likelihood based prediction error method

We use a ML based PEM using the CD-EKF to estimate the parameters. Let \mathcal{I}_N be a set of experimental data, i.e.

$$\mathcal{I}_{k+1} = \{y_{k+1}, u_k, d_k\} \cup \mathcal{I}_k, \quad \mathcal{I}_0 = \{y_0\}, \quad k = 0 \dots N-1. \quad (4.10)$$

The aim is to maximize the conditional probability density, $p(\mathcal{I}_N|\theta)$. Since we assume that the inputs, u_k , and disturbances, d_k , are deterministic, we can express the conditional probability density as

$$p(\mathcal{I}_N|\theta) = p(y_N, y_{N-1}, \dots, y_0|\theta). \quad (4.11)$$

Let the negative log-likelihood function

$$V(\theta) = -\log(p(\mathcal{Y}_N|\theta)), \quad (4.12)$$

be expressed as

$$V(\theta) = \frac{(N+1)n_y}{2} \log(2\pi) + \frac{1}{2} \sum_{k=0}^N \left(\log[\det(R_{e,k}(\theta))] + e_k(\theta)^T [R_{e,k}(\theta)]^{-1} e_k(\theta) \right). \quad (4.13)$$

Here, $n_y = 1$ and the innovation, e_k , and its covariance, $R_{e,k}$, are computed with the CD-EKF (4.2). The objective is to find the set of parameters, $\hat{\theta}$, that minimizes the negative log-likelihood function (4.13), i.e.,

$$\hat{\theta} = \arg \min_{\theta_l \leq \theta \leq \theta_u} V(\theta), \quad (4.14)$$

where $\hat{\theta} \sim N(\bar{\theta}, P_\theta)$ and with the constraints $\theta_l \leq \bar{\theta} \leq \theta_u$.

4.3.2.2 Fisher information matrix and parameter covariance

The Fisher information matrix, $H(\theta)$, is defined as the covariance of the gradient of the log-likelihood function

$$[H(\hat{\theta})]_{ij} \triangleq \mathbb{E}_\theta \left\{ \frac{\partial V}{\partial \theta_i}(\hat{\theta}) \frac{\partial V}{\partial \theta_j}(\hat{\theta}) \right\} = \mathbb{E}_\theta \left\{ \frac{\partial^2 V}{\partial \theta_i \partial \theta_j}(\hat{\theta}) \right\}, \quad (4.15)$$

or equivalently

$$H(\hat{\theta}) \triangleq \mathbb{E}_\theta \left\{ \nabla V(\hat{\theta}) \nabla V(\hat{\theta})' \right\} = \mathbb{E}_\theta \left\{ \nabla^2 V(\hat{\theta}) \right\}, \quad (4.16)$$

where

$$\frac{\partial V}{\partial \theta_i} = \sum_{k=0}^N \frac{1}{2} \text{tr} \left[R_{e,k}^{-1} \frac{\partial R_{e,k}}{\partial \theta_i} \right] + e_k' R_{e,k}^{-1} \frac{\partial e_k}{\partial \theta_i} - \frac{1}{2} e_k' R_{e,k}^{-1} \frac{\partial R_{e,k}}{\partial \theta_i} R_{e,k}^{-1} e_k, \quad (4.17)$$

The observed Fisher information matrix can be used to provide a lower bound on the covariance of the estimated parameters by the Cramér-Rao lower bound (CRLB) [81–83]

$$P_\theta = \text{Cov}(\hat{\theta}) \geq H^{-1}(\hat{\theta}). \quad (4.18)$$

If the number of data points is sufficiently large, the covariance of the parameter estimates, $\hat{\theta}$, can be approximated as the inverse of the Hessian [84], i.e.

$$\text{Cov}(\hat{\theta}) = H^{-1}(\hat{\theta}). \quad (4.19)$$

Consequently, the standard deviation of the parameter estimate, $\hat{\theta}_i$, is

$$\sigma_{\hat{\theta}_i} = \sqrt{(H^{-1})_{i,i}}. \quad (4.20)$$

Remark The Fisher information matrix can also be applied to evaluate the experimental design [85, 86].

4.3.2.3 Examples

Figure 4.5 shows an example of the data used for estimation and a simulation with the estimated parameters for one virtual participant from Appendix I, and Figure 4.6 shows the data and a simulation with the estimated parameters for a participant in the actual clinical trial from Appendix J and L. Clearly, the fit is more accurate in the simulation study. The data we received from each participant before the clinical trial was usually of poor quality with periods of missing CGM data and unannounced or misestimated meals. Therefore, we selected a subset of the data for estimation, which was usually less than 24 hours, and for some participants it was not possible to find more than a few hours of data without missing information. In practice, it was also necessary to fix some of the parameters. Choosing a suitable subset of the data and which parameters to fix was both a challenging and time-consuming task and was performed by trial and error. Conversely, the data in the simulation study had correctly announced meals and no missing data. Furthermore, the data received from the real participants included more variations in, e.g., the meal response, where meals of similar sizes with a corresponding insulin bolus resulted in different responses (see, e.g., the first and third meal in Figure 4.6). These variations might occur because of incorrectly announced meals, but can also happen because of physiological variability. We could have included incorrectly announced meals in the simulation study, but neither the control nor simulation model are able to describe the physiological variability in the meal response. The combined effects lead to much more accurate predictions in the AP in the simulation study compared to the real clinical trial.

4.3.3 Optimal control problem

We solve an OCP to compute the insulin or glucagon administration every 5 minutes when a new CGM measurement is received. The OCP is in the form

$$\min_{[x(t)]_{t_0}^{t_f}, \{u_k\}_{k=0}^{N-1}} \phi = \phi([x(t)]_{t_0}^{t_f}, \{u_k\}_{k=0}^{N-1}), \quad (4.21a)$$

subject to

$$x(t_0) = \hat{x}_0, \quad (4.21b)$$

$$\dot{x}(t) = f(t, x(t), u(t), d(t), \theta), \quad t \in [t_0, t_f], \quad (4.21c)$$

$$u(t) = u_k, \quad t \in [t_k, t_{k+1}[, \quad k = 0, \dots, N-1, \quad (4.21d)$$

$$d(t) = \hat{d}_k, \quad t \in [t_k, t_{k+1}[, \quad k = 0, \dots, N-1, \quad (4.21e)$$

$$u_{\min} \leq u_k \leq u_{\max}, \quad k = 0, \dots, N-1, \quad (4.21f)$$

where (4.21b) is the initial condition estimated with the CD-EKF, (4.21c) is the deterministic part of the extended MVP model, (4.21d)-(4.21e) are zero-order hold parametrizations of the manipulated inputs and announced disturbances, and (4.21f) are the constraints on the manipulated inputs. We use a control and prediction horizon of 6 hours

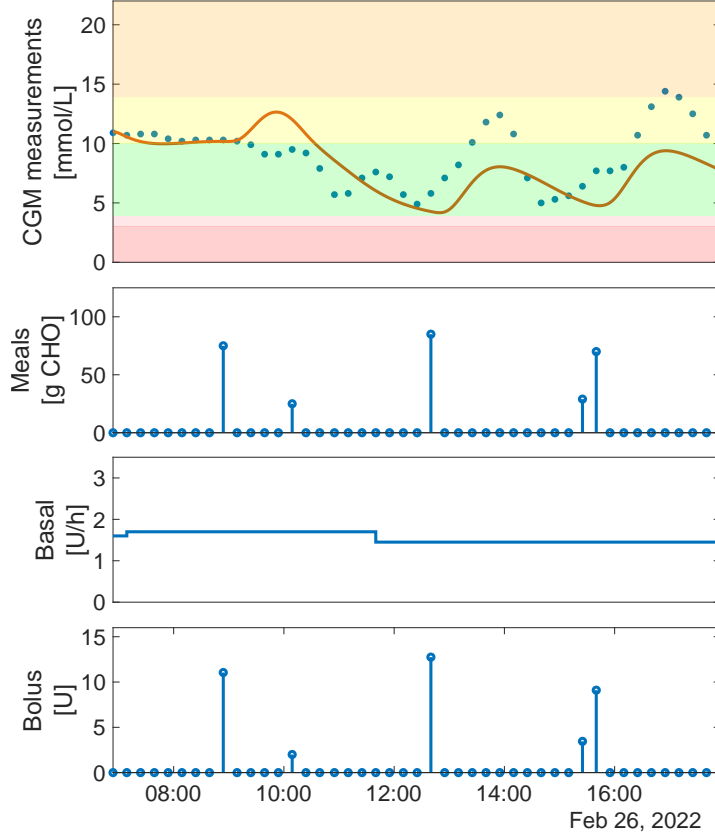


Figure 4.5: Parameter estimation for the example study. From the top: 1) CGM measurements (blue dots) and a simulation with the estimated parameters (red line), 2) announced meals, 3) basal insulin rate, and 4) bolus insulin.

for predicting sufficiently long to reach steady state while ensuring computational feasibility. We describe the objective function, ϕ , in Section 4.3.3.1.

4.3.3.1 Objective function

We define the objective function (4.21a) as

$$\phi = \int_{t_0}^{t_f} \rho_z(z(t))dt + \sum_{k=0}^{N-1} \rho_u(u_k), \quad (4.22)$$

to penalize deviations from the target glucose concentration and deviations from the nominal values of the manipulated inputs. We define the term that penalizes deviations from the target glucose concentration as

$$\rho_z(z) = \alpha_{\bar{z}}\rho_{\bar{z}}(z) + \alpha_{z_{\min}}\rho_{z_{\min}}(z) + \alpha_{z_{\max}}\rho_{z_{\max}}(z), \quad (4.23)$$

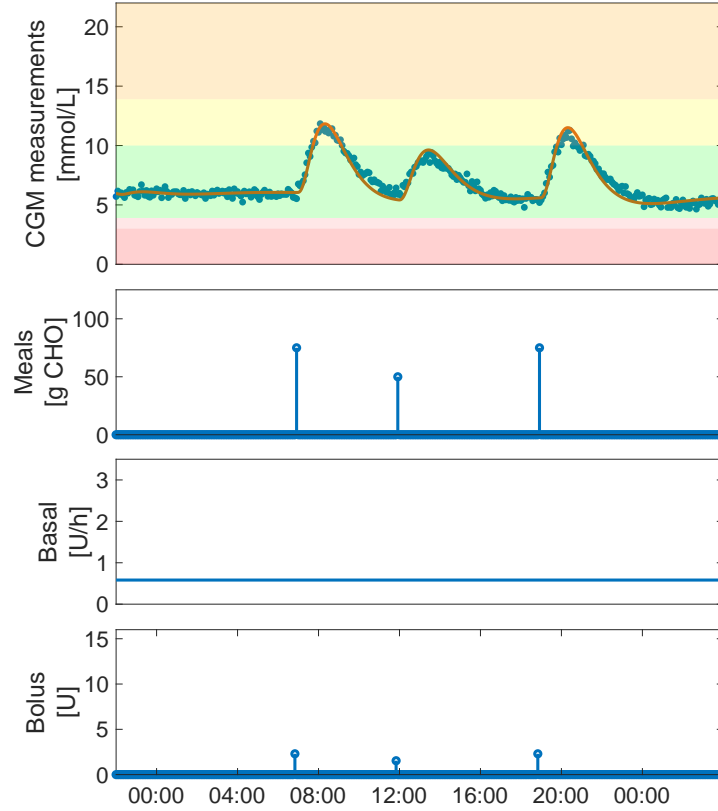


Figure 4.6: Parameter estimation for one virtual participant in the simulation study. From the top: 1) CGM measurements (blue dots) and a simulation with the estimated parameters (red line), 2) announced meals, 3) basal insulin rate, and 4) bolus insulin.

where

$$\rho_{\bar{z}}(z) = \frac{1}{2}(z - \bar{z})^2, \quad (4.24a)$$

$$\rho_{z_{\min}}(z) = \frac{1}{2}(\min\{0, z - z_{\min}\})^2, \quad (4.24b)$$

$$\rho_{z_{\max}}(z) = \frac{1}{2}(\max\{0, z - z_{\max}\})^2. \quad (4.24c)$$

We penalize 1) deviations of the blood glucose concentration from the setpoint, $\bar{z} = 6$ mmol/L, 2) hypoglycemia ($z < z_{\min} = 4.5$ mmol/L), and 3) hyperglycemia ($z > z_{\max} = 10.0$ mmol/L). Figure 4.7 shows the glucose penalty function when administering both glucagon and insulin. The weights in (4.23) are $\alpha_{\bar{z}} = 1$, $\alpha_{z_{\min}} = 10^6$, $\alpha_{z_{\max}} = 50$ when computing the insulin administration, and $\alpha_{z_{\max}} = 0$ when computing the glucagon administration. The penalty function is asymmetric to penalize hypoglycemia more than hyperglycemia i.e. $\alpha_{z_{\min}} > \alpha_{z_{\max}}$. The second penalty term is defined as

$$\rho_u(u_k) = \alpha_{u,ba}\rho_{u,ba}(u_{ba,k}) + \alpha_{u,bo}\rho_{u,bo}(u_{bo,k}), \quad (4.25)$$

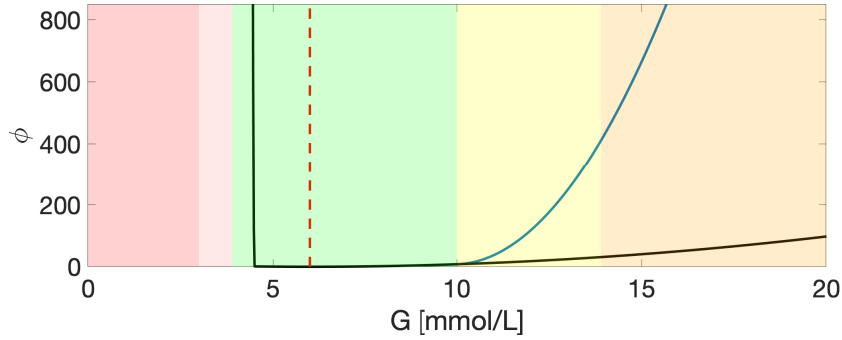


Figure 4.7: Asymmetric glucose penalty function when administering insulin (blue) and glucagon (black).

when administering insulin, where

$$\rho_{u,ba}(u_{ba,k}) = \|u_{ba,k} - \bar{u}_{ba,k}\|_2^2, \quad (4.26a)$$

$$\rho_{u,bo}(u_{bo,k}) = \|u_{bo,k}\|_1. \quad (4.26b)$$

Here, $\rho_{u,ba}(u_{ba,k})$ penalizes deviations from the nominal basal insulin rate $\bar{u}_{ba,k}$ in a 2-norm to promote small deviations and $\rho_{u,bo}(u_{bo,k})$ penalizes administering insulin boli, where the 1-norm promotes sparsity, i.e., few, but large insulin boli. We set the weights in (4.25) to $\alpha_{u,ba} = 0.5$ and $\alpha_{u,bo} = 0.01$. When administering glucagon, the penalty term is

$$\rho_u(u_k) = \alpha_{u,G} \|u_{G,k}\|_2^2. \quad (4.27)$$

Similar to the basal insulin penalty term, we also apply the 2-norm for glucagon administration to promote small deviations, but here the nominal value is zero. The weight is $\alpha_{u,G} = 100.0$.

4.3.3.2 Numerical solution

We use direct multiple-shooting [87] to transcribe the OCP (4.21) into an NLP. We discretize the dynamic constraint (4.21c) and the integral in the objective function with an explicit 4th order Runge-Kutta method with fixed step size. We solve the NLP with a SQP method [20, 88], where we solve the QP in each SQP iteration with a Riccati based primal-dual interior point algorithm [89, 90].

4.3.4 Heuristics

We use heuristics to 1) switch between insulin and glucagon administration, 2) compute bounds of the insulin and glucagon administration, 3) update controller parameters when exercise is announced, 4) round to pump resolution, and 5) a fall-back strategy if the

solution of the OCP (4.21) was prevented. In the nominal case, the setpoint, \bar{z} , and the switch limit is,

$$\bar{z} = 6.0 \text{ mmol/L}, \quad \text{switch limit} = 4.5 \text{ mmol/L}. \quad (4.28)$$

The setpoint is set to a value above the glucose level in healthy people as an extra safety measure to avoid hypoglycemia. Furthermore, the switch limit is slightly above the threshold for the hypoglycemic range to let the AP be able to administer glucagon proactively. Algorithm 1 lists the full control algorithm.

Algorithm 1: Control algorithm executed with 5 min intervals.

```

1 if CGM measurement available then
2   if a meal was consumed within the previous hour then
3     | set the insulin sensitivity diffusion coefficient,  $\sigma_{S_I}$ , to zero;
4   end
5   estimate the states,  $\hat{x}$ , Section 4.3.1;
6   clip insulin sensitivity,  $S_I(t)$ , (4.38);
7   update the constraints,  $u_{G,k}^{max}$ , (4.34),  $u_{ba,k}^{max}$ , (4.33), and,  $u_{bo,k}^{max}$ , (4.29);
8   if the exercise mode is active then
9     | update the setpoint,  $\bar{z}$ , and the switch limit, (4.36);
10  end
11  if the measured or estimated glucose level is below the switch limit then
12    | solve the OCP, (4.21), in glucagon mode;
13  else
14    | solve the OCP, (4.21), in insulin mode;
15    | if any glucose predictions within the next 30 min are below the switch
16    |   limit then
17    |   | go back and solve the OCP in glucagon mode;
18    |   end
19  end
20  if the optimal solution is obtained then
21    | proceed with the solution;
22  else
23    | use the open-loop fallback strategy, (4.39);
24  end
25  if exercise was just announced and  $G_{CGM} < 7 \text{ mmol/L}$  then
26    | stop insulin administration and give a glucagon bolus of 100  $\mu\text{g}$ , (4.37);
27  end
28 else
29   | use the open-loop fallback strategy, (4.39);
30 end
31 round to pump resolution and unit conversion, Section 4.3.10;

```

4.3.5 Switch logic

We use a simple switch logic to avoid administering insulin and glucagon simultaneously:

- If the measured or estimated glucose concentration is below switch limit, we set the insulin administration to zero and switch to the glucagon mode.
- If the glucose concentration is predicted to become below the switch limit within the next 30 minutes, we set the insulin administration to zero and switch to the glucagon mode.

The AP is always initialized in insulin mode.

4.3.6 Insulin administration logic

We allow insulin boli to be administered after meals or as a correction if the glucose concentration reaches hyperglycemia. We compute the upper bound on the allowed insulin bolus as

$$u_{bo,k}^{\max} = \max\{\epsilon, u_{bo,k}^{\text{corr}} + u_{bo,k}^{\text{meal}} - u_{bo,k}^{\text{hist}}\}, \quad (4.29)$$

where $\epsilon = 10^{-3}$, $u_{bo,k}^{\text{corr}}$ is the maximum correction bolus infusion rate, $u_{bo,k}^{\text{meal}}$ is the maximum meal bolus infusion rate, and $u_{bo,k}^{\text{hist}}$ is the sum of the insulin administration history over the last hour. The allowed correction bolus is computed as

$$u_{bo,k}^{\text{corr}} = \max\left\{0, \frac{1}{T_s} \frac{G_{CGM} - G_{\max}}{ISF}\right\}. \quad (4.30)$$

Here, $T_s = 5$ min is the sampling time, G_{CGM} [mmol/L] is the CGM measurement, $G_{\max} = 10$ mmol/L is the limit for when correction boli can be administered, and ISF [mmol/L/mU] is the insulin sensitivity factor provided by the participants. The correction bolus target is set to 10 mmol/L, as the aim is to correct the participants into range and not to the target. We allow meal boli for 1 hour after a meal is announced and compute the maximum allowed insulin bolus as

$$u_{bo,k}^{\text{meal}} = \max\left\{0, \frac{\gamma}{T_s} \frac{\hat{d}}{ICR}\right\}, \quad (4.31)$$

where \hat{d} [g CHO] is the announced amount of the carbohydrates in the meal, ICR [g/mU] is the ICR provided by the participants, and $\gamma = 1.15$ [unitless] allows the AP to administer 15% more insulin than the amount that would have been administered based on the ICR alone. If a meal was not consumed within the last hour, $u_{bo,k}^{\text{meal}} = 0$. The insulin bolus history is computed as

$$u_{bo,k}^{\text{hist}} = \sum_{j=1}^{N_{bo}^{\text{hist}}} u_{bo,k-j|k-j}, \quad (4.32)$$

where $u_{bo,k|k}$ is the insulin bolus infusion rate at the k 'th interval and $N_{bo}^{\text{hist}} = 11$ corresponds to 12 sampling intervals of 5 minutes, i.e., 1 hour. Finally, the maximum allowed insulin basal rate is

$$u_{ba,k}^{\max} = 2\bar{u}_{ba,k}, \quad (4.33)$$

where $\bar{u}_{ba,k}$ is the nominal basal rate of the participants.

4.3.7 Glucagon administration logic

The glucagon administration is constrained by

$$u_{G,k}^{\max} = \max\{\epsilon, \bar{u}_G^{\max} - u_{G,k}^{\text{hist}}\}. \quad (4.34)$$

Here, $\epsilon = 10^{-3}$, $\bar{u}_G^{\max} = 300 \mu\text{g}$ and the glucagon history is computed by

$$u_{G,k}^{\text{hist}} = \sum_{j=1}^{N_G^{\text{hist}}} u_{G,k-j|k-j}. \quad (4.35)$$

$u_{G,k|k}$ is the glucagon administration rate at the k 'th interval and $N_G^{\text{hist}} = 23$ which corresponds to 24 sampling intervals, i.e., 2 hours. The limit of $300 \mu\text{g}$ per 2 hours is based on the recommendations by the doctors at Steno Diabetes Center Copenhagen.

4.3.8 Exercise logic

We update certain parameters in the AP when exercise is announced as the prediction model does not include an exercise subsystem. We increase the setpoint, \bar{z} , and the switch limit to reduce insulin administration and allow the AP to administer glucagon earlier during exercise. The updated values are

$$\bar{z} = 7.0 \text{ mmol/L}, \quad \text{switch limit} = 7.0 \text{ mmol/L}. \quad (4.36)$$

Furthermore, if $G_{CGM} < 7 \text{ mmol/L}$ when exercise is announced, a glucagon bolus is administered

$$u_{G,k} = 100 \mu\text{g} \quad \text{if} \quad G_{CGM} < 7 \text{ mmol/L}. \quad (4.37)$$

4.3.9 Insulin sensitivity logic

We set the insulin sensitivity diffusion coefficient to zero for one hour after meals to prevent the meals from effecting the adaptive estimation of the insulin sensitivity. Furthermore, we restrict the estimated value of the insulin sensitivity, S_I , in the CD-EKF to be within the limits

$$\log S_I(0) - 1 \leq \log S_I(t) \leq \log S_I(0) + 1, \quad (4.38)$$

as a safety measure, where $S_I(0)$ is estimated during the parameter estimation.

4.3.10 Post-processing and fall-back strategy

We design a fall-back strategy to handle possible unforeseen problems. Specifically, the fall-back strategy is activated in case the solution of the OCP (4.21) is prevented (e.g., if the maximum number of iterations in the SQP algorithm is reached). The fall-back strategy is

$$u_{ba,k|k} = \begin{cases} 0 & G_{CGM} \leq 8.0 \text{ mmol/L}, \\ \bar{u}_{ba,k} & \text{otherwise,} \end{cases} \quad (4.39a)$$

$$u_{bo,k|k} = 0, \quad (4.39b)$$

$$u_{G,k|k} = \begin{cases} \min\{15 \text{ } \mu\text{g}, u_{G,k}^{\max}\} & G_{CGM} < 4.5 \text{ mmol/L}, \\ 0 & \text{otherwise.} \end{cases} \quad (4.39c)$$

If the solution of the OCP (4.21) is obtained, we round the manipulated inputs to the pump resolution which is 0.01 U/h for the insulin basal rate, 0.1 U/h for the bolus insulin and 0.01 $\mu\text{g/h}$ for the glucagon infusion rate.

4.4 Clinical trial

The DiaCon AP was tested in a clinical trial with adolescents with T1D. Appendix K describes the clinical trial and primary outcomes. Appendix L and J discuss the clinical trial from a technical perspective. Appendix L describes the results from each study individually and Appendix J summarizes the overall results and compares to the simulation study performed in Appendix I. Here, we provide an overview and discuss the most interesting learnings from a technical perspective and refer to the Appendices for more details. There were 3 participants in the phase 1 trial and 11 participants in the phase 2 trial. In the phase 1 trial, we only tested the DH configuration of the AP and in the phase 2 trial each participant had two visits, one with the DH configuration of the AP and one with the SH configuration of the AP. Figure 4.8 shows the protocol. The study lasted 26 hours and the participants entered the clinic at 17:00, had dinner at 19:00, slept from approximately 22:00 to 07:30, had breakfast at 08:00, lunch at 12:00, a snack at 15:00, had an exercise session of moderate intensity from 16:30-17:15, and the study ended at 19:00. The participants had a median of 54% TIR, 3% in level 1 and 2 hypoglycemia, and 43% in level 1 and 2 hyperglycemia with their normal treatment.

4.4.1 Technical difficulties and subset of participants

The studies were affected by a number of technical difficulties of varying impact including pressure induced sensor attenuations (PISAs), lost connections to the pumps, occlusions, and bent infusion sets. PISAs cause faulty CGM measurements of very low glucose concentrations, which causes the DH AP to administer glucagon to increase the glucose concentration. PISAs are less significant for SH APs as the only impact is a suspension

of the insulin administration until the next measurement is received. One approach to circumvent PISAs, is to, e.g., use two glucose sensors as in the Inreda system. Lost connections to the pumps can cause the AP to believe that the insulin or glucagon has been administered, which causes both the participants to not receive the adequate dose, but also the estimate of the insulin sensitivity to become incorrect. If the connection is lost briefly it has almost no effect, but prolonged disconnections can have a severe impact on the study outcome. The AP starts an alarm if the connection is lost for more than 15 minutes, but in one study the alarm was unnoticed. Glucagon occlusions are common and happen due to rapid fibrillation after reconstitution [91]. The occlusions prevent the glucagon from being delivered and causes issues in the AP as the administered amount is unknown. Finally, when inserting the infusion sets, the tubes may bend and prevent drug delivery. We make a subset of studies, where we exclude the studies that were heavily affected by technical difficulties. Furthermore, we also exclude the studies where no glucagon was administered in the DH study, as the algorithm is identical in both studies, in that case. The subset of selected participants ($n = 7$) excluded two participants, where no glucagon was administered in the DH study, a participant where the connection to the insulin pump was lost for approximately 7 hours in the DH study, and finally a participant where multiple PISAs occurred in the DH study and caused faulty glucagon administrations.

4.4.2 Results

We show the combined results from the phase 2 trial here and refer to Appendix J and L for discussions of the individual studies the results from the phase 1 trial. Figure 4.9 shows the mean time in the different ranges for all phase 2 studies, the selected studies, the worst-case studies (the studies where the participants spent most time in level 2 hypoglycemia), and the simulation study presented in Appendix I. Table 4.1 shows the outcomes for the glycemic targets [40] for all studies in the phase 2 trial as well as the selected studies and the simulation study, and Table 4.2 shows the insulin and glucagon administration. Finally, Figure 4.10 shows the median and span of all the phase 2 studies and the selected studies. The mean TIR was higher (not significantly different, see Appendix K) and the mean time in hypoglycemia was lower in the SH studies compared to the DH studies, when considering all studies. The TIR for both configurations was higher than the baseline TIR of the participants, but adherence during the clinical trial might also affect the TIR. If we consider the selected studies, the TIR was similar and all the glycemic targets were satisfied. In the worst-case SH study, the participant entered the clinic in level 2 hypoglycemia and did not reach normoglycemia before the study was started and both the meal and glucagon response was overestimated in the worst-case DH study, which resulted in too much insulin being administered. The insulin administration was similar in all studies although slightly more correction bolus insulin was administered in the DH studies. More glucagon was administered in the selected studies, where a mean of 912.91 μg glucagon was administered compared to a mean of 653.95 μg in all studies. Figure 4.10 shows that, the glucose concentration

was mainly in target over night and oscillated more during the day, and that the initial glucose concentration varied between each study. The initial condition should not have a large impact on the performance in a real life setting, where the participants wear the AP for extended periods of time, but can affect the outcomes in a 26 hour study. If we compare the outcomes from the clinical trial to the simulation study, both the DH and SH configuration achieved lower TIR and more TBR in the clinical trial. We believe future simulation studies could represent a real clinical better, if we designed the simulation study differently. Specifically, 1) the simulated data used for parameter estimation is of too high quality with no missing data and correctly announced meals, 2) the glucagon model was the same in both the simulation and control model in the simulation study which results in too accurate predictions of the glucagon response, and 3) the initial condition should not always be steady state. Furthermore, it could be interesting to include certain technical issues in a simulation study as suggested by, e.g., Formo et al. [92].

4.5 Summary

In this chapter, we introduced the DiaCon AP and summarized the results from a clinical trial with ($n = 11$) adolescents. Furthermore, we compared the overall features of the DiaCon AP to the closed-loop systems that are commercially available or in development. The DiaCon AP uses a Dexcom G6 CGM, two Dana Diabecare RS pumps, and the control algorithm is implemented in an Android smartphone. The control algorithm is an NMPC algorithm, where we use an extended stochastic version of the MVP model for prediction. Furthermore, we use a number of heuristics for additional safety measures and to switch between insulin and glucagon administration. We obtain the individualized model parameters with a ML based PEM from CGM, meal and insulin data before the trials. The clinical trials displayed that it is feasible to use NMPC for APs, where both the DH and SH configuration of the AP improved the TIR compared to the median baseline TIR of 54%, but obtaining a model for predictions is both very time-consuming

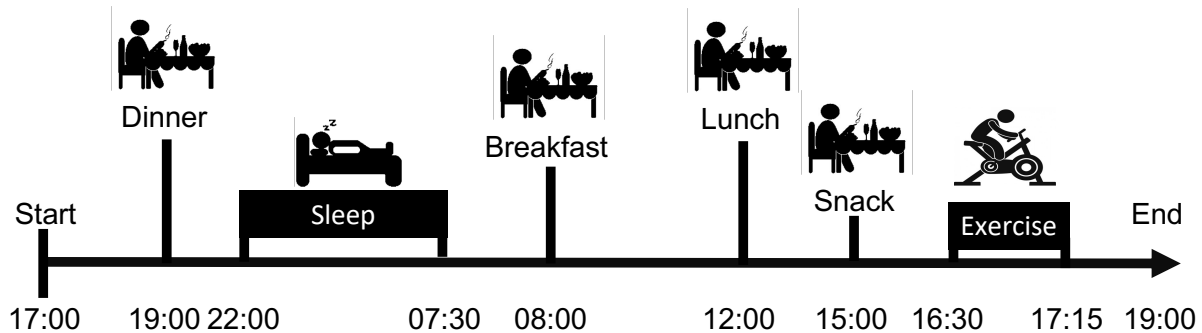


Figure 4.8: The protocol in the clinical trial. The protocol consists of a dinner, sleep, a breakfast, a lunch, a snack, and finally, exercise of moderate intensity.

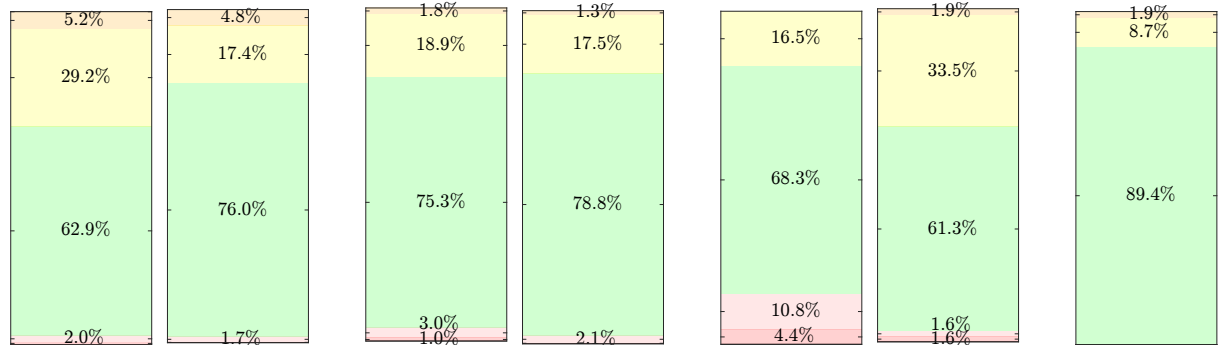


Figure 4.9: Time in ranges for the trial. From the left: 1) mean TIRs for the DH AP in all studies, 2) mean TIRs for the SH in all studies, 3) mean TIRs for the DH AP in selected studies, 4) mean TIRs for the SH AP in selected studies, 5) TIRs for the worst-case DH study, 6) TIRs for the worst-case SH study, and 7) TIRs for the DH simulation study.

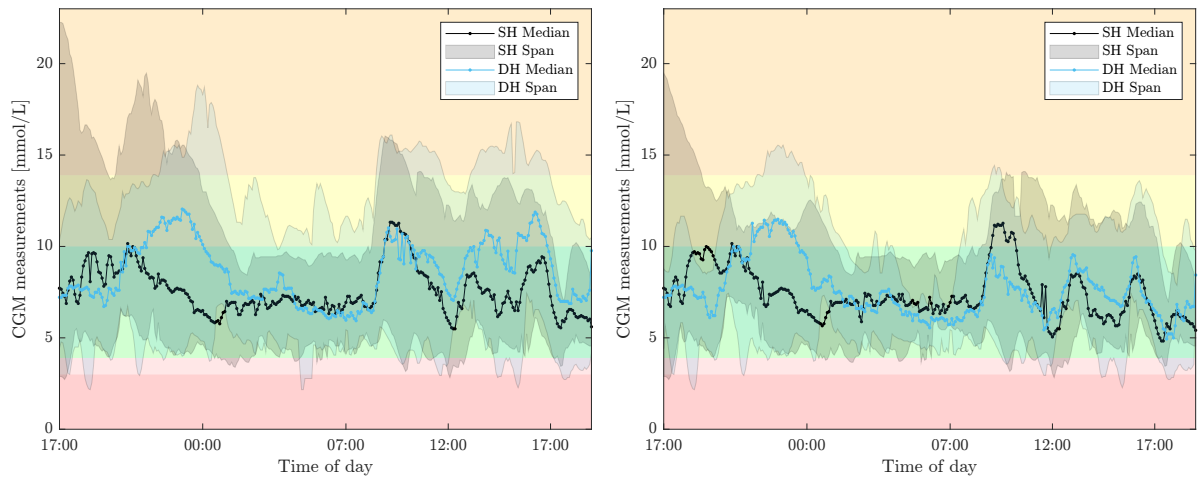


Figure 4.10: Left: median and span for all studies with SH in blue and DH in black. Right: median and span for selected studies with SH in black and DH in blue.

Table 4.1: Mean and standard deviation of the values for the glycemic targets [40] for the DH and SH AP in the clinical trial as well as the simulation study. The average glucose concentration is shown in [mmol/L] and the rest of the targets are displayed in [%].

Quantity	Target	DH all	SH all	DH selected	SH selected	DH sim.
Avg. gluc.	< 8.55	8.69 (1.57)	8.05 (1.15)	7.73 (0.91)	7.65 (0.66)	7.01 (0.41)
GMI	< 7	7.03 (0.70)	6.78 (0.50)	6.61 (0.41)	6.61 (0.29)	6.33 (0.18)
GV	≤ 36	29.81 (6.88)	33.93 (8.72)	31.34 (6.29)	31.74 (6.63)	29.95 (8.18)
Active CGM	100	99.97 (0.10)	100.0 (0.00)	100.0 (0.00)	100.0 (0.00)	100.0 (0.00)
2 hyper	< 5	5.2 (7.26)	4.8 (7.38)	1.8 (3.89)	1.3 (2.73)	1.9 (3.31)
1 and 2 hyper	< 25	34.3 (22.56)	22.2 (13.63)	20.7 (13.36)	18.8 (11.38)	10.56 (8.28)
normo	> 70	62.9 (20.94)	76.0 (13.63)	75.3 (12.70)	78.8 (11.90)	89.44 (7.16)
1 and 2 hypo	< 4	2.8 (4.65)	1.8 (1.63)	4.0 (5.52)	2.4 (1.42)	0.0 (0.00)
2 hypo	< 1	0.8 (1.50)	0.2 (0.48)	1 (1.75)	0.3 (0.60)	0.0 (0.00)

Table 4.2: Mean and standard deviation of the insulin and glucagon administration during the 26 h trial.

Quantity	DH all	SH all	DH selected	SH selected	DH sim.
Total ins. [U]	59.32 (20.65)	59.47 (17.15)	58.12 (18.44)	61.45 (18.89)	26.19 (7.34)
Basal ins. [U]	26.88 (9.45)	26.29 (7.96)	27.71 (9.01)	28.05 (7.99)	15.13 (4.59)
Meal bo. ins. [U]	25.94 (10.33)	28.64 (10.39)	26.89 (10.12)	30.64 (12.32)	10.12 (3.61)
Cor. bo. ins. [U]	6.50 (6.26)	4.54 (3.71)	3.53 (4.01)	2.76 (2.20)	0.94 (1.36)
Glucagon [μ g]	654.0 (499.6)	-	912.9 (415.2)	-	135.5 (74.3)

and very challenging. The TIR was not significantly different between the DH and SH configuration. The DH AP achieved a mean of 63% TIR and the SH AP achieved a mean of 76% TIR. Some studies were heavily affected by technical issues, such as, PISAs and lost connections to the pumps, and therefore we made a subset of selected participants ($n = 7$). For the selected participants, the DH AP achieved a mean of 75.3% TIR and the SH AP achieved a mean of 78.8% TIR.

CHAPTER 5

User interfaces

In this chapter, we describe and demonstrate two user interfaces for diabetes management. We show the GUI from the DiaCon AP application and a web application that lets people with diabetes and medical personnel view diabetes data from, e.g., an AP. The web application is a prototype hosted on the localhost and only includes virtual people and simulated data as described in Chapter 3, but it is designed to work with real data from, e.g., the AP as well. The web application is build with a Vue.js frontend application, a Java Spring Boot backend application, and the data is stored in a PostgreSQL database. We show a demonstration of the DiaCon app here, but it was primarily developed before the beginning of this project. During this project, we added functionality to the exercise announcement screen and corrected bugs. Appendix P describes the web application.

5.1 Artificial pancreas mobile application

The DiaCon app is a Java android application build with the model-view-presenter framework. The application is currently not connected to a database and saves the data in local CSV files as GDPR restricts the connection to the internet during the clinical trials. The application serves multiple purposes as it handles the connections to the pumps and sensor, calls the control algorithm, lets the user create a profile (name, *ICR*, *ISF*, nominal basal rate) and change settings, allows announcement of exercise and meals, and finally displays glucose, insulin, and glucagon time series and predictions. Figure 5.1 shows the *stats* page (front page) of the application on a smartphone and Figure 5.2 describes each component in the *stats* page. The *stats* page shows glucose, insulin, and glucagon data and lets the user activate or deactivate the automatic closed-loop mode. From the bottom menu, the user can navigate between the different pages. Figure 5.3 shows the *care* page that lets the user announce meals, give manual boluses, set temporary targets, and insert manual glucose measurements. Figure 5.4 shows the *exercise* page, where the user can announce exercise and shows the modifications to the *stats* page and *settings* page. While exercise is active, an icon is shown on the *stats* page to remind the user that exercise is active and during exercise it is not possible to change the settings from the *settings* page. Figure 5.5 shows the *profile* page that lets the user create new profiles and modify the existing ones (this is where the user enters, e.g., their *ICR*). Finally, Figure 5.6 shows the *settings* page, where the user connects the CGM and pumps. If the user selects virtual CGM and virtual pump, the app will run with

a simulator instead. The application also continuously monitors the connection to the CGM and pumps, and sounds an alarm if the connection to the sensor or pumps is lost for more than 15 minutes.

5.2 Web application

The web application allows users to login and view different representations of the data depending on their permissions. The aim of the web application is to let people with diabetes and medical personal view and analyze data, but, in the future, also to provide a GUI for the large scale virtual clinical trials described in Chapter 3 and enable remote monitoring of, e.g., the DiaCon AP. Figure 5.7 shows the architecture of the web application and the primary tools used to build each element. The web application is build with a Vue.js frontend application, a Java Spring Boot backend application, an API, and a PostgreSQL database. The backend and frontend application communicates through the API that is described with Swagger. Figure 5.8 shows the *login* page that handles the permission for each user. Currently, it is possible to log in as a *patient*, *doctor*, or *admin*. The *doctor* role has permissions to view the data from all the *patient* users, whereas the permissions of the *patient* only allow the user to view their own data. The *admin* role (e.g. a researcher) also enables the user to see statistics based on the entire population of *patients* similar to the results from Chapter 3, but this role is work in progress and will not be displayed here. Figure 5.9 shows the glucose page with the *doctor* login. The visualization of the data is the same for each role. The left bar lets the *doctor* search for



Figure 5.1: The DiaCon artificial pancreas Android application.

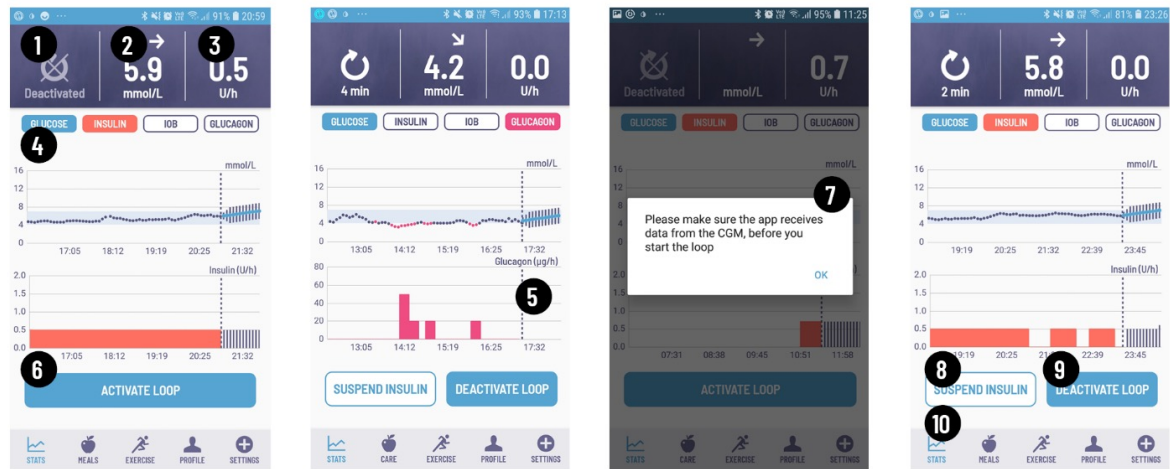


Figure 5.2: The stats page (front screen) in the DiaCon app. 1) Closed-loop status (active/inactive) and time since last update of the glucagon or insulin infusion rate, 2) current glucose concentration and trend, 3) current infusion rate, 4) historical glucose concentration and future predictions, 5) historical data for insulin, glucagon, or IOB (selected above 4.), 6) button to activate closed-loop. 7) reminder when activating closed-loop, 8) button to suspend insulin when closed-loop is active, 9) button to deactivate closed-loop, and 10) button that directs the user to the stats page.

specific *patients* and select who to visualize (this bar is not shown for *patients*). The top bar lets the user select data from a specific period, switch between mmol/L and mg/dL, and select between different pages with visualizations of the data. The second top bar and the right bar shows the values (black if the value is within target range and red if it is not in range) for the glycemic targets [40]. The *All time series* page shows meals, insulin administration, and exercise in addition to the glucose concentration as shown in Figure 5.10. Finally, the *Glucose statistics* page consists of two charts where 1) displays the time in ranges for each day in the selected period (see Figure 5.11) and 2) displays an overlay of the glucose concentration from each day in selected period (see Figure 5.12). The glucose statistics page indicates trends in the glucose concentration. The overlay of days in Figure 5.12 can indicate if the user has, e.g., a tendency of hypoglycemia in the morning and has a too high basal rate during the night or hyperglycemia after dinner and should administer a larger insulin bolus. The simulated data in Figure 5.12 has limited variations between the days and causes narrow confidence intervals. The daily time in ranges in Figure 5.11 can indicate if, e.g., the glucose concentration is usually poorly managed in weekends or if a new treatment improves the care as in the example in Figure 5.11, where the daily TIR is gradually improving.



Figure 5.3: The care menu in the DiaCon application. 1) Front page to announce meals, administer a manual insulin bolus, set temporary target or insert manual glucose measurement, 2) insert amount of carbohydrates in the meal, 3) select size and duration of manual insulin bolus, 4) icon on front page for administration of a meal bolus, 5) set temporary target, 6) icon that indicates that a temporary target is active, 7) the temporary target can be canceled by clicking the icon, and 8) enter manual glucose values.

5.3 Summary and future perspectives

In this chapter, we introduced the DiaCon app and a web application for diabetes management. The DiaCon app is a Java Android application that handles the setup and connection to the CGM and pumps, meal and exercise announcements, and displays the current status of the user and the treatment. The web application allows users to see different visualizations of diabetes data and see the glycemic targets for the selected periods. The web application is build with a Vue.js frontend application, a Java Spring

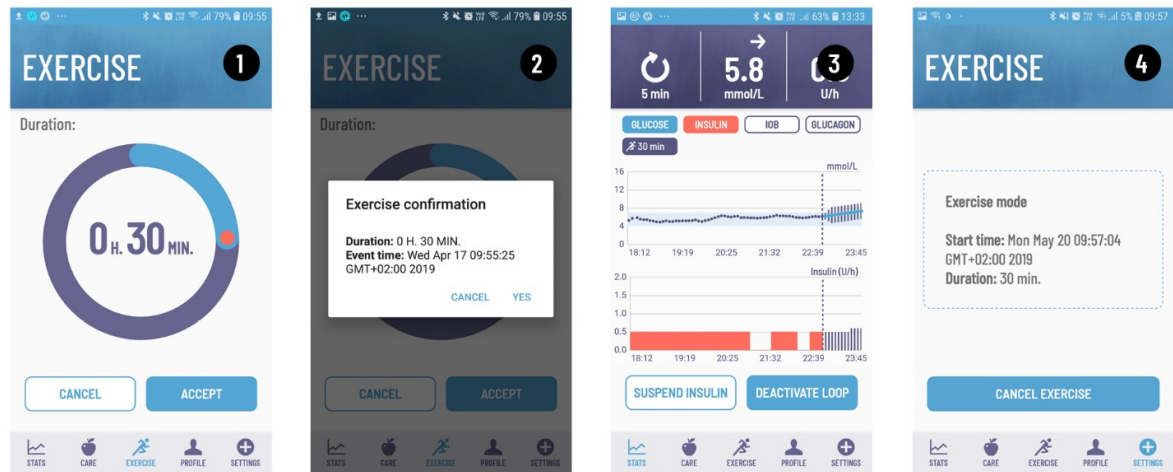


Figure 5.4: The exercise menu in the DiaCon application. 1) Front page to set exercise duration and accept, 2) confirm exercise announcement, 3) stats page after exercise announcement with an exercise icon in top-left corner, and 4) settings cannot be changed while exercise is active.

Boot backend application, an API, and a PostgreSQL database. Through the *login* page, the view changes depending on the permissions of the user, where *doctors* can see data from all their *patients*. *patients* can only see their personal data. There are however still several possible improvements to the web application and missing links before the concept from Figure 1.4 is achieved. Some of the first improvements should include adding the charts from Chapter 3 to the *admin* role and the possibility to sort the *patients* based on not only their name, but also, e.g., the TIR to let the *doctors* identify the *patients* that need care. Adding the charts from Chapter 3 requires some updates to the data structure and backend in order to handle the computations of population based statistics and reduce computation time. Furthermore, while both the virtual clinical trials from Chapter 3 and the web application are connected to a database, the two systems do not interact. In future versions, it should be possible to setup and start simulations (virtual clinical trials) from the web application for both educational purposes, and to perform and view results from large scale virtual clinical trials. Finally, the DiaCon app should be connected to the database to enable the web application for remote monitoring.

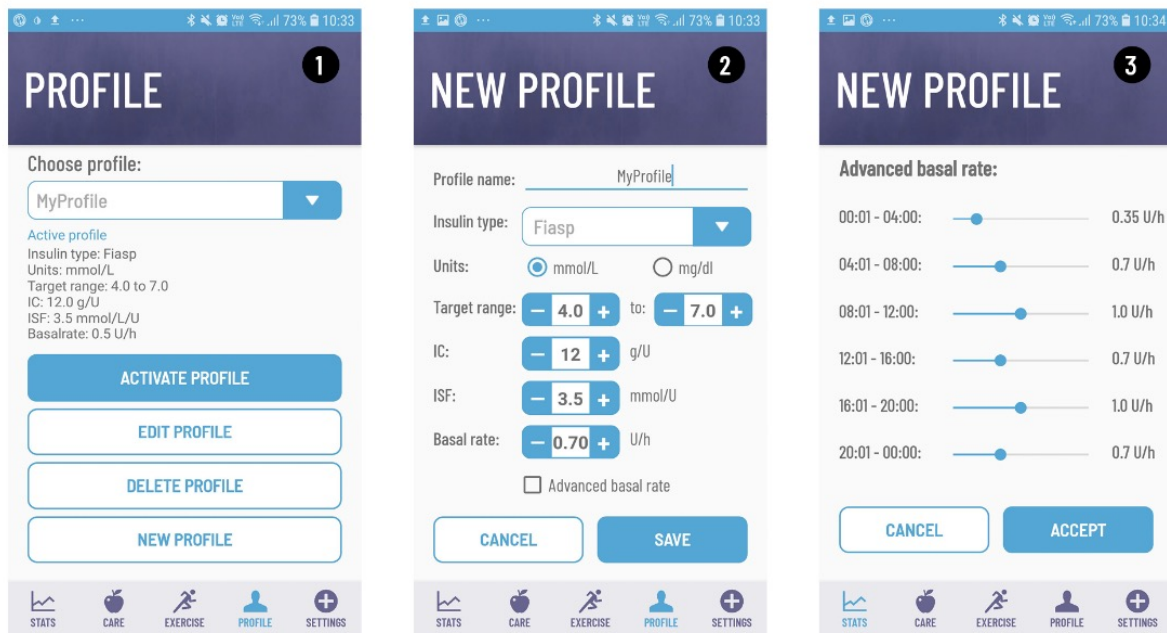


Figure 5.5: The profile menu in the DiaCon application. 1) The profile page, where profiles can be activated, edited, deleted, or created, 2) new profile page, where the user inserts information, and 3) settings for the advanced open loop basal rate (this feature is currently not implemented).

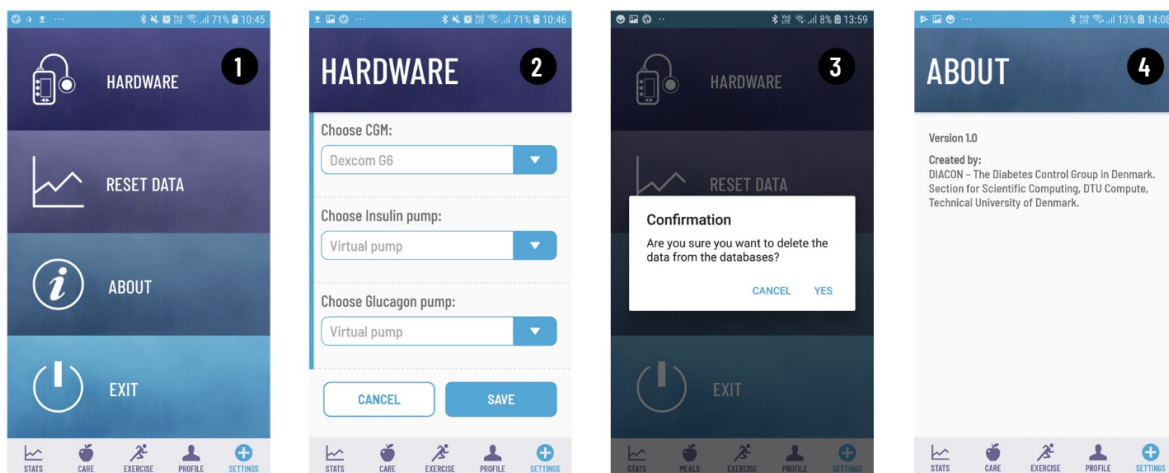


Figure 5.6: The settings menu in the DiaCon application. 1) The front page to connect hardware, reset data, receive general information about the application, and exit the application, 2) the hardware page, where the CGM and pumps are selected and connected, 3) confirmation for resetting data (this feature is inactive as no database is connected), and 4) the about page.

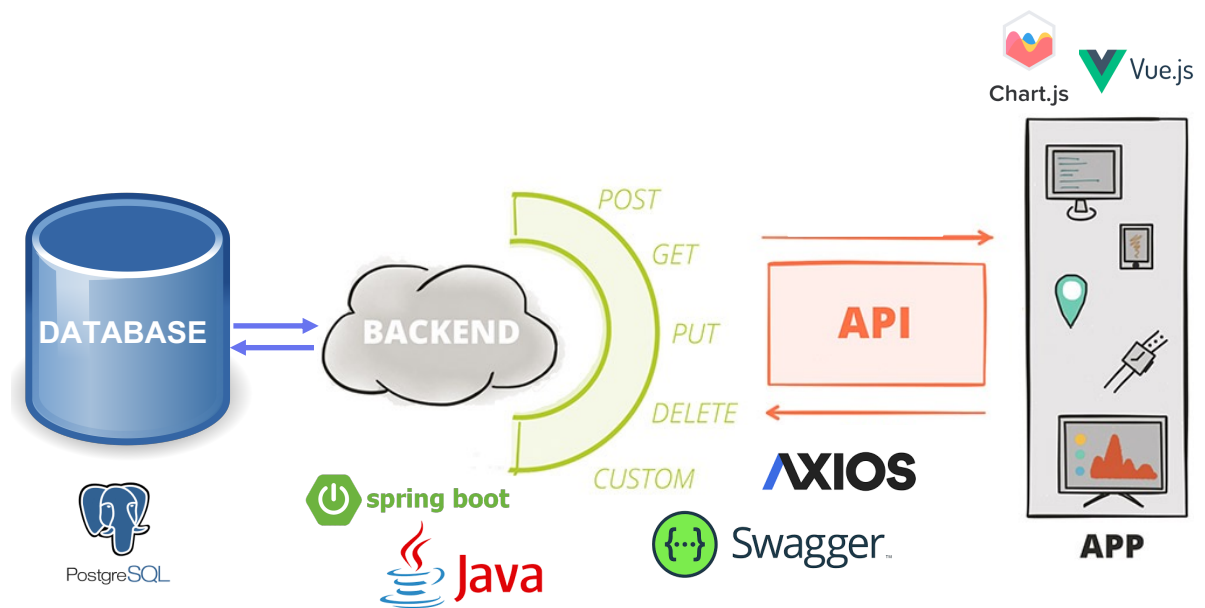


Figure 5.7: Architecture of the web application that consists of a PostgreSQL database, a Java Spring Boot backend application, an API, and a Vue.js frontend application. The charts in the frontend are build with Chart.js.

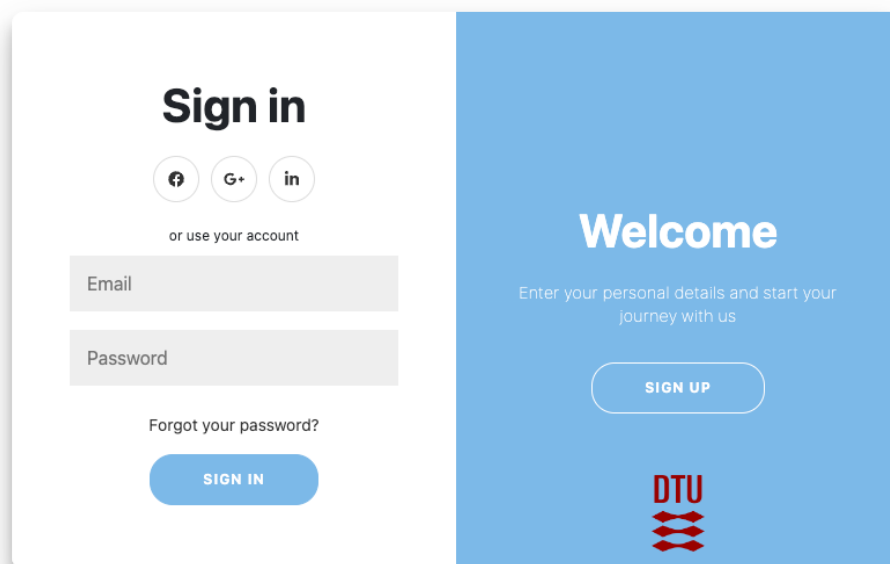


Figure 5.8: Login page to the web application. The login page allows the user to log in and view personalized pages. Currently, it is possible to log in as a *patient*, *doctor*, or *admin*.

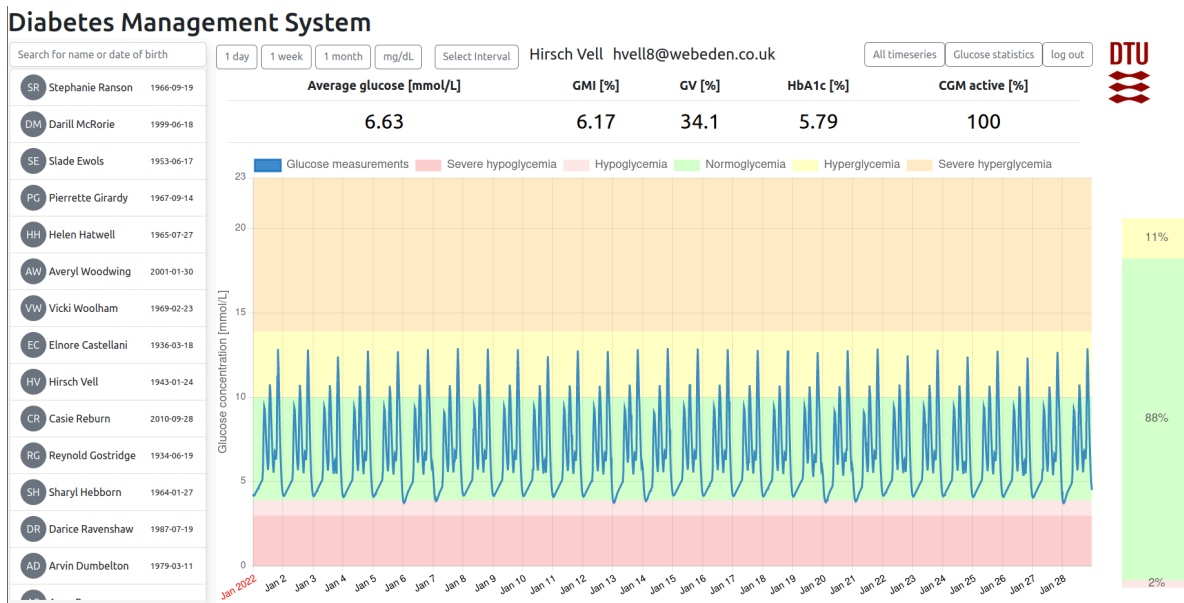


Figure 5.9: Glucose page with the *doctor* login. Left bar: search for specific *patients* and choose who to visualize. Top bar: select period of data to view, switch between mmol/L and mg/dL, and select between different visualizations of the data. Second top bar and right bar: values (the values are black if they are within target range and red if not) for the glycemic targets.

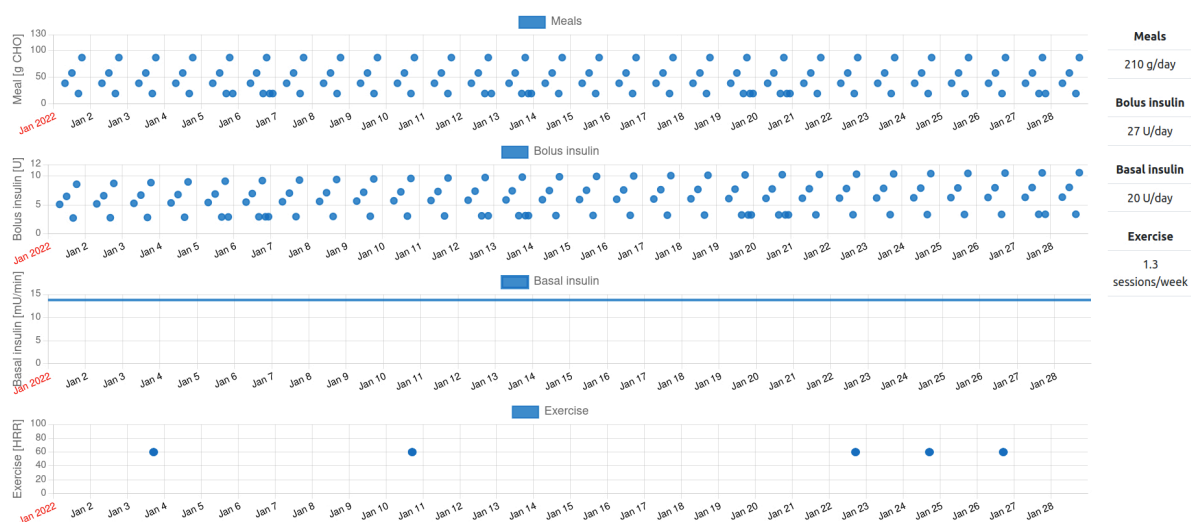


Figure 5.10: The *all time series* page. A glucose plot similar to Figure 5.9 is shown above, but does not fit in one screen. From the top: 1) meals, 2) insulin boli, 3) insulin basal rate, and 4) exercise sessions. Right bar: stats in the selected period for average daily amount of carbohydrates, average daily bolus insulin, average daily basal insulin, and average weekly exercise sessions.

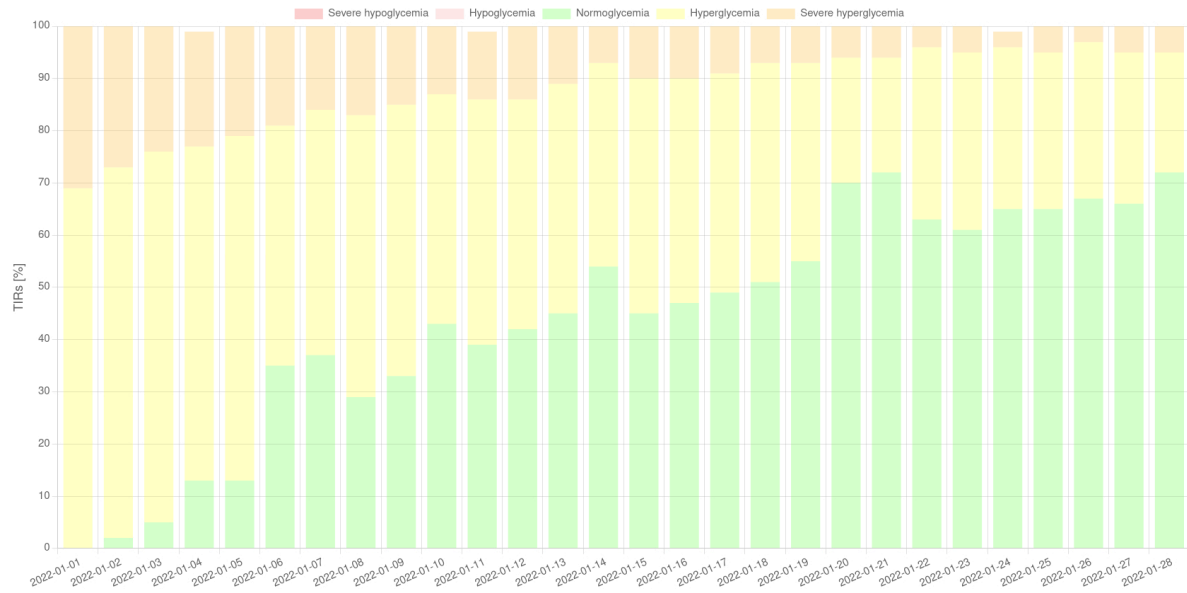


Figure 5.11: Chart that displays the time in ranges for each day in the selected period. The treatment for this virtual person improved during the period.

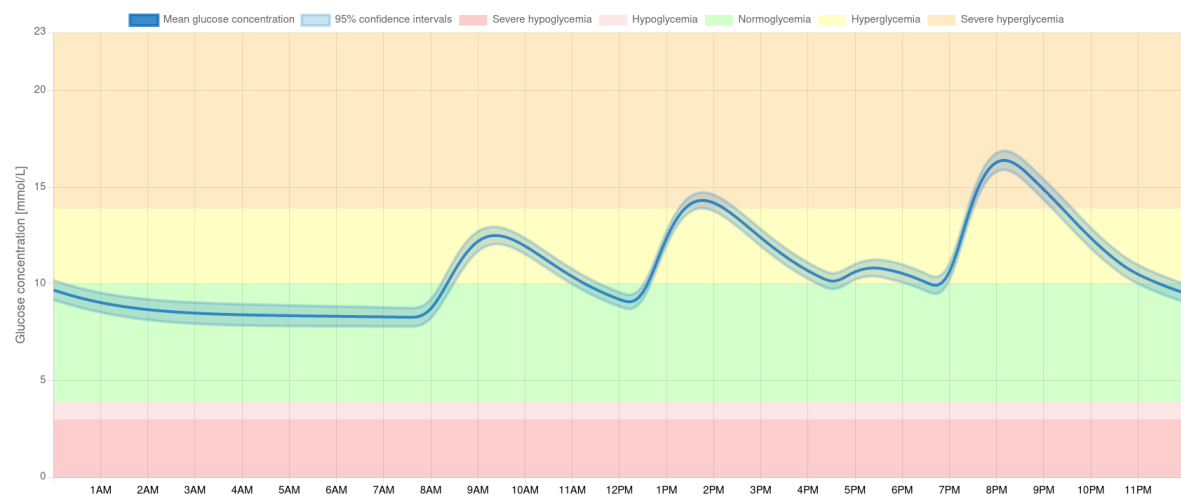


Figure 5.12: Chart that displays an overlay of each day to show the mean glucose concentration with a 95% confidence interval in the selected period.

CHAPTER 6

Conclusions

The main contributions of this thesis are

1. A high-performance Monte Carlo simulation toolbox to perform large-scale long-term virtual clinical trials of closed-loop diabetes treatments.
2. The DiaCon AP tested in a clinical trial with 11 adolescents.
3. A web application to visualize and analyze diabetes data.

In this work, we presented the models used and developed during the thesis. The models are a central component in both the DiaCon AP and the virtual clinical trials. We presented the models used for predictions in the DiaCon AP and the models used to represent virtual participants in the virtual clinical trials. We described and compared five different meal models and briefly discussed models for T2D and the ICU. Furthermore, we described the glucagon model and introduced the whole-body model developed during the thesis.

We developed a parallelized high-performance Monte Carlo simulation toolbox in C and applied it to perform large-scale long-term virtual clinical trials of closed-loop diabetes treatment. The virtual participants were represented by a combination of mathematical models, where each set of model parameters represent a unique participant. We designed protocols from a set of basis days and combined them to form weeks, months and years. The virtual participants and protocols are stored in a PostgreSQL database to make it straightforward to reuse, modify, or add more participants and protocols. We demonstrated the utility of the toolbox by comparing two different closed-loop algorithms in a population of 1 mio. virtual participants over a year (52 weeks) as well as by comparing the performance of a closed-loop system in two different virtual populations with 1 mio. participants in each over 1 year (52 weeks). The first virtual population was represented by the Hovorka model extended with the Haidar glucagon model, the Rashid exercise model, and a simplified version of the Facchinetti CGM model. The second virtual population was represented by the UVA/Padova model modified by Hovorka's meal model. The total computation time of each virtual clinical trial was less than 3 hours.

We developed the DiaCon AP that has both a DH and SH configuration. The DiaCon AP consists of a control algorithm implemented in an Android smartphone, a Dexcom G6 CGM, and two Dana Diabecare RS pumps for insulin or glucagon administration. The DiaCon AP is based on NMPC, where we used an extended version of the MVP model for predictions. We estimated the model parameters with a ML based PEM from

glucose, insulin, and meal data. The states were estimated with the CD-EKF that was also used in the PEM. Furthermore, we used a number of heuristics for 1) switching between insulin and glucagon administration, 2) updating controller hyperparameters during exercise, 3) a fall-back strategy in case the solution of the OCP was prevented, and 4) rounding the suggested administration rate to the pump resolution. The AP was tested in a clinical trial with 11 adolescents and we prepared the AP with a pre-clinical virtual clinical trial including 50 virtual participants. The virtual participants were represented by an extended version of Hovorka’s model. The clinical trial displayed that it is feasible to use NMPC for APs, where both the DH and SH configuration of the AP improved the TIR compared to the baseline (54% TIR). However, obtaining a model for predictions is both very time-consuming and very challenging. The TIR was not significantly different between the DH and SH configuration. The DH AP achieved a mean of 63% TIR and the SH AP achieved a mean of 76% TIR. Some studies were heavily affected by technical issues, such as, PISAs and lost connections to the pumps. The DH AP achieved a mean of 75.3% TIR and the SH AP achieved a mean of 78.8% TIR for the subset of selected participants ($n = 7$) without technical difficulties and where glucagon was administered in the DH studies.

Finally, we designed and developed a web application for visualizing and analyzing diabetes data. The web application was build with a Vue.js frontend application, an API, a Java Spring Boot backend application, and a PostgreSQL database. The web application is a prototype hosted on the localhost and only includes virtual people and simulated data. The web application allows users to login and see different views depending on their permissions. The web application allows users to inspect time-series data and the glycemic targets for specific periods. Furthermore, the user can view daily TIRs and an overlay of days in the selected period to inspect specific daily trends.

6.1 Suggestions for future work

In this section, we discuss suggestions for future work. We discuss future work and possible improvements for the Monte-Carlo simulation toolbox for large-scale virtual clinical trials, the DiaCon AP, and the web application, individually.

Large-scale virtual clinical trials. In this work, we generate virtual participants represented by two different models, 1) an extended version of the Hovorka model, and 2) a modified version of the UVA/Padova model. Both populations are based on limited data, and we suggest that virtual participants represented by more mathematical models are added to the library. Furthermore, we have attempted to construct a set of basis protocols that can be used as building blocks for longer protocols, but we suggest that protocols with more daily variations are added to the library. Furthermore, while we can solve OCPs in the Monte Carlo simulation toolbox, we were not able to achieve parallel scaling with IPOPT due to internal memory allocation. Here, a specialized thread-safe solver is required. Finally, we suggest adding a high-level interface to the toolbox, e.g.,

from the web application, to make it user friendly and available for people who are unfamiliar with C code.

DiaCon AP. Here, we displayed that it is feasible to use NMPC for APs and solve OCPs in a smartphone, but the major drawback of NMPC is the requirement of a prediction model. In this work, the model parameters are estimated from glucose, insulin and meal data from the participants with a ML based PEM, but it is a very time-consuming process that requires manual selection of suitable subsets of the data. Manual parameter estimation is not feasible in a commercial setting with, potentially, thousands of users. Therefore, either the parameter estimation procedure needs to be automated or the control algorithm should either depend on a simpler model or be completely model free. Furthermore, the clinical trial also provided valuable learnings for future development of DH APs: 1) the insulin sensitivity is adaptive and estimated with the CD-EKF, but we fixed it during and after meals. A similar approach should be implemented after administration of glucagon and 2) PISAs have a significant impact on the performance of DH APs. The impact of PISAs may be avoided by using two glucose sensors as in the Inreda system or by some fault-detection algorithm. Finally, in this work, we assumed that the glucagon response was the same for all participants as glucagon data from the participants was unavailable. With the data from the trials, it could be to estimate parameters in the Haidar glucagon model or the UPV glucagon model to compare and evaluate the differences.

Web application. The web application developed in this work is a prototype hosted on the localhost and only includes virtual people and simulated data. Evidently, several improvements are possible. The first and fastest improvement is to add the possibility to sort patients based on KPIs, such as, TIR in addition to their names and date of birth. This would allow medical personnel to quickly identify the people who need care. Furthermore, the *admin* role that allows for population based statistics needs to be finalized. The objective of the thesis from Figure 1.4 requires two significant updates to the web application, 1) the web application should be connected to the Monte Carlo simulation toolbox with a GUI to start simulations and 2) the data from DiaCon AP should be uploaded to the database and visualized. Connecting the DiaCon AP to a database is a relatively small task, but might be challenging due to GDPR.

Bibliography

- [1] International Diabetes Federation. *IDF Diabetes Atlas*. Tenth edition. 2021.
- [2] Michael Fang, Dan Wang, Josef Coresh, and Elizabeth Selvin. “Trends in Diabetes Treatment and Control in U.S. Adults, 1999–2018”. In: *The New England Journal of Medicine* 384.23 (2005), pages 2219–2228. DOI: 10.1056/NEJMsa2032271.
- [3] Katie Weinger and Elizabeth A. Beverly. “Barriers to Achieving Glycemic Targets: Who Omits Insulin and Why?” In: *Diabetes Care* 33.2 (2010), pages 450–452. DOI: 10.2337/dc09-2132.
- [4] Greet Van den Berghe, Pieter Wouters, Frank Weekers, Charles Verwaest, Frans Bruyninckx, Miet Schetz, Dirk Vlasselaers, Patrick Ferdinande, Peter Lauwers, and Roger Bouillon. “Intensive Insulin Therapy in Critically Ill Patients”. In: *New England Journal of Medicine* 345.19 (2001), pages 1359–1367. DOI: 10.1056/NEJMoa011300.
- [5] World Health Organization. *Classification of diabetes mellitus*. 2019.
- [6] Audren Fournel, Alysson Marlin, Anne Abot, Charles Pasquio, Carla Carillo, Patrice D. Cani, and Clause Knauf. “Glucosensing in the gastrointestinal tract: Impact on glucose metabolism”. In: *American Journal of Physiology - Gastrointestinal and Liver Physiology* 310.1 (2016), G645–58. DOI: 10.1152/ajpgi.00015.2016.
- [7] B. Wayne Bequette. “A critical assessment of algorithms and challenges in the development of a closed-loop artificial pancreas”. In: *Diabetes Technology and Therapeutics* 7.1 (2005), pages 28–47.
- [8] Paromita King, Ian Peacock, and Richard Donnelly. “The UK prospective diabetes study (UKPDS): clinical and therapeutic implications for type 2 diabetes”. In: *British Journal of Clinical Pharmacology* 363.4 (1999), pages 311–320. DOI: 10.1046/j.1365-2125.1999.00092.x.
- [9] Olesya Didyuk, Nicolas Econom, Angelica Guardia, Kelsey Livingston, and Ulrike Klueh. “Continuous Glucose Monitoring Devices: Past, Present, and Future Focus on the History and Evolution of Technological Innovation”. In: *Journal of Diabetes Science and Technology* 15.3 (2021), pages 676–683. DOI: 10.1177/1932296819899394.

- [10] Richard M. Bergenstal, William V. Tamborlane, Andrew Ahmann, John B. Buse, George Dailey, Stephen N. Davis, Carol Joyce, Tim Peoples, Bruce A. Perkins, John B. Welsh, Stevel M. Willi, and Michael A. Wood. “Effectiveness of Sensor-Augmented Insulin-Pump Therapy in Type 1 Diabetes”. In: *The New England Journal of Medicine* 363.5 (2010), pages 643–648. DOI: 10.1056/NEJMoa1002853.
- [11] Sophie Templer. “Closed-Loop Insulin Delivery Systems: Past, Present, and Future Directions”. In: *Frontiers in Endocrinology* 13 (2022), page 919942. DOI: 10.3389/fendo.2022.919942.
- [12] Joseph El Youssef, Jessica Castle, and W. Kenneth Ward. “A Review of Closed-Loop Algorithms for Glycemic Control in the Treatment of Type 1 Diabetes”. In: *Algorithms* 2.1 (2009), pages 518–532. DOI: doi.org/10.3390/a2010518.
- [13] Torben Biester, Judith Nir, Kerstin Remus, Alon Farfel, Ido Muller, Sarah Biester, Eran Atlas, Klemen Dovc, Nataša Bratina, Olga Kordonouri, Tadej Batelino, Moshe Philip, Thomas Danne, and Revital Nimri. “DREAM5: An open-label, randomized, cross-over study to evaluate the safety and efficacy of day and night closed-loop control by comparing the MD-Logic automated insulin delivery system to sensor augmented pump therapy in patients with type 1 diabetes at home”. In: *Diabetes, Obesity and Metabolism* 21.4 (2019), pages 822–828. DOI: 10.1111/dom.13585.
- [14] Lauren M. Huyett, Eyal Dassau, Howard C. Zisser, and Francis J. Doyle III. “Design and evaluation of a robust PID controller for a fully implantable artificial pancreas”. In: *Industrial and Engineering Chemistry Research* 54 (2015), pages 10311–10321. DOI: 10.1021/acs.iecr.5b01237.
- [15] John Bagterp Jørgensen, Dimitri Boiroux, and Zeinab Mahmoudi. “An artificial pancreas based on simple control algorithms and physiological insight”. In: *IFAC PapersOnLine* 52.1 (2019), pages 1018–1023. DOI: 10.1016/j.ifacol.2019.06.196.
- [16] Ankush Chakrabarty, Elizabeth Healey, Dawai Shi, Stamatina Zavitsanou, Francis J. Doyle III, and Eyal Dassau. “Embedded model predictive control for a wearable artificial pancreas”. In: *IEEE Transactions on Control Systems Technology* 28.6 (2020), pages 2600–2607. DOI: 10.1109/TCST.2019.2939122.
- [17] Mirko Messori, Gian Paolo Incremona, Claudio Cobelli, and Lalo Magni. “Individualized model predictive control for the artificial pancreas: In silico evaluation of closed-loop glucose control”. In: *IEEE Control Systems Magazine* 38.1 (2018), pages 86–104. DOI: 10.1109/MCS.2017.2766314.
- [18] Roman Hovorka, Valentina Canonico, Ludovic J. Chassin, Ulrich Haueter, Massimo Massi-Benedetti, Marco O. Federici, Thomas R. Pieber, Helga C. Schaller, Lukas Schaupp, Thomas Vering, and Malgorzata E. Wilinska. “Nonlinear Model Predictive Control of Glucose Concentration in Subjects with Type 1 Diabetes”. In: *Physiological Measurement* 25.4 (2004), pages 905–920. DOI: 10.1088/0967-3334/25/4/010.

- [19] Dimitri Boiroux, Anne Katrine Duun-Henriksen, Signe Schmidt, Kirsten Nørgaard, Sten Madsbad, Niels Kjølstad Poulsen, Henrik Madsen, and John Bagterp Jørgensen. “Overnight glucose control in people with type 1 diabetes”. In: *Biomedical Signal Processing and Control* 39 (2018), pages 503–512. DOI: 10.1016/j.bspc.2017.08.005.
- [20] Dimitri Boiroux and John Bagterp Jørgensen. “Nonlinear Model Predictive Control and Artificial Pancreas Technologies”. In: *2018 IEEE Conference on Decision and Control (CDC)*. 2018, pages 284–290. DOI: 10.1109/CDC.2018.8619521.
- [21] Kamuran Turksoy, Laurie Quinn, Elizabeth Littlejohn, and Ali Cinar. “Multi-variable Adaptive Identification and Control for Artificial Pancreas Systems”. In: *IEEE Transactions on Biomedical Engineering* 61.3 (2014), pages 883–891. DOI: 10.1109/TBME.2013.2291777.
- [22] Patricio Colmegna, Ricardo S. Sanchez Penã, Ravi Gondhalekar, Eyal Dassau, and Francis J. Doyle III. “Reducing Risks in Type 1 Diabetes Using H_∞ Control”. In: *Algorithms* 23.5 (2021), pages 367–375. DOI: 10.1089/dia.2020.0535.
- [23] Marc Breton, Anne Farret, Daniela Bruttomesso, Stacey Anderson, Lalo Magni, Stephen Patek, Chiara Dalla Man, Jerome Place, Susan Demartini, Simone Del Favero, Chiara Toffanin, Colleen Hughes-Karvetski, Eyal Dassau, Howard Zissar, Francis J Doyle III, Giuseppe De Nicolao, Angelo Avogaro, Claudio Cobelli, Eric Renard, and Boris Kovatchev. “Fully Integrated Artificial Pancreas in Type 1 Diabetes”. In: *Diabetes* 61.9 (2012), pages 2230–2237. DOI: 10.2337/db11-1445.
- [24] Satish K. Garg, Stuart A. Weinzimer, William V. Tamborlane, Bruce A. Buckingham, Bruce W. Bode, Timothy S. Bailey, Ronald L. Brazg, Jacob Ilany, Robert H. Slover, Stacey M. Anderson, Richard M. Bergenstal, Benyamin Grosman, Anirban Roy, Toni L. Cordero, John Shin, Scott W. Lee, and Francine R. Kaufman. “Glucose Outcomes with the In-Home Use of a Hybrid Closed-Loop Insulin Delivery System in Adolescents and Adults with Type 1 Diabetes”. In: *Diabetes Technology and Therapeutics* 19.3 (2017), pages 155–163. DOI: 10.1089/dia.2016.0421.
- [25] Sue A. Brown, Boris P. Kovatchev, Dan Raghinaru, John W. Lum, Bruce A. Buckingham, Yogish C. Kudva, Lori M. Laffel, Carol J. Levy, Jordan E. Pinsker, R. Paul Wadwa, Eyal Dassau, Francis J. Doyle III, Stacey M. Anderson, Mei Mei Church, Vikash Dadlani, Laya Ekhlaspour, Gregory P. Forlenza, Elvira Isganaitis, David W. Lam, Craig Kollman, and Roy W. Beck. “Six-Month Randomized, Multicenter Trial of Closed-Loop Control in Type 1 Diabetes”. In: *The New England Journal of Medicine* 381.18 (2019), pages 1707–1717. DOI: 10.1056/NEJMoa1907863.
- [26] Martin Tauschmann, Hood Thabit, Lia Bally, Janet M. Allen, Sara Hartnell, Malgorzata E. Wilinska, Yue Ruan, Judy Sibayan, Craig Kollman, Peiyao Cheng, Roy W. Beck, Carlo L. Acerini, Mark L. Evans, David B. Dunger, Daniela Elleri, Fiona Campbell, Richard M. Bergenstal, Amy Criege, Viral N. Shah, Lalantha Leelarathna, and Roman Hovorka. “Closed-loop insulin delivery in suboptimally controlled type 1 diabetes: a multicentre, 12-week randomised trial”. In: *Lancet* 392.10155 (2018), pages 1321–1329. DOI: 10.1016/S0140-6736(18)31947-0.

- [27] Anders L. Carlson, Jennifer L. Sherr, Dorothy I. Shulman, Satish K. Garg, Rodica Pop-Busui, Bruce W. Bode, David R. Lilienquist, Ron L. Brazg, Kevin B. Kaiserman, Mark S. Kipnes, James R. Thrasher, John H. Chip Reed, Robert H. Slover, Athena Philis-Tsimikas, Mark Christiansen, Benyamin Grosman, Anirban Roy, Melissa Vella, Richard A. M. Jonkers, Xiaoxiao Chen, John Shin, Toni L. Cordero, Scott W. Lee, Andrew S. Rhinehart, and Robert A. Vigersky. “Safety and Glycemic Outcomes During the MiniMed™ Advanced Hybrid Closed-Loop System Pivotal Trial in Adolescents and Adults with Type 1 Diabetes”. In: *Diabetes Technology and Therapeutics* 24.3 (2022), pages 178–189. DOI: 10.1089/dia.2021.0319.
- [28] Pierre-Yves Benhamou, Sylvia Franc, Yves Reznik, Charles Thivolet, Pauline Schaepelynck, Eric Renard, Bruno Guerci, Lucy Chaillous, Celine Lukas-Croisier, Nathalie Jeandidier, Helene Hanaire, Sophie Borot, Maeva Doron, Pierre Jallon, Ilham Xhaard, Vincent Melki, Laurent Meyer, Brigitte Delemer, Marie Guillouche, Laurene Schoumacker-Ley, Anne Farret, Denis Raccach, Sandrine Lablanche, Michael Joubert, Alfred Penfornis, and Guillaume Charpentier. “Closed-loop insulin delivery in adults with type 1 diabetes in real-life conditions: a 12-week multicentre, open-label randomised controlled crossover trial”. In: *Lancet Digital Health* 1 (2019), e17–e25. DOI: 10.1016/S2589-7500(19)30003-2.
- [29] Sue A. Brown, Gregory P. Forlenza, Bruce W. Bode, Jordan E. Pinsker, Carol J. Levy, Amy B. Criego, David W. Hansen, Irl B. Hirsch, Anders L. Carlson, Richard M. Bergenstal, Jennifer L. Sherr, Sanjeev N. Mehta, Lori M. Laffel, Viral N. Shah, Anuj Bhargava and Ruth S. Weinstock, Sarah A. MacLeish and Daniel J. DeSalvo, Thomas C. Jones, Grazia Aleppo, Bruce A. Buckingham, and Trang T. Ly. “Multicenter Trial of a Tubeless, On-Body Automated Insulin Delivery System With Customizable Glycemic Targets in Pediatric and Adult Participants With Type 1 Diabetes”. In: *Diabetes Care* 44 (2021), pages 1630–1640. DOI: 10.2337/dc21-0172.
- [30] Moshe Phillip, Revital Nimri, Richard M. Bergenstal, Katharine Barnard-Kelly, Thomas Danne, Roman Hovorka, Boris P. Kovatchev, Laurel H. Messer, Christopher G. Parkin, Louise Ambler-Osborn, Stephanie A. Amiel, Lia Bally, Roy W. Beck, Sarah Biester, Torben Biester, Julia E. Blanchette, Emanuele Bosi, Charlotte K. Boughton, Marc D. Breton, Sue A. Brown, Bruce A. Buckingham, Albert Cai, Anders L. Carlson, Jessica R. Castle, Pratik Choudhary, Kelly L. Close, Claudio Cobelli, Amy B. Criego, Elizabeth Davis, Carine de Beaufort, Martin I. de Bock, Daniel J. DeSalvo, J. Hans DeVries, Klemen Dovc, Francis J. Doyle III, Laya Ekhlaspour, Naama Fisch Shvalb, Gregory P. Forlenza, Geraldine Gallen, Satish K. Garg, Dana C. Gershenoff, Linda A. Gonder-Frederick, Ahmad Haidar, Sara Hartnell, Lutz Heinemann, Simon Heller, Irl B. Hirsch, Korey K. Hood, Diana Isaacs, David C. Klonoff, Olga Kordonouri, Aaron Kowalski, Lori Laffel, Julia Lawton, Rayhan A. Lal, Lalantha Leelarathna, David M. Maahs, Helen R. Murphy, Kirsten Nørsgaard, David O’Neal, Sean Oser, Tamara Oser, Eric Renard, Michael C. Riddell, David Rodbard, Steven J. Russell, Desmond A. Schatz, Viral N. Shah, Jennifer L. Sherr, Gregg D. Simonson, R. Paul Wadwa, Candice Ward, Stuart A.

- Weinzimer, Emma G. Wilmot, and Tadej Battelino. "Consensus Recommendations for the Use of Automated Insulin Delivery Technologies in Clinical Practice". In: *Endocrine Reviews* (2022), pages 1630–1640. DOI: 10.1210/endrev/bnac022.
- [31] Clara Viñals, Aleix Beneyto, Juan-Fernando Martín-SanJosé, Clara Furió-Novejarque, Arthur Bertachi, Jorge Bondia, Josep Vehi, Ignacio Conget, and Marga Giménez. "Artificial Pancreas With Carbohydrate Suggestion Performance for Unannounced and Announced Exercise in Type 1 Diabetes". In: *Journal of Clinical Endocrinology and Metabolism* 106.1 (2021), pages 55–63. DOI: 10.1210/clinem/dgaa562.
- [32] Luz E. Castellanos, Courtney A. Balliro, Jordan S. Sherwood, Rabab Jafri, Mallory A. Hillard, Evelyn Greaux, Rajendranath Selagamsetty, Hui Zheng, Firas H. El-Khatib, Edward R. Damiano, and Steven J. Russell. "Performance of the Insulin-Only iLet Bionic Pancreas and the Bihormonal iLet Using Dasiglucagon in Adults With Type 1 Diabetes in a Home-Use Setting". In: *Diabetes Care* 44.6 (2021), e118–e120. DOI: 10.2337/dc20-1086.
- [33] Bionic Pancreas Research Group. "Multicenter, Randomized Trial of a Bionic Pancreas in Type 1 Diabetes". In: *New England Journal of Medicine* 387.13 (2022), pages 1161–1172. DOI: 10.1056/NEJMoa2205225.
- [34] Helga Blauw, A. Joannet Onvlee, Michel Klaassen, Arianne C. Van Bon, and J. Hans DeVries. "Fully Closed Loop Glucose Control With a Bihormonal Artificial Pancreas in Adults With Type 1 Diabetes: An Outpatient, Randomized, Crossover Trial". In: *Diabetes Care* 44 (2021), pages 836–838. DOI: 10.2337/dc20-2106.
- [35] Karim Davari Benam, Hasti Khoshamadi, Marte Kierulf Åm, Øyvind Stavdahl, Sebastien Gros, and Anders Lyngvi Fougner. "Identifiable prediction animal model for the bi-hormonal intraperitoneal artificial pancreas". In: *Journal of Process Control* 121 (2023), pages 13–29. DOI: 10.1016/j.jprocont.2022.11.008.
- [36] Ahmad Haidar, Rémi Rabasa-Lhoret, Laurent Legault, Leif E. Lovblom, Rohan Rakheja, Virginie Messier, Emilie D'Aoust, C. Marcelo Falappa, Tara Justice, Andrej Orszag, Holly Tschirhart, Maryse Dallaire, Martin Ladouceur, and Bruce A. Perkins. "Single- and Dual-Hormone Artificial Pancreas for Overnight Glucose Control in Type 1 Diabetes". In: *Journal of Clinical Endocrinology and Metabolism* 101.1 (2016), pages 214–223. DOI: 10.1210/jc.2015-3003.
- [37] Ahmad Haidar. "Insulin-and-Glucagon Artificial Pancreas Versus Insulin-Alone Artificial Pancreas: A Short Review". In: *Diabetes Spectrum* 32.3 (2019), pages 215–221. DOI: 10.2337/ds18-0097.
- [38] John W. Lum, Ryan J. Bailey, Victoria Barnes-Lomen, Diana Naranjo, Korey K. Hood, Rayhan A. Lal, Brandon Arbiter, Adam S. Brown, Daniel J. DeSalvo, Jeremy Pettus, Peter Calhoun, and Roy W. Beck. "A Real-World Prospective Study of the Safety and Effectiveness of the Loop Open Source Automated Insulin Delivery System". In: *Diabetes Technology and Therapeutics* 2.1 (2009), pages 518–532. DOI: doi.org/10.3390/a2010518.

- [39] Signe Schmidt, Dimitri Boiroux, Ajenthen Ranjan, John Bagterp Jørgesen, Henrik Madsen, and Kirsten Nørgaard. “An artificial pancreas for automated blood glucose control in patients with type 1 diabetes”. In: *Therapeutic Delivery* 6.5 (2015), pages 609–619. DOI: 10.4155/tde.15.12.
- [40] Tadej Battelino, Thomas Danne, Richard M. Bergenstal, Stephanie A. Amiel, Roy Beck, Torben Biester, Emanuele Bosi, Bruce A. Buckingham, William T. Cefalu, Kelly L. Close, Claudio Cobelli, Eyal Dassau, J. Hans DeVries, Kim C. Donaghue, Klemen Dovc, Francis J. Doyle III, Satish Garg, George Grunberger, Simon Heller, Lutz Heinemann, Irl B. Hirsch, Roman Hovorka, Weiping Jia, Olga Kordonouri, Boris Kovatchev, Aaron Kowalski, Lori Laffel, Brian Levine, Alexander Mayorov, Chantal Mathieu, Helen R. Murphy, Revital Nimri, Kirsten Nørgaard, Christopher G. Parkin, Eric Renard, David Rodbard, Banshi Saboo, Desmond Schatz, Keaton Stoner, Tatsuiiko Urakami, Stuart A. Weinzimer, and Moshe Phillip. “Clinical Targets for Continuous Glucose Monitoring Data Interpretation: Recommendations From the International Consensus on Time in Range”. In: *Diabetes Care* 42.8 (2019), pages 1593–1603. DOI: 10.2337/dci19-0028.
- [41] Aylin Sertkaya, Rebecca DeVries, Amber Jessup, and Trinidad Beleche. “Estimated Cost of Developing a Therapeutic Complex Medical Device in the US”. In: *Journal of the American Medical Association* 5.9 (2022), e2231609. DOI: 10.1001/jamanetworkopen.2022.31609.
- [42] Claudio Cobelli, Chiara Dalla Man, Giovanni Sparacino, Lalo Magni, Giuseppe De Nicolao, and Boris P. Kovatchev. “Diabetes: Models, Signals, and Control”. In: *IEEE reviews in biomedical engineering* 2 (2009), pages 54–96. DOI: 10.1109/RBME.2009.2036073.
- [43] Malgorzata E. Wilinska, Ludovic J. Chassin, Carlo L. Acerini, Janet M. Allen, David B. Dunger, and Roman Hovorka. “Simulation Environment to Evaluate Closed-Loop Insulin Delivery Systems in Type 1 Diabetes”. In: *Journal of Diabetes Science and Technology* 4.1 (2010), pages 132–144. DOI: 10.1177/193229681000400117.
- [44] Chiara Dalla Man, Francesco Micheletto, Dayu Lv, Marc Breton, Boris Kovatchev, and Claudio Cobelli. “The UVA/PADOVA Type 1 Diabetes Simulator: New Features”. In: *Diabetes Technology and Therapeutics* 8.1 (2014), pages 26–34. DOI: 10.1177/1932296813514502.
- [45] Roberto Visentin, Enrique Campos-Náñez, Michele Schiavon, Dayu Lv, Martina Vettoretti, Marc Breton, Boris P. Kovatchev, Chiara Dalla Man, and Claudio Cobelli. “The UVA/Padova Type 1 Diabetes Simulator Goes From Single Meal to Single Day”. In: *Journal of Diabetes Science and Technology* 12.2 (2018), pages 273–281. DOI: 10.1177/1932296818757747.
- [46] Roman Hovorka, Fariba Shojaee-Moradie, Paul V. Carroll, Ludovic J. Chassin, Ian J. Gowrie, Nicola C. Jackson, Romulus S. Tudor, A. Margot Umpleby, and Richard H. Jones. “Partitioning glucose distribution/transport, disposal, and endogenous

- production during IVGTT". In: *American Journal of Physiology-Endocrinology and Metabolism* 282 (2002), E992–E1007. DOI: 10.1152/ajpendo.00304.2001.
- [47] Sayyar Ahmad, Charrise M. Ramkissoon, Aleix Beneyto, Ignacio Conget, Marga Giménez, and Josep Vehi. "Generation of Virtual Patient Populations That Represent Real Type 1 Diabetes Cohorts". In: *Mathematics* 9 (2021), page 1200. DOI: 10.3390/math9111200.
- [48] Ahmad Haidar, Malgorzata E. Wilinska, James A. Graveston, and Roman Hovorka. "Stochastic Virtual Population of Subjects With Type 1 Diabetes for the Assessment of Closed-Loop Glucose Controllers". In: *IEEE transactions on biomedical engineering* 60.12 (2013), pages 26–34. DOI: 10.1109/TBME.2013.2272736.
- [49] Onofre Orozco-López, Agustín Rodríguez-Herrero, Carlos E. Castañeda, Gema García-Sáez, and M. Elena Hernando. "Method to generate a large cohort in-silico for type 1 diabetes". In: *Computer Methods and Programs in Biomedicine* 193 (2020), page 105523. DOI: 10.1109/TBME.2013.2272736.
- [50] Navid Resalat, Joseph El Youssef, Nichole Tyler, Jessica Castle, and Peter G. Jacobs. "A statistical virtual patient population for the glucoregulatory system in type 1 diabetes with integrated exercise model". In: *PLoS One* 14.7 (2019), e0217301. DOI: 10.1371/journal.pone.0217301.
- [51] David Champagne, Amy Hung, and Olivier Leclerc. "The road to digital success in pharma". In: *McKinsey Global Institute* 22.18 (2015), pages 2014–2016.
- [52] Nithesh Naik, B. M. Zeeshan Hameed, Nilakshman Sooriyaperakasam, Shankeeth Vinayahalingam, Vathsala Patil, Komal Smriti, Janhavi Saxena, Milap Shah, Sufyan Ibrahim, Anshuman Singh, Hadis Karimi, Karthickeyan Naganathan, Dasharathraj K. Shetty, Bhavan Prasad Rai, Piotr Chlosta, and Bhaskar K. Somani. "Transforming healthcare through a digital revolution: A review of digital healthcare technologies and solutions". In: *Frontiers in Digital Health* 4 (2022), page 919985. DOI: 10.3389/fdgth.2022.919985.
- [53] Chiara Dalla Man, Robert A. Rizza, and Claudio Cobelli. "Meal simulation model of the glucose-insulin system". In: *IEEE Transactions on Biomedical Engineering* 54.10 (2007), pages 1740–1749. DOI: 10.1109/TBME.2007.893506.
- [54] Patricio Colmegna, Ke Wang, Jose Garcia-Tirado, and Marc D. Breton. "Mapping data to virtual patients in type 1 diabetes". In: *Control Engineering Practice* 103 (2020), page 104605. DOI: 10.1016/j.conengprac.2020.104605.
- [55] Sami S. Kanderian, Stu Weinzimer, Gayane Voskanyan, and Garry M. Steil. "Identification of Intraday Metabolic Profiles during Closed-Loop Glucose Control in Individuals with Type 1 Diabetes". In: *Journal of Diabetes Science and Technology* 3.5 (2009), pages 1047–1057. DOI: 10.1177/193229680900300508.

- [56] Dimitri Boiroux, Tobias K. S. Ritschel, Niels Kjølstad Poulsen, Henrik Madsen, and John Bagterp Jørgensen. “Efficient Computation of the Continuous-Discrete Extended Kalman Filter Sensitivities Applied to Maximum Likelihood Estimation”. In: *2019 IEEE 58th Conference on Decision and Control (CDC)*. 2019, pages 6983–6988. DOI: 10.1109/CDC40024.2019.9029672.
- [57] Ahmad Haidar, Claire Duval, Laurent Legault, and Rémi Rabasa-Lhoret. “Pharmacokinetics of insulin aspart and glucagon in type 1 diabetes during closed-loop operation”. In: *Journal of Diabetes Science and Technology* 7.6 (2013), pages 1507–1512. DOI: 10.1177/193229681300700610.
- [58] Saeed Masroor, Marloes G.J. van Dongen, Ricardo Alvarez-Jimenez, Koos Burggraaf, Lambertus A. Peletier, and Mark A. Peletier. “Mathematical modeling of the glucagon challenge test”. In: *Journal of Pharmacokinetics and Pharmacodynamics* 46.6 (2019), pages 553–564. DOI: 10.1007/s10928-019-09655-2.
- [59] Chiara Dalla Man, Michael Camilleri, and Claudio Cobelli. “A system model of oral glucose absorption: Validation on gold standard data”. In: *IEEE Transactions on Biomedical Engineering* 12.1 (2006), pages 2472–2478. DOI: 10.1109/TBME.2006.883792.
- [60] Andrea De Gaetano, Simona Panunzi, Alice Matone, Adeline Samson, Jana Vrbikova, Bela Bendlova, and Giovanni Pacini. “Routine OGTT: A robust model including incretin effect for precise identification of insulin sensitivity and secretion in a single individual”. In: *PLoS ONE* 8.8 (2013), e70875. DOI: 10.1371/journal.pone.0070875.
- [61] Oskar Alskär, Jonatan I. Bagger, Rikke M. Røge, Filip K. Knop, Mats O. Karlsson, Tina Vilsbøll, and Maria C. Kjellsson. “Semimechanistic model describing gastric emptying and glucose absorption in healthy subjects and patients with type 2 diabetes”. In: *The Journal of Clinical Pharmacology* 56.3 (2016), pages 340–348. DOI: 10.1002/jcph.602.
- [62] Thomas E. Moxon, Ourania Gouseti, and Serafim Bakalis. “*In silico* modelling of mass transfer and absorption in the human gut”. In: *Journal of Food Engineering* 176 (2016), pages 110–120. DOI: 10.1016/j.jfoodeng.2015.10.019.
- [63] Benjamin Guiastrennec, David P. Sonne, Morten Hansen, Jonathan I. Bagger, Asger Lund, Jens F. Rehfeld, Oskar Alskär, Mats O. Karlsson, Tina Vilsbøll, Filip K. Knop, and Martin Bergstrand. “Mechanism-Based Modeling of Gastric Emptying Rate and Gallbladder Emptying in Response to Caloric Intake”. In: *Pharmacometric and Systems Biology* 5.12 (2016), pages 692–700. DOI: 10.1002/psp4.12152.
- [64] Thomas E. Moxon, Philippe Nimmegeers, Dries Telen, Peter J. Fryer, Jan Van Impe, and Serafim Bakalis. “Effect of chyme viscosity and nutrient feedback mechanism on gastric emptying”. In: *Chemical Engineering Science* 171 (2017), pages 318–330. DOI: 10.1016/j.ces.2017.05.048.

- [65] Mudassir Rashid, Sediqeh Samadi, Mert Sevil, Iman Hajizadeh, Paul Kolodziej, Nicole Hobbs, Zacharie Maloney, Rachel Brandt, Jianyuan Feng, Minsun Park, Laurie Quinn, and Ali Cinar. “Simulation software for assessment of nonlinear and adaptive multivariable control algorithms: Glucose–insulin dynamics in Type 1 diabetes”. In: *Computers and Chemical Engineering* 130 (2019), page 106565. DOI: 10.1016/j.compchemeng.2019.106565.
- [66] Marc D. Breton. “Physical Activity - The Major Unaccounted Impediment to Closed Loop Control”. In: *Journal of Diabetes Science and Technology* 2.1 (2008), pages 169–174. DOI: 10.1177/193229680800200127.
- [67] Andrea Facchinetti, Simone Del Favero, Giovanni Sparacino, Jessica R. Castle, W. Kenneth Ward, and Claudio Cobelli. “Modeling the Glucose Sensor Error”. In: *IEEE Transactions on Biomedical Engineering* 61.3 (2014), pages 620–629. DOI: 10.1109/TBME.2013.2284023.
- [68] John Thomas Sorensen. “A physiological model of glucose metabolism in man and its use to design and assess improved insulin therapies for diabetes”. PhD thesis. Massachusetts Institute of Technology. Department of Chemical Engineering, 1985.
- [69] Roman Hovorka, Ludovic J. Chassin, Martin Ellmerer, Johannes Plank, and Malgorzata E Wilinska. “A simulation model of glucose regulation in the critically ill”. In: *Physiological Measurement* 29.8 (2008), pages 959–978. DOI: 10.1088/0967-3334/29/8/008.
- [70] Boris P. Kovatchev, Claudio Cobelli, and Chiara Dalla Man. *System, method and computer simulation environment for in silico trials in pre-diabetes and type 2 diabetes*. The U.S. Patent and Trademark Office. U.S. Patent Application Publication No. US 2022/0230762 A1, July 21, 2022. 2022.
- [71] Andreas Wächter and Lorenz T. Biegler. “On the implementation of an interior-point filter line-search algorithm for large-scale nonlinear programming”. eng. In: *Mathematical Programming* 106.1 (2006), pages 25–57. ISSN: 14364646, 00255610. DOI: 10.1007/s10107-004-0559-y.
- [72] Desmond J. Higham. “An algorithmic introduction to numerical simulation of stochastic differential equations”. In: *SIAM Review* 43.3 (2001), pages 525–546. DOI: 10.1137/S0036144500378302.
- [73] Boris P. Kovatchev, Marc D. Breton, Claudio Cobelli, and Chiara Dalla Man. *Method, System and Computer Simulation Environment for Testing of Monitoring and Control Strategies in Diabetes*. The U.S. Patent and Trademark Office. U.S. Patent Application Publication No. US 2010/0179768 A1, July 15, 2010. 2010.
- [74] Leonardo Dagum and Ramesh Menon. “OpenMP: an industry standard API for shared-memory programming”. In: *Computational Science and Engineering* 5.1 (1998), pages 46–55.
- [75] DTU Computing Center. *DTU Computing Center resources*. Technical University of Denmark. 2021. DOI: 10.48714/DTU.HPC.0001. URL: <https://doi.org/10.48714/DTU.HPC.0001>.

- [76] Message Passing Interface Forum. *MPI: A Message-Passing Interface Standard Version 4.0*. June 2021. URL: <https://www.mpi-forum.org/docs/mpi-4.0/mpi40-report.pdf>.
- [77] Andrew H. Jazwinski. *Stochastic processes and filtering theory*. Dover Publication, Inc., 2007. 376 pages. ISBN: 0486462749.
- [78] René Schneider and Christos Georgakis. “How To NOT Make the Extended Kalman Filter Fail”. In: *Industrial and Engineering Chemistry Research* 52.0 (2013), pages 3354–3362. DOI: 10.1021/ie300415d.
- [79] Zeinab Mahmoudi, Kirsten Nørgaard, Niels Kjølstad Poulsen, Henrik Madsen, and John Bagterp Jørgensen. “Fault and meal detection by redundant continuous glucose monitors and the unscented Kalman filter”. In: *Biomedical Signal Processing and Control* 38 (2017), pages 86–99. DOI: 10.1016/j.bspc.2017.05.004.
- [80] Zeinab Mahmoudi, Faye Comeron, Niels Kjølstad Poulsen, Henrik Madsen, B. Wayne Bequette, and Jonh Bagterp Jørgensen. “Sensor-based detection and estimation of meal carbohydrates for people with diabetes”. In: *Biomedical Signal Processing and Control* 48 (2019), pages 12–25. DOI: 10.1016/j.bspc.2018.09.012.
- [81] Henrik Madsen and Poul Thyregod. *Introduction to general and generalized linear models*. Chapman & Hall/CRC, 2010. ISBN: 1420091557.
- [82] C. Radhakrishna Rao. “Information and the accuracy attainable in the estimation of statistical parameters”. In: *Bulletin of the Calcutta Mathematical Society* 37.3 (1945), pages 81–91.
- [83] Harald Cramér. “A contribution to the theory of statistical estimation”. In: *Scandinavian Actuarial Journal* 29.1 (1946), pages 85–94.
- [84] Karl Johan Åström. “Maximum likelihood and prediction error methods”. In: *Automatica* 16.5 (1980), pages 551–574. DOI: 10.1016/0005-1098(80)90078-3.
- [85] Kathryn Chaloner and Isabella Verdinelli. “Bayesian experimental design: A review”. In: *Statistical Science* 10.3 (1995), pages 273–304. DOI: 10.1214/ss/1177009939.
- [86] Sylvie Retout, Stephen Duffull, and France Mentré. “Development and implementation of the population Fisher information matrix for the evaluation of population pharmacokinetic designs”. In: *Computer methods and Programs in Biomedicine* 65.2 (2001), pages 141–151. DOI: 10.1016/S0169-2607(00)00117-6.
- [87] H. G. Bock and K. J. Plitt. “A Multiple Shooting Algorithm For Direct Solution of Optimal Control Problems”. In: *IFAC proceedings volumes* 17.2 (1984), pages 1603–1608. DOI: 10.1016/S1474-6670(17)61205-9.
- [88] Jorge Nocedal and Stephen J. Wright. *Numerical optimization*. 2nd. Springer Science & Business Media, 2006. ISBN: 0-387-30303-0.
- [89] John Bagterp Jørgensen. “Moving horizon estimation and control”. PhD thesis. Department of Chemical Engineering, Technical University of Denmark, 2005.

- [90] Gianluca Frison and John Bagterp Jørgensen. “Efficient Implementation of the Riccati recursion for solving Linear-quadratic control problems”. In: *2013 IEEE International Conference on Systems and Control*. 2013, pages 1117–1122. DOI: 10.1109/CCA.2013.6662901.
- [91] Ajenthen G. Ranjan, Signe Schmidt, and Kirsten Nørgaard. “Glucagon for hypoglycaemia treatment in type 1 diabetes”. In: *Diabetes Metabolism Research and Reviews* (2020), e3409. DOI: 10.1002/dmrr.3409.
- [92] Mads Wikmark Formo, Oyvind Stavdahl, and Anders Lyngvi Fougner. “Modelling and simulation of occlusions in insulin pumps”. In: *Annual International Conference of the IEEE Engineering in Medicine and Biology Society*. 2021, pages 1499–1503. DOI: 10.1109/EMBC46164.2021.9630219.

Part II

Appendices

APPENDIX **A**

Conference Paper - FOSBE 2022

A whole-body multi-scale mathematical model for
dynamic simulation of the metabolism in man

Authors:

Peter Emil Carstensen, Jacob Bendtsen, Asbjørn Thode Reenberg, Tobias K. S. Ritschel,
John Bagterp Jørgensen

Published in:

IFAC-PapersOnLine, 55–23, 58–63, 2022.

Proceedings of the 9th IFAC Conference on Foundations of Systems Biology in Engineering (FOSBE), Cambridge, Massachusetts, USA, August 28-31, 2022.



A whole-body multi-scale mathematical model for dynamic simulation of the metabolism in man

Peter Emil Carstensen, Jacob Bendsen,
 Asbjørn Thode Reenberg, Tobias K. S. Ritschel,
 John Bagterp Jørgensen

*Department of Applied Mathematics and Computer Science,
 Technical University of Denmark, DK-2800 Kgs. Lyngby, Denmark*

Abstract: We propose a whole-body model of the metabolism in man as well as a generalized approach for modeling metabolic networks. Using this approach, we are able to write a large metabolic network in a systematic and compact way. We demonstrate the approach using a whole-body model of the metabolism of the three macronutrients, carbohydrates, proteins and lipids. The model contains 7 organs, 16 metabolites and 31 enzymatic reactions. All reaction rates are described by Michaelis-Menten kinetics with an addition of a hormonal regulator based on the two hormones insulin and glucagon. We incorporate ingestion of food in order to simulate metabolite concentrations during the feed-fast cycle. The model can simulate several days due to the inclusion of storage forms (glycogen, muscle protein and lipid droplets), that can be depleted if food is not ingested regularly. A physiological model incorporating complex cellular metabolism and whole-body mass dynamics can be used in virtual clinical trials. Such trials can be used to improve the development of medicine, treatment strategies such as control algorithms, and increase the likelihood of a successful clinical trial.

Copyright © 2022 The Authors. This is an open access article under the CC BY-NC-ND license (<https://creativecommons.org/licenses/by-nc-nd/4.0/>)

Keywords: Mathematical modeling, metabolism, systems biology, cyber-medical systems, multi-scale modeling, quantitative systems pharmacology

1. INTRODUCTION

In the human body, metabolites are constantly formed and broken down through a vast number of reactions. The metabolism functions in an organized manner to keep the body alive (Miesfeld and McEvoy, 2017). Whole-body modeling uses exactly this idea to describe the human body as a collective unit. Doing so can provide a predicted concentration of a metabolite in any specific organ, which is relevant e.g. to PK/PD drug development (Derendorf et al., 2020).

Depending on the modeling objective (i.e. the intended use of the model), there are several ways to model the human metabolism. We look at the system of organs and blood vessels as a whole-body model. The enzymatic reactions in the metabolic network occur in the organs, and the organs are connected with each other through the blood vessels. As the organs are not identical, different reactions and reaction rates are defined based on their role in the metabolism. Following this approach, it is possible to simulate the metabolism of man under various conditions.

There exist whole-body models in today's literature that describe the metabolism in man at different levels of complexity. Sorensen (1985) refined simple and inadequate models with focus on glucose, insulin and glucagon dynamics, using a simple whole-body model. More complex models have been developed in recent years. Panunzi

et al. (2020) focused on extending the model proposed by Sorensen (1985), by adding food intake. Other authors (Kim et al., 2007; Dash et al., 2008; Kurata, 2021) use whole-body models and expand into stoichiometry to include several metabolites. A simple and intuitive approach, in which the mathematical equations can easily be incorporated, is not readily available. By utilizing previous work and modeling principles described by Yasemi and Jolicoeur (2021), we propose such a mathematical approach.

In this work, we describe a whole-body model of the metabolism in man. Furthermore, we demonstrate a general, systematic and intuitive way to formulate the model equations. The five key organs included are the brain, the heart and lungs, the liver, the gut and the kidney. Further, the muscle tissue and the adipose tissue are each simplified as a single compartment and can therefore be considered as an organ. This results in a total of seven organs. The metabolism inside the organs are explained by the stoichiometry of the enzymatic reactions. We use Michaelis-Menten kinetics to describe the enzymatic reactions. Using the model, we simulate the feed-fast cycle to investigate how prolonged fasting affects selected metabolite concentrations and glucose flux. Further, we simulate intermittent fasting to investigate how it affects the carbohydrate, the protein and the lipid storage.

The remaining part of this paper is structured as follows. Section 2 describes the approach for whole-body modeling. In section 3, a biological model is formulated using the

* Corresponding author: J.B. Jørgensen (e-mail: jbj@dtu.dk).

mathematical approach. Section 4 presents the simulation results, and we discuss our formulated model and assumptions in Section 5. Finally, Section 6 concludes on our findings.

2. MATHEMATICAL APPROACH

The general model is described as a system in which metabolites flow in, are metabolized, and flow out. The dynamics of a single compartment is defined by the general differential equation

$$V \frac{dC}{dt} = M(Q_{in}C_{in} - Q_{out}C) + RV, \quad (1)$$

where V is the volume, C is a vector containing the concentration of the metabolites, M is the external and internal component ordering, Q_{in} is the flow rate of what goes in, C_{in} is a vector containing the concentration of the metabolites that flow in, Q_{out} is the flow rate of what goes out and R is the production rates. The compartments are coupled through concentration gradients in the blood vessels that connect the compartments. M is a square matrix containing only ones and zeros in the diagonal corresponding to the metabolites distributed through the blood vessels (circulating metabolites). For instance, the circulating metabolite, C_i , corresponds to $M_{i,i} = 1$. The production rate R is incorporated as a vector defined by

$$R = (TS)'Tr, \quad (2)$$

where T is a matrix of reactions that occur, S is a stoichiometric matrix containing all reactions and r is a vector with the kinetics for the reactions. T contains ones and zeros corresponding to which reactions from the stoichiometric matrix, that are present in the compartment. For instance, a compartment which involves reaction 1, 3 and 5 from the stoichiometric matrix have $T_{1,1} = 1, T_{2,3} = 1, T_{3,5} = 1$, and zeros elsewhere. The reaction rate vector, r , is a function of the concentration of each metabolite:

$$r = r(C). \quad (3)$$

To utilize (1), in a whole-body model, it must be formulated for each compartment.

3. MODEL

We now present a model containing 7 compartments, 16 metabolites and 31 reactions including the hormonal effect from two signal molecules, insulin and glucagon, on specific tissues. Fig. 1 shows a flow diagram of the whole-body model. The blood circulation is split into two parts, the arteries (red) and the veins (blue). The total blood flow, Q , is at all times preserved, and the local blood flow can be calculated using mixers and splitters. They are either explicitly modelled as organs, or implicitly as shown by the triangle (splitter) or square (mixer). A splitter divides the blood flow so $a_2 = a_1 + a_3$, and a mixer combines the blood flow so $v_1 + v_3 = v_2$. As blood flow is preserved, the flow coming into a compartment is the same as the flow coming out of a compartment.

We create the model using the same methodology as described in Section 2. The purpose is to describe the energy metabolism of the three macronutrients, carbohydrates, proteins and lipids. We include the major biochemical pathways, shown in Fig. 2, which these macronutrients

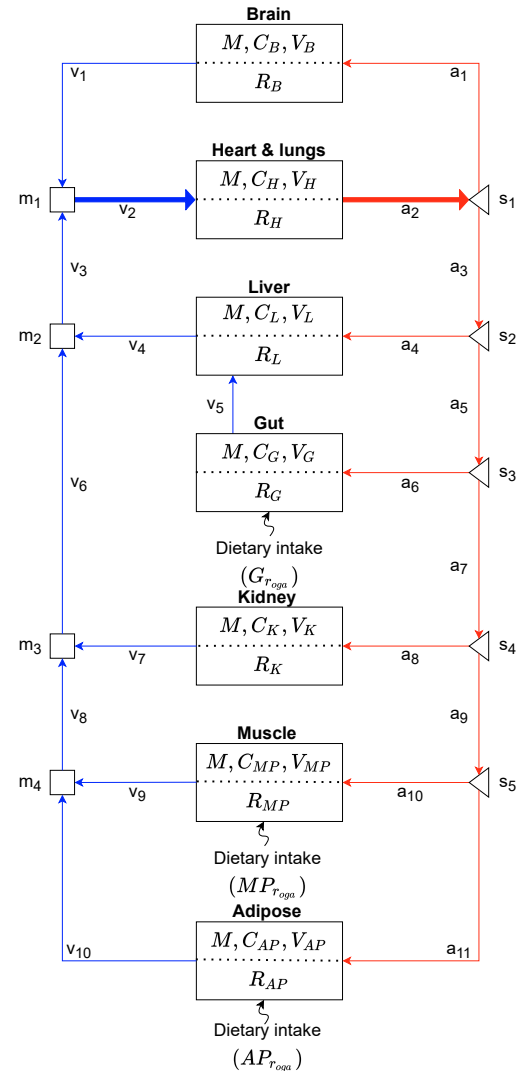


Fig. 1. Schematic representation of the whole-body model. Solid arrows represent blood circulation, where the right side is the arteries and the left side the veins. Thick arrows, a_2 and v_2 , represents joining of flows from other organs. M, C_k, V_k represents the blood tissue exchange and R_k represents the reactions happening inside the cell. The dotted lines in the compartments suggest free diffusion, as cell-permeability is not included.

are a part of, in order to simulate their behaviour under various conditions. Insulin and glucagon are included to add stability and avoid large transient periods in the simulation after food intake, as they are important anabolic and catabolic hormones, respectively. From Fig. 2, it follows that many pathways are cell specific. 10 of 31 reactions occur in all organs. The remaining 21 are tissue specific, as the different organs each have a specialized role. Insulin and glucagon secretion/clearance are incorporated as a single reaction each for simplicity, as they are not

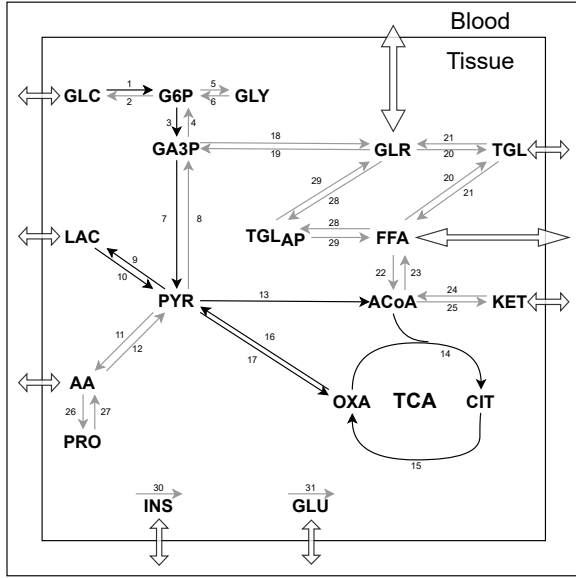


Fig. 2. Diagram of metabolic pathways in cell. The hollow double-sided arrows indicate that the metabolite is distributed through the blood. The black arrows indicate reactions that happen in all organs. The grey arrows indicate reactions that only happen in some organs. Metabolites are shown as 2-4 letter abbreviations. The stoichiometric matrix is formed from the numbering of the reactions.

created by nor metabolised into any included metabolite. Their reaction rates are inherited from Sorensen (1985), as described in Section 3.1.

The most accurate mathematical equations to describe each of these 31 metabolic reactions are not necessarily known, and vary from individual to individual. Therefore each of these reactions have been simplified. In the model, we describe the reaction rates using Michaelis-Menten kinetics. Michaelis-Menten kinetics are especially useful for describing enzyme reactions, as enzyme reactions have an upper limit on the reaction rate. Alternatives to Michaelis-Menten kinetics include altering the mathematical formula in the reaction rate vector to e.g. positive hyperbolic tangent functions as in Sorensen (1985) or simple first-order kinetics from Kim et al. (2007). If a reaction is excluded from an organ, it does not mean that the reaction never happens in reality. Instead, it means that the reaction is excluded for simplicity. An example is glycogen formation that also happens in the brain, heart and adipose tissue, but it is in such small quantities, that it becomes negligible (Gropper et al., 2018).

3.1 Inclusion of a hormonal model

Sorensen (1985) employs a very simple glucagon model that describes the pancreatic glucagon release. Sorensen found that the glucagon release and clearance could be described adequately by a one compartment model. Sorensen also formulated an insulin model described by a six compartment model. While it is possible to include

Table 1. Reactions affected by insulin and glucagon (Gropper et al., 2018; Miesfeld and McEvoy, 2017). \uparrow symbolizes increased stimulation and \downarrow symbolizes decreased stimulation.

Hormone	Effect	# R	Reaction	Affected Organs
Insulin	\uparrow	1	GLC \rightarrow G6P	Liver, muscle, adipose tissue
	\uparrow	3	G6P \rightarrow 2 GA3P	Liver, muscle tissue
	\uparrow	5	G6P \rightarrow GLY	Liver, muscle tissue
	\uparrow	13	PYR \rightarrow ACyA	Liver, muscle tissue
	\uparrow	21	TGL \rightarrow 3 FFA + GLR	Adipose tissue
	\uparrow	23	7 ACyA \rightarrow FFA	Liver
	\uparrow	26	AA \rightarrow PRO	Muscle tissue
	\uparrow	28	3 FFA + GLR \rightarrow TGLAP	Adipose tissue
	\downarrow	4	2 GA3P \rightarrow G6P	Liver
Glucagon	\uparrow	4	2 GA3P \rightarrow G6P	Liver
	\uparrow	6	GLY \rightarrow G6P	Liver
	\uparrow	29	TGLAP \rightarrow 3 FFA + GLR	Adipose tissue
	\downarrow	3	G6P \rightarrow 2 GA3P	Liver
	\downarrow	5	G6P \rightarrow GLY	Liver
	\downarrow	27	PRO \rightarrow AA	Muscle tissue
	\downarrow	29	TGLAP \rightarrow 3 FFA + GLR	Adipose tissue
	\downarrow	21	TGL \rightarrow 3 FFA + GLR	Adipose tissue
	\downarrow	23	7 ACyA \rightarrow FFA	Liver

the glucagon model as a single compartment model and insulin as a six compartment model, similar to Panunzi et al. (2020) and Sorensen (1985), we include insulin and glucagon in a whole-body seven compartment model. Insulin and glucagon are therefore included in the stoichiometric matrix as metabolites in order to calculate their production rates.

Table 1 contains the reactions that are affected by insulin and glucagon, as well as which organ is affected. While the qualitative effect of insulin and glucagon is known (see Table 1), the related model parameters for insulin and glucagon are not necessarily known. Miesfeld and McEvoy (2017) describe qualitatively which enzymes and hence reactions that insulin and glucagon affect. Accordingly, given the reciprocal effects of insulin (I) and glucagon (Γ), we use a simple function where the ratio between them allows us to determine whether or not they have an effect on the system. These functions alter the production rates of the reactions in Table 1. If only insulin have an effect on the reaction, the functions are

$$\text{Insulin activation: } \left(\frac{I_k}{I_k^B} \right)^{\mu_j} V_{max_j}, \quad (4)$$

$$\text{Insulin inhibition: } \left(\frac{I_k^B}{I_k} \right)^{\mu_j} V_{max_j}, \quad (5)$$

and if both insulin and glucagon have an effect on the same reaction (though with opposite effects), the insulin-to-glucagon or glucagon-to-insulin ratio is used instead,

$$\text{Insulin-to-Glucagon stimulation: } \left(\frac{\Gamma_k^B}{\Gamma_k} \frac{I_k}{I_k^B} \right)^{\mu_j} V_{max_j}, \quad (6)$$

$$\text{Glucagon-to-insulin stimulation: } \left(\frac{\Gamma_k}{\Gamma_k^B} \frac{I_k^B}{I_k} \right)^{\mu_j} V_{max_j}, \quad (7)$$

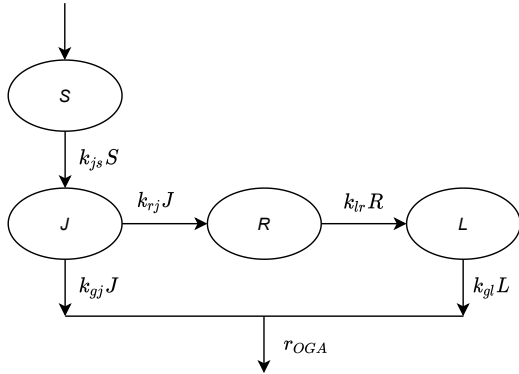


Fig. 3. Schematic representation of the digestive tract. S represents the amount of macronutrients in the stomach, J the jejunum, R a delay and L the amount in the ileum. r_{OGA} is a vector describing the uptake of the three macronutrients.

where j is the reaction, e.g. $GLC \rightarrow G6P$, k is the compartment and the superscript B indicates that it is the basal-value. V_{max_j} is the maximum rate in the Michaelis-Menten kinetics and μ_j is a scaling parameter for the hormonal effect. These simple functions are equal to V_{max_j} at steady state, which occurs when the blood glucose concentration is at 5 mmol/L, such that it is independent of μ_j in steady-state. This is an important property, since many of the parameters used in the reactions are estimated based on metabolite homeostasis.

3.2 Inclusion of a modified SIMO-model

A modified version of the simple interdependent glucose/insulin model, SIMO (Panunzi et al., 2020), is used to include the uptake of glucose, amino acids and lipids from ones diet. The rates are the same for all macronutrients, which is not physiologically accurate. It is known from Miesfeld and McEvoy (2017) that the macronutrients differ in terms of absorption given their molecular differences. Due to lack of data or other mathematical models describing the uptake of macronutrients, we adopt the SIMO model as it is the simplest choice. The resulting uptake of macronutrients is represented by

$$r_{OGA} = k_{gj}J + k_{gl}L = \begin{bmatrix} k_{gj}J_{GLC} + k_{gl}L_{GLC} \\ k_{gj}J_{AA} + k_{gl}L_{AA} \\ k_{gj}J_{TGL} + k_{gl}L_{TGL} \end{bmatrix}, \quad (8)$$

where k_{gj} and k_{gl} are uptake rates and r_{OGA} is a 3×1 vector, where the first two macronutrients, i.e. glucose and amino acids, are taken up by the gut. This is not the case for triglycerides, which enter the lymphatic system as chylomicrons and is transported to muscle and adipose tissue before it enters the blood circulation (Gropper et al., 2018). The triglycerides (TGL) from r_{OGA} is then delivered to muscle and adipose tissue, where a 50/50% distribution is assumed in the two tissues. As the specific uptake rates of amino acids and lipids are not explicitly known from the SIMO model, we utilize the uptake rate k_{gj} and k_{gl} from glucose. It is included in the model as the parameters:

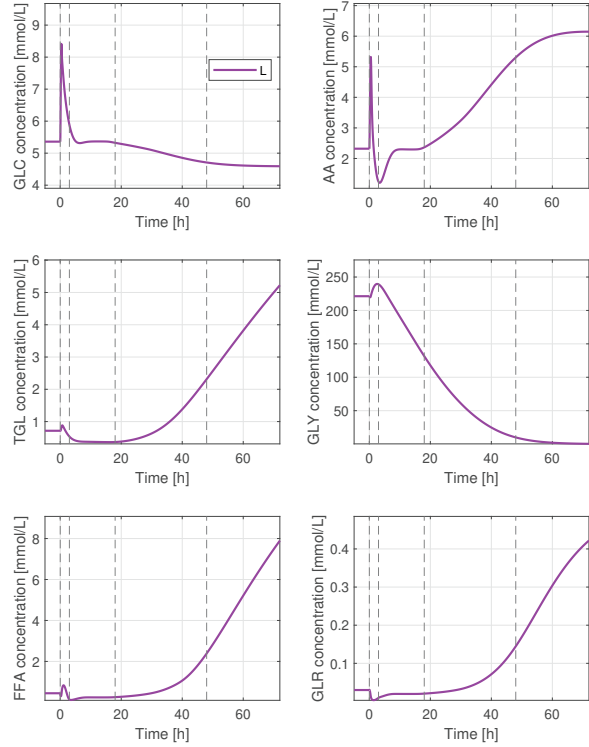


Fig. 4. The metabolite concentrations of glucose (GLC), amino acids (AA), triglycerides (TGL), glycogen storage (GLY), free fatty acids (FFA) and glycerol (GLR) in the liver after an initial meal of 60 g glucose, 24 g protein and 16 g fat and an accompanying fasting for 72 hours.

$$\begin{aligned} \text{Gut: } &G_{r_{OGA}} \\ \text{Muscle: } &MP_{r_{OGA}} \\ \text{Adipose: } &AP_{r_{OGA}} \end{aligned}$$

The modified SIMO model is included as additional inputs in the differential equations and not directly into the production rate vector R , as the modified SIMO model provides external inputs from meal consumption and is seen as an extension to the general methodology.

4. SIMULATION RESULTS

We now simulate the model presented in Section 3 in MATLAB. Initially we present the model with a single meal ingested at steady-state, and follow the development of the metabolites as an in silico patient refrains from eating or doing physical activity for the next 72 hours. Fig. 4 shows the glucose concentration, the amino acids, the triglycerides, the glycerol, the free fatty acids and the glycogen concentration. The plots for GLC , AA and TGL show the metabolites that are ingested through the modified SIMO model. After the initial meal, we see that, the glucose concentration initially rises and then returns to the baseline, where it remains constant for roughly 10 hours. The glucose concentration then starts to decrease as glycogen storage is reduced substantially. While the glucose concentration diminishes, the concentrations of

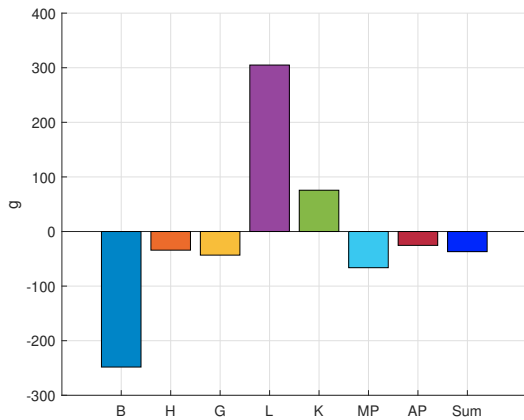


Fig. 5. Sum of the glucose fluxes in every organ after an initial meal and accompanying fasting for 72 hours. The organs are the brain (B), the heart and lungs (H), the gut (G), the liver (L), the kidneys (K), the muscle tissue (MP) and the adipose tissue (AP). The total sum of all the glucose fluxes is the rightmost column denoted 'Sum'.

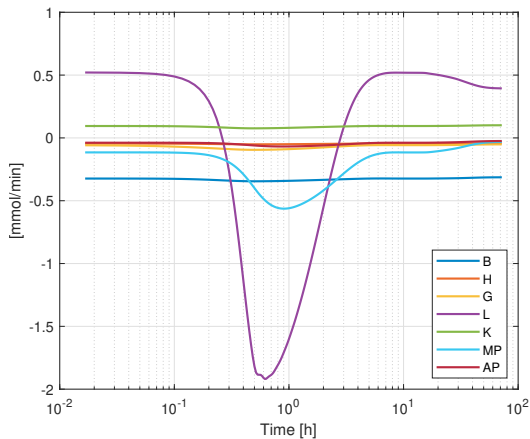


Fig. 6. The glucose fluxes in every organ after an initial meal and accompanying fasting for 72 hours. It shows the fluxes over time with a logarithmic scale on the x-axis.

the other metabolites start increasing. This is especially the glycerol concentration, the free fatty acids and the triglycerides, as the patient enters the starvation stage, where lipids are the main energy source for several organs. An increase in the triglycerides is seen during starvation as the triglyceride storage in the adipose tissue, TGL_{AP} , reduces. The free fatty acid levels increase substantially during starvation, which is to be expected based on articles that investigate the effects of starvation (Unger et al., 1963; Yaffe et al., 1980).

4.1 Fluxes inside the cells

While it is important to keep in mind that these simulation results are not physiologically accurate for all metabolites, we can plot the fluxes in order to investigate the dynamics.

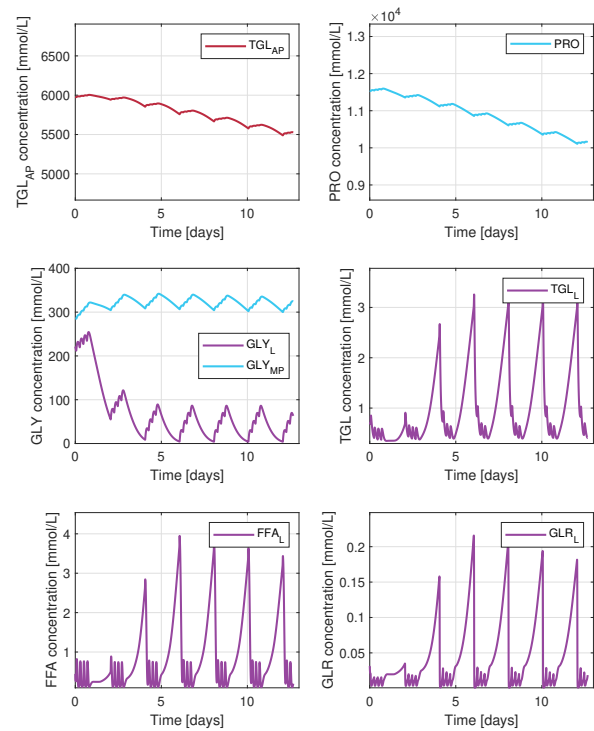


Fig. 7. The metabolite concentrations of the fat storage in the adipose tissue (TGL_{AP}), the protein storage in the muscle tissue (PRO), the glycogen storage in the liver (GLY_L) and in the muscle tissue (GLY_{MP}), the triglycerides in the liver (TGL_L), the free fatty acids in the liver (FFA_L) and the glycerol in the liver (GLR_L). The simulation is run for 13 days with intermittent fasting every other day.

Fig. 5 shows that the brain is a major consumer of glucose, and the liver is a major exporter of glucose, which is also what is expected from Miesfeld and McEvoy (2017). The rightmost column, Sum, shows the net flux of glucose in all organs, resulting in an overall consumption corresponding to a meal containing 60 g glucose. Fig. 6 shows which organs are the consumers of glucose over time. There is a large drop initially for the glucose flux in the liver and the muscle tissue as food is ingested and the blood glucose concentration is high. This is especially seen in the insulin stimulated tissues, as the effect described in Table 1 shows an increase in the glucose uptake as a result of high concentrations of insulin. As the blood glucose concentration reduces, the liver again produces glucose for the other organs in order to keep homeostasis, and thus increases its flux to a positive value.

4.2 Simulation of intermittent fasting

Fig. 7 shows a simulation over 13 days, with regular food intake every other day, resulting in intermittent fasting for 33 hours. We see a decrease in the concentration of lipid droplets, as they are metabolized to provide energy for the body. This is due to the energy balance of the system becoming skewed from a roughly equal calory

intake/consumption, to a 50% reduction in calory intake. Further, we see that the protein storage in the muscle tissue is also broken down, as food becomes a relatively scarce source for the body. Within a day we see a large drop in the concentration of glycogen after the last meal. Glycogen is initially used as an energy storage, but gets depleted quickly in the liver. The glycogen in the muscle tissue is relatively stable, as the in silico patient is at rest for the entire simulation. The lipid droplets are converted into *FFA* and *GLR* and utilized in different compartments. We see large spikes when the body enters the starvation phase after 18 hours without any food (see also Fig. 4). The simulation shows, that following this diet results in an effective weight loss, as TGL_{AP} (body fat) levels decrease. However there are adverse effects to this diet, as muscle proteins are also diminished. By simulating intermittent fasting, we are able to show both the effects of regular meal intake and fasting.

5. DISCUSSION

Diffusion across the cell membrane is assumed to happen infinitely fast, as the time it takes for the cell to be in equilibrium with the blood vessels happens at a much faster timescale compared to the timescale of our model. This assumption makes it possible to include organs as one compartment. If transporters and diffusion were to be incorporated in the model, it would be expected to divide the compartments in two, intracellular and extracellular, such that transporters could be explicitly modeled. The concentration is assumed to be the same across the entire compartment. We model each organ as a well-stirred tank. Therefore every metabolite is uniformly distributed in the organs. It is known, that the enzymatic reactions in each cell and organ happen at a fast timescale of 10^{-3} to 10^0 seconds (Yasemi and Jolicoeur, 2021). We are interested in simulating the model for up to several days. Therefore, we assume that the enzymatic reactions happen at a uniform rate across the spatial organs, allowing a simplification of enzymatic reactions to Michaelis-Menten kinetics.

It could be theorized, given the introduction of more metabolic inputs, that a model like this could be used to gain a better understanding of the dynamical changes in metabolite concentrations of an individual. Both a generalized model could be used, or one tailored to a specific person's parameters, thus introducing personalized modeling behaviour. Simulation of enzymatic defects to represent various diseases, could be done with the current format of the model. However, it would require validation of the model.

6. CONCLUSION

Using a systematic approach for modeling metabolic networks, we have developed a model that is capable of simulating the complex human metabolism. The approach makes it simple to expand the system through changes in the stoichiometric matrix, that match the chemistry and modeling objective. The core of the model is simply which parameters and reaction kinetics that are used in the production rate vector R_k . This is illustrated in the model, which involves 16 metabolites and 2 hormones in 7 organs. It results in a total of 126 differential equations.

We write these as 7 differential equations, one for each organ, as the entire reaction network is included in R_k . As shown, the modeling approach can readily be expanded to incorporate large networks of metabolic reactions in the body. The approach is applicable to not just a physiological model, but can easily be made to fit chemical systems, with containers, tubes and chemical reactions taking place. The modeling objective was to create the basis for a physiological whole-body model that can incorporate cellular metabolic processes, so that qualitative knowledge can be utilized in a quantitative manner and, when adequately tested, used for in silico trials.

REFERENCES

- Dash, R.K., Li, Y., Kim, J., Saidel, G.M., and Cabrera, M.E. (2008). Modeling cellular metabolism and energetics in skeletal muscle: Large-scale parameter estimation and sensitivity analysis. *IEEE Transactions on Biomedical Engineering*, 55(4), 1298–1318. doi: 10.1109/tbme.2007.913422.
- Derendorf, H., Schmidt, S., Rowland, M., and Tozer, T.N. (2020). *Rowland and Tozer's clinical pharmacokinetics and Pharmacodynamics: Concepts and applications*. Wolters Kluwer, 5 edition.
- Gropper, S.S., Smith, J.L., and Carr, T.P. (2018). *Advanced nutrition and human metabolism*. Cengage Learning, 7 edition.
- Kim, J., Saidel, G.M., and Cabrera, M.E. (2007). Multi-scale computational model of fuel homeostasis during exercise: Effect of hormonal control. *Annals of Biomedical Engineering*, 35(1), 69–90. doi:10.1007/s10439-006-9201-x.
- Kurata, H. (2021). Virtual metabolic human dynamic model for pathological analysis and therapy design for diabetes. *iScience*, 24(2), 102101. doi: 10.1016/j.isci.2021.102101.
- Miesfeld, R.L. and McEvoy, M.M. (2017). *Biochemistry*. W.W. Norton & Company.
- Panunzi, S., Pompa, M., Borri, A., Piemonte, V., and Gaetano, A.D. (2020). A revised sorenson model: Simulating glycemic and insulinemic response to oral and intra-venous glucose load. *PLoS ONE*, 15(8). doi: 10.1371/journal.pone.0237215.
- Sorensen, J.T. (1985). *A physiological model of glucose metabolism in man and its use to design and assess improved insulin therapies for diabetes*. Ph.D. thesis, Massachusetts Institute of Technology. Department of Chemical Engineering.
- Unger, R.H., Eisentraut, A.M., and Madison, L.L. (1963). The effects of total starvation upon the levels of circulating glucagon and insulin in man. *Journal of Clinical Investigation*, 42(7), 1031–1039. doi:10.1172/jci104788.
- Yaffe, S., Gold, A., and Sampugna, J. (1980). Effects of prolonged starvation on plasma free fatty acid levels and fatty acid composition of myocardial total lipids in the rat. *The Journal of Nutrition*, 110(12), 2490–2496. doi: 10.1093/jn/110.12.2490.
- Yasemi, M. and Jolicoeur, M. (2021). Modelling cell metabolism: A review on constraint-based steady-state and kinetic approaches. *Processes*, 9(2), 322. doi: 10.3390/pr9020322.

APPENDIX B

Conference Paper - Mathmod 2022

Assessment of a new model of glucagon action with
glucagon receptor dynamics

Authors:

Clara Furió-Novejarque, Ricardo Sanz, Asbjørn Thode Reenberg, Tobias K. S. Ritschel, Ajenthen G. Ranjan, Kirsten Nørgaard, José-Luis Díez, John Bagterp Jørgensen, Jorge Bondia

Published in:

IFAC-PapersOnLine, 55–22, 647–652, 2022.

Proceedings of the 10th Vienna International Conference on Mathematical Modelling
MATHMOD 2022: Vienna, Austria, 27–29 July, 2022.



Assessment of a new model of glucagon action with glucagon receptor dynamics

Clara Furió-Novejarque* Ricardo Sanz*
 Asbjørn Thode Reenberg** Tobias K. S. Ritschel**
 Ajenthon G. Ranjan*** Kirsten Nørgaard***
 José-Luis Díez*,**** John Bagterp Jørgensen**
 Jorge Bondia*,****

* Instituto Universitario de Automática e Informática Industrial,
 Universitat Politècnica de València, Valencia, Spain

** Department of Applied Mathematics and Computer Science,
 Technical University of Denmark, Kgs. Lyngby, Denmark

*** Steno Diabetes Center Copenhagen, Gentofte, Denmark

**** Centro de Investigación Biomédica en Red de Diabetes y
 Enfermedades Metabólicas Asociadas (CIBERDEM), Madrid, Spain

Abstract: In this work, a novel insulin-glucagon-glucose model is proposed, where the glucagon effect on the endogenous glucose production (EGP) is described by the dynamics of the glucagon receptors. In order to assess the quality of the model, its parameters are fitted in such a way that the influence of glucagon on EGP is isolated. Experimental data is used to validate the model structure and show that the receptor dynamics allow to explain some of the glucagon-related phenomena observed in the clinical data. This physiology-focused model will be useful in the development of artificial pancreas algorithms both for more realistic *in silico* validations and in the development of model-based control strategies.

Copyright © 2022 The Authors. This is an open access article under the CC BY-NC-ND license (<https://creativecommons.org/licenses/by-nc-nd/4.0/>)

Keywords: Diabetes, glucagon receptors, PK-PD model, parameter estimation, clinical data

1. INTRODUCTION

Type 1 diabetes (T1D) is a metabolic disease caused by the auto-immune destruction of the insulin-producing beta cells in the pancreas. This also results in glucagon-producing alpha cell dysfunction, partly due to lack of paracrine signalling between both cells (Unger and Cherrington, 2012). Insulin lowers blood glucose (BG) concentration by promoting glucose entrance into the cell, while glucagon has the opposite effect by promoting EGP. The lack of endogenous insulin secretion leads to an unhealthy state of too high BG concentration (hyperglycaemia). Therefore, diabetes treatment depends on exogenously injected insulin. However, too much insulin can result in too low BG concentrations (hypoglycaemia), leading to unconsciousness, coma and even death (Cryer et al., 2003). Exogenous glucagon infusion can be used to mitigate hypoglycaemia. Understanding and modelling the effect of both hormones is important to several aspects of diabetes treatment, e.g., automated insulin delivery systems, also referred as the artificial pancreas (AP).

AP systems aim to lessen the burden of glycaemic control for people with T1D. The main actor is a control algorithm

which adjusts the insulin dosage via an insulin pump, based on the glucose measurements below skin provided by a continuous glucose monitor. This is a challenging task since insulin infusion is a control action that acts in a single direction. Insulin stacking due to subcutaneous insulin absorption can provoke, for instance, late hypoglycaemia after a meal. As well, exercise can induce hypoglycaemia, which is difficult to resolve solely with insulin pump suspension (Zaharieva et al., 2017).

Dual-hormone AP systems add glucagon infusion as a counterregulatory control action. A review (Peters and Haidar, 2018) concluded that dual-hormone AP systems proved superior performance in reduction of hypoglycaemia overall and during exercise compared to single-hormone (insulin-only) AP systems. Contrary to the expected performance, benefits in postprandial control, reduction of severe hypoglycaemia, and mean BG remained unclear, which means there is room for improvement in the design of dual-hormone AP systems.

The design of an AP system relies heavily on *in silico* evaluations. Furthermore, many control algorithms are designed from control-oriented models, with simpler structure, which must capture the main dynamics between the control action and BG. Insulin pharmacokinetic-pharmacodynamic (PK-PD) models have been widely studied and few variations exist in the available simulators used in AP research (Hovorka et al., 2004; Dalla Man et al., 2014). However this is not the case with glucagon action and modelling differs significantly among authors.

* Corresponding author: J. Bondia (jbondia@isa.upv.es)

**This work was partially supported by: grant DPI2016-78831-C2-1-R funded by MCIN/AEI/10.13039/501100011033 and by “ERDF A way of making Europe”; grants PID2019-107722RB-C21, FPU17/03404 and EST19/00740, funded by MCIN/AEI/10.13039/501100011033; the IFD Grand solution project ADAPT-T2D (9068-00056B).

In Dalla Man et al. (2014), glucagon PK-PD is incorporated in the widely used UVA/Padova simulator. Glucagon action on EGP is modelled as an additive antagonistic effect with respect to insulin. A “delayed” glucagon action is considered proportional to plasma glucagon concentration (when above a basal threshold). The same additive effect is considered in the model proposed in Resalat et al. (2019), but in this case a composite term of glucagon action and its derivative are added to the EGP. Other authors have introduced a coupled effect of insulin and glucagon on EGP. Indeed, in El Youssef et al. (2014) a saturating effect of insulinemia on glucagon action is reported in euglycemic clamp studies with constant low-mid-high insulin infusion. In Wendt et al. (2017) a Michaelis-Menten-type glucagon action is proposed, modulated with a multiplicative effect of the delayed insulin action, proportional to plasma insulin. Emami et al. (2017) also resorts to consider this interaction with a multiplicative effect, reducing glucagon action the higher the insulin action is. Note that all the above models consider a functional relationship among plasma glucagon and EGP aimed at fitting experimental data, which does not provide any physiological insight.

Contrarily, in Masroor et al. (2019) a model of glucagon action on EGP is presented based on the glucagon receptor dynamics. In particular, internalization of glucagon receptors is proposed, with good fitting of experimental data from the “glucagon challenge test”, where endogenous insulin and glucagon secretion are inhibited by somatostatin, and are replaced by exogenous insulin and glucagon infusion to get a constant plasma insulin and rapidly changing plasma glucagon concentration 2-3-fold with respect to physiological levels. However, this experimental condition is far from being representative of physiological conditions in T1D insulin therapy.

This paper aims to assess the capacity of the glucagon-receptors-based proposal in Masroor et al. (2019), with no coupled effect with insulin, to explain the dose-response of glucagon from experimental data representative of T1D management, such as in a dual-hormone AP system, where glucagon delivery is expected as a response to hypoglycaemia, probably induced by an inadequate previous insulin bolus.

This paper is organized as follows: Section 2 presents the glucagon action model. Section 3 describes the complete glucoregulatory model. Experimental data is described in Section 4. Section 5 explains the model fitting procedure. Section 6 depicts the obtained results for the parameters and the fit to the data. Finally, in Section 7 the implications of the obtained results are discussed.

2. GLUCAGON ACTION MODEL WITH GLUCAGON RECEPTOR DYNAMICS

In this section, the glucagon action model proposed by Masroor et al. (2019) is described. As a key feature compared to current models used in artificial pancreas research, it incorporates dynamics of glucagon receptors, being more physiologically sustained. Glucagon receptors are mainly located on the liver membrane. These receptors bond to glucagon molecules and cause a chain reaction in protein signalling that leads to promotion of glycconeogenesis (synthesis of new glucose from non-carbohydrate

precursors such as aminoacids and lactate) and glycconeolysis (depletion of glycogen in the liver) while inhibiting glycolysis and glycogenesis (Müller et al., 2017). However, receptors undergo a recycling process in which they are internalized and become unavailable. Information about the behaviour of receptors is limited. In Masroor et al. (2019), this process is described by a three-compartmental model representing glucagon receptors at different states: the glucagon-bonded receptors $r_c(t)$, the available surface receptors $r(t)$, and the internalized receptors $r_i(t)$, expressed as normalized amounts with respect to the total (unknown) number of receptors, which is considered constant. Thus, the constraint $r_i(t) = 1 - r(t) - r_c(t)$ holds, and the model can be simplified to the following second order system (where no free receptors are internalized):

$$\frac{dr(t)}{dt} = -k_{on} \cdot V_h \cdot C(t) \cdot r(t) + k_{off} \cdot r_c(t) + k_{rec} \cdot (1 - r(t) - r_c(t)) \quad (1a)$$

$$\frac{dr_c(t)}{dt} = k_{on} \cdot V_h \cdot C(t) \cdot r(t) - k_{off} \cdot r_c(t) - k_{in} \cdot r_c(t) \quad (1b)$$

$$F_{hgp}(t) = \frac{V_r \cdot r_c(t)}{K_r + r_c(t)} \quad (1c)$$

where $C(t)$ (pg/ml) is the plasma glucagon concentration (model input), $F_{hgp}(t)$ ($\mu\text{mol/kg/min}$) represents the hepatic glucose production (model output) as a Michaelis-Menten dynamic of the relative number of glucagon-bonded receptors, V_h (ml) is the volume of the hepatic interstitial space, k_{on} ($(\text{pg/min})^{-1}$) is the association rate of glucagon to the receptor, k_{off} (min^{-1}) is the dissociation rate, k_{rec} (min^{-1}) is the recycling rate of the receptor, k_{in} (min^{-1}) is the internalization rate of the glucagon-bonded receptor, K_r (dimensionless) is the apparent dissociation constant, and V_r ($\mu\text{mol/kg/min}$) is the maximal glucagon-dependent hepatic glucose production rate.

3. COMPLETE GLUCOREGULATORY MODEL

In order to assess the capacity of the above model to describe glucagon dose-response, it must be integrated into a complete glucoregulatory model describing glucose regulation by subcutaneously infused insulin and glucagon. An adaptation of the model from Wendt et al. (2017) is considered in this work, where the insulin and glucagon effect on the EGP are substituted by the descriptions in Hovorka et al. (2004) and Masroor et al. (2019), respectively. It should be remarked that Wendt et al. (2017) was chosen as a baseline model because this work shares the same experimental data as the original model. Thus, it serves as a good comparator. An overview of the model subsystems is shown in Fig. 1, which are described next.

Insulin pharmacokinetics. A two-state system describes the pathway of insulin from subcutaneous administration to plasma:

$$\frac{dX_1(t)}{dt} = u_I(t) - \frac{X_1(t)}{t_{max}} \quad (2a)$$

$$\frac{dX_2(t)}{dt} = \frac{X_1(t)}{t_{max}} - \frac{X_2(t)}{t_{max}} \quad (2b)$$

$$I(t) = \frac{1}{t_{max}} \frac{X_2(t)}{W \cdot C_{I,F,I}} \cdot 10^6 + I_b \quad (2c)$$

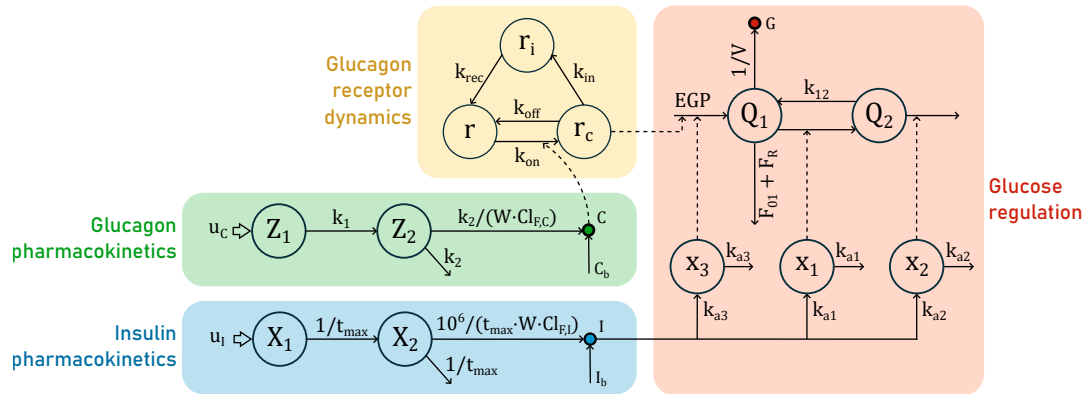


Fig. 1. Schematic of the proposed compartment model with glucagon receptor dynamics. The blue square contains insulin pharmacokinetics ((2a) to (2c)). The green square contains glucagon pharmacokinetics ((3a) to (3c)). The yellow square contains the glucagon receptors cycle ((1a) to (1c)), and the orange square contains the glucose regulation subsystem ((4a) to (4f)).

Here, $X_1(t)$ and $X_2(t)$ are the insulin mass due to exogenous dosing in the subcutaneous tissue and in plasma, respectively, measured in insulin units (U). t_{max} is the time from dose to maximum plasma concentration (min). $u_I(t)$ is insulin infusion as a deviation from basal (U/min). $I(t)$ is the insulin concentration in plasma, and I_b is its basal value (mU/l). W is the body weight (kg) and $Cl_{F,I}$ is the apparent insulin clearance (ml/kg/min). Note that dynamics in plasma are considered fast with respect to subcutaneous tissue, therefore equation (2c) represents the static behaviour.

Glucagon pharmacokinetics. Similar to the insulin subsystem, glucagon pharmacokinetics are described by:

$$\frac{dZ_1(t)}{dt} = u_c(t) - k_1 Z_1(t) \quad (3a)$$

$$\frac{dZ_2(t)}{dt} = k_1 Z_1(t) - k_2 Z_2(t) \quad (3b)$$

$$C(t) = \frac{k_2 Z_2(t)}{W \cdot Cl_{F,C}} + C_b \quad (3c)$$

Here $Z_1(t)$ and $Z_2(t)$ are the glucagon mass due to exogenous dosing in the subcutaneous tissue (pg). k_1 and k_2 are the absorption and elimination rate constants (min^{-1}). $Cl_{F,C}$ is the apparent glucagon clearance (ml/kg/min). $u_c(t)$ is glucagon infusion as a deviation from basal (pg/min). $C(t)$ and C_b are the glucagon concentration and its steady state value (pg/ml).

Glucose regulation. The model describing insulin action is composed by three states according to Hovorka et al. (2004). These states represent the effects of insulin on the glucose distribution, $x_1(t)$; glucose disposal, $x_2(t)$; and endogenous glucose production, $x_3(t)$:

$$\frac{dx_1(t)}{dt} = k_{a1} [I(t) - x_1(t)] \quad (4a)$$

$$\frac{dx_2(t)}{dt} = k_{a2} [I(t) - x_2(t)] \quad (4b)$$

$$\frac{dx_3(t)}{dt} = k_{a3} [I(t) - x_3(t)] \quad (4c)$$

k_{a1} , k_{a2} and k_{a3} are deactivation rate constants (min^{-1}).

Finally, the glucose dynamics for the accessible, $Q_1(t)$, and non-accessible, $Q_2(t)$, compartments, are described as:

$$\frac{dQ_1(t)}{dt} = -F_{01}(t) - F_R(t) - S_I x_1(t) Q_1(t) + k_{12} Q_2(t) + EGP(t) \quad (4d)$$

$$\frac{dQ_2(t)}{dt} = S_I x_1(t) Q_1(t) - Q_2(t) [k_{12} + S_D x_2(t)] \quad (4e)$$

$$G(t) = \frac{Q_1(t)}{V} \quad (4f)$$

where EGP is given by

$$EGP(t) = F_{hgp}(t) + EGP_0 (1 - S_I x_3(t)) \quad (4g)$$

F_{01} is the insulin-independent glucose flux ($\mu\text{mol/kg/min}$), F_R is the renal glucose clearance ($\mu\text{mol/kg/min}$) (see Wendt et al. (2017) for their definition), S_I and S_D are the insulin sensitivity to glucose transport and disposal, respectively ($\text{min}^{-1}/(\text{mU/l})$). k_{12} is the transfer rate constant from the non accessible to the accessible compartment (min^{-1}), EGP_0 is the EGP extrapolated to zero insulin concentration ($\mu\text{mol/kg/min}$), S_I is the hepatic insulin sensitivity ($(\text{mU/l})^{-1}$), V is the glucose distribution volume (ml/kg) and $G(t)$ is the BG (mmol/l).

Remark that the difference with the original model in Wendt et al. (2017) is provided by the new description of EGP given in (4g). For the sake of completeness, the original description was given by:

$$EGP(t) = \frac{1 - S_E x_3(t)}{1 - S_E I_b} \left((E_{max} - G_{GNG}) \frac{C(t)}{C_{E50} + C(t)} \right) + G_{GNG} \quad (5)$$

where S_E ($(\text{mU/l})^{-1}$) is the hepatic insulin sensitivity, E_{max} ($\mu\text{mol/kg/min}$) is the maximum EGP at basal insulin concentration, C_{E50} (pg/ml) represents the glucagon concentration yielding half of maximum EGP, and G_{GNG} ($\mu\text{mol/kg/min}$) represents glucose production by gluconeogenesis.

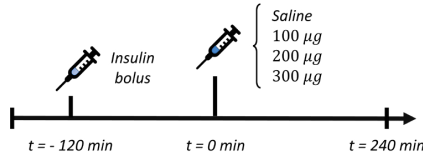


Fig. 2. Protocol in the clinical trial by Ranjan et al. (2016). After admission, patients were administered insulin in order to lower their glycemic values to 70 mg/dl. When glucose reached hypoglycaemia conditions ($t = 0$ min) a glucagon or saline bolus was injected.

4. EXPERIMENTAL DATA

The data used for the assessment of this model was obtained during the clinical trial carried out by Ranjan et al. (2016). Their study was designed to evaluate the effect of different glucagon doses from insulin-induced mild hypoglycaemia. Eight subjects with T1D participated in the study, and each one underwent four different arms of the trial. In all visits, patients were administered an insulin bolus to reach mild hypoglycaemia (BG concentration ≤ 70 mg/dl). Then, depending on the assigned randomization, they were administered either saline or a glucagon bolus of 100 μg , 200 μg or 300 μg (see Fig. 2).

Plasma glucose, plasma glucagon, plasma insulin, plasma growth hormone, cortisol, free fatty acids, triglycerides, blood pressure and heart rate were measured. However, for the purpose of this work, only glucose, insulin and glucagon data are relevant. Only the visits where glucagon was administered are considered. Consequently, three different sets of data are available per patient, each with a different glucagon dose, labelled henceforth Visit A, B and C, respectively.

Each of the datasets (3 datasets \times 8 patients) describes two parts: 1) the first segment of the study up to $t = 0$, where only insulin was administered and plasma glucagon kept its steady state value; and 2) from $t = 0$, when a glucagon bolus is administered and both the effect of plasma insulin and glucagon on EGP are present.

5. MODEL FITTING

5.1 Parameter identification

The purpose of this study is to assess the glucagon dose-response explanation capacity of a glucagon action model incorporating glucagon receptors as novelty. Thus, it is our interest to eliminate confounding factors unrelated to EGP that could hinder the explanatory performance of this model structure compared to other grey-box (functional) glucagon action models, such as the one in Wendt et al. (2017).

The main confounding factor in this case is the patient's insulin sensitivity, which varies over time and between patients (Heinemann (2002)). The model incorporates three insulin sensitivity parameters, of which S_T and S_D affect processes unrelated to EGP. Consequently, these parameters were identified for each patient visit. The initial value of $Q_2(t)$, denoted as Q_{20} , was also identified. In simulation studies, the initial state is sometimes associated

with equilibrium. However, it is difficult to achieve steady state conditions in real life, i.e., the starting point of the study is not in equilibrium. Contrary to the value of Q_{10} which is known from glucose measurements, Q_{20} must be identified for each visit. The rest of the model states were considered at equilibrium. Therefore, the following set of parameters θ_1 must be identified, for each patient (P) and for each visit (v):

$$\theta_{1P}^v = \{S_T, S_D, Q_{20}\}, \quad v = 1, 2, 3; \quad P = 1, 2, \dots, 8$$

The EGP model subsystem must be able to explain the dose-response from data in Visit A, B and C, so individualized parameter values must be considered. Regarding the glucagon action model, parameters k_{on} , K_r , and V_r were considered in the identification process, representing the activation rate of receptors, and the Michaelis-Menten parameters. Since the patients that underwent the "glucagon challenge test" in Masroor et al. (2019) were healthy people, it was deemed appropriate to tune the activation rate of the receptors. It could be discussed that glucagon action is impaired in people with diabetes and that could be explained by a deficit in the activation rate. The remaining parameters in (1) were taken from the work of Masroor et al. (2019), giving rise to the following to-be-identified parameter vector θ_2 per patient:

$$\theta_{2P} = \{k_{on}, K_r, V_r\}, \quad P = 1, 2, \dots, 8$$

Besides, parameters EGP_0 and S_I affecting insulin influence on EGP were also identified per patient:

$$\theta_{3P} = \{EGP_0, S_I\}, \quad P = 1, 2, \dots, 8$$

Thus, for each patient P , the complete parameter vector to be optimized is:

$$\Theta_P = \{\theta_{1P}^1, \theta_{1P}^2, \theta_{1P}^3, \theta_{2P}, \theta_{3P}\}$$

which was identified by minimizing the aggregated root-mean-squared error (RMSE) per visit

$$J_P = \sum_{v=1}^3 \sqrt{\frac{1}{n_v} \sum_{i=1}^{n_v} (\hat{y}_{i,P}^v - y_{i,P}^v)^2} \quad (6)$$

where n_v is the number of data, $\hat{y}_{i,P}^v$ is the simulated value, and $y_{i,P}^v$ is the real data point for visit v .

The identification was carried out in MATLAB R2018b, using the `fmincon` function.

The existence of many local minima is often observed in non-linear parameter estimation. Therefore, the identification was performed ten times using different random initial guesses of the parameter values within predefined limits based on the original values identified by Wendt et al. (2017).

5.2 Baseline comparison

In order to verify whether the use of the glucagon receptors in the description of glucagon action provides any improvements, we compared our model with the one presented by Wendt et al. (2017). In order to make a meaningful comparison, parameters were identified following the above-described procedure, giving rise to the following parameter set:

$$\Theta'_P = \{\theta_{1P}^1, \theta_{1P}^2, \theta_{1P}^3, S_E, E_{max}, C_{E50}\}$$

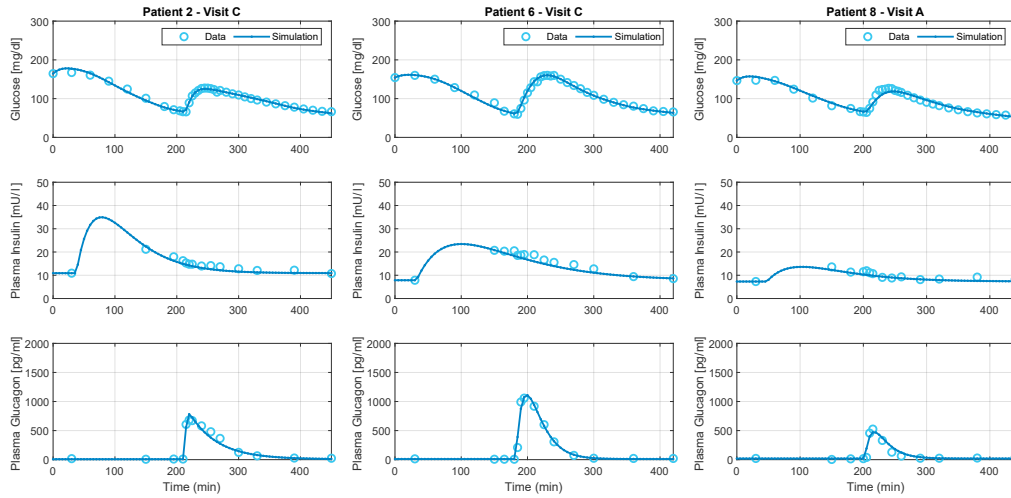


Fig. 3. Simulation results for Patient 2, visit C (300 μg glucagon dose); Patient 6, visit C and Patient 8, visit A (100 μg glucagon dose). Top graph depicts the glucose concentration in mg/dl, middle graph is the plasma insulin in mU/ml and bottom graph is the plasma glucagon in pg/ml.

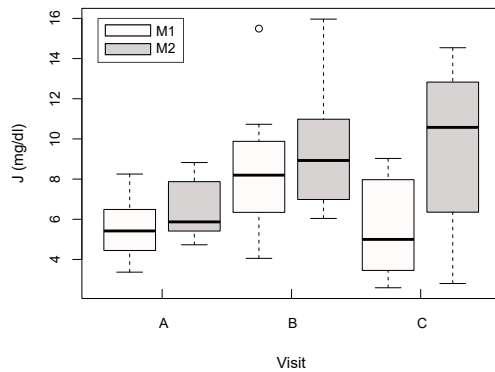


Fig. 4. J index distribution for our proposal (M1) and the model by Wendt et al. (2017) (M2).

6. RESULTS

Table 1 shows the identified parameter values. The parameters in θ_2 and θ_3 have a unique value per patient, whereas for θ_1 parameters (S_T, S_D, Q_{20}), the table shows the average value and standard deviation along the three visits for each patient. Results are reported as number or mean (standard deviation).

Figure 3 shows selected results obtained with the proposed model (Patients 2, 6 and 8). The results clearly show that the model successfully fits the data with different glucagon doses. These patients are illustrative of different behaviours with different glucagon doses. Remarkably, similar fits are obtained for all patients and visits.

After simulating all eight patients, we analyzed the obtained results for J_P (6) with both model structures. For our model (labelled M1), the mean J_P value is 19.65 (5.45) mg/dl, whereas for the model by Wendt et al. (2017) (labelled M2), the mean J_P is 25.57 (5.5) mg/dl. Normality tests were performed (Shapiro-Wilk, Kolmogorov-Smirnov

and Anderson-Darling) which prove that both data distributions were normal, so a t -test was applied to see if there were statistically significant differences between both approaches. The results for the paired t -test were: $t(7) = 3.20$, $p = 0.015^{**}$, Cohen's $d = 1.13$, proving that there was a significant difference between them.

The difference in the J_P values per visit was also analysed. The results show that the average error value is lower in every visit for the approach presented in this work (M1, Figure 4), especially in visit C (300 μg glucagon dose), where there is the greatest difference between both models. Note that a trend to increase residuals with respect to the glucagon dose is observed in the original model M2, contrary to our proposal. Table 2 details the average value of J_P per visit, as well as the t -test result, p -value and Cohen's d .

7. DISCUSSION AND CONCLUSION

This work validates a model which includes the dynamics of glucagon receptors using a set of clinical data with different glucagon doses. Our goal was to develop accurate models which can be used in the artificial pancreas environment, for both control and *in silico* validations. Therefore, it is necessary to find low-complexity models that properly describe the physiology.

The experimental conditions from the clinical trial by Ranjan et al. (2016) allowed us to assess the ability of the glucagon receptors dynamics proposed by Masroor et al. (2019) to describe the EGP variations due to different glucagon doses. The obtained results show the model proposed here successfully describes this effect.

Notice that the model from Wendt et al. (2017), as well as others (Resalat et al., 2019), include the influence of insulin on the glucagon effect. Moreover, the work by El Youssef et al. (2014) shows that high levels of plasma insulin inhibit glucagon effect. However, that clinical trial was performed under conditions of clamped plasma insulin. In

Table 1. Glucagon receptors and insulin PK identified parameters. For parameters with different values for each visit (S_T , S_D , Q_{20}), the mean and the standard deviation (SD) are shown.

Patient	$k_{on} \cdot 10^{-4}$ [(pg/min) $^{-1}$]	$K_r \cdot 10^{-4}$ [-]	V_r [μ mol/kg/min]	$S_I \cdot 10^{-4}$ [(mU/l) $^{-1}$]	EGP_0 [μ mol/kg/min]	$S_T \cdot 10^{-4}$ [min $^{-1}$ /(mU/l)]	$S_D \cdot 10^{-4}$ [min $^{-1}$ /(mU/l)]	Q_{20} [μ mol/kg]
1	0.37	184	63.9	170	7	33.9 (3.5)	5.1 (1.6)	2219 (318)
2	1.16	1778	120.4	100	10	27.0 (10.5)	3.8 (2.5)	1413 (389)
3	0.51	813	137.6	277	10	42.3 (9.9)	3.1 (2.2)	1891 (532)
4	0.19	152	85.3	100	6	18.7 (3.6)	1.3 (0.5)	1311 (1052)
5	0.10	108	70.0	100	6	32.3 (6.1)	1.2 (0.2)	1821 (620)
6	0.23	191	85.3	300	10	34.2 (14.9)	4.0 (1.8)	2077 (733)
7	0.57	2706	200.0	484	10	30.1 (17.5)	2.6 (0.8)	1687 (877)
8	0.23	146	64.7	500	2	42.9 (12.3)	2.7 (2.9)	1683 (578)
Mean (SD)	0.42 (0.34)	760 (975)	103.4 (47.2)	254 (167)	7.6 (2.8)	32.7 (11.8)	3.0 (2.0)	1763 (637)

Table 2. Means and standard deviations for J index of M1 and M2, t -test analysis, and Cohen's d .

Visit	M1	M2	t	p	Cohen's d
A	5.54 (1.46)	6.48 (1.44)	-2.17	0.066	-0.77
B	8.55 (3.28)	9.47 (3.00)	-1.57	0.161	-0.55
C	5.56 (2.32)	9.61 (3.85)	-3.10	0.017**	-1.10

contrast, the glucagon receptors model does not include information about insulin plasma levels in the glucagon action description. Despite of this, the model fits the data well. This suggests that further investigation into this effect is necessary. As well, a better understanding of the role of glucagon receptors and their internalization process is needed. Other phenomena such as lose of effectiveness of glucagon over time deem to be studied.

As a conclusion, based on the obtained results, the proposed model could help to improve the design of dual-hormone artificial pancreas systems.

ACKNOWLEDGEMENTS

The authors thank Dr. Juan Fernando Martín San José for assistance with statistical analysis and critical review of the manuscript.

REFERENCES

- Cryer, P., Davis, S., and Shamoon, H. (2003). Hypoglycemia in diabetes. *Diabetes Care*, 26(6), 1902–1912. doi:10.2337/diacare.26.6.1902.
- Dalla Man, C., Micheletto, F., Lv, D., Breton, M., Kovatchev, B., and Cobelli, C. (2014). The UVA/PADOVA type 1 diabetes simulator: New features. *Journal of Diabetes Science and Technology*, 8(1), 26–34. doi:10.1177/1932296813514502.
- El Youssef, J., Castle, J.R., Bakhtiani, P.A., Haidar, A., Branigan, D.L., Breen, M., and Ward, W.K. (2014). Quantification of the glycemic response to microdoses of subcutaneous glucagon at varying insulin levels. *Diabetes Care*, 37(11), 3054–3060. doi:10.2337/dc14-0803.
- Emami, A., Youssef, J.E., Rabasa-Lhoret, R., Pineau, J., Castle, J.R., and Haidar, A. (2017). Modeling Glucagon Action in Patients with Type 1 Diabetes. *IEEE Journal of Biomedical and Health Informatics*, 21(4), 1163–1171. doi:10.1109/JBHI.2016.2593630.
- Heinemann, L. (2002). Variability of Insulin Absorption and Insulin Action. *Diabetes Technology & Therapeutics*, 4(5), 673–682.
- Hovorka, R., Canonico, V., Chassin, L.J., Haueter, U., Massi-Benedetti, M., Federici, M.O., Pieber, T.R., Schaller, H.C., Schaupp, L., Vering, T., and Wilinska, M.E. (2004). Nonlinear model predictive control of glucose concentration in subjects with type 1 diabetes. *Physiological Measurement*, 25(4), 905–920. doi:10.1088/0967-3334/25/4/010.
- Masroor, S., van Dongen, M.G., Alvarez-Jimenez, R., Burggraaf, K., Peletier, L.A., and Peletier, M.A. (2019). Mathematical modeling of the glucagon challenge test. *Journal of Pharmacokinetics and Pharmacodynamics*, 46(6), 553–564. doi:10.1007/s10928-019-09655-2.
- Müller, T.D., Finan, B., Clemmensen, C., Di Marchi, R.D., and Tschöp, M.H. (2017). The new biology and pharmacology of glucagon. *Physiological Reviews*, 97(2), 721–766. doi:10.1152/physrev.00025.2016.
- Peters, T.M. and Haidar, A. (2018). Dual-hormone artificial pancreas: benefits and limitations compared with single-hormone systems. *Diabetic Medicine*, 35(4), 450–459. doi:10.1111/dme.13581.
- Ranjan, A., Schmidt, S., Madsbad, S., Holst, J.J., and Nørgaard, K. (2016). Effects of subcutaneous, low-dose glucagon on insulin-induced mild hypoglycaemia in patients with insulin pump treated type 1 diabetes. *Diabetes, Obesity and Metabolism*, 18(4), 410–418. doi:10.1111/dom.12627.
- Resalat, N., Youssef, J.E., Tyler, N., Castle, J., and Jacobs, P.G. (2019). A statistical virtual patient population for the glucoregulatory system in type 1 diabetes with integrated exercise model. *PLoS ONE*, 14(7), e0217301. doi:10.1371/journal.pone.0217301.
- Unger, R.H. and Cherrington, A.D. (2012). Glucagonocentric restructuring of diabetes: A pathophysiologic and therapeutic makeover. *Journal of Clinical Investigation*, 122(1), 4–12. doi:10.1172/JCI60016.
- Wendt, S.L., Ranjan, A., Möller, J.K., Schmidt, S., Knudsen, C.B., Holst, J.J., Madsbad, S., Madsen, H., Nørgaard, K., and Jørgensen, J.B. (2017). Cross-Validation of a Glucose-Insulin-Glucagon Pharmacodynamics Model for Simulation Using Data From Patients With Type 1 Diabetes. *Journal of diabetes science and technology*, 11(6), 1101–1111. doi:10.1177/1932296817693254.
- Zaharieva, D., Yavelberg, L., Jamnik, V., Cinar, A., Turksay, K., and Riddell, M.C. (2017). The effects of basal insulin suspension at the start of exercise on blood glucose levels during continuous versus circuit-based exercise in individuals with type 1 diabetes on continuous subcutaneous insulin infusion. *Diabetes Technology and Therapeutics*, 19(6), 370–378. doi:10.1089/dia.2017.0010.

APPENDIX C

Journal Paper - Computers in Biology and Medicine

Modeling the effect of glucagon on endogenous
glucose production in type 1 diabetes: on the role of
glucagon receptor dynamics

Authors:

Clara Furió-Novejarque, Ricardo Sanz, Tobias K. S. Ritschel, Asbjørn Thode Reenberg, Ajenthen G. Ranjan, Kirsten Nørgaard, José-Luis Díez, John Bagterp Jørgensen, Jorge Bondia

Published in:

Computers in Biology and Medicine, 154, 106605, 2023.



Contents lists available at ScienceDirect

Computers in Biology and Medicine

journal homepage: www.elsevier.com/locate/combiomed

Modeling the effect of glucagon on endogenous glucose production in type 1 diabetes: On the role of glucagon receptor dynamics

Clara Furió-Novejarque^a, Ricardo Sanz^a, Tobias K.S. Ritschel^b, Asbjørn Thode Reenberg^b,
Ajenthen G. Ranjan^{c,d}, Kirsten Nørgaard^c, José-Luis Díez^{a,e}, John Bagterp Jørgensen^b,
Jorge Bondia^{a,e,*}

^a Instituto Universitario de Automática e Informática Industrial, Universitat Politècnica de València, C/Camí de Vera, s/n, València, 46022, Spain

^b Department of Applied Mathematics and Computer Science, Technical University of Denmark, Anker Engelds Vej 1, Kgs. Lyngby, 2800, Denmark

^c Steno Diabetes Center Copenhagen, Borgmester Ib Juuls Vej 83, Herlev, 2730, Denmark

^d Danish Diabetes Academy, Sønder Blvd. 29, Odense, 5000, Denmark

^e Centro de Investigación Biomédica en Red de Diabetes y Enfermedades Metabólicas Asociadas, Instituto de Salud Carlos III, Av. Monforte de Lemos, 3-5, Madrid, 28029, Spain

ARTICLE INFO

Keywords:

Type 1 diabetes

Modeling

Endogenous glucose production

Glucagon receptors

ABSTRACT

This paper validates a glucoregulatory model including glucagon receptors dynamics in the description of endogenous glucose production (EGP). A set of models from literature are selected for a head-to-head comparison in order to evaluate the role of glucagon receptors. Each EGP model is incorporated into an existing glucoregulatory model and validated using a set of clinical data, where both insulin and glucagon are administered. The parameters of each EGP model are identified in the same optimization problem, minimizing the root mean square error (RMSE) between the simulation and the clinical data. The results show that the RMSE for the proposed receptors-based EGP model was lower when compared to each of the considered models (Receptors approach: 7.13 ± 1.71 mg/dl vs. 7.76 ± 1.45 mg/dl ($p = 0.066$), 8.45 ± 1.38 mg/dl ($p = 0.011$) and 8.99 ± 1.62 mg/dl ($p = 0.007$)). This raises the possibility of considering glucagon receptors dynamics in type 1 diabetes simulators.

1. Introduction

People with type 1 diabetes (T1D) suffer from an impairment in their blood glucose (BG) regulation. Due to the auto-immune destruction of the β cells in the pancreas, insulin is not produced, which is the hormone responsible of promoting glucose uptake by the cells. As a result, the body is unable to restore glucose concentration to normal values. People with T1D rely on external insulin administration with insulin pens or infusion pumps in order to regulate their BG levels. However, high doses of insulin could lead to low BG concentration if overdosed. Both a maintained high BG concentration (hyperglycaemia), and a low BG concentration (hypoglycaemia) are undesirable situations. The former, because it can cause several long-term vascular complications, such as retinopathy, foot amputations, heart attack and strokes, nephropathy, neuropathy, among others. Meanwhile, hypoglycaemia could induce dizziness, nausea, coma or even death in the most

severe cases [1]. This means people with T1D live with the colossal task of self-managing their diabetes on a daily basis.

In order to ease this duty, automated insulin delivery systems (also known as artificial pancreases (APs)) have recently appeared on the market. This term refers to the combination of (at least) three different elements: an insulin pump, a continuous glucose monitor (CGM) and a control algorithm (incorporated in the pump or in an external device such as a smartphone). The algorithm receives the glucose values provided by the CGM and provides an insulin infusion value to the pump every few minutes, according to a given control logic. Despite automation, hypoglycaemia prevention is challenging for single-hormone (insulin-only) systems, especially in situations like exercise or when overdosed. Thus, additional counterregulatory actions are needed, such as, intake of rescue carbohydrates or administration of glucagon.

* Corresponding author at: Instituto Universitario de Automática e Informática Industrial, Universitat Politècnica de València, C/Camí de Vera, s/n, València, 46022, Spain.

E-mail addresses: clafuno@upv.es (C. Furió-Novejarque), risanda@upv.es (R. Sanz), tobk@dtu.dk (T.K.S. Ritschel), athre@dtu.dk (A.T. Reenberg), ajenthen.ranjan@regionh.dk (A.G. Ranjan), kirsten.noergaard@regionh.dk (K. Nørgaard), jldiez@isa.upv.es (J.-L. Díez), jbo@dtu.dk (J.B. Jørgensen), jbondia@isa.upv.es (J. Bondia).

<https://doi.org/10.1016/j.combiomed.2023.106605>

Received 13 October 2022; Received in revised form 19 January 2023; Accepted 22 January 2023

Available online 24 January 2023

0010-4825/© 2023 Published by Elsevier Ltd.

Glucagon is a hormone produced in the pancreas by the α cells with an antagonist effect to insulin (it increases glucose concentration), promoting endogenous glucose production (EGP). The glucagon secretion is also impaired in people with T1D mainly due to the lack of signaling between β and α cells [2]. Glucagon is often used as stand-alone injections to rapidly rise glucose levels in case of severe hypoglycaemia. Soluble formulations of glucagon [3] have paved the way to dual-hormone AP systems infusing glucagon through dual-chamber pumps or an additional pump, in order to prevent hypoglycaemia. Dual-hormone APs have proven useful in glucose regulation in contrast to single-hormone APs, especially under exercise [4,5]. Integrating glucagon in APs allows to regulate glucose as the pancreas would, without needing any patient intervention, as it would be the case with the intake of rescue carbohydrates.

A fundamental step in the development of AP systems is the use of simulation tools to validate the algorithms. Clinical trials are expensive and may entail risks for the patients. Therefore, a lot of effort has been put towards developing mathematical models that reproduce physiology as accurately as possible. The use of these simulators allows to test algorithms in a quick and inexpensive way. The most commonly used models in the validation of AP algorithms are Dalla Man's model [6] (the UVA/Padova simulator) and Hovorka's model [7] (the Cambridge simulator and with some variations, OHSU and McGill simulators, for instance).

Whereas pharmacokinetics of insulin and glucagon are described in a similar fashion, other aspects can differ greatly among authors, such as EGP. This quantity is influenced by both insulin and glucagon and represents glucose production as a response to either hypoglycaemia or hyperglycemia. However, contrary to insulin, whose dynamics have been widely studied and there is a consensus in literature about describing its effect [6,8], glucagon effect description is more diverse. Although both insulin and glucagon are involved in EGP, their relationship has been described very differently in literature, and not many clinical trials study the relationship between both hormones. Their influence on EGP has been described as additive [9], multiplicative [10], or with a Michaelis–Menten function [11].

El Youssef et al. [12] reported a loss of glucagon effectiveness for high insulinemia under constant insulin infusion. A vanishing effect of glucagon effectiveness has also been reported. Whereas it has been proved that insulin and glucagon have a collaborative relationship, its physiological extent and mathematical description is still debated. One element that is sometimes overlooked in AP simulators development is glucagon receptors. The work by Masroor et al. [13] gave some insight into their dynamics.

The purpose of this work is to test an unconventional method for describing glucagon behavior. A physiology-based structure may prove useful in describing glucose dynamics more accurately. The glucagon receptors-based EGP model is compared to three other EGP models from literature. A set of clinical data is used to fit the models and to identify their parameters. In previous work, the authors carried out the validation of the receptors approach against just one other description of EGP [14]. This work adds two extra models to the comparison and changes the identification process so that the parameters in the baseline model used are common for all EGP definitions (the previous approach identified the models independently). The process will show how the receptors approach provides a good fit to the data, reducing the average error compared to the other models.

The paper is organized as follows: Section 2 describes the base model and the different EGP descriptions used for validation. Section 3 presents the identification procedure, divided into the description of the clinical data and the parameter identification method. Section 4 shows the main results and Section 5 discusses the implications of the results. Section 6 summarizes the conclusions.

2. Models

The evaluation of the EGP models was carried out using a baseline model that included descriptions of glucose regulation, insulin pharmacokinetics and glucagon pharmacokinetics. The submodel corresponding to EGP and glucagon effect was instantiated with the different EGP models to be evaluated.

Wendt et al. [11] presented the model used as reference, which is based on the widely used model by Hovorka et al. [8]. However, the former also incorporates glucagon pharmacokinetics and its effect on glucose. This model also fitted the purpose of the paper since it was identified using the same clinical dataset that is used to validate this work. Experimental data was obtained by Ranjan et al. [15] and it is described in more detail in Section 3.1.

The other EGP structures selected for comparison were chosen because their underlying structures were also based on Hovorka's model of glucose regulation. A total of four different definitions of EGP and glucagon effect are tested in this work:

1. The definition by Wendt et al. [11], which accompanies the baseline model. It will be labeled as *DTU* (Technical University of Denmark) which was Wendt's affiliation at the time of publication.
2. The EGP model proposed by Emami et al. [10]. This paper evaluates several definitions of EGP and presents a solution that is the one used in this work. It will be labeled as *McGill*, for McGill University in Montreal.
3. The proposal by Resalat et al. [9], which was first presented in [16]. It will be referred to as *OHSU* model, for the Oregon Health and Science University.
4. EGP based on receptors dynamics, this paper's new proposal, following the work by Masroor et al. [13]. It will be labeled as *Receptors* model.

The next sections will describe the baseline model and each one of the EGP definitions.

2.1. Baseline model

The baseline model can be divided into four different blocks: insulin pharmacokinetics, glucagon pharmacokinetics, EGP, and glucose regulation.

Fig. 1 provides an overview of the model compartments and their relationships. The block corresponding to EGP is left empty since its content will depend on the model being evaluated. Next, the equations and states of each subsystem are presented. Also, the model states are described in Table 1 and the parameters and their description can be found in Table 2.

2.1.1. Insulin pharmacokinetics

The insulin pharmacokinetics subsystem (blue block, Fig. 1) consists of two compartments ($X_1(t)$ and $X_2(t)$), the input being the insulin infusion ($u_I(t)$), expressed as a deviation with respect to basal insulin infusion, and the output, plasma insulin concentration ($I(t)$). The factor 10^6 in (1c) acts as unit conversion from U/ml to mU/l [11].

$$\frac{dX_1(t)}{dt} = u_I(t) - \frac{X_1(t)}{t_{max}} \quad (1a)$$

$$\frac{dX_2(t)}{dt} = \frac{X_1(t)}{t_{max}} - \frac{X_2(t)}{t_{max}} \quad (1b)$$

$$I(t) = \frac{1}{t_{max}} \frac{X_2(t)}{W \cdot C_{FI}} \cdot 10^6 + I_b \quad (1c)$$

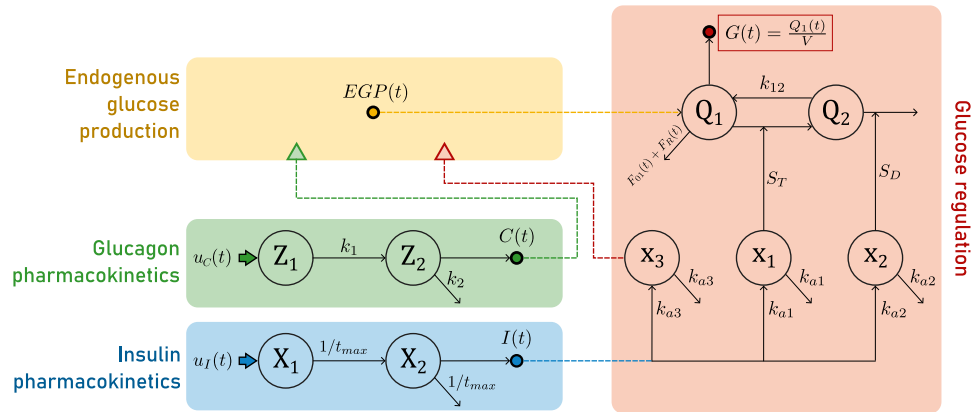


Fig. 1. Baseline model overview. Glucose regulation (red box), insulin pharmacokinetics (blue box) and glucagon pharmacokinetics (green box), corresponding to the model definition by Wendt et al. [11]. The EGP definition varies between the four definitions studied in this work (see Sections 2.2 to 2.5).

Table 1

Baseline model states units and description.

Magnitude	Units	Description
$u_I(t)$	U/min	Insulin infusion (as a deviation from basal)
$X_1(t)$	U	Insulin mass due to exogenous dosing in subcutaneous tissue
$X_2(t)$	U	Insulin mass due to exogenous dosing in plasma
$I(t)$	mU/l	Insulin plasma concentration
$u_C(t)$	pg/min	Glucagon infusion (as a deviation from basal)
$Z_1(t)$	pg	Glucagon mass due to exogenous dosing in subcutaneous tissue
$Z_2(t)$	pg	Glucagon mass due to exogenous dosing in plasma
$C(t)$	pg/ml	Glucagon concentration in plasma
$x_1(t)$	mU/l	Effect of insulin on glucose distribution
$x_2(t)$	mU/l	Effect of insulin on glucose disposal
$x_3(t)$	mU/l	Effect of insulin on endogenous glucose production
$EGP(t)$	$\mu\text{mol/kg/min}$	Endogenous glucose production
$Q_1(t)$	$\mu\text{mol/kg}$	Glucose mass in the accessible compartment
$Q_2(t)$	$\mu\text{mol/kg}$	Glucose mass in the non-accessible compartment
$G(t)$	mmol/l	Blood glucose

Table 2

Baseline model parameters units and description.

Parameter	Units	Description
t_{max}	min	Time from dose to maximum plasma concentration
W	kg	Weight
$Cl_{F,I}$	ml/kg/min	Apparent insulin clearance
I_b	mU/l	Basal insulin concentration
k_1, k_2	min^{-1}	Absorption elimination rate constants
$Cl_{F,C}$	ml/kg/min	Apparent glucagon clearance
C_b	pg/ml	Basal glucagon concentration
k_{a1}, k_{a2}, k_{a3}	min^{-1}	Deactivation rate constants
F_{0I}	$\mu\text{mol/kg/min}$	Insulin-independent glucose flux
F_R	$\mu\text{mol/kg/min}$	Renal glucose clearance
S_T	$\text{min}^{-1}/(\text{mU/l})$	Insulin sensitivity to glucose transport
S_D	$\text{min}^{-1}/(\text{mU/l})$	Insulin sensitivity to glucose disposal
k_{12}	min^{-1}	Transfer rate constant from the nonaccessible to the accessible compartment
V	ml/kg	Glucose distribution volume

2.1.2. Glucagon pharmacokinetics

The glucagon pharmacokinetics (green block, Fig. 1) is also represented as a two-compartment subsystem ($Z_1(t)$ and $Z_2(t)$), analogously to the insulin one, with input the glucagon infusion ($u_C(t)$), expressed as a deviation with respect to basal glucagon infusion (which is expected to be zero), and output plasma glucagon concentration ($C(t)$).

$$\frac{dZ_1(t)}{dt} = u_C(t) - k_1 \cdot Z_1(t) \quad (2a)$$

$$\frac{dZ_2(t)}{dt} = k_1 \cdot Z_1(t) - k_2 \cdot Z_2(t) \quad (2b)$$

$$C(t) = \frac{k_2 \cdot Z_2(t)}{W \cdot Cl_{F,C}} + C_b \quad (2c)$$

2.1.3. Glucose regulation

The glucose regulation subsystem (red block, Fig. 1) follows the Hovorka model [8]. It is composed by three states representing the

Table 3

EGP models parameters and states description. Parameters marked with (*) are the ones to be identified.

Magnitude	Units	Description
k_{off}	min^{-1}	Dissociation rate
k_{rec}	min^{-1}	Recycling rate
k_{in}	min^{-1}	Internalization rate of the glucagon-bonded receptor
k_{on} *	$(\text{pg}/\text{min})^{-1}$	Association rate of glucagon to the receptor
V_h	ml	Volume of the hepatic interstitial space
K_r *	unitless	Apparent dissociation constant
V_r *	$\mu\text{mol}/\text{kg}/\text{min}$	Maximal glucagon-dependent hepatic glucose production rate
EGP_0 *	$\mu\text{mol}/\text{kg}/\text{min}$	EGP extrapolated to zero insulin concentration
S_I *	$(\text{mU}/\text{l})^{-1}$	Hepatic insulin sensitivity
$r(t), r_C(t)$	unitless	Normalized amount of free and bonded receptors
$F_{hgg}(t)$	$\mu\text{mol}/\text{kg}/\text{min}$	Hepatic glucose production
S_E *	$(\text{mU}/\text{l})^{-1}$	Hepatic insulin sensitivity
E_{max} *	$\mu\text{mol}/\text{kg}/\text{min}$	Maximum EGP at basal insulin concentration
C_{E50} *	pg/ml	Glucagon concentration yielding half of maximum EGP
G_{NG} *	$\mu\text{mol}/\text{kg}/\text{min}$	Glucose production by gluconeogenesis
$G_{gg}(t)$	$\mu\text{mol}/\text{kg}/\text{min}$	Glucose production due to glycogenolysis
S *	$(\text{mU}/\text{l})^{-1}$	Hepatic insulin sensitivity
T *	$(\text{pg}/\text{ml})^{-1}$	Glucagon sensitivity
G_{ng} *	$\mu\text{mol}/\text{kg}/\text{min}$	Effect due to gluconeogenesis
K_{Gd} *	$(\mu\text{mol}/\text{kg})^{-1}$	Fractional deactivation rate constant
T_{Gd} *	$\mu\text{mol}/\text{kg}$	Glucagon rate of change sensitivity
$EGP_G(t)$	$\mu\text{mol}/\text{kg}/\text{min}$	Contribution to EGP from the rate of change of glucagon
EGP_0 *	$\mu\text{mol}/\text{kg}/\text{min}$	Basal endogenous glucose production at zero insulin concentration
S_f *	$(\text{mU}/\text{l})^{-1}$	Hepatic insulin sensitivity
k_{g3} *	min	Glucagon rate of change sensitivity
k_c *	$(\text{ng}/\text{l})^{-1}/\text{min}$	Glucagon sensitivity
k_d *	min^{-1}	Clearance rate of glucagon from the remote compartment
$Y(t)$	unitless	Effect of glucagon on EGP

effects of insulin on glucose transport, glucose disposal, and EGP.

$$\frac{dx_1(t)}{dt} = k_{a1} (I(t) - x_1(t)) \quad (3a)$$

$$\frac{dx_2(t)}{dt} = k_{a2} (I(t) - x_2(t)) \quad (3b)$$

$$\frac{dx_3(t)}{dt} = k_{a3} (I(t) - x_3(t)) \quad (3c)$$

Finally, the glucose dynamics for the accessible, $Q_1(t)$, and non-accessible, $Q_2(t)$, compartments, are described as follows:

$$\frac{dQ_1(t)}{dt} = -F_{01}(t) - F_R(t) - S_T \cdot x_1(t) \cdot Q_1(t) + k_{12} \cdot Q_2(t) + EGP(t) \quad (3d)$$

$$\frac{dQ_2(t)}{dt} = S_T \cdot x_1(t) \cdot Q_1(t) - Q_2(t) (k_{12} + S_D \cdot x_2(t)) \quad (3e)$$

$$G(t) = \frac{Q_1(t)}{V} \quad (3f)$$

where the definition of $EGP(t)$ will vary depending on the model used. Note that, as compared to Hovorka et al. [8], Eqs. (3a)–(3c) have unit static gain, being insulin sensitivities (gains) for glucose transport and uptake described by parameters S_T and S_D , respectively, in Eqs. (3d)–(3e). Hepatic insulin sensitivity will be defined by the corresponding model describing $EGP(t)$.

The following sections describe the different EGP models tested in this study. In the presentation of the subsequent models, the notation of parameters and states has been kept as similar as possible to the original respective works for the sake of clarity, as listed in Table 3.

2.2. DTU EGP model

The original Wendt model [11] described EGP as:

$$EGP(t) = G_{gg}(t) + G_{NG} \quad (4a)$$

where the signal $G_{gg}(t)$ determines the effect of glucagon and insulin on hepatic glucose production. This relationship is given by a Michaelis-Menten expression with maximum rate inhibited by insulin effect ($x_3(t)$) above basal insulin concentration I_b , with hepatic insulin sensitivity S_E (see Fig. 2):

$$G_{gg}(t) = \frac{1 - S_E \cdot x_3(t)}{1 - S_E \cdot I_b} \cdot \left((E_{max} - G_{NG}) \frac{C(t)}{C_{E50} + C(t)} \right) \quad (4b)$$

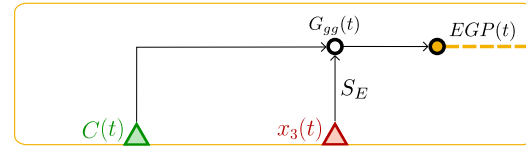


Fig. 2. DTU EGP model.

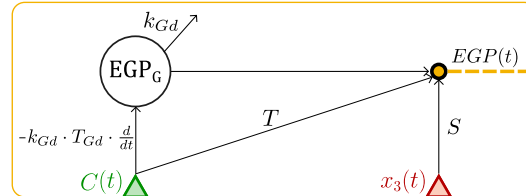


Fig. 3. McGill EGP model.

2.3. McGill EGP model

Emami et al. [10] perform a comparison of 8 different descriptions of EGP and validate them with a set of clinical data. The model concluded as the best description for EGP was defined as (see Fig. 3):

$$EGP(t) = H(1 - S \cdot x_3(t)) \cdot H(EGP_G(t) + T \cdot C(t)) + G_{ng} \quad (5a)$$

where $H(\cdot)$ is the unit step function, included to keep the expression positive. They consider that not only the level of plasma glucagon contributes to hepatic glucose production, but also its rate of change, defining the derivative of $EGP_G(t)$ as:

$$\frac{dEGP_G(t)}{dt} = -k_{Gd} \cdot EGP_G(t) - k_{Gd} \cdot T_{Gd} \left(\frac{dC(t)}{dt} \right) \quad (5b)$$

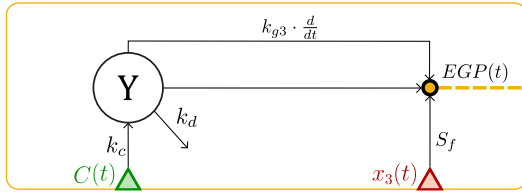


Fig. 4. OHSU EGP model.

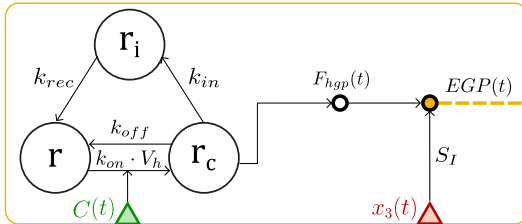


Fig. 5. Receptors EGP model.

Hepatic insulin sensitivity is given by parameter S . Similarly to Wendt et al. [11], insulin effect $x_3(t)$ inhibits glucagon effect on EGP as a multiplicative factor.

2.4. OHSU EGP model

Jacobs et al. [16] proposed a model based on Hovorka's model [8], incorporating glucagon dynamics. However, contrary to Wendt et al. [11], EGP is defined as (see Fig. 4):

$$EGP(t) = EGP_0 \left(1 - S_f \cdot x_3(t) + Y(t) + k_{g3} \cdot \frac{dY(t)}{dt} \right) \quad (6a)$$

where $Y(t)$ represents glucagon effect with dynamics given by:

$$\frac{dY(t)}{dt} = k_c \cdot C(t) - k_d \cdot Y(t) \quad (6b)$$

Note that the parameter S_f was added to the original formulation of the model, in order to match our definition of the unit-gain $x_3(t)$, as compared to Jacobs et al. [16]. Also, units of k_c are different with respect to the original definition, in order to match the units of the plasma glucagon signal.

Remark that, contrary to Wendt et al. [11] and Emami et al. [10], insulin and glucagon effects on EGP in this model are considered to be additive, instead of multiplicative. This means that contribution of glucagon to EGP is independent of insulin, and that the balance between glucagon and insulin antagonistic effects will determine EGP.

2.5. Receptors-based EGP model

More recently, the work from [13] proposed a three compartment system to describe glucagon receptors dynamics. Receptors are located on the surface membrane of the liver and they bond to plasma glucagon. This pairing triggers a chain of protein signaling that results in promoting glycogenolysis and glyconeogenesis [17]. After this, glucagon-bond receptors dissociate and internalize at different rates, becoming temporarily unavailable in this latter case. The authors represent this process with a three compartment model, one state variable for each state of the receptors: available ($r(t)$), bonded to glucagon ($r_c(t)$) and internalized ($r_i(t)$) (see Fig. 5). Assuming that the total number of receptors, although unknown, remains constant, this relationship can be simplified considering the constraint $r_i(t) = 1 - r(t) - r_c(t)$, where the state variables are expressed as relative to the total number of

receptors. As a result, a two-compartment model is obtained describing unbound and bonded (active) receptors, which is given by:

$$\frac{dr(t)}{dt} = -k_{on} \cdot V_h \cdot C(t) \cdot r(t) + k_{off} \cdot r_c(t) + k_{rec} (1 - r(t) - r_c(t)) \quad (7a)$$

$$\frac{dr_c(t)}{dt} = k_{on} \cdot V_h \cdot C(t) \cdot r(t) - k_{off} \cdot r_c(t) - k_{in} \cdot r_c(t) \quad (7b)$$

Then, glucagon effect on hepatic glucose production ($F_{hgp}(t)$) is made dependent on active glucagon receptors, as opposed to previous models which consider plasma glucagon concentration. This relation is modeled by means of a Michaelis-Menten relationship, as follows:

$$F_{hgp}(t) = \frac{V_r \cdot r_c(t)}{K_r + r_c(t)} \quad (7c)$$

When incorporating this effect into our model, the EGP expression was complemented by adding an additive effect of insulin on glucose production by the liver, which was not considered in the work by Masroor et al. [13]. With this, the expression of EGP is finally constituted as:

$$EGP(t) = F_{hgp}(t) + EGP_0 (1 - S_I \cdot x_3(t)) \quad (7d)$$

where S_I is the hepatic insulin sensitivity.

The original work by Masroor et al. [13] validated the model with glucagon-challenge test data on eight healthy subjects, and used a minimal glucoregulatory model, based on the [18] model. In this work, it is incorporated into a more detailed model and it is validated using data from people with T1D receiving subcutaneous glucagon injection of various doses, better describing the expected use of glucagon, as explained in the next section. This model proposal has already been proven useful in describing glucagon dynamics, as shown in the authors' previous work [14].

3. Identification procedure

3.1. Clinical data

The data used for the models evaluation was obtained in a clinical trial performed by Ranjan et al. [15]. The purpose of the trial was to test the efficacy of different glucagon doses in recovering from mild hypoglycaemia. Eight subjects with T1D took part in the study, who underwent four different arms in the trial.

The protocol for the study was the following: patients received an insulin bolus to reach mild hypoglycemic conditions (BG concentration lower than 70 mg/dl). At that point they received either saline or a glucagon bolus (100 µg, 200 µg or 300 µg) depending on the trial arm. The study finished four hours after the glucagon injection. A summary of the protocol is shown in Fig. 6. Plasma glucose, plasma glucagon, plasma insulin, plasma growth hormone, cortisol, free fatty acids, triglycerides, blood pressure, and heart rate were measured throughout the study. In the development of this work, only the information about plasma glucose, glucagon and insulin was used. Also, since the main interest was the modeling of glucagon effect on EGP, only the visits were glucagon was administered (100 µg, 200 µg or 300 µg) have been considered, which will be labeled as visit A, B and C henceforth.

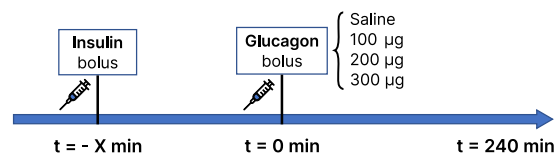


Fig. 6. Protocol in the clinical trial by Ranjan et al. [15]. After admission, patients were administered insulin in order to lower their glycemic values to 70 mg/dl. When glucose reached hypoglycaemia conditions ($t = 0$ min) a glucagon or saline bolus was injected.

3.2. Parameter identification

The main goal of this work is to test the receptors structure capability of describing observed glucose behavior against other proposals. This required identifying the model-specific parameters for each one of the aforementioned EGP models.

In a previous work, where a preliminary validation of the EGP model based on glucagon receptors was carried out, the identification was performed independently for each of the two models being tested [14]. However, since there are multiple EGP definitions, but the baseline model is common to all of them, the identification was revised taking into account that:

1. The parameters in the baseline model should be the same for each one of the complete models.
2. Instead of carrying out separate optimizations for each one of the models, the required set of parameters should be found for all of the models in the same optimization problem. This way, the parameters of the base model will be common to all EGP definitions.
3. The aim is to test each model structure, not finding a global model for all the patients. Hence, a different set of parameters will be identified for each patient.

With these premises in mind, the proposed identification method tries to find the best fit to the data for all the models while being equally fair. Note that most of the parameters for the baseline model (Table 2) are taken from [11], since they used the same set of clinical data as the present work.

In solving the optimization problem, each model runs three times, one for each visit to the clinic. Then, for each model, an index was calculated as the aggregated sum of the root mean square error (RMSE) per visit:

$$J_m = \sum_{v=1}^3 \sqrt{\frac{1}{n_v} \sum_{i=1}^{n_v} (\hat{y}_{i,P}^v - y_{i,P}^v)^2} \quad (8)$$

where m refers to the models, v refers to the visits, n_v is the number of data points in a specific visit, P refers to the patient, $\hat{y}_{i,P}^v$ is the simulated data point and $y_{i,P}^v$ is the measured data.

The total index to be optimized was the average value of J_m for the four models.

$$J = \frac{1}{4} \cdot \sum_{m=1}^4 J_m \quad (9)$$

Regarding the parameters to be identified, insulin sensitivities (S_T and S_D , (3d)–(3e)) were identified not only per patient but also per visit (i.e., each patient gets a different insulin sensitivity in each visit to the clinic). The reason behind this is that insulin sensitivity can present a wide variability, and change along time for a myriad of reasons [19]. Along with these parameters, the initial condition for the state $Q_2(t)$ (Q_{2_0}) was also identified for each visit. This allows to have a better fit to the data of each visit especially in the first part of the trial, where only insulin effect is present. In this way, simulated glucose and real glucose will be the closest possible at time $t = 0$ min, since from that point onwards is where our main area of interest will be.

The total vector of parameters can be divided into different sections. The first subset of parameters to identify will contain the constants from the base model.

$$\theta_{1P}^v = \{S_T^v, S_D^v, Q_{2_0}^v\}, \quad v = 1, 2, 3; \quad P = 1, 2, \dots, 8$$

For each of the EGP models, a subset of parameters is selected to be identified. These sets are identified per patient, but they are common across visits (the same EGP model should be able to explain the response of different glucagon doses). First, the subset for the DTU model will be:

$$\theta_{2P} = \{G_{NG}, S_E, E_{max}, C_{E50}\}, \quad P = 1, 2, \dots, 8$$

For the McGill model:

$$\theta_{3P} = \{G_{ng}, S, T, K_{Gd}, T_{Gd}\}, \quad P = 1, 2, \dots, 8$$

For the OHSU model:

$$\theta_{4P} = \{EGP_0, S_f, k_{g3}, k_g, k_c\}, \quad P = 1, 2, \dots, 8$$

And finally the Receptors model:

$$\theta_{5P} = \{EGP_0, S_f, k_{on}, K_r, V_r\}, \quad P = 1, 2, \dots, 8$$

The Receptors model included many parameters describing rates between the receptors compartments. In the original work by Masroor et al. [13], some of the parameters were identified whereas others were fixed according to previous works found in literature, based on the modeling of insulin receptors (k_{rec} based on [20]) or previous studies on glucagon receptors (k_{on} and k_{off} based on [21]). However, it was deemed appropriate to identify the activation rate (k_{on} , (7a)–(7b)) as a way of tailoring the process to each patient. Furthermore, to avoid identifiability issues, the value of k_{in} was fixed to the identified value in [13]. The components of the Michaelis-Menten expression (K_r and V_r , (7c)), were also included in the identification.

The complete parameter vector to be optimized will include all parameter subsets.

$$\theta_P = \{\theta_{1P}^1, \theta_{1P}^2, \theta_{1P}^3, \theta_{2P}, \theta_{3P}, \theta_{4P}, \theta_{5P}\}$$

This leaves an optimization problem with a total of 28 parameters per patient. The identification was carried out using the `fmincon` function in Matlab R2018b. This function makes use of the interior point algorithm to find the minimum of the specified cost index (9) [22]. This algorithm is the default solver in the `fmincon` function, and it is widely used for solving optimization problems. The interior point algorithm tries to iteratively approach the optimal solution from the interior of a feasible set. Since this is a local optimization solver, the optimization was repeated five times with different random starting points within the parameter bounds. These bounds are predefined based on the provided parameter values in each model's original work.

To solve the system of differential equations, Matlab provides the function `ode45`, that makes use of a Runge-Kutta method to solve the system over a specific time step. Specifically, the Dormand-Prince method [23]. In this work, the `ode45` function runs over 5 min intervals, with the solver applying a variable simulation step size within each interval.

4. Results

Fig. 7 shows the average fit of the models to the data. Each row corresponds to one model (DTU, McGill, OHSU and Receptors¹), and each column shows the different visits (A, B and C). All models present a reasonable fit to the data, however the Receptors model presents a better fit consistently across visits.

Fig. 8 shows the average fit to plasma insulin and plasma glucagon data. Since both these signals belong to the baseline pharmacokinetics models, they are common for all the studied models. Plasma insulin graph for visit B presents some unusual shape in the standard deviation graph. This is because only one patient's data was measured at some of the depicted timestamps. Hence, the standard deviation is zero for those points.

The parameter values obtained in the identification process are described in Tables 5–7. Table 5 shows the values of the parameters that were identified per visit (S_T , S_D and the initial value of Q_2). Tables 6 and 7 show the parameters values of each EGP model for the eight patients.

RMSE results for each model and period are summarized in Fig. 9. The RMSE values were analyzed at three different periods:

¹ From this point on, we refer to the models by name but they comprise the combination of the baseline model plus the corresponding EGP model.

Table 4

Means and standard deviations for the J_m index of each of the models against the receptors proposal, t -test analysis, and Cohen's d , separated by time period.

First period					
	Receptors		t	p	Cohen's d
DTU	7.22 ± 2.15		0.02	0.985	0.01
McGill	8.84 ± 3.01	7.21 ± 2.36	1.78	0.118	0.63
OHSU	8.64 ± 2.82		1.58	0.159	0.56
Second period					
	Receptors		t	p	Cohen's d
DTU	6.64 ± 1.58		2.43	0.046**	0.86
McGill	7.18 ± 1.32	5.90 ± 1.75	3.85	0.006**	1.36
OHSU	7.81 ± 1.75		3.06	0.018**	1.08
Overall					
	Receptors		t	p	Cohen's d
DTU	7.76 ± 1.45		2.18	0.066	0.77
McGill	8.45 ± 1.38	7.13 ± 1.71	3.44	0.011**	1.22
OHSU	8.99 ± 1.62		3.74	0.007**	1.32

Table 5

Identified values for the parameters S_d , S_t and Q_{20} . Bottom row shows the mean values and their standard deviation of each parameter.

Patient	Visit A			Visit B			Visit C		
	S_d	S_t	Q_{20}	S_d	S_t	Q_{20}	S_d	S_t	Q_{20}
1	$1.81 \cdot 10^{-4}$	$1.13 \cdot 10^{-3}$	860	$5.45 \cdot 10^{-4}$	$2.82 \cdot 10^{-3}$	2061	$3.08 \cdot 10^{-4}$	$4.92 \cdot 10^{-3}$	2999
2	$1.52 \cdot 10^{-4}$	$1.89 \cdot 10^{-3}$	1038	$3.16 \cdot 10^{-4}$	$3.05 \cdot 10^{-3}$	1508	$2.78 \cdot 10^{-5}$	$3.59 \cdot 10^{-3}$	2178
3	$2.08 \cdot 10^{-4}$	$5.62 \cdot 10^{-3}$	2990	$5.32 \cdot 10^{-4}$	$3.83 \cdot 10^{-3}$	1939	$5.97 \cdot 10^{-4}$	$8.90 \cdot 10^{-3}$	2992
4	$1.16 \cdot 10^{-5}$	$1.60 \cdot 10^{-4}$	218	$2.74 \cdot 10^{-4}$	$7.43 \cdot 10^{-4}$	802	$3.55 \cdot 10^{-1}$	$1.12 \cdot 10^{-4}$	121
5	$1.03 \cdot 10^{-5}$	$2.46 \cdot 10^{-3}$	1822	$9.64 \cdot 10^{-5}$	$2.19 \cdot 10^{-3}$	1126	$1.52 \cdot 10^{-4}$	$4.85 \cdot 10^{-3}$	1979
6	$2.79 \cdot 10^{-4}$	$5.50 \cdot 10^{-3}$	3000	$2.02 \cdot 10^{-2}$	$6.20 \cdot 10^{-4}$	3000	$4.69 \cdot 10^{-4}$	$4.77 \cdot 10^{-3}$	3000
7	$1.46 \cdot 10^{-4}$	$4.65 \cdot 10^{-3}$	2190	$1.54 \cdot 10^{-4}$	$4.12 \cdot 10^{-3}$	3000	$1.23 \cdot 10^{-4}$	$4.28 \cdot 10^{-3}$	2042
8	$6.33 \cdot 10^{-5}$	$5.53 \cdot 10^{-3}$	2503	$2.60 \cdot 10^{-4}$	$4.32 \cdot 10^{-3}$	2177	$9.71 \cdot 10^{-4}$	$9.01 \cdot 10^{-3}$	2999
	$1.31 \cdot 10^{-4} \pm 9.60 \cdot 10^{-5}$	$3.37 \cdot 10^{-3} \pm 2.21 \cdot 10^{-3}$	1828 ± 1033	$2.80 \cdot 10^{-3} \pm 7.03 \cdot 10^{-3}$	$2.71 \cdot 10^{-3} \pm 1.44 \cdot 10^{-3}$	1952 ± 798	$4.47 \cdot 10^{-2} \pm 1.25 \cdot 10^{-1}$	$5.05 \cdot 10^{-3} \pm 2.87 \cdot 10^{-3}$	2289 ± 991

Table 6

Identified values for the DTU and McGill EGP models parameters. Bottom row shows the mean values and their standard deviation of each parameter.

Patient	DTU				McGill				
	S_e	E_{max}	C_{E50}	G_{GNG}	S	T	K_{Gd}	T_{Gd}	G_{ng}
1	$1.33 \cdot 10^{-2}$	100	900	5	0.01	0.05	0.26	$1.93 \cdot 10^{-1}$	7
2	$1.03 \cdot 10^{-3}$	75	999	6	0.01	0.05	0.01	$4.66 \cdot 10^{-3}$	6
3	$1.02 \cdot 10^{-3}$	100	447	8	0.03	0.20	6.88	$4.32 \cdot 10^{-1}$	9
4	$1.17 \cdot 10^{-3}$	79	735	8	0.01	0.07	0.81	$3.65 \cdot 10^{-1}$	9
5	$2.98 \cdot 10^{-3}$	96	987	5	0.01	0.03	6.69	$5.54 \cdot 10^{-1}$	7
6	$1.00 \cdot 10^{-3}$	100	642	9	0.04	0.17	0.09	$4.16 \cdot 10^{-1}$	10
7	$2.14 \cdot 10^{-2}$	89	1000	3	0.01	0.05	6.65	$2.17 \cdot 10^{-3}$	3
8	$8.86 \cdot 10^{-3}$	100	631	1	0.01	0.06	0.07	$5.56 \cdot 10^{-1}$	5
	$6.34 \cdot 10^{-3} \pm 7.58 \cdot 10^{-3}$	92 ± 10	793 ± 209	6 ± 3	0.02 ± 0.01	0.09 ± 0.06	2.68 ± 3.37	$3.15 \cdot 10^{-1} \pm 2.24 \cdot 10^{-1}$	7 ± 2

Table 7

Identified values for the OHSU and Receptors EGP models parameters. Bottom row shows the mean values and their standard deviation of each parameter.

Patient	OHSU					Receptors				
	S_f	k_{g3}	k_c	k_d	EGP_0	S_f	k_{on}	K_r	V_r	EGP_0
1	$8.16 \cdot 10^{-6}$	$8.25 \cdot 10^{-6}$	$1.62 \cdot 10^{-3}$	0.26	7	$1.33 \cdot 10^{-2}$	$2.25 \cdot 10^{-6}$	$8.57 \cdot 10^{-3}$	135	8
2	$9.19 \cdot 10^{-6}$	$9.81 \cdot 10^{-6}$	$7.46 \cdot 10^{-3}$	1.00	6	$1.03 \cdot 10^{-3}$	$5.30 \cdot 10^{-5}$	$2.19 \cdot 10^{-1}$	200	9
3	$6.89 \cdot 10^{-5}$	$9.93 \cdot 10^{-6}$	$3.59 \cdot 10^{-3}$	0.34	10	$1.02 \cdot 10^{-3}$	$1.35 \cdot 10^{-5}$	$3.48 \cdot 10^{-2}$	195	10
4	$1.05 \cdot 10^{-5}$	$1.07 \cdot 10^{-5}$	$1.63 \cdot 10^{-3}$	0.27	9	$1.17 \cdot 10^{-3}$	$9.70 \cdot 10^{-6}$	$1.65 \cdot 10^{-2}$	80	10
5	$9.40 \cdot 10^{-6}$	$9.45 \cdot 10^{-6}$	$1.14 \cdot 10^{-3}$	0.20	7	$2.98 \cdot 10^{-3}$	$1.04 \cdot 10^{-6}$	$2.86 \cdot 10^{-3}$	101	6
6	$9.98 \cdot 10^{-5}$	$1.23 \cdot 10^{-5}$	$1.69 \cdot 10^{-3}$	0.32	12	$1.00 \cdot 10^{-3}$	$4.79 \cdot 10^{-6}$	$7.90 \cdot 10^{-3}$	109	10
7	$9.41 \cdot 10^{-5}$	$1.06 \cdot 10^{-5}$	$1.43 \cdot 10^{-2}$	1.00	3	$2.14 \cdot 10^{-2}$	$1.72 \cdot 10^{-5}$	$1.04 \cdot 10^{-1}$	200	5
8	$1.35 \cdot 10^{-5}$	$1.33 \cdot 10^{-5}$	$1.46 \cdot 10^{-3}$	0.13	5	$8.86 \cdot 10^{-3}$	$1.00 \cdot 10^{-6}$	$1.62 \cdot 10^{-3}$	103	4
	$3.92 \cdot 10^{-5} \pm 4.11 \cdot 10^{-5}$	$1.06 \cdot 10^{-5} \pm 1.62 \cdot 10^{-6}$	$4.11 \cdot 10^{-3} \pm 4.62 \cdot 10^{-3}$	0.44 ± 0.35	7 ± 3	$6.34 \cdot 10^{-3} \pm 7.58 \cdot 10^{-3}$	$1.28 \cdot 10^{-5} \pm 1.73 \cdot 10^{-5}$	$4.94 \cdot 10^{-2} \pm 7.64 \cdot 10^{-2}$	140 ± 50	8 ± 2

1. Considering the first part only (*First period*), from start time of the clinical trial until the glucagon bolus was administered ($t = -X$ to $t = 0$ min, see Fig. 6). This interval was analyzed to ensure that the behavior of the baseline model was consistent independent of the EGP model.
2. From the moment the glucagon was administered, onward (*Second period*), from $t = 0$ to $t = 240$ min. This would be the

main area of interest in this study, where the glucagon effect comes into play.

3. Along all the time of the experiment (*Overall*).

Table 4 details the mean RMSE (8) and its standard deviation for each of the models in each of the studied time periods. Several paired statistical analysis were performed, comparing each of the selected EGP models against the Receptors model. This comparison provided the

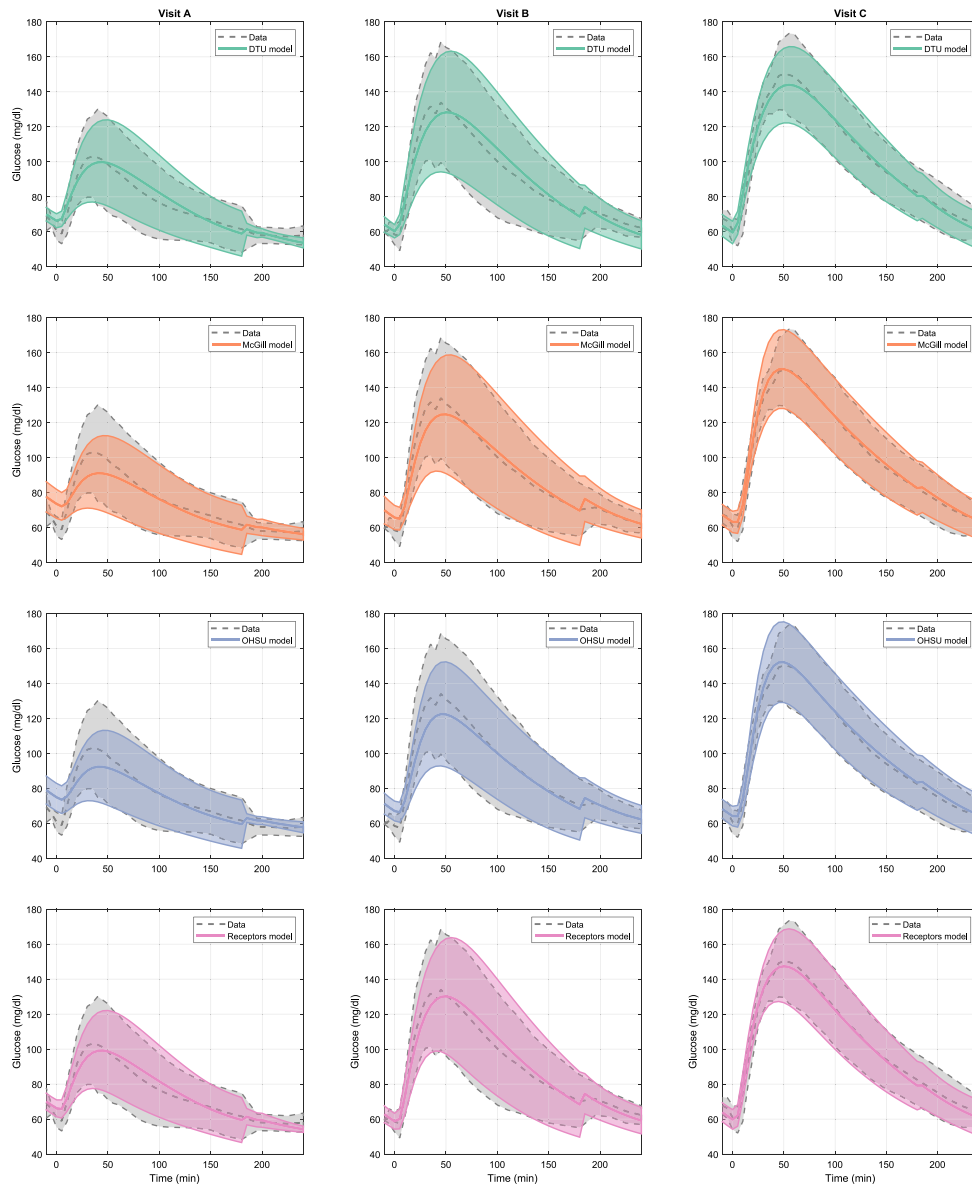


Fig. 7. Glucose simulation results. Figures show each of the studied models against the clinical data. Dashed/gray lines correspond to the data and continuous/colored lines show the simulation results. The central line for both data series represents the average of the eight patients, whereas the shaded area encloses standard deviation. Results show the response from $t = 0$ min to 240 min.

result of the t -test, its p -value and Cohen's d size effect. Results in the First period show that there is no statistically significant differences between any of the studied models and the Receptors model. However in the Second period, the difference is statistically significant for every pair of models. In the overall analysis, the pairs McGill-Receptors and OHSU-Receptors also present statistically significant differences. Across all the analysis it is also shown that the average error for the Receptors model is lower in every comparison.

5. Discussion

This work's results show how the EGP model including glucagon receptors dynamics provides an improvement in describing the glucagon effect when compared with other models from literature. Table 4 reflects this result, showing a lower average error value for the Receptors model, and a statistically significant difference for each of the comparisons in the Second period of the data, which is the main focus of our analysis. Also, Cohen's d values (larger than 0.8), confirm that

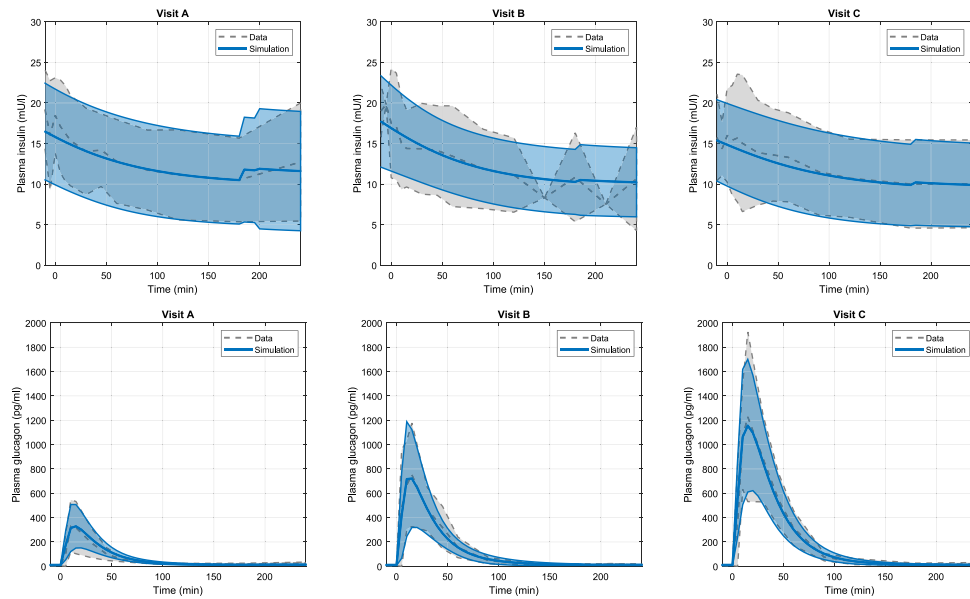


Fig. 8. Plasma insulin (top) and plasma glucagon (bottom) simulation results. Dashed/gray lines correspond to the data and continuous/colored lines show the simulation results. The central line for both data series represents the average of the eight patients, whereas the shaded area encloses standard deviation. Results show the response from $t = 0$ min to 240 min. Irregularities in insulin standard deviation graph are due to just one patient's data being measured in certain timestamps, making zero the standard deviation.

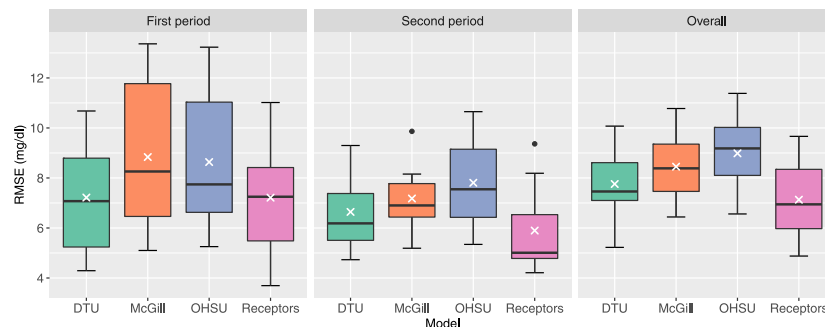


Fig. 9. Boxplots of RMSE values obtained per model for the First period of data (left), the Second period (middle) and Overall the time of the trial (right). White crosses mark mean values and black horizontal lines, median values.

there is a noticeable difference in the behavior between the analyzed pairs. In fact, for the Overall analysis, there is a statistically significant difference for all the comparisons but DTU-Receptors. However, the p -value is close to being lower than 0.05 and Cohen's d is also close to 0.8, meaning that the difference is not negligible.

Having no statistically significant difference in the First period agrees with what we expected, since in that interval, the EGP model only contributes as a constant (basal value) to the general model. Our hypothesis was that no matter the EGP model used, the behavior in the First period should be similar across models in order to provide a fair comparison. The First period also shows the greatest standard deviation in the error values. This is due to the scarce data available in the first part of the experiment, which caused the fits to have greater RMSEs, and also the great variability in the initial conditions (i.e., there is no information about the patients' state prior to arriving to the clinic).

The results obtained in this study will allow to incorporate EGP models including glucagon receptor dynamics into other T1D simulators. To our knowledge, they are not present in any widely-used simulator, but it could improve the accuracy of the *in silico* experiments providing a more physiology-based definition.

One question remains unanswered and that is, how decisive the influence of plasma insulin levels is on the glucagon effect. As shown in Fig. 8, plasma insulin levels were stable during the Second period, when glucagon was acting, with an average value of 15 mU/l approximately. According to the results reported by El Youssef et al. [12], maintained high plasma insulin may impair glucagon effect. Their results report a high plasma insulin concentration around 40 mU/l, which is not close to the conditions of the clinical data used in this work.

Limitations of this work include: (1) The reduced number of participants ($n = 8$) in the clinical dataset. This is a general limitation found in metabolic studies addressing glucagon modeling where cohorts are typically between 10 and 20 (see for instance [12,24,25]), due to the specific nature of the data to be collected in *ad-hoc* experiments (time series with frequent enough measurements of plasma glucose, insulin and glucagon are needed), as opposed to the use of tests part of the clinical routine such as the Oral Glucose Tolerance Test (OGTT), where larger cohorts are feasible (e.g. Contreras et al. [26]). Hence, given the reduced number of datasets available, this only allows to draw preliminary conclusions. Further research will be needed introducing

a larger dataset or several clinical trials as validation data in order to be able to guarantee the accuracy of the proposed model; (2) A slight inaccuracy in the first part of the data fit. As seen in Fig. 7, some models did not exactly reach the point of interest at $t = 0$, which might also indicate a limitation in the insulin pharmacokinetics models; (3) The large number of parameters to be identified. A long time was needed to solve the optimization problem, which makes it infeasible to be solved online within an AP algorithm; (4) Further validation should include different datasets in a variety of conditions, such as larger glucagon doses, higher plasma insulin concentrations or close in time repeated glucagon doses.

6. Conclusions

This work presents a glucagon receptors based EGP model, and performs a head to head comparison with three other models from literature. The evaluation consists in identifying parameters from the selected EGP models to fit data from a clinical trial. The results show an improvement in the data fitting with the proposed model. These outcomes will be useful in the study of T1D and AP development, allowing for more accurate *in silico* validations.

Funding

This work was supported by grant PID2019-107722RB-C21 funded by MCIN/AEI/10.13039/501100011033; C.F.N. received grant FPU17/03404 funded by MCIN/AEI/10.13039/501100011033 and “ERDF A way of making Europe”; grant CIPROM/2021/12 funded by Conselleria de Innovación, Universidades, Ciencia y Sociedad Digital from Generalitat Valenciana; A.G.R. received a postdoctoral fellowship from the Danish Diabetes Academy (PD002-19) supported by the Novo Nordisk Foundation and received a research grant from the Danish Diabetes Association; K. N. affiliation to Steno Diabetes Center Copenhagen is public funded by The Capital Region.

Declaration of competing interest

The authors declare that they have no known competing financial interests or personal relationships that could have appeared to influence the work reported in this paper.

References

- [1] P. Cryer, S. Davis, H. Shamon, Hypoglycemia in diabetes, *Diabetes Care* 26 (6) (2003) 1902–1912, <http://dx.doi.org/10.2337/diacare.26.6.1902>.
- [2] R.H. Unger, A.D. Cherrington, Glucagonocentric restructuring of diabetes: A pathophysiologic and therapeutic makeover, *J. Clin. Invest.* 122 (1) (2012) 4–12, <http://dx.doi.org/10.1172/JCI60016>.
- [3] U. Hövelmann, B.V. Bysted, U. Mouritzen, F. Macchi, D. Lamers, B. Kronshage, D.V. Möller, T. Heise, Pharmacokinetic and pharmacodynamic characteristics of dasiglucagon, a novel soluble and stable glucagon analog, *Diabetes Care* 41 (3) (2018) 531–537, <http://dx.doi.org/10.2337/dc17-1402>.
- [4] A. Weisman, J.W. Bai, M. Cardinez, C.K. Kramer, B.A. Perkins, Effect of artificial pancreas systems on glycaemic control in patients with type 1 diabetes: a systematic review and meta-analysis of outpatient randomised controlled trials, *Lancet Diabetes Endocrinol.* 5 (7) (2017) 501–512, [http://dx.doi.org/10.1016/S2213-8587\(17\)30167-5](http://dx.doi.org/10.1016/S2213-8587(17)30167-5).
- [5] T.M. Peters, A. Haidar, Dual-hormone artificial pancreas: benefits and limitations compared with single-hormone systems, *Diabetic Med.* 35 (4) (2018) 450–459, <http://dx.doi.org/10.1111/dme.13581>.
- [6] C. Dalla Man, F. Micheletto, D. Lv, M. Breton, B. Kovatchev, C. Cobelli, The UVA/PADOVA type 1 diabetes simulator: New features, *J. Diabetes Sci. Technol.* 8 (1) (2014) 26–34, <http://dx.doi.org/10.1177/1932296813514502>.
- [7] M.E. Wilinska, L.J. Chassin, C.L. Acerini, J.M. Allen, D.B. Dunger, R. Hovorka, Simulation environment to evaluate closed-loop insulin delivery systems in type 1 diabetes, *J. Diabetes Sci. Technol.* 4 (1) (2010) 132–144, <http://dx.doi.org/10.1177/193229681000400117>.
- [8] R. Hovorka, F. Shojae-Moradie, P.V. Carroll, L.J. Chassin, L.J. Gowrie, N.C. Jackson, R.S. Tudor, A. Margot Umpleby, R.H. Jones, Partitioning glucose distribution/transport, disposal, and endogenous production during IVGTT, *Am. J. Physiol. - Endocrinol. Metab.* 282 (5 45-5) (2002) 992–1007, <http://dx.doi.org/10.1152/ajpendo.00304.2001>.
- [9] N. Resalat, J.E. Youssef, N. Tyler, J. Castle, P.G. Jacobs, A statistical virtual patient population for the glucoregulatory system in type 1 diabetes with integrated exercise model, *PLoS ONE* 14 (7) (2019) e0217301, <http://dx.doi.org/10.1371/journal.pone.0217301>.
- [10] A. Emami, J.E. Youssef, R. Rabasa-Lhoret, J. Pineau, J.R. Castle, A. Haidar, Modeling glucagon action in patients with type 1 diabetes, *IEEE J. Biomed. Health Inf.* 21 (4) (2017) 1163–1171, <http://dx.doi.org/10.1109/JBHI.2016.2593630>.
- [11] S.L. Wendt, A. Ranjan, J.K. Möller, S. Schmidt, C.B. Knudsen, J.J. Holst, S. Madsbad, H. Madsen, K. Norgaard, J.B. Jørgensen, Cross-validation of a glucose-insulin-glucagon pharmacodynamics model for simulation using data from patients with type 1 diabetes, *J. Diabetes Sci. Technol.* 11 (6) (2017) 1101–1111, <http://dx.doi.org/10.1177/1932296817693254>.
- [12] J. El Youssef, J.R. Castle, P.A. Bakhtiani, A. Haidar, D.L. Branigan, M. Breen, W.K. Ward, Quantification of the glycemic response to microdoses of subcutaneous glucagon at varying insulin levels, *Diabetes Care* 37 (11) (2014) 3054–3060, <http://dx.doi.org/10.2337/dc14-0803>.
- [13] S. Masroor, M.G. van Dongen, R. Alvarez-Jimenez, K. Burggraaf, L.A. Peletier, M.A. Peletier, Mathematical modeling of the glucagon challenge test, *J. Pharmacokinetic. Pharmacodyn.* 46 (6) (2019) 553–564, <http://dx.doi.org/10.1007/s10928-019-09655-2>.
- [14] C. Furió-Novejarque, R. Sanz, A.T. Reenberg, T.K.S. Ritschel, A.G. Ranjan, K. Norgaard, J.-L. Díez, J.B. Jørgensen, J. Bondia, Assessment of a new model of glucagon action with glucagon receptor dynamics, *IFAC Proc. Vol. (IFAC-PapersOnline)* 55 (20) (2022) 647–652, <http://dx.doi.org/10.1016/j.ifacol.2022.09.169>.
- [15] A. Ranjan, S. Schmidt, S. Madsbad, J.J. Holst, K. Norgaard, Effects of subcutaneous, low-dose glucagon on insulin-induced mild hypoglycaemia in patients with insulin pump treated type 1 diabetes, *Diabetes, Obes. Metab.* 18 (4) (2016) 410–418, <http://dx.doi.org/10.1111/dom.12627>.
- [16] P.G. Jacobs, N. Resalat, J.E. Youssef, R. Reddy, D. Branigan, N. Preiser, J. Condon, J. Castle, Incorporating an exercise detection, grading, and hormone dosing algorithm into the artificial pancreas using accelerometry and heart rate, *J. Diabetes Sci. Technol.* 9 (6) (2015) 1175–1184, <http://dx.doi.org/10.1177/1932296815609371>.
- [17] T.D. Müller, B. Finan, C. Clemmensen, R.D. Di Marchi, M.H. Tschöp, The new biology and pharmacology of glucagon, *Physiol. Rev.* 97 (2) (2017) 721–766, <http://dx.doi.org/10.1152/physrev.00025.2016>.
- [18] R.N. Bergman, L.S. Phillips, C. Cobelli, Physiologic evaluation of factors controlling glucose tolerance in man. Measurement of insulin sensitivity and β -cell glucose sensitivity from the response to intravenous glucose, *J. Clin. Invest.* 68 (6) (1981) 1456–1467, <http://dx.doi.org/10.1172/JCI110398>, [arXiv: Bergman1981](https://arxiv.org/abs/1981).
- [19] L. Heinemann, Variability of insulin absorption and insulin action, *Diabetes Technol. Ther.* 4 (5) (2002) 673–682, <http://dx.doi.org/10.1089/152091502320798312>.
- [20] A.R. Sedaghat, A. Sherman, M.J. Quon, A mathematical model of metabolic insulin signaling pathways, *Am. J. Physiol. - Endocrinol. Metab.* 283 (5) (2002) 1084–1101, <http://dx.doi.org/10.1152/ajpendo.00571.2001>.
- [21] C. Ronald Kahn, Membrane receptors for hormones and neurotransmitters, *J. Cell Biol.* 70 (2) (1976) 261–286, <http://dx.doi.org/10.1083/jcb.70.2.261>.
- [22] J. Nocedal, S. Wright, Numerical Optimization, in: Springer Series in Operations Research and Financial Engineering, Springer New York, 2006.
- [23] J.R. Dormand, P.J. Prince, A family of embedded Runge-Kutta formulae, *J. Comput. Appl. Math.* 6 (1) (1980) 19–26.
- [24] A. Ranjan, S. Schmidt, C. Damm-Frydenberg, I. Steineck, T.R. Clausen, J.J. Holst, S. Madsbad, K. Norgaard, Low-carbohydrate diet impairs the effect of glucagon in the treatment of insulin-induced mild hypoglycemia: A randomized crossover study, *Diabetes Care* 40 (1) (2017) 132–135, <http://dx.doi.org/10.2337/dc16-1472>.
- [25] J.R. Castle, J.E. Youssef, P.A. Bakhtiani, Y. Cai, J.M. Stobbe, D. Branigan, K. Ramsey, P. Jacobs, R. Reddy, M. Woods, W.K. Ward, Effect of repeated glucagon doses on hepatic glycogen in type 1 Diabetes: Implications for a bihormonal Closed-Loop system, *Diabetes* 64 (11) (2015) 2115–2119, <http://dx.doi.org/10.2337/dc15-0754>.
- [26] S. Contreras, D. Medina-Ortiz, C. Conca, A. Olivera-Nappa, A novel synthetic model of the glucose-insulin system for patient-wise inference of physiological parameters from small-size OGTT data, *Front. Bioeng. Biotechnol.* 8 (2020) <http://dx.doi.org/10.3389/fbioe.2020.00195>.

APPENDIX D

Journal Paper - In preparation

Mathematical meal models for simulation of human metabolism

Authors:

Tobias K. S. Ritschel, Asbjørn Thode Reenberg, Peter Emil Carstensen, Jacob Bendsen, John Bagterp Jørgensen

Published in:

In preparation.

Mathematical meal models for simulation of human metabolism

Tobias K. S. Ritschel^a, Asbjørn Thode Reenberg^a, Peter Emil Carstensen^a, Jacob Bendsen^a and John Bagterp Jørgensen^{a,*}

^aDepartment of Applied Mathematics and Computer Science, Technical University of Denmark, Matematiktorvet, Building 303B, Kgs. Lyngby, DK-2800, Denmark

ARTICLE INFO

Keywords:

Gastrointestinal glucose absorption
Mathematical modeling
Simulation
Diabetes
Obesity

ABSTRACT

We present and critically discuss five commonly used mathematical models of the meal glucose rate of appearance in humans. Such models are key to simulation of the metabolism in healthy people, people with diabetes, and obese people, and they are central to developing effective treatments and prevention strategies. Furthermore, we discuss important aspects of systematic mathematical modeling of human metabolism, including meal consumption modeling, stoichiometry and reaction kinetics, and general-purpose model components.

1. Introduction

Mathematical modeling and simulation of the human metabolism are central to treating and preventing two of the major pandemics of the 21st century; diabetes and obesity (Pattaranit and van den Berg, 2008). Model-based simulation can both support scientific developments within physiology, help to improve drug development processes (Huang et al., 2009), and be used directly in support tools, e.g., in automated insulin delivery systems for people with diabetes (Lal et al., 2019). Specifically, modeling is a key component of virtual clinical trials (Reenberg et al., 2022; Ritschel et al., 2022), rigorous mathematical analysis (Cohen and Li, 2021), and of model-based algorithms for, e.g., monitoring, prediction, control, and optimization (Boiroux et al., 2018).

The human metabolism is a complex set of chemical reactions that are responsible for sustaining life. Their purposes are to 1) digest food, 2) convert the energy in the food into a form that can be used in cellular processes, 3) convert food into building blocks for nucleic acids, proteins, carbohydrates, and lipids, 4) transport substances into and between cells, and 5) eliminate waste from metabolic processes. Food digestion and absorption are particularly important to mathematical modeling in diabetes and obesity (Gouseti et al., 2019; Le Feunteun et al., 2020). Many models describe the dynamics of glucose and insulin and disregard other macronutrients (fat and protein) and hormones (e.g., glucagon, ghrelin, and incretins). Furthermore, it is common to describe meal glucose absorption using simple algebraic relations (Silber et al., 2010) or to only consider intravenous glucose injection (Silber et al., 2007). However, models that include the dynamics of glucagon (Adams and Lasseigne, 2018), ghrelin (Barnabei et al., 2022), and incretins (Jauslin et al., 2007), as well as the absorption of other macronutrients (Sicard et al., 2018), have also been

proposed. Recently, Pompa et al. (2021) compared three models commonly used in diabetes using a simulation study. However, they conclude that it is not possible to determine which of the models that is more physiologically accurate based on simulations alone. Noguchi et al. (2014) propose a model which accounts for the digestion and absorption of carbohydrates based on the glycemic index and carbohydrate bioavailability. Moxon et al. (2016) propose three models which include transport along the small intestine. Later, both Noguchi et al. (2016) and Moxon et al. (2017) extended their respective models with an upper bound on the glucose rate of appearance in the blood stream. We refer to the reviews by Smith et al. (2009), Palumbo et al. (2013), and Huard and Kirkham (2022) for further information on models in the literature.

Apart from the physiological phenomena included in the models, there are several differences between the underlying mathematical formulations. Some models are purely compartmental (De Gaetano et al., 2013) and described only by ordinary differential equations (ODEs). Others also use partial differential equations (PDEs), e.g., to describe the transport through the small intestine (Moxon et al., 2016). Similarly, there are models that represent delays exactly (Contreras et al., 2020; Cohen and Li, 2021) using delay differential equations (DDEs), and, in other cases, they are approximated (Alskär et al., 2016). Furthermore, meal consumption can either be represented as a finite flow rate of nutrients (Hovorka et al., 2004) or as instantaneous (Dalla Man et al., 2014). Finally, while most models are deterministic, some also include stochasticity (uncertainty), e.g., to model variations in the meal size and consumption time (Chudtong and De Gaetano, 2021). These different mathematical formulations are also discussed in the review by Makroglou et al. (2006).

In this work, we present a critical discussion of five commonly used mathematical models of meal glucose absorption: 1) the model proposed by Hovorka et al. (2004), 2) the UVA/Padova model presented by Dalla Man et al. (2006, 2007), 3) the SIMO model described by De Gaetano et al. (2013) and used in the revised Sorensen model by Panunzi et al. (2020), 4) the model by Alskär et al. (2016), and

*Corresponding author

✉ jbj@dtu.dk (J.B. Jørgensen)

ORCID(s): 0000-0002-5843-240X (T.K.S. Ritschel);

0000-0003-0015-7107 (A.T. Reenberg); 0000-0001-7511-2910 (J.B. Jørgensen)

Mathematical meal models

5) a model which represents the stomach as a continuous stirred-tank reactor (CSTR) and the small intestine as a plug-flow reactor (PFR) (Moxon et al., 2016, 2017). In the last model, we compare different models of the opening and closing of the pylorus valve, which connects the stomach to the duodenum in the small intestine. Furthermore, we discuss general aspects of mathematical modeling relevant to the human metabolism (representation of meals, delays, and general modeling components).

The remainder of the paper is structured as follows. In Section 2, we discuss the simulation of mathematical meal models, and in Section 3, we present modeling components that are relevant to modeling of the human metabolism in general. In Section 4, we present the five models of meal glucose absorption mentioned above, and in Section 5, we discuss and compare them based on simulations. Finally, we present conclusions in Section 6.

2. Mathematical models and simulation

We consider mathematical models of the meal nutrient absorption in the gastrointestinal tract, which are in the form of initial value problems involving ODEs:

$$\dot{x}(t) = f(x(t), d(t), p_f), \quad x(t_0) = x_0. \quad (1)$$

Here, t is time, x are the states, d are the meal inputs, and p_f are the parameters in the model, f . x_0 are the states at time t_0 . The states constitute the minimal amount of information necessary for simulating the future evolution of the system (1).

The outputs, y , are described by the function

$$y(t) = g(x(t), p_g), \quad (2)$$

where p_g is a parameter vector. The purpose of the model is to describe the relation between the outputs, y , and 1) the meal inputs, d , and 2) the parameters, p_f and p_g , which are specific to each person (and possibly also to each meal).

Remark 1. Models that contain PDEs or DDEs can be approximated by models that only contain ODEs by means of spatial discretizations and delay approximations, respectively.

2.1. Typical structure of nonlinear models

Nonlinear models of meal nutrient absorption are often more structured than the system (1). Specifically, many nonlinear models are affine in the meal inputs:

$$\begin{aligned} \dot{x}(t) &= f(x(t), d(t), p_f) \\ &= f_x(x(t), p_{f_x}) + f_d(x(t), p_{f_d})d(t), \quad x(t_0) = x_0. \end{aligned} \quad (3)$$

The first term describes the internal dynamics of the meal absorption and the second term describes the direct effect of the meal inputs on the states, e.g., the relation between the amount of glucose in the meal and in the stomach. The parameter vectors p_{f_x} and p_{f_d} contain the same parameters as p_f .

2.2. Linear models

Several meal models are linear in the states, x , and the meal inputs, d :

$$\dot{x}(t) = A_c(p_{f_x})x(t) + B_c(p_{f_d})d(t), \quad x(t_0) = x_0, \quad (4a)$$

$$y(t) = C_c(p_g)x(t). \quad (4b)$$

The subscript c on the system matrices, A_c , B_c , and C_c , indicate that it is a *continuous-time* linear state space model (as opposed to a *discrete-time* state space model).

Remark 2. The linear state space model (4) is a special case of the nonlinear model (1)–(2) where

$$f(x(t), d(t), p_f) = A_c(p_{f_x})x(t) + B_c(p_{f_d})d(t), \quad (5a)$$

$$g(x(t), p_g) = C_c(p_g)x(t). \quad (5b)$$

The dynamical equation in the linear state space model (4a) is also a special case of the meal input-affine model (3) where

$$f_x(x(t), p_{f_x}) = A_c(p_{f_x})x(t), \quad (6a)$$

$$f_d(x(t), p_{f_d}) = B_c(p_{f_d}). \quad (6b)$$

2.3. Meal inputs

Some models of meal nutrient absorption represent the meal inputs as flow rates, i.e., as step functions, and others represent them as instantaneous, i.e., as impulses.

2.3.1. Step inputs

When the meal inputs are represented using step functions, they are described by

$$d(t) = d_k = D_k/\Delta t, \quad t_k \leq t < t_{k+1}, \quad (7)$$

where D_k is the total meal size ingested in the interval $[t_k, t_{k+1}[$ and $\Delta t = t_{k+1} - t_k$. The response to a sequence of piecewise constant meal inputs of sizes $\{D_k\}_{k=0}^{M-1}$ may be simulated by setting $x(t_0) = x_0$ and solving the M initial value problems

$$x(t_k) = x_k, \quad (8a)$$

$$\dot{x}(t) = f(x(t), d_k, p_f), \quad t_k \leq t < t_{k+1}, \quad (8b)$$

$$x_{k+1} = x(t_{k+1}), \quad (8c)$$

for $k = 0, 1, \dots, M-1$. The result is the sequence of states $\{x_k\}_{k=0}^M$ that may be used to compute the corresponding sequence of outputs $\{y_k\}_{k=0}^M$ from (2).

2.3.2. Impulse inputs

For this type of meal input model, we only consider the input-affine model (3). A single meal of size D , which is consumed instantaneously at time t_0 , can be represented as an impulse,

$$d(t) = D\delta(t - t_0), \quad (9)$$

using the Dirac delta function, $\delta(t)$. We denote by t_0^- the time t_0 before the impulse and by t_0^+ the time t_0 immediately

Mathematical meal models

after the impulse. The impulse function has three relevant properties:

$$d(t_0) = \infty, \quad (10a)$$

$$d(t) = 0, \quad t_0 < t, \quad (10b)$$

$$\int_{t_0^-}^{t_0^+} d(t) dt = D. \quad (10c)$$

Consequently, the states immediately before and after the impulse are

$$x(t_0^-) = x_0^- = x_0, \quad (11a)$$

$$x(t_0^+) = x_0^+ = x_0^- + f_d(x_0^-, p_{f_d})D. \quad (11b)$$

Therefore, the initial value problem (3) with the meal input function (9) can be simulated by solving the initial value problem

$$\dot{x}(t) = f(x(t), 0, p_f) = f_x(x(t), p_{f_x}), \quad x(t_0^+) = x_0^+, \quad (12)$$

for $t \geq t_0^+$. The corresponding output, $y(t)$, computed by (2) is called the impulse response of the system (3) and (2) to the meal impulse, D , provided that $x(t_0) = x_0 = x_{ss}$ is a steady state, i.e., that x_{ss} satisfies $f(x_{ss}, 0, p_f) = f_x(x_{ss}, p_{f_x}) = 0$.

Multiple instantaneous meals (i.e., impulses) of sizes $\{D_k\}_{k=0}^{M-1}$ at times $\{t_k\}_{k=0}^{M-1}$ can be represented by the input function

$$d(t) = \sum_{k=0}^{M-1} D_k \delta(t - t_k). \quad (13)$$

This input function has the three properties

$$d(t_k) = \infty, \quad (14a)$$

$$d(t) = 0, \quad t_k < t < t_{k+1}, \quad (14b)$$

$$\int_{t_k^-}^{t_k^+} d(t) dt = D_k. \quad (14c)$$

The definitions of t_k^- and t_k^+ are analogous to those of t_0^- and t_0^+ , respectively. Because of these properties, the system (3) with the multiple meal impulse input function (13) may be simulated by using that $x_0^- = x_0$ and solving the M initial value problems

$$x(t_k^+) = x_k^- + f_d(x_k^-, p_{f_d})D_k, \quad (15a)$$

$$\dot{x}(t) = f_x(x(t), p_{f_x}), \quad t_k^+ < t < t_{k+1}^-, \quad (15b)$$

$$x_{k+1}^- = x(t_{k+1}^-), \quad (15c)$$

for $k = 0, \dots, M-1$. As mentioned previously,

$$f_x(x(t), p_{f_x}) = f(x(t), 0, p_f), \quad (16)$$

which means that the simulation can be carried out with the general dynamic model (1) using $d(t) = 0$ for $t_k < t < t_{k+1}$.

3. Model components

As the human metabolism is a set of chemical reactions, the gastrointestinal tract can be modeled mathematically using modeling techniques from chemical reaction engineering. In this section, we briefly outline a systematic modeling approach using stoichiometry and reaction kinetics in combination with ideal CSTRs and PFRs. Furthermore, delays play an important role in metabolic modeling (Voit, 2017), and we describe several mathematical models and approximations of delayed signals.

3.1. Stoichiometry and reaction kinetics

Consider a set of molecules C which are involved in a set of reactions R in the human metabolism. Let $S \in \mathbb{R}^{n_r \times n_c}$ be the matrix of stoichiometric coefficients for this set of reactions and molecules. n_c is the number of molecules and n_r is the number of reactions. Let c be the vector of concentrations such that we can express the rate vector, r , for this set of reactions as the function

$$r = r(c). \quad (17)$$

Consequently, the production rate vector for the molecules can be expressed as

$$R = S'r. \quad (18)$$

This general way of expressing the production rate, R , is useful because it only requires the specification of the chemical reaction stoichiometry (and the corresponding stoichiometric matrix, S) as well as the corresponding expression for the reaction rates, $r = r(c)$.

3.2. CSTR

Any part of the gastrointestinal tract where transport phenomena (i.e., advection and diffusion) are negligible can be represented as a CSTR. The mass balance for a CSTR is

$$V\dot{c} = (c_{in} - c)F + RV, \quad (19)$$

where V is volume, c is concentration, c_{in} is the inflow concentration, F is the volumetric in- and outflow rate, and R is the production rate. The volume is assumed to be constant, and the model can be reformulated as an ODE:

$$\dot{c} = (c_{in} - c)F/V + R. \quad (20)$$

3.3. PFR

The parts of the gastrointestinal tract where advective and diffusive transport phenomena are significant can be described as PFRs. A PFR is cylindrical and the concentration, $c = c(t, z, r, \theta) = c(t, z)$, only changes along the transport direction, z , i.e., it is constant along the radial and angular coordinates, r and θ .

The spatiotemporal evolution of the concentration is described by the PDE

$$\partial_t c = -\partial_z N + R + Q, \quad (21)$$

Mathematical meal models

where N is flux, R is the production rate, and Q is a source term. The flux is the sum of an advection term, N_a , and a diffusion term, N_d :

$$N = N_a + N_d. \quad (22)$$

These terms are

$$N_a = v c, \quad (23a)$$

$$N_d = -D_c \partial_z c, \quad (23b)$$

where v is velocity and D_c is the diffusion coefficient. The expression (23b) is called Fick's law.

3.4. Delays

Here, we describe different formulations and approximations of a model, where y is equal to the input signal u delayed by τ_d , i.e.,

$$y(t) = u(t - \tau_d). \quad (24)$$

The Laplace transform of (24) is

$$Y(s) = G(s)U(s), \quad (25a)$$

$$G(s) = e^{-\tau_d s}. \quad (25b)$$

Alternatively, the system (24) can be formulated as a series of M systems with smaller time delays:

$$y_i(t) = y_{i-1}(t - \tau_d/M), \quad i = 1, \dots, M, \quad (26)$$

where

$$y_0(t) = u(t), \quad (27a)$$

$$y(t) = y_M(t). \quad (27b)$$

The Laplace transform of this series of systems are

$$Y_i(s) = G_i(s)Y_{i-1}(s), \quad i = 1, \dots, M, \quad (28a)$$

$$G_i(s) = e^{-(\tau_d/M)s}, \quad (28b)$$

where

$$Y_0(s) = U(s), \quad (29a)$$

$$Y(s) = Y_M(s). \quad (29b)$$

Approximating G_i in (28) will typically result in a lower error than approximating G in (25) because the delay is smaller. However, the increased accuracy comes at the expense of higher computational cost. Below, we show different approximations based on a dynamical system in the form

$$\dot{x}(t) = A_c x(t) + B_c u(t), \quad (30a)$$

$$\tilde{y}(t) = C_c x(t) + D_c u(t). \quad (30b)$$

3.4.1. Lag approximation

The transfer function in (25b) can be approximated by the transfer function of a lag process, i.e.,

$$G(s) \approx \frac{1}{\tau_d s + 1} = \frac{1/\tau_d}{s + 1/\tau_d} = \frac{P(s)}{Q(s)} = \tilde{G}(s). \quad (31)$$

The system matrices in the corresponding linear state space realization, in observable canonical form (Hendricks et al., 2008, Chap. 3.9), are

$$A_c = -1/\tau_d, \quad B_c = 1/\tau_d, \quad (32a)$$

$$C_c = 1, \quad D_c = 0. \quad (32b)$$

We use the same approximation to the system (28):

$$\begin{aligned} G_i(s) &\approx \frac{1}{(\tau_d/M)s + 1} = \frac{M/\tau_d}{s + M/\tau_d} = \frac{P_i(s)}{Q_i(s)} \\ &= \tilde{G}_i(s). \end{aligned} \quad (33)$$

Again, we consider the corresponding state space realization in observable canonical form. In this case, the system matrices are

$$A_{c,ij} = \begin{cases} -M/\tau_d, & i = j, \\ M/\tau_d, & i = j - 1, \\ 0, & \text{otherwise,} \end{cases} \quad (34a)$$

$$B_{c,i} = \begin{cases} M/\tau_d, & i = 1, \\ 0, & \text{otherwise,} \end{cases} \quad (34b)$$

$$C_{c,i} = \begin{cases} 1, & i = M, \\ 0, & \text{otherwise,} \end{cases} \quad (34c)$$

$$D_c = 0, \quad (34d)$$

for $i = 1, \dots, M$ and $j = 1, \dots, M$.

3.4.2. Padé approximation

The Padé approximation (Wei et al., 2016) is another classical way used to approximate time delays. The first-order Padé approximation of $G(s) = e^{-\tau_d s}$ is

$$G(s) \approx \frac{-(\tau_d/2)s + 1}{(\tau_d/2)s + 1} = \frac{-s + 2/\tau_d}{s + 2/\tau_d} = \frac{P(s)}{Q(s)} = \tilde{G}(s). \quad (35)$$

The first-order Padé approximation (35) may be used to approximately realize (25) as the linear state space model (30), in observable canonical form, with the system matrices

$$A_c = -2/\tau_d, \quad B_c = 4/\tau_d, \quad (36a)$$

$$C_c = 1, \quad D_c = -1. \quad (36b)$$

The Padé approximation of G_i in (28) is

$$\begin{aligned} G_i(s) &\approx \frac{-(\tau_d/(2M))s + 1}{(\tau_d/(2M))s + 1} = \frac{-s + 2M/\tau_d}{s + 2M/\tau_d} \\ &= \frac{P_i(s)}{Q_i(s)} = \tilde{G}_i(s), \end{aligned} \quad (37)$$

Mathematical meal models

and the system matrices in the corresponding state space realization (in observer canonical form) are

$$A_{c,ij} = \begin{cases} -2M/\tau_d, & i = j, \\ (-1)^{i+j+1}4M/\tau_d, & i > j, \\ 0, & \text{otherwise,} \end{cases} \quad (38a)$$

$$B_{c,i} = (-1)^{i+1}4M/\tau_d, \quad (38b)$$

$$C_{c,i} = (-1)^{M+i}, \quad (38c)$$

$$D_c = (-1)^M, \quad (38d)$$

for $i = 1, \dots, M$ and $j = 1, \dots, M$.

3.4.3. Physical transport delay model

Delays can also be represented using transport processes. The input signal, u , constitutes the boundary condition,

$$c_{in}(t) = u(t), \quad (39)$$

and the initial boundary value problem

$$c(t, 0) = c_{in}(t), \quad (40a)$$

$$\partial_t c = -v\partial_z c, \quad t \geq 0, \quad 0 \leq z \leq L, \quad (40b)$$

has the analytical solution $y(t) = c(t, L) = c_{in}(t - \tau_d) = u(t - \tau_d)$ with the delay $\tau_d = L/v$.

Remark 3. A left-sided first-order finite difference discretization of the PDE (40), based on an equidistant grid with $M + 1$ nodes, is equivalent to the linear state space model (30) with the system matrices (34) obtained using a series of M lag approximations.

3.4.4. Algebraic delay approximation

For completeness, we also describe an algebraic delay approximation which is used in the literature, e.g., by Alskär et al. (2016). However, unlike the previous approximations, it is an algebraic expression rather than a linear state space model in the form (30). Furthermore, it specifically approximates a step in the input function, u , whereas the other approximations can be used for arbitrary input functions.

Let t_s denote the time at which the step in u occurs, i.e., $u(t) = 1$ for $t \geq t_s$ and $u(t) = 0$ otherwise. Then, the approximation is

$$y(t) \approx \frac{1}{1 + \exp(-\sigma(t - t_{50}))} = \tilde{y}(t), \quad (41)$$

where $t_{50} = t_s + \tau_d$ is the time at which \tilde{y} is halfway between the value of u before and after the step.

4. Meal models

In this section, we present five commonly used models of glucose absorption in the gastrointestinal tract: The model by Hovorka et al. (2004), the model by Dalla Man et al. (2006, 2007), the SIMO model by De Gaetano et al. (2013), the model by Alskär et al. (2016), and a CSTR-PFR model based on the ones proposed by Moxon et al. (2016, 2017).

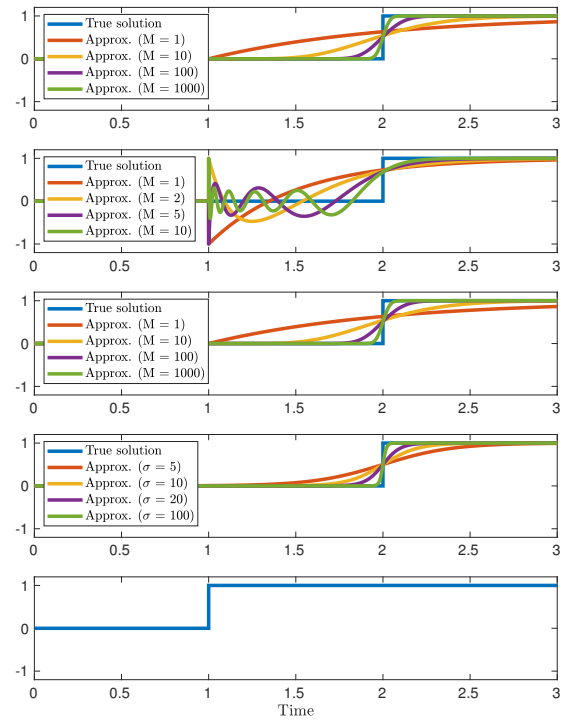


Figure 1: True, y , and approximate, \tilde{y} , delays of the input, u . Top: Lag approximation. Second from the top: Padé approximation. Third from the top: Finite difference discretization of physical transport delay model. Fourth from the top: Algebraic delay approximation. Bottom: Input, u .

For the CSTR-PFR model, we consider different descriptions of the pylorus sphincter (or valve) which connects the stomach to the small intestine.

Several of the models are linear. Specifically, they are in the form

$$\dot{x}(t) = A_c x(t) + B_c d(t), \quad (42a)$$

$$y(t) = C_c x(t), \quad (42b)$$

where d is the meal input and y is the glucose rate of appearance in the blood plasma. Furthermore, in Appendix B, we show that, for some of the models, y is a linear function of the total meal carbohydrate content, D . For brevity of notation, we omit the time dependency in the remainder of this section.

4.1. Hovorka's model

The model by Hovorka et al. (2004) contains two compartments, as illustrated in Fig. 2. The first compartment, D_1 , describes the amount of glucose in the stomach, and the second compartment, D_2 , describes the amount of glucose in the small intestine:

$$\dot{D}_1 = A_G d - R_{12}, \quad (43a)$$

$$\dot{D}_2 = R_{12} - R_2. \quad (43b)$$

Mathematical meal models

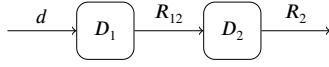


Figure 2: Sketch of the meal model presented by Hovorka et al. (2004).



Figure 3: Sketch of the meal model presented by Dalla Man et al. (2006).

Here, A_G describes the bioavailability of the carbohydrates in the meal, and $R_{12} = R_{12}(D_1)$ is the glucose flow rate between the stomach and the small intestine. Furthermore, $R_2 = R_2(D_2)$ describes the glucose absorption, and the glucose rate of appearance, $R_A = R_A(D_2)$, is a fraction, f , of R_2 :

$$R_{12} = D_1/\tau_D, \quad (44a)$$

$$R_2 = D_2/\tau_D, \quad (44b)$$

$$R_A = f R_2. \quad (44c)$$

The parameter τ_D is a time constant, and the model is a linear state space model in the form (42), where the system matrices are

$$A_c = \begin{bmatrix} \frac{-1}{\tau_D} & 0 \\ \frac{1}{\tau_D} & \frac{-1}{\tau_D} \end{bmatrix}, \quad B_c = \begin{bmatrix} A_G \\ 0 \end{bmatrix}, \quad C_c = \begin{bmatrix} 0 & f \end{bmatrix}. \quad (45)$$

4.2. Dalla Man's model

The model by Dalla Man et al. (2006, 2007) is sketched in Fig. 3, and it contains three compartments: The glucose in the solid and liquid phases of the stomach content, $Q_{sto,1}$ and $Q_{sto,2}$, respectively, and the amount of glucose in the small intestine, Q_{gut} . The compartments are described by

$$\dot{Q}_{sto,1} = d - R_{12}, \quad (46a)$$

$$\dot{Q}_{sto,2} = R_{12} - R_{sto,gut}, \quad (46b)$$

$$\dot{Q}_{gut} = R_{sto,gut} - R_{gut,pla}, \quad (46c)$$

where $R_{12} = R_{12}(Q_{sto,1})$ is the glucose flow rate between the liquid and solid phase in the stomach, $R_{sto,gut} = R_{sto,gut}(Q_{sto,1}, Q_{sto,2}, D)$ is the flow rate between the stomach and the small intestine, and D is the total carbohydrate content of the meal. Furthermore, $R_{gut,pla} = R_{gut,pla}(Q_{gut})$ is the glucose absorption rate, and the glucose rate of appearance in the blood plasma, $R_A = R_A(Q_{gut})$, is a fraction, f , of the glucose absorption rate:

$$R_{12} = k_{gri} Q_{sto,1}, \quad (47a)$$

$$R_{sto,gut} = k_{empt} Q_{sto,2}, \quad (47b)$$

$$R_{gut,pla} = k_{abs} Q_{gut}, \quad (47c)$$

$$R_A = f R_{gut,pla}. \quad (47d)$$

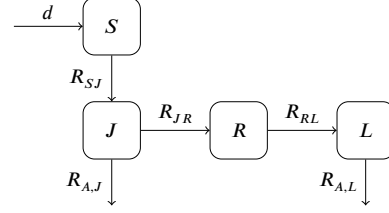


Figure 4: Sketch of the SIMO meal model presented by De Gaetano et al. (2013).

Here, k_{gri} and k_{abs} are the inverses of time constants, and the gastric emptying rate, $k_{empt} = k_{empt}(Q_{sto}, D)$, is

$$k_{empt} = k_{min} + \frac{k_{max} - k_{min}}{2} \left(\tanh(\alpha(Q_{sto} - bD)) - \tanh(\beta(Q_{sto} - cD)) + 2 \right), \quad (48a)$$

$$\alpha = \frac{5}{2D(1-b)}, \quad (48b)$$

$$\beta = \frac{5}{2Dc}, \quad (48c)$$

where $Q_{sto} = Q_{sto}(Q_{sto,1}, Q_{sto,2})$ is the total amount of glucose in the stomach:

$$Q_{sto} = Q_{sto,1} + Q_{sto,2}. \quad (49)$$

Furthermore, the parameters k_{min} and k_{max} are the minimum and maximum gastric emptying rates, and b and c are the percentages of D where the magnitude of the derivative of k_{empt} is $\frac{1}{2}(k_{max} - k_{min})$, i.e., at $Q_{sto} = bD$ and $Q_{sto} = cD$. Finally, as k_{empt} in (48a) is nonlinear in Q_{sto} , the model is not in the linear form (42).

4.3. The SIMO model

The SIMO model by De Gaetano et al. (2013) contains four compartments, and it is sketched in Fig. 4. The compartments represent the amounts of glucose in 1) the stomach, S , 2) the jejunum, J , 3) an artificial delay compartment, R , and 4) the ileum, L :

$$\dot{S} = d - R_{sj}, \quad (50a)$$

$$\dot{J} = R_{sj} - R_{jr} - R_{A,J}, \quad (50b)$$

$$\dot{R} = R_{jr} - R_{RL}, \quad (50c)$$

$$\dot{L} = R_{RL} - R_{A,L}. \quad (50d)$$

Here, the glucose flow rates between the stomach and the jejunum, $R_{sj} = R_{sj}(S)$, between the jejunum and the delay compartment, $R_{jr} = R_{jr}(J)$, and between the delay compartment and the ileum, $R_{RL} = R_{RL}(R)$, as well as the glucose absorption rates in the jejunum, $R_{A,J} = R_{A,J}(J)$, and the ileum, $R_{A,L} = R_{A,L}(L)$, are given by

$$R_{sj} = k_{js} S, \quad (51a)$$

Mathematical meal models

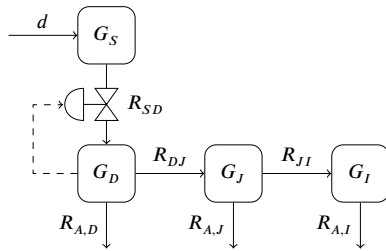


Figure 5: Sketch of the meal model presented by Alskär et al. (2016).

$$R_{JR} = k_{rj}J, \quad (51b)$$

$$R_{RL} = k_{lr}R, \quad (51c)$$

$$R_{A,J} = k_{gj}J, \quad (51d)$$

$$R_{A,L} = k_{gl}L. \quad (51e)$$

The coefficients, k_{js} , k_{rj} , k_{lr} , k_{gj} , and k_{gl} are the inverses of time constants, and the glucose rate of appearance, $R_A = R_A(J, L)$, is a fraction, f , of the total glucose absorption:

$$R_A = f(R_{A,J} + R_{A,L}). \quad (52)$$

This model is in the linear form (42), and the system matrices are given by

$$A_c = \begin{bmatrix} -k_{js} & 0 & 0 & 0 \\ k_{js} & -(k_{gj} + k_{rj}) & 0 & 0 \\ 0 & k_{rj} & -k_{lr} & 0 \\ 0 & 0 & k_{lr} & -k_{gl} \end{bmatrix}, \quad (53a)$$

$$B_c = \begin{bmatrix} 1 \\ 0 \\ 0 \\ 0 \end{bmatrix}, \quad (53b)$$

$$C_c = [0 \quad f k_{gj} \quad 0 \quad f k_{gl}]. \quad (53c)$$

4.4. Alskär's model

The model by Alskär et al. (2016) contains four compartments representing the amounts of glucose in the stomach, G_S , the duodenum, G_D , the jejunum, G_J , and the ileum, G_I , as illustrated in Fig. 5. They are described by

$$\dot{G}_S = d - R_{SD}, \quad (54a)$$

$$\dot{G}_D = R_{SD} - R_{DJ} - R_{A,D}, \quad (54b)$$

$$\dot{G}_J = R_{DJ} - R_{JI} - R_{A,J}, \quad (54c)$$

$$\dot{G}_I = R_{JI} - R_{A,I}, \quad (54d)$$

where the glucose flow rates between the stomach and duodenum, $R_{SD} = R_{SD}(G_S)$, between the duodenum and jejunum, $R_{DJ} = R_{DJ}(G_D)$, and between the jejunum and ileum, $R_{JI} = R_{JI}(G_J)$, are

$$R_{SD} = k_{SD}\tau G_S, \quad (55a)$$

$$R_{DJ} = k_{DJ}G_D, \quad (55b)$$

$$R_{JI} = k_{JI}G_J. \quad (55c)$$

The inverses of the time constants, $k_{SD} = k_{SD}(G_D)$, k_{DJ} , and k_{JI} , are

$$k_{SD} = k_w \left(1 - \frac{G_D^\gamma}{IG_{D50}^\gamma + G_D^\gamma} \right), \quad (56a)$$

$$k_{DJ} = \frac{1}{L_D T}, \quad (56b)$$

$$k_{JI} = \frac{1}{L_J T}. \quad (56c)$$

Here, k_{SD} represents the pylorus sphincter, and it is a function of the amount of glucose in the duodenum described using the Hill expression. For $G_D = 0$, k_{SD} is equal to its nominal value, k_w , and, as G_D increases, k_{SD} approaches zero. For large values of the Hill coefficient, γ , k_{SD} has a steep decrease around IG_{D50} . Furthermore, L_D and L_J are the relative lengths of the duodenum and jejunum (i.e., fractions of the total length of the small intestine), and T is the transit time through the small intestine. The lag coefficient (used to approximate a time delay) is given by

$$\tau = \frac{1}{1 + \exp(-\sigma(t - t_{50}))}, \quad (57)$$

as described in Section 3.4.4. The parameter σ determines the steepness, and t_{50} is the time at which τ is 0.5. The glucose absorption rates in the duodenum, $R_{A,D} = R_{A,D}(G_D)$, jejunum, $R_{A,J} = R_{A,J}(G_J)$, and ileum, $R_{A,I} = R_{A,I}(G_I)$, are described using Michaelis-Menten expressions, i.e.,

$$R_{A,D} = \frac{R_{D,\max} G_D}{K_{mG} + G_D}, \quad (58a)$$

$$R_{A,J} = \frac{R_{J,\max} G_J}{K_{mG} + G_J}, \quad (58b)$$

$$R_{A,I} = \frac{R_{I,\max} G_I}{K_{mG} + G_I}, \quad (58c)$$

where K_{mG} is the Michaelis constant and $R_{D,\max}$, $R_{J,\max}$, and $R_{I,\max}$ are the maximum glucose absorption rates in the duodenum, jejunum, and ileum, respectively. Finally, the glucose rate of appearance in the blood plasma, $R_A = R_A(G_D, G_J, G_I)$, is a fraction, F_P , of the total glucose absorption:

$$R_A = F_P(R_{A,D} + R_{A,J} + R_{A,I}). \quad (59)$$

4.5. CSTR-PFR model

The CSTR-PFR model presented here consists of a CSTR representing the stomach and a PFR representing the small intestine, as shown in Fig. 6 (see also Section 3.2 and 3.3). It is based on the second model presented by Moxon et al. (2016), and we describe three ways of modeling the opening and closing of the pylorus sphincter, which connects the stomach to the small intestine.

The amount of glucose in the stomach, m_s , is given by

$$\dot{m}_s = F_m - F_{sd}, \quad (60a)$$

$$F_{sd} = k_{sd}m_s, \quad (60b)$$

Mathematical meal models

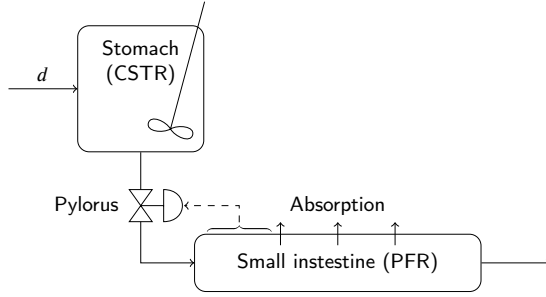


Figure 6: CSTR-PFR model with the feedback mechanism proposed by Alskär et al. (2016).

where $F_m = d$ is the meal input, F_{sd} is the glucose flow rate from the stomach to the duodenum, and k_{sd} is the inverse of a time constant. We either consider k_{sd} to be 1) constant (the pylorus sphincter is always completely open), 2) a function of the glucose rate of appearance in the blood (see Section 4.5.1), or 3) a function of the amount of glucose in the duodenum (see Section 4.5.2). The glucose concentration in the small intestine is described by the PDE

$$\partial_t c_{si} = -\partial_z N_p - Q_a, \quad z \in [z_0, z_f], \quad (61)$$

where z is the spatial coordinate along the small intestine, and the positions z_0 and z_f denote the beginning and end of the small intestine. The flux N_p describes the peristaltic movement in the small intestine, and it consists of an advection term, N_{ap} , and a diffusion term, N_{dp} :

$$N_p = N_{ap} + N_{dp}, \quad (62a)$$

$$N_{ap} = v_p c_{si}, \quad (62b)$$

$$N_{dp} = -D_p \partial_z c_{si}. \quad (62c)$$

The velocity, v_p , and the diffusion coefficient, D_p , are constant. The glucose absorption, Q_a , is given by

$$Q_a = \frac{2f}{r_{si}} q_a, \quad (63a)$$

$$q_a = v_a c_{si}, \quad (63b)$$

where r_{si} is the radius of the small intestine, and f is a factor describing 1) the increase in surface area (compared to that of a cylinder) due to villi, microvilli, and plicae circulares, and 2) the fact that glucose is only absorbed from a fraction of the surface. Furthermore, v_a is the glucose absorption rate. The flow rate from the stomach to the duodenum is represented as a boundary condition, i.e., the flux at the beginning of the small intestine times the cross-sectional area, A_{si} , must equal the glucose flow rate F_{sd} :

$$A_{si} N_p|_{z=z_0} = F_{sd}. \quad (64)$$

Finally, the glucose rate of appearance is the cross-sectional area times the integral of the glucose absorption rate over the

length of the small intestine:

$$R_A = A_{si} \int_{z_0}^{z_f} Q_a dz. \quad (65)$$

4.5.1. Moxon's feedback mechanism

Moxon et al. (2017) propose that the glucose flow rate between the stomach and duodenum is equal to 1) zero if the glucose rate of appearance, R_A , is above a certain threshold, $R_{A,max}$, and 2) k_{sd}^{max} otherwise. This is approximated by

$$k_{sd} = k_{sd}^{max} \frac{1}{1 + \exp(\sigma(R_A - R_{A,max}))}, \quad (66)$$

where the parameter σ determines the accuracy of the approximation, i.e., the steepness of k_{sd} around $R_{A,max}$.

4.5.2. Alskär's feedback mechanism

Alskär et al. (2016) propose that the glucose flow rate can be described using a Hill expression with a high Hill coefficient, γ , i.e., it approximates an on/off mechanism where the glucose flow rate is equal to zero if the amount of glucose in the duodenum, m_d , is above a threshold value, $m_{d,50}$, and k_{sd}^{max} otherwise. In addition to the original model of the feedback mechanism, we introduce a minimum value, k_{sd}^{min} :

$$k_{sd} = k_{sd}^{min} + (k_{sd}^{max} - k_{sd}^{min}) \left(1 - \frac{m_d^\gamma}{m_{d,50}^\gamma + m_d^\gamma} \right). \quad (67)$$

Finally, the duodenum constitutes the first part of the small intestine (from z_0 to z_d). Consequently, the amount of glucose in the duodenum is given by

$$m_d = A_{si} \int_{z_0}^{z_d} c_{si} dz. \quad (68)$$

Remark 4. If $k_{sd}^{min} = 0$ in (67), the glucose flow rate may become close to zero even though the duodenum is almost entirely empty. The reasons are that the velocity of the peristaltic movement, v_p , is relatively low and that it is independent of the glucose concentration. Consequently, a very short plug of chyme with a high glucose concentration will move through the duodenum, and once it enters into the jejunum, the duodenum again becomes empty, and the process repeats itself.

5. Discussion

Table 1 shows the main characteristics of the models described in Section 4: 1) the types of equations in the model, 2) the number of states, 3) whether it is a linear state space model or not, and 4) whether or not the glucose rate of appearance is linear in the total meal carbohydrate content, D . It is more straightforward to simulate models that only contain ODEs. The reason is that PDEs are typically approximated by a set of ODEs using spatial discretization (this

Mathematical meal models

is called the method of lines). However, this approximation is derived analytically, and it is problem-specific. In contrast, there exists general-purpose software for simulating models that only contain ODEs. In Appendix C and D, we describe two spatial discretization schemes that are relevant to meal models containing PDEs. The approximation often results in a large number of ODEs. Consequently, it is more computationally intensive to simulate models that contain PDEs because the computation time depends strongly on the number of states. Next, linear state space models are simpler to analyze than nonlinear models, and, in important special cases, explicit expressions for their solutions can be derived. Similarly, it can be exploited in both analysis and simulation if a model is linear in the total meal carbohydrate content, D . Specifically, if $R_A^{(1)}$ is the glucose rate of appearance over time for $D = 1$, the rate of appearance for any meal carbohydrate content is $R_A^{(1)}D$ if the model is linear in D .

Only the CSTR-PFR model contains a PDE (describing the glucose transport in the small intestine). Consequently, when discretized, it will contain more states than the other models, and it will be more computationally intensive to simulate. All the other models contain a small number of states. Furthermore, Hovorka's model and the SIMO model are linear. The CSTR-PFR model is also linear if the pylorus sphincter is modeled as always being open, i.e., if there is no feedback mechanism. The remaining models are nonlinear. Finally, Hovorka's and Dalla Man's models, the SIMO model, and the CSTR-PFR model without feedback are linear in the total meal carbohydrate content, D , (see Appendix B).

Fig. 7 shows the response to meals with different carbohydrate contents. The meal consumption is modeled as instantaneous (as described in Section 2.3). The parameter values used in the various models (see Appendix A) do not represent the same individual. Therefore, we show the glucose rate of appearance in the blood normalized with body weight. The meal responses predicted by the linear models, i.e., Hovorka's model, the SIMO model, and the CSTR-PFR model without feedback, are qualitatively similar. After an initial rise, the glucose rate of appearance slowly decays to zero. In contrast, Dalla Man's model predicts two peaks. After the initial rise, the rate of appearance decreases and then increases again before decaying to zero. The second peak represents the delayed carbohydrate absorption caused by, e.g., fat and protein in the meal. None of the other models predict more than one peak. In Alskär's model, there is a pronounced saturation effect, and the larger meals do not lead to significantly higher glucose absorption rates. Instead, the absorption is prolonged for larger meals. For the largest meal, the CSTR-PFR model using Moxon's feedback mechanism shows a similar saturation effect. However, for the two smaller meals, the saturation threshold is not reached and the simulations are almost identical to those obtained without a feedback mechanism. When Alskär's feedback mechanism is used in the CSTR-PFR model, the glucose rate of appearance does not saturate. Instead, after a fast but short rise where the duodenum is filled, it increases slowly. For larger meals,

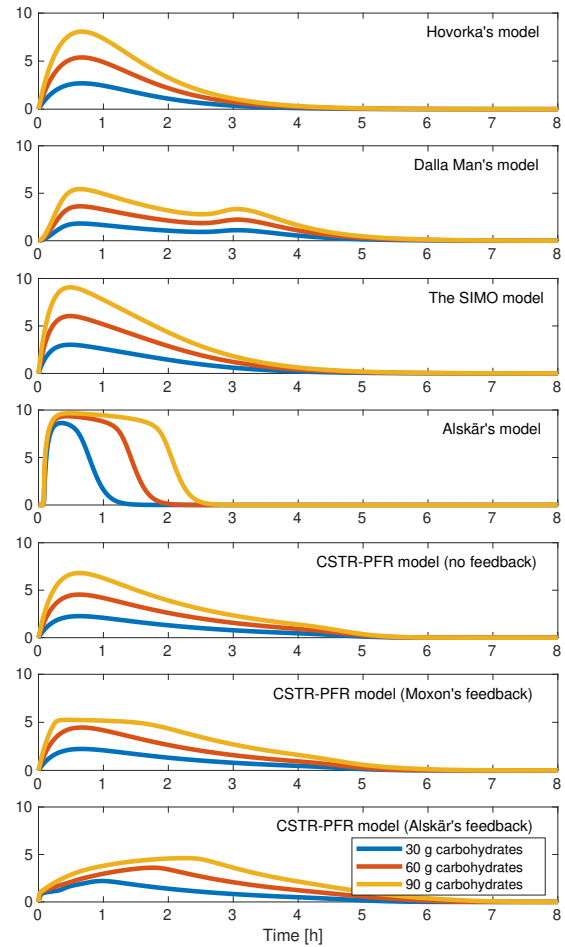


Figure 7: Glucose rate of appearance per body weight for different meal carbohydrate contents.

it increases for a longer time. Finally, the simulations clearly demonstrate that the glucose rate of appearance is linear in D for Hovorka's and Dalla Man's models, the SIMO model, and the CSTR-PFR model without feedback.

In Fig. 8, we compare the two meal input models discussed in Section 2.3, i.e., 1) the instantaneous model using an impulse function and 2) the constant flow rate model using a step function. The two representations are almost identical if the meal is consumed over 5 min. However, there is a pronounced lag for almost all of the models if the meal is consumed over 30 min. The exceptions are Alskär's model and the CSTR-PFR model using Alskär's feedback mechanism. The reason is that the feedback limits the amount of glucose that can enter into the duodenum. Consequently, the rate at which the stomach is filled has a smaller impact than in the other models.

Mathematical meal models

Table 1

Main characteristics of the meal models described in Section 4. For the CSTR-PFR model, the number of states depends on the discretization of the PDE (resulting in M ODEs). The models are considered linear if they are in the form of a linear state space model (42). The CSTR-PFR model is linear if k_{sd} in (60b) is constant and nonlinear if it is described by (66) or (67). In Appendix B, we show that the glucose rate of appearance is linear in the total meal carbohydrate content, D , for some of the models.

Model	Types of equations	Number of states	Linear	Linear in D
Hovorka et al. (2004)	ODEs	2	Yes	Yes
Dalla Man et al. (2006, 2007)	ODEs	3	No	Yes
De Gaetano et al. (2013)	ODEs	4	Yes	Yes
Alskär et al. (2016)	ODEs	4	No	No
CSTR-PFR (Moxon et al., 2016)	ODEs and PDEs	$1 + M$	Yes/no	Yes/no

6. Conclusions

We present a critical discussion of five commonly used mathematical models of gastrointestinal meal glucose absorption. We compare their predictions of the glucose rate of appearance in the blood plasma, and we provide an overview of key aspects of the models, including linearity and the types of equations in the models. The models are relevant to accurate simulation of the metabolism in healthy, diabetic, and obese people, and they can be used to test and develop treatment and prevention strategies. Furthermore, we discuss general modeling aspects relevant to systematic modeling of meal glucose absorption. Specifically, we discuss model structures, meal input representations, delay approximations, general formulations of stoichiometry and reaction kinetics, and general CSTR and PFR models which can represent different parts and processes in the human metabolism.

A. Parameter values

Table A.1 shows the parameter values used in the simulations presented in Section 5. Apart from the following exceptions, the parameter values are available in the papers referenced in the table. We use a value of σ in Alskär's model from an unpublished source, and we choose the value of k_{sd} in the CSTR-PFR model without feedback based on the interval considered by Moxon et al. (2016). In the CSTR-PFR model, D_p and $k_{sd,min}$ were not present in the original model. Therefore, we have chosen the values based on simulations. We have also chosen the value of σ in the CSTR-PFR model with Moxon's feedback mechanism. For models where the body weight, BW , is not provided, we use a value of 82 kg. Similarly, when f is not provided, we use a value of 1.

B. Linearity of the glucose rate of appearance

Here, we show that the glucose rate of appearance in the blood, as a function of time, is linear in the total meal carbohydrate content, D , for linear state space models and the model developed by Dalla Man et al. (2006, 2007), provided that the meal input, d , is linear in D . That is the case when d is an impulse or step function as described in Section 2.3. Consequently, the meal response can be

computed for $D = 1$ and scaled in order to obtain the response for any other value of D . For brevity of notation, we do not explicitly indicate the time-dependence of the states.

Remark 5. *There exist meal input functions, d , that are not linear in D . For instance, if d is a step function, the meal duration may increase linearly in D while the glucose flow rate remains constant.*

B.1. Linear models

The linear meal models are in the form

$$\dot{x} = A_c x + B_c d, \quad (\text{B.1a})$$

$$y = C_c x. \quad (\text{B.1b})$$

We introduce the normalized states, inputs, and outputs

$$\tilde{x} = x/D, \quad \tilde{d} = d/D, \quad \tilde{y} = y/D. \quad (\text{B.2a})$$

Note that, by assumption, \tilde{d} is independent of D . Then,

$$\dot{\tilde{x}} = \dot{x}/D = A_c \tilde{x} + B_c \tilde{d}, \quad (\text{B.3})$$

$$\tilde{y} = y/D = C_c \tilde{x}, \quad (\text{B.4})$$

and, given a simulation of this normalized system, the glucose rate of appearance can be obtained for any meal by scaling the normalized response, i.e., $y = \tilde{y}D$.

B.2. Dalla Man model

As for the linear state space models, we introduce the normalized state variables

$$q_{sto,1} = Q_{sto,1}/D, \quad q_{sto,2} = Q_{sto,2}/D, \quad (\text{B.5a})$$

$$q_{gut} = Q_{gut}/D, \quad q_{sto} = Q_{sto}/D, \quad (\text{B.5b})$$

and the normalized meal input $\tilde{d} = d/D$. Note that $q_{sto} = q_{sto,1} + q_{sto,2}$. The flow rates R_{12} and $R_{gut,pla}$ and the glucose rate of appearance, R_A , are linear in their arguments, and they do not depend directly on D , i.e.,

$$R_{12}(Q_{sto,1}) = R_{12}(q_{sto,1})D, \quad (\text{B.6})$$

$$R_{gut,pla}(Q_{gut}) = R_{gut,pla}(q_{gut})D, \quad (\text{B.7})$$

$$R_A(Q_{gut}) = R_A(q_{gut})D. \quad (\text{B.8})$$

In contrast, $R_{sto,gut}$ depends on the gastric emptying rate, $k_{empt} = k_{empt}(Q_{sto}, D)$, which 1) depends directly on D and

Mathematical meal models

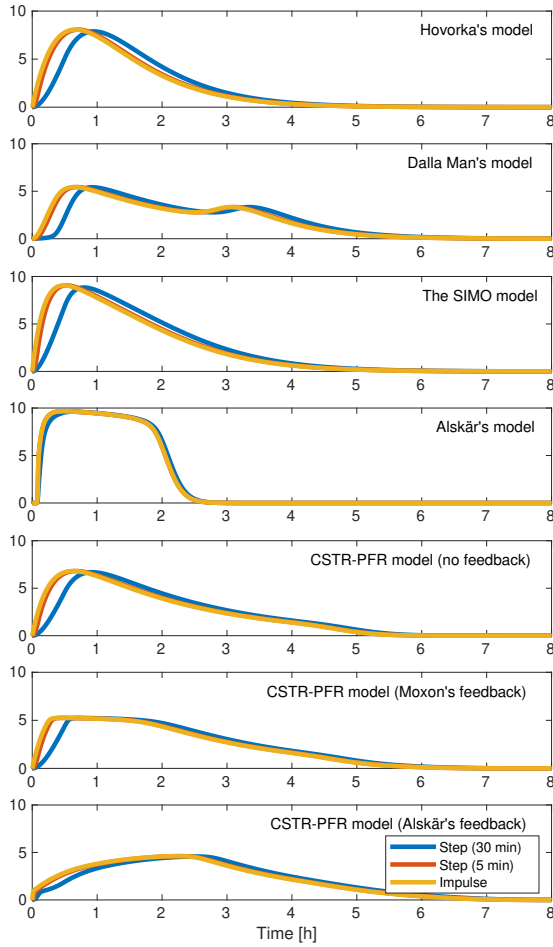


Figure 8: Responses to meals that are consumed instantaneously (i.e., modeled as an impulse function), over 5 min, and over 30 min (i.e., modeled as step functions). The meals contain 90 g carbohydrates.

2) is nonlinear in both its arguments. However, the arguments are not independent, and we show that k_{empt} is independent of D when $Q_{sto} = q_{sto}D$, i.e., that $k_{empt}(q_{sto}D, D) = k_{empt}(q_{sto})$. First, we note that

$$\alpha D = \frac{5}{2(1-b)}, \quad \beta D = \frac{5}{2c}. \quad (\text{B.9})$$

Next, using these expressions and substituting $Q_{sto} = q_{sto}D$,

$$\begin{aligned} \alpha(Q_{sto} - bD) &= \alpha(q_{sto}D - bD) = \alpha D(q_{sto} - b) \\ &= \frac{5}{2} \frac{q_{sto} - b}{1 - b}, \end{aligned} \quad (\text{B.10a})$$

$$\begin{aligned} \beta(Q_{sto} - cD) &= \beta(q_{sto}D - cD) = \beta D(q_{sto} - c) \\ &= \frac{5}{2} \frac{q_{sto} - c}{c}. \end{aligned} \quad (\text{B.10b})$$

Finally, we insert into the expression for the gastric emptying rate:

$$\begin{aligned} k_{empt} &= k_{min} + \frac{k_{max} - k_{min}}{2} \left(\tanh(\alpha(Q_{sto} - bD)) \right. \\ &\quad \left. - \tanh(\beta(Q_{sto} - cD)) + 2 \right) \\ &= k_{min} + \frac{k_{max} - k_{min}}{2} \left(\tanh\left(\frac{5}{2} \frac{q_{sto} - b}{1 - b}\right) \right. \\ &\quad \left. - \tanh\left(\frac{5}{2} \frac{q_{sto} - c}{c}\right) + 2 \right). \end{aligned} \quad (\text{B.11})$$

Clearly, k_{empt} is independent of D . Consequently, $R_{sto,gut}$ is linear in D for $Q_{sto,1} = q_{sto,1}D$ and $Q_{sto,2} = q_{sto,2}D$:

$$\begin{aligned} R_{sto,gut}(Q_{sto,1}, Q_{sto,2}, D) &= k_{empt}(Q_{sto}, D)Q_{sto,2} \\ &= k_{empt}(q_{sto}D, D)q_{sto,2}D \\ &= k_{empt}(q_{sto})q_{sto,2}D \\ &= R_{sto,gut}(q_{sto,1}, q_{sto,2})D. \end{aligned} \quad (\text{B.12})$$

In conclusion, the normalized variables are described by

$$\begin{aligned} \dot{q}_{sto,1} &= \dot{Q}_{sto,1}/D = d/D - R_{12}(Q_{sto,1})/D \\ &= \tilde{d} - R_{12}(q_{sto,1}), \end{aligned} \quad (\text{B.13a})$$

$$\begin{aligned} \dot{q}_{sto,2} &= \dot{Q}_{sto,2}/D \\ &= R_{12}(Q_{sto,1})/D - R_{sto,gut}(Q_{sto,1}, Q_{sto,2}, D)/D \\ &= R_{12}(q_{sto,1}) - R_{sto,gut}(q_{sto,1}, q_{sto,2}), \end{aligned} \quad (\text{B.13b})$$

$$\begin{aligned} \dot{q}_{gut} &= \dot{Q}_{gut}/D \\ &= R_{sto,gut}(Q_{sto,1}, Q_{sto,2}, D)/D \\ &\quad - R_{gut,pla}(Q_{gut})/D \\ &= R_{sto,gut}(q_{sto,1}, q_{sto,2}) - R_{gut,pla}(q_{gut}). \end{aligned} \quad (\text{B.13c})$$

Given a simulation of this system, the glucose rate of appearance for any meal carbohydrate content, D , can be computed as $R_A(q_{gut})D$.

C. Finite volume discretization

In this appendix, we present a finite volume discretization of the PFR model (21),

$$\partial_t c = -\partial_z N + Q, \quad (\text{C.1})$$

with the boundary condition

$$AN|_{z=z_0} = F. \quad (\text{C.2})$$

For simplicity, we ignore the reaction term, R , which is treated in the same way as the source term, Q . We discretize the cylindrical domain, Ω , as shown in Fig. C.1. That is, we split it into M smaller non-overlapping volumes (also

Mathematical meal models

cylinders) such that $\Omega = \bigcup_{i=0}^{M-1} \Omega_i$, where $\Omega_i = \{s = (z, r, \theta) | z \in [z_i, z_{i+1}], r \in [0, r_c], \theta \in [0, 2\pi[\}$ and r_c is the radius of the cylinder. First, we integrate over each volume, i.e.,

$$\begin{aligned} \int_{\Omega_i} \partial_t c \, ds &= - \int_{\Omega_i} \partial_z N \, ds + \int_{\Omega_i} Q \, ds, \\ &= -A \int_{z_i}^{z_{i+1}} \partial_z N \, dz + A \int_{z_i}^{z_{i+1}} Q \, dz, \end{aligned} \quad (\text{C.3})$$

for $i = 0, \dots, M-1$. We have interchanged integration and differentiation on the left-hand side, and exploited that the concentration is identical in the plane perpendicular to the motion through the cylinder. Next, we 1) use the definition of concentration to define the glucose mass $m_i = \int_{\Omega_i} c \, ds$, 2) apply Gauss' divergence theorem to the first term on the right-hand side, and 3) approximate Q as constant in each volume:

$$\dot{m}_i = -A(N_{i+1} - N_i) + F_i, \quad i = 0, \dots, M-1. \quad (\text{C.4})$$

Here, N_i is an approximation of the flux on the left boundary of the i 'th volume, and

$$F_i = A \Delta z_i Q_i, \quad i = 0, \dots, M-1, \quad (\text{C.5})$$

where $\Delta z_i = z_{i+1} - z_i$ and $Q_i = Q(c_i)$. Next, we 1) use the boundary condition (C.2), 2) use an upwind scheme to approximate the advection term, 3) use a first-order finite difference approximation of the spatial derivative in the diffusion term, and 4) assume that there's no diffusion at the end of the cylinder:

$$N_0 = F/A, \quad (\text{C.6a})$$

$$N_i = N_{a,i} + N_{d,i}, \quad i = 1, \dots, M, \quad (\text{C.6b})$$

$$N_{a,i} = v c_{i-1}, \quad i = 1, \dots, M, \quad (\text{C.6c})$$

$$N_{d,i} = -D_c \frac{c_i - c_{i-1}}{\Delta z_{c,i-1}}, \quad i = 1, \dots, M-1, \quad (\text{C.6d})$$

$$N_{d,M} = 0. \quad (\text{C.6e})$$

The center of the i 'th volume is

$$\begin{aligned} z_{c,i} &= z_i + \frac{1}{2} \Delta z_i = z_i + \frac{1}{2} (z_{i+1} - z_i) \\ &= \frac{z_{i+1} + z_i}{2}, \quad i = 0, \dots, M-1, \end{aligned} \quad (\text{C.7})$$

and the distance between the i 'th and $i+1$ 'th cell center is

$$\Delta z_{c,i} = z_{c,i+1} - z_{c,i}, \quad i = 0, \dots, M-2. \quad (\text{C.8})$$

For completeness, we also describe the discretization of

$$m_d = A \int_{z_0}^{z_d} c \, dz, \quad (\text{C.9})$$

which is used in the CSTR-PFR model with Alskär's feedback mechanism (68). Let K be the number of volumes for

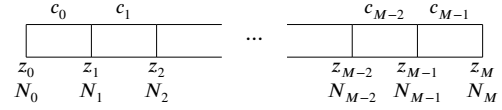


Figure C.1: Sketch of the spatially discrete grid used in the finite volume discretization of (C.1).

which $z_K \leq z_d < z_{K+1}$. Then, assuming that the glucose is evenly distributed in each volume,

$$\begin{aligned} m_d &= A \left(\int_{z_K}^{z_d} c \, dz + \sum_{i=0}^{K-1} \int_{z_i}^{z_{i+1}} c \, dz \right) \\ &\approx \frac{z_d - z_K}{z_{K+1} - z_K} m_K + \sum_{i=0}^{K-1} m_i. \end{aligned} \quad (\text{C.10})$$

First, we have split up the integral, and then, we have used the definition of concentration and the assumption of even distribution of the glucose.

D. Spectral Galerkin discretization

In this appendix, we describe a spectral Galerkin discretization (Kopriva, 2009) of the PFR model (21). As with the finite volume discretization, we disregard the reaction term, R , because it is discretized in the same way as the source term, Q . That is, we discretize the system

$$\partial_t c = -\partial_z N + Q, \quad (\text{D.1a})$$

$$AN|_{z=z_0} = F. \quad (\text{D.1b})$$

In this appendix, we assume that $z \in [-1, 1]$ (referred to as the computational domain). That is typically not the case. However, the actual physical domain can be mapped onto the computational domain and the system can be transformed accordingly, as described in Appendix D.3.

We approximate the solution, c , as a sum of products between time-dependent functions and space-dependent polynomials:

$$c(t, z) \approx \hat{c}(t, z) = \sum_{m=0}^M \hat{c}_m(t) \ell_m(z). \quad (\text{D.2})$$

Here, $\hat{c}_m = \hat{c}_m(t) = \hat{c}(t, z_m)$ is the m 'th time-dependent coefficient, $\{z_m\}_{m=0}^M$ is a set of collocation points, and $\ell_m = \ell_m(z)$ is the m 'th Lagrange polynomial (see Appendix D.2). An important property of such polynomials is that $\ell_m(z_i) = \delta_{im}$, i.e., it is equal to one when evaluated in the m 'th collocation point and zero when evaluated in any other collocation point. For brevity of notation, we often omit the dependency on time and space when functions are evaluated at t and z . Furthermore, for clarity, we explicitly indicate the arguments of the flux, N , and the source term, Q .

We require that the approximate solution, \hat{c} , satisfies the PDE weakly. Specifically,

$$\int_{z_0}^{z_f} (\partial_t \hat{c} + \partial_z N(\hat{c}) - Q(\hat{c})) \phi \, dz = 0 \quad (\text{D.3})$$

Mathematical meal models

must be satisfied for any test function ϕ that belongs to the same function space as the approximate solution, i.e., for any polynomial. As for the solution, we write the test function as a Lagrange polynomial:

$$\phi(t, z) = \sum_{n=0}^M \phi_n \ell_n. \quad (\text{D.4})$$

Here, $\phi_n = \phi_n(t) = \phi_n(t, z_n)$ is the n 'th time-dependent coefficient. We substitute the expression for the test function in (D.3):

$$\sum_{n=0}^M \phi_n \int_{z_0}^{z_f} (\partial_t \hat{c} + \partial_z N(\hat{c}) - Q(\hat{c})) \ell_n dz = 0. \quad (\text{D.5})$$

This equality must be satisfied for any polynomial ϕ , which means that it must be satisfied for any combination of values of $\{\phi_n\}_{n=0}^M$ at any point in time. Therefore, the integral must equal zero, i.e.,

$$\int_{z_0}^{z_f} (\partial_t \hat{c} + \partial_z N(\hat{c}) - Q(\hat{c})) \ell_n dz = 0, \quad (\text{D.6})$$

for $n = 0, \dots, M$. Next, we use integration by parts to rewrite the integral of the flux term. The result is

$$\int_{z_0}^{z_f} \partial_z N(\hat{c}) \ell_n dz = [N(\hat{c}) \ell_n]_{z_0}^{z_f} - \int_{z_0}^{z_f} N(\hat{c}) \frac{d\ell_n}{dz} dz, \quad (\text{D.7})$$

for $n = 0, \dots, M$. We insert this expression and the expression for the approximate concentration (D.2) into (D.6) in order to obtain

$$\sum_{m=0}^M \frac{d\hat{c}_m}{dt} \int_{z_0}^{z_f} \ell_m \ell_n dz + [N(\hat{c}) \ell_n]_{z_0}^{z_f} - \int_{z_0}^{z_f} N(\hat{c}) \frac{d\ell_n}{dz} dz - \int_{z_0}^{z_f} Q(\hat{c}) \ell_n dz = 0, \quad (\text{D.8})$$

for $n = 0, \dots, M$. We approximate the integrals using quadrature (see Appendix D.1). Consequently,

$$\begin{aligned} & \sum_{m=0}^M \frac{d\hat{c}_m}{dt} \sum_{l=0}^M \ell_m(z_l) \ell_n(z_l) w_l + [N(\hat{c}) \ell_n]_{z_0}^{z_f} \\ & - \sum_{l=0}^M N(\hat{c}(t, z_l)) \frac{d\ell_n}{dz}(z_l) w_l \\ & - \sum_{l=0}^M Q(\hat{c}(t, z_l)) \ell_n(z_l) w_l = 0, \end{aligned} \quad (\text{D.9})$$

for $n = 0, \dots, M$. We exploit that $\ell_m(z_l) = \delta_{ml}$ and that $\hat{c}(t, z_l) = \hat{c}_l(t)$:

$$\frac{d\hat{c}_n}{dt} w_n + [N(\hat{c}) \ell_n]_{z_0}^{z_f} - \sum_{l=0}^M N(\hat{c}_l) \frac{d\ell_n}{dz}(z_l) w_l$$

$$- Q(\hat{c}_n) w_n = 0, \quad n = 0, \dots, M. \quad (\text{D.10})$$

Finally, we rearrange terms in order to obtain the ODEs for each of the coefficients,

$$\begin{aligned} \frac{d\hat{c}_n}{dt} = & - \frac{1}{w_n} [N(\hat{c}) \ell_n(z)]_{z_0}^{z_f} \\ & + \frac{1}{w_n} \sum_{l=0}^M N(\hat{c}_l) \frac{d\ell_n}{dz}(z_l) w_l + Q(\hat{c}_n), \end{aligned} \quad (\text{D.11})$$

for $n = 0, \dots, M$.

Remark 6. When using Gauss-Lobatto quadrature, the boundary contribution in (D.11) (i.e., the first term on the right-hand side) is only nonzero for the boundary coefficient (i.e., for $n = 0$) because z_0 and z_f are collocation points. For Gauss quadrature, the boundary contribution is nonzero for all of the differential equations because z_0 and z_f are not collocation points.

D.1. Jacobi polynomials and quadrature

We denote by $P_k^{(\alpha, \beta)}$ a general k 'th order Jacobi polynomial (Kopriva, 2009), and we describe two special cases: 1) Legendre polynomials and 2) Chebyshev polynomials. Both polynomials can be used in a Gauss or Gauss-Lobatto quadrature rule:

$$\int_{z_0}^{z_f} f(z) w(z) dz \approx \sum_{l=0}^M f(z_l) w_l. \quad (\text{D.12})$$

The weight function w and the weights $\{w_l\}_{l=0}^M$ are specific to each Jacobi polynomial. Gauss quadrature rules are exact for polynomials of up to order $2M + 1$, but do not include the endpoints, z_0 and z_f . The endpoints are included in Gauss-Lobatto quadrature rules, which are only exact for polynomials of up to order $2M - 1$.

Remark 7. The Sturm-Liouville problem consists of the following differential equation combined with boundary conditions on u (not shown).

$$-\frac{d}{dz} \left(p(z) \frac{du}{dz} \right) + q(z)u = \lambda w(z)u, \quad a < z < b. \quad (\text{D.13})$$

Jacobi polynomials, $P_k^{(\alpha, \beta)}(z)$, are eigenfunctions of the specific Sturm-Liouville problem

$$\begin{aligned} & -\frac{d}{dz} \left((1-z)^{1+\alpha} (1+z)^{1+\beta} \frac{du}{dz} \right) \\ & = \lambda (1-z)^\alpha (1+z)^\beta u, \end{aligned} \quad (\text{D.14})$$

where $\alpha, \beta > -1$ and $-1 < z < 1$.

D.1.1. Legendre polynomials

The k 'th order Legendre polynomial, $L_k = P_k^{(0,0)}$, is obtained with $\alpha = \beta = 0$, and it is defined recursively starting with $L_0(z) = 1$ and $L_1(z) = z$. Subsequently,

$$L_{k+1}(z) = \frac{2k+1}{k+1} z L_k(z) - \frac{k}{k+1} L_{k-1}(z), \quad (\text{D.15})$$

Mathematical meal models

and the weight function is

$$w(z) = 1. \quad (\text{D.16})$$

The Legendre polynomials also satisfy

$$(2k+1)L_k(z) = \frac{dL_{k+1}}{dz}(z) - \frac{dL_{k-1}}{dz}(z). \quad (\text{D.17})$$

The Legendre Gauss collocation points, $\{z_l\}_{l=0}^M$, are the zeros of L_{M+1} , and the weights are

$$w_l = \frac{2}{(1-z_l^2) \left(\frac{dL_{M+1}}{dz}(z_l) \right)^2}, \quad l = 0, \dots, M. \quad (\text{D.18})$$

The Legendre Gauss-Lobatto collocation points, $\{z_l\}_{l=0}^M$, are -1, 1, and the zeros of $\frac{dL_M}{dz}$, and the weights are

$$w_l = \frac{2}{M(M+1)} \frac{1}{(L_M(z_l))^2}, \quad l = 0, \dots, M. \quad (\text{D.19})$$

D.1.2. Chebyshev polynomials

For Chebyshev polynomials, $\alpha = \beta = -1/2$ and the k 'th order polynomial is denoted by $T_k = P_k^{(-1/2, -1/2)}$. Chebyshev polynomials are given by the explicit expression

$$T_k(z) = \cos(k \cos^{-1}(z)), \quad (\text{D.20})$$

but they also satisfy a recursion. It starts with $T_0(z) = 1$ and $T_1(z) = z$ and is followed by

$$T_{k+1}(z) = 2zT_k(z) - T_{k-1}(z). \quad (\text{D.21})$$

They also satisfy

$$2T_k(z) = \frac{1}{k+1} \frac{dT_{k+1}}{dz}(z) - \frac{1}{k-1} \frac{dT_{k-1}}{dz}(z), \quad (\text{D.22})$$

and the weight function is

$$w(z) = \frac{1}{\sqrt{1-z^2}}. \quad (\text{D.23})$$

The Chebyshev Gauss collocation points and weights are given by

$$z_l = \cos\left(\frac{2l+1}{2M+2}\pi\right), \quad l = 0, \dots, M, \quad (\text{D.24a})$$

$$w_l = \frac{\pi}{M+1}, \quad l = 0, \dots, M, \quad (\text{D.24b})$$

and the Chebyshev Gauss-Lobatto collocation points and weights are

$$z_l = \cos\left(\frac{l\pi}{M}\right), \quad (\text{D.25a})$$

$$w_l = \begin{cases} \frac{\pi}{2M}, & l \in \{0, M\}, \\ \frac{\pi}{M}, & l = 1, \dots, M-1, \end{cases} \quad (\text{D.25b})$$

for $l = 0, \dots, M$.

D.2. Lagrange polynomials

Here, we describe the Lagrange polynomials which we use several times in the derivation of the spectral Galerkin method presented in this section. For arbitrary z , the m 'th Lagrange polynomial of order $M+1$ and its derivatives are (Berrut and Trefethen, 2004)

$$\ell_m(z) = \prod_{\substack{l=0 \\ l \neq m}}^M \frac{z - z_l}{z_m - z_l} = \frac{1}{s(z)} \frac{\tilde{w}_m}{z - z_m}, \quad (\text{D.26a})$$

$$\frac{d\ell_m}{dz}(z) = \frac{1}{s(z)} \left(\frac{-\tilde{w}_m}{(z - z_m)^2} - \ell_m(z) \frac{ds}{dz}(z) \right), \quad (\text{D.26b})$$

$$\frac{d^2\ell_m}{dz^2}(z) = \frac{1}{s(z)} \left(\frac{2\tilde{w}_m}{(z - z_m)^3} - 2 \frac{d\ell_m}{dz}(z) \frac{ds}{dz}(z) - \ell_m(z) \frac{d^2s}{dz^2}(z) \right), \quad (\text{D.26c})$$

where the corresponding weight is

$$\tilde{w}_m = \prod_{\substack{l=0 \\ l \neq m}}^M \frac{1}{z_m - z_l}, \quad (\text{D.27})$$

and the auxiliary function, s , and its derivatives are given by

$$s(z) = \sum_{l=0}^M \frac{\tilde{w}_l}{z - z_l}, \quad (\text{D.28a})$$

$$\frac{ds}{dz}(z) = \sum_{l=0}^M \frac{-\tilde{w}_l}{(z - z_l)^2}, \quad (\text{D.28b})$$

$$\frac{d^2s}{dz^2}(z) = \sum_{l=0}^M \frac{2\tilde{w}_l}{(z - z_l)^3}. \quad (\text{D.28c})$$

The above expressions for the derivative of ℓ_m cannot be evaluated in the collocation points, $\{z_m\}_{m=0}^M$, because it would result in division by zero. In the collocation points, the Lagrange polynomials and their derivatives are

$$\ell_m(z_l) = \delta_{ml}, \quad (\text{D.29a})$$

$$\frac{d\ell_m}{dz}(z_l) = \begin{cases} \frac{\tilde{w}_m}{\tilde{w}_l(z_l - z_m)}, & l \neq m, \\ -\sum_{\substack{j=0 \\ j \neq l}}^M \frac{d\ell_j}{dz}(z_l), & l = m, \end{cases} \quad (\text{D.29b})$$

$$\frac{d^2\ell_m}{dz^2}(z_l) = \begin{cases} -2 \frac{d\ell_m}{dz}(z_l) \left(-\frac{d\ell_l}{dz}(z_l) + \frac{1}{z_l - z_m} \right), & l \neq m, \\ -\sum_{\substack{j=0 \\ j \neq l}}^M \frac{d^2\ell_j}{dz^2}(z_l), & l = m. \end{cases} \quad (\text{D.29c})$$

Remark 8. There is a sign error in the last term in the parenthesis on the right-hand side of (9.4) in the paper by Berrut and Trefethen (2004).

Mathematical meal models

D.3. Domain transformation

If the physical spatial domain is not $[z_0, z_f] = [-1, 1]$, we transform the system by introducing the spatial coordinate $\xi = \xi(z) = 2 \frac{z-z_0}{z_f-z_0} - 1 \in [-1, 1]$. We use the inverse transformation, $z = z(\xi) = \frac{1}{2}(\xi + 1)(z_f - z_0) + z_0$, to express the PDE and the boundary condition in terms of ξ . For simplicity, in this appendix, we assume that the velocity, v , and the diffusion coefficient, D_c , are independent of space, z , and concentration, c . First, we use the chain rule to derive the partial derivatives of the concentration with respect to ξ :

$$\partial_\xi c = \partial_z c \frac{dz}{d\xi}, \quad (\text{D.30a})$$

$$\partial_{\xi\xi} c = \partial_{zz} c \left(\frac{dz}{d\xi} \right)^2 + \partial_z c \frac{d^2 z}{d\xi^2} = \partial_{zz} c \left(\frac{dz}{d\xi} \right)^2. \quad (\text{D.30b})$$

We have exploited that z is linear in ξ , i.e., $\frac{d^2 z}{d\xi^2} = 0$. Consequently,

$$\partial_z c = \partial_\xi c \left(\frac{dz}{d\xi} \right)^{-1}, \quad \partial_{zz} c = \partial_{\xi\xi} c \left(\frac{dz}{d\xi} \right)^{-2}. \quad (\text{D.31})$$

Next, we use the chain rule to express the partial derivatives of the flux:

$$\partial_\xi N = \partial_z N \frac{dz}{d\xi} = (v \partial_z c + \partial_z J) \frac{dz}{d\xi} = v \partial_\xi c + \partial_\xi J, \quad (\text{D.32a})$$

$$\partial_\xi J = \partial_z J \frac{dz}{d\xi} = -D_c \partial_{zz} c \frac{dz}{d\xi} = -D_c \partial_{\xi\xi} c \left(\frac{dz}{d\xi} \right)^{-1}. \quad (\text{D.32b})$$

Consequently,

$$\partial_t c = -\partial_z N + Q = -\partial_\xi N \left(\frac{dz}{d\xi} \right)^{-1} + Q, \quad (\text{D.33})$$

and

$$\partial_\xi N \left(\frac{dz}{d\xi} \right)^{-1} = v \left(\frac{dz}{d\xi} \right)^{-1} \partial_\xi c + \partial_\xi J \left(\frac{dz}{d\xi} \right)^{-1}, \quad (\text{D.34a})$$

$$\partial_\xi J \left(\frac{dz}{d\xi} \right)^{-1} = -D_c \left(\frac{dz}{d\xi} \right)^{-2} \partial_{\xi\xi} c. \quad (\text{D.34b})$$

Therefore, the transformed system

$$\partial_t c = -\partial_\xi \bar{N} + Q, \quad (\text{D.35})$$

where

$$\bar{N} = \bar{v} c + \bar{J}, \quad (\text{D.36a})$$

$$\bar{J} = -\bar{D}_c \partial_\xi c, \quad (\text{D.36b})$$

$$\bar{v} = v \left(\frac{dz}{d\xi} \right)^{-1}, \quad (\text{D.36c})$$

$$\bar{D}_c = D_c \left(\frac{dz}{d\xi} \right)^{-2}, \quad (\text{D.36d})$$

is in the form (D.1), and $\xi \in [-1, 1]$. The two main differences between the original and the transformed system are the velocity and the diffusion coefficient. Note that we have exploited that $\frac{dz}{d\xi}$ is independent of ξ (i.e., it is constant). The boundary condition in the transformed system is

$$A \bar{N}|_{z=z_0} = F, \quad (\text{D.37})$$

where

$$\bar{N} = \bar{v} c + \bar{J}, \quad (\text{D.38a})$$

$$\bar{J} = -D_c \partial_z c = -D_c \partial_\xi c \left(\frac{dz}{d\xi} \right)^{-1} = -\bar{D}_c \partial_\xi c, \quad (\text{D.38b})$$

$$\bar{D}_c = D_c \left(\frac{dz}{d\xi} \right)^{-1}. \quad (\text{D.38c})$$

Finally, we reformulate the integral in (68) in the CSTR-PFR model with Alskär's feedback mechanism. We use that $dz = \frac{dz}{d\xi} d\xi$:

$$m_d = A \int_{z_0}^{z_d} c dz = A \int_{\xi_0}^{\xi_d} c \frac{dz}{d\xi} d\xi, \quad (\text{D.39})$$

where $\xi_0 = -1$ and $\xi_d = \xi(z_d)$.

Remark 9. As $\frac{dz}{d\xi}$ is constant, the boundary condition (D.37) can also be formulated in terms of the transformed flux \bar{N} , i.e.,

$$A \bar{N}|_{z=z_0} = \bar{F}, \quad (\text{D.40})$$

where

$$\bar{F} = F \left(\frac{dz}{d\xi} \right)^{-1}. \quad (\text{D.41})$$

References

- Adams, C.L., Lasseigne, D.G., 2018. An extensible mathematical model of glucose metabolism. Part I: the basic glucose-insulin-glucagon model, basal conditions and basic dynamics. *Letters in Biomathematics* 5, 70–90. doi:10.1080/23737867.2018.1429332.
- Alskär, O., Bagger, J.I., Røge, R.M., Knop, F.K., Karlsson, M.O., Vilsbøll, T., Kjellsson, M.C., 2016. Semimechanistic model describing gastric emptying and glucose absorption in healthy subjects and patients with type 2 diabetes. *The Journal of Clinical Pharmacology* 56, 340–348. doi:10.1002/jcph.602.
- Barnabei, M., Borri, A., De Gaetano, A., Manes, C., Palumbo, P., Pires, J.G., 2022. A short-term food intake model involving glucose, insulin and ghrelin. *Discrete and Continuous Dynamical Systems Series B* 27, 1913–1926. doi:10.3934/dcdsb.2021114.
- Berrut, J.P., Trefethen, L.N., 2004. Barycentric Lagrange interpolation. *SIAM Review* 46, 501–517. doi:10.1137/S0036144502417715.
- Boiroux, D., Båtor, V., Hagdrup, M., Wendt, S.L., Poulsen, N.K., Madsen, H., Jørgensen, J.B., 2018. Adaptive model predictive control for a dual-hormone artificial pancreas. *Journal of Process Control* 68, 105–117. doi:10.1016/j.jprocont.2018.05.003.

Mathematical meal models

- Chudtong, M., De Gaetano, A., 2021. A mathematical model of food intake. *Mathematical Biosciences and Engineering* 18, 1238–1279. doi:10.3934/mbe.2021067.
- Cohen, R.B., Li, J., 2021. A novel model and its analysis on the metabolic regulations of glucose, insulin, and glucagon. *SIAM Journal on Applied Mathematics* 81, 2684–2703. doi:10.1137/21M1390876.
- Contreras, S., Medina-Ortiz, D., Conca, C., Olivera-Nappa, Á., 2020. A novel synthetic model of the glucose-insulin system for patient-wise inference of physiological parameters from small-size OGTT data. *Frontiers in Bioengineering and Biotechnology* 8, 195. doi:10.3389/fbioe.2020.00195.
- Dalla Man, C., Camilleri, M., Cobelli, C., 2006. A system model of oral glucose absorption: Validation on gold standard data. *IEEE Transactions on Biomedical Engineering* 53, 12. doi:10.1109/TBME.2006.883792.
- Dalla Man, C., Micheletto, F., Lv, D., Breton, M., Kovatchev, B., Cobelli, C., 2014. The UVA/PADOVA type 1 diabetes simulator: New features. *Journal of Diabetes Science and Technology* 8, 26–34. doi:10.1177/1932296813514502.
- Dalla Man, C., Rizza, R.A., Cobelli, C., 2007. Meal simulation model of the glucose-insulin system. *IEEE Transactions on Biomedical Engineering* 54, 1740–1749. doi:10.1109/TBME.2007.893506.
- De Gaetano, A., Panunzi, S., Matone, A., Samson, A., Vrbikova, J., Bendlova, B., Pacini, G., 2013. Routine OGTT: A robust model including incretin effect for precise identification of insulin sensitivity and secretion in a single individual. *PLoS ONE* 8, e70875. doi:10.1371/journal.pone.0070875.
- Gouseti, O., Bornhorst, G.M., Bakalis, S., Mackie, A., 2019. *Interdisciplinary Approaches to Food Digestion*. Springer.
- Hendricks, E., Jannerup, O., Sørensen, P.H., 2008. *Linear Systems Control: Deterministic and Stochastic Methods*. Springer. doi:10.1007/978-3-540-78486-9.
- Hovorka, R., Canonico, V., Chassin, L.J., Haueter, U., Massi-Benedetti, M., Federici, M.O., Pieber, T.R., Schaller, H.C., Schaupp, L., Vering, T., Wilinska, M.E., 2004. Nonlinear model predictive control of glucose concentration in subjects with type 1 diabetes. *Physiological Measurement* 25, 905–920. doi:10.1088/0967-3334/25/4/010.
- Huang, W., Lee, S.L., Yu, L.X., 2009. Mechanistic approaches to predicting oral drug absorption. *The AAPS Journal* 11, 217–224. doi:10.1208/s12248-009-9098-z.
- Huard, B., Kirkham, G., 2022. Mathematical modelling of glucose dynamics. *Current Opinion in Endocrine and Metabolic Research* 25, 100379. doi:10.1016/j.coemr.2022.100379.
- Jauslin, P.M., Silber, H.E., Frey, N., Gieschke, R., Simonsson, U.S.H., Jorga, K., Karlsson, M.O., 2007. An integrated glucose-insulin model to describe oral glucose tolerance test data in type 2 diabetics. *Journal of Clinical Pharmacology* 47, 1244–1255. doi:10.1177/0091270007302168.
- Kopriva, D.A., 2009. Implementing spectral methods for partial differential equations: Algorithms for scientists and engineers. *Scientific Computation*, Springer. doi:10.1007/978-90-481-2261-5.
- Lal, R.A., Ekhlaspour, L., Hood, K., Buckingham, B., 2019. Realizing a closed-loop (artificial pancreas) system for the treatment of type 1 diabetes. *Endocrine Reviews* 40, 1521–1546. doi:10.1210/er.2018-00174.
- Le Feunteun, S., Mackie, A.R., Dupont, D., 2020. *In silico* trials of food digestion and absorption: how far are we? *Current Opinions in Food Science* 31, 121–125.
- Makroglou, A., Li, J., Kuang, Y., 2006. Mathematical models and software tools for the glucose-insulin regulatory system and diabetes: an overview. *Applied Numerical Mathematics* 56, 559–573. doi:10.1016/j.apnum.2005.04.023.
- Moxon, T.E., Gouseti, O., Bakalis, S., 2016. *In silico* modelling of mass transfer & absorption in the human gut. *Journal of Food Engineering* 176, 110–120. doi:10.1016/j.jfoodeng.2015.10.019.
- Moxon, T.E., Nimmegeers, P., Telen, D., Fryer, P.J., Van Impe, J., Bakalis, S., 2017. Effect of chyme viscosity and nutrient feedback mechanism on gastric emptying. *Chemical Engineering Science* 171, 318–330. doi:10.1016/j.ces.2017.05.048.
- Noguchi, C.C.Y., Furutani, E., Sumi, S., 2014. Mathematical model of glucose-insulin metabolism in type 1 diabetes including digestion and absorption of carbohydrates. *SICE Journal of Control, Measurement, and System Integration* 7, 314–320. doi:10.9746/jcmsi.7.314.
- Noguchi, C.C.Y., Hashimoto, S., Furutani, E., Sumi, S., 2016. Model of gut absorption from carbohydrates with maximum rate of exogenous glucose appearance in type 1 diabetes. *SICE Journal of Control, Measurement, and System Integration* 9, 201–206. doi:10.9746/jcmsi.9.201.
- Palumbo, P., Ditlevsen, S., Bertuzzi, A., De Gaetano, A., 2013. Mathematical modeling of the glucose-insulin system: A review. *Mathematical Biosciences* 244, 69–81. doi:10.1016/j.mbs.2013.05.006.
- Panunzi, S., Pompa, M., Borri, A., Piemonte, V., De Gaetano, A., 2020. A revised Sorensen model: Simulating glycemic and insulinemic response to oral and intra-venous glucose load. *PLoS ONE* 15, e0237215. doi:10.1371/journal.pone.0237215.
- Pattaranit, R., van den Berg, H.A., 2008. Mathematical models of energy homeostasis. *Journal of the Royal Society Interface* 5, 1119–1135. doi:10.1098/rsif.2008.0216.
- Pompa, M., Panunzi, S., Borri, A., De Gaetano, A., 2021. A comparison among three maximal mathematical models of the glucose-insulin system. *PLoS ONE* 16, e0257789. doi:10.1371/journal.pone.0257789.
- Reenberg, A.T., Ritschel, T.K.S., Dammann, B., Jørgensen, J.B., 2022. High-performance uncertainty quantification in large-scale virtual clinical trials of closed-loop diabetes treatment, in: *Proceedings of the 2022 American Control Conference (ACC)*, Atlanta, Georgia, USA. pp. 1367–1372. doi:10.23919/ACC53348.2022.9867234.
- Ritschel, T.K.S., Reenberg, A.T., Jørgensen, J.B., 2022. Large-scale virtual clinical trials of closed-loop treatments for people with type 1 diabetes, in: *Proceedings of the 9th IFAC Conference on Foundations of Systems Biology in Engineering (FOSBE)*, Cambridge, Massachusetts, USA. Accepted.
- Sicard, J., Mirade, P.S., Portanguen, S., Clerjon, S., Kondjoyan, A., 2018. Simulation of the gastric digestion of proteins of meat bolus using a reaction-diffusion model. *Food and Function* 9, 6455–6469. doi:10.1039/c8fo01120f.
- Silber, H.E., Frey, N., Karlsson, M.O., 2010. An integrated glucose-insulin model to describe oral glucose tolerance test data in healthy volunteers. *The Journal of Clinical Pharmacology* 50, 246–256. doi:10.1177/0091270009341185.
- Silber, H.E., Jauslin, P.M., Frey, N., Gieschke, R., Simonsson, U.S.H., Karlsson, M.O., 2007. An integrated model for glucose and insulin regulation in healthy volunteers and type 2 diabetic patients following intravenous glucose provocations. *The Journal of Clinical Pharmacology* 47, 1159–1171. doi:10.1177/0091270007304457.
- Smith, J.M.D., Maas, J.A., Garnsworthy, P.C., Owen, M.R., Coombes, S., Pillay, T.S., Barrett, D.A., Symonds, M.E., 2009. Mathematical modeling of glucose homeostasis and its relationship with energy balance and body fat. *Obesity* 17, 632–639.
- Voit, E.O., 2017. The best models of metabolism. *Wiley Interdisciplinary Reviews. Systems Biology and Medicine* 9. doi:10.1002/wsbm.1391.
- Wei, Y., Hu, Y., Dai, Y., Wang, Y., 2016. A generalized Padé approximation of time delay operator. *International Journal of Control, Automation and Systems* 14, 181–187.

Mathematical meal models

Table A.1

Parameter values used in Section 5 to simulate the glucose rate of appearance for each of the models described in Section 4.

Symbol	Value	Unit	Description
Hovorka's model (Hovorka et al., 2004)			
A_G	0.8	—	Carbohydrate bioavailability
τ_D	40	min	Time constant
f	1	—	Percentage of absorbed glucose that appears in the blood
BW	82	kg	Body weight
Dalla Man's model (Dalla Man et al., 2006, 2007)			
k_{max}	0.0465	1/min	Maximum inverse of gastric emptying time constant
k_{min}	0.0076	1/min	Minimum inverse of gastric emptying time constant
k_{abs}	0.023	1/min	Inverse of intestinal glucose absorption time constant
k_{gri}	0.0465	1/min	Inverse of grinding (solid-to-liquid in the stomach) time constant
b	0.69	—	Percentage of total meal glucose content corresponding to left inflection point
c	0.17	—	Percentage of total meal glucose content corresponding to right inflection point
f	0.90	—	Percentage of absorbed glucose that appears in the blood
BW	91	kg	Body weight
The SIMO model (Panunzi et al., 2020, Table 4)			
k_{js}	0.026	1/min	Inverse of stomach-to-jejunum time constant
k_{rj}	0.033	1/min	Inverse of jejunum-to-delay compartment time constant
k_{lr}	0.030	1/min	Inverse of delay compartment-to-ileum time constant
k_{gj}	0.036	1/min	Inverse of time constant of glucose absorption in the jejunum
k_{gl}	0.027	1/min	Inverse of time constant of glucose absorption in the ileum
f	1	—	Percentage of absorbed glucose that appears in the blood
BW	82	kg	Body weight
Alskär's model (Alskär et al., 2016)			
k_w	0.14	1/min	Emptying rate for a noncaloric liquid (e.g., water)
IG_{D50}	7420	mg	Amount of glucose corresponding to a 50% reduction of the gastric emptying rate
γ	14	—	Hill factor
L_D	0.08	—	Length of duodenum relative to the length of the small intestine
L_J	0.37	—	Length of jejunum relative to the length of the small intestine
T	240	min	The time it takes the chyme to pass through the small intestine
σ	10	1/min	Parameter in the lag of the gastric emptying rate
t_{50}	5	min	Delay of the gastric emptying rate
K_{mG}	6320	mg	Amount of glucose corresponding to a 50% reduction of the absorption rate
$R_{D,max}$	580	mg/min	Maximum rate of glucose absorption in the duodenum
$R_{J,max}$	2060	mg/min	Maximum rate of glucose absorption in the jejunum
$R_{I,max}$	1330	mg/min	Maximum rate of glucose absorption in the ileum
F_P	1	—	Fraction of glucose absorption that appears in the blood
BW	82	kg	Body weight
CSTR-PFR model (Alskär et al., 2016; Moxon et al., 2016, 2017)			
z_0	0	m	Position of left end of small intestine
z_f	2.85	m	Position of right end of small intestine
v_p	0.0102	m/min	Advection velocity of the chyme due to peristaltic movement
D_p	0.0001	m ² /min	Coefficient of glucose diffusion in the chyme
r_{si}	0.018	m	Radius of small intestine
f	12	—	Factor accounting for villi, microvilli, plicae circulares, and effective absorption area
v_a	$6.4392 \cdot 10^{-6}$	m/min	Glucose absorption mass transfer coefficient
k_{sd}	0.06	1/min	Inverse of stomach-to-duodenum time constant (no feedback mechanism)
$k_{sd,max}$	0.0554	1/min	Maximum inverse of stomach-to-duodenum time constant (Moxon's feedback)
$k_{sd,max}$	0.14	1/min	Maximum inverse of stomach-to-duodenum time constant (Alskär's feedback)
$k_{sd,min}$	0.0116	1/min	Minimum inverse of stomach-to-duodenum time constant
$R_{A,max}$	420	mg/min	Maximum glucose rate of appearance
σ	0.1	—	Parameter in approximation of Moxon's feedback mechanism
$m_{d,50}$	7420	mg	Amount of glucose corresponding to a 50% reduction of the gastric emptying rate
γ	14	—	Hill factor
BW	82	kg	Body weight

APPENDIX E

Conference Paper - CDC 2021

A High-Performance Monte Carlo Simulation Toolbox for
Uncertainty Quantification of Closed-loop systems

Authors:

Morten Ryberg Wahlgreen, Asbjørn Thode Reenberg, Marcus Krogh Nielsen, Anton Rydahl, Tobias K. S. Ritschel, Bernd Dammann, John Bagterp Jørgensen

Published in:

Proceedings of the 2021 60th Conference on Decision and Control (CDC), December 13–15, 2021, Austin, Texas.

2021 60th IEEE Conference on Decision and Control (CDC)
December 13-15, 2021. Austin, Texas

A High-Performance Monte Carlo Simulation Toolbox for Uncertainty Quantification of Closed-loop Systems

Morten Ryberg Wahlgreen, Asbjørn Thode Reenberg, Marcus Krogh Nielsen,
Anton Rydahl, Tobias K. S. Ritschel, Bernd Dammann, John Bagterp Jørgensen

Abstract—We apply Monte Carlo simulation for performance quantification and tuning of controllers in nonlinear closed-loop systems. Computational feasibility of large-scale Monte Carlo simulation is achieved by implementation of a parallelized high-performance Monte Carlo simulation toolbox for closed-loop systems in C for shared memory architectures. The toolbox shows almost linear scale-up on 16 CPU cores on a single NUMA node, and a scale-up of 27.3 on two NUMA nodes with a total of 32 CPU cores. We demonstrate performance quantification and tuning of a PID controller for a bioreactor in fed-batch operation. We perform 30,000 closed-loop simulations of the fed-batch reactor within 1 second. This is approximately a 2300 times computational performance increase compared to a serial reference implementation in Matlab. Additionally, we apply Monte Carlo simulation to perform automatic tuning of the PID controller based on maximizing average produced biomass within 8 seconds.

I. INTRODUCTION

In closed-loop systems, we encounter unknown quantities that need to be estimated, e.g., model parameters. Additionally, it can be beneficial to quantify controller performance. Currently, there exist well-defined methods for parameters estimation [1], [2] and tuning of controllers in linear systems [3]–[5]. However, for nonlinear systems, quantification of controller performance and tuning is not as well developed. We propose a Monte Carlo simulation brute-force technique for automatic performance quantification and tuning of controllers in linear and nonlinear systems. With the Monte Carlo approach, we can tune controllers with any performance measure, e.g., maximizing economic yield or minimizing the risk of low production, such as in modern control applications [6], [7]. The Monte Carlo simulation technique is made computationally feasible by implementation of a high-performance Monte Carlo simulation toolbox parallelized for shared memory architectures in C.

Monte Carlo simulation is a widely used technique for quantification of uncertainties. It is applied in various areas, e.g., portfolio management and epidemiology [8]–[10]. Monte Carlo simulation uses random sampling to obtain numerical results about deterministic quantities. However, the method requires many samples to be effective, and thus computational efficiency becomes a bottleneck. The development in central processing unit (CPU) technology increases the number of possible applications for Monte

Carlo simulation. However, trends in CPU development show that the clock frequency of new CPUs is no longer increasing due to power consumption and heat issues [11]. Instead, new CPUs have increased performance by increasing the number of cores. Consequently, the full potential of modern CPUs is only achieved with parallelized software executed on multi-core processors. Not all problems are parallelizable, but Monte Carlo simulation is a prime example of a parallelizable problem, as each simulation is independent of all other simulations. To achieve the full potential of Monte Carlo simulation on modern CPUs, we require state-of-the-art parallelized software in high-performance languages.

In this paper, we present closed-loop systems based on a stochastic continuous-discrete model, a stochastic differential equation (SDE) solver, and a controller. We introduce our implementation of a high-performance Monte Carlo simulation toolbox for closed-loop systems. Additionally, we introduce the SDE solvers and controllers contained in the toolbox. Furthermore, we demonstrate applications of the toolbox on a bioreactor in fed-batch operation [12]. In particular, we demonstrate that Monte Carlo simulation can be used for performance quantification and tuning of a proportional–integral–derivative (PID) controller.

The remaining part of the paper is organized as follows. Section II introduces the stochastic continuous-discrete system, two SDE solvers, and four controllers of increasing complexity. Section III presents the Monte Carlo simulation scheme for closed-loop systems and introduces our toolbox for Monte Carlo simulation. Section IV presents an example application of the toolbox. Section V presents our conclusion.

II. CLOSED-LOOP SIMULATIONS

This section presents our representation of closed-loop systems for simulation. Our simulations consist of 1) an SDE model with discrete measurements, represented as a stochastic continuous-discrete model, 2) an SDE solver, and 3) a controller.

A. Stochastic continuous-discrete system

We consider stochastic continuous-discrete systems in the form

$$x(t_0) = x_0, \quad (1a)$$

$$dx(t) = f(t, x(t), u(t), d(t), p_f)dt + \sigma(t, x(t), u(t), d(t), p_\sigma)d\omega(t), \quad (1b)$$

$$y(t_k) = g(t_k, x(t_k), p_g) + v(t_k, p_v), \quad (1c)$$

$$z(t) = h(t, x(t), p_h), \quad (1d)$$

M. R. Wahlgreen, A. T. Reenberg, M. K. Nielsen, A. Rydahl, T. K. S. Ritschel, B. Dammann, and J. B. Jørgensen are with the Department of Applied Mathematics and Computer Science, Technical University of Denmark, DK-2800 Kgs. Lyngby, Denmark.

Corresponding author: J. B. Jørgensen (E-mail: jbj@dtu.dk).

where $x(t)$ are the states, $u(t)$ are inputs, $d(t)$ are disturbances, and p_f , p_σ , p_g , p_v , and p_h are parameters. Additionally, x_0 is a normally distributed initial condition, $\omega(t)$ is a standard Wiener process, and $v(t_k, p_v)$ is normally distributed measurement noise at discrete time, i.e.,

$$x_0 \sim N(\bar{x}_0, P_0), \quad (2a)$$

$$d\omega(t) \sim N_{iid}(0, Idt), \quad (2b)$$

$$v(t_k, p_v) \sim N_{iid}(0, R(t_k, p_v)). \quad (2c)$$

Measurements are sampled with sampling time Δt , such that, $t_{k+1} = t_k + \Delta t$. We use zero-order-hold parameterization of the inputs and disturbances:

$$u(t) = u_k, \quad t_k \leq t < t_{k+1}, \quad (3a)$$

$$d(t) = d_k, \quad t_k \leq t < t_{k+1}. \quad (3b)$$

B. Stochastic differential equation solvers

SDE solvers are required to simulate stochastic continuous-discrete systems in the form (1). We consider an explicit-explicit (Euler-Maruyama) solver and an implicit-explicit solver [13], [14].

1) Explicit-explicit (Euler-Maruyama):

$$t_{k,n+1} = t_{k,n} + \Delta t, \quad (4a)$$

$$x_{k,n+1} = x_{k,n} + f(t_{k,n}, x_{k,n}, u_k, d_k, p_f)\Delta t + \sigma(t_{k,n}, x_{k,n}, u_k, d_k, p_\sigma)\Delta\omega_{k,n}, \quad (4b)$$

2) Implicit-explicit:

$$t_{k,n+1} = t_{k,n} + \Delta t, \quad (5a)$$

$$x_{k,n+1} = x_{k,n} + f(t_{k,n+1}, x_{k,n+1}, u_k, d_k, p_f)\Delta t + \sigma(t_{k,n}, x_{k,n}, u_k, d_k, p_\sigma)\Delta\omega_{k,n}, \quad (5b)$$

where $t_{k,0} = t_k$, $x_{k,0} = x_k$, and $\Delta\omega_{k,n} \sim N_{iid}(0, I\Delta t)$.

Let N_k denote the number of steps of size Δt in the interval $[t_k, t_{k+1}]$. Then

$$t_{k+1} = t_{k,N_k}, \quad (6a)$$

$$x_{k+1} = x_{k,N_k}. \quad (6b)$$

The explicit-explicit solver is suitable for non-stiff systems, whereas the implicit-explicit solver is suitable for stiff systems.

We let Φ represent the discretization of the state equation, (1b), with either the explicit-explicit solver or the implicit-explicit solver. To compactly describe simulation of closed-loop systems, we introduce the notation for a discretized version of (1),

$$x_{k+1} = \Phi(t_k, x_k, u_k, d_k, w_k, p_f, p_\sigma), \quad (7a)$$

$$y_k = g(t_k, x_k, p_g) + v_k, \quad (7b)$$

$$z_k = h(t_k, x_k, p_h), \quad (7c)$$

where $v_k = v(t_k, p_v)$.

C. Controller

The digital discrete-time controller in typical model-based control applications is represented as the dynamic system

$$x_k^c = \kappa(t_{k-1}, x_{k-1}^c, y_k, u_{k-1}, p_\kappa), \quad (8a)$$

$$u_k = \lambda(t_k, x_k^c, p_\lambda), \quad (8b)$$

$$z_k^c = \mu(t_k, x_k^c, p_\mu), \quad (8c)$$

where x_k^c are estimated states, z_k^c are predictions of the outputs and manipulated inputs, $\kappa(\cdot)$ is a state estimator, $\lambda(\cdot)$ is a regulator, and $\mu(\cdot)$ is a predictor.

We consider four controllers of increasing complexity.

1) *Open-loop controller (no feedback)*: The open-loop controller does not include feedback and outputs a target value for the inputs

$$u_k = \lambda(\cdot) = \bar{u}_k. \quad (9)$$

The functions $\kappa(\cdot)$ and $\mu(\cdot)$ are not necessary for the open-loop controller.

2) *Proportional-integral-derivative controller*: The continuous PID controller is given by

$$u(t) = \bar{u}(t) + K_p e(t) + K_i \int_{t_0}^t e(\tau) d\tau + K_d \frac{de(t)}{dt}, \quad (10)$$

where K_p , K_i , and K_d are gain constants. The error, $e(t)$, is the difference between the set point, $\bar{y}(t)$, and the measurement, $y(t)$, i.e.,

$$e(t) = \bar{y}(t) - y(t). \quad (11a)$$

Notice, for the PID controller the output is assumed to be measured, i.e., $\bar{y}(t) = z(t)$. It can be advantageous to let the derivative term act on the measurements, $y(t)$, rather than the error, $e(t)$ [15], [16]. We get,

$$u(t) = \bar{u}(t) + K_p e(t) + K_i \int_{t_0}^t e(\tau) d\tau - K_d \frac{dy(t)}{dt}. \quad (12)$$

We discretize the PID controller (12) as

$$e_k = \bar{y}_k - y_k^F, \quad (13a)$$

$$P_k = K_p e_k, \quad (13b)$$

$$I_k = I_{k-1} + T_s K_i e_k, \quad (13c)$$

$$D_k = -\frac{K_d}{T_s} (y_k^F - y_{k-1}^F), \quad (13d)$$

$$u_k = \bar{u}_k + P_k + I_k + D_k, \quad (13e)$$

where T_s is the sampling time and filtered measurements, y_k^F , are computed from the discrete-time low-pass filter

$$y_k^F = (1 - \alpha)y_{k-1}^F + \alpha y_k, \quad (14)$$

with $\alpha \in [0, 1]$.

For the PID controller, $\lambda(\cdot)$ is given by (13e), $\kappa(\cdot)$ is given by (14), and $\mu(\cdot)$ is not necessary.

3) *PID controller with clipping*: We incorporate input bounds with clipping. The PID controller with clipping is,

$$\tilde{u}_k = \bar{u}_k + P_k + I_k + D_k, \quad (15a)$$

$$u_k = \max(u_{\min}, \min(u_{\max}, \tilde{u}_k)). \quad (15b)$$

4) *Nonlinear model predictive control*: The nonlinear model predictive controller (NMPC) includes a continuous-discrete extended Kalman filter (CD-EKF) based on (1) for state estimation and prediction [17], [18]. Given the filtered state-covariance pair, $\hat{x}_{k-1|k-1}$ and $P_{k-1|k-1}$, the CD-EKF obtains a one-step prediction

$$\hat{x}_{k|k-1} = \hat{x}_{k-1}(t_k), \quad (16a)$$

$$P_{k|k-1} = P_{k-1}(t_k), \quad (16b)$$

as the solution to

$$\frac{d}{dt}\hat{x}_{k-1}(t) = f(t, \hat{x}_{k-1}(t), u_{k-1}, d_{k-1}, p_f), \quad (17a)$$

$$\frac{d}{dt}P_{k-1}(t) = A_{k-1}(t)P_{k-1}(t) + P_{k-1}(t)A_{k-1}(t)' + \sigma_{k-1}(t)\sigma_{k-1}(t)', \quad (17b)$$

for $t_{k-1} \leq t \leq t_k$ with initial condition

$$\hat{x}_{k-1}(t_{k-1}) = \hat{x}_{k-1|k-1}, \quad (18a)$$

$$P_{k-1}(t_{k-1}) = P_{k-1|k-1}, \quad (18b)$$

and

$$A_{k-1}(t) = \frac{\partial}{\partial x}f(t, \hat{x}_{k-1}(t), u_{k-1}, d_{k-1}, p_f), \quad (19a)$$

$$\sigma_{k-1}(t) = \sigma(t, \hat{x}_{k-1}(t), u_{k-1}, d_{k-1}, p_\sigma). \quad (19b)$$

The CD-EKF obtains a filtered state estimate, $\hat{x}_{k|k}$, and its covariance, $P_{k|k}$, from the one-step prediction, $\hat{x}_{k|k-1}$ and $P_{k|k-1}$, and the measurement, y_k . The CD-EKF computes the predicted measurement and derivative,

$$\hat{y}_{k|k-1} = g(t_k, \hat{x}_{k|k-1}, p_g), \quad (20a)$$

$$C_k = \frac{\partial}{\partial x}g(t_k, \hat{x}_{k|k-1}, p_g), \quad (20b)$$

the innovation and its covariance,

$$e_k = y_k - \hat{y}_{k|k-1}, \quad (21a)$$

$$R_{e,k} = C_k P_{k|k-1} C_k' + R_k, \quad (21b)$$

and the Kalman gain,

$$K_{fx,k} = P_{k|k-1} C_k' R_{e,k}^{-1}. \quad (22)$$

We obtain the estimated state-covariance pair from (20)-(22) as

$$\hat{x}_{k|k} = \hat{x}_{k|k-1} + K_{fx,k} e_k, \quad (23a)$$

$$P_{k|k} = P_{k|k-1} - K_{fx,k} R_{e,k} K_{fx,k}'. \quad (23b)$$

The CD-EKF is the state estimator, $\kappa(\cdot)$, that computes filtered state estimates, $x_k^c = \hat{x}_{k|k}$, from measurements y_k , and one-step state prediction, $\hat{x}_{k|k-1}$.

The NMPC uses a regulator based on a weighted least-squares objective and regularization of the input rate-of-movement. This regulator can be expressed in terms of the optimal control problem (OCP)

$$\min_{x,u} \quad \varphi_k = \varphi_{z,k} + \varphi_{\Delta u,k}, \quad (24a)$$

$$s.t. \quad x(t_k) = \hat{x}_{k|k}, \quad (24b)$$

$$\dot{x}(t) = f(t, x, u, d, p_f), \quad t_k \leq t \leq t_k + T, \quad (24c)$$

$$z(t) = h(t, x, p_h), \quad (24d)$$

$$u(t) = u_{k+j}, \quad j \in \mathcal{N}, \quad t_{k+j} \leq t \leq t_{k+j+1}, \quad (24e)$$

$$d(t) = d_{k+j}, \quad j \in \mathcal{N}, \quad t_{k+j} \leq t \leq t_{k+j+1}, \quad (24f)$$

$$u_l \leq u_{k+j} \leq u_u, \quad j \in \mathcal{N}, \quad (24g)$$

$$\Delta u_l \leq \Delta u_{k+j} \leq \Delta u_u, \quad j \in \mathcal{N}, \quad (24h)$$

with $f(t, x, u, d, p_f) = f(t, x(t), u(t), d(t), p_f)$ and the objective terms

$$\varphi_{z,k} = \frac{1}{2} \int_{t_k}^{t_k+T} \|W_z(z(t) - \bar{z}(t))\|_2^2 dt, \quad (25a)$$

$$\varphi_{\Delta u,k} = \frac{1}{2} \sum_{j=0}^{N-1} \|\bar{W}_{\Delta u} \Delta u_{k+j}\|_2^2, \quad (25b)$$

where $\bar{W}_{\Delta u} = W_{\Delta u}/T_s$. The term $\varphi_{z,k}$ is output target tracking and $\varphi_{\Delta u,k}$ is input rate of movement penalty. We use the prediction and control horizon, T , defined as $T = NT_s$, where T_s is the sampling time and N is the discrete prediction and control horizon. Additionally, we define $\mathcal{N} = \{0, 1, \dots, N-1\}$ such that $t_{k+j} = t_k + jT_s$ for $j \in \mathcal{N}$. We solve the OCP with a simultaneous approach, where we discretize each control interval with M time steps using Euler's implicit method.

We denote the optimal solution $\{\hat{x}_{k+j+1|k}, \hat{u}_{k+j|k}\}_{j \in \mathcal{N}}$. The input corresponding to the first control interval, $u_k = \hat{u}_{k|k} = \lambda(\cdot)$, is part of the solution of this optimal control problem. Only u_k is implemented in the system. Furthermore, $\{\hat{z}_{k+j+1|k}, \hat{u}_{k+j|k}\}_{j=0}^{N-1} = z_k^c = \mu(\cdot)$ is the predicted output and the predicted manipulated inputs from the controller that can be used for visualization.

D. Simulation of closed-loop systems

We compactly write a closed-loop simulation as

$$y_k = g(t_k, x_k, p_g) + v_k, \quad (26a)$$

$$z_k = h(t_k, x_k, p_h), \quad (26b)$$

$$x_k^c = \kappa(t_{k-1}, x_{k-1}^c, y_k, u_{k-1}, p_\kappa), \quad (26c)$$

$$u_k = \lambda(t_k, x_k^c, p_\lambda), \quad (26d)$$

$$z_k^c = \mu(t_k, x_k^c, p_\mu), \quad (26e)$$

$$x_{k+1} = \Phi(t_k, x_k, u_k, d_k, w_k, p_f, p_\sigma), \quad (26f)$$

for $k = 0, 1, \dots, N_s - 1$.

III. MONTE CARLO SIMULATION

Our Monte Carlo simulations are based on the closed-loop simulation (26). We perform N_{mc} distinct closed-loop simulations for different, e.g., process noise realizations. Algorithm 1 presents an overview of the Monte Carlo simulation scheme. For sufficiently large N_{mc} , the computed Monte

Algorithm 1: Monte Carlo simulation

Result: Statistics and output data
 // Monte Carlo loop
for $i = 1, 2, \dots, N_{mc}$ **do**
 // Closed loop simulation
 for $k = 0, 1, \dots, N_s - 1$ **do**
 // Measurement
 $y_k^{(i)} = g(t_k, x_k^{(i)}, p_g^{(i)}) + v_k^{(i)}$
 // Output
 $z_k^{(i)} = h(t_k, x_k^{(i)}, p_h^{(i)})$
 // State estimation
 $x_k^{c,(i)} = \kappa(t_{k-1}, x_{k-1}^{c,(i)}, y_k^{(i)}, u_{k-1}^{(i)}, p_\kappa^{(i)})$
 // Regulator
 $u_k^{(i)} = \lambda(t_k, x_k^{c,(i)}, p_\lambda^{(i)})$
 // Output prediction
 $z_k^{c,(i)} = \mu(t_k, x_k^{c,(i)}, p_\mu^{(i)})$
 // Simulator
 $x_{k+1}^{(i)} = \Phi(t_k, x_k^{(i)}, u_k^{(i)}, d_k^{(i)}, w_k^{(i)}, p_f^{(i)}, p_\sigma^{(i)})$
end
 // Final measurement and output
 $y_{N_s}^{(i)} = g(t_{N_s}, x_{N_s}^{(i)}, p_g^{(i)}) + v_{N_s}^{(i)}$
 $z_{N_s}^{(i)} = h(t_{N_s}, x_{N_s}^{(i)}, p_h^{(i)})$
end

Carlo data can quantify uncertainties in the closed-loop system. Possible applications are; estimation of unknown model parameters, tuning controllers, and testing performance of controllers on different noise realizations.

A. Toolbox

We implement a Monte Carlo simulation toolbox for closed-loop systems in C. The toolbox provides an interface for closed-loop Monte Carlo simulations that currently includes implementations of

- an explicit-explicit Euler-Maruyama SDE solver,
- an implicit-explicit SDE solver,
- an open-loop controller,
- a single-input single-output (SISO) PID controller with clipping, and
- an NMPC based on the CD-EKF and a simultaneous approach combined with IPOPT [19].

The toolbox includes three test examples, and the user can provide a set of model functions for a system and perform Monte Carlo simulations with the toolbox. Additionally, the toolbox allows for user-provided controllers and SDE solvers with specific interfaces. This allows the user to test and benchmark controllers and SDE solvers using Monte Carlo simulations. The toolbox supports perturbations of model parameters, controller parameters, noise realizations, initial conditions, and disturbances.

We include a parallelized version with OpenMP for shared memory architectures. Each worker is assigned distinct closed-loop simulations. Such parallelization requires that

TABLE I
PARAMETERS FOR FED-BATCH REACTOR.

Variable	Value	Unit
μ_{\max}	0.37	1/h
K_S	0.021	kg/m ³
K_I	0.38	kg/m ³
γ_s	1.777	kg substrate/kg biomass
$c_{S,in}$	10.0	kg/m ³

TABLE II
INITIAL CONDITION AND OPERATIONAL BOUNDS.

Variable	Value	Unit
V_0	1.00	m ³
$c_{X,0}$	2.00	kg/m ³
$c_{S,0}$	0.0893	kg/m ³
V_{\max}	12.39	m ³
$c_{X,\max}$	2.00	kg/m ³
$c_{S,\max}$	3.00	kg/m ³
$F_{S,\max}$	10.00	m ³
$F_{W,\max}$	10.00	m ³

each worker has access to a local workspace for the SDE solver and the controller to avoid data races. Additionally, some controllers utilize information from previous steps, e.g., the integral term of a PID controller or the CD-EKF for an NMPC. Each worker also requires a local version of such information. The Monte Carlo simulation toolbox distributes memory blocks to each local worker, such that workers do not have overlapping cache lines. This consideration is essential for achieving optimal parallel performance.

We demonstrate some applications of the toolbox in section IV.

IV. BIOREACTOR IN FED-BATCH OPERATION**A. Model**

We consider the SDE model for a bioreactor in fed-batch operation [12],

$$dV = (F_S + F_W)dt + \sigma_1 d\omega_1(t), \quad (27a)$$

$$dm_X = (R_X V)dt + \sigma_2 d\omega_2(t), \quad (27b)$$

$$dm_S = (F_S c_{S,in} + R_S V)dt + \sigma_3 d\omega_3(t), \quad (27c)$$

where $m_X = c_X V$, $m_S = c_S V$, and

$$R_X = r, \quad r = \mu(c_S)c_X, \quad (28a)$$

$$R_S = -\gamma r, \quad \mu(c_S) = \mu_{\max} \frac{c_S}{K_S + c_S + c_S^2/K_I}. \quad (28b)$$

We represent the system as a stochastic continuous-discrete model in the form (1), where $x(t) = [V(t); m_X(t); m_S(t)]$, $y(t_k) = c_S(t_k) + v(t_k)$, and $z(t) = c_S(t)$.

Table I presents the parameters of the system and Table II presents the initial conditions and operational bounds of the system.

B. Control strategy

We operate the bioreactor with an open-loop input trajectory, $\bar{u} = [\bar{F}_W; \bar{F}_S]$. Additionally, we use a SISO PID

TABLE III
SYSTEM INFORMATION.

Architecture:	x86_64
CPU op-mode(s):	32-bit, 64-bit
CPU(s):	32
Thread(s) per core:	1
Core(s) per socket:	16
Socket(s):	2
NUMA node(s):	2
Model name:	Intel(R) Xeon(R) Gold 6226R CPU @ 2.90GHz
CPU MHz:	2900.000
L1d cache:	32 kB
L1i cache:	32 kB
L2 cache:	1024 kB
L3 cache:	22528 kB
RAM:	384 GB

controller with clipping, (15), that manipulate the substrate inlet, F_S , to achieve optimal substrate concentration, c_S^* , achieved at the maximum of $\mu(c_S)$,

$$c_S^* = \sqrt{K_I K_S}. \quad (29)$$

Thus, $\bar{z}(t) = c_S^*$. We use the bang-bang open-loop trajectory [12]. In the deterministic case, the bang-bang trajectory was one among infinitely many optimal solutions. However, it was the least sensitive to uncertainties. The inputs are computed as,

$$\bar{F}_W = \begin{cases} F_{W,\max}, & 0 \leq t \leq t_{\text{switch}}, \\ 0, & t_{\text{switch}} \leq t \leq t_f, \end{cases} \quad (30a)$$

$$\bar{F}_S = \frac{F_W c_S^* + \gamma_s \beta^*(t)}{c_{S,\text{in}} - c_S^*}, \quad (30b)$$

where

$$\beta^*(t) = \mu(c_S^*) c_{X,\max} V_0 \exp(\mu(c_S^*) t). \quad (31)$$

C. Simulation of the true system

We simulate the fed-batch reactor in closed-loop with an Euler-Maruyama solver. The reactor runs for 10 hours from time $t_0 = 0$ to $t_f = 10$ h. The sampling time is $T_s = 36$ seconds resulting in $N_s = 1000$ steps. At each step, we solve the SDE with $N_k = 10$ Euler-Maruyama steps.

D. Monte Carlo simulations of fed-batch reactor

Here, we demonstrate an application of the Monte Carlo simulation toolbox. The simulations are conducted on a dual-socket Intel(R) Xeon(R) Gold 6226R CPU @ 2.90GHz system (see Table III for CPU details).

1) *Scaling*: Fig. 1 shows the wall time and the scale-up for 10,000 Monte Carlo simulations. We observe close to linear scaling within one non-uniform memory access (NUMA) node, and slightly decreasing scale-up when exceeding one socket. We point out that the toolbox is not optimized to utilize multiple NUMA nodes, so a decrease in performance on more than one socket is expected.

2) *Open-loop controller*: We perform Monte Carlo simulations for the fed-batch reactor in open-loop. Fig. 3(a) shows a probability density function (PDF) plot for 30,000 realizations of process noise. The mean produced biomass is $\bar{m}_X(t_f) = 20.69$ kg.

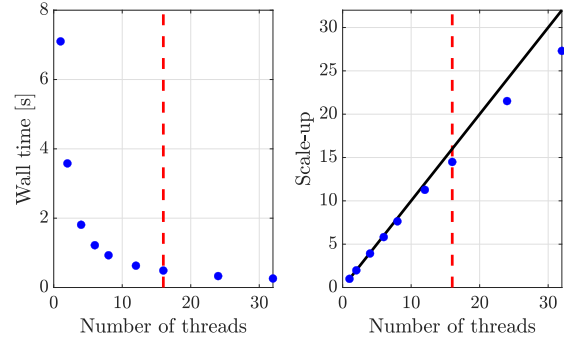


Fig. 1. Wall time and scale-up plots for 10,000 Monte Carlo simulations. The red dashed line is the number of cores on a single NUMA node. We get a scale-up of 27.3 on 32 cores.

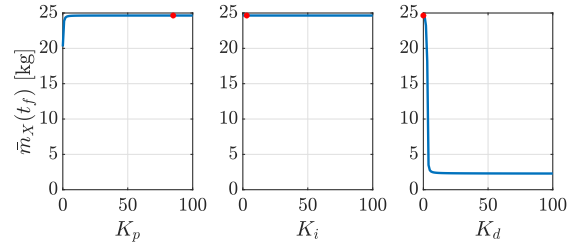
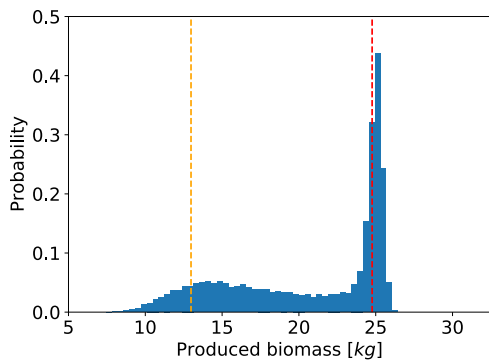


Fig. 2. Tuning of PID gains. Left: locate $K_p = 85$ as the optimum. Middle: locate $K_i = 3$ as the optimum. Right: locate $K_d = 0$ as the optimum. Total Monte Carlo simulations: $3 \cdot 101,000 = 303,000$. Computation time: ~ 7.50 seconds.

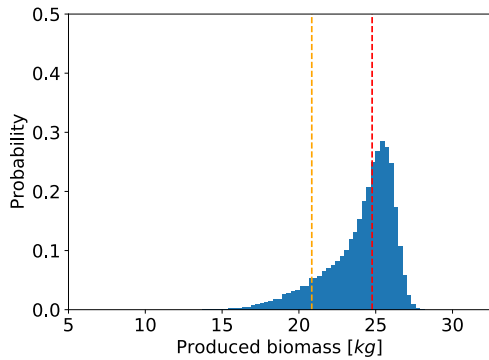
3) *Quantification of PID controller performance*: Consider a PID controller with $K_p = 1.0$, $K_i = 0.0$, and $K_d = 0.0$. We perform a Monte Carlo simulation with 30,000 process noise realizations. Fig. 3(b) presents a PDF plot of the produced biomass. The PDF follows a long-tailed distribution towards the lower values of produced biomass with mean produced biomass $\bar{m}_X(t_f) = 24.04$ kg, i.e., a 16.19% increase in biomass production compared to the open-loop controller. However, low produced biomass, for some realizations of process noise, indicates poor controller performance. The computation time of the Monte Carlo simulation is 0.77s. That is approximately a 2300 times speed-up compared to a reference serial implementation in Matlab.

4) *Tuning*: We apply Monte Carlo simulation to tune the value of K_p , K_i , and K_d in the PID controller. The tuning is based on maximizing the average produced biomass, $\bar{m}_X(t_f)$, for 1000 realizations of process noise. We point out that the tuning could have been based on other factors, e.g., maximizing the 10% quantile. We investigate 101 equidistant values in $[0, 100]$ of K_p , K_i , and K_d . Thus, the tuning of each gain requires 101,000 closed loop simulations. Fig. 2 shows the tuning results of the PID controller. The optimal parameters for the PID gains are $K_p = 85$, $K_i = 3$, and $K_d = 0$.

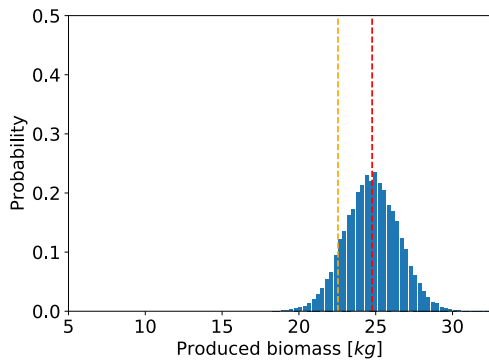
Fig. 3(c) shows a PDF plot for 30,000 noise realizations



(a) Open-loop controller. Computation time: 0.78s.



(b) Sub-optimal PID controller. Computation time: 0.77s.



(c) Optimal PID controller. Computation time: 0.76s.

Fig. 3. Probability density function of biomass production computed from 30,000 closed-loop simulations with different process noise realizations. The closed-loop consists of the fed-batch model, the Euler-Maruyama SDE solver, and a controller specified in the subplot. The red dashed line is the produced biomass in a simulation without process noise and the orange dashed line is the 10% quantile.

with the tuned PID controller. The PDF is almost normally distributed with mean produced biomass, $\bar{m}_X(t_f) = 24.76$. Compared to the non-optimal PID controller, the tuned controller results in an 2.98% increased average biomass

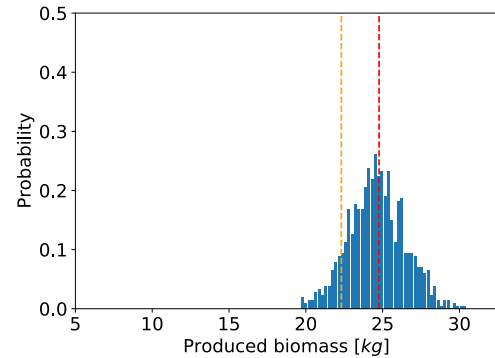


Fig. 4. Probability density function of biomass production computed from 1000 NMPC closed-loop simulations with different process noise realizations. The red dashed line is the produced biomass in a simulation without process noise and the orange dashed line is the 10% quantile. The computation time is ~ 30 min.

production and reduced risk of low biomass production. It is evident that the tuning improved the performance of the PID controller.

5) *NMPC*: Initial investigation of an NMPC based on the open source optimization software, IPOPT, does not show the same scaling as the PID controller. We observe a significant stall time in the memory allocation with `malloc()`, when increasing the number of threads. These calls to `malloc()` are located in IPOPT and give reason to believe that IPOPT has internal memory allocation. Each memory allocation has a lock that interrupts all activity, i.e., stalling all threads. In future work, we will expand the toolbox to include an NMPC based on optimization software that does not have internal memory allocation. We believe that scaling similar to the PID case can be achieved with such an NMPC. Fig. 4 presents a PDF plot for 1000 process noise realizations. The NMPC and the tuned PID controller show similar performance. The experiment is conducted on 6 cores as performance decreases above 6 cores due to the problem mentioned above. The computation time is ~ 30 min.

V. CONCLUSION

The paper presents a Monte Carlo simulation approach for performance quantification and tuning of controllers in linear and nonlinear systems. The approach is computationally feasible due to the implementation of a parallel high-performance Monte Carlo simulation toolbox in C for closed-loop systems. In particular, we demonstrate performance quantification and tuning of a PID controller for a bioreactor in fed-batch operation. Our results show that large-scale Monte Carlo simulations can be performed within seconds. The computational performance of the toolbox show approximately a 2300 times speed-up compared to a serial reference implementation in Matlab.

High-performance closed-loop Monte-Carlo simulations, as illustrated in this paper, has countless applications in systems and control. Drug dosing, as in treatment of diabetes,

is a very prominent example of this where several dosing strategies must be compared by their probability density functions [20], [21].

REFERENCES

- [1] D. Boiroux, T. K. S. Ritschel, N. K. Poulsen, H. Madsen, and J. B. Jørgensen, "Efficient Computation of the Continuous-Discrete Extended Kalman Filter Sensitivities Applied to Maximum Likelihood Estimation," *58th Conference on Decision and Control*, pp. 6983–6988, 2019.
- [2] H. G. Bock, E. Kostina, and J. P. Schlöder, "Numerical Methods for Parameter Estimation in Nonlinear Differential Algebraic Equations," *GAMM-Mitteilungen*, vol. 30, no. 2, pp. 376–408, 2007.
- [3] S. Skogestad, "Simple analytic rules for model reduction and PID controller tuning," *Journal of Process Control*, p. 291–309, 2003.
- [4] D. Olesen, J. K. Huusom, and J. B. Jørgensen, "A Tuning Procedure for ARX-based MPC," *IEEE Multi-conference on Systems and Control*, pp. 188–193, 2013.
- [5] D. H. Olesen, J. K. Huusom, and J. B. Jørgensen, "A tuning procedure for ARX-based MPC of multivariate processes," *American Control Conference*, pp. 1721–1726, 2013.
- [6] T. K. S. Ritschel, D. Boiroux, M. K. Nielsen, J. K. Huusom, S. B. Jørgensen, and J. B. Jørgensen, "Economic Optimal Control of a U-loop Bioreactor using Simultaneous Collocation-based Approaches," in *2019 IEEE Conference on Control Technology and Applications (CCTA)*. IEEE, 2019, pp. 933–938.
- [7] —, "Economic Nonlinear Model Predictive Control of a U-loop Bioreactor," in *2020 European Control Conference (ECC)*. IEEE, 2020, pp. 208–213.
- [8] L. J. Hong, S. Juneja, and J. Luo, "Estimating sensitivities of portfolio credit risk using Monte Carlo," *Inform Journal on Computing*, vol. 26, no. 4, pp. 848–865, 2014.
- [9] A. Shlyakhter, L. Mirny, A. Vlasov, and R. Wilson, "Monte Carlo Modeling of Epidemiologic Studies," *Human and Ecological Risk Assessment*, vol. 2, no. 4, pp. 920–936, 1996.
- [20] J. B. Jørgensen, D. Boiroux, and Z. Mahmoudi, "An artificial pancreas based on simple control algorithms and physiological insight," *12th Symposium IFAC on Dynamics and Control of Process Systems, including Biosystems (DYCOPS 2019)*, Florianópolis - SC, Brazil, April 23–26 2019.
- [10] S. J. Ratick and G. Schwarz, "Monte Carlo Simulation," in *Encyclopedia of Human Geography (Second Edition)*. Elsevier, 2009, ch. 14, pp. 175–185.
- [11] P. Ross, "Why CPU Frequency Stalled," *IEEE Spectrum*, vol. 45, no. 4, p. 72, 2008.
- [12] T. E. Ryde, M. R. Wahlgreen, M. K. Nielsen, S. Hørsholt, S. B. Jørgensen, and J. B. Jørgensen, "Optimal Feed Trajectories for Fed-batch Fermentation with Substrate Inhibition Kinetics," *International Symposium on Advanced Control of Chemical Processes, Accepted*, 2021.
- [13] D. J. Higham, "An Algorithmic Introduction to Numerical Simulation of Stochastic Differential Equations," *SIAM Review*, vol. 43, no. 3, pp. 525–546, 2001.
- [14] T. Tian and K. Burrage, "Implicit Taylor methods for stiff stochastic differential equations," *Applied Numerical Mathematics*, vol. 38, pp. 167–185, 2001.
- [15] B. Wittenmark, K. Johan Åström, and K.-E. Årzén, in *Computer Control: An Overview*. IFAC professional brief, 2009.
- [16] K. J. Åström and R. M. Murray, *Feedback Systems: An Introduction for Scientists and Engineers*. Princeton University Press, 2008.
- [17] M. R. Wahlgreen, E. Schroll-Fleischer, D. Boiroux, T. K. S. Ritschel, H. Wu, J. K. Huusom, and J. B. Jørgensen, "Nonlinear Model Predictive Control for an Exothermic Reaction in an adiabatic CSTR," *6th Conference on Advances in Control and Optimization of Dynamical Systems ACODS, Chennai, India*, February 16–19 2020.
- [18] J. B. Jørgensen, T. K. S. Ritschel, D. Boiroux, E. Schroll-Fleischer, M. R. Wahlgreen, M. K. Nielsen, H. Wu, and J. K. Huusom, "Simulation of NMPC for a Laboratory Adiabatic CSTR with an Exothermic Reaction," *Proceedings of 2020 European Control Conference*, pp. 202–207, 2020.
- [19] A. Wächter and L. T. Biegler, "On the implementation of an interior-point filter line-search algorithm for large-scale nonlinear programming," *Mathematical Programming*, vol. 106, no. 1, pp. 25–57, 2006.
- [21] D. Boiroux and J. Jørgensen, "Nonlinear Model Predictive Control and Artificial Pancreas Technologies," *IEEE Conference on Decision and Control (CDC)*, Miami Beach, Florida, USA, December 17–19 2018.

APPENDIX F

Conference Paper - ACC 2022

High-performance Uncertainty Quantification in
Large-scale Virtual Clinical Trials of Closed-loop
Diabetes Treatment

Authors:

Asbjørn Thode Reenberg, Tobias K. S. Ritschel, Bernd Dammann, John Bagterp Jørgensen

Published in:

Proceedings of the 2022 American Control Conference (ACC), Atlanta, USA, June 8-10, 2022.

2022 American Control Conference (ACC)
Atlanta, USA, June 8-10, 2022

High-performance Uncertainty Quantification in Large-scale Virtual Clinical Trials of Closed-loop Diabetes Treatment

Asbjørn Thode Reenberg, Tobias K. S. Ritschel, Bernd Dammann, John Bagterp Jørgensen

Abstract—In this paper, we propose a virtual clinical trial for assessing the performance and identifying risks in closed-loop diabetes treatments. Virtual clinical trials enable fast and risk-free tests of many treatment variations for large populations of fictive patients (represented by mathematical models). We use closed-loop Monte Carlo simulation, implemented in high-performance software and hardware, to quantify the uncertainty in treatment performance as well as to compare the performance in different scenarios or of different closed-loop treatments. Our software can be used for testing a wide variety of control strategies ranging from heuristical approaches to nonlinear model predictive control. We present an example of a virtual clinical trial with one million patients over 52 weeks, and we use high-performance software and hardware to conduct the virtual trial in 1 h and 22 min.

I. INTRODUCTION

Clinical trials of medical treatments are crucial to ensuring a high level of safety and efficacy. However, they are also very expensive and time-consuming. Therefore, it is important to assess the treatment performance, identify potential risks, and rigorously compare with state-of-the-art prior to the trials. *Virtual* clinical trials are used for exactly this purpose. In a virtual clinical trial, each patient is represented by a mathematical model and the clinical trial is simulated using high-performance software and hardware. The simulation is carried out for a large population of virtual patients, many different scenarios, and several variations of the treatment. This allows for thorough and *fast* testing of a large variety of different treatment designs.

In this paper, we specifically consider the treatment of type 1 diabetes (T1D). One in eleven adults suffer from diabetes (both types), and in 2019, 10% of the global health expenditure (USD 760 billion) was spent on diabetes [1]. Due to autoimmune destruction of β -cells, people with T1D are unable to produce insulin. Consequently, life-long treatment involving daily injections of insulin is necessary to avoid elevated blood glucose (BG) levels (hyperglycemia), which can lead to several complications and chronic conditions [2]. The BG concentration must be measured in order to determine an appropriate insulin dose. While too little insulin results in hyperglycemia, too much insulin results in hypoglycemia (low BG levels), which can be fatal in very severe cases.

As monitoring the BG and determining the appropriate insulin dose is laborious, there is significant interest in auto-

mated closed-loop diabetes treatment systems. Such systems are referred to as artificial pancreases (APs), and they consist of 1) a continuous glucose monitor (CGM), 2) a control algorithm that determines the insulin dose, and 3) a pump which delivers the insulin to the patient (it is possible to use other hormones, e.g., glucagon or amylin, in addition to insulin). Many AP algorithms have been proposed and the majority is based on heuristics [3], proportional-integral-derivative (PID) control [4], fuzzy logic [5], linear model predictive control (MPC) [6]–[8], or nonlinear MPC [9], [10].

All AP algorithms contain hyperparameters, e.g., the gains in a PID controller, and performance assessment is essential to choosing suitable values for these. There exist both process-independent performance measures for this purpose, e.g., setpoint deviation and variance, and process-specific measures [11]–[13]. For diabetes treatment, including closed-loop systems, time-in-range (TIR), Hb1Ac values, and the probability of severe hypoglycemia [14]–[18] are commonly used (process-specific) performance measures. The performance of an AP can vary significantly between T1D patients due to differences in physiology (e.g., in pharmacodynamics and pharmacokinetics). Therefore, it is necessary to evaluate the performance measures for a large population of patients in order to accurately estimate the uncertainty. However, due to computational limitations of standard software, it is common to evaluate the performance using only a small number of patients and over a short time span (days or a few weeks).

In this work, we describe an approach for high-performance uncertainty quantification of the performance of AP algorithms in large-scale long-term virtual clinical trials. The approach involves mathematical models based on stochastic differential equations (SDEs), and we use closed-loop Monte Carlo simulation to quantify the performance uncertainty. Furthermore, we propose multiple ways of 1) visualizing the uncertainty in the performance measures and 2) comparing the performance for different scenarios or AP algorithms. We implement the Monte Carlo simulation and the AP in parallelized high-performance C code, and the computations are carried out on a high-performance computing (HPC) cluster. Finally, we present a numerical example of a virtual clinical trial with one million patients over 52 weeks which can be carried out in 1 h and 22 min.

The remaining part of this paper is organized as follows. In Section II, we describe the virtual clinical trial, and in Section III, we present the approach for uncertainty quantification of AP algorithms. Section IV contains the numerical examples, and conclusions are presented in Section V.

This work was partially funded by the IFD Grand Solution project ADAPT-T2D (9068-00056B). *A. T. Reenberg, T. K. S. Ritschel, Bernd Dammann, and J. B. Jørgensen are with the Department of Applied Mathematics and Computer Science, Technical University of Denmark, DK-2800 Kgs. Lyngby, Denmark. Corresponding author: J. B. Jørgensen (E-mail: jbj@dtu.dk).

II. VIRTUAL CLINICAL TRIAL

The virtual clinical trial consists of 1) a population of patients, 2) a protocol containing the trial activities (size and duration of meals, intensity and duration of exercise, etc.), 3) one or more mathematical models of the patients, 4) values of the model parameters, and 5) one or more APs (i.e., control algorithms). Furthermore, it is possible to include both incorrectly announced and unannounced meals and exercise which are some of the key challenges that an AP should be able to address. Finally, the virtual clinical trial allows for *stochastic* mathematical models which can represent unmodeled physiological phenomena, uncertain model parameters, and uncertainty related to meals and exercise, as well as noisy sensor measurements.

A. Patients

The virtual clinical trial contains one million fictive patients. Each patient is represented by the same information that would be available for a real patient. Specifically, each fictive patient is associated with a unique ID and a set of attributes including first and last name, date and place of birth, sex, height, body weight, and resting heart rate. The height, the body weight and the resting heart rate are sampled from normal distributions, and the date of birth is sampled from a uniform distribution.

B. Protocols

A protocol consists of a sequence of model *disturbances*, i.e., uncontrolled inputs to the patient model. Common disturbances are meals and exercise. Each protocol has an ID and for each disturbance, it contains the disturbance type and size as well as time stamps indicating the beginning and end of the disturbance.

Next, to illustrate the concept, we describe a protocol designed to mimic a Northern European lifestyle in terms of meal times, seasons, work weeks, and the number of vacation weeks and public holidays. Furthermore, the protocol involves a high-carb diet (in particular during winter and autumn), which is challenging for APs. We divide the year into 4 seasons each consisting of 13 weeks, and we assume 6 weeks of vacation and 10 public holidays, represented as an additional 2 weeks of vacation. Each season is a different combination of three basis weeks; a *standard week*, an *active week*, and a *vacation week*. Furthermore, each basis week is a different combination of four basis days; a *standard day*, an *active day*, a day with a *movie night*, and a day with a *late night*. Table I shows the compositions of the seasons and the weeks.

The patients are less active and eat more during vacation weeks, they also eat more during winter and autumn, and active weeks contain more active days. Compared to the standard day, 1) the active day has an exercise session, 2) the movie night has an additional snack in the evening, and 3) the late night has two additional snacks in the evening. Fig. 1 shows schematics of the basis days, and Table II shows the meal sizes which depend on the body weight.

TABLE I
COMPOSITIONS OF THE SEASONS AND THE WEEKS

Compositions of the seasons			
Season	Standard week	Active week	Vacation week
Winter	6	4	3
Spring	6	6	1
Summer	7	3	3
Autumn	9	3	1

Compositions of the weeks				
Week type	Standard day	Active day	Movie night	Late night
Standard	4	1	1	1
Active	3	3	1	0
Vacation	5	0	0	2

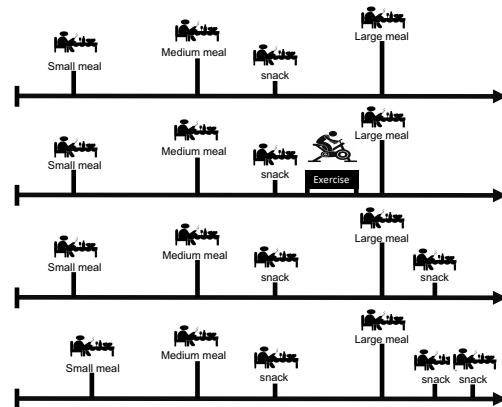


Fig. 1. Overview of the basis days in winter and autumn. From the top, we show 1) the *standard day*, 2) the *active day*, 3) the *movie night*, and 4) the *late night*. During the summer and spring, the dinner is a *medium meal* and the snack is before lunch.

C. Database

A key component of the virtual clinical trial is a database containing the fictive patients, protocols, model parameters, and simulation results. We use the open-source database system PostgreSQL. Using a database makes it straightforward to share the virtual clinical trial and compare performance results for the exact same patients and protocols. It also allows the user to carry out the clinical trial for a specific demographic, e.g., people with a certain body weight or sex. Furthermore, the database includes several basis days and weeks which the user can combine to form new protocols. Finally, the database can be extended with a graphical user interface in order to 1) visualize the AP performance and characteristics of the patients and protocols and 2) add

TABLE II
WEIGHT-DEPENDENT MEAL SIZES

Meal size	Amount of carbohydrates	For a 70 kg patient
Large meal	1.29 g CHO/kg	90 g CHO
Medium meal	0.86 g CHO/kg	60 g CHO
Small meal	0.57 g CHO/kg	40 g CHO
Snack	0.29 g CHO/kg	20 g CHO

new elements such as patients, protocols, and mathematical models to the database.

III. CLOSED-LOOP MONTE CARLO SIMULATION

In Monte Carlo simulation, the uncertainty of a quantity of interest (e.g., the TIR for a T1D patient) is estimated by simulating the system (i.e., the clinical trial) with different values of the uncertain quantities (e.g., the model parameters). In this work, we extend the high-performance toolbox for closed-loop Monte Carlo simulation developed by Wahlgreen et al. [19] with a low-memory implementation which circumvents the high storage requirements associated with large numbers of long-term simulations.

A. Mathematical model

The virtual clinical trial can be used for mathematical models of patient physiology in the general stochastic form

$$x(t_0) = x_0, \quad (1a)$$

$$dx(t) = f(t, x(t), u(t), d(t), p)dt + \sigma(t, x(t), u(t), d(t), p)dw(t), \quad (1b)$$

$$z(t) = h(t, x(t), p) \quad (1c)$$

$$y(t_k) = g(t_k, x(t_k), p) + v(t_k). \quad (1d)$$

Here, t is time, and the virtual clinical trial starts at time t_0 . The states, x , represent the physiological state of the patient, e.g., the BG concentration and amount of insulin in the body, and x_0 are the initial states. The manipulated inputs, u , are the quantities computed by the AP, e.g., the insulin flow rate. The disturbance variables, d , represent the uncontrolled inputs, e.g., meals and exercise, and p are model parameters. The first term in (1b) is the deterministic drift term and the second term is the stochastic diffusion term.

The AP receives measurements of the observed variables, y , obtained from the measurement function, g , at discrete points in time, t_k , and the outputs, z , obtained from the output function, h , are the quantities relevant to the control objective of the AP. The standard Wiener process w is used to represent uncertainty. Its increment is distributed as $dw(t) \sim N_{iid}(0, Idt)$, and the measurement noise is assumed to be normally distributed: $v(t_k) \sim N_{iid}(0, R(t_k))$. Furthermore, the inputs are assumed to be piecewise constant between sampling times:

$$u(t) = u_k, \quad t \in [t_k, t_{k+1}[, \quad (2a)$$

$$d(t) = d_k, \quad t \in [t_k, t_{k+1}[. \quad (2b)$$

Finally, we stress that the form (1b) also includes *deterministic* dynamical systems, i.e., ordinary differential equations (ODEs), where σ is zero.

B. Control algorithm

At time t_k , 1) the control state, x_k^c , is updated, and 2) the AP (i.e., the closed-loop feedback control strategy) computes values of the manipulated inputs based on the previous control state and the measurements, $y_k = y(t_k)$:

$$x_{k+1}^c = \kappa_k(x_k^c, y_k, \bar{u}_k, \bar{y}_k, \hat{d}_k, p_\kappa), \quad (3a)$$

$$u_k = \lambda_k(x_k^c, y_k, \bar{u}_k, \bar{y}_k, \hat{d}_k, p_\mu). \quad (3b)$$

Here, \bar{u}_k and \bar{y}_k are setpoints, and \hat{d}_k are estimates of the disturbances. This form can represent many types of closed-loop control strategies including heuristic strategies based on physiological insight, PID-based strategies, and MPC (including state estimation). Many different values of the hyperparameters p_μ and p_κ can be tested using the virtual clinical trial.

C. Software and hardware

The closed-loop Monte Carlo simulation, the mathematical models, and the AP are implemented using high-performance C code which we parallelize for shared-memory architectures using OpenMP. Whenever a simulation is completed, we immediately compute its contribution to performance indicators such as TIR as well as mean, minimum, and maximum BG concentration as functions of time. Subsequently, the simulation is only stored if it is worse than previous simulations according to some criterion (e.g., lowest BG concentration reached).

We use two AMD EPYC 7542 32-core processors with a clock speed of 2.9 GHz [20]. As the Monte Carlo simulation is highly parallelizable, the speedup in computational performance increases almost linearly with the number of cores. Consequently, the parallel implementation runs almost 64 times faster than a corresponding sequential implementation. Furthermore, it would be computationally infeasible to carry out large-scale long-term virtual clinical trials using a sequential Matlab implementation [19] or similar.

IV. EXAMPLE OF A VIRTUAL CLINICAL TRIAL

In this section, we present an example of a virtual clinical trial involving a million virtual patients following the example protocol described in Section II-B. We briefly describe the mathematical model of the patients' physiology and the AP used in the trial, and we demonstrate how to visualize the uncertainty in the AP performance. Furthermore, we also show how to compare the performance of the AP in two different scenarios; one where the basal rate is correct (trial A) and another where it is underestimated by 50% (trial B). Finally, the computation time is 1 h and 22 min (with a time step size of 30 s in the simulations). Consequently, several virtual clinical trials can be carried out in a single day.

A. Performance measures

We divide the BG concentration into 5 ranges [14] given in mmol/L. Red: severe hypoglycemia (below 3). Light red: hypoglycemia (3–3.9). Green: normoglycemia (3.9–10). Yellow: hyperglycemia (10–13.9). Orange: severe hyperglycemia (above 13.9). Furthermore, we also consider the distributions of the total daily basal and bolus insulin as well as bolus glucagon.

B. Patient model

We use an extension of the model presented by Hovorka et al. [9] to represent the pharmacokinetic and pharmacodynamical responses of the virtual patients to carbohydrate absorption and subcutaneous infusion of insulin and glucagon.

The model is extended with 1) a one-state model of the measured BG concentration, 2) a two-state pharmacokinetic model of subcutaneous glucagon injection [21], and 3) a three-state model of the effect of exercise on the plasma BG concentration [22].

The model parameters related to the measured BG concentration, glucagon infusion, and exercise have the same values for all virtual patients. We sample the remaining model parameters from the distributions presented by Hovorka et al. [23]. We only use parameter sets where the parameter values are nonnegative, the normally distributed parameters are within one standard deviation from the mean, and the insulin basal rate is at least 0.4 U/h.

C. Artificial pancreas

We demonstrate the capabilities of the virtual clinical trial using a dual-hormone AP which switches between an insulin mode and a glucagon mode. Glucagon is used to mitigate hypoglycemia. The insulin mode involves 1) microadjustments of the basal rate, 2) a meal bolus calculator, 3) superboli, and 4) an insulin-to-carb ratio estimator. In the glucagon mode, only microboli are administered. In both modes, a 100 μ g glucagon bolus is administered at the beginning of exercise if the blood glucose concentration is below 7 mmol/L. No insulin is administered in the glucagon mode, and no glucagon, apart from the exercise bolus, is administered in the insulin mode. The AP uses filtered estimates of the glucose concentration obtained with a low-pass filter, and several hyperparameters have different values depending on whether the patient is exercising or not.

Fig. 2 shows week 14 of a simulation for a single patient. The AP administers insulin boli at meal times, the basal rate is turned off for a period after the meals, and a small glucagon bolus is administered during exercise, i.e., it is not the 100 μ g bolus at the beginning of exercise. As is evident, the TIR is high for the shown period.

D. Performance of the artificial pancreas

Fig. 3 shows the amount of time spent below different BG concentrations. It allows us to inspect the worst-case patient (lowest BG concentration reached), the population average, and the values reached by at least one patient (the span). The worst-case patient is useful for identifying weaknesses in the AP. Here, it seems unlikely that the basal rate is too high because the patient suffers from severe hyperglycemia almost 40% of the time. This can also be seen from the stacked bar chart in the middle of Fig. 4. The population mean can reveal systemic issues. On average, the patients spend almost all of their time above the target of 6 mmol/L. Perhaps too little insulin is administered. Finally, the shaded area can be used to conclude that, e.g., 1) no patient spends more than 6% of their time below 3.9 mmol/L and 2) nobody is above 13.9 mmol/L more than 40% of the time.

Whereas the two stacked bar charts in the left of Fig. 4 provide an intuitive overview, the box plot on the right gives a comprehensive picture of the TIR for the entire population. The red markers show that only a few patients experience

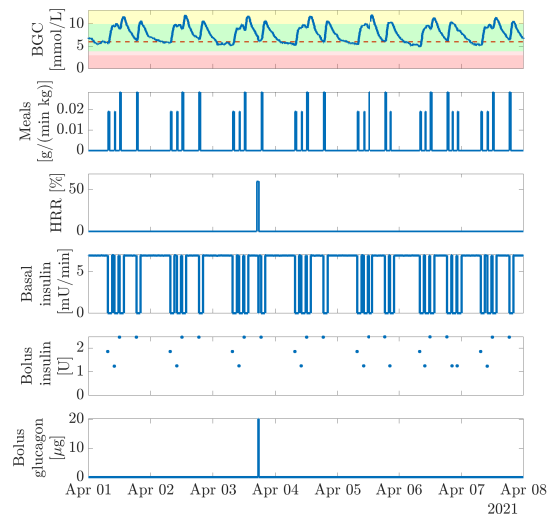


Fig. 2. Week 14 of a simulation for 1 patient. From the top we show: 1) The BG concentration (BGC), 2) the meal carbohydrate content (shown as a rate dependent on the body weight), 3) the resting heart rate reserve (HRR), 4) the administered insulin basal rate, 5) the insulin boli, and 6) the glucagon boli.

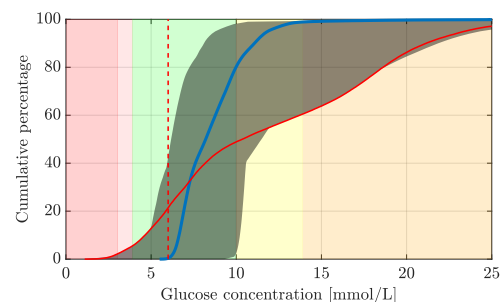


Fig. 3. Cumulative distribution of the BG concentration in a virtual clinical trial with 1 million patients over 52 weeks. Blue solid line: The mean BG concentration. Red solid line: The worst-case patient. Red dashed line: The setpoint. Grey shaded area: The span of all the patients.

hypoglycemia. On average, the patients spend 77% of their time in range, and for most patients, this value is at least 55%. However, a significant part spends between 5% and 40% above 13.9 mmol/L. Finally, Fig. 5 shows distributions of the total insulin and glucagon administered per day. These distributions can be compared with dosage guidelines to see if extreme amounts are administered. For instance, it is positive that for the most part, only small amounts of glucagon are administered here.

E. Comparison of scenarios

When comparing different scenarios or APs, the plots in Fig. 3–5 can be overlaid or combined as shown in Fig. 6–8. It is clear from Fig. 6 that the basal rate is too low in trial B. However, the worst-case patients reach equally low

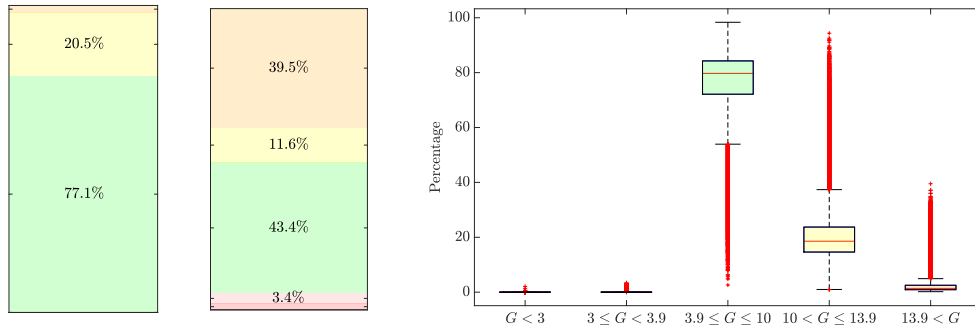


Fig. 4. Distribution of the TIRs for a virtual clinical trial with 1 million patients over 52 weeks. Left: Mean TIRs for all patients. Middle: TIRs for the worst-case patient. Right: Box plot of the TIRs for all patients.

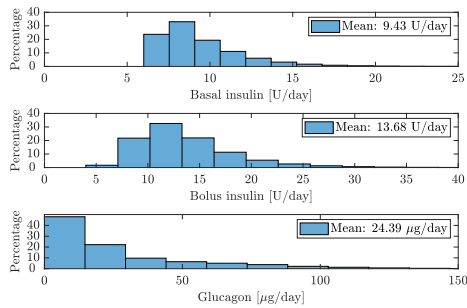


Fig. 5. Distributions of the total daily basal and bolus insulin and bolus glucagon for a virtual clinical trial with 1 million patients over 52 weeks. Top: Basal insulin. Middle: Bolus insulin. Bottom: Bolus glucagon.

BG concentrations in both trials. Fig. 7 also clearly shows that far better TIRs are reached with the correct basal rate although the worst-case patient experiences hypoglycemia more often with the correct basal rate. Fig. 8 allows for direct comparison of how much insulin and glucagon that is administered on a daily basis. Obviously, less basal insulin is administered in trial B, and as a result, more bolus insulin is given. Consequently, more glucagon is given in trial B.

V. CONCLUSION

In this paper, we present a virtual clinical trial for assessing the uncertainty in the performance of closed-loop diabetes treatments. We use a high-performance closed-loop Monte Carlo method for quantifying the uncertainty, and we evaluate the performance by examining 1) the distributions of the TIRs for the patient population and 2) the distributions of the total daily doses of basal and bolus insulin as well as bolus glucagon. Furthermore, this approach can be used to compare the performance in different scenarios and for different closed-loop treatments. Finally, we demonstrate that a virtual clinical trial with one million patients over 52 weeks can be completed in 1 h and 22 min by using parallel high-performance software and hardware. The developed software can be used for closed-loop systems with any drug

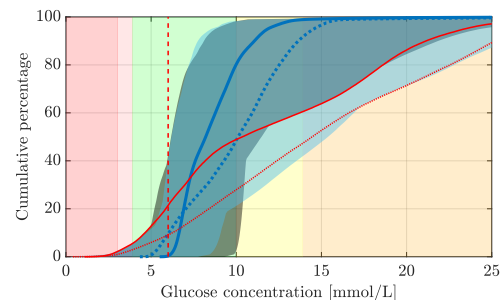


Fig. 6. Cumulative distribution of the BG concentration in two virtual clinical trials of 1 million patients over 52 weeks. Blue solid line: The mean BG concentration of trial A. Blue dotted line: The mean BG concentration of trial B. Red solid line: The patient that reaches the lowest BG concentration in trial A. Red dotted line: The patient that reaches the lowest BG concentration in trial B. Red dashed line: The setpoint. Grey shaded area: The span of all patients in trial A. Light blue shaded area: The span of all patients in trial B.

administration device (pump or pen) and measurement device (CGM or self-monitoring of blood glucose (SMBG) device).

REFERENCES

- [1] International Diabetes Federation, "IDF diabetes atlas 9th edition," 2019, ISBN: 978-2-930229-87-4.
- [2] American Diabetes Association, "Diabetes technology: Standards of medical care in diabetes," *Diabetes Care*, vol. 41, no. 1, 2018.
- [3] I. Capel, M. Rigla, G. García-Saez, A. Rodríguez-Herrero, B. Pons, D. Subias, F. García-García, M. Gallach, M. Aguilar, C. Perez-Gandia, E. J. Gomez, A. Caixas, and M. E. Hernando, "Artificial pancreas using a personalized rule-based controller achieves overnight normoglycemia in patients with type 1 diabetes," *Diabetes Technology and Therapeutics*, vol. 16, no. 3, pp. 172–179, 2014.
- [4] G. Marchetti, M. Barolo, L. Jovanovic, H. Zisser, and D. E. Seborg, "An improved PID switching control strategy for type 1 diabetes," *IEEE Transactions on Biomedical Engineering*, vol. 55, no. 3, pp. 857–865, 2008.
- [5] T. Biester, J. Nir, K. Remus, A. Farfel, I. Muller, S. Biester, E. Atlas, K. Dovc, N. Bratina, O. Kordonouri, T. Battelino, M. Philip, T. Danne, and R. Nimri, "DREAM5: An open-label, randomized, cross-over study to evaluate the safety and efficacy of day and night closed-loop control by comparing the MD-Logic automated insulin delivery system to sensor augmented pump therapy in patients with type 1 diabetes at home," *Diabetes, Obesity and Metabolism*, vol. 21, no. 4, pp. 822–828, 2019.

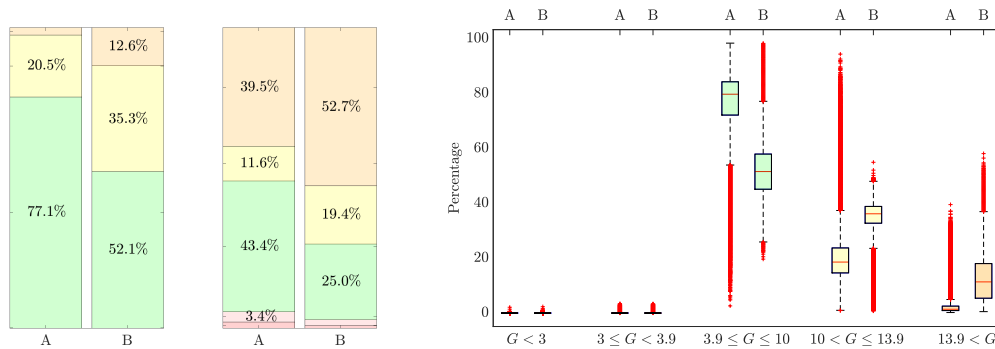


Fig. 7. Distribution of the TIRs for two virtual clinical trials of 1 million patients over 52 weeks. Left: Mean TIRs for all patients in trial A and trial B. Middle: TIRs for the worst-case patients in trial A and trial B. Right: Box plot of the TIRs for all patients in trial A and trial B.

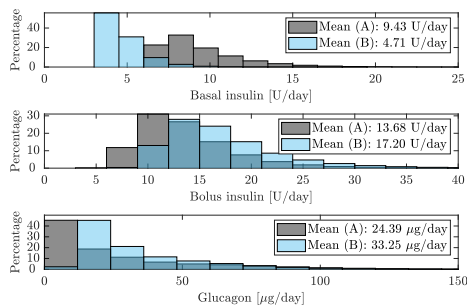


Fig. 8. Distributions of the total daily basal and bolus insulin and bolus glucagon for two virtual clinical trials with 1 million patients over 52 weeks. Top: Basal insulin. Middle: Bolus insulin. Bottom: Bolus glucagon. Grey: Trial A. Light blue: Trial B.

- [6] M. Eren-Oruklu, A. Cinar, L. Quinn, and D. Smith, "Adaptive control strategy for regulation of blood glucose levels in patients with type 1 diabetes," *Journal of Process Control*, vol. 19, no. 8, pp. 1333–1346, 2009.
- [7] S. Schmidt, D. Boiroux, A. K. Duun-Henriksen, L. Frössing, O. Skyggebjerg, J. B. Jørgensen, N. K. Poulsen, H. Madsen, S. Madsbad, and K. Nørgaard, "Model-based closed-loop glucose control in type 1 diabetes: The DiaCon experience," *Journal of Diabetes Science and Technology*, vol. 7, no. 5, pp. 1255–1264, 2013.
- [8] D. Boiroux, A. K. Duun-Henriksen, S. Schmidt, K. Nørgaard, S. Madsbad, N. K. Poulsen, H. Madsen, and J. B. Jørgensen, "Overnight glucose control in people with type 1 diabetes," *Biomedical Signal Processing and Control*, vol. 39, pp. 503–512, 2018.
- [9] R. Hovorka, V. Canonico, L. Chassin, U. Haueter, M. Massi-Benedetti, M. Federici, T. Pieber, H. Schaller, L. Schaupp, T. Vering, and M. Wilinska, "Nonlinear model predictive control of glucose concentration in subjects with type 1 diabetes," *Physiological Measurement*, vol. 25, no. 4, pp. 905–920, 2004.
- [10] D. Boiroux and J. B. Jørgensen, "Nonlinear model predictive control and artificial pancreas technologies," in *2018 IEEE Conference on Decision and Control (CDC)*, 2018, pp. 284–290.
- [11] K. J. Åström, "Assessment of achievable performance of simple feedback loops," Department of Automatic Control, Lund Institute of Technology, Tech. Rep. TFRT-7411, 1989.
- [12] T. J. Harris, "Assessment of control loop performance," *The Canadian Journal of Chemical Engineering*, vol. 67, pp. 856–861, 1989.
- [13] M. Jelali, "An overview of control performance assessment technology and industrial applications," *Control Engineering Practice*, vol. 14, pp. 441–446, 2006.
- [14] R. I. G. Holt, J. H. DeVries, A. Hess-Fischl, I. B. Hirsch, M. S. Kirkman, T. Klupa, B. Ludwig, K. Nørgaard, J. Pettus, E. Renard, J. S. Skyler, F. J. Snoek, R. S. Weinstock, and A. L. Peters, "The management of type 1 diabetes in adults. A consensus report by the American Diabetes Association (ADA) and the European Association for the Study of Diabetes (EASD)," *Diabetes Care*, vol. 44, pp. 2589–2625, 2021.
- [15] H. Calsbeek, N. A. B. M. Ketelaar, M. J. Faber, M. Wensing, and J. Braspenning, "Performance measurements in diabetes care: The complex task of selecting quality indicators," *International Journal for Quality in Health Care*, vol. 25, no. 6, pp. 704–709, 2013.
- [16] R. A. Lal, C. L. Maikawa, D. Lewis, S. W. Baker, A. A. A. Smith, G. A. Roth, E. C. Gale, L. M. Stapleton, J. L. Mann, A. C. Yu, S. Correa, A. K. Grosskopf, C. S. Liong, C. M. Meis, D. Chan, J. P. Garner, D. M. Maahs, B. A. Buckingham, and E. A. Appel, "Full closed loop open-source algorithm performance comparison in pigs with diabetes," *Clinical and Translational Medicine*, vol. 11, p. e387, 2021.
- [17] I. Hajizadeh, S. Samadi, M. Sevil, M. Rashid, and A. Cinar, "Performance assessment and modification of an adaptive model predictive control for automated insulin delivery by a multivariable artificial pancreas," *Industrial & Engineering Chemistry Research*, vol. 58, pp. 11 506–11 520, 2019.
- [18] M. Sejersen, D. Boiroux, S. E. Engell, T. K. S. Ritschel, A. T. Reenberg, and J. B. Jørgensen, "Initial titration for people with type 1 diabetes using an artificial pancreas," *IFAC PapersOnLine*, vol. 54, no. 15, pp. 484–489, 2021.
- [19] M. R. Wahlgreen, A. T. Reenberg, M. K. Nielsen, A. Rydahl, T. K. S. Ritschel, B. Dammann, and J. B. Jørgensen, "A high-performance Monte Carlo simulation toolbox for uncertainty quantification of closed-loop systems," in *2021 IEEE Conference on Decision and Control (CDC)*, 2021, pp. 6755–6761.
- [20] DTU Computing Center, "DTU Computing Center resources," 2021, Technical University of Denmark. [Online]. Available: <https://doi.org/10.48714/DTU.HPC.0001>
- [21] S. L. Wendt, J. K. Møller, C. B. Knudsen, H. Madsen, A. Haidar, and J. B. Jørgensen, "PK/PD modelling of glucose-insulin-glucagon dynamics in healthy dogs after a subcutaneous bolus administration of native glucagon or a novel glucagon analogue," Technical University of Denmark, Tech. Rep. 2, 2016.
- [22] M. Rashid, S. Samadi, M. Sevil, I. Hajizadeh, P. Kolodziej, N. Hobbs, Z. Maloney, R. Brandt, J. Feng, M. Park, L. Quinn, and A. Cinar, "Simulation software for assessment of nonlinear and adaptive multivariable control algorithms: Glucose-insulin dynamics in type 1 diabetes," *Computers & Chemical Engineering*, vol. 130, p. 106565, 2019.
- [23] R. Hovorka, F. Shojae-Moradie, P. V. Carroll, L. J. Chassin, I. J. Gowrie, N. C. Jackson, R. S. Tudor, A. M. Umpleby, and R. H. Jones, "Partitioning glucose distribution/transport, disposal, and endogenous production during IVGTT," *American Journal of Physiology-Endocrinology and Metabolism*, vol. 282, pp. E992–E1007, 2002.

APPENDIX G

Conference Paper - FOSBE 2022

Large-scale Virtual Clinical Trials of Closed-loop
Treatments for People with Type 1 Diabetes

Authors:

Tobias K. S. Ritschel, Asbjørn Thode Reenberg, John Bagterp Jørgensen

Published in:

IFAC-PapersOnLine, 55–23, 169–174, 2022.

Proceedings of the 9th IFAC Conference on Foundations of Systems Biology in Engineering (FOSBE), Cambridge, Massachusetts, USA, August 28-31, 2022.



Large-scale Virtual Clinical Trials of Closed-loop Treatments for People with Type 1 Diabetes

Tobias K. S. Ritschel, Asbjørn Thode Reenberg,
John Bagterp Jørgensen

Department of Applied Mathematics and Computer Science,
Technical University of Denmark, DK-2800 Kgs. Lyngby, Denmark
(e-mail: jbjo@dtu.dk).

Abstract: We propose a virtual clinical trial for assessing the safety and efficacy of closed-loop diabetes treatments prior to an actual clinical trial. Such virtual trials enable rapid and risk-free pretrial testing of algorithms, and they can be used to compare different treatment variations for large and diverse populations. The participants are represented by multiple mathematical models, consisting of stochastic differential equations, and we use Monte Carlo closed-loop simulations to compute detailed statistics of the closed-loop treatments. We implement the virtual clinical trial using high-performance software and hardware, and we present an example trial with two mathematical models of one million participants over 52 weeks (i.e., two million simulations), which can be completed in 2 h 9 min.

Copyright © 2022 The Authors. This is an open access article under the CC BY-NC-ND license (<https://creativecommons.org/licenses/by-nc-nd/4.0/>)

Keywords: Virtual clinical trials, Diabetes, Stochastic modeling, High-performance computing

1. INTRODUCTION

Clinical trials ensure the safety and efficacy of medical treatments, but they are also time-consuming and expensive. Furthermore, they might result in a negative outcome, e.g., that the proposed treatment is not safe. Therefore, prior to the actual clinical trial, it is important to 1) evaluate the potential treatment performance, 2) identify shortcomings and risks, and 3) assess the advantages of the treatment over alternative treatments. This is the purpose of *virtual* clinical trials which involve virtual participants that are represented by a mathematical model (often consisting of differential equations). By using high-performance computing (HPC) software and hardware, such virtual trials can involve large populations and long-term protocols, which allows for extensive and fast testing of different treatment variations.

In this paper, we consider virtual clinical trials of closed-loop diabetes treatment systems. These are also referred to as *artificial pancreases* (APs). Worldwide, one in ten adults suffer from diabetes, and according to the International Diabetes Federation (2021), it accounted for 9% of the 2021 global health expenditure (USD 966 billion). Specifically, we consider type 1 diabetes (T1D) where, due to autoimmune destruction of the β -cells, the pancreas does not produce any insulin. People with T1D require daily treatment with exogenous insulin in order to avoid high blood glucose concentrations (hyperglycemia). Prolonged hyperglycemia can lead to a number of health complications and chronic conditions, e.g., chronic kidney disease, cardiovascular disease, and damage to the eyes and nerves. Conversely, the insulin treatment can lead to low

blood glucose concentrations (hypoglycemia), which can result in acute complications such as loss of consciousness and seizures.

Clearly, given the risks associated with hyper- and hypoglycemia, it is not straightforward for people with T1D to manage their insulin treatment. Therefore, over the last few decades, there have been significant developments within AP systems which can decrease this burden (Lal et al., 2019). APs typically consist of 1) a continuous glucose monitor (CGM), 2) an insulin pump, and 3) a control algorithm implemented on a smartphone or a dedicated device. The control algorithm repeatedly computes an appropriate insulin flow rate based on measurements from the CGM device and communicates it to the insulin pump. There exist a variety of control algorithms for computing the insulin flow rate, e.g., based on heuristics, fuzzy logic, proportional-integral-derivative (PID) control (Huyett et al., 2015; Sejersen et al., 2021), and model predictive control (MPC) (Boiroux and Jørgensen, 2018; Chakrabarty et al., 2020). All of these algorithms contain algorithmic parameters which must be tuned based on simulation, i.e., based on a virtual clinical trial. As the human physiology and behavior vary significantly between people and over time, this is a nontrivial task. In spite of this, the tuning is typically based on short-term simulations of one or a few virtual participants who are only represented by a single mathematical model. In contrast, if large-scale long-term virtual clinical trials (involving multiple mathematical models) are used to identify candidate algorithms and algorithmic parameters, the chances of a successful real-world clinical trial increase significantly.

In this work, we develop an approach for performing large-scale long-term virtual clinical trials of AP algorithms (i.e.,

* This work was partially funded by the IFD Grand Solution project ADAPT-T2D (9068-00056B).

Monte Carlo closed-loop simulations). The approach is an extension of our recent work (Reenberg et al., 2022; Wahlgreen et al., 2021) which allows the virtual participants to be represented by multiple mathematical models. Specifically, we use 1) the model described by Hovorka et al. (2002) combined with a CGM model and 2) a modification of the model described by Dalla Man et al. (2007) and Colmegna et al. (2020). Furthermore, we extend both models to incorporate uncertainty about the physiology and the CGM measurements, i.e., we formulate the models as stochastic differential equations (describing the dynamics) and stochastic algebraic equations (describing the CGM measurements). We implement the approach using high-performance C code, and we use an HPC cluster (DTU Computing Center, 2021) to carry out the computations. Finally, we demonstrate the utility of the virtual clinical trial by comparing the performance of an AP algorithm for the two models. Specifically, we simulate one million participants over 52 weeks with both models (i.e., two million in total) which takes 2 h 9 min.

The remainder of this paper is structured as follows. In Section 2, we describe the virtual clinical trial, and in Section 3, we describe the two models used in this work. Next, we present the results of the virtual clinical trial in Section 4, and finally, we present conclusions in Section 5.

2. VIRTUAL CLINICAL TRIAL

The virtual clinical trial involves a population of people with T1D, a protocol describing, e.g., the size and duration of meals, mathematical models, model parameter values, and AP algorithms. Additionally, meals and other activities can be incorrectly announced to the AP algorithm (as is often the case in reality). Furthermore, the mathematical models can be either deterministic (no uncertainty) or stochastic (uncertain dynamics and measurements). The uncertainty can, for instance, represent physiological phenomena that are not included in the model or unknown model parameters.

2.1 Virtual people

The virtual clinical trial contains one million virtual people. Each person is represented by the same pieces of information as real people, e.g., a unique ID, given name, family name, date of birth, place of birth, sex, height, and body weight. Additionally, each person is associated with a set of mathematical models and model parameter values.

2.2 Protocols

A protocol describes the participants' activities during the virtual trial. Typical examples include the time and carbohydrate contents of meals as well as the duration and intensity of physical activity. Furthermore, each protocol has its own ID, and it contains IDs, time stamps (start and end time), and type and size for each activity.

In Section 4, we demonstrate the virtual clinical trial using a protocol based on a Northern European lifestyle with respect to 1) meal times, 2) work weeks, 3) vacation weeks, 4) public holidays, and 5) seasons. The year is divided into 4 seasons consisting of 13 weeks. In total, there are

Table 1. The seasons, weeks, and meal carbohydrate contents (Reenberg et al., 2022).

Compositions of the seasons

Season	Standard weeks	Active weeks	Vacation weeks
Winter	6	4	3
Spring	6	6	1
Summer	7	3	3
Autumn	9	3	1

Compositions of the weeks

Type	Standard days	Active days	Movie nights	Late nights
Standard	4	1	1	1
Active	3	3	1	0
Vacation	5	0	0	2

Body weight-dependent meal carbohydrate contents

Meal size	Amount of carbohydrates	For a 70 kg person
Large meal	1.29 g CHO/kg	90 g CHO
Medium meal	0.86 g CHO/kg	60 g CHO
Small meal	0.57 g CHO/kg	40 g CHO
Snack	0.29 g CHO/kg	20 g CHO

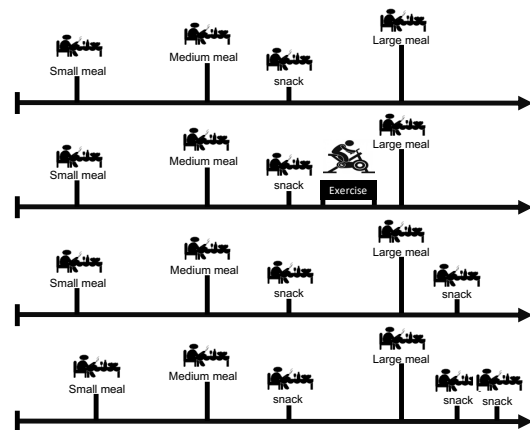


Fig. 1. Schematic of the different types of days during autumn and winter (Reenberg et al., 2022). Top: A standard day. Second from the top: An active day. Third from the top: A day with a movie night. Bottom: A day with a late night. In the spring and summer, the snack is consumed between breakfast and lunch, and the dinner is a medium meal.

8 weeks of vacation (2 of them represent public holidays). All weeks are either a standard week, an active week, or a vacation week. Similarly, all days are categorized as either a standard day, an active day, a day with a movie night, or a day with a late night. Each type of week contains a different combination of the days, and each season contains a different combination of the weeks. Table 1 gives an overview of the weeks and seasons as well as the carbohydrate contents of the different meals in the trial. During autumn, winter, and vacation weeks, the participants are less active and eat more. Furthermore, in addition to the meals consumed during a standard day, active days have an additional exercise session, days with a movie night have an additional snack in the evening, and days with a late night have two additional snacks in the evening.

2.3 Database

The virtual participants, model parameters, protocols, and results from the virtual clinical trial are stored in a database. We use PostgreSQL which is an open-source database system. The database enables direct comparison of the performance of different AP systems on different populations, e.g., people with high body weights or low insulin sensitivity (provided that this sensitivity is a model parameter). Additionally, the database contains basic components for building protocols, e.g., the 4 types of days used in the protocol described in Section 2.2. The user can construct their own protocols based on these basic components. Finally, the database can be used together with a graphical user interface to select and visualize the results of the virtual clinical trial, show statistics of certain demographics and protocols, and add new elements (for instance, virtual people, mathematical models and parameters, or protocols).

3. MODELS

In this section, we describe the two models used in the virtual clinical trial. In Section 3.1, we describe the model developed by Hovorka et al. (2002) combined with a CGM model, and in Section 3.2, we describe the model developed by Dalla Man et al. (2007) and Colmegna et al. (2020) where the meal model is replaced with that proposed by Hovorka et al. (2002). In order to simplify the demonstration of the virtual clinical trial in Section 4, we do not include exercise in the models or in the protocol.

3.1 An extension of Hovorka's model

The insulin subsystem is described by

$$\dot{S}_1(t) = u_I(t) - \frac{S_1(t)}{\tau_S}, \quad (1a)$$

$$\dot{S}_2(t) = \frac{S_1(t)}{\tau_S} - \frac{S_2(t)}{\tau_S}, \quad (1b)$$

$$\dot{I}(t) = \frac{1}{V_I} \frac{S_2(t)}{\tau_S} - k_e I(t), \quad (1c)$$

where S_1 and S_2 [mU] constitute a two-compartment chain representing the absorption of insulin, I [mU/L] is the insulin concentration in the plasma, τ_S [min] is the insulin absorption time constant, V_I is the volume in which insulin is distributed, k_e [1/min] is an elimination rate, and u_I [mU/min] is the insulin infusion rate. The insulin action subsystem is described by the three compartments

$$\dot{x}_1(t) = k_{b1} I(t) - k_{a1} x_1(t), \quad (2a)$$

$$\dot{x}_2(t) = k_{b2} I(t) - k_{a2} x_2(t), \quad (2b)$$

$$\dot{x}_3(t) = k_{b3} I(t) - k_{a3} x_3(t), \quad (2c)$$

where x_i [1/min] are the insulin effect on the glucose distribution ($i = 1$), the disposal of glucose ($i = 2$), and the endogenous glucose production ($i = 3$). Furthermore, k_{bi} [(L/mU)/min²] are activation rates and k_{ai} [1/min] are deactivation rates (for $i = 1, 2, 3$). The meal subsystem is described by a two-compartment chain:

$$\dot{D}_1(t) = A_G D(t) - \frac{D_1(t)}{\tau_D}, \quad (3a)$$

$$\dot{D}_2(t) = \frac{D_1(t)}{\tau_D} - \frac{D_2(t)}{\tau_D}. \quad (3b)$$

Here, D [mmol/min] is the meal carbohydrate content (per minute), D_1 and D_2 [mmol] represent the meal absorption, A_G [-] is the bioavailability of the carbohydrates, and τ_D [min] is a time constant. The glucose subsystem is also described by two compartments, i.e.,

$$\begin{aligned} \dot{Q}_1(t) = & \frac{D_2(t)}{\tau_D} - F_{01,c}(t) - F_R(t) - x_1(t)Q_1(t) \\ & + k_{12}Q_2(t) + EGP_0(1 - x_3(t)), \end{aligned} \quad (4a)$$

$$\dot{Q}_2(t) = x_1(t)Q_1(t) - k_{12}Q_2(t) - x_2Q_2(t), \quad (4b)$$

where Q_1 and Q_2 [mmol] are the accessible and non-accessible glucose compartments, k_{12} [1/min] is a transfer rate, EGP_0 [mmol] is the endogenous glucose production (extrapolated to an insulin concentration of zero). Furthermore,

$$F_{01,c}(t) = \begin{cases} F_{01} & G(t) \geq 4.5 \text{ mmol/L}, \\ F_{01}G(t)/4.5 & \text{otherwise}, \end{cases} \quad (5a)$$

$$F_R(t) = \begin{cases} 0.003(G(t) - 9)V_G & G(t) \geq 9 \text{ mmol/L}, \\ 0 & \text{otherwise}, \end{cases} \quad (5b)$$

$$G(t) = \frac{Q_1(t)}{V_G}, \quad (5c)$$

where $F_{01,c}$ and F_{01} [mmol/min] are the corrected and nominal total non-insulin dependent glucose fluxes, F_R [mmol/min] is the renal glucose clearance, G [mmol/L] is the glucose plasma concentration, and V_G [L] is the volume in which the glucose is distributed. Finally, the CGM subsystem is

$$\dot{G}_I(t) = \frac{G(t)}{\tau_{IG}} - \frac{G_I(t)}{\tau_{IG}}. \quad (6)$$

Here, G_I [mmol/L] is the interstitial glucose concentration measured by the CGM and τ_{IG} [1/min] is a time constant.

3.2 A modification of the UVA/Padova model

In the UVA/Padova model, the glucose subsystem is described by

$$\begin{aligned} \dot{G}_p(t) = & EGP(t) + Ra_m(t) - U_{ii}(t) - E(t) \\ & - k_1 G_p(t) + k_2 G_t(t), \end{aligned} \quad (7a)$$

$$\dot{G}_t(t) = -U_{id}(t) + k_1 G_p(t) - k_2 G_t(t), \quad (7b)$$

$$G(t) = \frac{G_p(t)}{V_g}, \quad (7c)$$

where G_p and G_t [mg/kg] are the plasma glucose in rapidly and slowly equilibrating tissues, respectively, EGP [(mg/kg)/min] is the endogenous glucose production, Ra_m [(mg/kg)/min] is the glucose rate of appearance, U_{ii} and U_{id} [(mg/kg)/min] are the insulin-independent and insulin-dependent glucose utilization, E [(mg/kg)/min] represents renal excretion, k_1 and k_2 [1/min] are rate parameters, G [mg/dL] is the glucose concentration, and V_g [dL/kg] is the glucose distribution volume. Next, the insulin subsystem is represented by

$$\dot{I}_\ell(t) = -(m_1 + m_3)I_\ell(t) + m_2 I_p(t), \quad (8a)$$

$$\dot{I}_p(t) = -(m_2 + m_4)I_p(t) + m_1 I_\ell(t) + Ra_{Isc}(t), \quad (8b)$$

$$I(t) = \frac{I_p(t)}{V_i}, \quad (8c)$$

where I_ℓ and I_p [pmol/kg] are insulin in the plasma and liver, m_i [1/min] for $i = 1, \dots, 4$ are rate parameters.

ters, Ra_{Isc} [(pmol/kg)/min] is the insulin rate of appearance, I [pmol/L] is the plasma insulin concentration, and V_i [L/kg] is the insulin distribution volume. Furthermore,

$$m_2 = \frac{3CL}{5HE_bV_iBW}, \quad (9a)$$

$$m_3 = \frac{HE_b m_1}{1 - HE_b}, \quad (9b)$$

$$m_4 = \frac{2CL}{5V_iBW}. \quad (9c)$$

Here, CL [L/min] is the insulin clearance, HE_b [-] is the basal hepatic insulin extraction, and BW [kg] is the body weight. The insulin-independent and insulin-dependent glucose utilization are given by

$$U_{ii}(t) = F_{cns}, \quad (10a)$$

$$U_{id}(t) = \frac{(V_{m0} + V_{mx}X(t))G_t(t)}{K_{m0} + G_t(t)}, \quad (10b)$$

$$\dot{X}(t) = -p_{2U}X(t) + p_{2U}(I(t) - I_b), \quad (10c)$$

where F_{cns} [(mg/kg)/min] is the glucose uptake of the erythrocytes and the brain, V_{mx} [mg L/(kg pmol min)] and K_{m0} [mg/kg] are parameters, X [pmol/L] is the insulin concentration in the interstitial fluid, p_{2U} [1/min] is the rate of the insulin action on the peripheral glucose utilization, I_b [pmol/L] is the basal insulin plasma concentration, and V_{m0} [(mg/kg)/min] is

$$V_{m0} = \frac{(EGP_b - F_{cns})(K_{m0} + G_{tb})}{G_{tb}}, \quad (11a)$$

$$G_{tb} = \frac{F_{cns} - EGP_b + k_1 G_{pb}}{k_2}, \quad (11b)$$

where EGP_b [(mg/kg)/min], G_{tb} [mg/kg], and G_{pb} [mg/kg] are the basal endogenous glucose production and the basal plasma glucose masses. The model of the oral glucose absorption is similar to that in (3):

$$\dot{D}_1(t) = A_G D(t) - \frac{D_1(t)}{\tau_D}, \quad (12a)$$

$$\dot{D}_2(t) = \frac{D_1(t)}{\tau_D} - \frac{D_2(t)}{\tau_D}, \quad (12b)$$

$$Ra_m(t) = \frac{D_2(t)}{BW\tau_D}. \quad (12c)$$

Again, D [mg/min] is the meal carbohydrate rate, D_1 and D_2 [mg] describe the meal absorption, A_G [-] is the carbohydrate bioavailability, and τ_D [min] is a time constant. The endogenous glucose production is

$$EGP(t) = \max\{0, EGP_b - k_{p2}(G_p(t) - G_{pb}) - k_{p3}(I_d(t) - I_b)\}, \quad (13a)$$

$$\dot{I}_d(t) = -k_i(I_d(t) - I_1(t)), \quad (13b)$$

$$\dot{I}_1(t) = -k_i(I_1(t) - I(t)), \quad (13c)$$

where k_{p2} [1/min] and k_{p3} [mg L/(kg pmol min)] are the liver glucose effectiveness and the amplitude of the insulin action of the liver, I_d and I_1 [pmol/L] constitute a two-compartment delayed insulin signal chain, and k_i [1/min] is a rate parameter. Next, the renal excretion is given by

$$E(t) = \max\{0, k_{e1}(G_p(t) - k_{e2})\}. \quad (14)$$

Here, k_{e1} [1/min] and k_{e2} [mg/kg] are the glomerular filtration rate and the renal glucose threshold. The subcutaneous insulin delivery is described by

$$\dot{I}_{sc1}(t) = -(k_d + k_{a1})I_{sc1}(t) + \frac{u_I(t)}{BW}, \quad (15a)$$

$$\dot{I}_{sc2}(t) = k_d I_{sc1}(t) - k_{a2} I_{sc2}(t), \quad (15b)$$

$$Ra_{Isc}(t) = k_{a1} I_{sc1}(t) + k_{a2} I_{sc2}(t), \quad (15c)$$

where I_{sc1} and I_{sc2} [pmol/kg] are insulin in a non-monomeric and monomeric state, k_d , k_{a1} , and k_{a2} [1/min] are rate parameters accounting for subcutaneous insulin kinetics, and u_I [pmol/min] is the insulin infusion rate. Finally, the subcutaneous glucose concentration, G_{sc} [mg/dL], is

$$\dot{G}_{sc}(t) = -k_{sc}G_{sc}(t) + k_{sc}G(t), \quad (16)$$

and k_{sc} [1/min] is the inverse of a time constant.

3.3 General mathematical form and simulation

The two models described in this section are in the form

$$x(t_0) = x_0, \quad (17a)$$

$$dx(t) = f(t, x(t), u(t), d(t), p)dt + \sigma(t, x(t), u(t), d(t), p)dw(t), \quad (17b)$$

$$z(t) = h(t, x(t), p), \quad (17c)$$

$$y(t_k) = g(t_k, x(t_k), p) + v(t_k). \quad (17d)$$

Here, t is time, t_0 is the initial time, x are the states (i.e., the physiological state), x_0 are the initial states, u are manipulated inputs computed by the AP algorithm (e.g., the insulin infusion rate), d are disturbance variables (e.g., the meal carbohydrate content), and p are model parameters (specific to each person). The first term in (17b) is the deterministic (drift) term, and the second term is the stochastic (diffusion) term. At time t_k (e.g., every 5 min), the AP receives a CGM measurement, y , which is corrupted by noise, v . Furthermore, the outputs, z , are used to evaluate the AP algorithm. The measurement noise is normally distributed, and w is a standard Wiener process, i.e., $v(t_k) \sim N(0, R)$ and $dw(t) \sim N(0, Idt)$ where I is an identity matrix. In between measurements, the manipulated inputs and the disturbance variables are modeled as constant:

$$u(t) = u_k, \quad t \in [t_k, t_{k+1}[, \quad (18a)$$

$$d(t) = d_k, \quad t \in [t_k, t_{k+1}[. \quad (18b)$$

Finally, when the AP algorithm (represented by the functions κ_k and λ_k) receives a measurement, it updates its internal state, x_k^c , and computes the manipulated inputs based on the measurement, $y_k = y(t_k)$, the targets \bar{u}_k and \bar{y}_k , an estimate of the disturbance variables, \hat{d}_k , and the hyperparameters p_κ and p_μ :

$$x_{k+1}^c = \kappa_k(x_k^c, y_k, \bar{u}_k, \bar{y}_k, \hat{d}_k, p_\kappa), \quad (19a)$$

$$u_k = \lambda_k(x_k^c, y_k, \bar{u}_k, \bar{y}_k, \hat{d}_k, p_\mu). \quad (19b)$$

In Section 3.1 and 3.2, we described the models without uncertainty, i.e., with $\sigma = 0$. In Section 4, we use uncertain models where we 1) add a stochastic term to the plasma glucose compartments (4a) and (7a) with (equivalent) diffusion coefficients of $1.5 \text{ mmol/min}^{3/2}$ and $270.24/BW \text{ mg/(kg min}^{3/2})$, and 2) add measurement noise with a variance of $0.1 \text{ mmol/L} \approx 1.8 \text{ mg/dL}$.

We use the Euler-Maruyama method with a step size of 0.5 min to simulate each participant, and we only store statistics and the worst-case simulation. We implement

the virtual clinical trial using parallel high-performance C code for shared-memory architectures and two 2.9 GHz AMD EPYC 7542 32-core processors.

4. VIRTUAL CLINICAL TRIAL RESULTS

In this section, we demonstrate how the virtual clinical trial can be used to assess the safety and efficacy of an AP algorithm. We use the protocol described in Section 2 (without exercise), and for each model, we include one million participants. In the analysis, we consider the first 4 weeks a titration period and disregard them. In the following, we refer to the models presented in Section 3.1 and 3.2 as model A and B, respectively. We choose the algorithmic hyperparameters based on deterministic simulations with model A. The total computation time is 2 h 9 min.

We demonstrate the virtual clinical trial using a simple algorithm based on physiological insight and concepts from proportional-integral-derivative (PID) control. It uses two integrators (I-controllers) to estimate the basal and bolus insulin requirements, and a PD-controller to mitigate smaller variations in the blood glucose. It also uses deadbands, error truncation, a hypoglycemia amplification factor, switching logic, and a few heuristics. Fig. 2 shows how the controller doses insulin during 4 days of the virtual clinical trial for a single participant.

We evaluate the algorithm using the performance measures and targets described by Holt et al. (2021). The measures are 1) average glucose, 2) glucose management index (GMI), 3) glucose variation (GV) computed as the coefficient of variation, 3) time above range (TAR), 4) time in range (TIR), and 5) time below range (TBR). All of these are based on CGM measurements. The 5 ranges used to compute TAR, TIR, and TBR are as follows (all values are in mmol/L, and the colors are used throughout this section). Level 2 hypoglycemia: $[0, 3[$ (red). Level 1 hypoglycemia: $[3, 3.9[$ (light red). Normoglycemia: $[3.9, 10]$ (green). Level 1 hyperglycemia: $]10, 13.9]$ (yellow). Level 2 hyperglycemia: $]13.9, \infty[$ (orange).

For model A, τ_{IG} has the same value for all participants. All other parameters are sampled from normal distributions based on the sample means and variances of the parameter values presented by Hovorka et al. (2002). For model B, we generate normal distributions based on the means and variances reported by Colmegna et al. (2020). For the remaining parameters, we use the means and variances of the values reported by Kovatchev et al. (2010) and Dalla Man et al. (2007). For both models, we discard parameter sets if 1) all parameters are not within one standard deviation of the mean, 2) the basal rate is lower than 0.4 U/h (corresponding to a blood glucose concentration of 6 mmol/L), 3) any time constant or inverse rate parameter is not within one order of magnitude of the corresponding mean, and 4) the steady state is not physical. For model B, we also discard parameter sets if the steady state blood glucose concentration, in the absence of insulin, is above 43.93 mmol/L (the highest obtained with model A).

Fig. 3 shows the mean and worst-case (i.e., the participant with the lowest CGM measurement) time in ranges (TIRs) as well as a box plot of the distributions of the TIRs. The

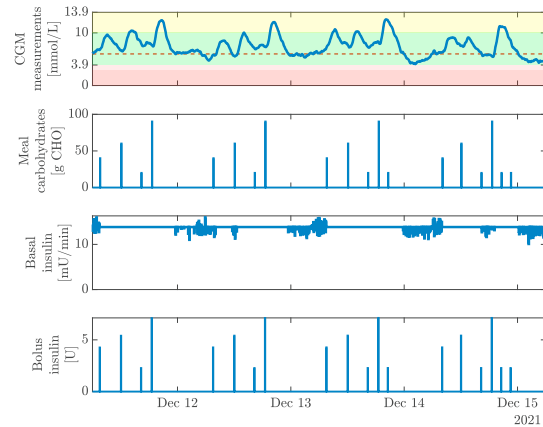


Fig. 2. CGM measurements (top), meal carbohydrate contents (second from the top), basal insulin infusion rate (third from the top), and insulin boluses (bottom) for a single participant (represented with model B) over a period of 4 days.

Table 2. Comparison based on the glycemic targets described by Holt et al. (2021).

Quantity	Target	A	B
Average glucose	< 154 mg/dL	76.87%	84.19%
GMI	< 7%	77.48%	84.82%
GV	≤ 36%	91.37%	89.46%
TAR (level 2)	< 5%	85.80%	88.35%
TAR (level 1 and 2)	< 25%	68.92%	58.57%
TIR (normoglycemia)	> 70%	78.01%	75.09%
TBR (level 1 and 2)	< 4%	100.00%	100.00%
TBR (level 2)	< 1%	100.00%	100.00%
All targets		68.10%	58.46%

mean TIRs are similar for the two models, and the worst-case TIRs are better for model B. The box plot gives a more thorough overview and illustrates that, for model B, the distributions of TIR and TAR (level 1) are more narrow. Fig. 4 shows the total daily doses (TDDs) of basal and bolus insulin. Both distributions are shifted towards higher TDDs for model B. Fig. 5 shows the cumulative distributions of the CGM measurements. The distribution is more narrow for model B, and the mean and worst-case trajectories are similar for the two models. Finally, Table 2 shows that the AP performs better for model B on some but not all glycemic targets. For both models, the target on TAR (level 1 and 2) appears to be the most challenging.

5. CONCLUSIONS

We present an approach for conducting large-scale long-term virtual clinical trials for evaluating APs prior to the actual clinical trials. The participants are represented by multiple mathematical models consisting of stochastic differential equations. We use Monte Carlo closed-loop simulations, implemented with HPC software and hardware, to compute detailed treatment statistics. Finally, we present results from a virtual clinical trial with one million participants (represented by two mathematical models) over 52 weeks, which is conducted in 2 h 9 min.

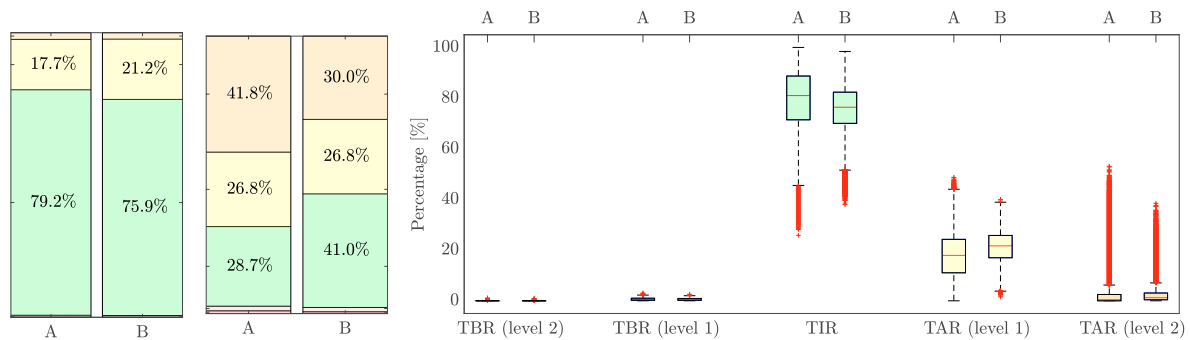


Fig. 3. Left: Mean TIRs. Middle: TIRs for the worst-case participants. Right: Box plots of the TIRs for all participants.

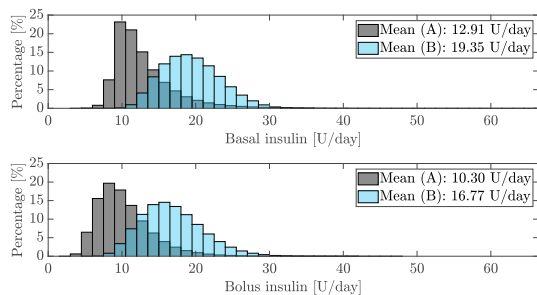


Fig. 4. Histograms of the insulin basal and bolus TDDs.

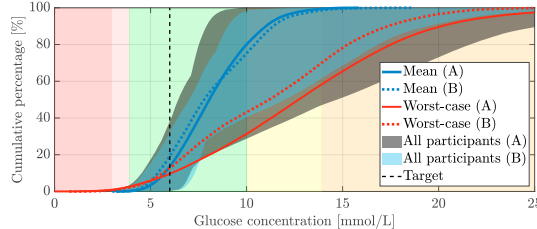


Fig. 5. Cumulative distributions of the CGM measurements.

REFERENCES

- Boiroux, D. and Jørgensen, J.B. (2018). Nonlinear model predictive control and artificial pancreas technologies. In *Proceedings of the 2018 IEEE Conference on Decision and Control (CDC)*, 284–290.
- Chakrabarty, A., Healey, E., Shi, D., Zavitsanos, S., Doyle III, F.J., and Dassau, E. (2020). Embedded model predictive control for a wearable artificial pancreas. *IEEE Transactions on Control Systems Technology*, 28(6), 2600–2607.
- Colmegna, P., Wang, K., Garcia-Tirado, J., and Breton, M.D. (2020). Mapping data to virtual patients in type 1 diabetes. *Control Engineering Practice*, 103, 104605.
- Dalla Man, C., Rizza, R.A., and Cobelli, C. (2007). Meal simulation model of the glucose-insulin system. *IEEE Transactions on Biomedical Engineering*, 54(10), 1740–1749.
- DTU Computing Center (2021). DTU Computing Center resources. doi:10.48714/DTU.HPC.0001. URL <https://doi.org/10.48714/DTU.HPC.0001>. Technical

- University of Denmark.
- Holt, R.I.G., DeVries, J.H., Hess-Fischl, A., Hirsch, I.B., Kirkman, M.S., Klupa, T., Ludwig, B., Nørgaard, K., Pettus, J., Renard, E., Skyler, J.S., Snoek, F.J., Weinstock, R.S., and Peters, A.L. (2021). The management of type 1 diabetes in adults. A consensus report by the American Diabetes Association (ADA) and the European Association for the Study of Diabetes (EASD). *Diabetologia*, 64, 2609–2652.
- Hovorka, R., Shojaei-Moradie, F., Carroll, P.V., Chassin, L.J., Gowrie, I.J., Jackson, N.C., Tudor, R.S., Umpleby, A.M., and Jones, R.H. (2002). Partitioning glucose distribution/transport, disposal, and endogenous production during IVGTT. *American Journal of Physiology-Endocrinology and Metabolism*, 282, E992–E1007.
- Huyett, L.M., Dassau, E., Zisser, H.C., and Doyle III, F.J. (2015). Design and evaluation of a robust PID controller for a fully implantable artificial pancreas. *Industrial & Engineering Chemistry Research*, 54(42), 10311–10321.
- International Diabetes Federation (2021). IDF diabetes atlas, 10th edition. ISBN: 978-2-930229-98-0.
- Kovatchev, B.P., Breton, M.D., Cobelli, C., and Dalla Man, C. (2010). Method, system and computer simulation environment for testing of monitoring and control strategies in diabetes. The U.S. Patent and Trademark Office. U.S. Patent Application Publication No. US 2010/0179768 A1, July 15, 2010.
- Lal, R.A., Ekhlaspour, L., Hood, K., and Buckingham, B. (2019). Realizing a closed-loop (artificial pancreas) system for the treatment of type 1 diabetes. *Endocrine Reviews*, 40(6), 1521–1546.
- Reenberg, A.T., Ritschel, T.K.S., Dammann, B., and Jørgensen, J.B. (2022). High-performance uncertainty quantification in large-scale virtual clinical trials of closed-loop diabetes treatment. In *Proceedings of the 2022 American Control Conference (ACC)*. Accepted.
- Sejersens, M., Boiroux, D., Engell, S.E., Ritschel, T.K.S., Reenberg, A.T., and Jørgensen, J.B. (2021). Initial titration for people with type 1 diabetes using an artificial pancreas. *IFAC PapersOnLine*, 54(15), 484–489.
- Wahlgreen, M.R., Reenberg, A.T., Nielsen, M.K., Rydahl, A., Ritschel, T.K.S., Dammann, B., and Jørgensen, J.B. (2021). A high-performance Monte Carlo simulation toolbox for uncertainty quantification of closed-loop systems. In *Proceedings of the 60th IEEE Conference on Decision and Control (CDC)*, 6755–6761.

APPENDIX H

Technical Report

Protocols and virtual participants for large-scale
long-term virtual clinical trials of closed-loop diabetes
treatment

Authors:

Asbjørn Thode Reenberg, Tobias K. S. Ritschel, John Bagterp Jørgensen

Submitted to:

arXiv 2023.



Protocols and virtual participants for large-scale long-term virtual clinical trials of closed-loop diabetes treatment

Technical report

Asbjørn Thode Reenberg
Tobias K. S. Ritschel
John Bagterp Jørgensen

Department of Applied Mathematics and Computer Science,
Technical University of Denmark, DK-2800 Kgs. Lyngby, Denmark

DTU Compute
Department of Applied Mathematics and Computer Science
Technical University of Denmark

Matematiktorvet
Building 303B
2800 Kongens Lyngby, Denmark
Phone +45 4525 3031
compute@compute.dtu.dk
www.compute.dtu.dk

Summary

In this technical report, we describe and discuss how we design protocols and generate virtual participants for large-scale long-term virtual clinical trials of closed-loop diabetes treatment. We design the protocols from a set basis days that function as building blocks to form weeks, months and years. The virtual participants are represented by a mathematical model with a set of parameters generated from a distribution. We use an extended version of the Hovorka model to represent a population of 1 mio. virtual participants and a modified version of the UVA/Padova model to represent another population of 1 mio. virtual participants. We show how both the protocols and virtual participants are stored in a database. The database make existing protocols and virtual participants sortable and reusable and allows the user to add new protocols and participants.

Contents

Summary	i
Contents	iii
1 Introduction	1
2 Protocols	3
2.1 Days	3
2.2 Weeks	4
2.3 Months and years	4
2.4 Database	5
3 Virtual participants	11
3.1 Personal information	11
3.2 Mathematical models	11
3.3 Parameters	19
4 Conclusions	23
Bibliography	25

CHAPTER 1

Introduction

In this technical report, we describe how the protocols and virtual participants are designed and generated in Reenberg et al. [1] and Ritschel et al. [2] in more detail and we list the model parameters. Furthermore, we show how the protocols and virtual participants are stored in a database. Virtual clinical trials make it possible to evaluate the potential performance of, e.g., closed-loop diabetes treatment and identify potential shortcomings prior to a real clinical trial. The virtual clinical trials involve a population of virtual people with type 1 diabetes described by a mathematical model, a protocol to describe, e.g., the size and duration of meals and some treatment strategy. The mathematical models can be either deterministic or stochastic. The uncertainty represents, e.g., unknown model parameters or physiological phenomena that are not described by the mathematical models. The mathematical models we consider, can be written in the form

$$x(t_0) = x_0, \quad (1.1a)$$

$$dx(t) = f(t, x(t), u(t), d(t), p)dt + \sigma(t, x(t), u(t), d(t), p)dw(t), \quad (1.1b)$$

$$z(t) = h(t, x(t), p), \quad (1.1c)$$

$$y(t_k) = g(t_k, x(t_k), p) + v(t_k), \quad (1.1d)$$

where t is time, t_0 is the initial time, x are the states, x_0 are the initial states, u are manipulated inputs (e.g., insulin administration), d are disturbance variables (e.g., the meals described in the protocols), and p are model parameters (unique to each virtual participant). The first term in (1.1b) is the deterministic (drift) term, and the second term is the stochastic (diffusion) term. y are the measurements (e.g., from a CGM) with measurement noise, v . z , are the outputs and are used in, e.g., a control algorithm. The measurement noise, v , is normally distributed, and w is a standard Wiener process, i.e., $v(t_k) \sim N(0, R)$ and $dw(t) \sim N(0, Idt)$ where I is an identity matrix. We assume that the manipulated inputs and the disturbance variables are piecewise constant, i.e.

$$u(t) = u_k, \quad t \in [t_k, t_{k+1}[, \quad (1.2a)$$

$$d(t) = d_k, \quad t \in [t_k, t_{k+1}[, \quad (1.2b)$$

and we use the Euler-Maruyama method to solve the system of SDEs. In Section 3.2.1 and 3.2.2, we describe the models without uncertainty, i.e., with $\sigma = 0$, but a stochastic term can be added to the plasma glucose compartments that will be described in (3.9a)

and (3.22a). In Reenberg et al. [1] and Ritschel et al. [2], we used diffusion coefficients of $1.5 \text{ mmol}/\text{min}^{3/2}$ and $270.24/BW \text{ mg}/(\text{kg min}^{3/2})$ and added measurement noise with a variance of $0.1 \text{ mmol}/\text{L} \approx 1.8 \text{ mg}/\text{dL}$.

Protocols The protocols are represented by the disturbances, d , in (1.1). The protocols describe the activities or events that happen during a clinical trial. In a real clinical trial the inputs, u , can also be described in a protocol, but here we assume that the inputs are controlled by a control algorithm and not decided from the protocol. The protocols include meals and exercise, and we design a set of days that each should describe a typical day. We combine the days to form different weeks, e.g., an active week where the participant exercises more, and use the different weeks to form months and years. The protocols depend on the season, and we assume that the participants eat more during winter and autumn compared to during summer and spring.

Virtual participants The virtual participants are described by a mathematical model as described in (1.1b), where each participant is represented by a unique set of parameters, p . We use two mathematical models to represent two populations of each 1 mio. virtual participants. The first model is an extended version of the Hovorka model [3] and the second model is a modified version of the UVA/Padova model [4, 5].

Database We use a the open-source PostgreSQL database to store the protocols and virtual participants. The database enables the user to store, reuse and combine different protocols and use the existing virtual participants or add more participants. Furthermore, it also enables the user to sort, e.g., the participants based on certain demographics or select specific protocols. The database also enables storage of the results from a virtual clinical trial, such that two trials can be directly compared. Finally, the database enables the use of a graphical user interface to visualize the results, protocols and participants.

Virtual clinical trial Reenberg et al. [1] and Ritschel et al. [2] each show examples of results from a virtual clinical trials. Reenberg et al. [1] shows an example virtual clinical trial used to assess the difference in performance between two different treatment strategies and Ritschel et al. [2] tests a closed-loop system in two different virtual populations. We refer to these publications for example results from a virtual clinical trial and only describe the protocols and virtual participants in this technical report.

Structure of the report In Chapter 2, we describe the protocols used in the virtual clinical trials and how they are stored in a database and in Chapter 3, we describe the demographics and the mathematical models used to represent the virtual participants. In Chapter 3, we also list the model parameters and show how they are stored in a database. Finally, we provide conclusions in Chapter 4.

CHAPTER 2

Protocols

In this chapter, we describe how we design and generate protocols for the virtual clinical trials. The protocols describe the activities or events (e.g. meals or exercise) that happen during a clinical trial. We consider the protocols as disturbances, d , in (1.1), and the protocols are translated to piecewise constant rates as described in (1.2). Each disturbance has a start time and an end time to make it possible to include that, e.g., it is faster to eat a snack than a large meal. Furthermore, each disturbance has a size and an indicator for the type of disturbance. We design the protocols from a set of basis days that we combine to form weeks, months and years. The aim is to imitate a northern european lifestyle w.r.t. 1) meal times, 2) work weeks, 3) vacation weeks, and 4) public holidays. Here, the size and timing of the events are deterministic to make it easy to use and understand, but similar protocols could be made where the events are randomly generated. Table 2 shows the disturbances that can be included in the protocols. In the protocols created in this technical report, we do not include stress and only consider meals and exercise.

Table 2.1: Types of disturbances that can be included in the protocols and the corresponding indicator.

Type	Indicator
Meal size dependent on body weight [g CHO/kg]	1
Heart rate [bpm]	2
Stress [-]	3
Meal size rate [g CHO/min]	4
Absolute meal size [g CHO]	5
Heart rate reserve [%]	6

2.1 Days

We design a set of days that can either be used on their own or used as building blocks for longer protocols. We construct four basis days that change depending on the season. Figure 2.1 shows the basis days during autumn and winter where the standard day consists of three meals and a snack, the active day consists of three meals, a snack, and an exercise session (of 60% heart rate reserve (HRR)), the movie night consists of three

meals and two snacks, and finally the late night consists of three meals (with a later breakfast) and three snacks. Figure 2.2 shows the basis days during spring and summer where the snack instead is before lunch and the dinner is a medium meal. Table 2.1 shows the size of the different meals. The meal sizes are dependent on the body weight, which creates variation between the participants. The large meal is a relatively high amount of carbohydrates, but does not represent, e.g., a pizza.

Table 2.2: Body weight-dependent meal carbohydrate contents.

Meal size	Amount of carbohydrates	For a 70 kg person
Large meal	1.29 g CHO/kg	90 g CHO
Medium meal	0.86 g CHO/kg	60 g CHO
Small meal	0.57 g CHO/kg	40 g CHO
Snack	0.29 g CHO/kg	20 g CHO

2.2 Weeks

We use the basis days to build three different weeks: 1) the standard week consisting of 4 standard days, 1 active day, 1 movie night, and 1 late night, 2) the active week consisting of 3 standard days, 3 active days, and 1 movie night, and 3) the vacation week consisting of 5 standard days and 2 late nights. The weeks are designed such that the participants exercise more in the active weeks and have more late nights (more snacks) in vacation weeks. Table 2.2 shows the composition of days in the different weeks.

Table 2.3: Compositions of the weeks.

Type	Standard days	Active days	Movie nights	Late nights
Standard	4	1	1	1
Active	3	3	1	0
Vacation	5	0	0	2

2.3 Months and years

We combine the weeks to form months (4 weeks), seasons (12 weeks), and years (52 weeks). Table 2.4 shows the composition of weeks in each season that together forms a year. We assume that the participants are more active during spring and summer and eat more during autumn and winter. We add combined Christmas and winter holidays, easter holidays, summer holidays and autumn holidays. We include 8 vacation weeks in total, where the vacation weeks also include public holidays. Figure 2.3 shows where the vacation weeks are placed during the year.

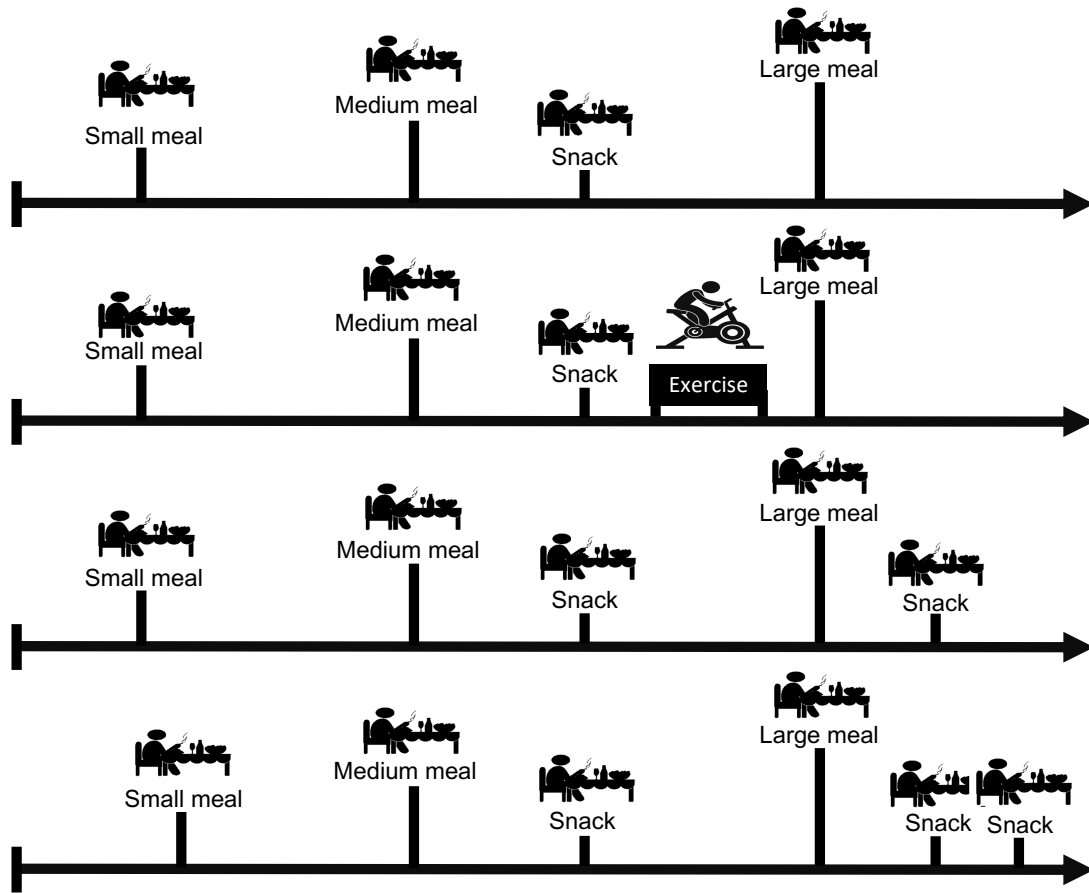


Figure 2.1: Basis days during autumn and winter. From the top: 1) the standard day, 2) the active day, 3) the movie night, and 4) the late night .

Table 2.4: Compositions of the seasons.

Season	Standard weeks	Active weeks	Vacation weeks
Winter	6	4	3
Spring	6	6	1
Summer	7	3	3
Autumn	9	3	1

2.4 Database

We store the protocols in a PostgreSQL database to make them reusable and to make it straightforward to add more protocols and distinguish between them. Each protocol is stored in the database with a unique ID and a name and it is possible to combine, e.g., *the standard week* and *the active week* as a new protocol. Table 2.5, 2.6, 2.7, and 2.8

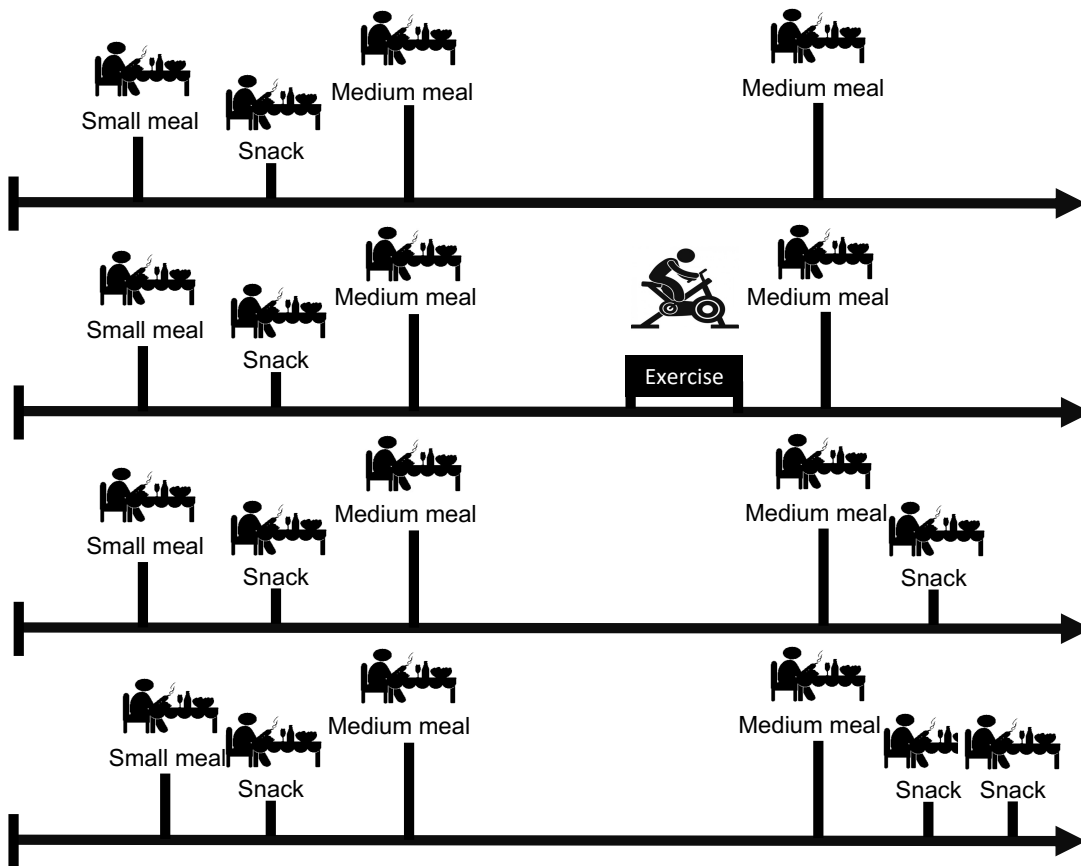


Figure 2.2: Sample days during spring and summer. From the top: 1) the standard day, 2) the active day, 3) the movie night, and 4) the late night.

show the data format and exact timestamps for the four basis days during autumn and winter and Table 2.9, 2.10, 2.11, and 2.12 show the days during spring and summer. We only store the start and end time, size and type of the disturbance in the database. The protocols are automatically translated into the form (1.1) before simulations are started. If we consider, e.g., a meal of type 1 (body weight dependent meal size), we correct for the body weight, and then divide by the time it took the participant to eat the meal, to convert it to a rate.

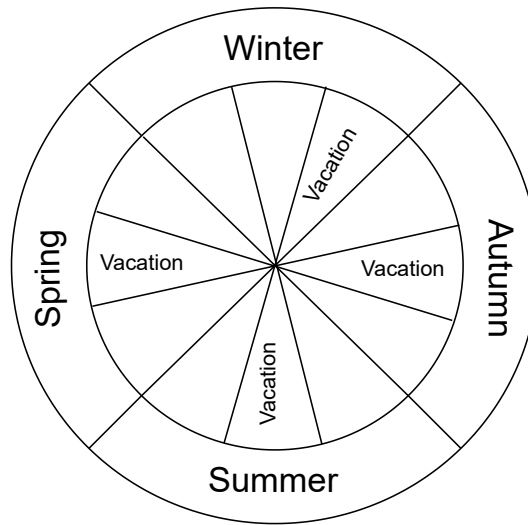


Figure 2.3: A year with seasons and approximate vacations.

Table 2.5: Standard winter day.

start time	end time	size	type
0000-01-01T07:30	0000-01-01T08:00	0.57g CHO/kg	1
0000-01-01T12:00	0000-01-01T12:30	0.86g CHO/kg	1
0000-01-01T16:15	0000-01-01T16:30	0.29g CHO/kg	1
0000-01-01T18:30	0000-01-01T19:00	1.29g CHO/kg	1

Table 2.6: Active winter day.

start time	end time	size	type
0000-01-01T07:30	0000-01-01T08:00	0.57g CHO/kg	1
0000-01-01T12:00	0000-01-01T12:30	0.86g CHO/kg	1
0000-01-01T16:15	0000-01-01T16:30	0.29g CHO/kg	1
0000-01-01T16:45	0000-01-01T17:30	60% HRR	6
0000-01-01T18:30	0000-01-01T19:00	1.29g CHO/kg	1

Table 2.7: Winter movie night.

start time	end time	size	type
0000-01-01T07:30	0000-01-01T08:00	0.57g CHO/kg	1
0000-01-01T12:00	0000-01-01T12:30	0.86g CHO/kg	1
0000-01-01T16:15	0000-01-01T16:30	0.29g CHO/kg	1
0000-01-01T18:30	0000-01-01T19:00	1.29g CHO/kg	1
0000-01-01T20:30	0000-01-01T20:45	0.29g CHO/kg	1

Table 2.8: Winter late night.

start time	end time	size	type
0000-01-01T08:00	0000-01-01T08:30	0.57g CHO/kg	1
0000-01-01T12:00	0000-01-01T12:30	0.86g CHO/kg	1
0000-01-01T16:15	0000-01-01T16:30	0.29g CHO/kg	1
0000-01-01T18:30	0000-01-01T19:00	1.29g CHO/kg	1
0000-01-01T20:30	0000-01-01T20:45	0.29g CHO/kg	1
0000-01-01T22:30	0000-01-01T22:45	0.29g CHO/kg	1

Table 2.9: Standard Summer day.

start time	end time	size	type
0000-01-01T07:30	0000-01-01T08:00	0.57g CHO/kg	1
0000-01-01T10:00	0000-01-01T10:15	0.29g CHO/kg	1
0000-01-01T12:00	0000-01-01T12:30	0.86g CHO/kg	1
0000-01-01T18:30	0000-01-01T19:00	1.29g CHO/kg	1

Table 2.10: Active Summer day.

start time	end time	size	type
0000-01-01T07:30	0000-01-01T08:00	0.57g CHO/kg	1
0000-01-01T10:00	0000-01-01T10:15	0.29g CHO/kg	1
0000-01-01T12:00	0000-01-01T12:30	0.86g CHO/kg	1
0000-01-01T16:45	0000-01-01T17:30	60% HRR	6
0000-01-01T18:30	0000-01-01T19:00	1.29g CHO/kg	1

Table 2.11: Summer movie night.

start time	end time	size	type
0000-01-01T07:30	0000-01-01T08:00	0.57g CHO/kg	1
0000-01-01T10:00	0000-01-01T10:15	0.29g CHO/kg	1
0000-01-01T12:00	0000-01-01T12:30	0.86g CHO/kg	1
0000-01-01T18:30	0000-01-01T19:00	1.29g CHO/kg	1
0000-01-01T20:30	0000-01-01T20:45	0.29g CHO/kg	1

Table 2.12: Summer late night.

start time	end time	size	type
0000-01-01T07:30	0000-01-01T08:00	0.57g CHO/kg	1
0000-01-01T10:00	0000-01-01T10:15	0.29g CHO/kg	1
0000-01-01T12:00	0000-01-01T12:30	0.86g CHO/kg	1
0000-01-01T18:30	0000-01-01T19:00	1.29g CHO/kg	1
0000-01-01T20:30	0000-01-01T20:45	0.29g CHO/kg	1
0000-01-01T22:30	0000-01-01T22:45	0.29g CHO/kg	1

CHAPTER 3

Virtual participants

In this chapter, we describe how we generate participants for the virtual clinical trials. Each virtual person is represented by some personal information similar to a real person, i.e., a unique ID, given name, family name, date of birth, place of birth, sex, height, resting heart rate, and body weight. Additionally, each virtual participant is associated with a set of parameters in a mathematical model.

3.1 Personal information

We generate the personal information with Mockaroo <https://www.mockaroo.com> (Accessed: January 18th, 2023). Mockaroo lets users generate test data of anything from names to IP addresses or unique IDs. Table 3.1 shows an example of a participant generated with Mockaroo. Figure 3.1 shows the distribution of the virtual participants' age, body weight, and resting heart rate. We only include adult people and assume that their age is uniformly distributed. We use approximate average values of the adult human population to generate normal distributions for the body weight and resting heart rate. Using normal distributions for the body weight and resting heart rate are very crude approximations and result in, e.g., the body weights being between 35 kg and 100 kg which is not representative of all humans. The exact distributions of the parameters are listed in Section 3.3. The patient class value is used to distinguish between types of participants and virtual populations where real people have class 0 and virtual people have class 1.

3.2 Mathematical models

In this section, we describe the two mathematical models that represent the virtual participants in the virtual clinical trials. We consider the participants represented by each model, a virtual population. The first model is an extension of Hovorka's model and the second model is a modified version of the UVA/Padova model. The models are also described in Reenberg et al. [1] and Ritschel et al. [2]. The dynamics in the models are different and result in different outcomes of the trials. Therefore, it would also be valuable to add more mathematical models (populations) to the framework. We list the parameters used in both models in Section 3.3. We do not have distributions for the parameters related to the glucagon model, the exercise model, and the CGM model and

Table 3.1: Example of a virtual participant.

ID	321781
First name	Hilly
Last name	Hehir
Sex	Male
Height	187.0 cm
Body weight	88.4 kg
Resting heart rate	67
Date of birth	1991-06-18
Country of birth	Russia
Patient class	1

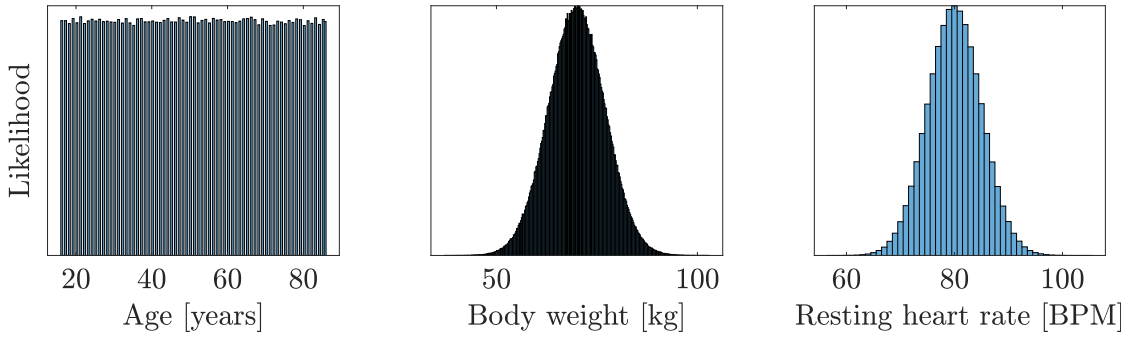


Figure 3.1: Distributions of the personal parameters that affect the simulation models. From the left: 1) The age of the participants with a mean of 51 years, 2) the body weight of the participants with a mean of 70 kg, and 3) the resting heart rate of the participants with a mean of 80 BPM.

use the same parameters for all participants. We translate the exercise intensity in heart rate reserve to heart rate by

$$HR = HR_R(HR_{max} - HR_{rest}) + HR_{rest}, \quad (3.1)$$

where HR [BPM] is the target heart rate, HR_R [%] is the heart rate reserve, HR_{max} [BPM] is the maximum heart rate and HR_{rest} [BPM] is the resting heart rate. We compute the maximum heart rate based on the participants age by

$$HR_{max} = 220 - age. \quad (3.2)$$

3.2.1 Extended Hovorka model

The model by Hovorka et al [3, 6] consists of an insulin subsystem, a meal subsystem, and a glucose subsystem. We extend it with a glucagon subsystem [7], an exercise subsystem [8], and a simplified version of the CGM subsystem by Facchinetti et al. [9]. Table 3.3 in Section 3.3 describes the parameters.

Insulin subsystem The insulin subsystem describes the insulin absorption and the insulin concentration by

$$\dot{S}_1(t) = u_I(t) - \frac{S_1(t)}{\tau_S}, \quad (3.3a)$$

$$\dot{S}_2(t) = \frac{S_1(t)}{\tau_S} - \frac{S_2(t)}{\tau_S}, \quad (3.3b)$$

$$\dot{I}(t) = \frac{1}{V_I} \frac{S_2(t)}{\tau_S} - k_e I(t), \quad (3.3c)$$

where S_1 and S_2 [mU] represent the insulin absorption as a two-compartment chain, τ_S [min] is the insulin absorption time constant, I [mU/L] is the plasma insulin concentration, V_I [L] is the insulin distribution volume, and k_e [1/min] is the elimination rate. $u_I = u_{ba} + u_{bo}$ [mU/min] is the insulin infusion rate where u_{ba} [mU/min] is the basal infusion rate and u_{bo} [mU/min] is the bolus infusion rate.

Insulin action subsystem The insulin action subsystem describes the insulin action on the glucose kinetics by

$$\dot{x}_1(t) = k_{b1}I(t) - k_{a1}x_1(t), \quad (3.4a)$$

$$\dot{x}_2(t) = k_{b2}I(t) - k_{a2}x_2(t), \quad (3.4b)$$

$$\dot{x}_3(t) = k_{b3}I(t) - k_{a3}x_3(t), \quad (3.4c)$$

where x_1 [1/min], x_2 [1/min], and x_3 [1/min] describe the effects of insulin on the glucose distribution, the glucose disposal, and the endogenous glucose production. k_{bi} [(L/mU)/min²] and k_{ai} [1/min] for $i = 1, 2, 3$ are the activation and deactivation rate constants.

Meal subsystem The meal subsystem describes the meal absorption by

$$\dot{D}_1(t) = A_G D(t) - \frac{D_1(t)}{\tau_D}, \quad (3.5a)$$

$$\dot{D}_2(t) = \frac{D_1(t)}{\tau_D} - \frac{D_2(t)}{\tau_D}. \quad (3.5b)$$

Here, D_1 [mmol] and D_2 [mmol] represent the meal absorption as a two-compartment chain, D [mmol/min] is the carbohydrate content of the meal as a rate, A_G [-] is the

carbohydrate bioavailability, and τ_D [min] is the meal time constant. We convert carbohydrates in the meal, $D(t)$ [mmol/min], to $d(t)$ [g CHO/min] by

$$D(t) = \frac{1000}{M_{wG}} d(t), \quad (3.6)$$

where $M_{wG} = 180.1577$ [g/mol] is the molecular weight of glucose.

Glucagon subsystem The glucagon subsystem describes the glucagon absorption by

$$\dot{Q}_1^G(t) = u_G(t) - \frac{Q_1^G(t)}{\tau_{Glu}}, \quad (3.7a)$$

$$\dot{Q}_2^G(t) = \frac{Q_1^G(t)}{\tau_{Glu}} - \frac{Q_2^G(t)}{\tau_{Glu}}, \quad (3.7b)$$

where Q_1^G [μ g] and Q_2^G [μ g] represent the glucagon absorption as a two-compartment chain, u_G [μ g/min] is the glucagon infusion rate, and τ_{Glu} [min] is a time constant.

Exercise subsystem The exercise subsystem describes short-term and long-term effects of physical activity on the glucose consumption and insulin sensitivity. The effect of high-intensity exercise is not modeled. The exercise subsystem consists of

$$\dot{E}_1(t) = \frac{HR(t) - HR_0 - E_1(t)}{\tau_{HR}}, \quad (3.8a)$$

$$\dot{T}_E(t) = \frac{c_1 f_{E1}(t) + c_2 - T_E(t)}{\tau_{ex}}, \quad (3.8b)$$

$$\dot{E}_2(t) = - \left(\frac{f_{E1}(t)}{\tau_{in}} + \frac{1}{T_E(t)} \right) E_2(t) + \frac{f_{E1}(t) T_E(t)}{c_1 + c_2}, \quad (3.8c)$$

$$f_{E1}(t) = \frac{\left(\frac{E_1(t)}{a \cdot HR_0} \right)^n}{1 + \left(\frac{E_1(t)}{a \cdot HR_0} \right)^n}. \quad (3.8d)$$

Here, E_1 [BPM] is the short-term effect, E_2 [min] is the long-term effect, T_E [min] is the characteristic time for the long-term effect, HR [BPM] is the heart rate, HR_0 [BPM] is the resting heart rate, τ_{HR} [min] is a time constant, c_1 [min] and c_2 [min] define the steady state value for T_E , τ_{ex} [min] is a time constant for how fast T_E reaches steady state, and a [-], n [-], and τ_{in} [min] specify the intensity and time constant of the long-term effect on the insulin sensitivity.

Glucose subsystem The glucose subsystem describe the glucose kinetics modeled as two compartments (accessible and non-accessible) and is represented by

$$\dot{Q}_1(t) = \frac{D_2(t)}{\tau_D} - F_{01,c}(t) - F_R(t) - x_1(t)Q_1(t) \quad (3.9a)$$

$$+ k_{12}Q_2(t) + EGP(t) + Q_G(t) - Q_{E21}(t),$$

$$\dot{Q}_2(t) = x_1(t)Q_1(t) - k_{12}Q_2(t) - x_2Q_2(t) \quad (3.9b)$$

$$+ Q_{E21}(t) - Q_{E22}(t) - Q_{E1}(t),$$

where

$$EGP(t) = EGP_0(1 - x_3(t)), \quad (3.10a)$$

$$Q_G(t) = K_{Glu}V_GQ_2^G(t), \quad (3.10b)$$

$$Q_{E21}(t) = \alpha E_2(t)^2 x_1(t)Q_1(t), \quad (3.10c)$$

$$Q_{E22}(t) = \alpha E_2(t)^2 x_2(t)Q_2(t), \quad (3.10d)$$

$$Q_{E1}(t) = \beta \frac{E_1(t)}{HR_0}, \quad (3.10e)$$

and

$$F_{01,c}(t) = \begin{cases} F_{01} & G(t) \geq 4.5 \text{ mmol/L}, \\ F_{01}G(t)/4.5 & \text{otherwise,} \end{cases} \quad (3.11a)$$

$$F_R(t) = \begin{cases} 0.003(G(t) - 9)V_G & G(t) \geq 9 \text{ mmol/L}, \\ 0 & \text{otherwise,} \end{cases} \quad (3.11b)$$

$$G(t) = \frac{Q_1(t)}{V_G}. \quad (3.11c)$$

Here, Q_1 [mmol] and Q_2 [mmol] represent the accessible and non-accessible compartments, k_{12} [1/min] is the transfer rate, F_{01} [mmol/min] and $F_{01,c}$ [mmol/min] are the nominal and corrected total non-insulin dependent glucose flux, F_R [mmol/min] is the renal glucose clearance, V_G [L] is the glucose distribution volume, EGP_0 [mmol] is the endogenous glucose production, K_{Glu} [(mmol/L)/ μ g/min] is the glucagon gain, α [1/min²] is the exercise-induced insulin action, β [mmol/min] is the exercise-induced insulin-independent glucose uptake rate, and G [mmol/L] is the glucose concentration.

CGM subsystem The CGM subsystem describes the glucose concentration in the interstitial tissue by

$$\dot{G}_I(t) = \frac{G(t)}{\tau_{IG}} - \frac{G_I(t)}{\tau_{IG}}, \quad (3.12)$$

where G_I [mmol/L] is the interstitial glucose concentration and τ_{IG} is a time constant.

3.2.2 Modified UVA/Padova model

The second model we use to describe a virtual population of participants, is a modified version of the UVA/Padova model [4, 5]. We use the meal model from the Hovorka model as the original UVA/Padova model only allows simulations of a single meal. This model does not include exercise or glucagon, but can be extended with the equations described in Section 3.2.1. Table 3.4 in Section 3.3 lists the parameters.

Insulin subsystem The insulin subsystem describes the insulin in the plasma and the liver by

$$\dot{I}_p = -(m_2 + m_4)I_p + m_1I_l + R_{ai}, \quad (3.13a)$$

$$\dot{I}_l = -(m_1 + m_3)I_l + m_2I_p. \quad (3.13b)$$

I_p [pmol/kg] is the insulin in the plasma and I_l [pmol/kg] is the insulin in the liver. R_{aisc} [(pmol/kg)/min] is the rate of appearance described by

$$R_{ai} = k_{a1}I_{sc1} + k_{a2}I_{sc2}, \quad (3.14)$$

where m_1 is a rate parameters, and m_2 , m_3 , and m_4 [1/min] are rate parameters computed as

$$m_2 = \frac{3CL}{5HE_bV_lBW}, \quad (3.15a)$$

$$m_3 = \frac{HE_b m_1}{1 - HE_b}, \quad (3.15b)$$

$$m_4 = \frac{2CL}{5V_lBW}. \quad (3.15c)$$

Here, CL [L/kg] is the insulin clearance, HE_b [-] is the basal hepatic insulin extraction, and BW [kg] is the body weight. The plasma insulin concentration, I [pmol/L] (note that 1 pmol/L = 3/1000 ng/mL [10].), is

$$I = I_p/V_l. \quad (3.16)$$

Subcutaneous insulin subsystem The subcutaneous insulin subsystem describes the kinetics of insulin subcutaneous insulin administration by

$$\dot{I}_{sc1} = -(k_d + k_{a1})I_{sc1} + \frac{u_I}{BW}, \quad (3.17a)$$

$$\dot{I}_{sc2} = k_d I_{sc1} - k_{a2} I_{sc2}, \quad (3.17b)$$

where I_{sc1} and I_{sc2} [pmol/kg] represent the insulin in a non-monomeric and monomeric state, k_d , k_{a1} , and k_{a2} [1/min] are rate parameters, and u_I [pmol/min] is the insulin infusion rate.

Glucose utilization subsystem The glucose utilization subsystem describes the insulin-independent and insulin-dependent glucose utilization by

$$U_{ii} = F_{cns}, \quad (3.18a)$$

$$U_{id} = \frac{(V_{m0} + V_{mx}X)G_t}{K_{m0} + G_t}, \quad (3.18b)$$

where U_{ii} [(mg/kg)/min] is the insulin-independent glucose utilization, U_{id} [(mg/kg)/min] is the insulin-dependent glucose utilization, F_{CNS} [(mg/kg)/min] is the glucose uptake of the erythrocytes in the brain, V_{mx} [mg L/(kg pmol min)] and K_{m0} [mg/kg] are parameters, X [pmol/L] is the insulin concentration in the interstitial fluid described by

$$\dot{X} = -p_{2U}X + p_{2U}(I - I_b), \quad (3.19)$$

where p_{2U} [1/min] is the rate of the insulin action on the peripheral glucose utilization, I_b [pmol/L] is the basal plasma insulin concentration, and V_{m0} [(mg/kg)/min] is

$$V_{m0} = \frac{(EGP_b - F_{cns})(K_{m0} + G_{tb})}{G_{tb}}, \quad (3.20a)$$

$$G_{tb} = \frac{F_{cns} - EGP_b + k_1G_{pb}}{k_2}, \quad (3.20b)$$

where EGP_b [(mg/kg)/min] is the basal endogenous glucose production, and G_{tb} and G_{pb} [mg/kg] are the plasma glucose masses.

Meal subsystem The meal subsystem is identical to (3.5) and describes the meal absorption by

$$\dot{D}_1 = A_G D - \frac{D_1}{\tau_D}, \quad (3.21a)$$

$$\dot{D}_2 = \frac{D_1}{\tau_D} - \frac{D_2}{\tau_D}. \quad (3.21b)$$

Here, D_1 [mmol] and D_2 [mmol] represents the meal absorption as a two-compartment chain, D [mmol/min] is carbohydrate content of the meal as a rate, A_G [-] is the carbohydrate bioavailability, and τ_D [min] is the meal time constant.

Glucose subsystem The glucose subsystem describes the plasma glucose in the rapidly and slowly equilibrating tissues as

$$\dot{G}_p = EGP + R_a - U_{ii} - E - k_1G_p + k_2G_t, \quad (3.22a)$$

$$\dot{G}_t = -U_{id} + k_1G_p - k_2G_t. \quad (3.22b)$$

G_p and G_t [mg/kg] are the plasma glucose in the rapidly and slowly equilibrating tissues, respectively. EGP [(mg/kg)/min] is the endogenous glucose production, R_a

$[(\text{mg/kg})/\text{min}]$ is the glucose rate of appearance, U_{ii} , and U_{id} is the insulin-independent and insulin-dependent glucose utilization as described in (3.18), E $[(\text{mg/kg})/\text{min}]$ is the renal excretion, k_1 and k_2 $[1/\text{min}]$ are rate parameters, and V_g $[\text{dL/kg}]$ is the glucose distribution volume. The plasma glucose concentration is computed by

$$G = G_p/V_G, \quad (3.23)$$

the glucose rate of appearance by

$$R_{am} = \frac{D_2}{BW\tau_D}, \quad (3.24)$$

and renal excretion is described by

$$E = \begin{cases} k_{e1}(G_p - k_{e2}), & \text{if } G_p > k_{e2}, \\ 0, & \text{if } G_p \leq k_{e2}. \end{cases} \quad (3.25)$$

Here, k_{e1} $[1/\text{min}]$ is the glomerular filtration rate and k_{e2} $[\text{mg/kg}]$ is the renal glucose threshold.

Endogenous glucose production subsystem The endogenous glucose productions is described as

$$EGP = \max\{0, EGP_b - k_{p2}(G_p - G_{pb}) - k_{p3}(I_d - I_b)\}, \quad (3.26)$$

where k_{p2} $[1/\text{min}]$ is the liver glucose effectiveness and k_{p3} $[\text{mg L}/(\text{kg pmol min})]$ is the amplitude of the insulin action on the liver. I_l and I_d $[\text{pmol/L}]$ are a two-compartment chain for the insulin effect on the EGP described by

$$\dot{I}_1 = -k_i(I_1 - I), \quad (3.27a)$$

$$\dot{I}_d = -k_i(I_d - I_1), \quad (3.27b)$$

where k_i $[1/\text{min}]$ is a rate parameter.

Subcutaneous glucose subsystem The subcutaneous glucose subsystem describes the glucose concentration in the subcutaneous tissue (e.g. the tissue a CGM measures from) by

$$\dot{G}_s = -k_{sc}G_s + k_{sc}G, \quad (3.28)$$

where k_{sc} $[1/\text{min}]$ is a rate parameter.

3.3 Parameters

This section lists the parameters of the models described in Section 3.2. Table 3.2 shows the distribution of the personal parameters. The height is not used in any of the models, but we generate it such that it is possible to compute, e.g., the BMI. If the sampled body weight is below 35 kg, we set it to 70 kg and if the resting heart rate is below 35 BPM, we set it to 80 BPM. Table 3.3 shows the parameters used in the extended Hovorka model and Table 3.4 shows the parameters used in the modified UVA/Padova model. The data used to construct the parameter distributions is sparse and we assume that the parameters are not correlated. Therefore, the parameters distributions are crude approximations. We require that 1) the generated parameters are within one standard deviation of the mean, 2) the generated time constants are within one order of magnitude of the mean, 3) the basal rate is above 0.4 U/h, and 4) the steady state is physical. If these criteria are not satisfied, we discard the parameters and sample a new set. Furthermore, we also discard parameters sets that lead to a steady state glucose concentration above 44 [mmol/L] when no insulin is administered. As also mentioned in the introduction, we describe the models in the original form as ODEs here, i.e., with $\sigma = 0$, but a stochastic term can be added to the plasma glucose compartments, (3.9a) and (3.22a). In Reenberg et al. [1] and Ritschel et al. [2], we used diffusion coefficients of $1.5 \text{ mmol}/\text{min}^{3/2}$ and $270.24/BW \text{ mg}/(\text{kg min}^{3/2})$ and added measurement noise with a variance of $0.1 \text{ mmol/L} \approx 1.8 \text{ mg/dL}$.

3.3.1 Database

We store the virtual participants (i.e. the information shown in Table 3.1) and parameters (i.e. the parameters generated from the distributions listed in Table 3.3 and Table 3.4) in a Postgresql database. The database allows the user to reuse the generated parameters, but also to sort the population based on certain demographics and simulate a subset of the population. Each set of parameters is associated with a unique id. The database also makes it easy to add parameters for a new population or add more virtual people to the existing populations. Figure 3.2 shows the example virtual participant from Table 3.1 directly in the database. In the database, we add an additional universally unique identifier (UUID).

Table 3.2: Distributions of the personal parameters.

Symbol	Value or distribution	Unit	Description
BW	$N(70, 7^2)$	kg	Body weight
$Height$	$N(170, 7^2)$	cm	Height
Age	$U(17, 87)$	years	Age
HR_0	$N(80, 5^2)$	BPM	Resting heart rate

Table 3.3: Model parameters in the extended Hovorka model.

Symbol	Value or distribution	Unit	Description
Parameters presented by Boiroux et al. [11] (see also Wilinska and Hovorka et al. [12, 3])			
EGP_0	$N(0.0161, 0.0039^2)$	mmol/min	Liver gluc. prod. at 0 ins.
F_{01}	$N(0.0097, 0.0022^2)$	mmol/min	Ins. indep. gluc. cons.
A_g	$U(0.7, 1.2)$	-	CHO utilization
k_{12}	$N(0.0649, 0.0282^2)$	1/min	Transfer Rate
k_{a1}	$N(0.0055, 0.0056^2)$	1/min	Deactivation Rate
k_{a2}	$N(0.0683, 0.0507^2)$	1/min	Deactivation Rate
k_{a3}	$N(0.0304, 0.0235^2)$	1/min	Deactivation Rate
SIT	$N(51.2, 32.09^2)$	$((L/mU)/min) \cdot 10^{-4}$	Transport ins. sens.
SID	$N(8.2, 7.84^2)$	$((L/mU)/min) \cdot 10^{-4}$	Disposal ins. sens.
SIE	$N(520, 306.2^2)$	$((L/mU)/min) \cdot 10^{-4}$	EGP ins. sens.
k_{b1}	$k_{a1} \cdot SIT$	$(L/mU)/min^2$	Activation Rate
k_{b2}	$k_{a2} \cdot SID$	$(L/mU)/min^2$	Activation Rate
k_{b3}	$k_{a3} \cdot SIE$	$(L/mU)/min^2$	Activation Rate
ke	$N(0.14, 0.035^2)$	1/min	Ins. elim. rate
V_I	$N(0.12, 0.012^2)$	L	Ins. dist. volume
$\ln(V_G)$	$N(\ln(0.15), 0.23^2)$	L	Gluc. dist. volume
$\ln(1/\tau_D)$	$N(-3.689, 0.25^2)$	min	Carb. abs. time const.
$1/\tau_S$	$N(0.018, 0.0045^2)$	min	Ins. abs. time const.
Model parameters in the model by Rashid et al. [8].			
a	0.77	-	Ex. param.
t_{HR}	5	min	Ex. param.
t_{in}	1	min	Ex. param.
n	3	-	Ex. param.
t_{ex}	200	min	Ex. param.
c_1	500	min	Ex. param.
c_2	100	min	Ex. param.
β	0.78	mmol/min	Ex-ind. ins. indep. gluc. upt.
α	1.79	-	Ex-ind. in. action
Model parameters in the model by Haider et al. [7] and Facchinetti et al. [9].			
τ_{IG}	6.7	min	Interst. gluc. time const.
τ_{Glu}	19	min	Glucagon time const.
K_{Glu}	0.075	$(mmol/dL)/(\mu g/min)$	Glucagon gain

uuid	id	first_name	last_name	gender	height	body_weight	resting_heart_rate	date_of_birth	country_of_birth	patient_type
54f771d2b-6822-4dcb-83ae-28825bf2c3dc	824576	Hilly	Mehir	Male	187	88.4	67	1991-06-18	Russia	1

Figure 3.2: The example virtual participant as it is stored in the database.

Table 3.4: Model parameters in the modified UVA/Padova model.

Symbol	Distribution or value	Unit	Description
Parameter values based on data collected by Colmegna et al. [5]			
V_G	$N(1.8700, 0.1020^2)$	dL/kg	Distribution volume
k_1	$N(0.0810, 0.0230^2)$	1/min	Rate parameter
k_2	$N(0.1370, 0.0530^2)$	1/min	Rate parameter
K_{m0}	$N(224.2810, 12.2640^2)$	mg/kg	Glucose mass (MM)
k_{p2}	$N(0.0050, 0.0040^2)$	1/min	Hep. gluc. effectiveness
V_{mx}	$N(0.0810, 0.0330^2)$	mg L/(kg min pmol)	Ins. sens. on gluc. util.
EGP_b	$N(2.5040, 0.3910^2)$	mg/(kg min)	Basal endo. gluc. prod.
CL	$N(1.0210, 0.3080^2)$	L/min	Insulin clearance
Parameter values based on data collected by Kovatchev et al. [13]			
V_I	$N(0.0646, 0.0175^2)$	L/kg	Distribution volume
G_b	$N(147.4100, 8.9390^2)$	mg/dL	Basal blood gluc. conc.
m_1	$N(0.2109, 0.1362^2)$	1/min	Rate parameter
k_{p3}	$N(0.0106, 0.0068^2)$	mg L/(kg min pmol)	Hepatic ins. sens.
k_i	$N(0.0069, 0.0027^2)$	1/min	Delayed ins. action rate
p_{2U}	$N(0.0246, 0.0120^2)$	1/min	Ins. action rate
I_b	$N(92.7470, 19.6618^2)$	pmol/L	Basal plasma ins. conc.
k_{a1}	$N(0.0016, 0.0005^2)$	1/min	Rate parameter
k_{a2}	$N(0.0149, 0.0052^2)$	1/min	Rate parameter
k_d	$N(0.0161, 0.0017^2)$	1/min	Rate parameter
k_{sc}	$N(0.1033, 0.0376^2)$	1/min	Rate parameter
Parameter values presented by Dalla Man et al. [4]			
F_{cns}	1.0	mg/(kg min)	Ins.-indep. gluc. util.
k_{e1}	0.0005	1/min	Glomerular filt. rate
k_{e2}	339.0	mg/kg	Renal threshold of gluc.
HE_b	0.6	-	Basal hep. excre. of ins.
Parameters presented by Boiroux et al. [11] (see also Wilinska and Hovorka et al. [12, 3])			
$\log(1/\tau_D)$	$N(-3.689, 0.25^2)$	min	Carb. abs.
A_g	$U(0.7, 1.2)$	-	Carb. bioavailability

CHAPTER 4

Conclusions

In this technical report, we described how we design protocols and generate virtual participants for large-scale long-term virtual clinical trials of closed-loop diabetes treatment. We design four different season dependent days consisting of meals and exercise, and use them as building blocks for longer protocols. We describe and list the parameters for two mathematical models to each represent a population of 1 mio. virtual participants and generate the personal details with Mockaroo. The protocols and virtual participants are stored in a PostgreSQL database to make them reusable and make it straightforward to add new protocols and participants.

Bibliography

- [1] Asbjørn Thode Reenberg, Tobias K. S. Ritschel, Bernd Dammann, and John Bagterp Jørgensen. “High-performance uncertainty quantification in large-scale virtual clinical trials of closed-loop diabetes treatment”. In: *Proceedings of the 2022 American Control Conference (ACC)*. 2022, pages 1367–1372. DOI: 10.23919/ACC53348.2022.9867234.
- [2] Tobias K. S. Ritschel, Asbjørn Thode Reenberg, and John Bagterp Jørgensen. “Large-scale Virtual Clinical Trials of Closed-loop Treatments for People with Type 1 Diabetes”. In: *IFAC-PapersOnLine* 55.23 (2022), pages 169–174. DOI: 10.1016/j.ifacol.2023.01.037.
- [3] Roman Hovorka, Fariba Shojaee-Moradie, Paul V. Carroll, Ludovic J. Chassin, Ian J. Gowrie, Nicola C. Jackson, Romulus S. Tudor, A. Margot Umpleby, and Richard H. Jones. “Partitioning glucose distribution/transport, disposal, and endogenous production during IVGTT”. In: *American Journal of Physiology-Endocrinology and Metabolism* 282 (2002), E992–E1007. DOI: 10.1152/ajpendo.00304.2001.
- [4] Chiara Dalla Man, Robert A. Rizza, and Claudio Cobelli. “Meal simulation model of the glucose-insulin system”. In: *IEEE Transactions on Biomedical Engineering* 54.10 (2007), pages 1740–1749. DOI: 10.1109/TBME.2007.893506.
- [5] Patricio Colmegna, Ke Wang, Jose Garcia-Tirado, and Marc D. Breton. “Mapping data to virtual patients in type 1 diabetes”. In: *Control Engineering Practice* 103 (2020), page 104605. DOI: 10.1016/j.conengprac.2020.104605.
- [6] Roman Hovorka, Valentina Canonico, Ludovic J. Chassin, Ulrich Haueter, Massimo Massi-Benedetti, Marco O. Federici, Thomas R. Pieber, Helga C. Schaller, Lukas Schaupp, Thomas Vering, and Malgorzata E. Wilinska. “Nonlinear Model Predictive Control of Glucose Concentration in Subjects with Type 1 Diabetes”. In: *Physiological Measurement* 25.4 (2004), pages 905–920. DOI: 10.1088/0967-3334/25/4/010.
- [7] Ahmad Haidar, Claire Duval, Laurent Legault, and Rémi Rabasa-Lhoret. “Pharmacokinetics of insulin aspart and glucagon in type 1 diabetes during closed-loop operation”. In: *Journal of Diabetes Science and Technology* 7.6 (2013), pages 1507–1512. DOI: 10.1177/193229681300700610.

- [8] Mudassir Rashid, Sediqeh Samadi, Mert Sevil, Iman Hajizadeh, Paul Kolodziej, Nicole Hobbs, Zacharie Maloney, Rachel Brandt, Jianyuan Feng, Minsun Park, Laurie Quinn, and Ali Cinar. “Simulation software for assessment of nonlinear and adaptive multivariable control algorithms: Glucose–insulin dynamics in Type 1 diabetes”. In: *Computers & Chemical Engineering* 130 (2019), page 106565. ISSN: 0098-1354. DOI: 10.1016/j.compchemeng.2019.106565.
- [9] Andrea Facchinetti, Simone Del Favero, Giovanni Sparacino, Jessica R. Castle, W. Kenneth Ward, and Claudio Cobelli. “Modeling the Glucose Sensor Error”. In: *IEEE Transactions on Biomedical Engineering* 61.3 (2014), pages 620–629. DOI: 10.1109/TBME.2013.2284023.
- [10] Angus G. Jones and Andrew T. Hattersly. “The clinical utility of C-peptide measurement in the care of patients with diabetes”. In: *Diabetic Medicine* 30.7 (2013), pages 803–817. DOI: 10.1111/dme.12159.
- [11] Dimitri Boiroux, Anne Katrine Duun-Henriksen, Signe Schmidt, Kirsten Nørgaard, Sten Madsbad, Niels Kjølstad Poulsen, Henrik Madsen, and John Bagterp Jørgensen. “Overnight glucose control in people with type 1 diabetes”. English. In: *Biomedical Signal Processing and Control* 39 (2018), pages 503–512. ISSN: 1746-8094. DOI: 10.1016/j.bspc.2017.08.005.
- [12] Malgorzata E. Wilinska, Ludovic J. Chassin, Carlo L. Acerini, Janet M. Allen, David B. Dunger, and Roman Hovorka. “Simulation Environment to Evaluate Closed-Loop Insulin Delivery Systems in Type 1 Diabetes”. In: *Journal of Diabetes Science and Technology* 4.1 (2010), pages 132–144. DOI: 10.1177/193229681000400117.
- [13] Boris P. Kovatchev, Marc D. Breton, Claudio Cobelli, and Chiara Dalla Man. *Method, System and Computer Simulation Environment for Testing of Monitoring and Control Strategies in Diabetes*. The U.S. Patent and Trademark Office. U.S. Patent Application Publication No. US 2010/0179768 A1, July 15, 2010. 2010.

APPENDIX |

Conference Paper - DYCOPS 2022

Nonlinear Model Predictive Control and System
Identification for a Dual-hormone Artificial Pancreas

Authors:

Asbjørn Thode Reenberg, Tobias K. S. Ritschel, Emilie B. Lindkvist, Christian Lauge-
sen, Jannet Svensson, Ajenthen G. Ranjan, Kirsten Nørgaard, John Bagterp Jørgensen

Published in:

IFAC-PapersOnLine, 55–7, 915–921, 2022.

Proceedings of the 13th IFAC Symposium on Dynamics and Control of Process Systems,
including Biosystems DYCOPS 2022: Busan, Republic of Korea, 14–17 June, 2022.



Nonlinear Model Predictive Control and System Identification for a Dual-hormone Artificial Pancreas

Asbjørn Thode Reenberg*, Tobias K. S. Ritschel*,
Emilie B. Lindkvist**, Christian Laugesen**,
Jannet Svensson**, Ajenthen G. Ranjan**,
Kirsten Nørgaard**, John Bagterp Jørgensen*

* *Department of Applied Mathematics and Computer Science,
Technical University of Denmark, DK-2800 Kgs. Lyngby, Denmark.*

** *Steno Diabetes Center Copenhagen, Clinical Research, DK-2730
Herlev, Denmark.*

Abstract: In this work, we present a switching nonlinear model predictive control (NMPC) algorithm for a dual-hormone artificial pancreas (AP), and we use maximum likelihood estimation (MLE) to identify the model parameters. A dual-hormone AP consists of a continuous glucose monitor (CGM), a control algorithm, an insulin pump, and a glucagon pump. The AP is designed with a heuristic to switch between insulin and glucagon as well as state-dependent constraints. We extend an existing glucoregulatory model with glucagon and exercise for simulation, and we use a simpler model for control. We test the AP (NMPC and MLE) using in silico numerical simulations on 50 virtual people with type 1 diabetes. The system is identified for each virtual person based on data generated with the simulation model. The simulations show a mean of 89.3% time in range (3.9–10 mmol/L) and no hypoglycemic events.

Copyright © 2022 The Authors. This is an open access article under the CC BY-NC-ND license (<https://creativecommons.org/licenses/by-nc-nd/4.0/>)

Keywords: Artificial Pancreas, Model Predictive Control, System Identification, Optimal Control, Physiological modeling

1. INTRODUCTION

Type 1 diabetes (T1D) is a chronic metabolic disorder which prevents the pancreas from producing insulin. People with T1D require life-long treatment with daily injections of insulin in order to prevent hyperglycemia (i.e., high blood glucose concentrations). Prolonged hyperglycemia leads to a range of health complications, e.g., cardiovascular disease, chronic kidney disease, and damage to the nerves and eyes. Over 9% of the world population suffers from diabetes, 5–10% of those have T1D, and 10% of the 2019 global health expenditure (USD 760 billion) was spent on diabetes (International Diabetes Federation, 2019).

The treatment of T1D is tedious and time-consuming, and if managed poorly, it can lead to both hyper- and hypoglycemia (low blood glucose concentrations). Hypoglycemia can, in severe cases, cause a variety of acute complications including loss of consciousness, seizures, and death. Therefore, there is a significant interest in developing closed-loop diabetes treatment systems based on feedback control. Such systems are referred to as *artificial pancreases* (APs). They consist of 1) a continuous glucose monitor (CGM) (the sensor), 2) a control algorithm (e.g., implemented on a smartphone or a dedicated device), and 3) an insulin pump (the actuator). Many control strategies have been proposed for

this purpose, including fuzzy logic (Biester et al., 2019), proportional-integral-derivative (PID) control (Sejerssen et al., 2021; Huyett et al., 2015; Jørgensen et al., 2019), and model predictive control (MPC). MPC is a closed-loop feedback strategy that uses the moving horizon optimization principle, i.e., it involves solving a sequence of open-loop optimal control problems (OCs). Both linear MPC (LMPC) (Chakrabarty et al., 2020; Messori et al., 2018), and nonlinear MPC (NMPC) (Hovorka et al., 2004; Boiroux et al., 2018b; Boiroux and Jørgensen, 2018) have been considered.

Most algorithms are designed for *single-hormone* systems where only insulin is administered. Consequently, they are unable to actively counteract low blood sugar concentrations which can occur in a variety of situations, e.g., in connection with physical activity. Therefore, researchers currently investigate *dual-hormone* systems that administer both insulin and glucagon (Peters and Haidar, 2018; Infante et al., 2021). In contrast to insulin, glucagon causes an increase in the blood glucose level. Moscardo et al. (2019) develop a dual-hormone control algorithm based on proportional-derivative (PD) control, and Boiroux et al. (2018a) develop LMPC algorithms based on a variety of different transfer function models. Other hormones than glucagon have also been considered, e.g., pramlintide which slows down gastric emptying (Haidar et al., 2020).

In this work, we present a dual-hormone NMPC algorithm for administering insulin and glucagon. The algorithm is

¹ Corresponding author: J. B. Jørgensen (E-mail: jbjo@dtu.dk).

based on an extended Medtronic Virtual patient (MVP) model (Kanderian et al., 2009), and we use maximum likelihood estimation (MLE) to identify the model parameters. We use the continuous-discrete extended Kalman filter (CD-EKF) in both the parameter estimation and in the NMPC algorithm. Furthermore, we use a state-dependent heuristic for switching between administering insulin and glucagon (which cannot be administered simultaneously). We use an extension of the model developed by Hovorka et al. (2002) to perform closed-loop simulations. It is extended with 1) a model of the measurement delay of the CGM (Facchinetti et al., 2014), 2) a pharmacokinetic model of subcutaneous glucagon injection (Haidar et al., 2013), and 3) a model of the effect of physical activity (Rashid et al., 2019). We present numerical results for 50 virtual people with T1D and demonstrate that the AP, including the parameter estimation, satisfies the time in range (TIR) targets described by Holt et al. (2021).

The remainder of the paper is structured as follows. We present the extension of the model by Hovorka et al. in Section 2 and the MVP model in Section 3. In Section 4, we describe the parameter estimation problem, and we describe the NMPC algorithm in Section 5. We present the state-dependent switching heuristic in Section 6, and we discuss the numerical results in Section 7. Finally, conclusions are given in Section 8.

2. SIMULATION MODEL

The model by Hovorka et al. (2002, 2004) consists of an insulin subsystem, a meal subsystem, and a glucose subsystem. We extend it with a glucagon subsystem (Haidar et al., 2013), an exercise subsystem (Rashid et al., 2019), and a CGM subsystem (Facchinetti et al., 2014).

2.1 Insulin subsystem

The insulin absorption and insulin concentration are described by

$$\dot{S}_1(t) = u_I(t) - \frac{S_1(t)}{\tau_S}, \quad (1a)$$

$$\dot{S}_2(t) = \frac{S_1(t)}{\tau_S} - \frac{S_2(t)}{\tau_S}, \quad (1b)$$

$$\dot{I}(t) = \frac{1}{V_I} \frac{S_2(t)}{\tau_S} - k_e I(t), \quad (1c)$$

where S_1 and S_2 [mU] are a two compartment chain representing the insulin absorption, τ_S [min] is the insulin absorption time constant, I [mU/L] is the plasma insulin concentration, V_I [L] is the insulin distribution volume, and k_e [1/min] is the elimination rate. $u_I = u_{ba} + u_{bo}$ [mU/min] is the insulin infusion rate where u_{ba} [mU/min] is the basal infusion rate and u_{bo} [mU/min] is the bolus infusion rate.

2.2 Insulin action subsystem

The insulin action on the glucose kinetics is described by

$$\dot{x}_1(t) = k_{b1} I(t) - k_{a1} x_1(t), \quad (2a)$$

$$\dot{x}_2(t) = k_{b2} I(t) - k_{a2} x_2(t), \quad (2b)$$

$$\dot{x}_3(t) = k_{b3} I(t) - k_{a3} x_3(t), \quad (2c)$$

where x_1 [1/min], x_2 [1/min], and x_3 [1/min] represent the effects of insulin on the glucose distribution, the glucose disposal, and the endogenous glucose production. Furthermore, k_{bi} [(L/mU)/min²] and k_{ai} [1/min] for $i = 1, 2, 3$ are the activation and deactivation rate constants.

2.3 Meal subsystem

The meal absorption subsystem is represented by

$$\dot{D}_1(t) = A_G D(t) - \frac{D_1(t)}{\tau_D}, \quad (3a)$$

$$\dot{D}_2(t) = \frac{D_1(t)}{\tau_D} - \frac{D_2(t)}{\tau_D}, \quad (3b)$$

where D_1 [mmol] and D_2 [mmol] are a two compartment chain representing the meal absorption, D [mmol/min] is the meal carbohydrate content, A_G [-] is the carbohydrate bioavailability, and τ_D [min] is the meal time constant.

2.4 Glucagon subsystem

The glucagon subsystem is described by

$$\dot{Q}_1^G(t) = u_G(t) - \frac{Q_1^G(t)}{\tau_{Glu}}, \quad (4a)$$

$$\dot{Q}_2^G(t) = \frac{Q_1^G(t)}{\tau_{Glu}} - \frac{Q_2^G(t)}{\tau_{Glu}}, \quad (4b)$$

where Q_1^G [μ g] and Q_2^G [μ g] are a two-compartment chain representing the glucagon absorption, u_G [μ g/min] is the glucagon infusion rate, and τ_{Glu} [min] is a time constant.

2.5 Exercise subsystem

The exercise model describes the increased glucose consumption and insulin sensitivity during and after physical activity. The effect of high-intensity exercise is not modeled. The exercise subsystem consists of

$$\dot{E}_1(t) = \frac{HR(t) - HR_0 - E_1(t)}{\tau_{HR}}, \quad (5a)$$

$$\dot{T}_E(t) = \frac{c_1 f_{E1}(t) + c_2 - T_E(t)}{\tau_{ex}}, \quad (5b)$$

$$\dot{E}_2(t) = - \left(\frac{f_{E1}(t)}{\tau_{in}} + \frac{1}{T_E(t)} \right) E_2(t) + \frac{f_{E1}(t) T_E(t)}{c_1 + c_2}, \quad (5c)$$

$$f_{E1}(t) = \frac{\left(\frac{E_1(t)}{a \cdot HR_0} \right)^n}{1 + \left(\frac{E_1(t)}{a \cdot HR_0} \right)^n}, \quad (5d)$$

where E_1 [BPM] is the short-term effect, E_2 [min] is the long-term effect, T_E [min] is the characteristic time for the long-term effect, HR [BPM] is the heart rate, HR_0 [BPM] is the resting heart rate, τ_{HR} [min] is the time constant, c_1 [min] and c_2 [min] define the steady state value for T_E , τ_{ex} [min] is the time constant for how fast T_E reaches steady state, and a [-], n [-], and τ_{in} [min] specify the intensity and time constant of the long-term effect on the insulin sensitivity.

2.6 Glucose subsystem

The glucose kinetics are represented by

$$\dot{Q}_1(t) = \frac{D_2(t)}{\tau_D} - F_{01,c}(t) - F_R(t) - x_1(t)Q_1(t) \quad (6a)$$

$$+ k_{12}Q_2(t) + EGP(t) + Q_G(t) - Q_{E21}(t),$$

$$\dot{Q}_2(t) = x_1(t)Q_1(t) - k_{12}Q_2(t) - x_2Q_2(t) \quad (6b)$$

$$+ Q_{E21}(t) - Q_{E22}(t) - Q_{E1}(t),$$

where

$$EGP(t) = EGP_0(1 - x_3(t)), \quad (7a)$$

$$Q_G(t) = K_{Glu}V_GQ_2^G(t), \quad (7b)$$

$$Q_{E21}(t) = \alpha E_2(t)^2 x_1(t)Q_1(t), \quad (7c)$$

$$Q_{E22}(t) = \alpha E_2(t)^2 x_2(t)Q_2(t), \quad (7d)$$

$$Q_{E1}(t) = \beta \frac{E_1(t)}{HR_0}, \quad (7e)$$

and

$$F_{01,c}(t) = \begin{cases} F_{01} & G(t) \geq 4.5 \text{ mmol/L}, \\ F_{01}G(t)/4.5 & \text{otherwise}, \end{cases} \quad (8a)$$

$$F_R(t) = \begin{cases} 0.003(G(t) - 9)V_G & G(t) \geq 9 \text{ mmol/L}, \\ 0 & \text{otherwise}, \end{cases} \quad (8b)$$

$$G(t) = \frac{Q_1(t)}{V_G}, \quad (8c)$$

where Q_1 [mmol] and Q_2 [mmol] represent the accessible and non-accessible compartments, k_{12} [1/min] is the transfer rate, F_{01} [mmol/min] and $F_{01,c}$ [mmol/min] are the nominal and corrected total non-insulin dependent glucose flux, F_R [mmol/min] is the renal glucose clearance, V_G [L] is the glucose distribution volume, EGP_0 [mmol] is the endogenous glucose production, K_{Glu} [(mmol/L)/μg/min] is the glucagon gain, α [1/min²] is the exercise-induced insulin action, β [mmol/min] is the exercise-induced insulin-independent glucose uptake rate, and G [mmol/L] is the glucose concentration.

2.7 CGM subsystem

The CGM subsystem describes the glucose transfer from the plasma to the interstitial tissue by

$$\dot{G}_I(t) = \frac{G(t)}{\tau_{IG}} - \frac{G_I(t)}{\tau_{IG}}, \quad (9)$$

where G_I [mmol/L] is the interstitial glucose concentration and τ_{IG} is a time constant.

3. CONTROL MODEL

In the AP, we use an extension of the Medtronic Virtual patient (MVP) model (Kanderian et al., 2009) represented as a system of coupled stochastic differential equations. The MVP model describes the glucose-insulin dynamics and we extend it with the meal subsystem, the glucagon subsystem and the CGM subsystem from the simulation model described in Section 2.

3.1 Insulin subsystem

The insulin absorption subsystem consists of

$$dI_{SC}(t) = k_1 \left(\frac{u_{ba}(t) + u_{bo}(t)}{C_I} - I_{SC}(t) \right) dt, \quad (10a)$$

$$dI_P(t) = k_2 (I_{SC}(t) - I_P(t)) dt, \quad (10b)$$

where I_{SC} [mU/L] is the subcutaneous insulin concentration, I_P [mU/L] is the plasma insulin concentration,

$k_2 = k_1$ [1/min] is the inverse insulin absorption time constant, and C_I [L/min] is the insulin clearance rate.

3.2 Glucose subsystem

Here, we describe the insulin effect, the blood glucose concentration and insulin sensitivity. The blood glucose concentration and insulin sensitivity is modeled as stochastic differential equations:

$$dI_{EFF}(t) = p_2 (S_I(t)I_P(t) - I_{EFF}(t)) dt, \quad (11a)$$

$$dG(t) = [-(GEZI + I_{EFF}(t))G(t) + EGP \quad (11b)$$

$$+ R_A(t) + K_{Glu}Q_2^G(t)]dt + \sigma_G dw_G(t),$$

$$d \log(S_I(t)) = \sigma_{S_I} dw_{S_I}(t), \quad (11c)$$

where I_{EFF} [1/min] is the insulin effect, $p_2 = k_1$ [1/min] is the inverse insulin action time constant, S_I [(L/mU)/min] is the insulin sensitivity, $GEZI$ [1/min] is the glucose effectiveness, EGP [(mmol/L)/min] is the endogenous glucose production, σ_G and σ_{S_I} are the glucose and insulin sensitivity diffusion coefficients, and w_G and w_{S_I} are standard Wiener processes. The meal rate of appearance, R_A [(mmol/L)/min], is

$$R_A(t) = \frac{k_m D_2(t)}{V_G}, \quad (12)$$

where k_m [1/min] is a time constant.

4. PARAMETER ESTIMATION

We use MLE based on the CD-EKF to estimate the parameters in the MVP model given $N + 1$ CGM measurements of the blood glucose concentration, $\mathcal{Y}_N = \{y_0, y_1, \dots, y_N\}$. The MVP model is in the form

$$dx(t) = f(t, x(t), u(t), d(t), \theta)dt + \sigma(\theta)dw(t), \quad (13a)$$

$$y_k = g(t_k, x_k, \theta) + v_k, \quad (13b)$$

where t is the time, x are the states, u are the manipulated inputs, d are the disturbances, θ are the parameters, and $y_k = y(t_k)$ are the measured variables. σ is the diffusion coefficient, w is a standard Wiener process (i.e., $dw(t) \sim N(0, Idt)$), and $v_k \sim N(0, R)$ is the measurement noise.

The MLE of the parameters, $\hat{\theta}$, is given by

$$\hat{\theta} = \arg \min_{\theta} V(\theta), \quad (14)$$

where V is the negative log-likelihood function:

$$V(\theta) = -\log p(\mathcal{Y}_N|\theta). \quad (15)$$

Here, $p(\mathcal{Y}_N|\theta)$ is the conditional probability density function of the stochastic observations in the system (13) evaluated at the observed blood glucose concentrations for a given set of parameters, θ . The negative log-likelihood function is given by

$$V(\theta) = \frac{(N+1)n_y}{2} \log(2\pi) + \frac{1}{2} \sum_{k=0}^N \log[\det(R_{e,k}(\theta))] \\ + e_k(\theta)^T [R_{e,k}(\theta)]^{-1} e_k(\theta), \quad (16)$$

where $n_y = 1$ and $e_k(\theta)$ is the innovation:

$$e_k(\theta) = y_k - \hat{y}_{k|k-1}(\theta). \quad (17)$$

Given an initial estimate of the states (which is also estimated) and their covariance, $\hat{x}_0(\theta)$ and P_0 , we use the CD-EKF to compute the one-step predictions of the observed variables, $\hat{y}_{k|k-1}(\theta)$, and the covariance of the innovations, $R_{e,k}(\theta)$. We refer to the paper by Boiroux et al. (2019) for more details.

5. NONLINEAR MODEL PREDICTIVE CONTROL

The NMPC algorithm receives a CGM measurement of the blood glucose concentration every 5 minutes. Subsequently, the CD-EKF is used to compute a filtered estimate of the states which is used as the initial states, \hat{x}_0 , when solving the following OCP for the manipulated inputs.

$$\min_{[x(t)]_{t_0}^{t_f}, \{u_k\}_{k=0}^{N-1}} \phi = \phi([x(t)]_{t_0}^{t_f}, \{u_k\}_{k=0}^{N-1}), \quad (18a)$$

subject to

$$x(t_0) = \hat{x}_0, \quad (18b)$$

$$\dot{x}(t) = f(t, x(t), u(t), d(t), \theta), \quad t \in [t_0, t_f], \quad (18c)$$

$$u(t) = u_k, \quad t \in [t_k, t_{k+1}[, \quad k = 0, \dots, N-1, \quad (18d)$$

$$d(t) = \hat{d}_k, \quad t \in [t_k, t_{k+1}[, \quad k = 0, \dots, N-1, \quad (18e)$$

$$u_{\min} \leq u_k \leq u_{\max}, \quad k = 0, \dots, N-1. \quad (18f)$$

The prediction and control horizon, $[t_0, t_f]$, is 6 h, and each of the N control intervals is 5 min. The objective function in (18a) is described in Section 5.1, (18b) is the initial condition, (18c) is the MVP model where the process noise is disregarded, (18d)–(18e) are zero-order-hold parametrizations of the manipulated inputs and the estimated disturbance variables, and (18f) are bounds on the manipulated inputs. Only the first set of manipulated inputs, u_0 , are administered before a new CGM measurement is received and the horizon $[t_0, t_f]$ is shifted by one control interval.

5.1 Objective function

The objective function depends on whether insulin or glucagon is administered. In both cases, it is in the form

$$\phi = \int_{t_0}^{t_f} \rho_z(z(t))dt + \sum_{k=0}^{N-1} \rho_u(u_k), \quad (19)$$

where ρ_z and ρ_u are penalty functions and the outputs (the CGM measurements of the blood glucose concentration) are $z(t) = g(t, x(t), \theta)$.

The penalty function in the first term of (19) is

$$\rho_z(z) = \alpha_{\bar{z}} \rho_{\bar{z}}(z) + \alpha_{z_{\min}} \rho_{z_{\min}}(z) + \alpha_{z_{\max}} \rho_{z_{\max}}(z), \quad (20)$$

where 1) the first term penalizes the deviation of the blood glucose from the setpoint $\bar{z} = 6$ mmol/L, 2) the second term penalizes hypoglycemia ($z < z_{\min} = 4.5$ mmol/L), and 3) the third term penalizes hyperglycemia ($z > z_{\max} = 10$ mmol/L):

$$\rho_{\bar{z}}(z) = \frac{1}{2}(z - \bar{z})^2, \quad (21a)$$

$$\rho_{z_{\min}}(z) = \frac{1}{2}(\min\{0, z - z_{\min}\})^2, \quad (21b)$$

$$\rho_{z_{\max}}(z) = \frac{1}{2}(\max\{0, z - z_{\max}\})^2. \quad (21c)$$

The weights in (20) are $\alpha_{\bar{z}} = 1$, $\alpha_{z_{\min}} = 10^6$, $\alpha_{z_{\max}} = 50$ when computing the insulin flow rates, and $\alpha_{z_{\max}} = 0$ when computing the glucagon flow rate. The penalty function is shown in Fig. 1. As is evident, preventing hypoglycemia has the highest priority.

When computing the insulin flow rates, the penalty function in the second term of (19) is

$$\rho_u(u_k) = \rho_{u,ba}(u_{ba,k}) + \rho_{u,bo}(u_{bo,k}), \quad (22)$$

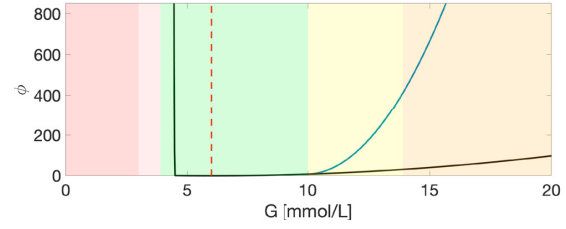


Fig. 1. Blood glucose penalty function when administering insulin (blue) and glucagon (black).

where

$$\rho_{u,ba}(u_{ba,k}) = \|u_{ba,k} - \bar{u}_{ba,k}\|_2^2, \quad (23a)$$

$$\rho_{u,bo}(u_{bo,k}) = \|u_{bo,k}\|_1, \quad (23b)$$

in order to penalize excursions from the nominal basal rate $\bar{u}_{ba,k}$ and to promote the administration of fewer larger insulin boluses. When computing the glucagon flow rate,

$$\rho_u(u_k) = \|u_{G,k}\|_2^2, \quad (24)$$

in order to minimize the administered glucagon.

5.2 Numerical solution

We use a multiple-shooting approach (Bock and Plitt, 1984) to transcribe (18) by discretizing the dynamic constraint (18c) and the integral in (19) using an explicit Runge-Kutta method with fixed step size. The result is a nonlinear program which we solve using a sequential quadratic programming (SQP) method (Nocedal and Wright, 2006).

6. HEURISTICS

In the NMPC algorithm, we use a set of heuristics to 1) switch between administering insulin and glucagon, 2) compute upper bounds on the manipulated inputs, 3) modify algorithmic hyperparameters during exercise, and 4) post-process the manipulated inputs computed by solving the OCP (18).

6.1 Switching between insulin and glucagon administration

Insulin and glucagon should not be administered simultaneously. Therefore, we switch between them based on the blood glucose concentration. If the blood glucose concentration becomes lower than 4.5 mmol/L, the AP switches to glucagon administration. Conversely, if it becomes higher than 5 mmol/L, the AP switches to administering insulin. However, for 1 h after each meal, only insulin can be administered.

6.2 Bounds and meal-specific heuristics

The upper bounds on the insulin and glucagon boli are updated at the beginning of every control interval (i.e., whenever a CGM measurement is obtained). Furthermore, the upper bound on the insulin basal rate is twice the target basal rate, i.e., $2\bar{u}_{ba,k}$, and the lower bounds on all three manipulated inputs are 0.

The upper bound on the insulin bolus is

$$u_{bo,k}^{\max} = \max\{\epsilon, u_{bo,k}^{\text{corr}} + u_{bo,k}^{\text{meal}} - u_{bo,k}^{\text{hist}}\}, \quad (25)$$

where $\epsilon = 10^{-3}$ [–], $u_{bo,k}^{\text{corr}}$ is the maximum correction bolus infusion rate, $u_{bo,k}^{\text{meal}}$ is the maximum meal bolus infusion rate, and $u_{bo,k}^{\text{hist}}$ is the sum of the insulin bolus infusion rates administered during the previous 11 control intervals. If a meal was announced at time t_k , or if no meal was announced in the last hour,

$$u_{bo,k}^{\text{corr}} = \max \left\{ 0, \frac{1}{T_s} \frac{G - 10 \text{ mmol/L}}{ISF} \right\}, \quad (26)$$

where ISF [(mmol/L)/mU] is the insulin sensitivity factor and $T_s = 5$ min is the sampling time. Otherwise, $u_{bo,k}^{\text{corr}} = u_{bo,k-1}^{\text{corr}}$. If a meal was consumed within the last hour, the maximum meal bolus is

$$u_{bo,k}^{\text{meal}} = \max \left\{ 0, \frac{\gamma}{T_s} \frac{\hat{d}}{ICR} \right\}, \quad (27)$$

where \hat{d} [g CHO] is the announced carbohydrate content of the last meal, $\gamma = 1.15$ [–] is a bolus allowance factor, and ICR [g/mU] is the insulin-to-carb ratio. Otherwise, $u_{bo,k}^{\text{meal}} = 0$. Finally, the insulin bolus history is

$$u_{bo,k}^{\text{hist}} = \sum_{j=1}^{11} u_{bo,k-j|k-j}, \quad (28)$$

where $u_{bo,k|k}$ is the insulin bolus infusion rate in the k 'th control interval. When a meal is announced, we set $u_{bo,k}^{\text{hist}} = 0$. The history spans 11 control intervals in order to bound the amount of bolus insulin over each 1 h period.

The maximum glucagon bolus is computed by

$$u_{G,k}^{\text{max}} = \max \{ \epsilon, \bar{u}_G^{\text{max}} - u_{G,k}^{\text{hist}} \}, \quad (29)$$

where $\bar{u}_G^{\text{max}} = 300 \mu\text{g}$ and the glucagon bolus history is

$$u_{G,k}^{\text{hist}} = \sum_{j=1}^{23} u_{G,k-j|k-j}. \quad (30)$$

Here, $u_{G,k|k}$ is the glucagon infusion rate in the k 'th control interval. As for the insulin bolus history, the glucagon history spans 23 control intervals in order to bound the amount of glucagon administered over each 2 h period.

Finally, to avoid that the insulin sensitivity is adjusted after a meal, the insulin sensitivity diffusion coefficient is set to zero if a meal was consumed within the last hour. Otherwise, it is set to the value estimated during the parameter estimation. Additionally, in the CD-EKF, we set the state variance of $\log S_I$ as well as the corresponding covariances with the other states to zero when a meal is announced, and we enforce that

$$\log S_I(0) - 1 \leq \log S_I(t) \leq \log S_I(0) + 1 \quad (31)$$

using clipping, where $\log S_I(0)$ is estimated during the parameter estimation.

6.3 Exercise logic

During physical activity, the setpoint, \bar{z} , is increased from 6 mmol/L to 7 mmol/L, the glucagon switching threshold is increased to 7 mmol/L, and a glucagon dose of 100 μg is administered if the blood glucose concentration is below 7 mmol/L when the physical activity is initiated.

6.4 Post-processing and open-loop fallback strategy

Once the solution to the OCP (18) has been obtained, the resulting manipulated inputs in the first control interval are rounded to the pump resolution which is 0.01 U/h for the insulin basal rate, 0.1 U for the bolus insulin, and 0.01 $\mu\text{g/h}$ for the glucagon infusion rate.

Furthermore, the AP algorithm is intended to be used by real people, e.g., in clinical trials. Therefore, as a safety measure, we implement the following open-loop strategy if unforeseen circumstances prevent the solution of the OCP (18).

$$u_{ba,k|k} = \begin{cases} 0 & G \leq 8.0 \text{ mmol/L}, \\ \bar{u}_{ba,k} & \text{otherwise}, \end{cases} \quad (32a)$$

$$u_{bo,k|k} = 0, \quad (32b)$$

$$u_{G,k|k} = \begin{cases} \min\{15 \mu\text{g}, u_{G,k}^{\text{max}}\} & G < 4.5 \text{ mmol/L}, \\ 0 & \text{otherwise}. \end{cases} \quad (32c)$$

7. RESULTS

In this section, we present the results from testing both the system identification and the artificial pancreas in a virtual clinical trial with 50 virtual people with T1D. We estimate the parameters in the control model from data generated with the simulation model individually for each person. We estimate the parameters k_m , τ_D , V_G , EGP , σ_G , and σ_{S_I} as well as the initial states in the MVP model. The remaining parameters are fixed. We estimate ICR as described by Sejersen et al. (2021) and $ISF = 2$ mmol/L/U for all participants. We show the generated data and a simulation (without process noise) with the estimated model in Fig. 2 for one virtual person. In the virtual clinical trial, we use the protocol shown in Fig. 3. In Fig. 4, we show the closed-loop simulation for the person identified in Fig. 2. We divide the blood glucose concentration into the following 5 ranges (Holt et al., 2021) given in mmol/L. Red: severe hypoglycemia (below 3). Light red: hypoglycemia (3–3.9). Green: normoglycemia (3.9–10). Yellow: hyperglycemia (10–13.9). Orange: severe hyperglycemia (above 13.9). For this person, the administered meal bolus is at the limit for most of the meals, but for the snack, we see that only a part of the allowed bolus is administered. The AP is allowed to give the remaining bolus insulin for 1 hour after the snack. The basal rate is increased after the meals where the bolus size is constrained, as the control model predicts the meal to have a larger effect than what the allowed bolus can correct for. Due to the high insulin dose after the dinner, the AP administers a small dose of glucagon. Furthermore, we see that the AP is allowed to give a small correction bolus after the dinner, but once the blood glucose concentration is below 10 mmol/L, the correction bolus is no longer allowed. It is desired to administer a larger meal bolus and compensate by decreasing the basal rate to reduce the postprandial peak. However, for safety reasons, we have a limit on the maximum bolus even though it can decrease the performance of the AP for some people. After the person begins to exercise, the setpoint is increased and a glucagon bolus of 100 μg is administered. Fig. 5 and 6 show the TIR for all 50 virtual people. The average time in normoglycemia is very high at 89.3%, with 8.7% in hyperglycemia, 2% in severe hyperglycemia and no

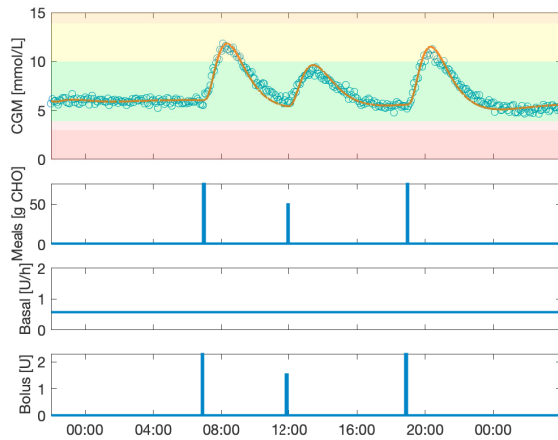


Fig. 2. Generated data and simulation with the estimated model for one virtual person. From the top: 1) the CGM data (blue circles) and simulation (red line), 2) the meal carbohydrate content, 3) the insulin basal rate, and 4) the insulin boli.

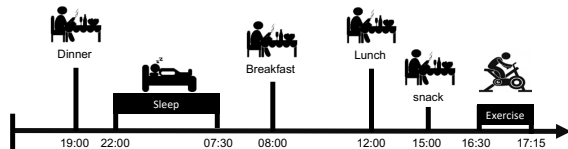


Fig. 3. The protocol used in the virtual clinical trial. The protocol consists of a dinner of 75 g CHO, sleep, a breakfast of 50 g CHO, a lunch of 75 g CHO, a snack of 15 g CHO, and finally, exercise of moderate intensity.

time in hypoglycemia. The person with the lowest time in normoglycemia still spends more than 70% of the time in normoglycemia which is the minimum recommended by Holt et al. (2021). From Fig. 6, we see that the 50 virtual people receive relatively low total daily insulin doses and are sensitive to insulin. The amount of administered glucagon is fairly low and at a reasonable level.

8. CONCLUSION

In this paper, we present a dual-hormone AP algorithm for controlling the blood glucose concentration in people with T1D. The AP is based on a switching NMPC algorithm, and we use an extension of the MVP model for prediction. Furthermore, we use MLE to estimate the model parameters. The CD-EKF is used in both the NMPC and the MLE algorithm. We test the algorithm using an extension of the model by Hovorka et al. (2002), and we demonstrate that the average TIR for 50 virtual people with T1D in a virtual clinical trial is 89.3%. Furthermore, none of the virtual people experience any hypoglycemic events.

REFERENCES

- Biester, T., Nir, J., Remus, K., Farfel, A., Muller, I., Biester, S., Atlas, E., Dovc, K., Bratina, N., Kordonouri, O., Battelino, T., Philip, M., Danne, T., and Nimri, R. (2019). DREAM5: An open-label, randomized, cross-over study to evaluate the safety and efficacy of day and

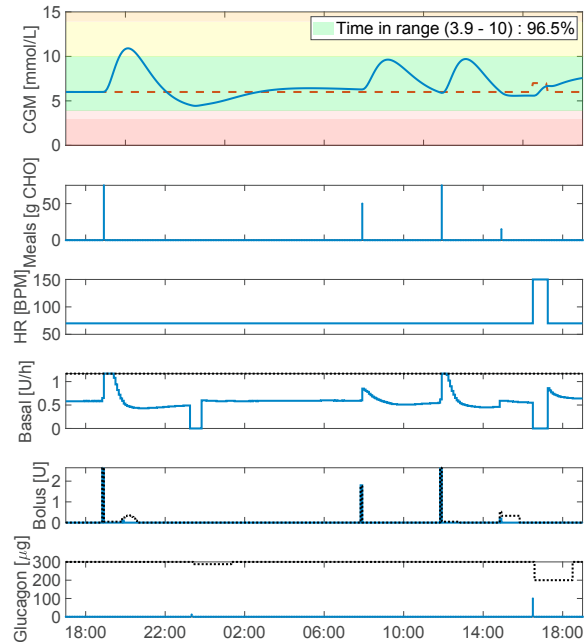


Fig. 4. Closed-loop simulation for one virtual person. From the top: 1) The CGM measurement and the setpoint, 2) the meal carbohydrate content, 3) the heart rate, 4) the administered insulin basal rate and the maximum allowed basal rate, 5) the insulin boli and maximum allowed insulin boli, and 6) the glucagon boli and the maximum allowed glucagon boli. The black dotted lines are the upper bounds.

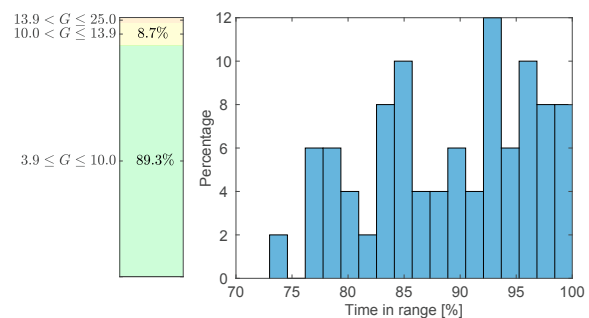


Fig. 5. Time in ranges for the 50 virtual people with T1D. Left: mean time in ranges, Right: distribution of time in range.

- night closed-loop control by comparing the MD-Logic automated insulin delivery system to sensor augmented pump therapy in patients with type 1 diabetes at home. *Diabetes, Obesity and Metabolism*, 21(4), 822–828.
- Bock, H.G. and Plitt, K.J. (1984). A multiple shooting algorithm for direct solution of optimal control problems. *IFAC Proceedings Volumes*, 17(2), 1603–1608.
- Boiroux, D., Batora, V., Hagdrup, M., Wendt, S.L., Poulsen, N.K., Madsen, H., and Jørgensen, J.B. (2018a). Adaptive model predictive control for a dual-hormone artificial pancreas. *Journal of Process Control*, 68, 105–

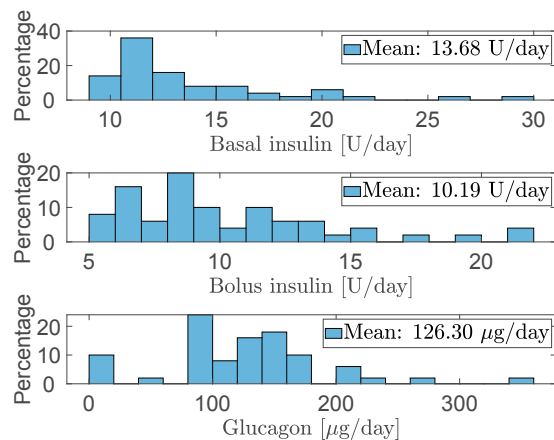


Fig. 6. Distributions of the total daily basal and bolus insulin and bolus glucagon for the 50 virtual people. Top: Basal insulin. Middle: Bolus insulin. Bottom: Bolus glucagon.

- 117.
- Boiroux, D., Duun-Henriksen, A.K., Schmidt, S., Nørgaard, K., Madsbad, S., Poulsen, N.K., Madsen, H., and Jørgensen, J.B. (2018b). Overnight glucose control in people with type 1 diabetes. *Biomedical Signal Processing and Control*, 39, 503–512.
- Boiroux, D. and Jørgensen, J.B. (2018). Nonlinear model predictive control and artificial pancreas technologies. In *2018 IEEE Conference on Decision and Control (CDC)*, 284–290.
- Boiroux, D., Ritschel, T.K.S., Poulsen, N.K., Madsen, H., and Jørgensen, J.B. (2019). Efficient computation of the continuous-discrete extended Kalman filter sensitivities applied to maximum likelihood estimation. *2019 IEEE 58th Conference on Decision and Control (CDC)*, 6983–6988.
- Chakrabarty, A., Healey, E., Shi, D., Zavitsanos, S., Doyle III, F.J., and Dassau, E. (2020). Embedded model predictive control for a wearable artificial pancreas. *IEEE Transactions on Control Systems Technology*, 28(6), 2600–2607.
- Facchinetti, A., Favero, S.D., Sparacino, G., Castle, J.R., Ward, W.K., and Cobelli, C. (2014). Modeling the glucose sensor error. *IEEE Transactions on Biomedical Engineering*, 61(3), 620–629.
- Haidar, A., Duval, C., Legault, L., and Rabasa-Lhoret, R. (2013). Pharmacokinetics of insulin aspart and glucagon in type 1 diabetes during closed-loop operation. *Journal of Diabetes Science and Technology*, 7(6), 1507–1512.
- Haidar, A., Tsoukas, M.A., Bernier-Twardy, S., Yale, J.F., Rutkowski, J., Bossy, A., Pytka, E., Fathi, A.E., Strauss, N., and Legault, L. (2020). A novel dual-hormone insulin-and-pramlintide artificial pancreas for type 1 diabetes: A randomized controlled crossover trial. *Diabetes Care*, 43(3), 597–606.
- Holt, R.I., DeVries, J.H., Hess-Fischl, A., Hirsch, I.B., Kirkman, M.S., Klupa, T., Ludwig, B., Nørgaard, K., Pettus, J., Renard, E., Skyler, J.S., Snoek, F.J., Weinstock, R.S., and Peters, A.L. (2021). The management of type 1 diabetes in adults. A consensus report by the American Diabetes Association (ADA) and the European Association for the Study of Diabetes (EASD). *Diabetologia*, 64, 2609–2652.
- Hovorka, R., Shojaei-Moradie, F., Carroll, P.V., Chassin, L.J., Gowrie, I.J., Jackson, N.C., Tudor, R.S., Umpleby, A.M., and Jones, R.H. (2002). Partitioning glucose distribution/transport, disposal, and endogenous production during IVGTT. *American Journal of Physiology-Endocrinology and Metabolism*, 282, E992–E1007.
- Hovorka, R., Canonico, V., Chassin, L.J., Haueter, U., Massi-Benedetti, M., Federici, M.O., Pieber, T.R., Schaller, H.C., Schaupp, L., Vering, T., and Wilinska, M.E. (2004). Nonlinear model predictive control of glucose concentration in subjects with type 1 diabetes. *Physiological Measurement*, 25(4), 905–920.
- Huyett, L.M., Dassau, E., Zisser, H.C., and Doyle III, F.J. (2015). Design and evaluation of a robust PID controller for a fully implantable artificial pancreas. *Industrial & Engineering Chemistry Research*, 54, 10311–10321.
- Infante, M., Baidal, D.A., Rickels, M.R., Fabbri, A., Skyler, J.S., Alejandro, R., and Ricordi, C. (2021). Dual-hormone artificial pancreas for management of type 1 diabetes: Recent progress and future directions. *Artificial Organs*, 45(9), 968–986.
- International Diabetes Federation (2019). IDF diabetes atlas 9th edition. ISBN: 978-2-930229-87-4.
- Jørgensen, J.B., Boiroux, D., and Mahmoudi, Z. (2019). An artificial pancreas based on simple control algorithms and physiological insight. *IFAC PapersOnLine*, 52(1), 1018–1023.
- Kandarian, S.S., Weinzimer, S., Voskanyan, G., and Steil, G.M. (2009). Identification of intraday metabolic profiles during closed-loop glucose control in individuals with type 1 diabetes. *Journal of Diabetes Science and Technology*, 3(5), 1047–1057.
- Messori, M., Incremona, G.P., Cobelli, C., and Magni, L. (2018). Individualized model predictive control for artificial pancreas: In silico evaluation of the closed-loop glucose control. *IEEE Control Systems Magazine*, 38(1), 86–104.
- Moscardo, V., Herrero, P., Diez, J.L., Gimenez, M., Rossetti, P., Georgiou, P., and Bondia, J. (2019). Coordinated dual-hormone artificial pancreas with parallel control structure. *Computers and Chemical Engineering*, 128, 322–328.
- Nocedal, J. and Wright, S.J. (2006). *Numerical optimization*. Springer Science & Business Media, 2nd edition.
- Peters, T.M. and Haidar, A. (2018). Dual-hormone artificial pancreas: Benefits and limitations compared with single-hormone systems. *Diabetic Medicine*, 35(4), 450–459.
- Rashid, M., Samadi, S., Sevil, M., Hajizadeh, I., Kolodziej, P., Hobbs, N., Maloney, Z., Brandt, R., Feng, J., Park, M., Quinn, L., and Cinar, A. (2019). Simulation software for assessment of nonlinear and adaptive multivariable control algorithms: Glucose-insulin dynamics in type 1 diabetes. *Computers & Chemical Engineering*, 130, 106565.
- Sejersén, M., Boiroux, D., Engell, S.E., Ritschel, T.K.S., Reenberg, A.T., and Jørgensen, J.B. (2021). Initial titration for people with type 1 diabetes using an artificial pancreas. *IFAC PapersOnLine*, 54(15), 484–489.

APPENDIX J

Journal Paper - In preparation

A Dual- and Single-Hormone Artificial Pancreas based on Nonlinear Model Predictive Control in a Clinical Trial with Adolescents

Authors:

Asbjørn Thode Reenberg, Tobias K. S. Ritschel, Dimitri Boiroux, Maria Sejersen, Emilie B. Lindkvist, Christian Laugesen, Jannet Svensson, Ajenthen G. Ranjan, Kirsten Nørgaard, John Bagterp Jørgensen

Published in:

In preparation.

A Dual- and Single-Hormone Artificial Pancreas based on Nonlinear Model Predictive Control in a Clinical Trial with Adolescents

Asbjørn Thode Reenberg^a, Tobias K. S. Ritschel^a, Dimitri Boiroux^a, Maria Sejersen^a, Emilie B. Lindkvist^b, Christian Laugesen^b, Jannet Svensson^b, Ajenthen G. Ranjan^b, Kirsten Nørgaard^b and John Bagterp Jørgensen^{a,*}

^aDepartment of Applied Mathematics and Computer Science, Technical University of Denmark, Kgs. Lyngby, DK-2800, Denmark

^bSteno Diabetes Center Copenhagen, Clinical Research, Herlev, DK-2730, Denmark

ARTICLE INFO

Keywords:

Nonlinear model predictive control
System identification
Artificial pancreas
Dual-hormone
Insulin and glucagon
Type 1 diabetes
Clinical trial
Adolescents

ABSTRACT

In this work, we present the DiaCon dual- and single-hormone artificial pancreas (AP) for controlling the blood glucose concentration (BGC) in people with type 1 diabetes. A dual-hormone AP can administer insulin to lower the BGC and glucagon to increase the BGC. A single-hormone AP is limited to insulin administration and is therefore unable to actively prevent low BGCs (hypoglycemia). Severe hypoglycemia can have acute consequences, such as loss of consciousness and seizures. A dual-hormone AP consists of a continuous glucose monitor (CGM), an insulin pump, a glucagon pump, and a control algorithm. The control algorithm is implemented using a smartphone that also receives the sensor measurements and sends instructions to the pumps. The control algorithm computes the insulin or glucagon infusion rate that is administered until the next measurement is received. The DiaCon AP is based on a nonlinear model predictive control (NMPC) algorithm that uses heuristics to switch between insulin and glucagon administration. The heuristics also ensure that insulin and glucagon are never administered simultaneously. The NMPC algorithm is based on stochastic differential equations and we estimate the states using the continuous-discrete extended Kalman filter (CD-EKF). The model parameters are estimated using a prediction error method (PEM). We present the hardware components and show how it is technically feasible to solve NMPC problems on a smartphone. We discuss the limitations and potential of the dual-hormone AP as well as the NMPC algorithm. The dual- and single-hormone AP has been tested in a clinical trial with adolescents with type 1 diabetes. The AP achieved a mean of 62.9% and 76.0% TIR time in range (TIR) (3.9–10 mmol/L) for the DH and SH configuration respectively, and 75.3% and 78.8% TIR when disregarding the studies where there were significant technical issues or where no glucagon was administered. The technical issues included pressure induced sensor attenuations (PISAs) and loss of connection to the pumps.


1. Introduction

Type 1 diabetes (T1D) is a chronic metabolic disorder which leads to an autoimmune destruction of the pancreatic β cells and prevents insulin production. Therefore, people with T1D require life-long insulin treatment to prevent high blood glucose levels (hyperglycemia). Extended periods of hyperglycemia can lead to a range of complications, e.g., cardiovascular disease, chronic kidney disease and damage to the nerves and eyes. Conversely, too much insulin can lead to low blood glucose levels (hypoglycemia). Hypoglycemia can in severe cases lead to acute complications, such as loss of consciousness and seizures. Managing the treatment is thus necessary, but also tedious and time-consuming. Therefore, there is an increasing interest in developing safe automatic closed-loop diabetes treatment systems based on feedback control. Such systems are known as *artificial pancreases* (APs). APs consist of 1) a continuous glucose monitor (CGM), 2) a control algorithm (here, implemented using a smartphone), and 3) one or more pumps. The control algorithm computes the insulin or glucagon infusion rates administered through the pumps. A variety of control algorithms have been applied, including fuzzy logic

(Biester et al., 2019), proportional-integral-derivative (PID) control (Huyett et al., 2015; Jørgensen et al., 2019; Sejersen et al., 2021), linear model predictive control (LMPC) (Chakrabarty et al., 2020; Messori et al., 2018), nonlinear model predictive control (NMPC) (Boiroux et al., 2018b; Boiroux and Jørgensen, 2018; Hovorka et al., 2004), and algorithms based on a modular architecture (Breton et al., 2012).

There are currently only single hormone (SH) APs commercially available. SH APs are only able to administer insulin and are unable to actively prevent low blood sugar concentrations, which may occur because of, e.g., exercise, over-bolused meals, stress and physiological variability. Therefore, researchers investigate dual-hormone (DH) APs where glucagon can be administered in addition to insulin (Bionic Pancreas Research Group, 2022; Blauw et al., 2021; Infante et al., 2021; Peters and Haidar, 2018). Glucagon causes an increase in the blood glucose concentration. A number of approaches have been suggested for DH algorithms. Moscardo et al. (2019) suggested a coordinated control strategy based on PD control and Boiroux et al. (2018a) suggested LMPC algorithms based on transfer functions, but currently no DH APs based on NMPC have been tested in a clinical trial. There are also systems that use other hormones, such as pramlintide that slows gastric emptying (Haidar et al., 2020). However, previous clinical evaluations of DH APs have not

*Corresponding author

 jbo@dtu.dk (J.B. Jørgensen)
ORCID(s):

<A Dual- and Single-Hormone Artificial Pancreas based on NMPC>

demonstrated the expected improved performance compared to SH systems (Haidar, 2019; Haidar et al., 2016). Some studies have indicated improved performance during and after exercise (Castle et al., 2018; Taleb et al., 2016) and in the more recent studies, the iLet bionic pancreas by Beta Bionics and the Inreda Diabetic AP showed improved outcomes for the DH AP compared to the SH AP (Bionic Pancreas Research Group, 2022; Blauw et al., 2021; Castellanos et al., 2021). Children and adolescents have proven more challenging for closed-loop systems (Fushimi et al., 2020) and only the trial by Bionic Pancreas Research Group (2022) included children and adolescents.

In Reenberg et al. (2022), we introduced the DiaCon DH AP system based on NMPC, described how it was prepared for clinical trials and tested using in silico simulations. In this work, we show the hardware that is used in the trial, present the algorithm, and describe the optimal control problem (OCP) we solve using the smartphone. We discuss the benefits and technical challenges related to using APs in general and the specific challenges related to DH APs. Furthermore, we summarize and discuss the results from a clinical trial where the DH AP and SH AP was tested for adolescents ($n = 11$) and compare with the results from the simulations in Reenberg et al. (2022). The insulin algorithm is identical for the DH and SH configuration of the AP. The clinical trial and primary outcomes are presented in detail in Lindkvist et al. (2023). We evaluate the performance of the APs based on the targets specified by Battelino et al. (2019). The remainder of the paper is structured as follows. We introduce AP systems and present the DiaCon AP system and hardware in Section 2. In Section 3, we introduce the Medtronic virtual patient (MVP) model. We describe the state estimation in Section 4 and the system identification in Section 5. In Section 6, we present the OCP, and describe how we solve it. We present the safety constraints and heuristics used to switch between insulin and glucagon administration in Section 7. In Section 8, we describe the clinical trial and summarize and discuss the results. Finally, we conclude in Section 9.

2. Artificial pancreas systems

The development of artificial pancreas systems has been accelerating over the last 20 years (Templer, 2022). The first hybrid closed-loop system (Medtronic MiniMed 670G) became approved for commercial use in 2016. Hybrid closed-loop systems require the users to manually announce, e.g., meals and exercise. Contrarily, fully automatic closed-loop systems require no interactions from the user. Currently, only hybrid closed-loop single-hormone systems are commercially available in Europe or the US, but both fully automatic and multihormonal closed-loop systems are an active field of research.

2.1. DiaCon AP system

The DiaCon AP system is categorized as a hybrid multihormonal closed-loop system as it requires the user to announce meals and exercise, but can administer both insulin



Figure 1: The DiaCon AP system. The system consists of 1) an Android smartphone, 2) a Dexcom G6 sensor, 4) a Dana Diabcare RS pump for insulin administration, and 5) another Dana Diabcare RS pump for glucagon administration.

and glucagon. The system consists of two Dana Diabcare RS pumps (one for insulin and one for glucagon), a Dexcom G6 sensor, and a Samsung galaxy A5 2017 smartphone. Fig. 1 shows a picture of the hardware. The DiaCon app is installed on the smartphone and provides an interface for the AP. Both the graphical user-interface and the underlying numerical methods are implemented in Java. The smartphone performs all computations and communicates with the sensor and pumps through a bluetooth connection. Therefore, the AP also works without connection to the internet. However, the AP requires estimation of model parameters and we require the user to provide glucose, insulin and meal data before the AP can be used. The parameter estimation is performed on a computer and the parameters are provided to the smartphone. The model parameters are the same for both the DH and SH configuration of the AP. Fig. 2 shows a flowchart of the closed-loop system as well as the pre-trial preparations.

3. Model

We use an extension of the MVP model (Kanderian et al., 2009) in the AP. The model consists of the glucose-insulin dynamics from the MVP model, the meal subsystem by Hovorka et al. (2004), the glucagon subsystem by Haidar et al. (2013), and the CGM subsystem by Facchinetti et al. (2014). Fig. 3 shows an overview of the model. We can write the model as an uncertain dynamical system in the form

$$dx(t) = f(t, x(t), u(t), d(t), \theta)dt + \sigma(\theta)dw(t), \quad (1a)$$

$$y_k = g(t_k, x_k, \theta) + v_k. \quad (1b)$$

Here, $f(\cdot)dt$ represents the deterministic part of the model. t is the time, x are the states, u are the manipulated inputs (i.e., insulin and glucagon administration), d are the disturbances (meals), y_k are the measured variables and σ are the diffusion

<A Dual- and Single-Hormone Artificial Pancreas based on NMPC>

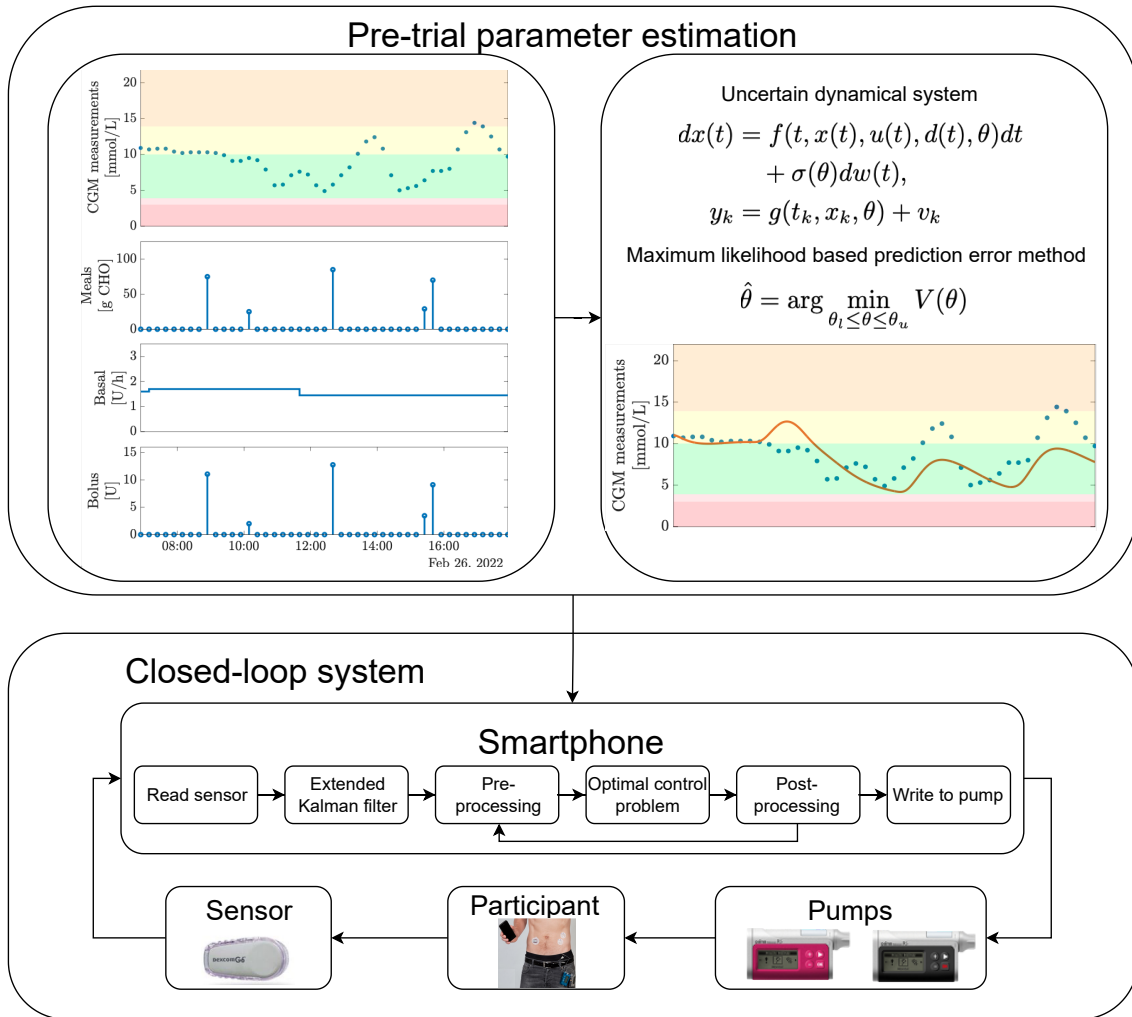


Figure 2: Flowchart of the pre-trial preparations and the DiaCon AP as a closed-loop system. Top left: Example of CGM, meal, and insulin data received before the studies. Top right: Parameter estimation using the data provided by the participants. Bottom: We enter the model parameters in the smartphone that is connected to the sensor and pumps. The smartphone reads the sensor and estimates the states using the extended Kalman filter based on the measurement. We then update the constraints, select either insulin or glucagon administration and solve the optimal control problem. The post-processing routine evaluates the solution, checks the predictions, and rounds the input to the pump resolution before writing the instructions to the pump. The full control algorithm is described in Algorithm 1.

model coefficients. The measurement noise, v_k , and the process noise, $d\omega$, are standard Wiener processes, i.e.,

$$d\omega(t) \sim N_{iid}(0, I dt), \quad (2)$$

$$v_k \sim N_{iid}(0, R). \quad (3)$$

3.1. Insulin subsystem

The insulin subsystem describes the absorption of the insulin administered by the insulin pump. The pump administers insulin in subcutaneous tissue, but only the insulin in the plasma affects the glucose concentration. The insulin subsystem is represented by

$$dI_{SC}(t) = k_1 \left(\frac{u_{ba}(t) + u_{bo}(t)}{C_I} - I_{SC}(t) \right) dt, \quad (4a)$$

<A Dual- and Single-Hormone Artificial Pancreas based on NMPC>

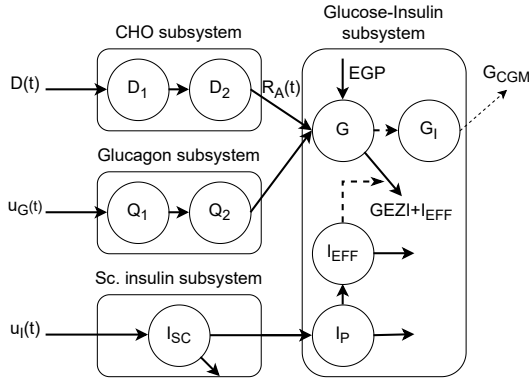


Figure 3: A diagram of the extended version of the MVP model. The MVP model is used for prediction in the AP.

$$dI_P(t) = k_2 (I_{SC}(t) - I_P(t)) dt, \quad (4b)$$

where I_{SC} [mU/L] is the subcutaneous insulin concentration, I_P [mU/L] is the insulin concentration in the plasma, u_{ba} [mU/min] represents the basal insulin infusion rate and $u_{bo}(t)$ is the bolus insulin infusion rate, that both enter through the subcutaneous tissue, and the total insulin infusion rate is thus $u_I(t) = u_{ba}(t) + u_{bo}(t)$, $k_2 = k_1$ [1/min] is the inverse insulin absorption time constant, and C_I [L/min] is the insulin clearance rate.

3.2. Meal subsystem

The meal absorption subsystem is described by

$$\dot{D}_1(t) = A_G D(t) - \frac{D_1(t)}{\tau_D}, \quad (5a)$$

$$\dot{D}_2(t) = \frac{D_1(t)}{\tau_D} - \frac{D_2(t)}{\tau_D}. \quad (5b)$$

Here, D_1 [mmol] and D_2 [mmol] form a two-compartment chain to describe the meal absorption from the stomach into the intestine before it appears in the blood, D [mmol/min] represents the amount of carbohydrates in the meals, A_G [-] is the carbohydrate bioavailability, and τ_D [min] is the meal absorption time constant.

3.3. Glucagon subsystem

The glucagon subsystem is represented by

$$\dot{Q}_1(t) = u_G(t) - \frac{Q_1(t)}{\tau_{Glu}}, \quad (6a)$$

$$\dot{Q}_2(t) = \frac{Q_1(t)}{\tau_{Glu}} - \frac{Q_2(t)}{\tau_{Glu}}. \quad (6b)$$

Q_1 [μ g] and Q_2 [μ g] are a two-compartment chain to describe the glucagon absorption from the subcutaneous tissue to the plasma, u_G [μ g/min] is the glucagon infusion rate and τ_{Glu} [min] is the glucagon absorption time constant.

3.4. Glucose subsystem

The glucose subsystem is represented as a set of stochastic differential equations

$$dI_{EFF}(t) = p_2 (S_I(t)I_P(t) - I_{EFF}(t)) dt, \quad (7a)$$

$$dG(t) = [- (GEZI + I_{EFF}(t))G(t) + EGP + R_A(t) + K_{Glu}Q_2(t)]dt + \sigma_G dw_G(t), \quad (7b)$$

$$d \log(S_I(t)) = \sigma_{S_I} dw_{S_I}(t), \quad (7c)$$

where I_{EFF} [1/min] is the insulin effect, $p_2 = k_1$ [1/min] is a time constant, S_I [(L/mU)/min] is the insulin sensitivity, $GEZI$ [1/min] is the glucose effectiveness, EGP [(mmol/L)/min] is the endogenous glucose production, σ_G is the glucose diffusion coefficient, σ_{S_I} is the insulin sensitivity diffusion coefficient, and w_G and w_{S_I} are standard wiener processes. The insulin sensitivity, S_I , is adaptive and updated using the CD-EKF. The adaptive insulin sensitivity describes the change in insulin sensitivity that happens during and after exercise. Furthermore, the log-transform ensures that it remains positive. Finally, the rate of appearance, R_A [(mmol/L)/min], is represented by

$$R_A(t) = \frac{k_m D_2(t)}{V_G}, \quad (8)$$

where k_m [1/min] is a time constant.

3.5. CGM subsystem

Since a CGM measures the glucose concentration in the interstitial tissue, we extend the MVP model with the CGM subsystem

$$\dot{G}_I(t) = \frac{G(t)}{\tau_{IG}} - \frac{G_I(t)}{\tau_{IG}}, \quad (9)$$

to describe the interstitial glucose concentration, G_I [mmol/L], where τ_{IG} is a time constant.

4. Extended Kalman filter

When a new CGM measurement is received, the states and insulin sensitivity are estimated using a continuous-discrete extended Kalman filter (CD-EKF) (Jazwinski, 2007).

4.1. Filtering

The CD-EKF computes the filtered state, $\hat{x}_{k|k}$, and its covariance, $P_{k|k}$, given the previous one-step prediction, $\hat{x}_{k|k-1}$, and, $P_{k|k-1}$, and a measurement, y_k . The predicted measurement and its derivative is given by

$$\hat{y}_{k|k-1} = g(t_k, \hat{x}_{k|k-1}, \theta), \quad (10a)$$

$$C_k = \frac{\partial g}{\partial x}(t_k, \hat{x}_{k|k-1}, \theta). \quad (10b)$$

From the predicted measurement, the innovation and covariance of the innovation, can be computed as

$$e_k = y_k - \hat{y}_{k|k-1}, \quad (11a)$$

<A Dual- and Single-Hormone Artificial Pancreas based on NMPC>

$$R_{e,k} = C_k P_{k|k-1} C_k^T + R, \quad (11b)$$

and the Kalman gain as

$$K_{f,x,k} = P_{k|k-1} C_k^T R_{e,k}^{-1}. \quad (12)$$

We then obtain the estimated state-covariance pair

$$\hat{x}_{k|k} = \hat{x}_{k|k-1} + K_{f,x,k} e_k, \quad (13a)$$

$$P_{k|k} = P_{k|k-1} - K_{f,x,k} R_{e,k} K_{f,x,k}^T. \quad (13b)$$

We can guarantee positive definiteness of the covariance of the filtered state, $P_{k|k}$, by using the Joseph stabilized form (Schneider and Georgakis, 2013)

$$P_{k|k} = (I - K_{f,x,k} C_k) P_{k|k-1} (I - K_{f,x,k} C_k)^T + K_{f,x,k} R K_{f,x,k}^T. \quad (14)$$

4.2. Prediction

From the estimated state-covariance pair (13), we can obtain the one-step prediction

$$\hat{x}_{k+1|k} = \hat{x}_k(t_{k+1}), \quad (15a)$$

$$P_{k+1|k} = P_k(t_{k+1}), \quad (15b)$$

as the solution to

$$\frac{d}{dt} \hat{x}_k(t) = f(t, \hat{x}_k(t), u_k, d_k, \theta), \quad (16a)$$

$$\begin{aligned} \frac{d}{dt} P_k(t) &= A_k(t) P_k(t) + P_k(t) A_k(t)^T \\ &\quad + \sigma_k(t) \sigma_k(t)^T, \end{aligned} \quad (16b)$$

for $t_k \leq t \leq t_{k+1}$, where

$$A_k(t) = \frac{\partial f}{\partial x}(t, \hat{x}_k(t), u_k, d_k, \theta), \quad (17a)$$

$$\sigma_k(t) = \sigma(t, \hat{x}_k(t), u_k, d_k, \theta), \quad (17b)$$

with the initial condition

$$\hat{x}_k(t_k) = \hat{x}_{k|k}, \quad (18a)$$

$$P_k(t_k) = P_{k|k}. \quad (18b)$$

5. System identification

We receive data from each participant to identify the system before the clinical trials. The data consists of CGM values, meal information and insulin infusion rates. We estimate the parameters in the MVP model with a maximum likelihood based PEM using the CD-EKF. We refer to Boiroux et al. (2019) for more details.

5.1. Maximum likelihood based prediction error method

Let \mathcal{I}_N be a set of experimental data, i.e.

$$\mathcal{I}_{k+1} = \{y_{k+1}, u_k, d_k\} \cup \mathcal{I}_k, \quad \mathcal{I}_0 = \{y_0\}. \quad (19)$$

The aim is to maximize the conditional probability density, $p(\mathcal{I}_N | \theta)$. Since we assume that the inputs, u_k , and disturbances, d_k , are deterministic, we can express the conditional probability density as

$$p(\mathcal{I}_N | \theta) = p(y_N, y_{N-1}, \dots, y_0 | \theta). \quad (20)$$

Let the negative log-likelihood function

$$V(\theta) = -\log(p(\mathcal{I}_N | \theta)), \quad (21)$$

be expressed as

$$\begin{aligned} V(\theta) &= \frac{(N+1)n_y}{2} \log(2\pi) + \frac{1}{2} \sum_{k=0}^N (\log[\det(R_{e,k}(\theta))] \\ &\quad + e_k(\theta)^T [R_{e,k}(\theta)]^{-1} e_k(\theta)), \end{aligned} \quad (22)$$

where $n_y = 1$ and the innovation, e_k , and its covariance, $R_{e,k}$, are computed with the CD-EKF (11). The objective is to find the set of parameters, $\hat{\theta}$, that minimizes the negative log-likelihood function (22), i.e.,

$$\hat{\theta} = \arg \min_{\theta_l \leq \theta \leq \theta_u} V(\theta), \quad (23)$$

where $\hat{\theta} \sim N(\bar{\theta}, P_{\theta})$ and with the constraints $\theta_l \leq \bar{\theta} \leq \theta_u$.

6. Optimal control problem

Every 5 minutes, we solve an OCP to compute the insulin or glucagon dose. We assume zero-order hold parametrization of the manipulated inputs, $u(t)$, and disturbances, $d(t)$, i.e.,

$$u(t) = u_k, \quad t_k \leq t < t_{k+1}, \quad (24a)$$

$$d(t) = d_k, \quad t_k \leq t < t_{k+1}. \quad (24b)$$

We solve an OCP in the form

$$\min_{[x(t)]_{t_0}^{t_f}, \{u_k\}_{k=0}^{N-1}} \phi = \phi([x(t)]_{t_0}^{t_f}, \{u_k\}_{k=0}^{N-1}), \quad (25a)$$

subject to

$$x(t_0) = \hat{x}_0, \quad (25b)$$

$$\dot{x}(t) = f(t, x(t), u(t), d(t), \theta), \quad t \in [t_0, t_f], \quad (25c)$$

$$u(t) = u_k, \quad t \in [t_k, t_{k+1}], \quad k = 0, \dots, N-1, \quad (25d)$$

$$d(t) = \hat{d}_k, \quad t \in [t_k, t_{k+1}], \quad k = 0, \dots, N-1, \quad (25e)$$

$$u_{\min} \leq u_k \leq u_{\max}, \quad k = 0, \dots, N-1. \quad (25f)$$

We describe the objective function (25) in section 6.1. (25b) is the initial condition, (25c) is the deterministic version of the extended MVP model described in Section 3, (25d)-(25e) are the zero-order hold parametrizations of the manipulated inputs and estimated disturbances, and (25f) are the bounds on the manipulated inputs. We use a control and prediction horizon of 6 hours which is sufficient to reach steady state while retaining computational feasibility.

<A Dual- and Single-Hormone Artificial Pancreas based on NMPC>

6.1. Objective function

We use the objective function described in Reenberg et al. (2022) in the AP. We use different objective functions for insulin and glucagon administration. The objective function is

$$\phi = \int_{t_0}^{t_f} \rho_z(z(t))dt + \sum_{k=0}^{N-1} \rho_u(u_k), \quad (26)$$

where ρ_z is the output penalty function and ρ_u is the input penalty function. $z(t) = g(t, x(t), \theta)$ are the outputs (blood glucose concentration). We define the first penalty function, ρ_z , in (26) as

$$\rho_z(z) = \alpha_z \rho_{\bar{z}}(z) + \alpha_{z_{\min}} \rho_{z_{\min}}(z) + \alpha_{z_{\max}} \rho_{z_{\max}}(z), \quad (27)$$

that penalizes 1) deviations of the blood glucose concentration from the setpoint, $\bar{z} = 6$ mmol/L, 2) hypoglycemia ($z < z_{\min} = 4.5$ mmol/L), and 3) hyperglycemia ($z > z_{\max} = 10.0$ mmol/L):

$$\rho_{\bar{z}}(z) = \frac{1}{2}(z - \bar{z})^2, \quad (28a)$$

$$\rho_{z_{\min}}(z) = \frac{1}{2}(\min\{0, z - z_{\min}\})^2, \quad (28b)$$

$$\rho_{z_{\max}}(z) = \frac{1}{2}(\max\{0, z - z_{\max}\})^2, \quad (28c)$$

where $\alpha_z = 1$, $\alpha_{z_{\min}} = 10^6$, and $\alpha_{z_{\max}} = 50$ when computing insulin administration and $\alpha_z = 1$, $\alpha_{z_{\min}} = 10^6$, and $\alpha_{z_{\max}} = 0$ when computing glucagon administration. $\alpha_{z_{\min}}$ is set to a large value as preventing hypoglycemia has the highest priority. Fig. 4 shows the penalty function. When computing the insulin administration, we define the second penalty term in (26) as

$$\rho_u(u_k) = \alpha_{u,ba} \rho_{u,ba}(u_{ba,k}) + \alpha_{u,bo} \rho_{u,bo}(u_{bo,k}), \quad (29)$$

where the weights are $\alpha_{u,ba} = 0.5$ and $\alpha_{u,bo} = 0.01$ and

$$\rho_{u,ba}(u_{ba,k}) = \|u_{ba,k} - \bar{u}_{ba,k}\|_2^2, \quad (30a)$$

$$\rho_{u,bo}(u_{bo,k}) = \|u_{bo,k}\|_1. \quad (30b)$$

The first term penalizes deviations from the nominal basal rate, \bar{u}_k , where the 2-norm promotes small deviations from the nominal basal rate. The second term penalizes the administration insulin boluses, where the 1-norm promotes few, but large insulin boluses. When computing the glucagon administration, we instead use

$$\rho_u(u_k) = \alpha_{u,G} \|u_{G,k}\|_2^2, \quad (31)$$

to penalize the administration of glucagon with $\alpha_{u,G} = 100.0$. This expression is identical to (30a), but the nominal glucagon rate is zero.

6.2. Numerical Solution

We use direct multiple-shooting (Bock and Plitt, 1984) to transcribe (25) by discretizing the dynamic constraint

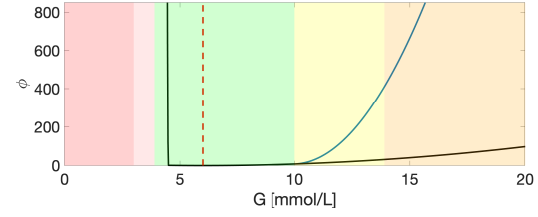


Figure 4: Blood glucose penalty function when administering insulin (blue) and glucagon (black).

(25c) and the integral in the objective function (26) using an explicit 4th order Runge-Kutta scheme with fixed step size. We solve the resulting nonlinear program using a sequential quadratic programming (SQP) method (Boiroux and Jørgensen, 2018; Nocedal and Wright, 2006). We solve the quadratic program (QP) in each SQP iteration using a structured primal-dual interior point algorithm, where we use Riccati recursions to compute the Newton iterations (Frison and Jørgensen, 2013; Jørgensen, 2005).

7. Heuristics

In the AP, we use several heuristics to 1) switch between insulin and glucagon administration, 2) compute upper bounds on the manipulated inputs, 3) modify controller hyperparameters during exercise, and 4) a post-processing and fall-back strategy to round to pumps and handle possible issues in the solution of the OCP (25) (Reenberg et al., 2022). In the nominal case, the setpoint, \bar{z} , is

$$\bar{z} = 6.0 \text{ mmol/L}, \quad (32)$$

and the switch limit is

$$\text{switch limit} = 4.5 \text{ mmol/L}. \quad (33)$$

The switch limit is slightly above the hypoglycemic range to allow the AP to administer glucagon to proactively prevent hypoglycemic events. We show the control algorithm used in the AP in algorithm 1.

7.1. Switch logic

To avoid simultaneous administration of insulin and glucagon, we use a switch with the following logic (the system is always initialized in insulin mode):

- If the measured or estimated glucose concentration is below switch limit, we switch off the insulin administration and switch to the glucagon mode.
- If the glucose concentration is predicted to become below the switch limit within the next 30 minutes, we switch off the insulin administration and switch to the glucagon mode.

7.2. Insulin administration logic

For safety reasons, we update the constraint for the maximum allowed insulin bolus in the beginning of each

<A Dual- and Single-Hormone Artificial Pancreas based on NMPC>

Algorithm 1: Control algorithm executed with 5 min intervals.

```

1 if CGM measurement available then
2   if a meal was consumed within the previous
     hour then
3     set the insulin sensitivity diffusion
       coefficient,  $\sigma_{S_I}$ , to zero;
4   end
5   estimate the states,  $\hat{x}$ , Section 4;
6   clip insulin sensitivity,  $S_I(t)$ , (44);
7   update the constraints,  $u_{G,k}^{max}$ , (39),  $u_{ba,k}^{max}$ , (38),
     and,  $u_{bo,k}^{max}$ , (34);
8   if the exercise mode is active then
9     update the setpoint,  $\bar{z}$ , (41), and the switch
       limit, (42);
10  end
11  if the measured or estimated glucose level is
     below the switch limit then
12    solve the OCP, (25), in glucagon mode;
13  else
14    solve the OCP, (25), in insulin mode;
15    if any glucose predictions within the next 30
       min are below the switch limit then
16      go back and solve the OCP in glucagon
        mode;
17    end
18  end
19  if the optimal solution is obtained then
20    proceed with the solution;
21  else
22    use the open-loop fallback strategy, (45);
23  end
24  if exercise was just announced and
      $G_{CGM} < 7$  mmol/L then
25    stop insulin administration and give a
      glucagon bolus of 100  $\mu$ g, (43);
26  end
27 else
28   use the open-loop fallback strategy, (45);
29 end
30 round to pump resolution and unit conversion,
    Section 7.6;

```

control interval. We allow insulin boli to be administered after meals or as a correction if the glucose concentration becomes too high. We compute the upper bound on the allowed insulin bolus as

$$u_{bo,k}^{max} = \max\{\epsilon, u_{bo,k}^{corr} + u_{bo,k}^{meal} - u_{bo,k}^{hist}\}, \quad (34)$$

where $\epsilon = 10^{-3}$, $u_{bo,k}^{corr}$ is the maximum correction bolus infusion rate, $u_{bo,k}^{meal}$ is the maximum meal bolus infusion rate, and $u_{bo,k}^{hist}$ is the sum of the history of the insulin administration over the last hour. The allowed correction bolus is computed

as

$$u_{bo,k}^{corr} = \max\left\{0, \frac{1}{T_s} \frac{G_{CGM} - G_{max}}{ISF}\right\}, \quad (35)$$

where $T_s = 5$ min is the sampling time, G_{CGM} [mmol/L] is the CGM measurement, $G_{max} = 10$ mmol/L is the limit for when correction boli are allowed, and ISF [(mmol/L)/mU] is the insulin sensitivity factor provided by the participants. For 1 hour after a meal is consumed, the allowed meal bolus is computed as

$$u_{bo,k}^{meal} = \max\left\{0, \frac{\gamma}{T_s} \frac{\hat{d}}{ICR}\right\}, \quad (36)$$

where \hat{d} [g CHO] is the announced amount of the carbohydrates in the meal, ICR [g/mU] is the insulin to carb ratio provided by the participants, and $\gamma = 1.15$ [-] is a bolus allowance factor. If a meal was not consumed within the last hour, $u_{bo,k}^{meal} = 0$. The insulin bolus history is computed as

$$u_{bo,k}^{hist} = \sum_{j=1}^{N_{bo}^{hist}} u_{bo,k-j|k-j}, \quad (37)$$

where $u_{bo,k|k}$ is the insulin bolus infusion rate at the k 'th interval and $N_{bo}^{hist} = 11$ to compute the history for 1 hour. Finally, we constraint the maximum insulin basal infusion rate to

$$u_{ba,k}^{max} = 2\bar{u}_{ba,k}, \quad (38)$$

where $\bar{u}_{ba,k}$ is the nominal basal rate of the participants.

7.3. Glucagon administration logic

Similarly, we restrict the maximum glucagon administration rate by

$$u_{G,k}^{max} = \max\{\epsilon, \bar{u}_G^{max} - u_{G,k}^{hist}\}, \quad (39)$$

where $\epsilon = 10^{-3}$, $\bar{u}_G^{max} = 300$ μ g, and the glucagon history is computed by

$$u_{G,k}^{hist} = \sum_{j=1}^{N_G^{hist}} u_{G,k-j|k-j}, \quad (40)$$

where $u_{G,k|k}$ is the glucagon administration rate at the k 'th interval and $N_G^{hist} = 23$ which corresponds to a history of 2 hours.

7.4. Exercise logic

When exercise is announced, a number of hyperparameters in the AP are updated as the control model does not describe the effect of exercise. We increase the setpoint

$$\bar{z} = 7.0 \text{ mmol/L}, \quad (41)$$

<A Dual- and Single-Hormone Artificial Pancreas based on NMPC>

to make the AP less aggressive w.r.t. insulin administration and we increase the limit for switching to glucagon administration

$$\text{switch limit} = 7.0 \text{ mmol/L}, \quad (42)$$

to allow the AP to administer glucagon before the participants approach hypoglycemia. Finally, if $G_{CGM} < 7 \text{ mmol/L}$ when exercise is announced, a glucagon bolus is administered

$$u_{G,k} = 100 \mu\text{g} \quad \text{if } G_{CGM} < 7 \text{ mmol/L}. \quad (43)$$

7.5. Insulin sensitivity logic

After meals, we set the insulin sensitivity diffusion coefficient to zero for 1 hour to avoid adjusting the insulin sensitivity to the postprandial peaks, and we restrict the estimated value of the insulin sensitivity, S_I , in the CD-EKF to be within the limits

$$\log S_I(0) - 1 \leq \log S_I(t) \leq \log S_I(0) + 1, \quad (44)$$

where $S_I(0)$ is estimated during the parameter estimation.

7.6. Post-processing and fall-back strategy

After the solution of the OCP (25), the manipulated inputs for the first control interval are rounded to the pump resolution which is 0.01 U/h for the insulin basal rate, 0.1 U/h for the bolus insulin and 0.01 $\mu\text{g/h}$ for the glucagon infusion rate.

In the rare case, where the solution of the OCP (25) is prevented (e.g., if the maximum number of iterations in the SQP algorithm is reached or if no measurement is received), we use the following fall-back strategy as a safety measure

$$u_{ba,k|k} = \begin{cases} 0 & G_{CGM} \leq 8.0 \text{ mmol/L}, \\ \bar{u}_{ba,k} & \text{otherwise}, \end{cases} \quad (45a)$$

$$u_{bo,k|k} = 0, \quad (45b)$$

$$u_{G,k|k} = \begin{cases} \min\{15 \mu\text{g}, u_{G,k}^{\max}\} & G_{CGM} < 4.5 \text{ mmol/L}, \\ 0 & \text{otherwise}. \end{cases} \quad (45c)$$

8. Summary and insights from the clinical trial

In this section, we summarize and discuss the results from the clinical trial to understand the performance of the NMPC algorithm and compare with the results from the simulation study performed in Reenberg et al. (2022). The DH and SH AP was tested in a clinical trial with adolescents with T1D ($n = 11$). Lindkvist et al. (2023) describes the clinical trial and outcomes in detail. Each study in the trial consisted of one 26 hour visit with the SH configuration of the AP and another 26 hour visit with the DH configuration of the AP (in a randomized order). Both studies followed the same schedule: the closed-loop system was started at 17:00, the participants had dinner at 19:00, breakfast at 08:00, lunch

at 12:00, a snack at 15:00, a 45 min exercise session of moderate intensity (50% heart rate reserve) from 16:30 to 17:15, and at 19:00 the participants left the clinic. The participants slept from approximately 22:00 to 07:30. See Fig. 5. The participants were between 13 and 18 years old and had a median of 54% baseline TIR with 3% in level 1 and 2 hypoglycemia and 43% in level 1 and 2 hyperglycemia. All participants already used a CGM (the participants used different CGMs with different accuracy and sampling times) and an insulin pump and some participants used commercially available closed-loop systems. We evaluate the outcomes from the trial based on the targets specified by Battelino et al. (2019) where Table 1 shows the target glucose ranges. We show the results from one example DH study, where we show both the system identification as well as the time series of all inputs and outputs during the study. We compare with a simulation study for one virtual participant. Furthermore, we give an overview of the results from the trial. However, some studies were either heavily affected by technical challenges or no glucagon was administered in the DH study. Therefore, we also make a subset of studies ($n = 7$), where we require that there were no major technical issues and that glucagon was administered in the DH study. We show both the combined results from all studies and the results from the remaining 7 selected studies and compare with results from the simulation study. The studies we consider as heavily affected by technical issues, were because of 1) multiple pressure induced sensor attenuations (PISAs), and 2) lost connection to the insulin pump for extended periods of time. We also experienced minor challenges with the infusion sets and occlusions in the glucagon pump, but do not exclude those studies. The CGM measurements deviated from the Yellow Springs Instruments (YSI) measurements in some studies, but we do not consider that as a major technical issue. PISAs cause faulty measurements of very low blood glucose levels and can occur if the participant, e.g., sleeps on the CGM. Therefore, the position of the CGM can influence the performance of the AP. PISAs are especially challenging for DH systems as glucagon may be administered when faulty glucose measurements are received. In the appendix, Fig. 13 shows the results from participant 5 where multiple PISAs occurred during the DH study and caused administration of glucagon. Algorithms for detection of PISAs have been suggested by, e.g., Baysal et al. (2014), but false PISA detections can potentially be dangerous if the hypoglycemic event is not handled. Furthermore, Fig. 12 shows the results for participant 3 where the connection to the insulin pump was lost for an extended period of time during the DH study.

8.1. Example study

We show the system identification from the participant in the example study in Fig. 7 and the results from the DH study in Fig. 9. We received approximately 2 weeks of data from the participants before the studies, but the quality of the data varied because of mistimed or misestimated meals, lost connections to the CGM or insulin pump, or missed meal boluses. Therefore, we selected a subset of the data

<A Dual- and Single-Hormone Artificial Pancreas based on NMPC>

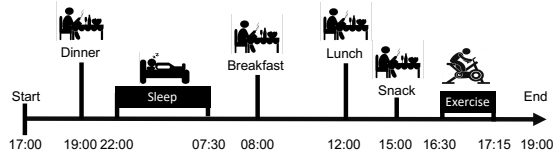


Figure 5: The protocol used in the clinical trial. The protocol consists of a dinner, sleep, a breakfast, a lunch, a snack, and finally, exercise of moderate intensity.

Table 1

The five glycemic ranges described by Battelino et al. (2019).

Category	Range [mmol/L]	Color
Level 2 hyperglycemia	$]13.9, \infty[$	Orange
Level 1 hyperglycemia	$]10.0, 13.9]$	Yellow
Normoglycemia	$[3.9, 10.0]$	Green
Level 1 hypoglycemia	$[3.0, 3.9[$	Light red
Level 2 hypoglycemia	$[0.0, 3.0[$	Red

that appeared to be without missing information. It can be a time-consuming process to select a subset of the data that allows for an accurate identification of the system, and as is evident from Fig. 7, the fit was not perfect. There are many non-measured factors and the model structure is not able to describe the varying meal responses from similar carbohydrate and insulin amounts. It was, in most cases, also necessary to fix some of the parameters even though the MVP model in theory is identifiable (Boiroux et al., 2019). We tuned the fixed parameters by hand to match the data and get feasible values of the remaining parameters. We tuned *GEZI* to reach a basal rate, \bar{u} , close to what the participants normally used. Importantly, we did not receive any glucagon or exercise data from the participants. Therefore, we fixed the parameters related to the glucagon model and did not include an exercise subsystem in the control model. The example study resulted in 78.3% TIR and approximately 100 μg glucagon was administered around 06:00 and 10:00. The glucagon administration increased the blood glucose levels in both cases and seemed to reduce the time in level 1 hypoglycemia around 10:00. The meal responses were very different despite the similar amount of carbohydrates and insulin, where the postprandial peak was very large at the dinner, but almost not visible at breakfast. The meal insulin boli were limited by the safety constraints, and the large postprandial peak after the dinner caused administration of a number of correction boli. Ideally, the correction boli should have been administered earlier to reduce the peak and avoid the glucagon administration around 06:00. The insulin basal rate remained close to the nominal basal rate, \bar{u} , for most of the study, but the basal rate was increased slightly over the night. This was due to the adaptation of the insulin sensitivity, S_I , which also caused the basal rate to increase slightly after meals on the second day. No glucagon was administered during or after exercise as the glucose concentration was above 7 mmol/L when exercise was announced and remained in range during the exercise

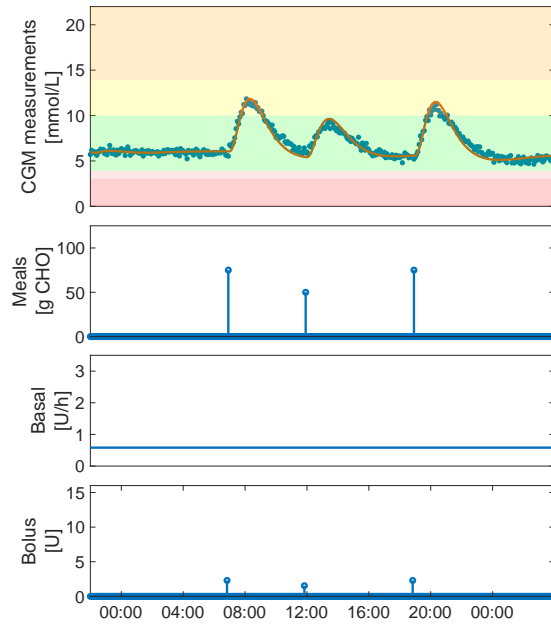


Figure 6: Parameter estimation for one virtual participant in the simulation study. From the top: 1) CGM measurements (blue dots) and a simulation with the estimated parameters (red line), 2) announced meals, 3) basal insulin rate, and 4) bolus insulin.

session. The AP handled the potential low glucose levels with glucagon and reduced the hyperglycemia with correction boli, as desired. Overall, the CGM measurements had high accuracy in this study with only minor differences from the YSI measurements. For comparison, we show the parameter estimation in Fig. 6 and simulation result in Fig. 8 for one virtual participant in the simulation study. The main differences are that the identified model was more accurate in the simulation study and provides more accurate predictions. Furthermore, the simulations began in steady state which was not the case in the example study where the initial glucose concentration lead to high glucose concentrations after dinner. Finally, much less insulin was administered in the simulation study, which was due to the high insulin sensitivity in the simulation model.

8.2. All studies

In this section, we show the combined results from the selected studies and all the studies. In Fig. 10, we show the TIRs for all studies, selected studies, worst-case studies (defined as the studies with the most time in level 2 hypoglycemia), and the simulation study and in Fig. 11, we show the median and span for the SH and DH studies. We show the average values of all clinical targets described by Battelino et al. (2019) in Table 2. The DH AP achieved lower TIR than the SH AP when we consider all studies, but statistically insignificant Lindkvist et al. (2023). In the selected studies, the performance was similar and all clinical targets were

<A Dual- and Single-Hormone Artificial Pancreas based on NMPC>

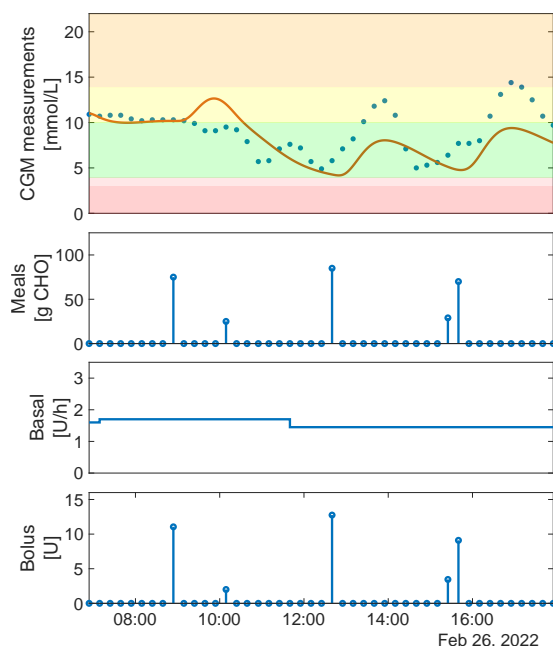


Figure 7: Parameter estimation for the example study. From the top: 1) CGM measurements (blue dots) and a simulation with the estimated parameters (red line), 2) announced meals, 3) basal insulin rate, and 4) bolus insulin.

satisfied by both APs. However, the SH AP still achieved higher TIR and less time in hypoglycemia compared to the DH AP. In the worst-case DH study both the meal and glucagon response were overestimated which caused too much insulin to be administered. In the worst-case SH study the participant entered the clinic in level 2 hypoglycemia and did not reach normoglycemia before the study was started. Both the DH and SH AP increased the TIR on average without increasing the time in hypoglycemia compared to the baseline TIRs of the participants. Fig. 11 shows that the glucose levels were mostly in target over the night and there were more variations during the day and after meals. The initial blood glucose levels varied notably between the studies and some participants also reached hypoglycemia immediately after the study was started. The AP assumed that the participants were at steady state when the study was started which clearly was not the case. We could have used previous data from the participants to update the initial condition, which might have improved the performance when the study was only 26 hours, but in a real life setting, the initial condition is not as significant. The span of the DH studies had a larger and later postprandial peak from the dinner that we believe was due to the participants that reached hypoglycemia in the beginning of the studies and thus received glucagon just before the dinner. Table 3 shows the insulin and glucagon administration in the studies, where there was almost no difference in the insulin administration. A mean of 653.95 μg glucagon was administered during

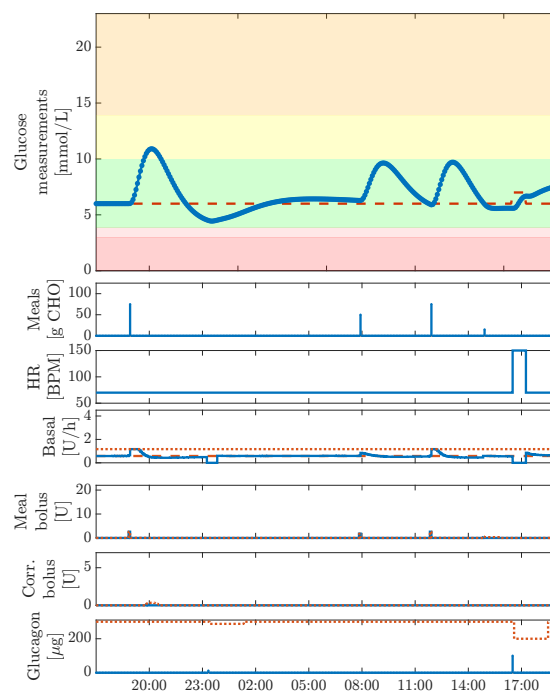


Figure 8: Results from one virtual participant in the simulation study. From the top: 1) CGM measurements (blue dotted line) with 96.5% time in range, 2) meals, 3) exercise, 4) basal insulin (blue line) and maximum allowed basal insulin (red dots), 5) meal boli (blue line) and maximum allowed meal boli (red dots), 6) correction insulin boli (blue line) and maximum allowed correction boli (red dots), and 7) glucagon boli (blue line) and maximum allowed glucagon boli (red dots).

all the DH studies and a mean of 912.91 μg glucagon was administered in the selected DH studies. If we compare to the simulation study with a cohort of 50 virtual participants, the TIR is higher in the simulation study with no time in level 1 and 2 hypoglycemia. The virtual participants required much less insulin and on average received less glucagon. The simulation result depends on the simulation model, but some factors could be improved in the design of future simulation studies to better represent a real clinical trial, 1) the simulated data used for parameter estimation is of too high quality, i.e., there was no missing data and all the meals were correctly announced, 2) The model of the glucose-insulin dynamics are different in the simulation and control model, but the glucagon model was the same and results in too accurate predictions of the glucagon response, and 3) The initial condition should not always be steady state.

9. Conclusion

In this paper, we presented the DiaCon DH and SH AP system. The system consists of an Android smartphone, a Dexcom G6 sensor and two Dana Diabecare RS pumps for insulin and glucagon administration. The AP is based on

<A Dual- and Single-Hormone Artificial Pancreas based on NMPC>

Table 2

Mean and standard deviation of the values for the glycemic targets described in Battelino et al. (2019) for the DH and SH AP.

Quantity	Target	DH all	SH all	DH selected	SH selected	DH simulation
Average glucose [mmol/L]	< 8.55	8.69 (1.57)	8.05 (1.15)	7.73 (0.91)	7.65 (0.66)	7.01 (0.41)
GMI [%]	< 7	7.03 (0.70)	6.78 (0.50)	6.61 (0.41)	6.61 (0.29)	6.33 (0.18)
GV [%]	≤ 36	29.81 (6.88)	33.93 (8.72)	31.34 (6.29)	31.74 (6.63)	29.95 (8.18)
Active CGM [%]	100	99.97 (0.10)	100.0 (0.00)	100.0 (0.00)	100.0 (0.00)	100.0 (0.00)
level 2 hyperglycemia [%]	< 5	5.2 (7.26)	4.8 (7.38)	1.8 (3.89)	1.3 (2.73)	1.9 (3.31)
level 1 and 2 hyperglycemia [%]	< 25	34.3 (22.56)	22.2 (13.63)	20.7 (13.36)	18.8 (11.38)	10.56 (8.28)
TIR (normoglycemia) [%]	> 70	62.9 (20.94)	76.0 (13.63)	75.3 (12.70)	78.8 (11.90)	89.44 (7.16)
level 1 and 2 hypoglycemia [%]	< 4	2.8 (4.65)	1.8 (1.63)	4.0 (5.52)	2.4 (1.42)	0.0 (0.00)
level 2 hypoglycemia [%]	< 1	0.8 (1.50)	0.2 (0.48)	1.0 (1.75)	0.3 (0.60)	0.0 (0.00)

Table 3

Mean and standard deviation of the insulin and glucagon administration during the 26 h trial.

Quantity	DH all	SH all	DH selected	SH selected	DH simulation
Total insulin [U]	59.32 (20.65)	59.47 (17.15)	58.12 (18.44)	61.45 (18.89)	26.19 (7.34)
Basal insulin [U]	26.88 (9.45)	26.29 (7.96)	27.71 (9.01)	28.05 (7.99)	15.13 (4.59)
Meal bolus insulin [U]	25.94 (10.33)	28.64 (10.39)	26.89 (10.12)	30.64 (12.32)	10.12 (3.61)
Correction bolus insulin [U]	6.50 (6.26)	4.54 (3.71)	3.53 (4.01)	2.76 (2.20)	0.94 (1.36)
Glucagon [μg]	653.95 (499.55)	-	912.91 (415.21)	-	135.47 (74.34)

a NMPC algorithm as well as several heuristics used to 1) switch between insulin and glucagon administration, 2) provide additional safety constraints and a fall-back strategy, 3) update controller hyperparameters during exercise, and 4) round to the pump resolution. We use an extension of the MVP model for prediction and estimate the model parameters using a maximum likelihood based PEM. The CD-EKF is used in both in the NMPC and the PEM. We analyze and summarize the results from a clinical trial with adolescents with type 1 diabetes ($n = 11$) and compare with the results from a simulation study. Each study in the clinical trial lasted 26 hours, included 4 meals, and a 45 min exercise session of moderate intensity. It is technically feasible to use NMPC for AP systems and both APs were able to control the glucose concentration, but obtaining a model for predictions is difficult and time-consuming and inaccurate models may limit performance. Both the DH and SH AP improved the TIR without increasing the time in hypoglycemia compared to the baseline TIR of the participants. Some studies were affected by technical issues, such as, PISAs or loss of connection to the pumps. PISAs can especially be challenging for DH APs, as glucagon can be administered. The DH AP achieved a mean of 62.9% TIR and the SH achieves a mean of 76.0% TIR. For the selected studies without technical difficulties and where glucagon was administered in the DH study ($n = 7$), the mean TIR was 75.3% for the DH AP and 78.8% for the SH AP, and all the clinical targets specified by Battelino et al. (2019) were satisfied for both the DH and SH AP. The DH and SH AP achieved lower TIR in the clinical trial compared to the simulation study. In the simulation study, the data used for parameter estimation did not include, e.g., missing data or misestimated meals and we used the same glucagon model for simulation and control which caused the predictions to

more accurate than in the clinical trial. Furthermore, the simulation study did not include technical difficulties.

10. Appendix

References

- Battelino, T., Danne, T., Bergenstal, R., Amiel, S.A., Beck, R., Biester, T., Bosi, E., Buckingham, B.A., Cefalu, W.T., Close, K.L., Cobelli, C., Dassau, E., DeVries, J.H., Donaghue, K.C., Dovc, K., Doyle III, F.J., Garg, S., Grunberger, G., Heller, S., Heinemann, L., Hirsch, I.B., Hovorka, R., Jia, W., Kordonouri, O., Kovatchev, B., Kowalski, A., Laffel, L., Levine, B., Mayorov, A., Mathieu, C., Murphy, H.R., Nimri, R., Nørgaard, K., Parkin, C.G., Renard, E., Rodbard, D., Saboo, B., Schatz, D., Stoner, K., Urakami, T., Weinzimer, S.A., Phillip, M., 2019. Clinical targets for continuous glucose monitoring data interpretation: Recommendations from the international consensus on time in range. *Diabetes Care* 42, 1593–1603.
- Baysal, N., Cameron, F., Buckingham, B.A., Wilson, D.M., Chase, H.P., Maahs, D.M., Bequette, B.W., 2014. A novel method to detect pressure-induced sensor attenuations (PISA) in an artificial pancreas. *Journal of Diabetes Science and Technology* 8, 1091–1096.
- Biester, T., Nir, J., Remus, K., Farfel, A., Muller, I., Biester, S., Atlas, E., Dovc, K., Bratina, N., Kordonouri, O., Battelino, T., Phillip, M., Danne, T., Nimri, R., 2019. DREAM5: An open-label, randomized, cross-over study to evaluate the safety and efficacy of day and night closed-loop control by comparing the MD-Logic automated insulin delivery system to sensor augmented pump therapy in patients with type 1 diabetes at home. *Diabetes, Obesity and Metabolism* 21, 822–828.
- Bionic Pancreas Research Group, 2022. Multicenter, randomized trial of a bionic pancreas in type 1 diabetes. *N Engl J Med* 387, 1161–1172.
- Blauw, H., onvlee, A.J., Klaassen, M., Bon, A.C.V., DeVries, J.H., 2021. Fully closed loop glucose control with a bi-hormonal artificial pancreas in adults with type 1 diabetes: An outpatient, randomized, crossover trial. *Diabetes Care* 44, 836–838.
- Bock, H.G., Plitt, K.J., 1984. A multiple shooting algorithm for direct solution of optimal control problems. *IFAC proceedings volumes* 17, 1603–1608.

<A Dual- and Single-Hormone Artificial Pancreas based on NMPC>

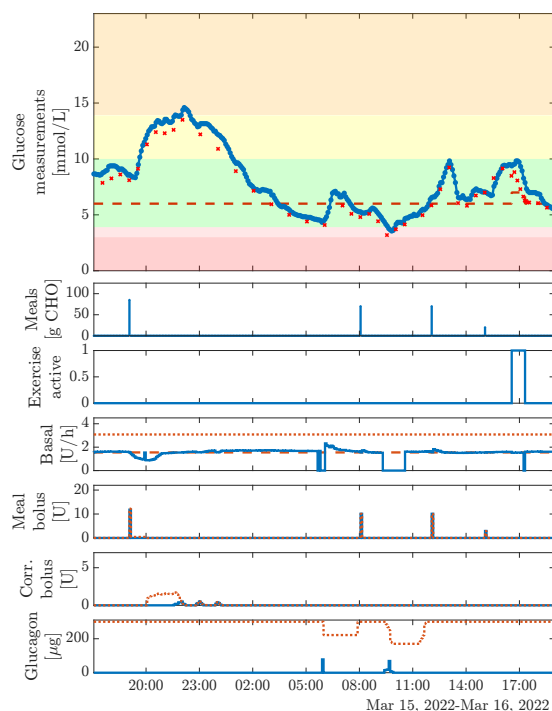


Figure 9: Results from the example study. From the top: 1) CGM measurements (blue dotted line) with 78.3% time in range, YSI measurements (red crosses), and setpoint (red dashed line), 2) meals, 3) exercise, 4) basal insulin (blue line) and maximum allowed basal insulin (red dots), 5) meal boli (blue line) and maximum allowed meal boli (red dots), 6) correction insulin boli (blue line) and maximum allowed correction boli (red dots), and 7) glucagon boli (blue line) and maximum allowed glucagon boli (red dots).

Boiroux, D., Batora, V., Hagdrup, M., Wendt, S.L., Poulsen, N.K., Madsen, H., Jørgensen, J.B., 2018a. Adaptive model predictive control for a dual-hormone artificial pancreas. *Journal of Process Control* 68, 105–117.

Boiroux, D., Duun-Henriksen, A.K., Schmidt, S., Nørgaard, K., Madsbad, S., Poulsen, N.K., Madsen, H., Jørgensen, J.B., 2018b. Overnight glucose control in people with type 1 diabetes. *Biomedical Signal Processing and Control* 39, 503–512.

Boiroux, D., Jørgensen, J.B., 2018. Nonlinear model predictive control and artificial pancreas technologies, in: 2018 IEEE Conference on Decision and Control (CDC), pp. 284–290.

Boiroux, D., Ritschel, T.K.S., Kjølstad Poulsen, N., Madsen, H., Jørgensen, J.B., 2019. Efficient computation of the continuous-discrete extended Kalman filter sensitivities applied to maximum likelihood estimation. 2019 IEEE 58th Conference on Decision and Control (CDC), 6983–6988.

Breton, M., Farret, A., Bruttomesso, D., Anderson, S., Magni, L., Patek, S., Man, C.D., Place, J., Demartini, S., Favero, S.D., Toffanin, C., Hughes-Karvetski, C., Dassau, E., Zissar, H., Doyle III, F.J., Nicolao, G.D., Avogaro, A., Cobelli, C., Renard, E., Kovatchev, B., 2012. Fully integrated artificial pancreas in type 1 diabetes. *Diabetes* 61, 2230–2237.

Castellanos, L.E., Balliro, C.A., Sherwood, J.S., Jafri, R., Hillard, M.A., Greux, E., Selagamsetty, R., Zheng, H., El-Khatib, F.H., Damiano, E.R., Russell, S.J., 2021. Performance of the insulin-only iLet bionic pancreas and the bi-hormonal iLet using dasiglucagon in adults with type 1 diabetes in a home-use setting. *Diabetes Care* 44, e118–e120.

Castle, J.R., Youssef, J.E., Wilson, L.M., Reddy, R., Resalat, N., Branigan, D., Ramsey, K., Leitschuh, J., Rajbharrysingh, U., Senf, B., Sugarman, S.M., Gabo, V., Jacobs, P.G., 2018. Randomized outpatient trial of single- and dual-hormone closed-loop systems that adapt to exercise using wearable sensors. *Diabetes Care* 41, 1471–1477.

Chakrabarty, A., Healey, E., Shi, D., Zavitsanos, S., Doyle III, F.J., Dassau, E., 2020. Embedded model predictive control for a wearable artificial pancreas. *IEEE Transactions on Control Systems Technology* 28, 2600–2607.

Facchinetti, A., Favero, S.D., Sparacino, G., Castle, J.R., Ward, W.K., Cobelli, C., 2014. Modeling the glucose sensor error. *IEEE Transactions on Biomedical Engineering* 61, 620–629.

Frison, G., Jørgensen, J.B., 2013. Efficient implementation of the Riccati recursion for solving linear-quadratic control problems, in: 2013 IEEE International Conference on Systems and Control, pp. 1117–1122.

Fushimi, E., Sefafini, M.C., Battista, H.D., Garelli, F., 2020. Automatic glycemic regulation for the pediatric population based on switched control and time-varying IOB constraints: an in silico study. *Medical & Biological Engineering & Computing* 58, 2325–2337.

Haidar, A., 2019. Insulin-and-glucagon artificial pancreas versus insulin-alone artificial pancreas: A short review. *Diabetes Spectrum* 32, 215–221.

Haidar, A., Duval, C., Legault, L., Rabasa-Lhoret, R., 2013. Pharmacokinetics of insulin aspart and glucagon in type 1 diabetes during closed-loop operation. *Journal of Diabetes Science and Technology* 7, 1507–1512.

Haidar, A., Rabasa-Lhoret, R., Legault, L., Lovblom, L.E., Rakheja, R., Messier, V., D'Aoust, E., Falappa, C.M., Justice, T., Orszag, A., Tschirhart, H., Dallaire, M., Ladouceur, M., Perkins, B.A., 2016. Single- and dual-hormone artificial pancreas for overnight glucose control in type 1 diabetes. *Journal of Clinical Endocrinology and Metabolism* 101, 214–223.

Haidar, A., Tsoukas, M.A., Bernier-Twardy, S., Yale, J.F., Rutkowski, J., Bossy, A., Pytko, E., Fathi, A.E., Strauss, N., Legault, L., 2020. A novel dual-hormone insulin-and-pramlintide artificial pancreas for type 1 diabetes: A randomized controlled crossover trial. *Diabetes Care* 43, 597–606.

Hovorka, R., Canonico, V., Chassin, L.J., Haueter, U., Massi-Benedetti, M., Federici, M.O., Pieber, T.R., Schaller, H.C., Schaupp, L., Vering, T., Wilinska, M.E., 2004. Nonlinear model predictive control of glucose concentration in subjects with type 1 diabetes. *Physiological Measurement* 25, 905–920.

Huyett, L.M., Dassau, E., Zisser, H.C., Doyle III, F.J., 2015. Design and evaluation of a robust PID controller for a fully implantable artificial pancreas. *Industrial & Engineering Chemistry Research* 54, 10311–10321.

Infante, M., Baidal, D.A., Rickels, M.R., Fabbri, A., Skyler, J.S., Alejandro, R., Ricordi, C., 2021. Dual-hormone artificial pancreas for management of type 1 diabetes: Recent progress and future directions. *Artificial Organs* 45, 968–986.

Jazwinski, A.H., 2007. *Stochastic processes and filtering theory*. Dover Publication, Inc.

Jørgensen, J.B., Boiroux, D., Mahmoudi, Z., 2019. An artificial pancreas based on simple control algorithms and physiological insight. *IFAC PapersOnLine* 52, 1018–1023.

Jørgensen, J.B., 2005. *Moving horizon estimation and control*. Ph.D. thesis. Department of Chemical Engineering, Technical University of Denmark.

Kanderian, S.S., Weinzimer, S., Voskanyan, G., Steil, G.M., 2009. Identification of intraday metabolic profiles during closed-loop glucose control in individuals with type 1 diabetes. *Journal of Diabetes Science and Technology* 3, 1047–1057.

Lindkvist, E.B., Laugesen, C., Reenberg, A.T., Ritschel, T.K.S., Svensson, J., Jørgensen, J.B., Nørgaard, K., Ranjan, A.G., 2023. Performance of a dual-hormone closed-loop system versus insulin-only closed-loop system in adolescents with type 1 diabetes. A single-blind, randomized, controlled, crossover trial. *Frontiers in Endocrinology* 14, 1073388.

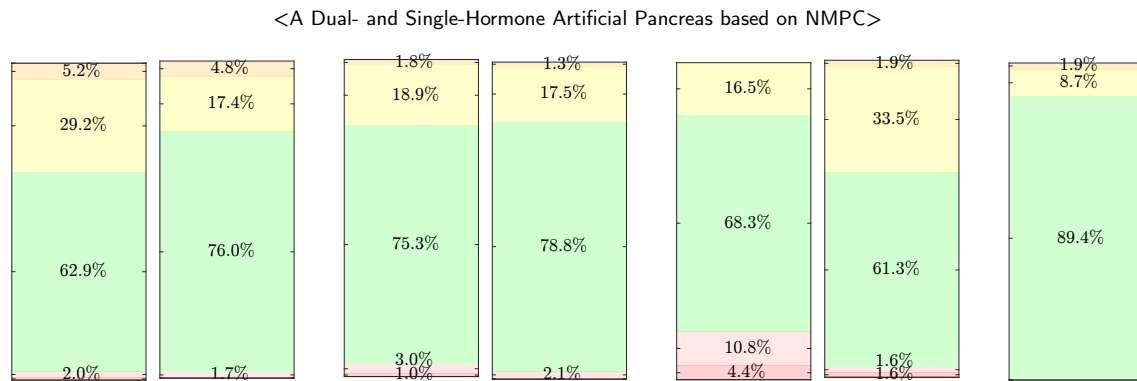


Figure 10: Time in ranges for the trial. From the left: 1) mean TIRs for the DH AP in all studies, 2) mean TIRs for the SH AP in all studies, 3) mean TIRs for the DH AP in selected studies, 4) mean TIRs for the SH AP in selected studies, 5) TIRs for the worst-case DH study, 6) TIRs for the worst-case SH study, and 7) TIRs for the DH simulation study.

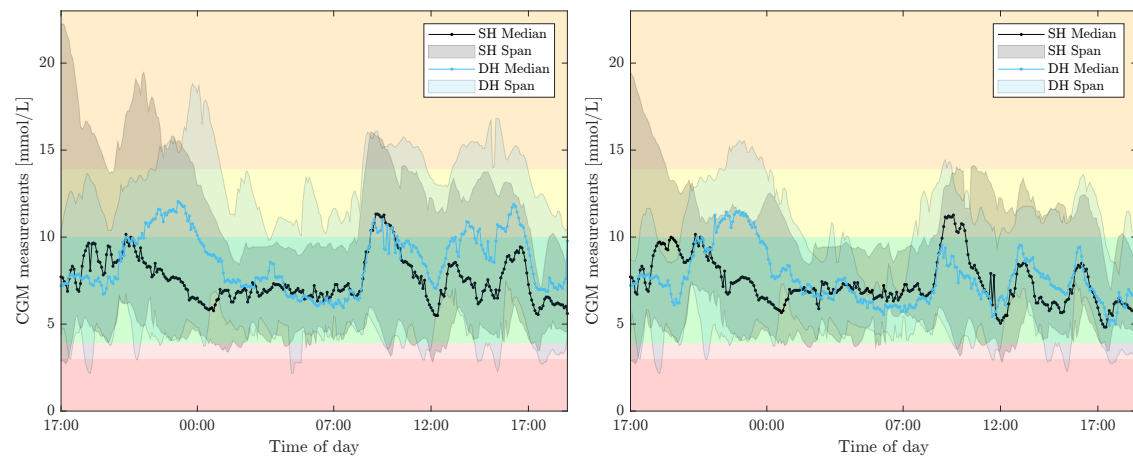


Figure 11: Left: median and span for all studies with SH in blue and DH in black. Right: median and span for selected studies with SH in black and DH in blue.

Messori, M., Incremona, G.P., Cobelli, C., Magni, L., 2018. Individualized model predictive control for the artificial pancreas: In silico evaluation of closed-loop glucose control. *IEEE Control Systems Magazine* 38, 86–104.

Moscardo, V., Herrero, P., Diez, J.L., Gimenez, M., Rossetti, P., Georgiou, P., Bondia, J., 2019. Coordinated dual-hormone artificial pancreas with parallel control structure. *Computers and Chemical Engineering* 128, 322–328.

Nocedal, J., Wright, S.J., 2006. Numerical optimization. 2nd ed., Springer Science & Business Media.

Peters, T.M., Haidar, A., 2018. Dual-hormone artificial pancreas: Benefits and limitations compared with single-hormone systems. *Diabetic Medicine* 35, 450–459.

Reenberg, A.T., Ritschel, T.K.S., Lindkvist, E.B., Laugesen, C., Svensson, J., Ranjan, A.G., Nørgaard, K., Jørgensen, J.B., 2022. Nonlinear model predictive control and system identification for a dual-hormone artificial pancreas. 13th IFAC Symposium on Dynamics and Control of Process Systems, including Biosystems (DYCOPS).

Schneider, R., Georgakis, C., 2013. How to not make the extended Kalman filter fail. *Industrial & Engineering Chemistry Research* 52, 3354–3362.

Sejersen, M., Boiroux, D., Engell, S.E., Ritschel, T.K.S., Reenberg, A.T., Jørgensen, J.B., 2021. Initial titration for people with type 1 diabetes using an artificial pancreas. *IFAC PapersOnLine* 54, 484–489.

Taleb, N., Emami, A., Suppere, C., Messier, V., Legault, L., Ladouceur, M., Chiasson, J.L., Haidar, A., Rabasa-Lhoret, R., 2016. Efficacy of single-hormone and dual-hormone artificial pancreas during continuous and interval exercise in adult patients with type 1 diabetes: Randomised controlled crossover trial. *Diabetologia* 59, 2561–2571.

Templer, S., 2022. Closed-loop insulin delivery systems: Past, present, and future directions. *Frontiers in Endocrinology* 13, 919942.

<A Dual- and Single-Hormone Artificial Pancreas based on NMPC>

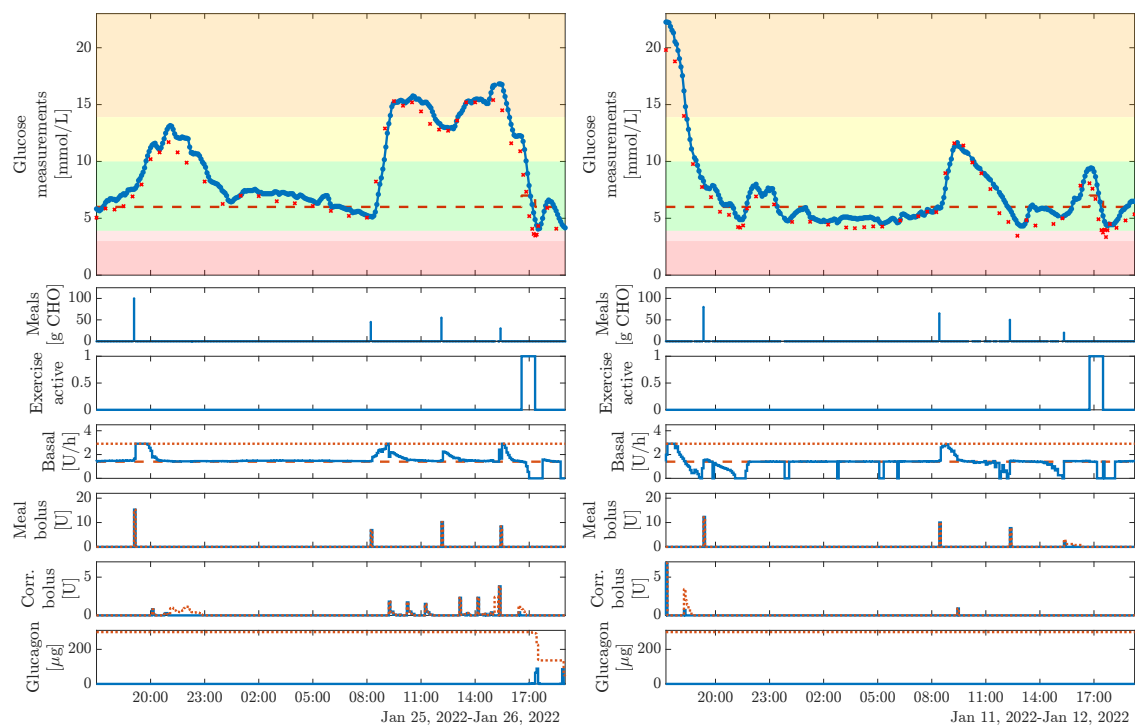


Figure 12: Participant 3. Left: results from the DH trial for participant 3 where the connection to the insulin pump was lost with 57.3% time in range. Right: results from the SH trial for participant 3 with 89.0% time in range. From the top: 1) CGM measurements (blue dotted line), YSI measurements (red crosses), and setpoint (red dashed line), 2) meals, 3) exercise, 4) basal insulin (blue line) and maximum allowed basal insulin (red dots), 5) meal boli (blue line) and maximum allowed meal boli (red dots), 6) correction insulin boli (blue line) and maximum allowed correction boli (red dots), and 7) glucagon boli (blue line) and maximum allowed glucagon boli (red dots).

APPENDIX **K**

Journal Paper - Frontiers in Endocrinology

Performance of a Dual-Hormone Closed-Loop System
Versus Insulin-Only Closed-loop System in Adolescents
with Type 1 Diabetes. A Single-Blind, Randomized,
Controlled Crossover Trial

Authors:

Emilie B. Lindkvist, Christian Laugesen, Asbjørn Thode Reenberg, Tobias K. S. Ritschel,
John Bagterp Jørgensen, Kirsten Nørgaard, Ajenthen G. Ranjan

Published in:

Frontiers in Endocrinology. 14:1073388, 2023.



OPEN ACCESS

EDITED BY

Valentino Cherubini,
Azienda Ospedaliero Universitaria Ospedali
Riuniti, Italy

REVIEWED BY

Siddharth Narayanan,
Nationwide Children's Hospital,
United States
Leah Wilson,
Oregon Health and Science University,
United States

*CORRESPONDENCE

Emilie Bundgaard Lindkvist
✉ Emilie.lindkvist@regionh.dk

SPECIALTY SECTION

This article was submitted to
Pediatric Endocrinology,
a section of the journal
Frontiers in Endocrinology

RECEIVED 18 October 2022

ACCEPTED 09 January 2023

PUBLISHED 23 January 2023

CITATION

Lindkvist EB, Laugesen C, Reenberg AT,
Ritschel TK, Svensson J, Jørgensen JB,
Nørgaard K and Ranjan AG (2023)
Performance of a dual-hormone closed-
loop system versus insulin-only closed-
loop system in adolescents with type 1
diabetes. A single-blind, randomized,
controlled, crossover trial.
Front. Endocrinol. 14:1073388.
doi: 10.3389/fendo.2023.1073388

COPYRIGHT

© 2023 Lindkvist, Laugesen, Reenberg,
Ritschel, Svensson, Jørgensen, Nørgaard and
Ranjan. This is an open-access article
distributed under the terms of the [Creative
Commons Attribution License \(CC BY\)](#). The
use, distribution or reproduction in other
forums is permitted, provided the original
author(s) and the copyright owner(s) are
credited and that the original publication in
this journal is cited, in accordance with
accepted academic practice. No use,
distribution or reproduction is permitted
which does not comply with these terms.

Performance of a dual-hormone closed-loop system versus insulin-only closed-loop system in adolescents with type 1 diabetes. A single-blind, randomized, controlled, crossover trial

Emilie Bundgaard Lindkvist^{1,2*}, Christian Laugesen^{1,2},
Asbjørn Thode Reenberg³, Tobias Kasper Skov Ritschel³,
Jannet Svensson^{1,4}, John Bagterp Jørgensen³,
Kirsten Nørgaard^{1,2} and Ajenthen G. Ranjan^{1,5}

¹Copenhagen University Hospital - Steno Diabetes Center Copenhagen, Herlev, Denmark, ²Department of Clinical Medicine, Faculty of Health and Medical Sciences, University of Copenhagen, Copenhagen, Denmark, ³Department of Applied Mathematics and Computer Science, Technical University of Denmark, Kgs. Lyngby, Denmark, ⁴Department of Pediatrics, Herlev and Gentofte University Hospital, Herlev, Denmark, ⁵Danish Diabetes Academy, Odense, Denmark

Objective: To assess the efficacy and safety of a dual-hormone (DH [insulin and glucagon]) closed-loop system compared to a single-hormone (SH [insulin only]) closed-loop system in adolescents with type 1 diabetes.

Methods: This was a 26-hour, two-period, randomized, crossover, inpatient study involving 11 adolescents with type 1 diabetes (nine males [82%], mean \pm SD age 14.8 ± 1.4 years, diabetes duration 5.7 ± 2.3 years). Except for the treatment configuration of the DiaCon Artificial Pancreas: DH or SH, experimental visits were identical consisting of: an overnight stay (10:00 pm until 7:30 am), several meals/snacks, and a 45-minute bout of moderate intensity continuous exercise. The primary endpoint was percentage of time spent with sensor glucose values below range (TBR [<3.9 mmol/L]) during closed-loop control over the 26-h period (5:00 pm, day 1 to 7:00 pm, day 2).

Results: Overall, there were no differences between DH and SH for the following glycemic outcomes (median [IQR]): TBR 1.6 [$0.0, 2.4$] vs. 1.28 [$0.16, 3.19$]%, $p=1.00$; time in range (TIR [3.9 - 10.0 mmol/L]) 68.4 [$48.7, 76.8$] vs. 75.7 [$69.8, 87.1$]%, $p=0.08$; and time above range (TAR [>10.0 mmol/L]) 28.1 [$18.1, 49.8$] vs. 23.3 [$12.3, 27.2$]%, $p=0.10$. Mean (\pm SD) glucose was higher during DH than SH (8.7 (± 3.2) vs. 8.1 (± 3.0) mmol/L, $p<0.001$) but coefficient of variation was similar (34.8 (± 6.8) vs. 37.3 (± 8.6)%, $p=0.20$). The average amount of rescue carbohydrates was similar between DH and SH (6.8 (± 12.3) vs. 9.5 (± 15.4) grams/participant/visit, $p=0.78$). Overnight, TIR was higher, TAR was lower during the SH visit compared to DH. During and after exercise (4:30 pm until 7 pm) the SH configuration produced higher TIR, but similar TAR and TBR compared to the DH configuration.

Conclusions: DH and SH performed similarly in adolescents with type 1 diabetes during a 26-hour inpatient monitoring period involving several metabolic challenges including feeding and exercise. However, during the night and around exercise, the SH configuration outperformed DH.

KEYWORDS

type 1 diabetes mellitus, adolescents, dual-hormone, advanced hybrid closed-loop, artificial pancreas, non-linear model predictive control, moderate intensity continuous exercise

1 Introduction

People with type 1 diabetes (T1D) are advised to aim for near-normal blood glucose levels to reduce the risk of diabetes late complications (1, 2). However, achieving optimal metabolic control is challenging and many fail to meet recommended guidelines – especially adolescents (3).

The most advanced commercially available technology is a single-hormone (SH) closed-loop system, also known as an artificial pancreas (AP). These systems automatically adjust insulin pump delivery based on real-time values from a continuous glucose monitor (CGM). Relative to insulin pump and CGM systems without automated insulin dosing, APs have been shown to improve glucose control (4–6). Despite these technological improvements, adolescents with T1D still frequently experience non-severe hypoglycemia (<3.9 mmol/L) (5, 7). Furthermore, around exercise the risk of hypoglycemia is higher due to increased insulin sensitivity, insulin absorption, glucose uptake in combination with an impaired glucagon secretion (8).

A potential means of reducing the risk of hypoglycemia using closed-loop systems is to add the glucose-elevating hormone glucagon. Such dual-hormone (DH) hybrid closed-loop systems are not currently commercially available but have generated interest in research trials investigating their performance relative to SH systems. A meta-analysis found that both SH and DH closed-loop systems resulted in more time spent in the target glucose range (TIR [3.9–10.0 mmol/L]) compared to non-automated delivery systems. Furthermore, DH was superior to SH in increasing TIR and decreasing time below range (TBR [< 3.9 mmol/L]) (9). Limited data exist comparing DH and SH closed-loop treatments during and after exercise, however, some studies have found DH to minimize TBR in such circumstances (10–13).

Our group has developed the DiaCon AP (14) which can run in two configurations; SH and DH. A previous version of the system was tested among adults with T1D showing improvements in TIR during exercise and a lesser need for hypoglycemic-CHO treatments when using the DH configuration (15). However, the updated system is yet to be tested in an adolescent T1D cohort.

Abbreviations: AP, Artificial Pancreas; CGM, Continuous Glucose Monitoring; CHO, Carbohydrate intake; DH, Dual-Hormone; PG, Plasma Glucose; SG, Sensor Glucose; SH, Single-Hormone; T1D, Type 1 diabetes; TAR, Time above range; TBR, Time below range; TIR, Time in range.

The aim of this study was therefore to test our hypothesis, that the updated DiaCon AP DH configuration would be safe and effective to use in individuals with T1D between 13–17 years old and that it would be *superior* in managing glycemia compared to the DiaCon AP SH configuration.

2 Materials and methods

2.1 Methods

This was a randomized, single-blind, two-period, crossover study in adolescents with T1D recruited from Herlev and Gentofte Hospital Pediatric Department Outpatient Clinics and the Steno Diabetes Center Copenhagen. Enrollment was conducted from September 1st, 2021 until March 7th, 2022. All study participants' parents or legal guardians provided written informed consent and participants ≥ 15 -years provided written, informed assent before participation. The study was approved by the Regional Committee in Health Research Ethics (H-21000207), the Danish Data Protection Agency (P-2021-326), and the Danish Medicines Agency (2020-005836-31). The trial was registered with ClinicalTrials.gov (NCT04949867).

Participants were included if they were: 13–17 years old; diagnosed with T1D for ≥ 2 years; used an insulin pump for ≥ 1 year; used a real-time or intermittently scanned CGM, had an HbA1c ≤ 7.5 mmol/mol; and used carbohydrate counting as well as the pump bolus calculator for all meals. Main exclusion criteria were known allergy to glucagon or lactose, use of diabetes medication other than insulin, and hypoglycemia unawareness.

2.2 Study device and drugs

We used our DiaCon system consisting of two Dana Diabecare RS insulin pumps (one for insulin and one for glucagon/saline), a Dexcom G6 sensor (Dexcom, San Diego, CA) and a smartphone (Samsung Galaxy A5 2017 Android phone) containing the DiaCon algorithm (14) to adjust the pump deliveries based on the CGM values. One pump was filled with insulin aspart (Fiasp[®], Novo Nordisk, Bagsværd, Denmark) and the other with either glucagon (GlucaGen[®], Novo Nordisk, Bagsværd, Denmark) or isotonic saline (sodium chloride 9 mg/dL). The glucagon pump was refilled with fresh glucagon every 22 hours after the first pump filling. The

individual parameter estimates for the insulin algorithm were set up using insulin pump, CGM and carbohydrate intake (CHO) data from each participant. The algorithm computed the insulin and glucagon administration based on predictions obtained with a mathematical model of the blood glucose response to CHO, insulin, and glucagon, i.e., based on nonlinear model predictive control (NMPC). Safety constraints on bolus and basal insulin were based on participants' insulin pump settings and the glucagon algorithm was constrained to deliver maximally 300 μ g glucagon over a two hour period (14). Meals and exercise were announced to the DiaCon AP. The NMPC utilized insulin-carbohydrate-ratio and the announced meal carbohydrates when dosing meal boluses. Exercise mode increased target glucose from 6 to 7 mmol/L and the limit for when glucagon could be administered was increased from 4.5 to 7.0 mmol/L. If SG was \leq 7.0 mmol/L at exercise announcement 100 μ g glucagon was administered (14).

2.3 Study design

Participants went through a screening visit and two 26-h in-clinic visits with a wash-out period of at least three days. During each in-clinic visit, participants wore the DiaCon system set-up to run in either the DH or SH configuration depending on the randomization order. Except for the DH and SH configurations, the study visits were identical (Figure 1).

At the screening visit, participants' medical history (i.e., allergies, medications, other illnesses, diabetes complications) as well as results of blood and urine analyses were reviewed. A clinical examination was performed to assess height, weight, and blood pressure. Finally, 14 days of insulin pump and CGM data were downloaded to register the mean values for basal rate delivery, insulin sensitivity factor, insulin-carbohydrate-ratio, CHO, TBR, TIR, time above range (TAR [$>$ 10.0 mmol/L]) and mean glucose.

Two days prior to each in-clinic visit, participants inserted the Dexcom G6 sensor which linked to the Dexcom receiver. On visit days, participants arrived at the research facility at 4 pm following a three hour fast. Upon arrival, the Dexcom sensor was linked to the study equipment, an intravenous canula was inserted for blood sampling, and participants were fitted with an activity tracker (ActiGraph GT9X Link, Pensacola, FL). Intervention with one of the two closed-loop configurations was initiated at 5:00 pm and continued for the following 26-h (Figure 2). Meals (7:00 pm, 8:00 am and 12:00 noon) and snacks (3:00 pm) were served throughout the

inpatient period and their CHO contents were based on the participants' average daily CHO intake entered in their own pumps evaluated over a seven-day period. Participants eating $<$ 100 g daily received 30 g CHO per meal, 100-150 g daily received 50 g CHO per meal, 150-200 g daily received 60 g CHO per meal, and $>$ 200 g per day received 70 g CHO per meal. The snack consisted of 1/3 of the CHO given per meal, and the dinner consisted of 1.5 times the CHO content of the other regular meals. The dinner was from McDonalds and the CHO content was determined using their nutrition calculator by the study personnel (16), who also prepared the remaining meals incl. snack. The CHO contents of all meals were blinded from participants, who made estimations which were used as the value entered into the DiaCon AP at the start of each meal. Though meals were kept identical between visits, participants' estimations could differ.

Participants were instructed to be in bed, and sleep, if possible, from 10:00 pm to 7:30 am.

After resting during the day, at 4:30 pm on day two, participants performed a 45-minute bout of moderate intensity continuous exercise at an intensity equivalent to \sim 50% of their heart rate (HR) reserve (17). Participants were fitted with a chest strap telemetry monitor that linked to the ActiGraph and the stationary bike. Exercise duration was announced to the DiaCon AP upon initiation of exercise. During the entirety of the study period, participants were asked to stay around the research facility, not to exercise and eat, and to only be away from the research room within the 30-minute window between plasma samples.

Venous blood samples were drawn every 30 minutes during the day, every 60 minutes during sleep (10:00 pm until 7:30 am) and every five to ten minutes during and immediately after exercise (4:30 pm until 5:30 pm). Plasma glucose (PG) was measured via the YSI 2300 STAT Plus Analyzer (YSI Life Sciences, Yellow Springs, OH).

If PG dropped $<$ 3.0 mmol/L at any time during the intervention, 15 grams of oral rescue carbohydrate (dextrose) tablets were provided to the participants, and plasma sampling was performed every five minutes. The treatment was repeated every 15 minutes until PG was $>$ 3.9 mmol/L. If PG was $>$ 12 mmol/L for more than two hours or $>$ 14 mmol/L (not in relation to a meal), blood ketones were measured in 15 minutely intervals and the study devices were checked for issues. After an hour, if blood ketones were \geq 0.6 mmol/L and PG remained $>$ 14 mmol/L, insulin was administered with an injection pen based on the participants' insulin-sensitivity factor aiming for PG of 7.0 mmol/L.

During each visit, participants scored side effects using a visual analog scale (VAS; 0-100) at seven specified timepoints (day 1: 5:00

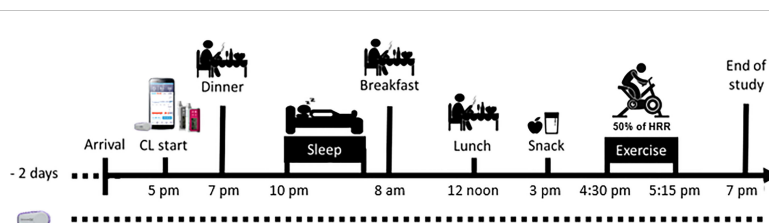
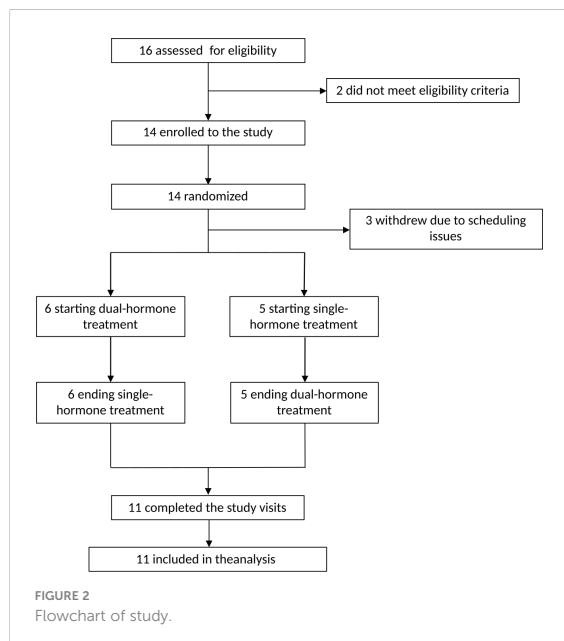


FIGURE 1
Schematic overview of the study days.



pm and 7:00 pm and day 2: 8:00 am, 12:00 noon, 3:00 pm, 4:30 pm and 7:00 pm). Clinically significant side effects were defined as a VAS score ≥ 15 (18–20).

2.4 Outcomes

The primary outcome was percentage of TBR_{SG} during the 26-h intervention period. Secondary outcomes were: percentage of TBR_{PG}, percentage of TIR_{SG&PG} and TAR_{SG&PG}, mean SG and PG, coefficient of variation (CV) and number of rescue CHO interventions. Study outcomes were also reviewed separately overnight (10:00 pm to 7:30 am) as well as during and after exercise (4:30 pm to 7:00 pm).

2.5 Statistical analysis

To be able to detect a difference in percentage of time with SG < 3.9 mmol/L of 2.3%-points (approximately 30 minutes) with 90% power, a 5% significance level, and a presumed 3.0%-points standard deviation (10), it was established that 20 participants were to be included in the study (2-sided test). Categorical variables were reported as frequencies (percentage), whereas continuous variables were reported as mean (SD) or median (interquartile range [IQR]). Continuous data was assessed for normality using Shapiro-Wilk test. For normally distributed variables, paired student's t-test was used to conduct pairwise comparisons between the two groups. For skewedly distributed variables despite log-transformation, the non-parametric Wilcoxon signed-rank test was used. Missing glucose data were estimated using linear interpolation. We used McNemar's test to assess the significance of the difference in the incidence of level 2 hypoglycemia between the two study arms. Analyses were

performed on an intention-to-treat basis. Statistical analyses were performed using RStudio version 1.4.

3 Results

As per protocol, we performed an interim analysis to assess efficiency of the DiaCon algorithm, where we found DH to be inferior to SH for TIR and TAR and to be non-superior for TBR, therefore the inclusion was truncated. At that time, 16 had been screened and 14 were included and enrolled in the study. Two adolescents were not eligible due to hypoglycemia unawareness. Before initiation of the first study visit, three participants withdrew due to scheduling issues [e.g., school absence and lack of time (Figure 2)]. Thus, 11 participants completed both visits (Table 1), and no differences were observed between completers and non-completers on age, sex, BMI, HbA1c, diabetes duration or daily insulin dose.

3.1 Entire study period

3.1.1 Glycemic metrics

For the 26-h study period we found no differences in TBR_{SG}, TIR_{SG}, or TAR_{SG} between the two study arms (Table 2). The mean (\pm SD) SG was higher during the DH compared to the SH study arm (8.7 (\pm 3.0) mmol/L vs. 8.1 (\pm 3.0) mmol/L, $p < 0.001$), with no difference in CV. Similarly, no differences were found in PG-derived measures (Table 2), except for TAR_{PG} (33.2 [16.1, 40.7] vs. 11.5 [3.83, 23.0]%, $p = 0.02$) and mean_{PG} (8.84 (\pm 2.83) vs. 7.51 (\pm 2.98), $p = 0.03$) both of which were higher during DH.

During DH, six events of SG-derived level 2 hypoglycemia (< 3.0 mmol/L) were registered in three participants compared to two events in two participants during SH ($p = 0.65$). In contrast, four episodes of PG-derived level 2 hypoglycemia were registered in three participants during DH compared to five episodes in four participants during SH

TABLE 1 Baseline characteristics of the 11 participants who completed both study visits.

Baseline characteristics	Mean (\pm SD) or median [IQR]
Sex (males [%])	9 (82%)
Age (years)	14.8 (\pm 1.47)
HbA1c (mmol/mol)	54.6 (\pm 9.20)
BMI (kg/m ²)	21.4 (\pm 2.42)
Diabetes duration (years)	5.73 (\pm 2.45)
Total daily insulin (U/kg)	0.94 (\pm 0.26)
Time below range (%)	3.0 [1.5, 6.5]
Time in range (%)	54.0 [46.0, 73.0]
Time above range (%)	43.0 [22.5, 52.0]

Age, HbA1c, BMI, diabetes duration and total daily insulin are expressed as mean (\pm SD). Time below (< 3.9 mmol/L), in (3.9–10.0 mmol/L) and above range (> 10.0 mmol/L) are expressed as median [interquartile range]. Sex is presented as absolute number and percentage.

TABLE 2 Sensor and plasma glucose values during entire study, overnight and exercise and post-exercise period.

	Sensor Glucose Measures			Plasma Glucose Measures		
	Dual-Hormone (n=11)	Single-Hormone (n=11)	P-value	Dual-Hormone (n=11)	Single-Hormone (n=11)	P-value
Entire study period (5:00 pm, day 1 – 7:00 pm, day 2)						
Starting glucose for period (mmol/L)	7.33 (± 1.90)	9.35 (± 6.61)	0.64 ^w	6.61 (± 1.71)	9.14 (± 4.90)	0.21
Time below range (%)	1.60 [0, 2.4]	1.28 [0.16, 3.19]	1.00 ^w	0.958 [0, 3.83]	2.56 [0.479, 8.47]	0.26 ^w
Time in range (%)	68.4 [48.7, 76.8]	75.7 [69.8, 87.1]	0.09	66.8 [56.9, 78.9]	79.6 [75.2, 87.4]	0.06
Time above range (%)	28.1 [18.1, 49.8]	23.3 [12.3, 27.2]	0.10	33.2 [16.1, 40.7]	11.5 [3.83, 23.0]	0.02
Mean glucose (mmol/L)	8.7 (± 3.02)	8.1 (± 3.0)	<0.001	8.84 (± 2.83)	7.51 (± 2.98)	0.03
Coefficient of variation (%)	34.8 (± 6.8)	37.3 (± 8.6)	0.20	33.59 (± 8.17)	39.63 (± 8.72)	0.17
Overnight period (10:00 pm – 7:30 am)						
Starting glucose for period (mmol/L)	10.3 (± 3.55)	9.34 (± 3.66)	0.54	9.66 (± 3.53)	8.22 (± 3.71)	0.24
Time below range (%)	0 [0, 0]	0 [0, 3.48]	0.10 ^w	0 [0, 0]	0 [0, 5.22]	0.36 ^w
Time in range (%)	73.0 [53.9, 87.4]	96.5 [84.3, 100]	0.02^w	67.8 [60.4, 89.6]	89.6 [82.6, 100]	0.07 ^w
Time above range (%)	27.0 [12.6, 42.6]	0 [0, 10.0]	0.02^w	32.2 [5.22, 37.8]	0 [0, 5.22]	0.02^w
Mean glucose (mmol/L)	8.49 (± 2.97)	7.25 (± 2.25)	0.04	8.34 (± 2.70)	6.88 (± 2.38)	0.01
Coefficient of variation (%)	35.0 (± 10.8)	31.0 (± 8.9)	0.39	32.34 (± 11.62)	34.66 (± 9.78)	0.69
Exercise and post-exercise period (4:30 pm – 7:00 pm)						
Starting glucose for period (mmol/L)	10.1 (± 3.15)	9.31 (± 2.30)	0.35	9.40 (± 2.92)	7.71 (± 2.25)	0.14
Time below range (%)	0 [0, 0]	0 [0, 0]	0.42 ^w	0 [0, 4.84]	0 [0, 14.5]	0.78 ^w
Time in range (%)	64.5 [50.0, 91.9]	83.9 [80.6, 100]	0.02^w	67.7 [32.3, 99.4]	93.5 [82.3, 100]	0.10 ^w
Time above range (%)	22.6 [0, 37.1]	12.9 [0, 17.7]	0.06 ^w	1.18 [0, 58.1]	0 [0, 3.23]	0.09 ^w
Mean glucose (mmol/L)	7.92 (± 2.92)	6.81 (± 1.91)	0.13	7.91 (± 2.70)	6.06 (± 1.76)	0.05
Coefficient of variation (%)	37.0 (± 9.6)	28.2 (± 7.7)	0.65	34.16 (± 11.51)	29.10 (± 7.49)	0.49
Change _{during-exercise} (mmol/L)	-2.5 (± 1.6)	-3.2 (± 1.0)	0.14	-2.5 (± 1.8)	-2.7 (± 1.7)	0.73
Heart Rate Telemetry during exercise (4:30 pm – 5:15 pm)						
HR target _{during-exercise} (BPM)	133 (± 4.6)	132 (± 4.8)	0.33			
HR target accuracy _{during-exercise} (%)	94.6 (± 5.7)	94.2 (± 4.6)	0.52			

Time below (<3.9 mmol/L), in (3.9–10.0 mmol/L) and above range (>10.0 mmol/L) are reported as median [interquartile range], starting glucose, mean glucose and coefficient of variation are reported as mean (± SD) and level 2 hypoglycemia is presented as events/participant. Time in range 3.9–10.0 mmol/L, time below range <3.9 mmol/L and time above range >10.0 mmol/L.

^wnon-parametric test. For level 2 hypoglycemic events McNemars test was performed. HR, Heart Rate; BPM, Beats per minute. Measures notated with _{during-exercise} depicts the 45-minutes bout of exercise time period.

P-values marked with w have been analysed using non-parametric test. Otherwise, paired t-tests have been applied. P-values < 0.05 were considered statistically significant (marked bold).

(p=0.71). Of those, two of the events were prolonged (>20 minutes) during DH compared to one during SH.

Figure 3 shows the SG profile during the total study period, overnight and the period during and after exercise. Individual SG profiles are provided in the Supplemental Material, Figure 1S.

3.1.2 Insulin and glucagon

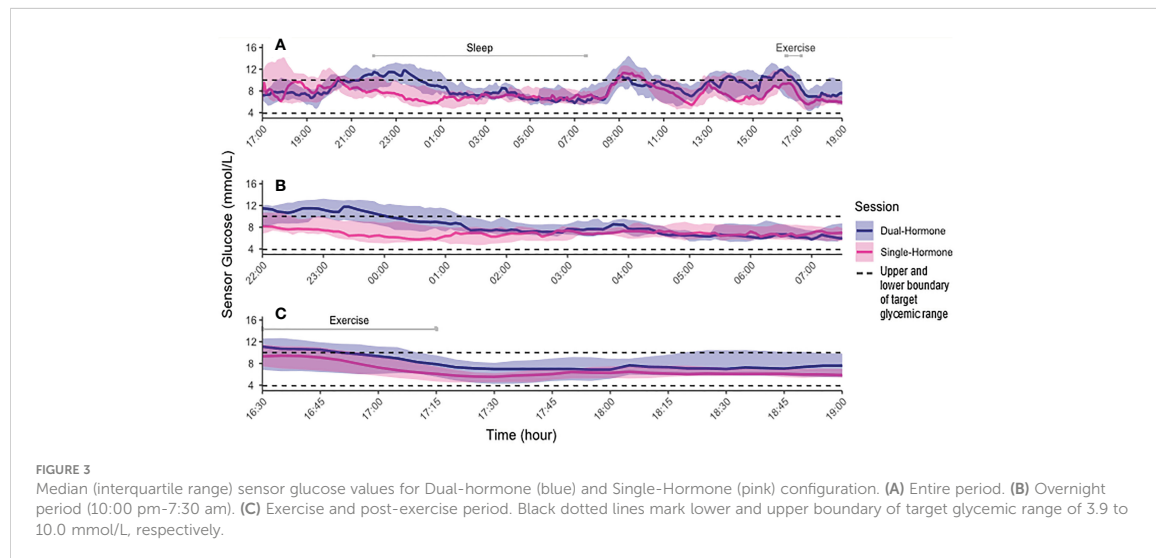
There were no differences in insulin delivery, either total insulin delivery or average basal rate, between the DH and SH study arms (Table 3, Supplemental Material Figures 2–5S). For the entire study

period, all received glucagon with a median [IQR] administration of 549 [229, 1034] µg (Figures 6–7S).

3.1.3 Carbohydrates (rescue interventions and meals)

The mean amount of rescue CHO provided was similar between the two arms (DH: 6.8 (± 12.3) grams/participant/visit vs. SH: 9.5 (± 15.4) grams/participant/visit, p=0.78).

The median [IQR] amount of CHO provided for each meal was 72 [70, 94] g for dinner, 60 [55, 70] g for breakfast, 60 [55, 70] g for lunch and



21 [19, 24]g for snacks, and we found no difference in the accuracy (%) of the participants' CHO estimations between the two study arms.

3.2 Overnight period

During the overnight period, the SH configuration outperformed the DH with more TIR_{SG} (96.5 [84.3, 100] vs. 73.0 [53.9, 87.4]%, $p=0.02$), less TAR_{SG} (0 [0.0, 10.0] vs. 27.0 [12.6, 42.6]%, $p=0.02$) and

lower mean SG (Table 2). There were no differences in TBR_{SG} or CV. TAR_{PG} was higher during DH than during SH, with no differences in TIR_{PG} or TBR_{PG} (Table 2). The overnight amount of total insulin delivered was lower during SH than during DH (Table 3). Seven participants received glucagon overnight by the DH system (549 [409, 599] μ g). Data for the entire study population is depicted in Table 3.

Overnight we found one and zero SG-derived hypoglycemic episodes, respectively, in the DH and SH arm. We did, however,

TABLE 3 Study medication administration. Insulin measures are reported as mean (SD) and glucagon as median [IQR].

Insulin and glucagon delivery	Dual-Hormone (N=11)	Single-Hormone (N=11)	P-value
Entire study period (5:00 pm, day 1 – 7:00 pm, day 2)			
Total insulin delivery (U/24h)	54.8 (19.0)	54.6 (15.4)	0.95
Basal insulin delivery (U/h)	1.03 (0.36)	1.01 (0.30)	0.77 ^w
Bolus insulin delivery (U/24h)	29.9 (12.4)	30.3 (9.6)	0.92
Glucagon delivery (μ g/26-h)	549 [229, 1034]	-	-
Overnight period (10:00 pm – 7:30 am)			
Total insulin delivery (U/night)	12.94 (4.14)	10.51 (3.08)	0.01
Basal insulin delivery (U/h)	1.09 (0.37)	1.05 (0.34)	0.15 ^w
Bolus insulin delivery (U/night)	2.55 (2.50)	0.5 (1.13)	0.04^w
Glucagon delivery (μ g/night)	298 [0, 462]	-	-
Exercise and post-exercise period (4:30 pm – 7:00 pm)			
Total insulin delivery (U/exercise)	2.24 (1.07)	2.19 (0.98)	0.88
Basal insulin delivery (U/h)	0.80 (0.38)	0.87 (0.40)	0.51
Bolus insulin delivery (U/exercise)	0.25 (0.47)	0.01 (0.03)	0.14 ^w
Glucagon delivery (μ g/period)	1 [0, 275]	-	-

P-values marked with w have been analysed using non-parametric test. Otherwise, paired t-tests have been applied. P-values < 0.05 were considered statistically significant (marked bold).

not provide any rescue glucose interventions as PG was never <3.0 mmol/L in either arm.

3.3 Exercise period

For the exercise and post-exercise phases, the SH system performed superiorly to DH with more TIR_{SG} (83.9 [80.6, 100.0] vs. 64.5 [50.0, 91.9]%, $p=0.02$). There were no differences in TAR_{SG}, TBR_{SG}, mean SG, CV or in PG (Table 2). For this period, there was no difference in amount of insulin delivered. A total of five participants received glucagon during and after exercise (300 [250, 300] μ g) (Table 3).

One participant received rescue CHO following exercise in the DH arm, and two participants received one and two rescue CHO interventions, respectively, in the SH arm. The participant needing two rescue interventions around exercise experienced level 2 hypoglycemia during exercise, and the exercise bout was therefore cut short. None of the DH exercise sessions were interrupted.

The exercise starting SG and drop in SG during exercise (4:30 to 5:15 pm) were comparable between the two study visits (Table 2). Furthermore, we found no difference in the estimated HR target during exercise or in the accuracy (%) of which participants reached their target between the two visits (Table 2).

3.4 Side effects

No severe adverse events were observed. Three participants (27%) reported a clinically significant measure of nausea during the DH arm compared with none in the SH arm. Headache was reported by four (36%) in both the SH and the DH arm. Stomach-ache was reported by two (18%) in the DH arm and one (9%) in the SH arm. None experienced vomiting. All reported side effects were mild in severity and, besides from hypoglycemic- and hyperglycemic episodes, required no intervention.

3.5 Technological issues

During the study, there were a few technological issues. One participant (during the DH visit) experienced prolonged pressure induced sensor attenuation causing the sensor to register level 2 hypoglycemia, while PG was well within range. This caused wrongful glucagon administration and subsequent hyperglycemia. During two DH study visits, glucagon occluded the pump which required a change of infusion set. During both study arms, the phone lost connection to the sensor. However, all connection issues were automatically reestablished without intervention from the study personnel. These phone-sensor connection issues only triggered an alarm if they lasted more than 15 minutes, thus shorter connection losses may have been present, without the study personnel being aware. Once during a DH study visit, there was a disconnection between the phone and the insulin pumps which was resolved by restarting the entire system.

4 Discussion

In this 26-h inpatient study, we compared the performance of the DiaCon DH and SH configurations in adolescents with type 1 diabetes. For the entire study period, we found no differences in TBR_{SG}/PG, TIR_{SG}/PG, TAR_{SG}/PG, or in the amount of rescue glucose needed. However, despite equivalency in TBR_{SG} during the overnight period and around exercise, SH achieved more TIR_{SG} and less TAR_{SG} compared to DH.

The DiaCon AP has previously been tested in adults with type 1 diabetes (15), showing that DH was superior to SH in handling hypoglycemia. These findings were in line with two systematic reviews and meta-analyses performed in 2018, finding that DH was superior to SH for TBR and TIR (4, 9). Still, only two studies have performed head-to-head comparison of DH and SH in adolescents with type 1 diabetes (21, 22). In line with our findings, the first study showed no significant differences in TIR, TAR or TBR between SH and DH for the adolescents during a 24-h observation period (21). Further, they found a tendency for SH to achieve higher TIR than DH during the overnight period (11:00 pm to 8:00 am), but it did not reach statistical significance. The other study was an overnight study showing that the addition of glucagon significantly improved TIR and reduced the time in level 1 hypoglycemia, but had similar time in level 2 hypoglycemia when compared with SH (22). Both studies included a third study arm with usual care, and generally both SH and DH achieved better glycemic control compared to this arm. Recently, a pooled analysis was performed for nocturnal control in children and adolescents using SH and DH. They found superiority in favor of the DH configuration for TIR, level 1 hypoglycemia and level 2 hyperglycemia (23).

Even though our SH configuration managed to ensure good glycemic control comparable to that of the commercially available APs with a TIR_{SG} of 75% for the whole study period, 83% during exercise and 95% overnight, hypoglycemia still posed a challenge (4, 5). Indeed, seven (64%) participants had at least one hypoglycemic event, whilst six experienced recurrent events. This issue was not resolved by addition of glucagon in our DH configuration. The reason may be attributed to the different conditions for parameter estimations in the DiaCon AP rather than glucagon *per se*. While the insulin algorithm was individualized and parameter estimates were based on individual insulin pump and CGM data, the parameter estimates for the glucagon algorithm were generic and similar for all participants. The uncertainty of the individual glucose response to glucagon (median[IQR] glucagon administration 549 [229, 1034] μ g), therefore, produced equally uncertain glucose predictions for the system, resulting in less correct insulin dosing in the DH configuration. In this study, the glucagon sensitivity was not adaptive, and we did not have the data to estimate individual glucagon parameters. Whether addition of these features would have improved the DH study results remain uncertain. The DiaCon AP was further challenged by known technical issues, i.e., glucagon pump occlusions and pressure induced sensor attenuation, both of which unfortunately affected the DiaCon AP predictions and hence, its performance during the DH study days. Glucagon occlusions happen quite commonly when using native glucagon due to rapid fibrillation after reconstitution (12, 24–26), and although we tried to avoid them by changing glucagon every 22 hours, they still occurred. Future algorithms would therefore benefit immensely from being able to detect occlusions and pressure induced sensor

attenuations to avoid miscommunication between the systems' predictions and the actual CGM data and hormonal delivery. Still, even with improved occlusion detection in the algorithms, a stable formulation of glucagon is required before it is feasible to be used in a real-world setting. New, soluble formulations have been developed (Dasiglucagon[®], Baqsimi[™] and Gvoke[®]/XeriSol[®]), but are still only approved for treatment of severe hypoglycemia. Recently published and ongoing clinical trials have shown promising results in using soluble glucagon for treatment of non-severe hypoglycemia, regardless of whether glucagon has been delivered through automated pumps or *via* pen-injections (13, 27, 28).

In the overnight period participants were administered higher doses of bolus insulin during DH compared to SH (2.55 [± 2.50] vs. 0.5 [± 1.13] IE). This was most likely due to a couple of different factors. During the DH arm some participants were administered glucagon right before dinner announcement, resulting in inadequate meal bolus insulin, and subsequent hyperglycemia. Due to restrictions in the DiaCon AP around meals this led to insulin corrections being administered in the night hours (14). Another possible explanation could be the occurrence of pressure induced sensor augmentations. These caused wrongful glucagon administration and hyperglycemia, which was followed by increased insulin supply when the augmentation was resolved. Furthermore, a few participants experienced oscillating sensor glucose levels, as they were overcorrected and entered a glucagon-insulin oscillating cycle. With the result from the SH arm in mind (TIR 96.5%) it is fair to speculate whether a specific night setting should be developed, making the glucagon algorithm during the night less aggressive, but as our study was rather small and the glucagon algorithm was faced with several challenges, we still think it is too unsafe to conclude (10).

Initially, we hypothesized that the addition of glucagon could have counteracted the increased risk for hypoglycemia during physical activity (8). However, we found that SH was superior to DH with more TIR_{SG}, and no difference in TAR_{SG} or TBR_{SG/PG} during and after exercise. We speculate whether the higher starting glucose level before exercise for DH (10.1 [± 3.15] vs. 9.31 [± 2.30], *p*=0.35), though not statistically significant, may have reduced the need for glucagon around exercise – causing a systematic error when interpreting the glucose data that are in favor for SH. In fact, only five participants received glucagon in relation to exercise. Among four adult head-to-head studies, DH was found to be superior to SH in avoiding hypoglycemia during exercise, whereas only one of the studies also included adolescents (11–13, 15). In the combined adult and adolescent study, no differences were found between the two hormonal configurations (21). Unfortunately, no subgroup analysis – adult versus adolescents – for the exercise period was reported. Our study period ended 1 hour and 45 minutes after the exercise bout, and we were therefore only able to investigate a small window of the post-exercise period. Previous studies, however, have shown that SH systems could sufficiently keep glucose in range during the post-exercise period (21, 29). This could indicate that glucagon may be especially beneficial during aerobic exercise, where blood glucose changes rapidly and insulin reduction or suspension is inadequate, but requirement may waiver in the post-exercise period

when the pronounced acute glycemic declines induced by exercise have passed (10).

The side effects experienced in this study were mild and self-limiting, but the adolescents reported more clinically significant events of nausea during DH than during SH (27% vs. 0%). The other side effects were equally distributed across both study visits, as reported by other study groups (26). A new outpatient study investigating dasiglucagon pen treatment for non-severe hypoglycemia found a higher occurrence of mild nausea with glucagon treatment, but the participants would still incorporate it into their regular diabetes treatment if possible (30). Taken collectively nausea remains a limitation of DH use and finding ways to resolve such should be a major consideration in future developments.

The current study had some limitations. Firstly, a small sample size makes the generalizability of the study results difficult. Furthermore, the current DiaCon AP set-up was too comprehensive for commercial pump use. Simpler set-up versions of the DiaCon AP, should be developed. The use of native glucagon limited the possibility to be used in real-world settings, but the current data show that soluble glucagon has a similar response. Furthermore, we conducted our study on adolescents of 13-17-years-old. This age group is different from all other due to the considerable hormonal and physiological changes over time. Therefore, it is important that studies with DH and SH APs also include adolescents before concluding whether it is beneficial in this age group. We chose a McDonalds meal as dinner, which is not typically classified as a balanced and healthy meal, however, we decided to do so in order to test our configurations maximally during the limited study time. Meals with a high carbohydrate and fat content are usually more difficultly handled for people with type 1 diabetes and testing our system in such a situation was therefore important. Furthermore, McDonalds is known worldwide making the approach universally applicable. Our participants were overall better regulated during the study days than in their everyday lives, though, we did not have a usual care control arm to test whether the superior glycemic control achieved by the DiaCon AP would persist in an inpatient setting. This was the first 26-h inpatient study, during which the DH configuration was tested during multiple metabolic challenges.

5 Conclusion

To conclude, the two configurations performed equally well; but during night and exercise, SH achieved better glucose control than DH with equal amount of rescue glucose needed.

Whether it is justifiable to add glucagon to the AP systems remains unanswered. Our SH configuration managed to yield good glycemic control, but hypoglycemia still posed a challenge which neither of our configurations managed to overcome. However, as we become more familiar with the use of glucagon and with more stable glucagon formulations readily available, improved DH algorithms can potentially be a key player in resolving this.

Data availability statement

The original contributions presented in the study are included in the article/**Supplementary Material**. Further inquiries can be directed to the corresponding authors.

Ethics statement

The study was approved by the Regional Committee in Health Research Ethics (H-21000207), the Danish Data Protection Agency (P-2021-326), and the Danish Medicines Agency (2020-005836-31). Written informed consent to participate in this study was provided by the participants' legal guardian/next of kin.

Author contributions

KN, JS, CL, ATR, JJ, and AGR contributed to conceive and design the study. EL, ATR, CL, AGR, and TR conducted the clinical trial. EL performed data analysis and wrote the manuscript. AGR, KN, JS, and CL supervised. All authors read and approved the final manuscript. All authors contributed to the article and approved the submitted version.

Funding

The project was investigator initiated. Investigator salaries, equipment, medications, and consumables are covered by the research unit at Steno Diabetes Center Copenhagen and Technical University of Denmark. None of the investigators have personal financial interest in the conduct or the outcome of the project. The study received a grant by Danish Diabetes Academy, and AGR was partly funded by the Danish Diabetes Academy (Grant ID PD002-19).

Acknowledgments

The authors would like to thank all participants and their parents for engaging with the study. Furthermore, a special thank you should be paid to biomedical scientist, Sandra Tawfik, for contributing to the conduction of the study and to Olivia McCarthy for proof reading and providing feedback on the final manuscript.

References

1. Gubitosi-Klug RA, Lachin JM, Backlund JYC, Lorenzi GM, Brillou DJ, Orchard TJ. Intensive diabetes treatment and cardiovascular outcomes in type 1 diabetes: The DCCT/EDIC study 30-year follow-up. *Diabetes Care* (2016) 39:686–93. doi: 10.2337/dc15-1990
2. Nathan DM, Cleary PA, Backlund J-YC, Genuth SM, Lachin JM, Orchard TJ, et al. Intensive diabetes treatment and cardiovascular disease in patients with type 1 diabetes. *N Engl J Med* (2005) 353:2643–53. doi: 10.1056/NEJMoa052187

Conflict of interest

The authors declare that the research was conducted in the absence of any commercial or financial relationships that could be construed as a potential conflict of interest.

Publisher's note

All claims expressed in this article are solely those of the authors and do not necessarily represent those of their affiliated organizations, or those of the publisher, the editors and the reviewers. Any product that may be evaluated in this article, or claim that may be made by its manufacturer, is not guaranteed or endorsed by the publisher.

Supplementary material

The Supplementary Material for this article can be found online at: <https://www.frontiersin.org/articles/10.3389/fendo.2023.1073388/full#supplementary-material>

FIGURE 1S:

Individual SG measures for participant during the entire study period for dual-hormone (blue) and single-hormone (pink). Black dotted lines mark the lower and upper boundary of target glycemic range of 3.9 mmol/L to 10.0 mmol/L, respectively.

FIGURE 2S:

Mean (\pm SD) basal insulin (IE) delivered during the entire study period for dual-hormone (blue) and single-hormone (pink). Sleep and exercise periods marked in the figure.

FIGURE 3S:

Mean (\pm SD) total insulin (IE) delivered during the entire study period for dual-hormone (blue) and single-hormone (pink). Sleep and exercise periods marked in the figure.

FIGURE 4S:

Mean (\pm SD) bolus insulin (IE) delivered during the entire study period for dual-hormone (blue) and single-hormone (pink). Sleep and exercise periods marked in the figure.

FIGURE 5S:

Individual insulin delivery for each participant during the entire study period for dual-hormone (blue) and single-hormone (pink).

FIGURE 6S:

Mean glucagon delivery during the entire dual-hormone study period. Sleep and exercise periods marked in the figure.

FIGURE 7S:

Individual glucagon delivery for each participant during the entire dual-hormone study period.

5. Schiaffini R, Deodati A, Nicoletti MC, Carducci C, Ciampalini P, Lorubbio A, et al. Comparison of two advanced hybrid closed loop in a pediatric population with type 1 diabetes: a real-life observational study. *Acta Diabetol* (2022) 59:59–64. doi: 10.1007/s00592-022-01886-z
6. Phillip M, Nimri R, Barnard-Kelly K, Bergenstal R, Norgaard K. Consensus recommendations for the use of automated insulin delivery (AID) technologies in clinical practice 2022. *Endocrine Rev* (2022) 00:1–27. doi: 10.1210/endrev/bnac022
7. Boscarì F, Ferretto S, Cavallin F, Bruttomesso D. Switching from predictive low glucose suspend to advanced hybrid closed loop control: Effects on glucose control and patient reported outcomes. *Diabetes Res Clin Pract* (2022) 185:109784. doi: 10.1016/j.diabres.2022.109784
8. Sylow L, Kleinert M, Richter EA, Jensen TE. Exercise-stimulated glucose uptake — regulation and implications for glycaemic control. *Nat Rev Endocrinol* (2017) 13:133–48. doi: 10.1038/nrendo.2016.162
9. Bekiarì E, Kitsios K, Thabit H, Tauschmann M, Athanasiadou E, Karagiannis T, et al. Artificial pancreas treatment for outpatients with type 1 diabetes: systematic review and meta-analysis. *BMJ* (2018) 361:k1310. doi: 10.1136/bmj.k1310
10. Peters TM, Haidar A. Dual-hormone artificial pancreas: benefits and limitations compared with single-hormone systems. *Diabetes Med* (2018) 35:450–9. doi: 10.1111/dme.13581
11. Taleb N, Emami A, Suppere C, Messier V, Legault L, Ladouceur M, et al. Efficacy of single-hormone and dual-hormone artificial pancreas during continuous and interval exercise in adult patients with type 1 diabetes: randomised controlled crossover trial. *Diabetologia* (2016) 59:2561–71. doi: 10.1007/s00125-016-4107-0
12. Castle JR, El Youssef J, Wilson LM, Reddy R, Resalat N, Branigan D, et al. Randomized outpatient trial of single- and dual-hormone closed-loop systems that adapt to exercise using wearable sensors. *Diabetes Care* (2018) 41:1471–7. doi: 10.2337/dc18-0228
13. Wilson LM, Jacobs PG, Ramsey KL, Resalat N, Reddy R, Branigan D, et al. Dual-hormone closed-loop system using a liquid stable glucagon formulation versus insulin-only closed-loop system compared with a predictive low glucose suspend system: An open-label, outpatient, single-center, crossover, randomized controlled trial. *Diabetes Care* (2020) 43:2721–9. doi: 10.2337/dc19-2267
14. Reenberg AT, Ritschel TKS, Lindkvist EB, Laugesen C, Svensson J, Ranjan AG, et al. Nonlinear model predictive control and system identification for a dual-hormone artificial pancreas. *IFAC-Pap* (2022) 55:915–21. doi: 10.1016/j.ifacol.2022.07.561
15. Ranjan AG, Boiroux D, Laugesen C, Schmidt S, Reenberg AT, Jørgensen JB, et al. Performance of a dual hormone closed-loop system vs. an insulin-only closed-loop system during challenging inpatient conditions: A single-blinded randomized. *Diabetes* (2021) 70 (Supplement_1):215-OR. doi: https://doi.org/10.2337/db21-215-OR
16. McDonald's nutrition calculator: Calories and more. Available at: <https://www.mcdonalds.com/us/en-us/about-our-food/nutrition-calculator.html>.
17. Ciccone ZS, Holmes CJ, Fedewa MV, MacDonald HV, Esco MR. Age-based prediction of maximal heart rate in children and adolescents: A systematic review and meta-analysis. *Res Q Exerc Sport* (2019) 90:417–28. doi: 10.1080/02701367.2019.1615605
18. Lundqvist C, Benth J, Grande R, Aaseth K, Russell M. A vertical VAS is a valid instrument for monitoring headache pain intensity. *Cephalalgia* (2009) 29:1034–41. doi: 10.1111/j.1468-2982.2008.01833.x
19. Hendey GW, Donner NF, Fuller K. Clinically significant changes in nausea as measured on a visual analog scale. *Ann Emerg Med* (2005) 45:77–81. doi: 10.1016/j.annemergmed.2004.07.446
20. Gallagher EJ, Bijur PE, Latimer C, Silver W. Reliability and validity of a visual analog scale for acute abdominal pain in the ED. *Am J Emerg Med* (2002) 20:287–90. doi: 10.1053/ajem.2002.33778
21. Haidar A, Legault L, Messier V, Mitre TM, Leroux C, Rabasa-Lhoret R. Comparison of dual-hormone artificial pancreas, single-hormone artificial pancreas, and conventional insulin pump therapy for glycaemic control in patients with type 1 diabetes: an open-label randomised controlled crossover trial. *Lancet Diabetes Endocrinol* (2015) 3:17–26. doi: 10.1016/S2213-8587(14)70226-8
22. Haidar A, Legault L, Matteau-Pelletier L, Messier V, Dallaire M, Ladouceur M, et al. Outpatient overnight glucose control with dual-hormone artificial pancreas, single-hormone artificial pancreas, or conventional insulin pump therapy in children and adolescents with type 1 diabetes: an open-label, randomised controlled trial. *Lancet Diabetes Endocrinol* (2015) 3:595–604. doi: 10.1016/S2213-8587(15)00141-2
23. Wu Z, Lebbar M, Taleb N, Legault L, Messier V, Rabasa-Lhoret R. Comparing dual-hormone and single-hormone automated insulin delivery systems on nocturnal glucose management among children and adolescents with type 1 diabetes: A pooled analysis. *Diabetes Obes Metab* (2023). 25:310–3 doi: 10.1111/dom.14850. n/a.
24. Ranjan AG, Schmidt S, Norgaard K. Glucagon for hypoglycaemia treatment in type 1 diabetes. *Diabetes Metab Res Rev* (2021) 37:e3409. doi: 10.1002/dmrr.3409
25. Russell SJ, El-Khatib FH, Sinha M, Magyar KL, McKeon K, Goergen LG, et al. Outpatient glycemic control with a bionic pancreas in type 1 diabetes. *N Engl J Med* (2014) 371:313–25. doi: 10.1056/NEJMoa1314474
26. El-Khatib FH, Balliro C, Hillard MA, Magyar KL, Ekhlaspour L, Sinha M, et al. Home use of a bi-hormonal bionic pancreas versus insulin pump therapy in adults with type 1 diabetes: a multicentre randomised crossover trial. *Lancet Lond Engl* (2017) 389:369–80. doi: 10.1016/S0140-6736(16)32567-3
27. Laugesen C, Ranjan AG, Schmidt S, Norgaard K. Low-dose dasiglucagon versus oral glucose for prevention of insulin-induced hypoglycemia in people with type 1 diabetes: A phase 2, randomized, three-arm crossover study. *Diabetes Care* (2022) 45:1391–9. doi: 10.2337/dc21-2304
28. Castellanos LE, Balliro CA, Sherwood JS, Jafri R, Hillard MA, Greau E, et al. Performance of the insulin-only iLet bionic pancreas and the bi-hormonal iLet using dasiglucagon in adults with type 1 diabetes in a home-use setting. *Diabetes Care* (2021) 44: e118–20. doi: 10.2337/dc20-1086
29. Haidar A, Rabasa-Lhoret R, Legault L, Lovblom LE, Rakheja R, Messier V, et al. Single- and dual-hormone artificial pancreas for overnight glucose control in type 1 diabetes. *J Clin Endocrinol Metab* (2016) 101:214–23. doi: 10.1210/jc.2015-3003
30. Laugesen C, Ranjan A, Schmidt S, Norgaard K. 257-OR: Pen-administered low-dose dasiglucagon vs. usual care for prevention and treatment of nonsevere hypoglycemia in people with type 1 diabetes during free-living conditions: A phase 2, randomized, two-period, crossover outpatient study. *Diabetes* (2022) 71(Supplement_1):257-OR. doi: 10.2337/db22-257-OR

APPENDIX L

Technical Report

DiaCon: Clinical trials of a dual- and single-hormone artificial pancreas for adolescents

Authors:

Asbjørn Thode Reenberg, Tobias K. S. Ritschel, Emilie B. Lindkvist, Christian Laugesen, Jannet Svensson, Ajenthen G. Ranjan, Kirsten Nørgaard, John Bagterp Jørgensen

Submitted to:

arXiv 2023.



DiaCon: Clinical trials of a dual- and single-hormone artificial pancreas for adolescents

Conducted in 2021–2022

Technical report

Asbjørn Thode Reenberg

Tobias K. S. Ritschel

Emilie Bundgaard Lindkvist

Christian Laugesen

Jannet Svensson

Ajenthien G. Ranjan

Kirsten Nørgaard

John Bagterp Jørgensen

Department of Applied Mathematics and Computer Science,
Technical University of Denmark, DK-2800 Kgs. Lyngby, Denmark

Clinical Research,
Steno Diabetes Center Copenhagen, DK-2730 Herlev, Denmark

DTU Compute
Department of Applied Mathematics and Computer Science
Technical University of Denmark

Matematiktorvet
Building 303B
2800 Kongens Lyngby, Denmark
Phone +45 4525 3031
compute@compute.dtu.dk
www.compute.dtu.dk

Summary

In this technical report, we describe the individual parameter estimation and results of a phase 1 and a phase 2 clinical trial of the DiaCon dual-hormone artificial pancreas based on nonlinear model predictive in adolescents with type 1 diabetes from a technical perspective. The two trials were conducted between October, 2021 and April, 2022, and the 14 participants were between 13 and 17 years old at the time of recruitment. In the phase 1 trial, there is one visit for each of 3 participants (only dual-hormone treatment), and there are two visits for each of 11 participants in the phase 2 trial (both single- and dual-hormone treatment). The AP was primarily developed by John Bagterp Jørgensen's research group at the Department of Applied Mathematics and Computer Science, Technical University of Denmark, and the clinical trials were primarily carried out by Kirsten Nørgaard's research group at Clinical Research, Steno Diabetes Center Copenhagen.

Executive summary

Objective

- Test a dual-hormone (DH) and a single-hormone (SH) artificial pancreas (AP) in a clinical trial with adolescents.
- Test the feasibility of using nonlinear model predictive control (NMPC) for APs.
- Phase 1 trial: Identify and adress minor issues with the AP.
- Phase 2 trial: Evaluate performance and compare the DH configuration to the SH configuration of the AP.

Artificial pancreas

- The AP consists of 1) a Dexcom G6 sensor, 2) two Dana Diabecare RS pumps, and 3) a control algorithm.
- The control algorithm is based on an adaptive NMPC algorithm.
- The AP uses an extension of the Medtronic Virtual Patient (MVP) model.
- The optimal control problem (OCP) is solved using a multiple-shooting approach combined with a sequential quadratic programming (SQP) algorithm.
- The AP algorithm switches between two modes where it administers either insulin or glucagon. In the single-hormone AP, it is not possible to switch to administering glucagon. All other aspects of the two APs are the same.

Pre-trial parameter estimation

- The parameters were estimated using a maximum likelihood (ML) based prediction error method (PEM) from CGM measurements, meal carbohydrate estimates, and basal and meal bolus insulin administration from the participants.
- The amount of data available for estimation was different for each participant. For all data sets, there appeared to be several meals without a corresponding estimate of the carbohydrate content.

- We selected a subset of the data for estimation where there appeared to be no missing information. This period of time was typically short, e.g., less than 24 h and sometimes only a few hours.
- The estimation required many decisions based on experience as well as trial and error to choose, e.g., the subset of the data used for estimation, which parameters to estimate, and the values of parameters that are not estimated from data.
- We evaluated the estimated parameters with a deterministic simulation that should fit the data used for estimation and by simulation of the meal response for insulin boli computed from different insulin-to-carb (ICR) ratios.

Clinical trials

- Phase 1 trial: The phase 1 trial ($n = 3$) only involved a single visit where the dual-hormone AP was tested.
- Phase 2 trial: The phase 2 trial ($n = 11$) involved two visits; one with the single-hormone AP and one with the dual-hormone AP.
- Each visit lasted 26 h. The visits started at 17:00 on the first day and ends at 19:00 on the second day. The participants had dinner at 19:00 on day one and slept from 22:00 to 07:30. The participants had breakfast at 08:00, lunch at 12:00, and a snack at 15:00 on day two. Finally, the participants exercised from 16:30 to 17:15 with moderate intensity.

Outcomes

- The trials displayed that it is feasible to use NMPC for APs and that both the DH and SH AP were able to control the blood glucose concentration.
- Identifying a model can be a challenging and time-consuming process due to missing data and sometimes also incorrectly announced meals and insulin boli.
- During the studies, we started to set, e.g., the ICR to a value that seemed reasonable instead of using the participants' average value. We also shifted the timing of some of the meals to match the peaks in the glucose concentration instead of directly using the reported data. These adaptations seemed to improve the performance of the AP.
- Pressure induced sensor attenuations (PISAs) are challenging for DH APs as glucagon can be administered even if the glucose concentration is not low. Occlusions in the glucagon pump and lost connections also influenced the performance of the AP.
- The predicted glucagon response was inaccurate for many participants as we used the same parameters for all participants.

- Many participants received too much insulin after glucagon was administered and caused oscillations in some of the DH studies.
- Despite the challenges related to administration of glucagon in some studies it also prevented hypoglycemia and the need for rescue carbs in others.

Contents

Summary	i
Executive summary	iii
Contents	vii
1 Introduction	1
2 Phase 1 trial	5
2.1 Participant 1	5
2.2 Participant 2	10
2.3 Participant 3	15
3 Phase 2 trial	21
3.1 Participant 1	21
3.2 Participant 2	26
3.3 Participant 3	30
3.4 Participant 4	34
3.5 Participant 5	38
3.6 Participant 6	42
3.7 Participant 7	46
3.8 Participant 8	50
3.9 Participant 9	54
3.10 Participant 10	58
3.11 Participant 11	62
4 Conclusions	67
Bibliography	69

CHAPTER 1

Introduction

In this technical report, we describe the individual parameter estimation and results of a phase 1 and a phase 2 trial of a dual-hormone and a single-hormone artificial pancreas (AP) for controlling the blood glucose concentration in adolescents with type 1 diabetes (T1D) from a technical perspective. We describe each study in the trials individually and we refer to Lindkvist et al. [2] for a clinical description of the trial outcomes and Reenberg et al. [3] for the mathematical details. In this section, we summarize the key details of the clinical trials and provide an outline of the report.

Objective The objective of the clinical trials was to test an AP which can administer both insulin and glucagon and an AP that can only administer insulin in terms the targets specified in [1] where Table 1.1 shows the target glucose ranges. Furthermore, we tested the feasibility of using nonlinear model predictive control (NMPC) for APs. The purpose of the phase 1 trial was to identify and address minor issues with the AP, and the purpose of the phase 2 trial was to evaluate the performance and compare a dual-hormone AP to a single-hormone AP.

Artificial pancreas We used a dual-hormone AP consisting of 1) a sensor, 2) two actuators, and 3) a control algorithm. The sensor was a Dexcom G6 continuous glucose monitor¹ (CGM), and the actuators were two Dana Diabecare RS pumps² from the company Sooil. The pumps were used to administer insulin and glucagon, and the control algorithm was implemented in an Android app, which is ran on a Samsung Galaxy A5 (2017) smartphone³. The dual-hormone AP algorithm switches between two modes where it administers either insulin or glucagon. The switch is based on measurements of the subcutaneous glucose concentration as well as estimates and predictions of the blood glucose concentration. In the single-hormone AP, it is not possible to switch to administering glucagon. All other aspects of the two APs are the same.

The control algorithm is based on an adaptive NMPC algorithm. It uses an extension of the Medtronic Virtual Patient (MVP) model. The (deterministic) optimal control problem (OCP) is solved using a multiple-shooting approach combined with a sequential quadratic programming (SQP) algorithm. The states and the initial condition in the OCP are estimated using the continuous-discrete extended Kalman filter (CD-EKF), which also (simultaneously) estimates the insulin sensitivity (a parameter in the MVP

¹www.dexcom.com/g6-cgm-system (Accessed: June 27th, 2022)

²www.sooil.com/eng/product/dana-rs.php (Accessed: June 27th, 2022)

³www.samsung.com/dk/support/model/SM-A520FZKANEE (Accessed: June 27th, 2022)

Table 1.1: The five glycemic ranges described by Batteline et al. [1].

Category	Range [mmol/L]	Color	Target [%]
Missing measurements	-	Grey	0
Level 2 hyperglycemia]13.9, ∞ [Orange	<5.0
Level 1 hyperglycemia]10.0, 13.9]	Yellow	<20.0
Normoglycemia	[3.9, 10.0]	Green	>70.0
Level 1 hypoglycemia	[3.0, 3.9[Light red	<4.0
Level 2 hypoglycemia	[0.0, 3.0[Red	<1.0

model). As the control algorithm updates a model parameter based on feedback (CGM measurements), it is adaptive.

The parameters in the MVP model were estimated using a maximum likelihood (ML) based prediction error method (PEM) based on the participants' own CGM measurements, meal carbohydrate estimates, and basal and meal bolus insulin administration. Furthermore, we received the participants' own values for their insulin-to-carb (ICR) ratio and their insulin-sensitivity-factor (ISF). The amount of data available for estimation was different for each participant, and for all data sets, there appeared to be several meals without a corresponding estimate of the carbohydrate content. Therefore, for each participant, we selected a period of time where the majority of the meal carbohydrate contents appeared to be properly estimated and used this subset of the data to estimate the parameter values. This period of time was typically short, e.g., less than 24 h. Furthermore, the estimation was not fully automatic. It required many decisions based on experience as well as trial and error to choose, e.g., the subset of the data used for estimation, which parameters to estimate, and the values of parameters that are not estimated from data. We evaluated the estimated parameters with a deterministic simulation that should fit the data used for estimation and by simulation of the meal response for insulin boli computed from different ICRs. The simulation of the meal response was used to verify that meals result in a post-prandial peak and that the corresponding insulin bolus causes the blood glucose concentration to decrease within a reasonable amount of time.

Time period The phase 1 trial was conducted between October 6th, 2021 and November 3rd, 2021, and the phase 2 trial was conducted between November 23rd, 2022 and April 26th, 2022.

Protocol The phase 1 trial only involved a single visit where the dual-hormone AP was tested. The phase 2 trial involved two visits; one with the single-hormone AP and one with the dual-hormone AP. Each visit lasted 26 h. In the phase 1 trial, the visit started at 17:00 on the first day and ends at 19:00 on the second day. The participant consumed a meal at 19:00 on day one and slept from 22:00 (day one) to 07:30 (day two). Next, breakfast and lunch were consumed at 08:00 and 12:00, respectively, and a snack was consumed at 15:00. Finally, the participant exercised from 16:30 to 17:15 using an

indoor bike trainer. Fig. 1.1 shows the protocol. In the phase 2 trial, two participants' visits sometimes overlapped. In that case, one visit would proceed as in the phase 1 trial, and all aspects of the other visit were delayed by 15 minutes, i.e., it lasted from 17:15 on day one to 19:15 on day two. Otherwise, the protocol was identical in the two studies. For some participants, there were slight variations in the actual starting time due to specific details of the individual visits.

Participants The participants were between 13 and 17 years old when they were recruited for the trials. There were 3 participants in the phase 1 trial, and 11 participants in the phase 2 trial. In their daily lives, the participants used a CGM and an insulin pump in either an open- or a closed-loop configuration.

DIACON partners DIACON is a collaboration between 1) John Bagterp Jørgensen's research group at the Department of Applied Mathematics and Computer Science, Technical University of Denmark, and 2) Kirsten Nørgaard's research group at Clinical Research, Steno Diabetes Center Copenhagen. The control algorithm and the app was developed by Jørgensen's group with assistance from Nørgaard's group. The clinical trials were carried out at Steno Diabetes Center Copenhagen by Nørgaard's group with assistance from Jørgensen's group.

Jørgensen's group consists of Dimitri Boiroux, Maria Sejersen, Tobias K. S. Ritschel, and Asbjørn Thode Reenberg. Nørgaard's group consists of Jannet Svensson, Ajenthen G. Ranjan, Christian Laugesen, and Emilie Bundgaard Lindkvist.

Structure of the report In Chapter 2, we describe the parameter estimation and results of the phase 1 trial and the modifications made to the AP after each visit. In Chapter 3, we describe and discuss the parameter estimation and results of each of the phase 2 trials, and in Chapter 4, we provide conclusions based on the clinical trial.

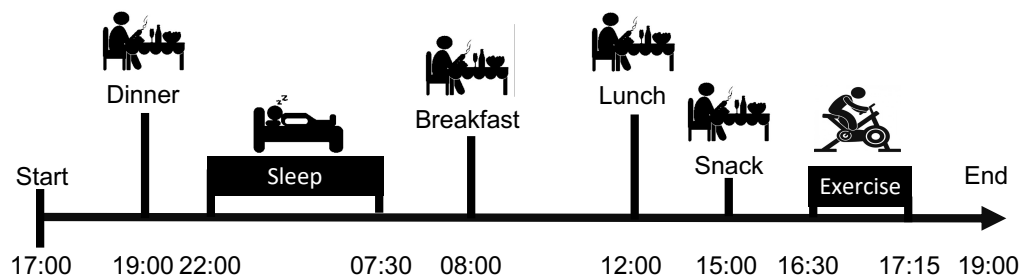


Figure 1.1: Schematic of the protocol used in the clinical trials.

CHAPTER 2

Phase 1 trial

In this chapter, we show the parameter estimation and results from all the studies in the phase 1 trial. The studies are shown in chronological order. The app was updated to save all values from the control algorithm after the phase 1 trial. Therefore, we are unable to definitively distinguish between insulin meal boli and correction boli in the phase 1 trial and show the combined insulin boli in the figures. Furthermore, the YSI measurements from participant 2 in the phase 1 trial are missing.

2.1 Participant 1

2.1.1 Parameter estimation

We used around 40 hours of data with multiple meals and insulin boli. Figure 2.1 shows the data used for estimation and a simulation with the estimated parameters. For this participant, we fixed EGP , k_1 , and Q_{logSI} , and $1/V_g$ was on the boundary. $GEZI$ was tuned to correct the basal rate to match the participants' normal basal rate which was ~ 25 mU/min. ICR and ISF were set to the mean values. Table 2.1 shows the estimated parameters. Figure 2.2 shows the meal response with an insulin bolus computed from different insulin-to-carb (ICR) ratios.

2.1.2 Results

Table 2.2 and Figure 2.3 shows the outcomes for the glycemic targets and Figure 2.4 shows the results. The blood glucose concentration oscillates a lot and the controller should not give as much insulin after glucagon. The glucagon response was much larger than we expected. We verified that the controller and heuristics were working as expected. The controller is more aggressive with glucagon than in the adult study, which was also as expected. The insulin basal rate for the participant (1.5 U/h) seemed to be a bit high. We noted that, there was a problem, where the app crashed after multiple missing measurements. We increased the penalty of deviating from the basal rate after this study to administer less insulin after glucagon administration to reduce oscillations.

Table 2.1: Participant 1. Parameter estimates for participant 1 in the phase 1 trial.

Parameter	Initial guess	Lower bound	Estimate	Upper bound	Unit
k_1	0.0167	0.00667	0.02	0.2	1/min
EGP	0.96	0.1	0.7	3	mg/(dL min)
$1/V_g$	0.0074	0.005	0.005	0.125	1/dL
k_m	0.027	0.00667	0.0184	0.1	1/min
Q_g	15	0	22.7	30	(mg/(dL min ^{1/2})) ²
$\log(Q_{\log SI})$	-11.5	-11.5	-11.5	-11.5	(L/(mU min ^{3/2})) ²
$I_{Sc}(0)$	0.0005	0	89.7	1e+06	mU/L
$I_P(0)$	34.3	0	2.99	1e+06	mU/L
$I_{Eff}(0)$	0.0567	0	0.00696	1e+06	1/min
$G(0)$	123	0	123	1e+06	mg/dL
$D_1(0)$	0.5	0	0.00494	0.005	mg
$D_2(0)$	0.5	0	0.00493	0.005	mg
$\log(SI(0))$	-6.65	-10	-8.3	0	$\log(L/(mU \text{ min}))$
$GEZI$	—	—	0.0023	—	1/min
ICR	—	—	6.71	—	g/U
ISF	—	—	1.93	—	mmol/(L U)

Table 2.2: Participant 1. Values of the glycemic targets for participant 1 in the phase 1 trial.

Quantity	Target	DH
Average glucose [mmol/L]	< 8.55	7.26
GMI [%]	< 7	6.44
GV [%]	≤ 36	39.16
Active CGM [%]	100	99.37

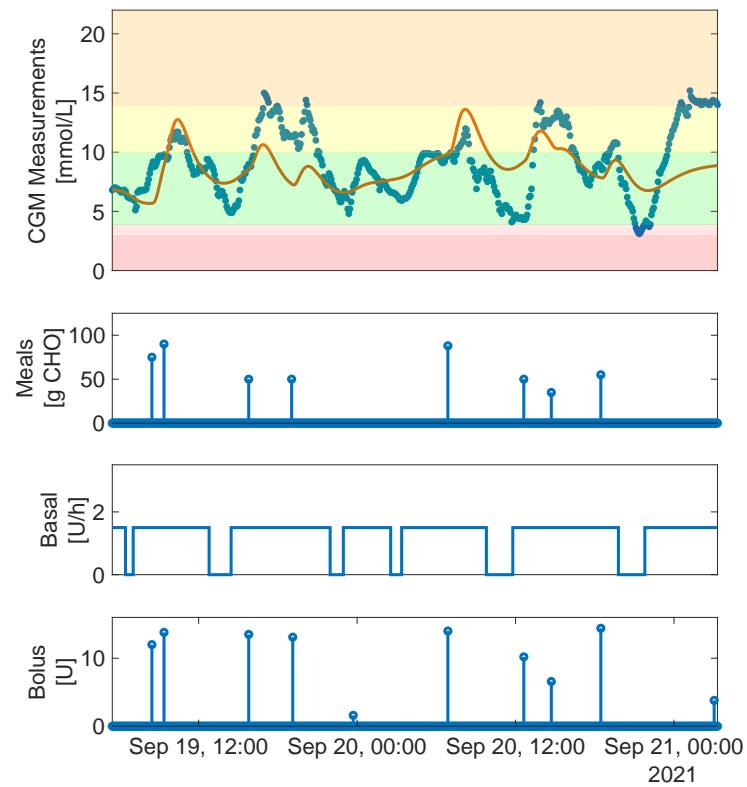


Figure 2.1: Participant 1. Parameter estimation for participant 1 in the phase 1 trial. From the top: 1) CGM measurements (blue dots) and a deterministic simulation with the estimated parameters (red line), 2) announced meals, 3) basal insulin rate, and 4) bolus insulin.

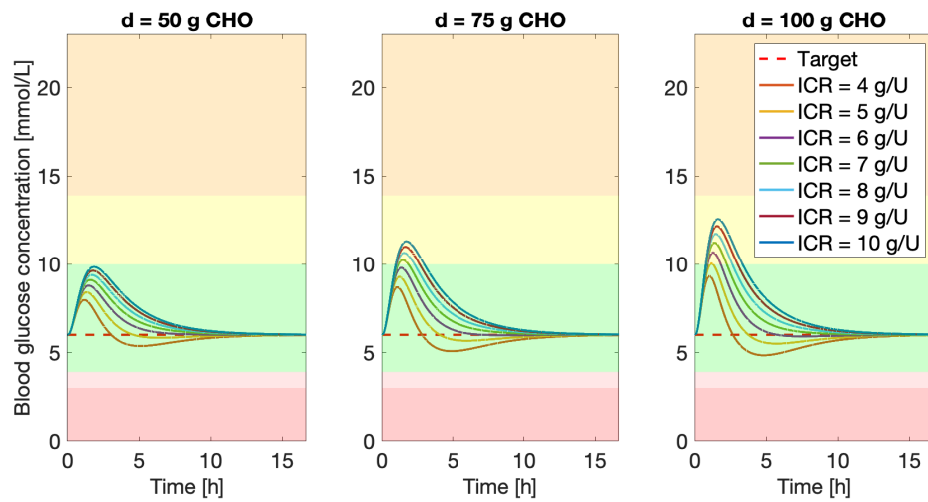


Figure 2.2: Participant 1. Evaluation of the meal response for participant 1 in the phase 1 trial with an insulin bolus computed using different ICRs.

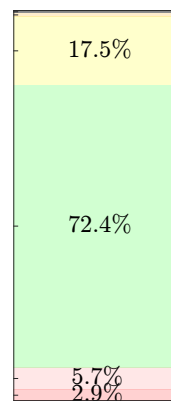


Figure 2.3: Participant 1. TIRs for the DH study for participant 1 in the phase 1 trial.

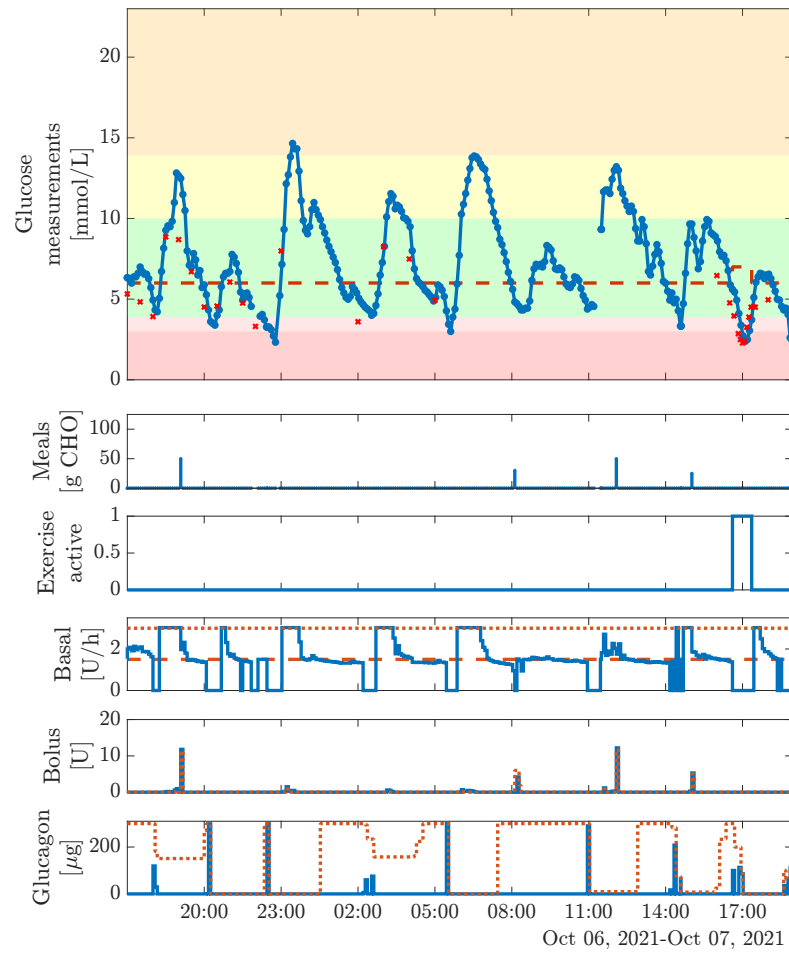


Figure 2.4: Participant 1. Results from the DH study for participant 1 in the phase 1 trial with 72.4% time in range. From the top: 1) CGM measurements (blue dotted line), YSI measurements (red crosses), and setpoint (red dashed line), 2) meals, 3) exercise, 4) basal insulin (blue line) and maximum allowed basal insulin (red dots), 5) insulin boli (blue line) and maximum allowed insulin boli (red dots), and 6) glucagon boli (blue line) and maximum allowed glucagon boli (red dots).

2.2 Participant 2

2.2.1 Parameter estimation

We used around 20 hours of data with 3 meals that all had a corresponding insulin bolus. Figure 2.5 shows the data used for estimation and a simulation with the estimated parameters. The fit for this participant was very good. In this study, we fixed EGP , k_m , and Q_{logSI} , and $1/V_g$ was on the boundary. $GEZI$ was tuned to make the estimated basal rate match the participants' normal basal rate which was ~ 18.68 mU/min. We computed ICR and ISF as the mean values for the participant. Table 2.3 shows the estimated parameters. Figure 2.6 shows the meal response for an insulin bolus computed from different ICRs.

2.2.2 Results

Table 2.4 and Figure 2.7 shows the outcomes for the glycemic targets and Figure 2.8 shows the results. This study went very well with nearly 100% TIR. Glucagon was administered to prevent hypoglycemic events after dinner and also kept the participant in range during exercise. After the study, we discussed if the penalty on hyperglycemia should be changed, but we did not make any changes after this study.

Table 2.3: Participant 2. Parameter estimates for participant 2 in the phase 1 trial.

Desc	Param.	init.	lb.	estim.	ub.	unit
inv. ins. TC	k_1	0.0167	0.00667	0.0169	0.2	1/min
ins. sens.	$\log(SI(0))$	-6.65	-10	-8	0	$\log((1/(\text{mU/L}))/\text{min})$
Endo. gluc. prod	EGP	0.96	0.1	0.6	3	(mg/dL)/min
inv. dist. vol.	$1/V_g$	0.0952	0.005	0.005	0.125	1/dL
inv. meal TC	k_m	0.027	0.00667	0.02	0.1	1/min
IC ins. sub.	$I_{Sc}(0)$	0.0005	0	68.6	1e+06	mU/L
IC ins. plas.	$I_P(0)$	34.3	0	0.834	1e+06	mU/L
IC ins. eff.	$I_{Eff}(0)$	0.0567	0	0.119	1e+06	1/min
IC gluc. conc.	$G(0)$	187	0	188	1e+06	mg/dL
IC meal 1	$D_1(0)$	0.5	0	111	300	mg
IC meal 2	$D_2(0)$	0.5	0	230	300	mg
gluc. cov.	Q_g	15	0	14.4	30	-
ins. cov.	$\log(Q_{\log SI})$	-11.5	-11.5	-11.5	-11.5	-
gluc. eff.	$GEZI$	-	-	0.00146	-	1/min
ins. to carb. rat.	ICR	-	-	7.04	-	g/U
ins. sens. fac.	ISF	-	-	1.16	-	mmol/L/U

Table 2.4: Participant 2. Values of the glycemic targets for participant 2 in the phase 1 trial.

Quantity	Target	DH
Average glucose [mmol/L]	< 8.55	6.25
GMI [%]	< 7	6.00
GV [%]	≤ 36	21.13
Active CGM [%]	100	100.0

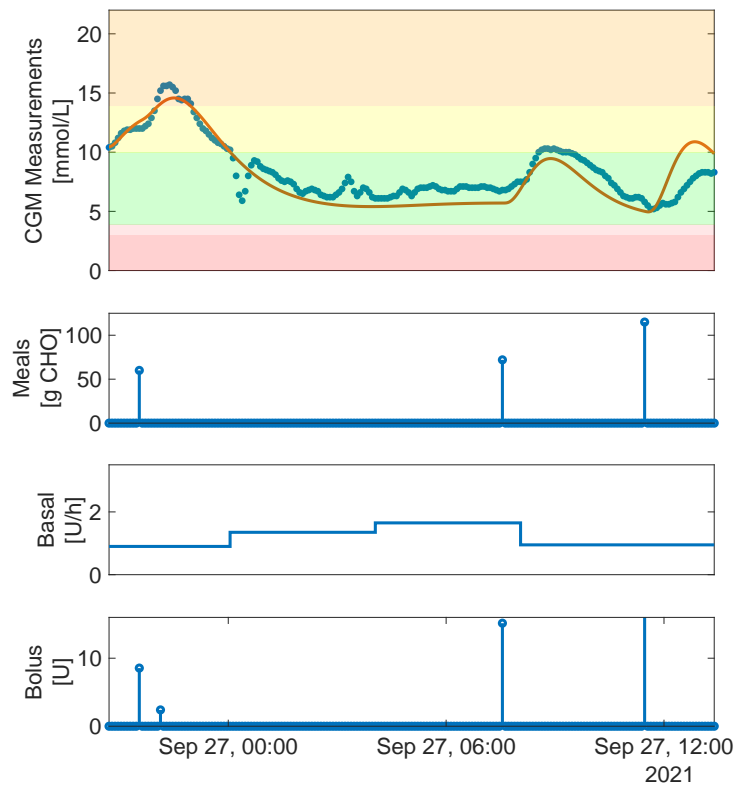


Figure 2.5: Participant 2. Parameter estimation for participant 2 in the phase 1 trial. From the top: 1) CGM measurements (blue dots) and a deterministic simulation with the estimated parameters (red line), 2) announced meals, 3) basal insulin rate, and 4) bolus insulin.

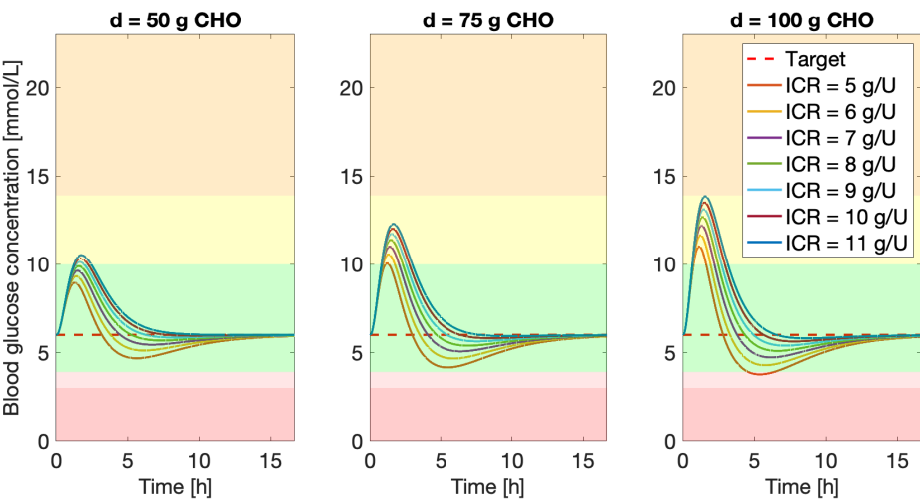


Figure 2.6: Participant 2. Evaluation of the meal responses participant 2 in the phase 1 trial with an insulin bolus computed from different ICRs.

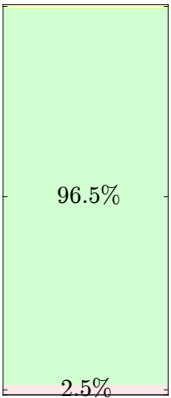


Figure 2.7: Participant 2. TIRs for the DH study for participant 2 in the phase 1 trial.

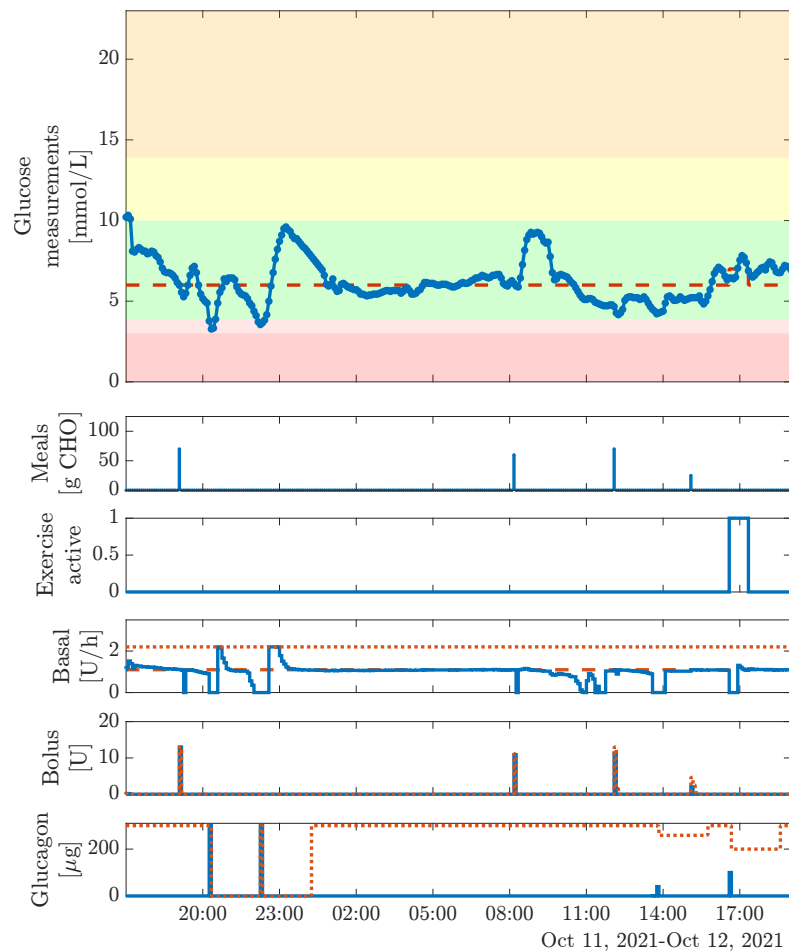


Figure 2.8: Participant 2. Results from the DH study for participant 2 in the phase 1 trial with 96.5% time in range. From the top: 1) CGM measurements (blue dotted line) and setpoint (red dashed line), 2) meals, 3) exercise, 4) basal insulin (blue line) and maximum allowed basal insulin (red dots), 5) insulin boli (blue line) and maximum allowed insulin boli (red dots), and 6) glucagon boli (blue line) and maximum allowed glucagon boli (red dots).

2.3 Participant 3

2.3.1 Parameter estimation

We used around 13 hours of data with 3 meals that had a corresponding insulin bolus. There seems to be a missing meal around 10:00, but this was the best data we could find. Figure 2.9 shows the data used for estimation and a simulation with the estimated parameters. The fit is very good over night, but the meal responses are less accurate, which could be because of a missing meal. In this study, we fixed EGP , k_m , k_1 , and Q_{logSI} and $1/V_g$ was on the boundary. $GEZI$ was tuned to make the estimated basal rate match the participants' normal basal rate which was ~ 14.76 mU/min. For the 2 previous participants the meal time constant was for 1) fixed at 50 minutes and for 2) estimated to be around 50 minutes, but we observed that the model predicted that meals had a longer response, than what the results showed. Therefore, we fixed the meal time constant to 40 minutes for this participant, which also seemed to match the data used for estimation. We computed ICR and ISF as the mean values for the participant. Table 2.5 shows the estimated parameters and Figure 2.10 shows the meal response for an insulin bolus computed from different ICRs.

2.3.2 Results

Table 2.6 and Figure 2.11 shows the outcomes for the glycemic targets and Figure 2.12 shows the results. This study also resulted in a high TIR and a low amount of time in hypoglycemia, but the app crashed around 11:00, which meant not all glucagon was administered. Therefore, the participant also required rescue carbs. If the app had not crashed, the peak before the snack could possibly have been avoided. We decided to continue to calibrate xDrip before the studies as the CGM and YSI measurements were consistent. After this study, we decided to reduce the allowed meal bolus factor from 1.3 to 1.15 based on the results from the phase 1 trial and decided that the AP was ready to start phase 2.

Table 2.5: Participant 3. Parameter estimates for participant 3 in the phase 1 trial.

Desc	Param.	init.	lb.	estim.	ub.	unit
inv. ins. TC	k_1	0.0167	0.00667	0.0167	0.2	1/min
ins. sens.	$\log(SI(0))$	-6.65	-10	-7.68	0	$\log((1/(\text{mU/L}))/\text{min})$
Endo. gluc. prod	EGP	0.96	0.1	0.6	3	(mg/dL)/min
inv. dist. vol.	$1/V_g$	0.0952	0.005	0.005	0.125	1/dL
inv. meal TC	k_m	0.027	0.00667	0.025	0.1	1/min
IC ins. sub.	$I_{Sc}(0)$	0.0005	0	33	1e+06	mU/L
IC ins. plas.	$I_P(0)$	34.3	0	0.000837	1e+06	mU/L
IC ins. eff.	$I_{Eff}(0)$	0.0567	0	0.0163	1e+06	1/min
IC gluc. conc.	$G(0)$	119	0	120	1e+06	mg/dL
IC meal 1	$D_1(0)$	0.5	0	10	10	mg
IC meal 2	$D_2(0)$	0.5	0	10	10	mg
gluc. cov.	Q_g	15	0	18.5	30	-
ins. cov.	$\log(Q_{\log SI})$	-11.5	-11.5	-11.5	-11.5	-
gluc. eff.	$GEZI$	-	-	0.0011	-	1/min
ins. to carb. rat.	ICR	-	-	9.75	-	g/U
ins. sens. fac.	ISF	-	-	3	-	mmol/L/U

Table 2.6: Participant 3. Values of the glycemic targets for participant 3 in the phase 1 trial.

Quantity	Target	DH
Average glucose [mmol/L]	< 8.55	7.36
GMI [%]	< 7	6.48
GV [%]	≤ 36	26.47
Active CGM [%]	100	96.86

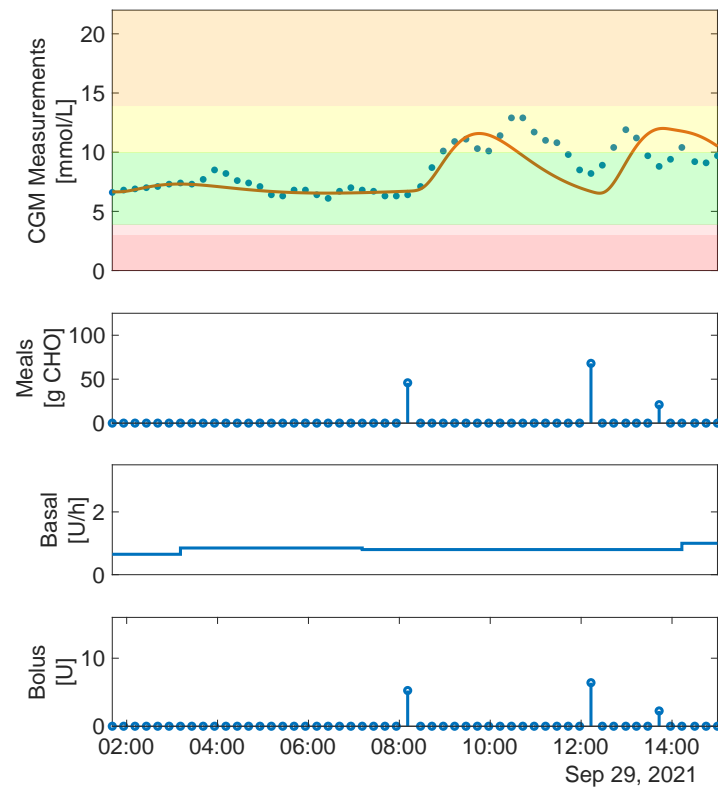


Figure 2.9: Participant 3. Parameter estimation for participant 3 in the phase 1 trial. From the top: 1) CGM measurements (blue dots) and a deterministic simulation with the estimated parameters (red line), 2) announced meals, 3) basal insulin rate, and 4) bolus insulin.

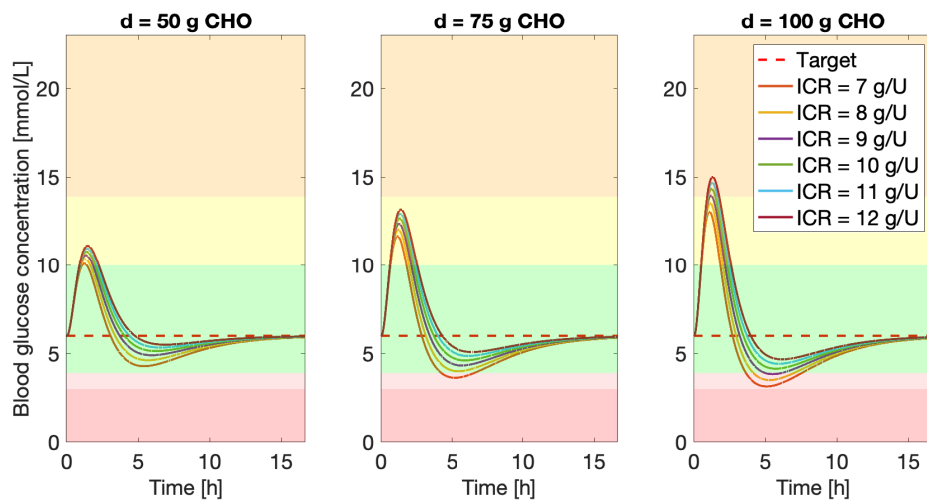


Figure 2.10: Participant 3. Evaluation of the meal responses for participant 3 in the phase 1 trial with an insulin bolus computed from different ICRs.

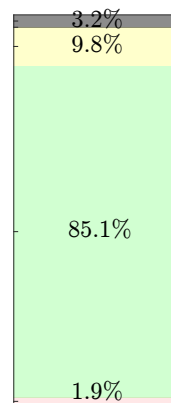


Figure 2.11: Participant 3. TIRs for the DH study for participant 3 in the phase 1 trial.

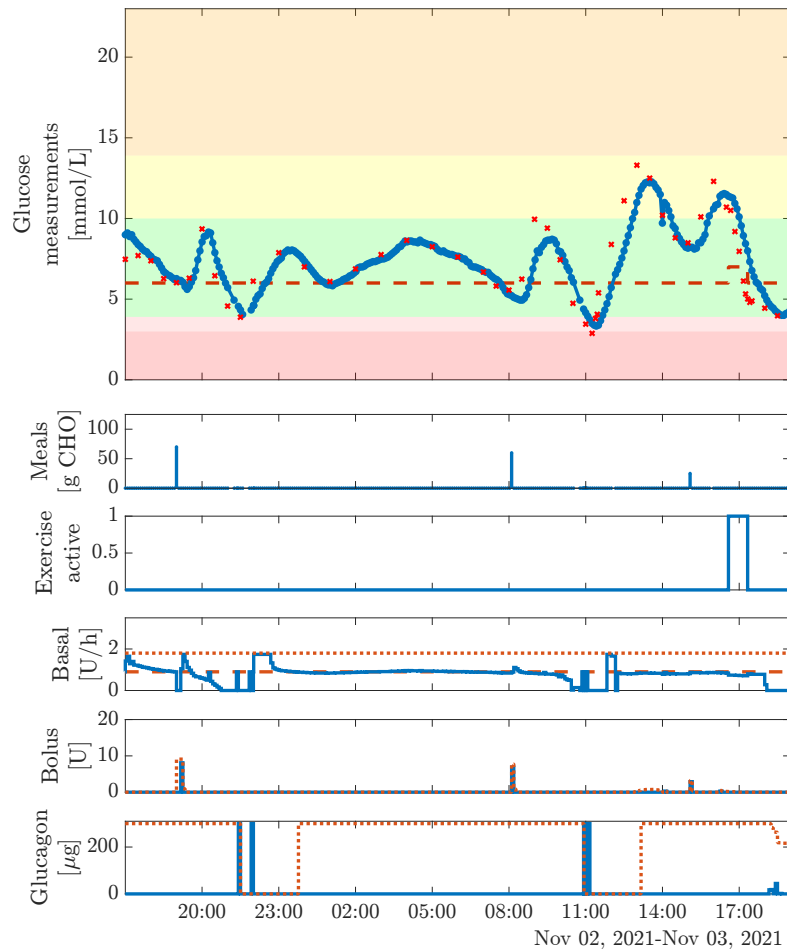


Figure 2.12: Participant 3. Results from the DH study for participant 3 in the phase 1 trial with 85.1% time in range. From the top: 1) CGM measurements (blue dotted line), YSI measurements (red crosses), and setpoint (red dashed line), 2) meals, 3) exercise, 4) basal insulin (blue line) and maximum allowed basal insulin (red dots), 5) insulin boli (blue line) and maximum allowed insulin boli (red dots), and 6) glucagon boli (blue line) and maximum allowed glucagon boli (red dots).

CHAPTER 3

Phase 2 trial

In this chapter, we show the parameter estimation and results from all the DH and SH studies in the phase 2 trial. Here, the studies are shown in the order of when both the DH and SH study was completed. Therefore, e.g. participant 4 had their first visit before participant 3. We did not make any changes to the algorithm during the phase 2 trial. However, we changed the time series charts to show dots instead of lines in the app, as the chart library had a memory leak in the line chart. The memory leak was also the reason why the app sometimes crashed during the phase 1 trial.

3.1 Participant 1

3.1.1 Parameter estimation

We had trouble finding suitable data for this participant and ended using data from only one night and breakfast. Figure 3.1 shows the data used for estimation and a simulation with the estimated parameters. The meal response seems to fit relatively well, but the fit over night is less accurate which indicates that the basal rate was hard to estimate. In this study, we fixed EGP , k_1 , and Q_{logSI} . $GEZI$ was tuned to make the estimated basal rate match the participants' normal basal rate which was ~ 11.94 mU/min. We computed ICR and ISF as the mean values for the participant. In the phase 1 trial, we observed that the meals have had a longer and larger response in the predictions than what the actual data showed. Therefore, we reduced the lower bound on $1/Vg$ in this study. We ended up increasing the lower bound on $1/Vg$ again later in the phase 2 trial, as it did not have the desired effect. Table 3.2 shows the estimated parameters. Fig 3.2 shows the meal response for an insulin bolus computed from different ICRs. The meal responses indicated that the algorithm would most likely be conservative with the meal boli to avoid hypoglycemia.

3.1.2 Results

Table 3.2 and Figure 3.3 shows the outcomes for the glycemic targets and Figure 3.4 shows the results. Overall, the participant received too little insulin in both studies, which also lead to a high amount of time in hyperglycemia. The meal effect seemed to be underestimated and correction boli were administered in both studies. We believe this was, partly, because the lower bound on $1/Vg$ was reduced in the parameter estimation.

Table 3.1: Participant 1. Parameter estimates for participant 1 in the phase 2 trial.

Parameter	Initial guess	Lower bound	Estimate	Upper bound	Unit
k_1	0.0167	0.00667	0.02	0.2	1/min
EGP	0.96	0.1	0.5	3	mg/(dL min)
$1/V_g$	0.0952	0.00333	0.00369	0.125	1/dL
k_m	0.027	0.00667	0.0487	0.1	1/min
Q_g	15	0	7.27	30	$(\text{mg}/(\text{dL min}^{1/2}))^2$
$\log(Q_{\log SI})$	-11.5	-11.5	-11.5	-11.5	$(\text{L}/(\text{mU min}^{3/2}))^2$
$I_{Sc}(0)$	0.0005	0	3.05e-05	1e+06	mU/L
$I_P(0)$	34.3	0	4.38e-05	1e+06	mU/L
$I_{Eff}(0)$	0.0567	0	0.0103	1e+06	1/min
$G(0)$	133	0	128	1e+06	mg/dL
$D_1(0)$	0.5	0	10	10	mg
$D_2(0)$	0.5	0	2.44e-05	10	mg
$\log(SI(0))$	-6.65	-10	-7.87	0	$\log(\text{L}/(\text{mU min}))$
$GEZI$	—	—	0.0015	—	1/min
ICR	—	—	8.29	—	g/U
ISF	—	—	2.35	—	mmol/(L U)

In both studies there also seemed to be a dawn effect. In the SH study, the dinner meal bolus was given manually without the algorithm knowing, as there was a problem with the insulin pump. The glucose concentration was stabilized over night in the SH study, due to the multiple correction boli that was administered after dinner. The amount of carbs in the breakfast was underestimated and caused a large post prandial peak and a correction bolus. In the DH study, the participant entered the clinic with slight hypoglycemia and received glucagon. The AP was unable to stabilize the glucose concentration over night. After the lunch, the basal rate is set to 0 due to the predictions (possibly the connection was also lost), which causes the following increase in the glucose concentration. In the DH study, the CGM measurements were higher than the YSI measurements in most of the study.

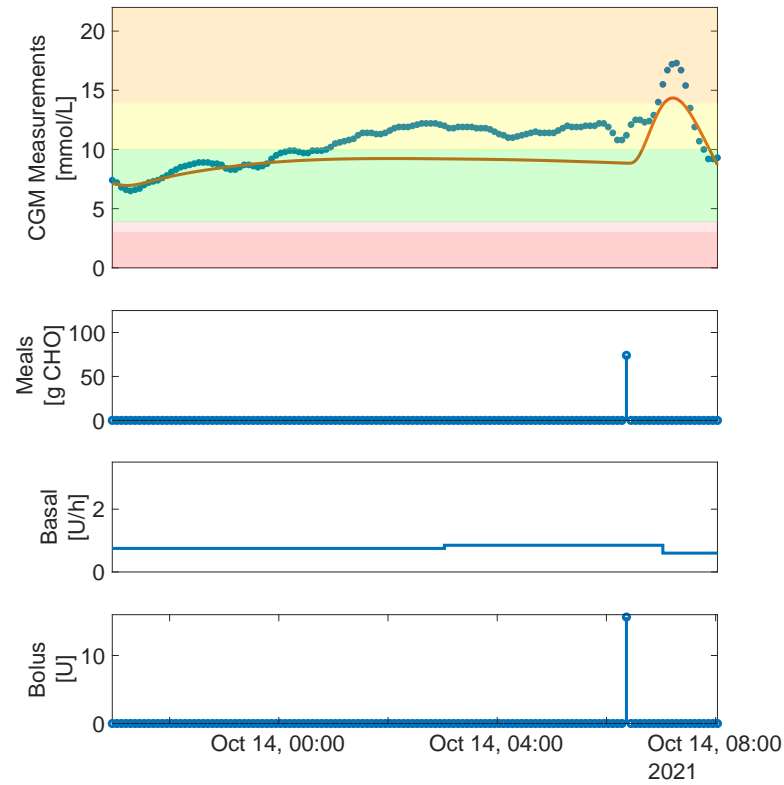


Figure 3.1: Participant 1. Parameter estimation for participant 1 in the phase 2 trial. From the top: 1) CGM measurements (blue dots) and a simulation with the estimated parameters (red line), 2) announced meals, 3) basal insulin rate, and 4) bolus insulin.

Table 3.2: Values of the glycemic targets for participant 1 in the phase 2 trial.

Quantity	Target	DH	SH
Average glucose [mmol/L]	< 8.55	10.19	10.81
GMI [%]	< 7	7.70	7.97
GV [%]	≤ 36	26.90	31.94
Active CGM [%]	100	100.0	100.0

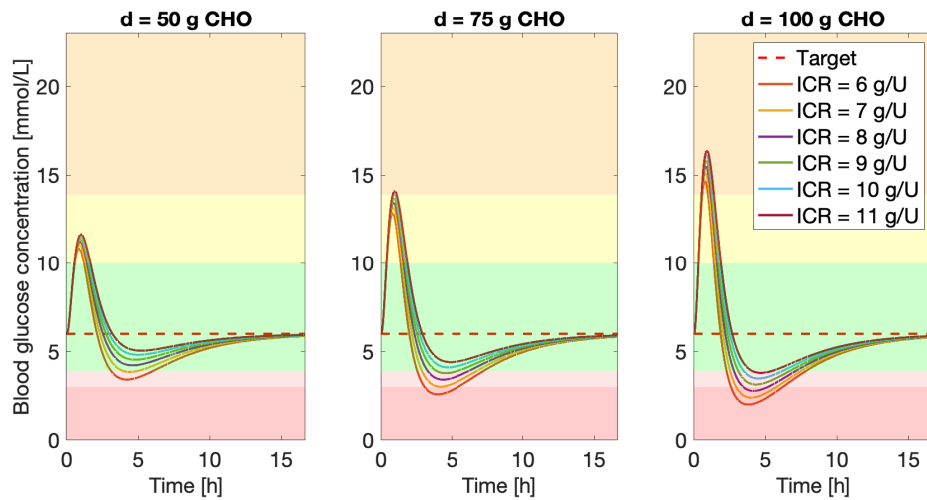


Figure 3.2: Participant 1. Evaluation of the meal responses for participant 1 in the phase 2 trial with an insulin bolus computed from different ICRs.

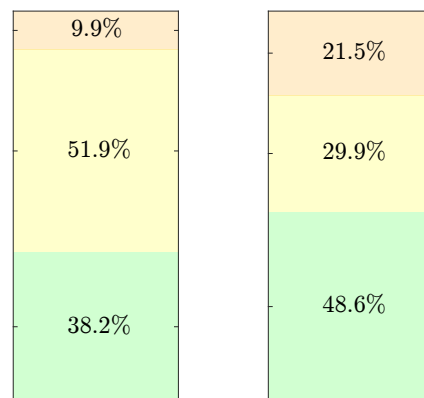


Figure 3.3: Participant 1. Left: TIRs for the DH study for participant 1 in the phase 2 trial. Right: TIRs for the SH study for participant 1 in the phase 2 trial.

3.1 Participant 1

25

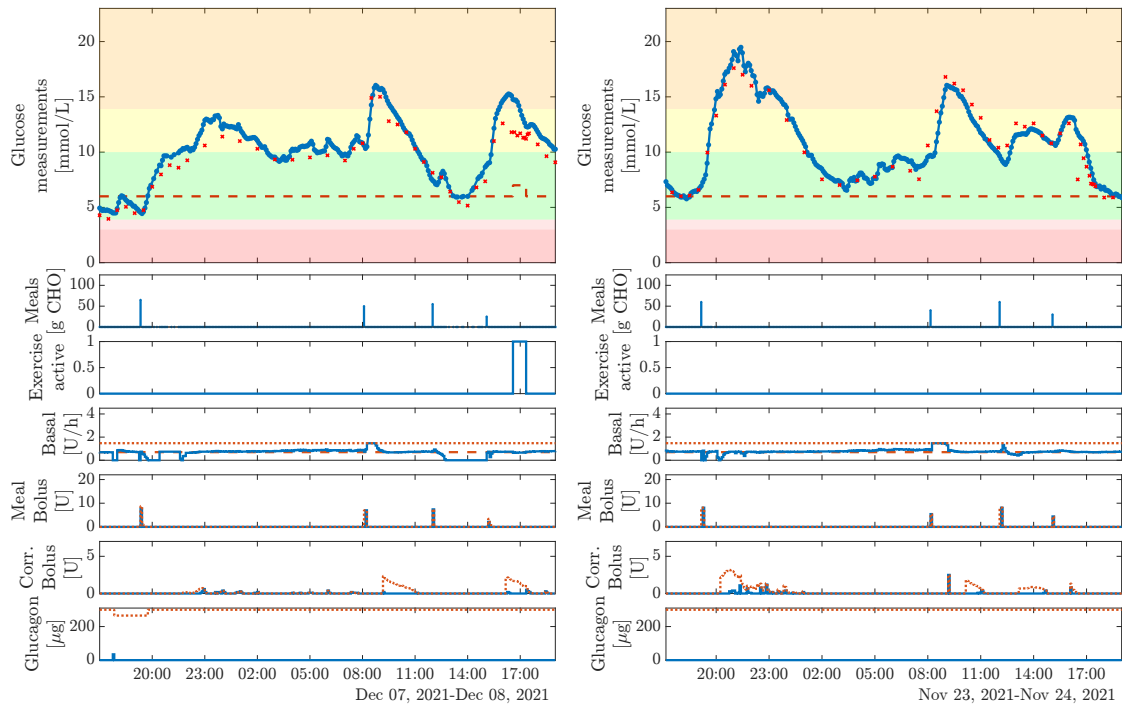


Figure 3.4: Participant 1. Left: Results from the DH study for participant 1 in the phase 2 trial with 38.2% time in range. Right: Results from the SH study for participant 1 in the phase 2 trial with 46.6% time in range. From the top: 1) CGM measurements (blue dotted line), YSI measurements (red crosses), and setpoint (red dashed line), 2) meals, 3) exercise, 4) basal insulin (blue line) and maximum allowed basal insulin (red dots), 5) meal boli (blue line) and maximum allowed meal boli (red dots), 6) correction insulin boli (blue line) and maximum allowed correction boli (red dots), and 7) glucagon boli (blue line) and maximum allowed glucagon boli (red dots).

3.2 Participant 2

3.2.1 Parameter estimation

The data for this patient was quite challenging. Again, we used data from one night and a breakfast and it seemed like unannounced rescue carbs were consumed after the breakfast, but this was the best data available. The meal was shifted 20 minutes earlier to fit the peak in glucose concentration. Figure 3.5 shows the data used for estimation and a simulation with the estimated parameters. Overall, the fit was relatively good, but the model was unable to describe the increases after breakfast which could be because of unannounced carbohydrates. We fixed EGP , k_m , k_1 , and Q_{logSI} for this participant, and $1/V_g$ was at its lower bound. $GEZI$ was tuned to correct the basal rate to the participants' normal basal rate which was ~ 14.13 mU/min. We computed ICR and ISF as mean values for the participant. Table 3.4 shows the estimated parameters. Figure 3.6 shows the meal response for an insulin bolus computed from different ICRs. A bolus corresponding to the participants regular ICR results in slight hypoglycemia, which causes the AP to be conservative with the meal boli, but we were unable to avoid it with the data from this participant.

3.2.2 Results

Table 3.4 and Figure 3.7 shows the outcomes for the glycemic targets and Figure 3.8 shows the results. In both studies the meal boli seemed to be too small. The AP was allowed to administer more insulin, but did not. In retrospect, we could have predicted that based on the meal responses from the parameter estimation. Instead the AP administers some correction boli after the predictions are updated, but the participant still

Table 3.3: Parameter estimates for participant 2 in the phase 2 trial.

Desc	Param.	init.	lb.	estim.	ub.	unit
inv. ins. TC	k_1	0.0167	0.00667	0.02	0.2	1/min
ins. sens.	$\log(SI(0))$	-6.65	-10	-7.13	0	$\log((1/(\text{mU/L}))/\text{min})$
Endo. gluc. prod	EGP	0.96	0.1	1	3	(mg/dL)/min
inv. dist. vol.	$1/V_g$	0.00667	0.00455	0.00455	0.125	1/dL
inv. meal TC	k_m	0.027	0.00667	0.025	0.1	1/min
IC ins. sub.	$I_{Sc}(0)$	0.0005	0	19.3	1e+06	mU/L
IC ins. plas.	$I_P(0)$	34.3	0	70.1	1e+06	mU/L
IC ins. eff.	$I_{Eff}(0)$	0.0567	0	0.0914	1e+06	1/min
IC gluc. conc.	$G(0)$	164	0	167	1e+06	mg/dL
IC meal 1	$D_1(0)$	0.5	0	100	100	mg
IC meal 2	$D_2(0)$	0.5	0	100	100	mg
gluc. cov.	Q_g	15	0	15	30	-
ins. cov.	$\log(Q_{logSI})$	-11.5	-11.5	-11.5	-11.5	-
gluc. eff.	$GEZI$	-	-	0.0016	-	1/min
ins. to carb. rat.	ICR	-	-	8.5	-	g/U
ins. sens. fac.	ISF	-	-	2.12	-	mmol/L/U

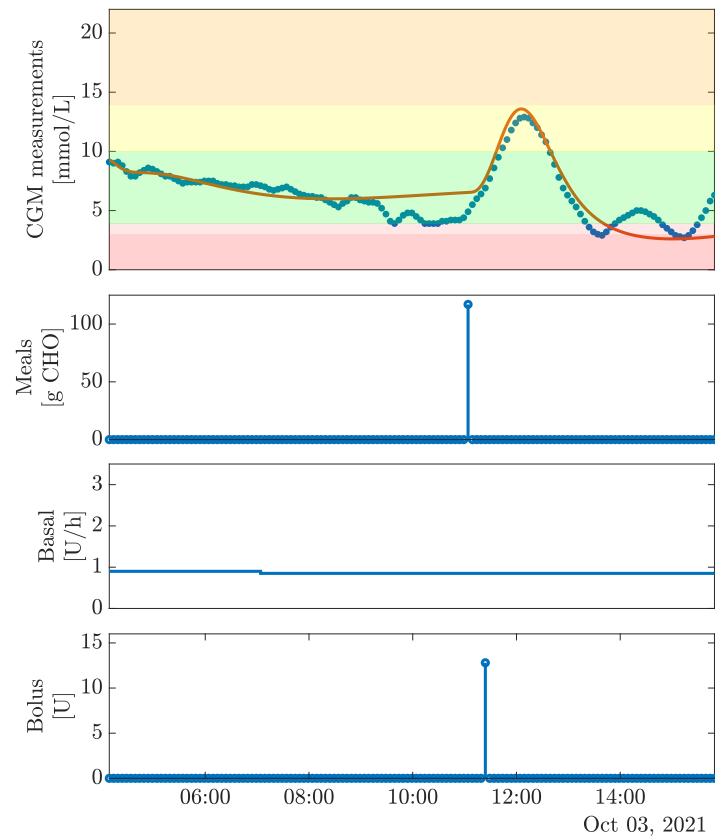


Figure 3.5: Participant 2. Parameter estimation for participant 2 in the phase 2 trial. From the top: 1) CGM measurements (blue dots) and a simulation with the estimated parameters (red line), 2) announced meals, 3) basal insulin rate, and 4) bolus insulin.

receives too little insulin. The participant started the SH study in hypoglycemia and received dextrose. During the SH study it seemed like multiple pressure induced sensor attenuations (PISAs) occurred, where the most significant one was before breakfast. In the DH study, the AP administered glucagon when the participant was approaching hypoglycemia. The glucagon response was very large and the basal rate was increased, which caused oscillations during the night. During the day, the meal boli are too small and even though correction boli are administered, the glucose concentration remained high.

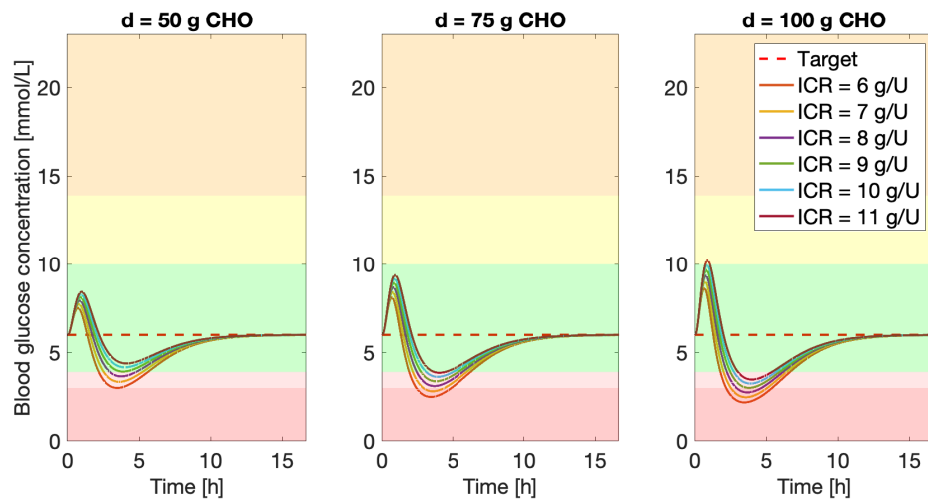


Figure 3.6: Participant 2. Evaluation of the meal responses for participant 2 in the phase 2 trial with an insulin bolus computed from different ICRs.

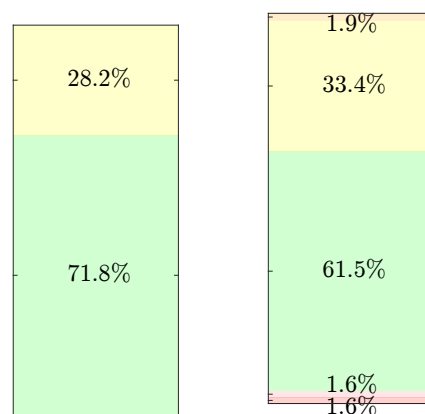


Figure 3.7: Participant 2. Left: TIRs for the DH study for participant 2 in the phase 2 trial. Right: TIRs for the SH study for participant 2 in the phase 2 trial.

Table 3.4: Values of the glycemic targets for participant 2 in the phase 2 trial.

Quantity	Target	DH	SH
Average glucose [mmol/L]	< 8.55	8.62	8.74
GMI [%]	< 7	7.03	7.08
GV [%]	≤ 36	22.42	31.94
Active CGM [%]	100	100.0	100.0

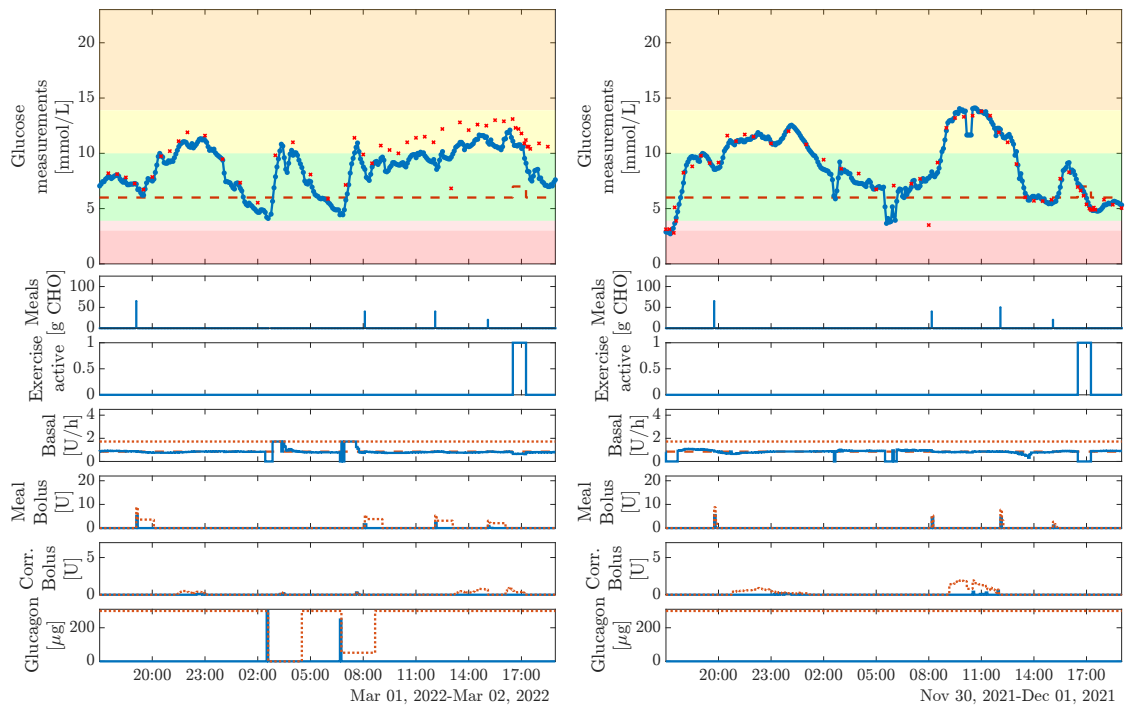


Figure 3.8: Participant 2. Left: Results from the DH study for participant 2 in the phase 2 trial with 71.8% time in range. Right: Results from the SH study for participant 2 in the phase 2 trial with 61.5% time in range. From the top: 1) CGM measurements (blue dotted line), YSI measurements (red crosses), and setpoint (red dashed line), 2) meals, 3) exercise, 4) basal insulin (blue line) and maximum allowed basal insulin (red dots), 5) meal bolus (blue line) and maximum allowed meal bolus (red dots), 6) correction insulin bolus (blue line) and maximum allowed correction bolus (red dots), and 7) glucagon bolus (blue line) and maximum allowed glucagon bolus (red dots).

3.3 Participant 3

3.3.1 Parameter estimation

This participant was using a closed-loop system and therefore all the administered insulin comes from insulin boli. The basal rate acts as a fallback mode and was active for around 2 hours around 15:00. Figure 3.9 shows the data used for estimation and a simulation with the estimated parameters. The meal response in the simulation was rather large, but that did also seem to match the data and overall this seemed to be one of the better fits. We fixed k_m , k_1 , and EGP for this participant. $GEZI$ was tuned to correct the basal rate to match the participants' normal basal rate which was ~ 23.61 mU/min. Here, we set the ICR slightly below the average as it seemed to be higher for dinner and during the night compared to breakfast. We computed ISF as the mean value for the participant. Table 3.5 shows the estimated parameters. Figure 3.10 shows the meal response for an insulin bolus computed from different ICRs.

3.3.2 Results

Table 3.6 and Figure 3.11 shows the outcomes for the glycemic targets and Figure 3.12 shows the results. Overall, the AP performed very well for this participant, but unfortunately the connection to the pump was lost for most of the day during the DH study. In both studies, the AP managed to stabilize the participant at the setpoint over night and achieved high TIR. The participant entered the clinic in level 2 hyperglycemia in the SH study and received both a manual bolus before the study and correction boli when the AP was activated. The participant was not in hypoglycemia, but felt hypoglycemic and specifically asked for carbs. The AP reduced the basal rate, but the

Table 3.5: Parameter estimates for participant 3 in the phase 2 trial.

Desc	Param.	init.	lb.	estim.	ub.	unit
inv. ins. TC	k_1	0.0167	0.0111	0.0167	0.2	1/min
ins. sens.	$\log(SI(0))$	-8.15	-10	-8.6	0	$\log((1/(\text{mU/L}))/\text{min})$
Endo. gluc. prod	EGP	1.11	0.1	0.4	3	(mg/dL)/min
inv. dist. vol.	$1/V_g$	0.005	0.00455	0.00455	0.125	1/dL
inv. meal TC	k_m	0.02	0.0111	0.025	0.1	1/min
IC ins. sub.	$I_{Sc}(0)$	14.8	0	16.9	1e+06	mU/L
IC ins. plas.	$I_P(0)$	80.1	0	6.79e-06	1e+06	mU/L
IC ins. eff.	$I_{Eff}(0)$	0.0212	0	0.0147	1e+06	1/min
IC gluc. conc.	$G(0)$	140	0	151	1e+06	mg/dL
IC meal 1	$D_1(0)$	10	0	10	10	mg
IC meal 2	$D_2(0)$	10	0	10	10	mg
gluc. cov.	Q_g	20.3	0	22.3	30	-
ins. cov.	$\log(Q_{\log SI})$	-9.21	-11.5	-9.35	-9.21	-
gluc. eff.	$GEZI$	-	-	0.00073	-	1/min
ins. to carb. rat.	ICR	-	-	7.500	-	g/U
ins. sens. fac.	ISF	-	-	1.800	-	mmol/L/U

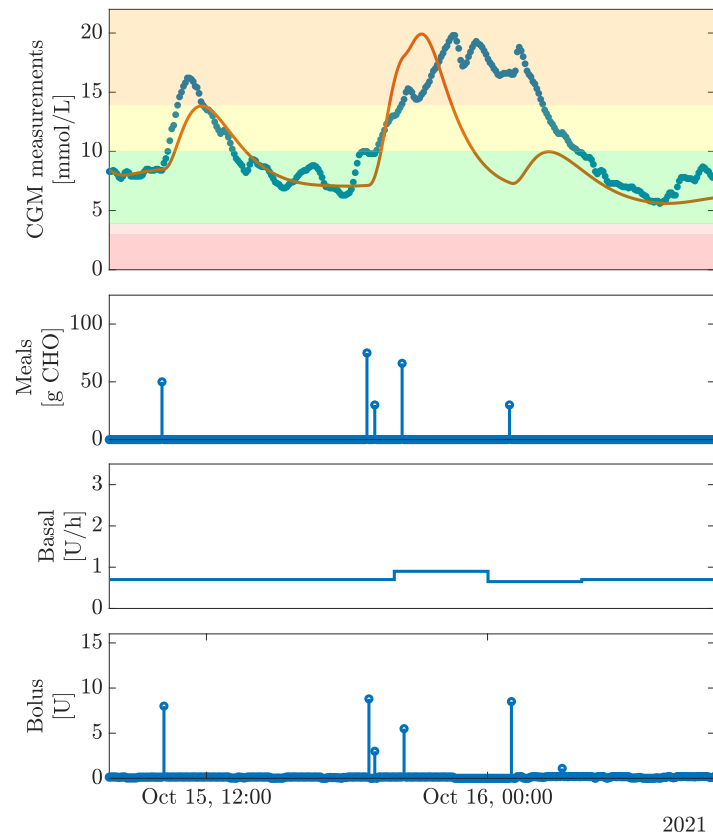


Figure 3.9: Participant 3. Parameter estimation for participant 3 in the phase 2 trial. From the top: 1) CGM measurements (blue dots) and a simulation with the estimated parameters (red line), 2) announced meals, 3) basal insulin rate, and 4) bolus insulin.

carbs might have prevented hypoglycemia. In the DH study, the AP handled both the dinner and night very well, but after breakfast, the connection to the insulin pump was lost until around 15:20. A large amount of insulin was administered after the insulin pump was reconnected. The high amount of insulin was administered just before the exercise session and resulted in administration of glucagon to prevent hypoglycemia.

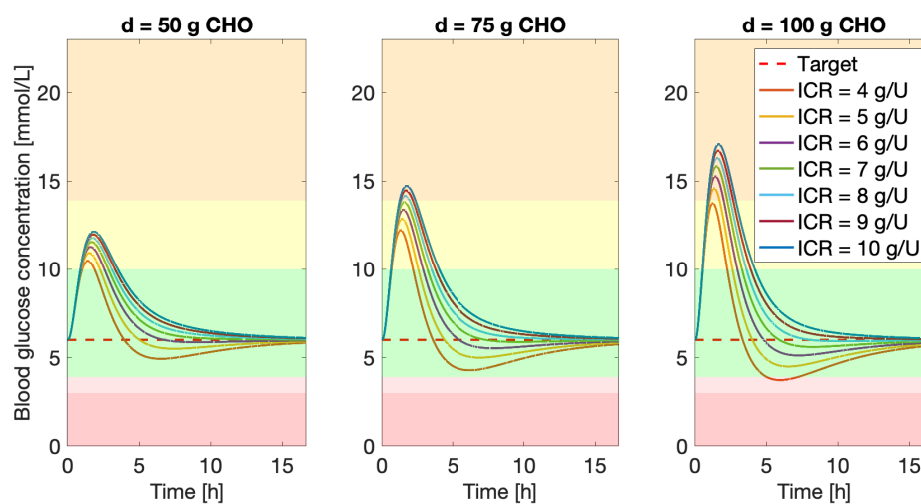


Figure 3.10: Participant 3. Evaluation of the meal responses with an insulin bolus computed from different ICRs.

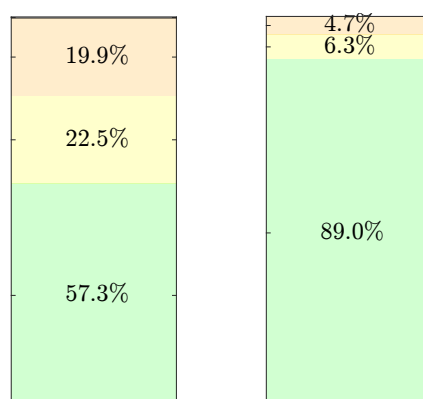


Figure 3.11: Participant 3. Left: TIRs for the DH study for participant 3 in the phase 2 trial. Right: TIRs for the SH study for participant 3 in the phase 2 trial.

Table 3.6: Values of the glycemic targets for participant 3 in the phase 2 trial.

Quantity	Target	DH	SH
Average glucose [mmol/L]	< 8.55	9.63	7.02
GMI [%]	< 7	7.46	6.33
GV [%]	≤ 36	38.43	47.97
Active CGM [%]	100	99.68	100.0

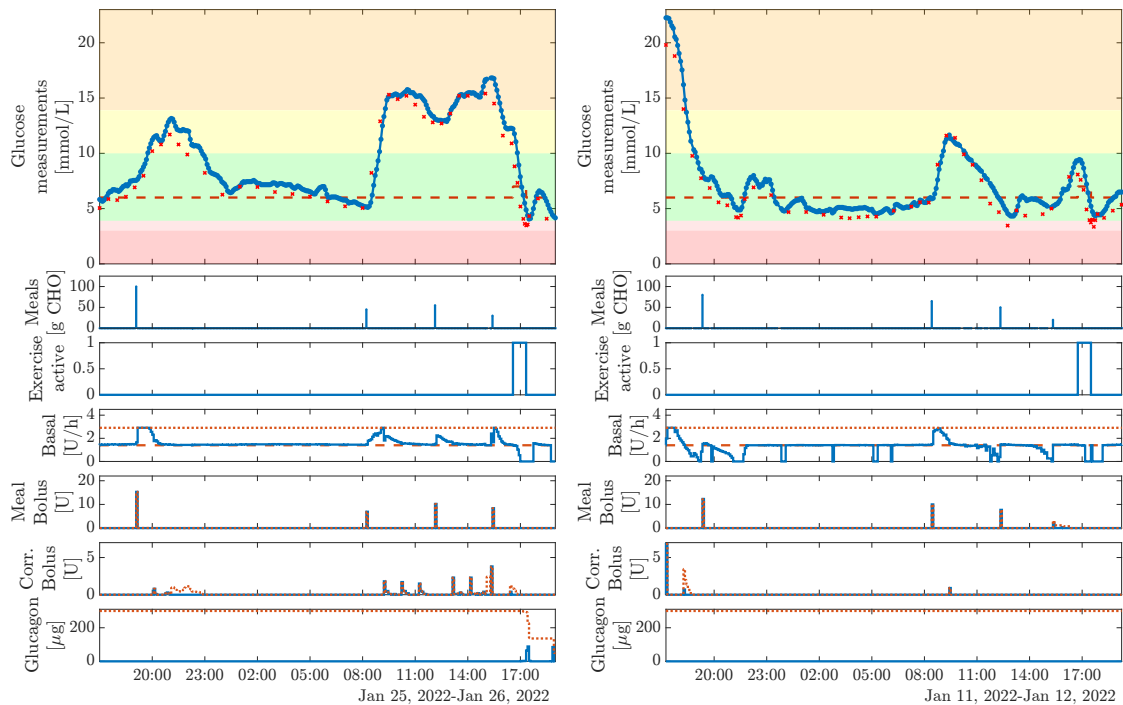


Figure 3.12: Participant 3. Left: Results from the DH study for participant 3 in the phase 2 trial with 57.3% time in range. Right: Results from the SH study for participant 3 in the phase 2 trial with 89.0% time in range. From the top: 1) CGM measurements (blue dotted line), YSI measurements (red crosses), and setpoint (red dashed line), 2) meals, 3) exercise, 4) basal insulin (blue line) and maximum allowed basal insulin (red dots), 5) meal boli (blue line) and maximum allowed meal boli (red dots), 6) correction insulin boli (blue line) and maximum allowed correction boli (red dots), and 7) glucagon boli (blue line) and maximum allowed glucagon boli (red dots).

3.4 Participant 4

3.4.1 Parameter estimation

This participant also used a closed-loop system. We used data from one night and a breakfast to estimate the parameters. Figure 3.13 shows the data used for estimation and a simulation with the estimated parameters. There might have been an unannounced snack during the night or evening, which caused the closed-loop system to administer a correction bolus. The meal response was rather small for a meal with around 100g carbohydrates compared to the other participants, but this was the best data available. We fixed k_m , k_1 , and $Q_{\log SI}$ for this participant and $GEZI$ was tuned to correct the basal rate to match the participants' normal basal rate which was ~ 9.028 mU/min. We computed ISF as the mean values for the participant. The participant used ICR values between 8 and 21 g/U in the closed-loop system. For the meals where the ICR is set to 21 g/U, the participant seemed to rely on correction boli that are automatically administered by the closed-loop system. Therefore, we chose to set the ICR to 13 even though the weighted mean was 19 g/U. Table 3.7 shows the estimated parameters and Figure 3.14 shows the meal response for an insulin bolus computed from different ICRs.

3.4.2 Results

Table 3.8 and Figure 3.15 shows the outcomes for the glycemic targets and Figure 3.16 shows the results. The DH study resulted in a very low TIR and high time in hyperglycemia compared to the SH study. No glucagon was administered during the DH study which means the control algorithm was identical for the 2 studies. Around 10U insulin more was administered in the DH study compared to the SH study and a

Table 3.7: Parameter estimates for participant 4 in the phase 2 trial.

Desc	Param.	init.	lb.	estim.	ub.	unit
inv. ins. TC	k_1	0.0182	0.0111	0.0167	0.2	1/min
ins. sens.	$\log(SI(0))$	-7.5	-10	-7.32	0	$\log((1/(\text{mU/L}))/\text{min})$
Endo. gluc. prod	EGP	0.96	0.5	0.5	3	(mg/dL)/min
inv. dist. vol.	$1/V_g$	0.00402	0.005	0.00515	0.125	1/dL
inv. meal TC	k_m	0.027	0.0111	0.02	0.1	1/min
IC ins. sub.	$I_{Sc}(0)$	0.0005	0	0.00114	1e+06	mU/L
IC ins. plas.	$I_P(0)$	34.3	0	3.84	1e+06	mU/L
IC ins. eff.	$I_{Eff}(0)$	0.0567	0	0.0202	1e+06	1/min
IC gluc. conc.	$G(0)$	106	0	105	1e+06	mg/dL
IC meal 1	$D_1(0)$	0.5	0	10	10	mg
IC meal 2	$D_2(0)$	0.5	0	10	10	mg
gluc. cov.	Q_g	5	0	13.6	30	-
ins. cov.	$\log(Q_{\log SI})$	-11.5	-11.5	-11.5	-9.21	-
gluc. eff.	$GEZI$	-	-	0.0006	-	1/min
ins. to carb. rat.	ICR	-	-	13.000	-	g/U
ins. sens. fac.	ISF	-	-	3.446	-	mmol/L/U

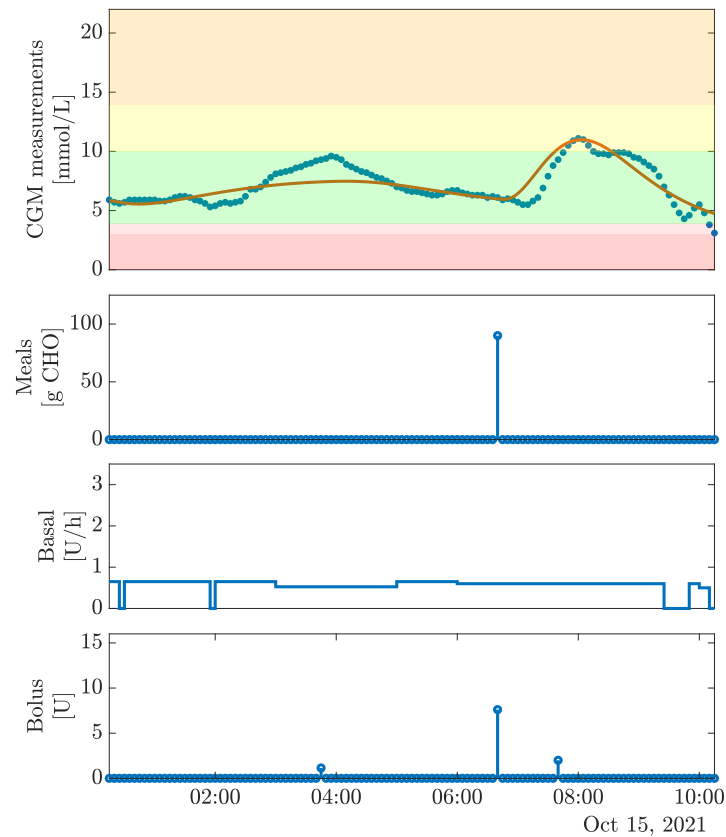


Figure 3.13: Participant 4. Parameter estimation for participant 4 in the phase 2 trial. From the top: 1) CGM measurements (blue dots) and a simulation with the estimated parameters (red line), 2) announced meals, 3) basal insulin rate, and 4) bolus insulin.

manual correction bolus of 2.5 U was also administered during the night of the DH study. In both studies, it seemed like the basal rate was estimated to be too low and the AP increased the basal rate during both studies. The CGM measurements are higher than the YSI measurements during most of the DH study. In the DH study the response from the dinner seemed to be rather large and delayed as the peak happened around midnight.

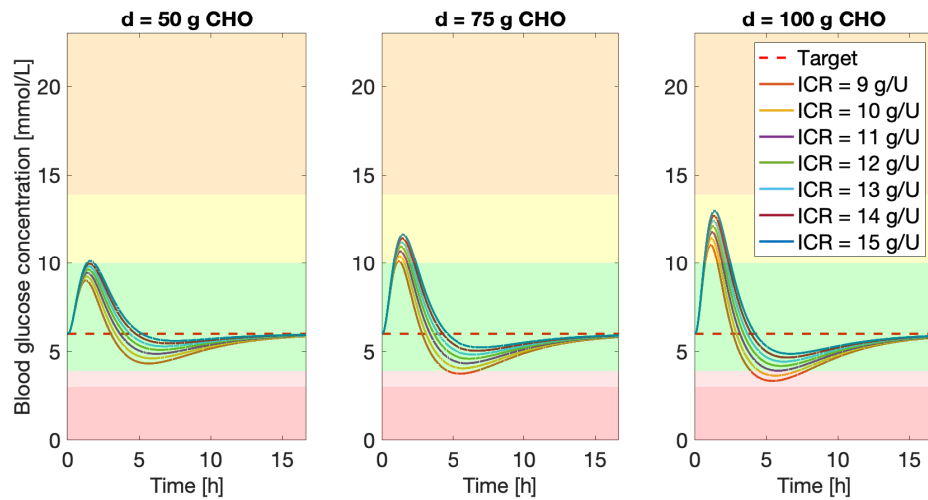


Figure 3.14: Participant 4. Evaluation of the meal responses for participant 4 in the phase 2 trial with an insulin bolus computed from different ICRs.

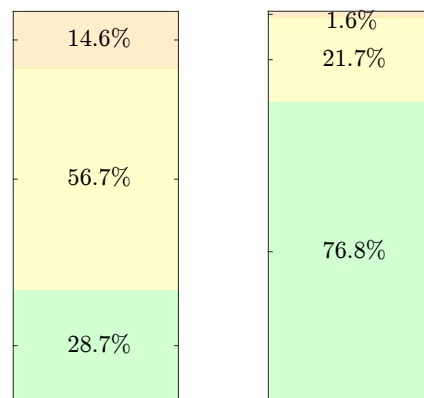


Figure 3.15: Participant 4. Left: TIRs for the DH study for participant 4 in the phase 2 trial. Right: TIRs for the SH study for participant 4 in the phase 2 trial.

Table 3.8: Values of the glycemic targets for participant 4 in the phase 2 trial.

Quantity	Target	DH	SH
Average glucose [mmol/L]	< 8.55	11.48	8.92
GMI [%]	< 7	8.26	7.15
GV [%]	≤ 36	20.78	24.24
Active CGM [%]	100	100.0	100.0

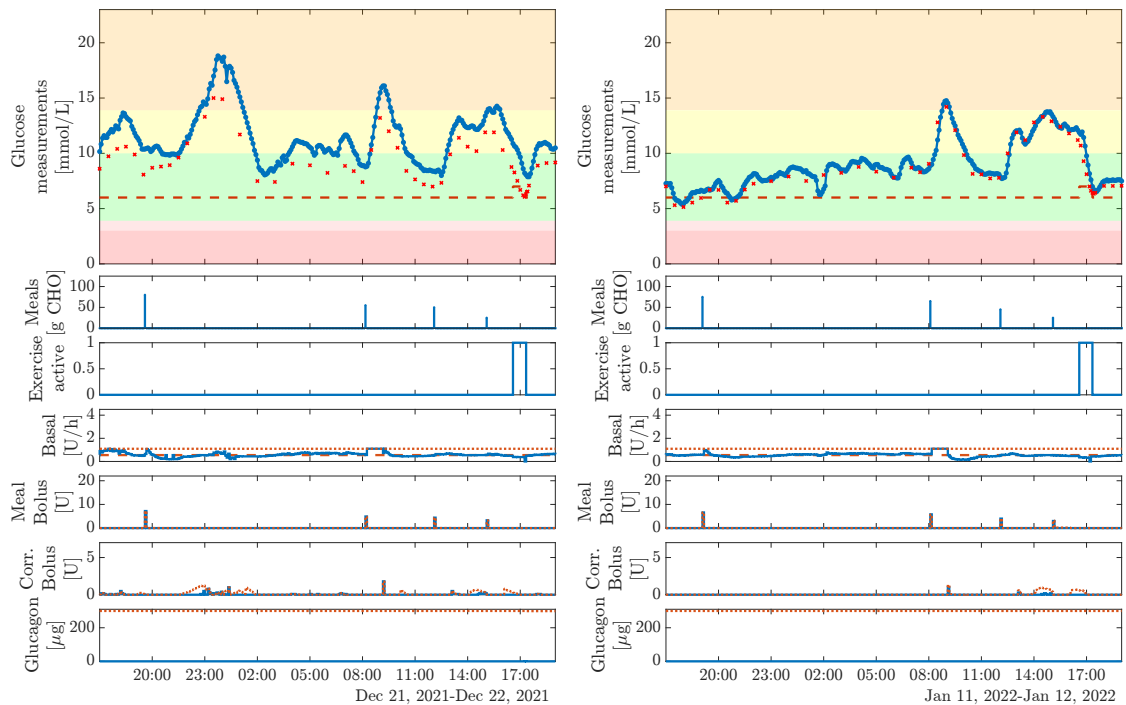


Figure 3.16: Participant 4. Left: Results from the DH study for participant 4 in the phase 2 trial with 28.7% time in range. Right: Results from the SH study for participant 4 in the phase 2 trial with 76.8% time in range. From the top: 1) CGM measurements (blue dotted line), YSI measurements (red crosses), and setpoint (red dashed line), 2) meals, 3) exercise, 4) basal insulin (blue line) and maximum allowed basal insulin (red dots), 5) meal boli (blue line) and maximum allowed meal boli (red dots), 6) correction insulin boli (blue line) and maximum allowed correction boli (red dots), and 7) glucagon boli (blue line) and maximum allowed glucagon boli (red dots).

3.5 Participant 5

3.5.1 Parameter estimation

We were only able to find around 5 hours of data for this participant. Figure 3.17 shows the data used for estimation and a simulation with the estimated parameters. Clearly, the fit matched the data, but the meal response was very small and from Figure 3.18, we saw that the AP would be conservative with the meal boli as the meal response in the model was relatively small and sensitive to insulin. We fixed EGP , k_m , and Q_{logSI} for this participant and $1/V_g$ was at its lower bound. $GEZI$ was tuned to correct the basal rate to match the participants' normal basal rate which was ~ 19.06 mU/min. We computed ICR and ISF as mean values for the participant. Table 3.11 shows the estimated parameters.

3.5.2 Results

Table 3.10 and Figure 3.19 shows the outcomes for the glycemic targets and Figure 3.20 shows the results. In both studies, the AP administered correction boli in the beginning as the participant entered the clinic in hyperglycemia with a rising glucose concentration. In the SH study, the meal bolus should have been larger, but the performance of the AP was relatively good. The DH study was affected by multiple PISAs during the night which caused administration of multiple large glucagon boli even though the participant already had a high glucose concentration. The participant was wearing the sensor on the arm while most of the other participants wore the sensor on their stomach. During the day in the DH study, the predictions were very inaccurate and the AP administered too little insulin and even when it was allowed to give correction boli, almost no additional

Table 3.9: Parameter estimates for participant 5 in the phase 2 trial.

Desc	Param.	init.	lb.	estim.	ub.	unit
inv. ins. TC	k_1	0.0217	0.00667	0.0213	0.2	1/min
ins. sens.	$\log(SI(0))$	-7.4	-10	-7.38	0	$\log((1/(mU/L))/min)$
Endo. gluc. prod	EGP	0.9	0.1	0.87	3	(mg/dL)/min
inv. dist. vol.	$1/V_g$	0.00364	0.00364	0.00364	0.125	1/dL
inv. meal TC	k_m	0.0333	0.00667	0.0333	0.1	1/min
IC ins. sub.	$I_{Sc}(0)$	26.3	0	23.7	1e+06	mU/L
IC ins. plas.	$I_P(0)$	9.61e-06	0	0.000426	1e+06	mU/L
IC ins. eff.	$I_{Eff}(0)$	0.0233	0	0.023	1e+06	1/min
IC gluc. conc.	$G(0)$	119	0	119	1e+06	mg/dL
IC meal 1	$D_1(0)$	10	0	10	10	mg
IC meal 2	$D_2(0)$	10	0	10	10	mg
gluc. cov.	Q_g	2.97	0	2.97	30	-
ins. cov.	$\log(Q_{logSI})$	-11.5	-11.5	-11.5	-11.5	-
gluc. eff.	$GEZI$	-	-	0.0001	-	1/min
ins. to carb. rat.	ICR	-	-	9.17	-	g/U
ins. sens. fac.	ISF	-	-	2	-	mmol/L/U

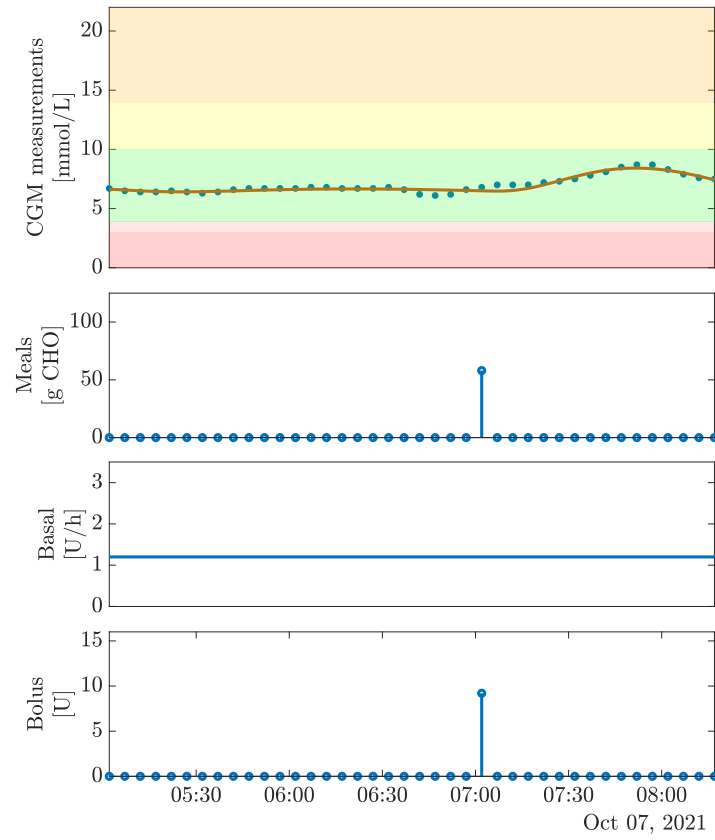


Figure 3.17: Participant 5. Parameter estimation for participant 5 in the phase 2 trial. From the top: 1) CGM measurements (blue dots) and a simulation with the estimated parameters (red line), 2) announced meals, 3) basal insulin rate, and 4) bolus insulin.

insulin was administered. This could be because the insulin sensitivity was adapted based on the faulty CGM measurements during the night.

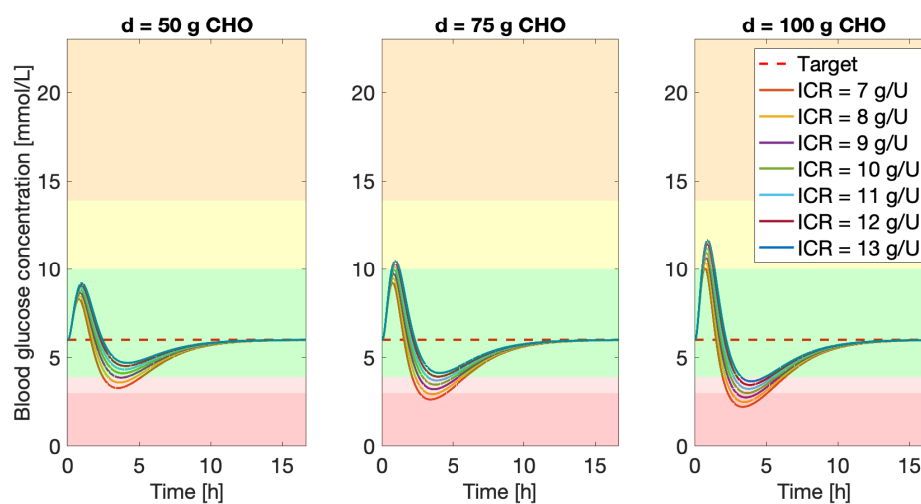


Figure 3.18: Participant 5. Evaluation of the meal responses for participant 5 in the phase 2 trial with an insulin bolus computed from different ICRs.

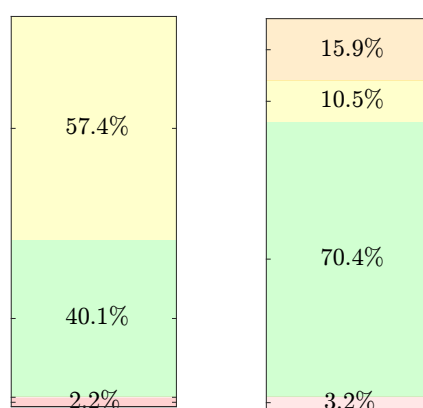


Figure 3.19: Participant 5. Left: TIRs for the DH study for participant 5 in the phase 2 trial. Right: TIRs for the SH study for participant 5 in the phase 2 trial.

Table 3.10: Values of the glycemic targets for participant 5 in the phase 2 trial.

Quantity	Target	DH	SH
Average glucose [mmol/L]	< 8.55	10.16	8.26
GMI [%]	< 7	7.69	6.87
GV [%]	≤ 36	22.36	46.92
Active CGM [%]	100	100.0	100.0

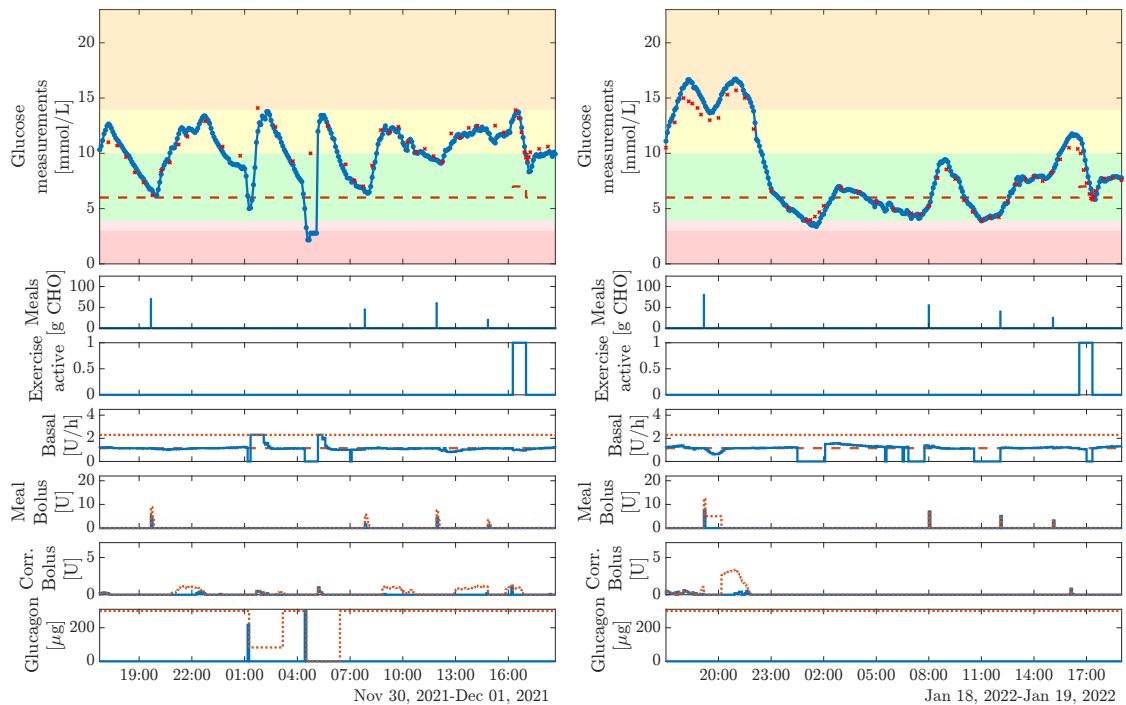


Figure 3.20: Participant 5. Left: Results from the DH study for participant 5 in the phase 2 trial with 40.1% time in range. Right: Results from the SH study for participant 5 in the phase 2 trial with 70.4% time in range. From the top: 1) CGM measurements (blue dotted line), YSI measurements (red crosses), and setpoint (red dashed line), 2) meals, 3) exercise, 4) basal insulin (blue line) and maximum allowed basal insulin (red dots), 5) meal boli (blue line) and maximum allowed meal boli (red dots), 6) correction insulin boli (blue line) and maximum allowed correction boli (red dots), and 7) glucagon boli (blue line) and maximum allowed glucagon boli (red dots).

3.6 Participant 6

3.6.1 Parameter estimation

This participant also used a closed-loop system. Again, we used data from one night and a breakfast. Figure 3.21 shows the data used for estimation and a simulation with the estimated parameters. It seemed like the meal response was slightly delayed compared to the announcement of the meal, but overall, the fit seemed decent. We fixed k_m , k_1 , and EGP and $GEZI$ was tuned to correct the basal rate to match the participants' normal basal rate with was ~ 16.667 mU/min. The closed-loop system had multiple pump programs and therefore the basal rate was tuned to the value recommended by Jannet Svensson. We computed ISF as the mean value for the participant and ICR was computed as the mean of the values during the day (the participants used an ICR of 13 g/U during the night). We estimated the ICR to 8.575g/U and the values ranged from 8.4-8.7g/U during the day in the closed-loop system. Table 3.11 shows the estimated parameters. The time constants $1/k_1$ and $1/k_m$ were relatively small for this participant, but it looked reasonable from inspection of the post-prandial peaks in the data. Figure 3.22 shows the meal response for an insulin bolus computed from different ICRs.

3.6.2 Results

Table 3.12 and Figure 3.23 shows the outcomes for the glycemic targets and Figure 3.24 shows the results. In the SH study, the participant entered the clinical in hyperglycemia and the CGM measurements were consistently higher than the YSI measurements. The participant received rescue carbs before lunch and during exercise. The response from the dinner was almost not visible and maybe the basal rate was a little too high. In

Table 3.11: Parameter estimates for participant 6 in the phase 2 trial.

Desc	Param.	init.	lb.	estim.	ub.	unit
inv. ins. TC	k_1	0.0182	0.0111	0.0222	0.2	1/min
ins. sens.	$\log(SI(0))$	-7.5	-10	-7.72	0	$\log((1/(\text{mU/L}))/\text{min})$
Endo. gluc. prod	EGP	0.96	0.1	0.6	3	(mg/dL)/min
inv. dist. vol.	$1/V_g$	0.00402	0.005	0.005	0.125	1/dL
inv. meal TC	k_m	0.027	0.0111	0.025	0.1	1/min
IC ins. sub.	$I_{Sc}(0)$	0.0005	0	0.000247	1e+06	mU/L
IC ins. plas.	$I_P(0)$	34.3	0	77.6	1e+06	mU/L
IC ins. eff.	$I_{Eff}(0)$	0.0567	0	0.00475	1e+06	1/min
IC gluc. conc.	$G(0)$	115	0	119	1e+06	mg/dL
IC meal 1	$D_1(0)$	0.5	0	10	10	mg
IC meal 2	$D_2(0)$	0.5	0	10	10	mg
gluc. cov.	Q_g	5	0	15.8	30	-
ins. cov.	$\log(Q_{\log SI})$	-11.5	-9.21	-9.21	-9.12	-
gluc. eff.	$GEZI$	-	-	0.00054	-	1/min
ins. to carb. rat.	ICR	-	-	8.575	-	g/U
ins. sens. fac.	ISF	-	-	2.135	-	mmol/L/U

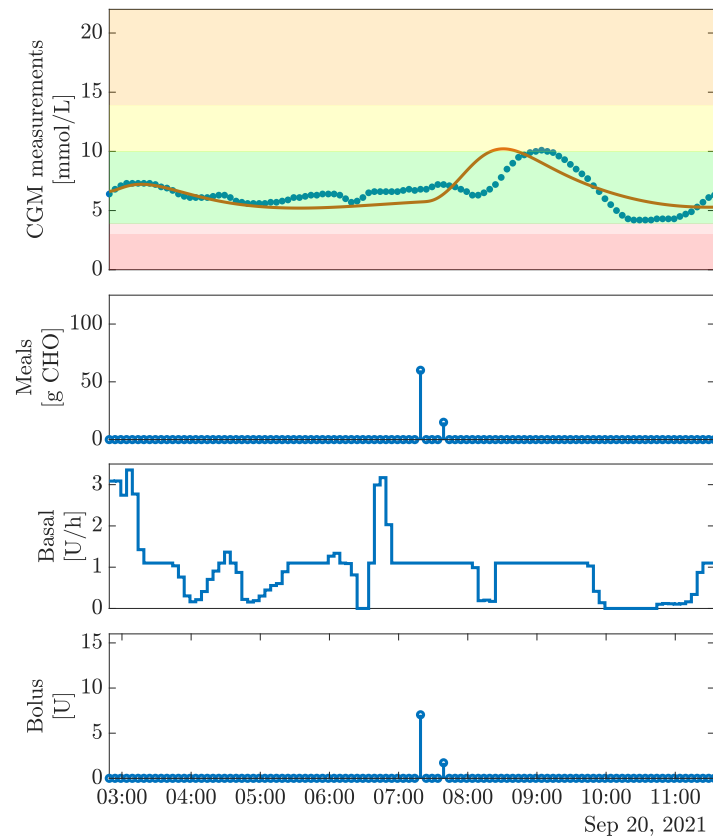


Figure 3.21: Participant 6. Parameter estimation for participant 6 in the phase 2 trial. From the top: 1) CGM measurements (blue dots) and a simulation with the estimated parameters (red line), 2) announced meals, 3) basal insulin rate, and 4) bolus insulin.

the DH study, the dinner was handled well and the glucagon administration seemed to prevent hypoglycemia and stabilize the participant over night. There appeared to be a PISA just before the breakfast which caused glucagon to be administered and resulted in very large post-prandial peak. The glucagon pump occluded between breakfast and lunch and we don't know how much glucagon was actually administered.

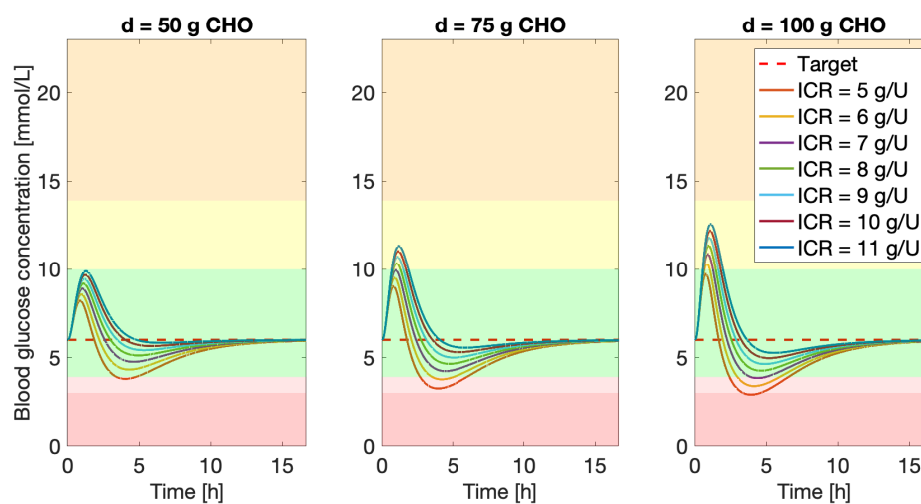


Figure 3.22: Participant 6. Evaluation of the meal responses for participant 6 in the phase 2 trial with an insulin bolus computed from different ICRs.

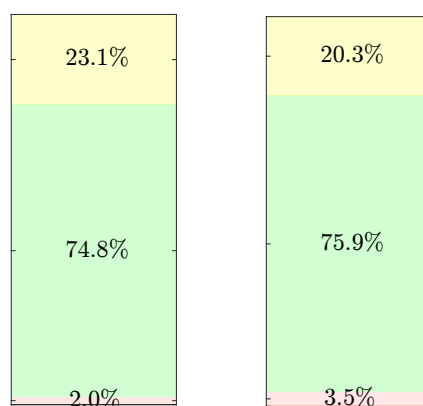


Figure 3.23: Participant 6. Left: TIRs for the DH study for participant 6 in the phase 2 trial. Right: TIRs for the SH study for participant 6 in the phase 2 trial.

Table 3.12: Values of the glycemic targets for participant 6 in the phase 2 trial.

Quantity	Target	DH	SH
Average glucose [mmol/L]	< 8.55	7.69	7.79
GMI [%]	< 7	6.62	6.67
GV [%]	≤ 36	30.70	30.48
Active CGM [%]	100	100.0	100.0

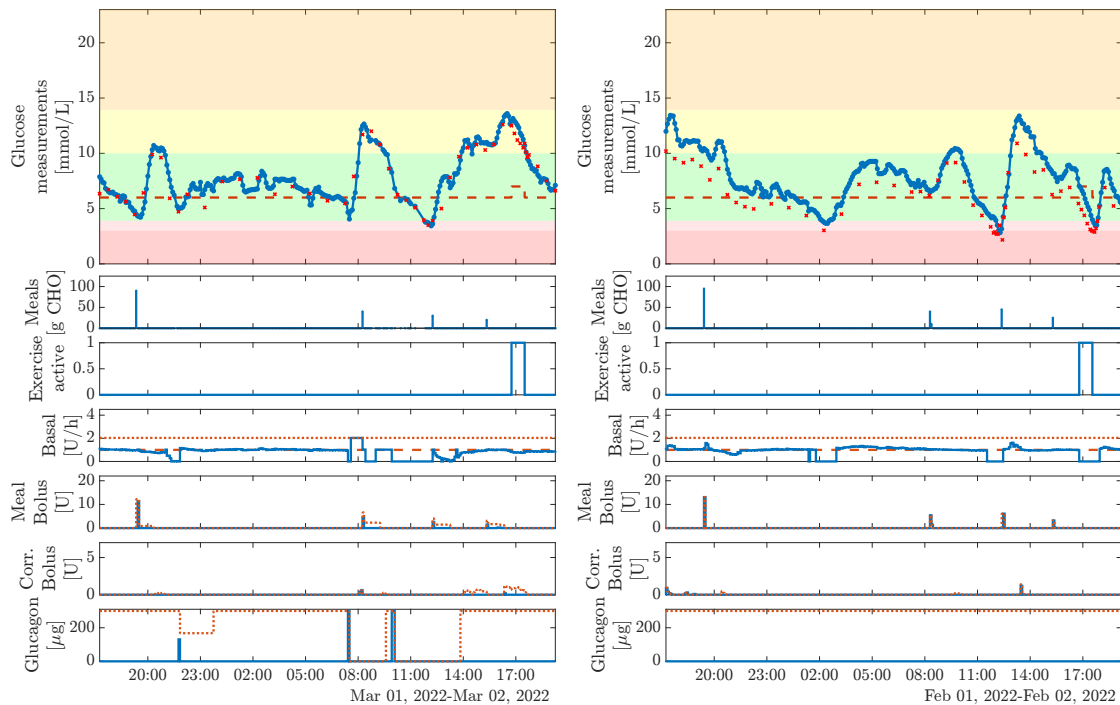


Figure 3.24: Participant 6. Left: Results from the DH study for participant 6 in the phase 2 trial with 74.8% time in range. Right: Results from the SH study for participant 6 in the phase 2 trial with 75.9% time in range. From the top: 1) CGM measurements (blue dotted line), YSI measurements (red crosses), and setpoint (red dashed line), 2) meals, 3) exercise, 4) basal insulin (blue line) and maximum allowed basal insulin (red dots), 5) meal boli (blue line) and maximum allowed meal boli (red dots), 6) correction insulin boli (blue line) and maximum allowed correction boli (red dots), and 7) glucagon boli (blue line) and maximum allowed glucagon boli (red dots).

3.7 Participant 7

3.7.1 Parameter estimation

This participant used a closed-loop system and did not announce meals in a conventional way. The participant used an ICR between 2 and 2.5 and only announced a part of the meal. The doctors decided together with the participant that we should set the *ICR* to 7 g/U. Therefore, we also increased the size of the meals in the data by the same factor, i.e., $7/2 = 3.5$. Figure 3.25 shows the data used for estimation and a simulation with the estimated parameters. We moved the meals 20 minutes earlier to match the increase in the glucose concentration around noon. Therefore, the parameters related to the effect of meals were very uncertain for this participant. We fixed k_m , k_1 , and *EGP* and $1/V_g$ is on the boundary. *GEZI* was tuned to the correct basal rate to match the participants' normal basal rate which is ~ 24.236 mU/min and *ISF* was computed as the mean value. Table 3.13 shows the estimated parameters and Figure 3.26 shows the meal response for an insulin bolus computed from different ICRs.

3.7.2 Results

Table 3.14 and Figure 3.27 shows the outcomes for the glycemic targets and Figure 3.28 shows the results. The participant entered the clinic with a rapidly decreasing glucose concentration in the DH study and the AP immediately administered glucagon. In the SH study, the participant entered the clinic in hypoglycemia and received both a banana and dextrose before the study was started. The oscillations in the beginning of DH study also caused almost no meal bolus to be administered for the dinner and resulted in a large post-prandial peak. In general, the AP struggled to predict the effect of glucagon

Table 3.13: Parameter estimates for participant 7 in the phase 2 trial.

Desc	Param.	init.	lb.	estim.	ub.	unit
inv. ins. TC	k_1	0.0182	0.0111	0.0167	0.2	1/min
ins. sens.	$\log(SI(0))$	-7.5	-10	-7.51	0	$\log((1/(\text{mU/L}))/\text{min})$
Endo. gluc. prod	<i>EGP</i>	0.96	0.1	1.1	3	(mg/dL)/min
inv. dist. vol.	$1/V_g$	0.00402	0.00455	0.00667	0.00667	1/dL
inv. meal TC	k_m	0.027	0.0111	0.0182	0.1	1/min
IC ins. sub.	$I_{Sc}(0)$	0.0005	0	60.7	1e+06	mU/L
IC ins. plas.	$I_P(0)$	34.3	0	0.000476	1e+06	mU/L
IC ins. eff.	$I_{Eff}(0)$	0.0567	0	0.0311	1e+06	1/min
IC gluc. conc.	$G(0)$	110	0	117	1e+06	mg/dL
IC meal 1	$D_1(0)$	0.5	0	10	10	mg
IC meal 2	$D_2(0)$	0.5	0	10	10	mg
gluc. cov.	Q_g	5	0	5.3	30	-
ins. cov.	$\log(Q_{\log SI})$	-11.5	-9.21	-9.21	-9.12	-
gluc. eff.	<i>GEZI</i>	-	-	0.0014	-	1/min
ins. to carb. rat.	<i>ICR</i>	-	-	7.000	-	g/U
ins. sens. fac.	<i>ISF</i>	-	-	1.742	-	mmol/L/U

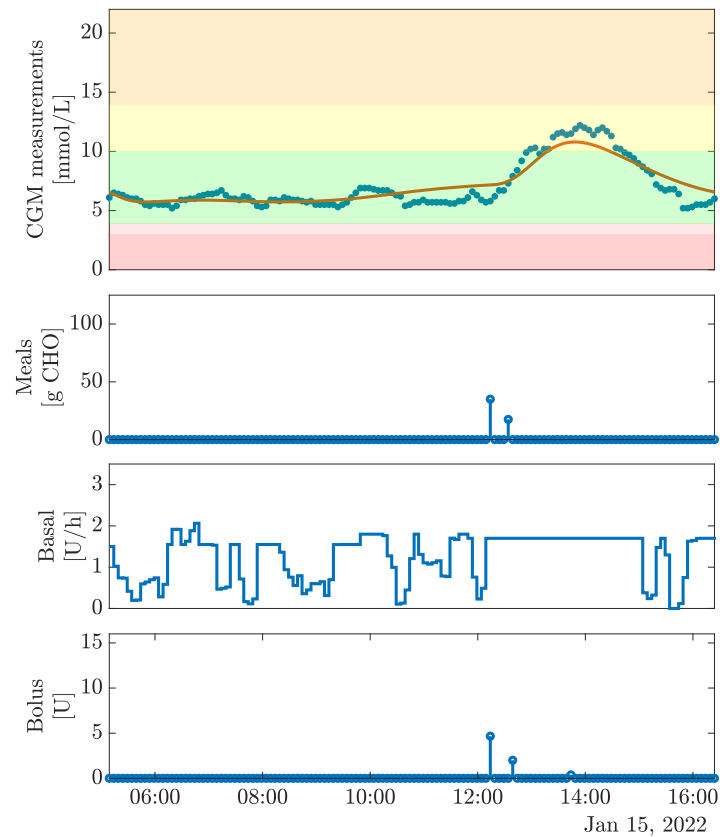


Figure 3.25: Participant 7. Parameter estimation for participant 7 in the phase 2 trial. From the top: 1) CGM measurements (blue dots) and a simulation with the estimated parameters (red line), 2) announced meals, 3) basal insulin rate, and 4) bolus insulin.

for the participant and administered too much insulin. Glucagon was administered right before breakfast and the combined effect caused the glucose concentration to remain high until after lunch. The phone briefly lost the connection to the CGM and pumps before breakfast and the participant received rescue carbs after exercise. In the SH study, only one YSI measurement is not in range, but there was an offset between the CGM and YSI measurements. It looks like the participant might have received additional carbs before exercise, even though it is not registered.

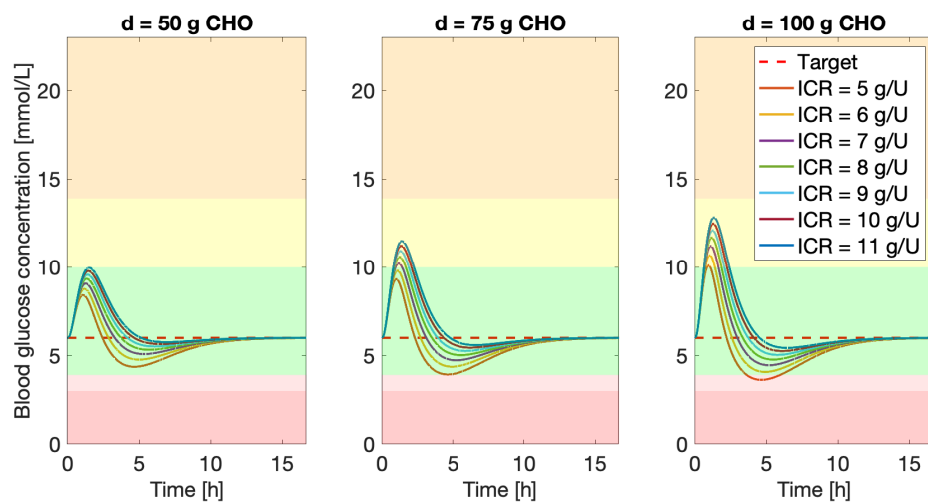


Figure 3.26: Participant 7. Evaluation of the meal responses for participant 7 in the phase 2 trial with an insulin bolus computed from different ICRs.

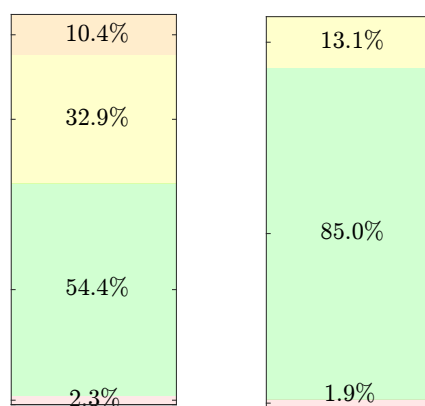


Figure 3.27: Participant 7. Left: TIRs for the DH study for participant 7 in the phase 2 trial. Right: TIRs for the SH study for participant 7 in the phase 2 trial.

Table 3.14: Values of the glycemic targets for participant 7 in the phase 2 trial.

Quantity	Target	DH	SH
Average glucose [mmol/L]	< 8.55	8.95	7.18
GMI [%]	< 7	7.16	6.40
GV [%]	≤ 36	38.08	29.62
Active CGM [%]	100	100.0	100.0

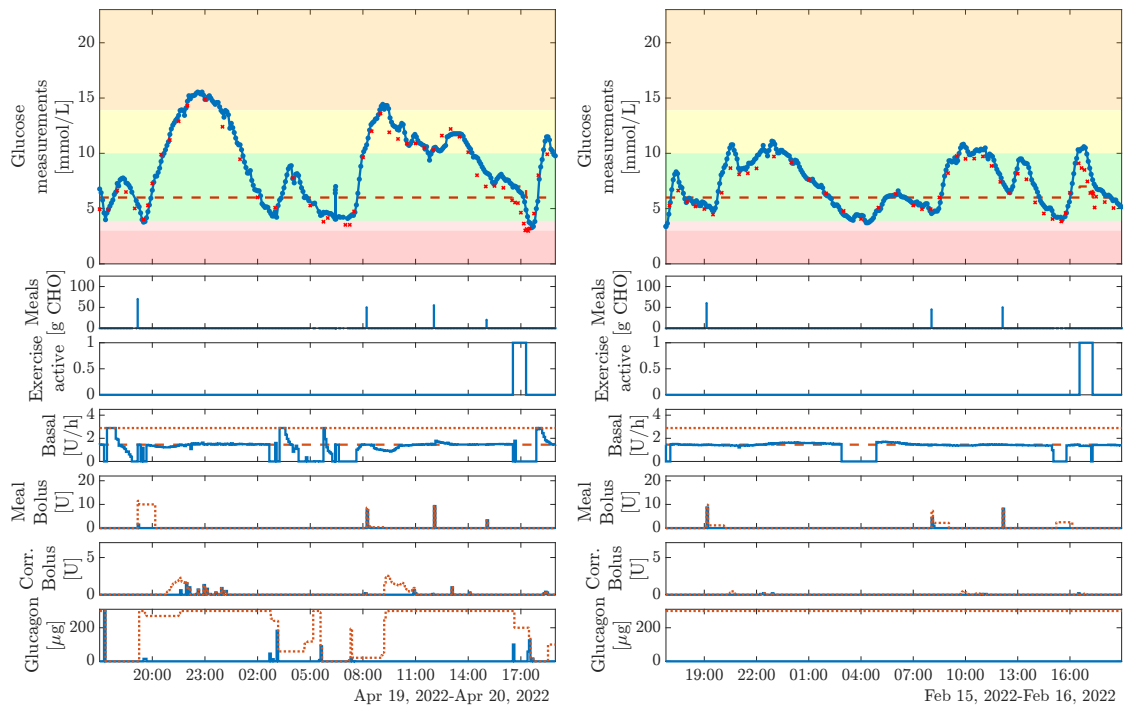


Figure 3.28: Participant 7. Left: Results from the DH study for participant 7 in the phase 2 trial with 54.4% time in range. Right: Results from the SH study for participant 7 in the phase 2 trial with 85.0% time in range. From the top: 1) CGM measurements (blue dotted line), YSI measurements (red crosses), and setpoint (red dashed line), 2) meals, 3) exercise, 4) basal insulin (blue line) and maximum allowed basal insulin (red dots), 5) meal boli (blue line) and maximum allowed meal boli (red dots), 6) correction insulin boli (blue line) and maximum allowed correction boli (red dots), and 7) glucagon boli (blue line) and maximum allowed glucagon boli (red dots).

3.8 Participant 8

This participant had participated in an earlier study where the settings for the basal rate were incorrect. The basal rate settings were tuned to the basal rate profile from the participants pump, but the participant was not using that pump program. Therefore, the study was restarted and the first visit erased.

3.8.1 Parameter estimation

We were also only able to find data from one night and one meal for this participant. Figure 3.29 shows the data used for estimation and a simulation with the estimated parameters. This participant was using the Medtronic 780G closed-loop system, which means the basal rate is registered as multiple small insulin boli. Therefore, we tuned the basal rate to the doctors recommendation. The participant used an ICR of 8 g/U during the day and 13 g/U during the night. We chose an ICR of 8 g/U, which also corresponds well with the meal responses in Figure 3.30. We fixed k_m , k_1 , and $Q_{\log SI}$ for this participant and used *GEZI* to tune the basal rate to match the doctors recommendation which was ~ 15.0 mU/min. Table 3.15 shows the estimated parameters.

3.8.2 Results

Table 3.16 and Figure 3.31 shows the outcomes for the glycemic targets and Figure 3.32 shows the results. The participant had administered a correction bolus before entering the clinic and had a rapidly decreasing glucose concentration in the DH study which caused immediate administration of glucagon. Still, the participant went into level 2 hypoglycemia. The AP had trouble predicting the effect of glucagon as in some of

Table 3.15: Parameter estimates for participant 8 in the phase 2 trial.

Desc	Param.	init.	lb.	estim.	ub.	unit
inv. ins. TC	k_1	0.0182	0.0111	0.0167	0.2	1/min
ins. sens.	$\log(SI(0))$	-7.5	-10	-8.09	0	$\log((1/(\text{mU/L}))/\text{min})$
Endo. gluc. prod	EGP	0.96	0.1	0.35	3	(mg/dL)/min
inv. dist. vol.	$1/V_g$	0.00402	0.00444	0.00444	0.125	1/dL
inv. meal TC	k_m	0.027	0.0111	0.02	0.1	1/min
IC ins. sub.	$I_{Sc}(0)$	0.0005	0	14	1e+06	mU/L
IC ins. plas.	$I_P(0)$	34.3	0	3.51e-05	1e+06	mU/L
IC ins. eff.	$I_{Eff}(0)$	0.0567	0	0.0214	1e+06	1/min
IC gluc. conc.	$G(0)$	103	0	104	1e+06	mg/dL
IC meal 1	$D_1(0)$	0.5	0	10	10	mg
IC meal 2	$D_2(0)$	0.5	0	10	10	mg
gluc. cov.	Q_g	5	0	11.3	30	-
ins. cov.	$\log(Q_{\log SI})$	-11.5	-11	-11	-9.21	-
gluc. eff.	<i>GEZI</i>	-	-	0.00015	-	1/min
ins. to carb. rat.	<i>ICR</i>	-	-	8.000	-	g/U
ins. sens. fac.	<i>ISF</i>	-	-	2.000	-	mmol/L/U

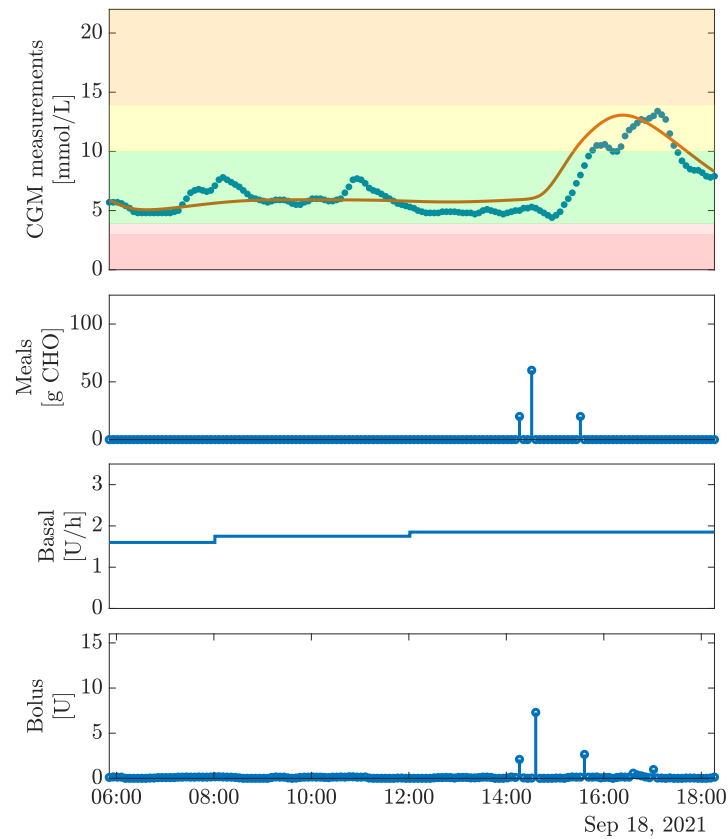


Figure 3.29: Participant 8. Parameter estimation for participant 8 in the phase 2 trial. From the top: 1) CGM measurements (blue dots) and a simulation with the estimated parameters (red line), 2) announced meals, 3) basal insulin rate, and 4) bolus insulin.

the previous studies. The TIR in the DH study was very high despite the oscillatory behavior and the AP handled the potential hypoglycemic event after the dinner. In the SH study, there was a slight offset between the CGM and YSI measurements. The TIR was also above the target with a low amount of time in hypoglycemia in the SH study even though the participant entered the clinic in level 1 hyperglycemia.

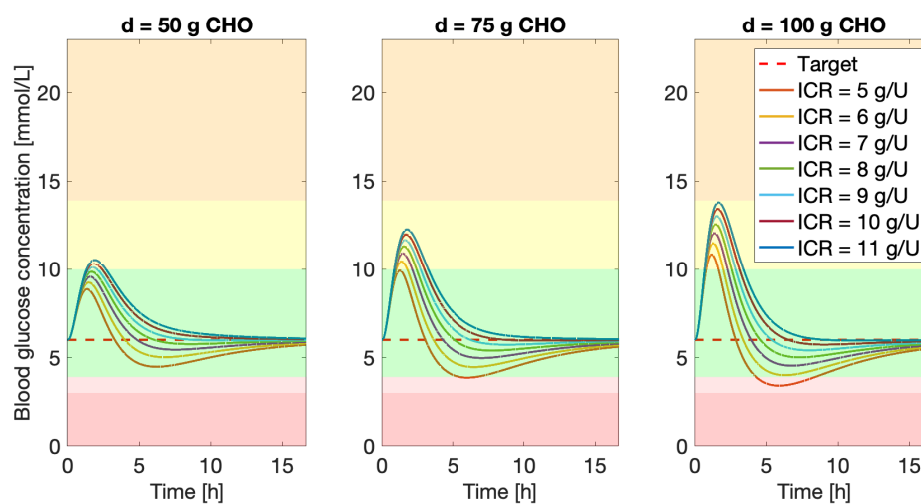


Figure 3.30: Participant 8. Evaluation of the meal responses with an insulin bolus computed from different ICRs.

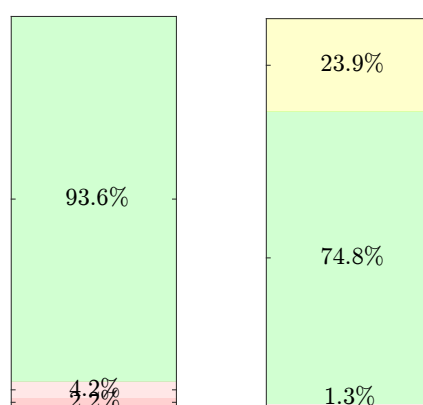


Figure 3.31: Participant 8. Left: TIRs for the DH study for participant 8 in the phase 2 trial. Right: TIRs for the SH study for participant 8 in the phase 2 trial.

Table 3.16: Values of the glycemic targets for participant 8 in the phase 2 trial.

Quantity	Target	DH	SH
Average glucose [mmol/L]	< 8.55	6.24	7.98
GMI [%]	< 7	6.00	6.75
GV [%]	≤ 36	24.77	31.38
Active CGM [%]	100	100.0	100.0

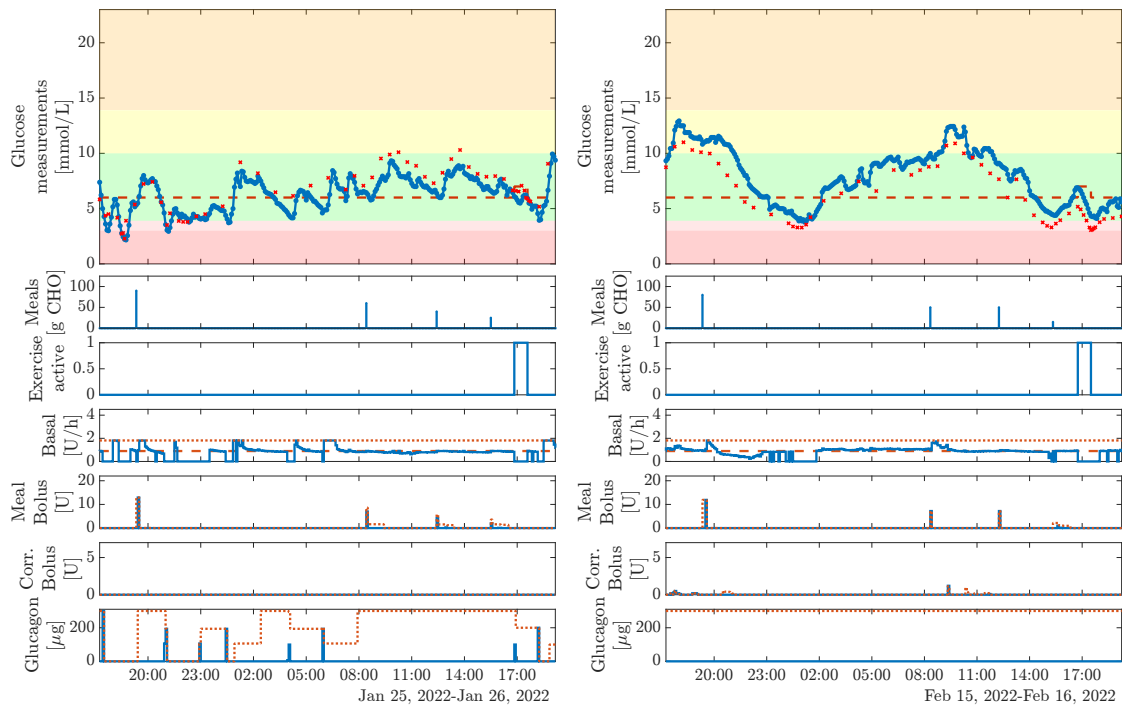


Figure 3.32: Participant 8. Left: Results from the DH study for participant 8 in the phase 2 trial with 93.6% time in range. Right: Results from the SH study for participant 8 in the phase 2 trial with 74.8% time in range. From the top: 1) CGM measurements (blue dotted line), YSI measurements (red crosses), and setpoint (red dashed line), 2) meals, 3) exercise, 4) basal insulin (blue line) and maximum allowed basal insulin (red dots), 5) meal boli (blue line) and maximum allowed meal boli (red dots), 6) correction insulin boli (blue line) and maximum allowed correction boli (red dots), and 7) glucagon boli (blue line) and maximum allowed glucagon boli (red dots).

3.9 Participant 9

3.9.1 Parameter estimation

We used data from a night followed by breakfast and lunch for this participant. We shifted the meals 15 minutes earlier to match the meal response. The meal response from the lunch seemed rather large which could indicate that the amount of carbs is underestimated. Figure 3.33 shows the data used for estimation and a simulation with the estimated parameters. We fixed k_m , k_1 , and EGP for this participant. We tuned $GEZI$ to correct the basal rate to match the participants' normal basal rate which was ~ 13.75 mU/min. The participant used different ICRs during day (5 g/U in the morning, 6 g/U for lunch, and 8 g/U in the afternoon and evening). We set the ICR to 6 g/U to not be too restrictive. We computed ISF as the mean value. Table 3.17 shows the estimated parameters. V_g was rather small for this participant. That means the glucose concentration was predicted to reach a relatively high level after meals which is also clear from the meal responses in Figure 3.33.

3.9.2 Results

Table 3.18 and Figure 3.35 shows the outcomes for the glycemic targets and Figure 3.36 shows the results. The AP administered the maximum allowed meal bolus for all meals and also turns up the basal rate after meals, which might have been the reason for the high time in hypoglycemia for this participant. The TIR was very high in the SH study, but the exercise session was stopped preemptively and the participant received rescue carbs. We also predicted that the participant would receive a lot of insulin for the meals based on the meal responses during the parameter estimation and could have considered

Table 3.17: Parameter estimates for participant 9 in the phase 2 trial.

Desc	Param.	init.	lb.	estim.	ub.	unit
inv. ins. TC	k_1	0.0182	0.0111	0.0167	0.2	1/min
ins. sens.	$\log(SI(0))$	-7.5	-10	-8.13	0	$\log((1/(\text{mU/L}))/\text{min})$
Endo. gluc. prod	EGP	0.96	0.1	0.47	3	(mg/dL)/min
inv. dist. vol.	$1/V_g$	0.00402	0.005	0.00759	0.125	1/dL
inv. meal TC	k_m	0.027	0.0111	0.02	0.1	1/min
IC ins. sub.	$I_{Sc}(0)$	0.0005	0	34.4	1e+06	mU/L
IC ins. plas.	$I_P(0)$	34.3	0	2.83	1e+06	mU/L
IC ins. eff.	$I_{Eff}(0)$	0.0567	0	0.015	1e+06	1/min
IC gluc. conc.	$G(0)$	142	0	143	1e+06	mg/dL
IC meal 1	$D_1(0)$	0.5	0	5	5	mg
IC meal 2	$D_2(0)$	0.5	0	5	5	mg
gluc. cov.	Q_g	5	0	13.5	30	-
ins. cov.	$\log(Q_{\log SI})$	-11.5	-11.5	-9.21	-9.21	-
gluc. eff.	$GEZI$	-	-	0.00159	-	1/min
ins. to carb. rat.	ICR	-	-	6.000	-	g/U
ins. sens. fac.	ISF	-	-	2.200	-	mmol/L/U

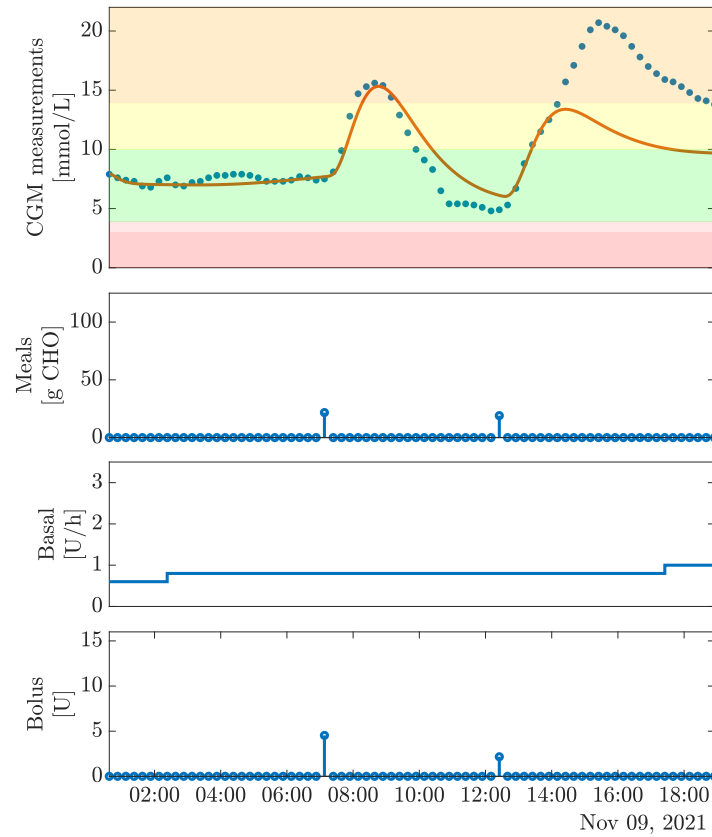


Figure 3.33: Parameter estimation for participant 9 in the phase 2 trial. From the top: 1) CGM measurements (blue dots) and a simulation with the estimated parameters (red line), 2) announced meals, 3) basal insulin rate, and 4) bolus insulin.

to manually adapt the parameters. The high amount of insulin might also be the reason for the comparably small glucagon response in the DH study and high amount of time in hypoglycemia.

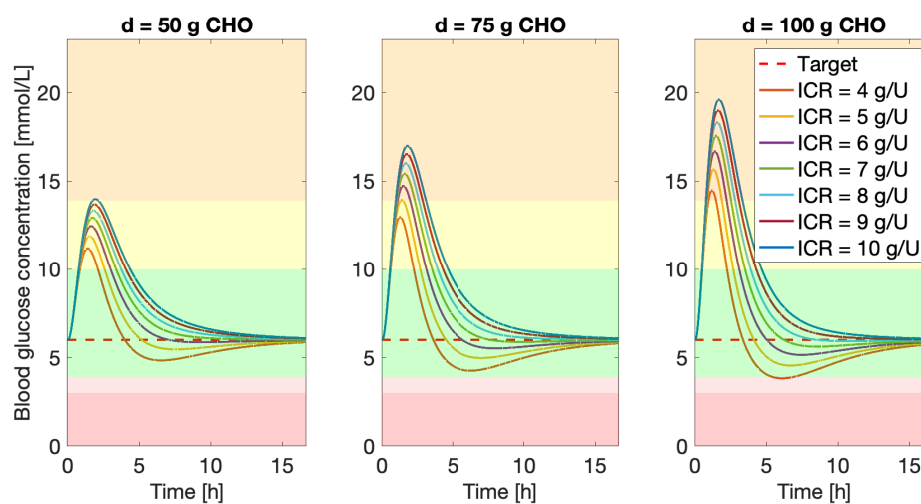


Figure 3.34: Participant 9. Evaluation of the meal responses for participant 9 in the phase 2 trial with an insulin bolus computed from different ICRs.

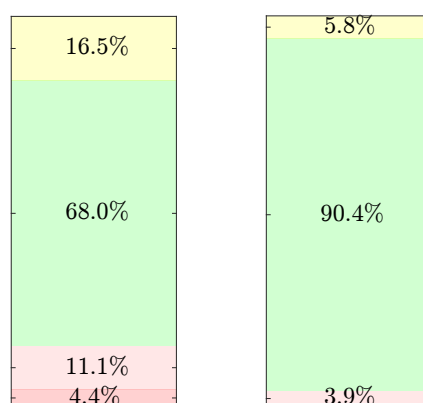


Figure 3.35: Participant 9. Left: TIRs for the DH study for participant 9 in the phase 2 trial. Right: TIRs for the SH study for participant 9 in the phase 2 trial.

Table 3.18: Values of the glycemic targets for participant 9 in the phase 2 trial.

Quantity	Target	DH	SH
Average glucose [mmol/L]	< 8.55	7.20	7.03
GMI [%]	< 7	6.41	6.34
GV [%]	≤ 36	37.74	24.40
Active CGM [%]	100	100.0	100.0

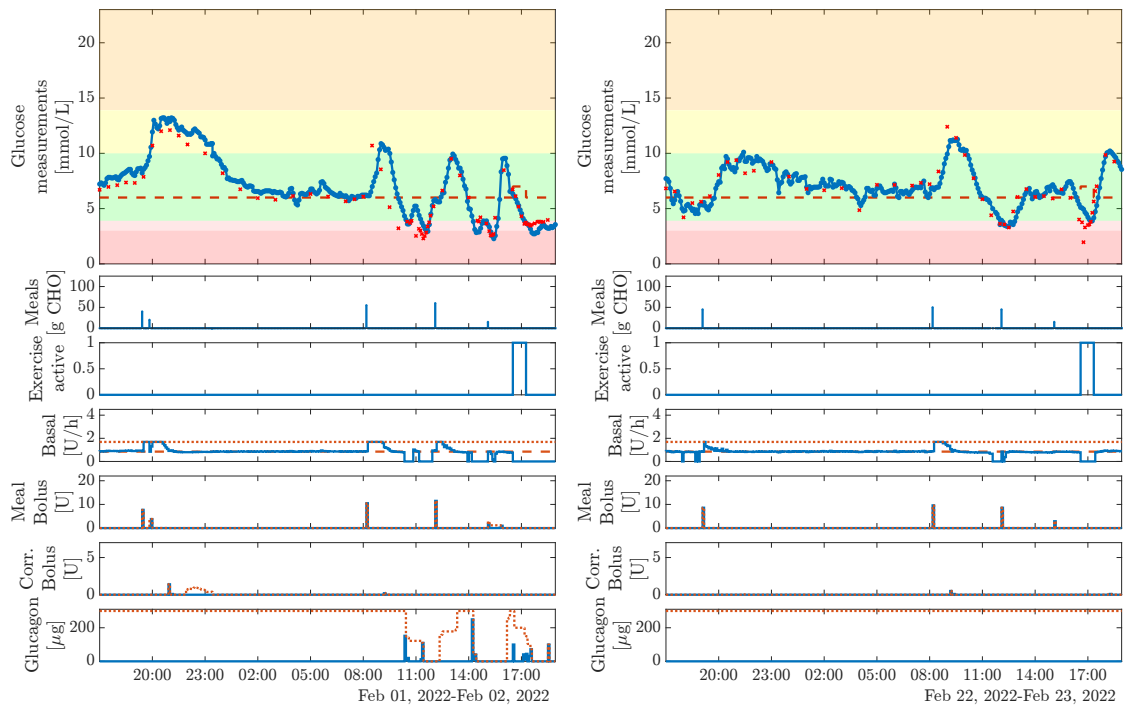


Figure 3.36: Participant 9. Left: Results from the DH study for participant 9 in the phase 2 trial with 68.0% time in range. Right: Results from the SH study for participant 9 in the phase 2 trial with 90.4% time in range. From the top: 1) CGM measurements (blue dotted line), YSI measurements (red crosses), and setpoint (red dashed line), 2) meals, 3) exercise, 4) basal insulin (blue line) and maximum allowed basal insulin (red dots), 5) meal boli (blue line) and maximum allowed meal boli (red dots), 6) correction insulin boli (blue line) and maximum allowed correction boli (red dots), and 7) glucagon boli (blue line) and maximum allowed glucagon boli (red dots).

3.10 Participant 10

3.10.1 Parameter estimation

We used data from around one day that consisted of 3 meals. There were many missing CGM measurements and the meals seemed to have been announced very late. Therefore, we shifted the meals by 45 minutes in the estimation. Figure 3.37 shows the data used for estimation and a simulation with the estimated parameters. We fixed k_m , k_1 , and EGP and $1/V_g$ was on the boundary. EGP was estimated and then fixed to a slightly higher value. We tuned $GEZI$ to the correct basal rate to match the participants' normal basal rate which was ~ 25.764 mU/min. We used the ISF reported by the participant. The participant used an ICR of 8 g/U during the day and 10 g/U over night. Therefore, we set it to 8 g/U. Table 3.19 shows the estimated parameters. Figure 3.38 shows the meal response for an insulin bolus computed from different ICRs.

3.10.2 Results

Table 3.20 and Figure 3.39 shows the outcomes for the glycemic targets and Figure 3.40 shows the results. The participant entered the clinic in hyperglycemia in the SH study and therefore the TIR was lower. The meal response after breakfast was very low in both studies. Therefore, glucagon was administered in the DH study and rescue carbs were given in the SH study. The AP handled the potential hypoglycemic events with glucagon in the DH study and also reduced the post-prandial peak with correction boli after dinner. In general, the AP worked well for this participant even though the achieved TIR was not the highest.

Table 3.19: Parameter estimates for participant 10 in the phase 2 trial.

Desc	Param.	init.	lb.	estim.	ub.	unit
inv. ins. TC	k_1	0.02	0.0111	0.02	0.2	1/min
ins. sens.	$\log(SI(0))$	-7.61	-10	-7.59	0	$\log((1/(\text{mU/L}))/\text{min})$
Endo. gluc. prod	EGP	0.92	0.1	0.96	3	(mg/dL)/min
inv. dist. vol.	$1/V_g$	0.005	0.005	0.005	0.125	1/dL
inv. meal TC	k_m	0.025	0.0111	0.025	0.1	1/min
IC ins. sub.	$I_{sc}(0)$	1	0	1	1	mU/L
IC ins. plas.	$I_P(0)$	0.999	0	1	1	mU/L
IC ins. eff.	$I_{Eff}(0)$	0.0164	0	0.0168	1e+06	1/min
IC gluc. conc.	$G(0)$	198	0	198	1e+06	mg/dL
IC meal 1	$D_1(0)$	0.0012	0	1.12e-05	10	mg
IC meal 2	$D_2(0)$	10	0	10	10	mg
gluc. cov.	Q_g	30	0	30	30	-
ins. cov.	$\log(Q_{\log SI})$	-9.12	-9.21	-9.12	-9.12	-
gluc. eff.	$GEZI$	-	-	0.00023	-	1/min
ins. to carb. rat.	ICR	-	-	8.000	-	g/U
ins. sens. fac.	ISF	-	-	2.200	-	mmol/L/U
Basal rate	u_{ba}	-	-	1.546	-	U/h

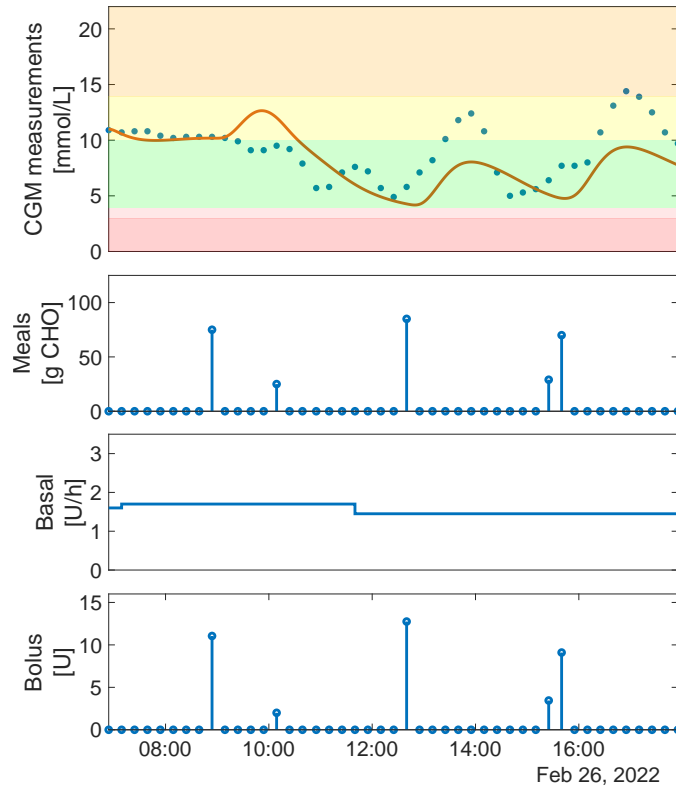


Figure 3.37: Participant 10. Parameter estimation for participant 10 in the phase 2 trial. From the top: 1) CGM measurements (blue dots) and a simulation with the estimated parameters (red line), 2) announced meals, 3) basal insulin rate, and 4) bolus insulin.

Table 3.20: Values of the glycemic targets for participant 10 in the phase 2 trial.

Quantity	Target	DH	SH
Average glucose [mmol/L]	< 8.55	8.00	7.94
GMI [%]	< 7	6.76	6.73
GV [%]	≤ 36	36.27	45.67
Active CGM [%]	100	100.0	100.0

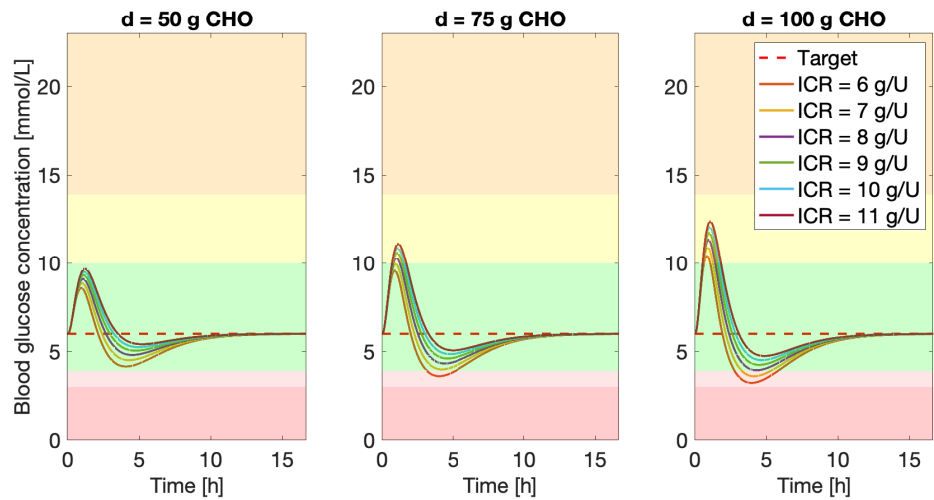


Figure 3.38: Participant 10. Evaluation of the meal responses for participant 10 in the phase 2 trial with an insulin bolus computed from different ICRs.

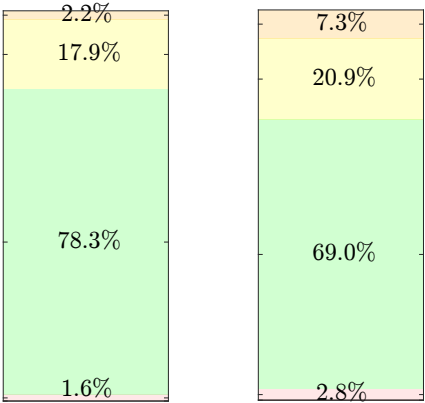


Figure 3.39: Participant 10. Left: TIRs for the DH study for participant 10 in the phase 2 trial. Right: TIRs for the SH study for participant 10 in the phase 2 trial.

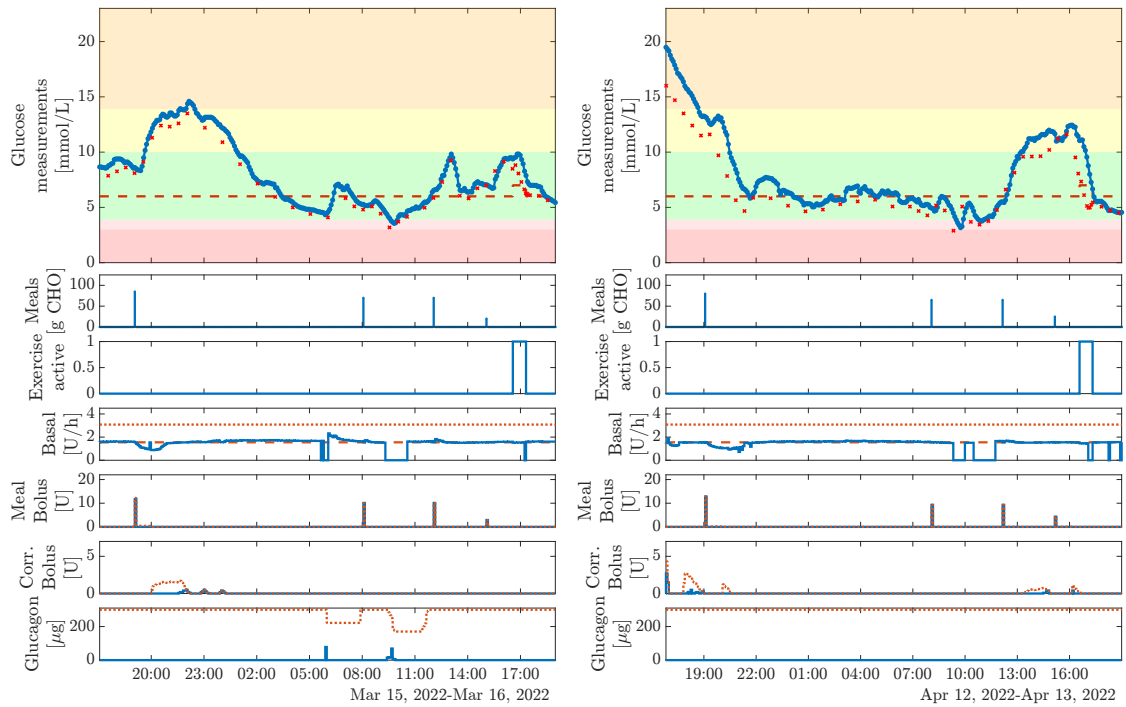


Figure 3.40: Participant 10. Left: Results from the DH study for participant 10 in the phase 2 trial with 78.3% time in range. Right: Results from the SH study for participant 10 in the phase 2 trial with 69.0% time in range. From the top: 1) CGM measurements (blue dotted line), YSI measurements (red crosses), and setpoint (red dashed line), 2) meals, 3) exercise, 4) basal insulin (blue line) and maximum allowed basal insulin (red dots), 5) meal boli (blue line) and maximum allowed meal boli (red dots), 6) correction insulin boli (blue line) and maximum allowed correction boli (red dots), and 7) glucagon boli (blue line) and maximum allowed glucagon boli (red dots).

3.11 Participant 11

3.11.1 Parameter estimation

The parameter estimation for this participant was very challenging as often either the meals or CGM measurements were missing in the data. We ended up using around 10 hours of data, but had to shift the announcement of both meals. The first meal was shifted 1 h back in time and the other meal was shifted 15 min back. Figure 3.41 shows the data used for estimation and a simulation with the estimated parameters. We fixed k_m , k_1 , and EGP and tuned $GEZI$ to the correct basal rate to match the participants' normal base rate which was ~ 31.944 mU/min. In general, this participant received a lot of insulin, but still spent a lot of time in hyperglycemia. We computed ISF and ICR based on the participants' settings during the day and evening and not during the night and morning. Table 3.21 shows the estimated parameters. We focused on getting a meal response in Figure 3.42 for 75-100g CHO meal and an ICR of 5 g/U that would reach around 4.5 mmol/L due to the challenging data.

3.11.2 Results

Table 3.22 and Figure 3.43 shows the outcomes for the glycemic targets and Figure 3.44 shows the results. In general, the AP works very well in both studies, but rescue carbs were required before the snack in the SH study. The AP was most likely unable to prevent the requirement for rescue carbs due to the offset between the CGM and YSI measurements on the second day in the SH study. The participant entered the clinic in hypoglycemia in the DH study and received carbs before the study was started.

Table 3.21: Parameter estimates for participant 11 in the phase 2 trial.

Desc	Param.	init.	lb.	estim.	ub.	unit
inv. ins. TC	k_1	0.02	0.0111	0.02	0.2	1/min
ins. sens.	$\log(SI(0))$	-8.44	-10	-8.42	-6	$\log((1/(\text{mU/L}))/\text{min})$
Endo. gluc. prod	EGP	0.48	0.1	0.52	3	(mg/dL)/min
inv. dist. vol.	$1/V_g$	0.005	0.005	0.005	0.125	1/dL
inv. meal TC	k_m	0.025	0.0111	0.025	0.1	1/min
IC ins. sub.	$I_{sc}(0)$	39.1	0	51.8	1e+06	mU/L
IC ins. plas.	$I_P(0)$	23.9	0	14.1	1e+06	mU/L
IC ins. eff.	$I_{Eff}(0)$	0.022	0	0.0232	1e+06	1/min
IC gluc. conc.	$G(0)$	104	0	104	1e+06	mg/dL
IC meal 1	$D_1(0)$	10	0	10	10	mg
IC meal 2	$D_2(0)$	10	0	10	10	mg
gluc. cov.	Q_g	3.88	0	4.12	30	-
ins. cov.	$\log(Q_{\log SI})$	-9.21	-9.21	-9.21	-9.12	-
gluc. eff.	$GEZI$	-	-	0.000127	-	1/min
ins. to carb. rat.	ICR	-	-	5.000	-	g/U
ins. sens. fac.	ISF	-	-	1.400	-	mmol/L/U
Basal rate	u_{ba}	-	-	1.917	-	U/h

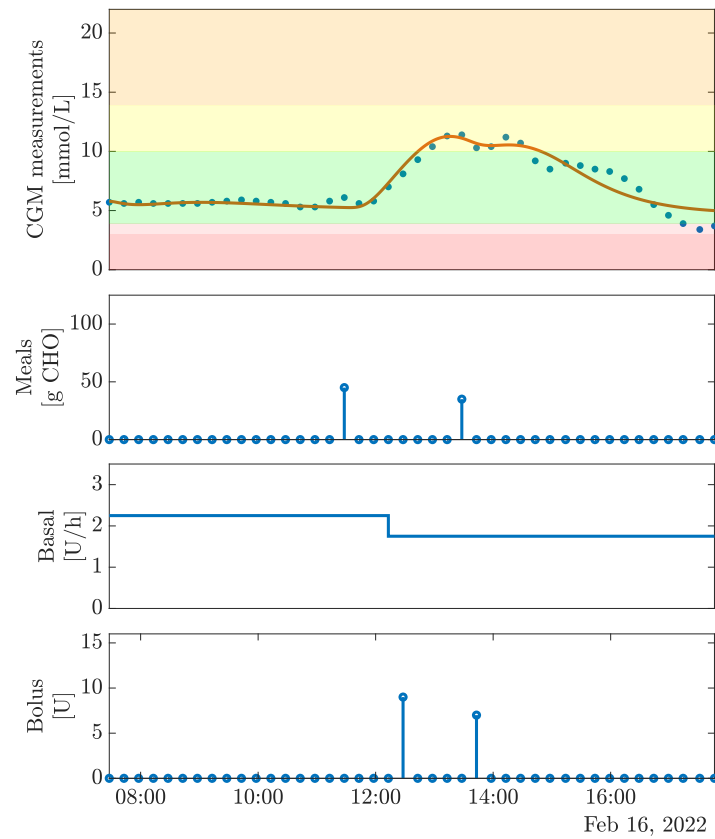


Figure 3.41: Participant 11. Parameter estimation for participant 11 in the phase 2 trial. From the top: 1) CGM measurements (blue dots) and a simulation with the estimated parameters (red line), 2) announced meals, 3) basal insulin rate, and 4) bolus insulin.

Therefore, the AP immediately increased the basal rate to the maximum in the DH study. The participant had a relatively high response to the glucagon administered after the dinner compared to the glucagon administered during the day. The TIR was slightly lower in the DH study, but glucagon prevented the need for rescue carbs and also seemed to prevent hypoglycemia during exercise.

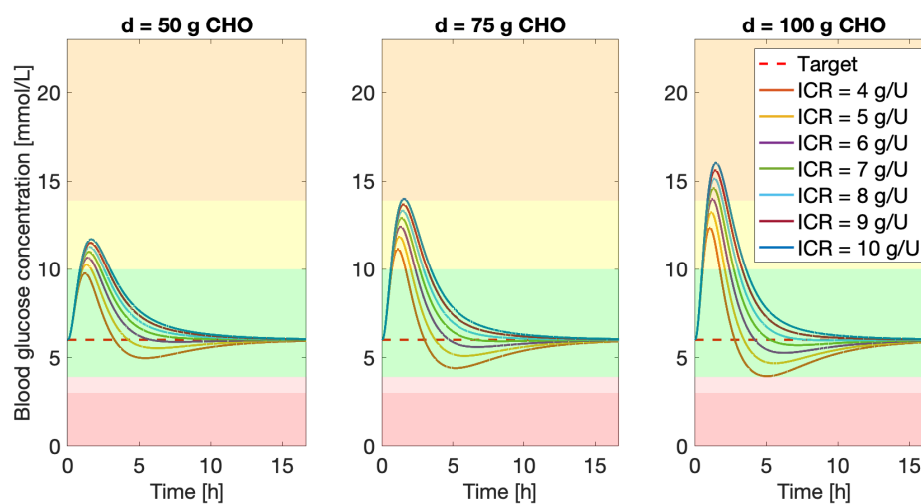


Figure 3.42: Participant 11. Evaluation of the meal responses for participant 11 in the phase 2 trial with an insulin bolus computed from different ICRs.

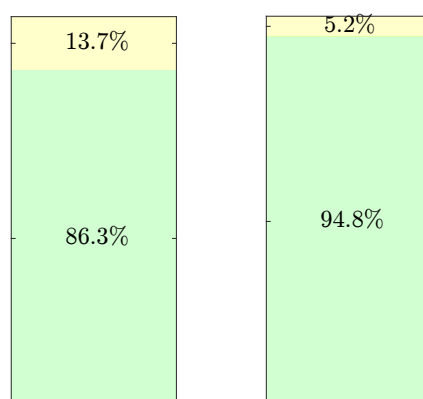


Figure 3.43: Participant 11. Left: TIRs for the DH study for participant 11 in the phase 2 trial. Right: TIRs for the SH study for participant 11 in the phase 2 trial.

Table 3.22: Values of the glycemic targets for participant 11 in the phase 2 trial.

Quantity	Target	DH	SH
Average glucose [mmol/L]	< 8.55	7.39	6.88
GMI [%]	< 7	6.27	6.27
GV [%]	≤ 36	29.41	28.70
Active CGM [%]	100	100.0	100.0

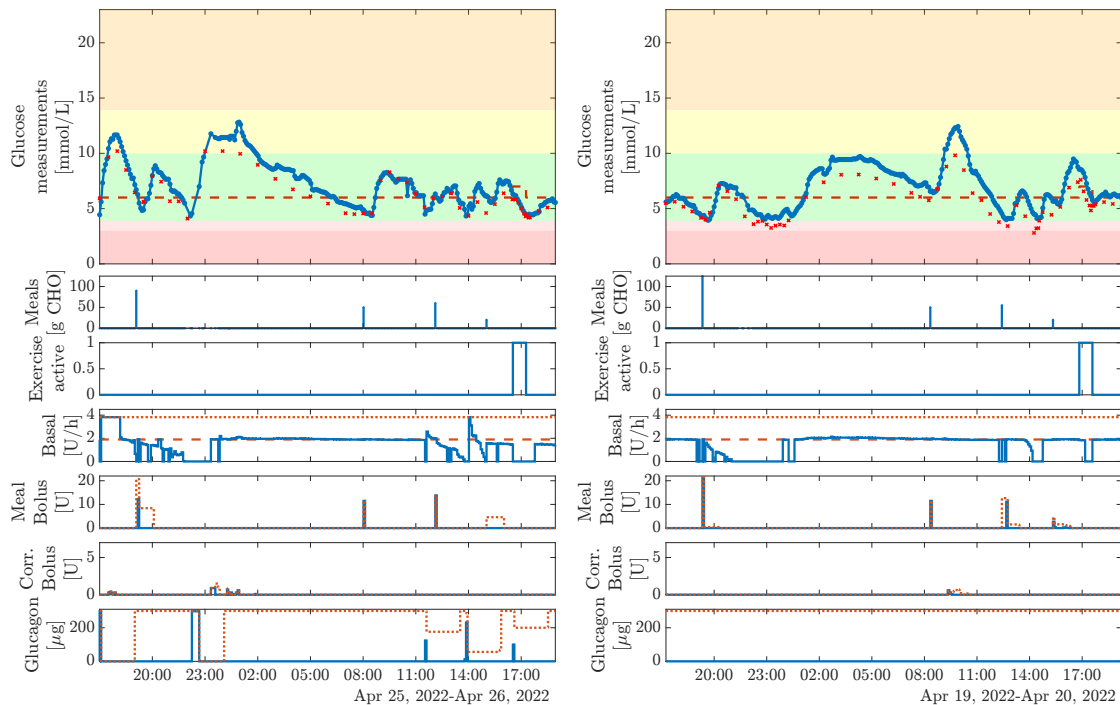


Figure 3.44: Participant 11. Left: Results from the DH study for participant 11 in the phase 2 trial with 86.3% time in range. Right: Results from the SH study for participant 11 in the phase 2 trial with 94.8% time in range. From the top: 1) CGM measurements (blue dotted line), YSI measurements (red crosses), and setpoint (red dashed line), 2) meals, 3) exercise, 4) basal insulin (blue line) and maximum allowed basal insulin (red dots), 5) meal boli (blue line) and maximum allowed meal boli (red dots), 6) correction insulin boli (blue line) and maximum allowed correction boli (red dots), and 7) glucagon boli (blue line) and maximum allowed glucagon boli (red dots).

CHAPTER 4

Conclusions

In this technical report, we described the phase 1 and phase 2 trial of the Diacon dual- and single hormone artificial pancreas in adolescents. We described both the parameter estimation and study outcomes for each participant individually. Each study lasted 26 hours and consisted of 3 meals, a snack and an exercise session of moderate intensity. There were 3 participants in the phase 1 trial and 11 participants in the phase 2 trial. The trials displayed that it is feasible to use NMPC for APs and that both the DH and SH AP are able to control the blood glucose concentration, but identifying a model is a challenging and time-consuming process due to missing data and sometimes also incorrectly announced meals and insulin boli. Identifying a good model is also a learning process and during the studies, we started to set, e.g., the ICR to a value that seemed reasonable instead of using the participants' average value. We also shifted the timing of some of the meals to match the peaks in the glucose concentration instead of directly using the reported data. These adaptations seemed to improve the performance of the AP. There were some technical difficulties that influenced the performance of the AP. PISAs are especially challenging for DH APs as glucagon can be administered even if glucose concentration is not low. That was the case for, e.g., participant 5. Occlusions in the glucagon pump and lost connections also influenced the performance of the AP. It was a limitation that we did not have any data on how the participants would respond to glucagon and used the same parameters for all participants. That caused the predicted glucagon response to be very inaccurate for many participants. Therefore, many participants received too much insulin after glucagon was administered and caused oscillations. We cannot expect to be able to receive glucagon data from each participant, but we could consider to make the parameters related to glucagon adaptive as it is the case for the insulin sensitivity. Despite the challenges related to administration of glucagon in some studies it also prevented hypoglycemia and the need for rescue carbs in others.

Bibliography

- [1] Tadej Battelino, Thomas Danne, Richard Bergenstal, Stephanie Amiel, Roy Beck, Torben Biester, Emanuele Bosi, Bruce Buckingham, William Cefalu, Kelly Close, Claudio Cobelli, Eyal Dassau, J DeVries, Kim Donaghue, Klemen Dovc, Francis Doyle, Shefally Garg, George Grunberger, Simon Heller, and Moshe Phillip. “Clinical Targets for Continuous Glucose Monitoring Data Interpretation: Recommendations From the International Consensus on Time in Range”. In: *Diabetes Care* 42.8 (2019), pages 1593–1603. DOI: 10.2337/dci19-0028.
- [2] Emilie B. Lindkvist, Christian Laugesen, Asbjørn Thode Reenberg, Tobias K. S. Ritschel, Jannet Svensson, John Bagterp Jørgensen, Kirsten Nørgaard, and Ajenthen G. Ranjan. “Performance of a Dual-Hormone Closed-Loop System Versus Insulin-Only Closed-Loop System in Adolescents with Type 1 Diabetes. A Single-Blind, Randomized, Controlled, Crossover Trial”. In: *Frontiers In Endocrinology* 14 (2023), page 1073388. DOI: 10.3389/fendo.2023.1073388.
- [3] Asbjørn Thode Reenberg, Tobias K. S. Ritschel, Emilie B. Lindkvist, Christian Laugesen, Jannet Svensson, Ajenthen G. Ranjan, Kirsten Nørgaard, and John Bagterp Jørgensen. “Nonlinear Model Predictive Control and System Identification for a Dual-hormone Artificial Pancreas”. In: *IFAC-PapersOnLine* 55.7 (2022), pages 915–921. DOI: 10.1016/j.ifacol.2022.07.561.

$$\sqrt{17} \int \delta e^{i\pi} = -1$$

$\{2.7182818284\}$ θ φ ε ρ τ υ θ ι ο π σ δ φ γ η ξ κ λ

$$\chi^2 \gg \approx$$
$$\Sigma ! ,$$

•

APPENDIX M

Conference Paper - ECC 2023

A one-size-fits-all artificial pancreas for people with type 1 diabetes based on physiological insight and feedback control

Authors:

Tobias K. S. Ritschel, Asbjørn Thode Reenberg, Emilie B. Lindkvist, Christian Lauge-sen, Jannet Svensson, Ajenthen G. Ranjan, Kirsten Nørgaard, Bernd Dammann, John Bagterp Jørgensen

Submitted to:

2023 European Control Conference (ECC), accepted.

A one-size-fits-all artificial pancreas for people with type 1 diabetes based on physiological insight and feedback control

Tobias K. S. Ritschel, Asbjørn Thode Reenberg, Emilie B. Lindkvist, Christian Laugesen, Jannet Svensson, Ajenthen G. Ranjan, Kirsten Nørgaard, Bernd Dammann, John Bagterp Jørgensen

Abstract—We propose a model-free artificial pancreas (AP) for people with type 1 diabetes. The algorithmic parameters are tuned to a virtual population of 1,000,000 individuals, and the AP repeatedly estimates the basal and bolus insulin requirements necessary for maintaining normal blood glucose levels. Therefore, the AP can be used without healthcare personnel or engineers customizing the algorithm to each user. The estimates are based on bodyweight, measurements from a continuous glucose monitor (CGM), and estimates of the meal carbohydrate contents. In a virtual clinical trial with all 1,000,000 individuals (i.e., a Monte Carlo closed-loop simulation), the AP achieves a mean time in range of more than 87% and over 88% of the participants satisfy several glycemic targets.

I. INTRODUCTION

Diabetes is a chronic disease where the pancreas produces insufficient amounts of insulin or the body is resistant to insulin. More than 10% of the world's adult population suffers from this disease, and in 2021, USD 966 billion dollars were spent on diabetes (which corresponds to 9% of the global health expenditure) [1]. Type 1 diabetes (T1D) accounts for 5–10% of all cases, and it is caused by autoimmune destruction of the pancreatic insulin-producing cells. Consequently, the pancreas does not produce any insulin. Therefore, people with T1D require daily insulin treatment in order to prevent high blood glucose concentrations (referred to as hyperglycemia). Long periods of hyperglycemia can cause damage to the nerves and eyes and lead to chronic kidney disease and cardiovascular disease. Additionally, incorrect insulin treatment can lead to low blood glucose concentrations (referred to as hypoglycemia). Severe hypoglycemia can lead to a number of acute complications, e.g., loss of consciousness and seizures.

People with T1D spend significant amounts of time on self-treatment. Therefore, there is considerable interest in developing automated insulin delivery systems which can assist them. Such systems are referred to as *artificial pancreases* (APs) [2], and they typically consist of 1) a sensor, often a continuous glucose monitor (CGM), 2) a control system, usually a control algorithm implemented on a smartphone or a dedicated device, and 3) an actuator, e.g., an insulin pump.

This work was partially funded by the IFD Grand Solution project ADAPT-T2D (9068-00056B). A. T. Reenberg, T. K. S. Ritschel, B. Dammann, and J. B. Jørgensen are with the Department of Applied Mathematics and Computer Science, Technical University of Denmark, DK-2800 Kgs. Lyngby, Denmark. E. B. Lindkvist, C. Laugesen, J. Svensson, A. G. Ranjan, and K. Nørgaard are with Steno Diabetes Center Copenhagen, Clinical Research, DK-2730 Herlev, Denmark. Corresponding author: J. B. Jørgensen (E-mail: jbj@dtu.dk).

Many control algorithms have been considered for this purpose. They can be divided into model-free and model-based algorithms. Model-based algorithms typically use model predictive control (MPC) [3]–[6] where a model is used to predict the body's response to, e.g., meal carbohydrates and insulin. MPC is a well-proven control methodology that has been applied to many different types of processes [7]. However, it requires an accurate model. Automatic generation of such a model based on historical data (e.g., CGM measurements, administered insulin, and meal carbohydrates) is an ongoing field of research. Consequently, it remains difficult to make model-based APs widely available because a model must be developed for each individual. In contrast, model-free controllers only rely on a few pieces of information about the body for which estimates are readily available, e.g., the bodyweight, the basal insulin requirement, the insulin-to-carb ratio (ICR), and the insulin sensitivity factor (ISF). These controllers are often based on heuristics [8], fuzzy logic [9], or proportional-integral-derivative (PID) control. PID controllers have been successfully applied in many different industrial applications [10], and several researchers have proposed APs based on concepts from PID control. Marchetti et al. [11] proposed a PID controller which is switched off when a meal is announced and switched back on based on heuristical rules. Huyett et al. [12] described a PID control algorithm for intraperitoneal insulin delivery (whereas most APs deliver insulin subcutaneously which results in a more delayed insulin effect). However, these AP algorithms have not been tested on large numbers of real or virtual people. Therefore, it is currently unknown whether they can be adopted without healthcare personnel or engineers tuning the algorithms specifically for each individual (or group of individuals).

In this work, we present a one-size-fits-all AP algorithm with a single set of controller parameters tuned to a population of 1,000,000 virtual individuals with T1D. It simultaneously estimates the basal insulin and the meal insulin bolus curve. Therefore, it is straightforward for a user to start using the system, and it can also be used for titration. Furthermore, we demonstrate that, for a given objective function, the optimal meal insulin bolus is a nonlinear function of the meal carbohydrate content, and we argue that it can be approximated well by a piecewise linear function. The AP algorithm is an extension of our previous work [13], [14], where we also estimated the basal rate using concepts from PID control but assumed the meal insulin bolus curve to be known (and linear). We test the AP using a previously

developed virtual clinical trial with 1,000,000 participants over 52 weeks [15]. The participants are represented by an extension of the model by Hovorka et al. [16], and the mean time in range (TIR) is 87.2%. Furthermore, all of the participants meet the target on time in level 2 hypoglycemia, and over 88% of the participants meet all targets on TIR, time above range (TAR), time below range (TBR), average glucose, and glucose management indicator (GMI) [17].

The remainder of this paper is organized as follows. In Section II, we analyze the optimal insulin bolus as a function of the meal carbohydrate content, and in Section III, we present the AP. We present the results of the virtual clinical trial in Section IV, and conclusions are given in Section V.

II. ANALYSIS

In this section, we present a dynamic optimization problem for determining the optimal meal insulin bolus as a function of the meal size. We only use this optimization problem to analyze the meal insulin bolus curve. It is not used in the AP algorithm presented in Section III because it would require a model of each person using the AP.

A. The dynamic optimization problem

The dynamic optimization problem determining the optimal meal insulin bolus flow rate is in the form

$$\min_{u_0} \quad \phi = \int_{t_0}^{t_f} \rho(z(t)) dt, \quad (1a)$$

subject to

$$x(t_0) = x_0, \quad (1b)$$

$$\dot{x}(t) = f(x(t), u(t), d(t), \theta), \quad t \in [t_0, t_f], \quad (1c)$$

$$z(t) = g(x(t), \theta), \quad t \in [t_0, t_f], \quad (1d)$$

$$u(t) = u_k, \quad t \in [t_k, t_{k+1}[, \quad k = 0, \dots, N-1, \quad (1e)$$

$$d(t) = d_k, \quad t \in [t_k, t_{k+1}[, \quad k = 0, \dots, N-1, \quad (1f)$$

$$u_{\min} \leq u_0 \leq u_{\max}. \quad (1g)$$

The objective function in (1a) is the integral of the penalty function ρ over the time horizon $[t_0, t_f] = [0, 12]$ h, and N is the number of control intervals. Furthermore, t is time, x are the state variables, u is a vector of manipulated inputs (i.e., the basal and bolus insulin flow rates), d are disturbance variables (i.e., the meal carbohydrate flow rate), z is the output (i.e., the CGM measurement), and θ are model parameters. The initial condition (1b) is the steady state corresponding to a blood glucose concentration of 6 mmol/L, and the dynamical constraint (1c) is the model presented by Hovorka et al. [16] extended with a CGM model [18]. Next, (1d) is an output equation, and (1e)–(1f) are zero-order-hold (ZOH) parametrizations of the manipulated inputs and the disturbance variables. Finally, u_{\min} and u_{\max} in (1g) are lower and upper bounds on the manipulated inputs in the first control interval.

In the first control interval ($k = 0$), the person consumes a meal with a specified meal carbohydrate flow rate, d_0 , and an insulin bolus is administered. For the remaining control intervals ($k > 0$), the disturbances and the bolus insulin flow

TABLE I
THE FIVE GLYCEMIC RANGES DESCRIBED BY HOLT ET AL. [17].

Category	Range [mmol/L]	Color
Level 2 hyperglycemia]13.9, ∞ [Orange
Level 1 hyperglycemia]10.0, 13.9]	Yellow
Normoglycemia	[3.9, 10.0]	Green
Level 1 hypoglycemia	[3.0, 3.9[Light red
Level 2 hypoglycemia	[0.0, 3.0[Red

rate are zero. The insulin basal rate is equal to its steady state value (corresponding to 6 mmol/L) in all control intervals, i.e., it is not a decision variable. Finally, the lower bound on the insulin bolus flow rate in the first control interval ($k = 0$) is 0 and the upper bound is infinity.

The penalty function penalizes the deviation from the setpoint $\bar{z} = 6$ mmol/L and the violation of the soft lower bound $z_{\min} = 3.9$ mmol/L (see also Table I), i.e.,

$$\rho(z(t)) = \bar{\rho}(z(t)) + \kappa \rho_{\min}(z(t)), \quad (2)$$

where

$$\bar{\rho}(z(t)) = \frac{1}{2}(z(t) - \bar{z})^2, \quad (3a)$$

$$\rho_{\min}(z(t)) = \frac{1}{2} \max\{0, z_{\min} - z(t)\}^2. \quad (3b)$$

As the main priority is to avoid hypoglycemia, $\kappa = 10^6$.

B. Optimal insulin bolus curves

For 6 virtual people with type 1 diabetes (i.e., 6 different sets of parameters, θ), Fig. 1 shows the values of the objective function in (1a) for different combinations of (absolute) meal carbohydrate contents and insulin boluses. The black lines indicate the optimal boluses found by solving the dynamic optimization problem (1) using a single-shooting approach. The optimal insulin bolus curve is more nonlinear for some sets of parameters than others. For instance, a linear insulin bolus curve is a worse approximation for person 6 than for person 4. The first kink in the optimal insulin bolus curve (starting from the left) appears because the total non-insulin-dependent glucose flux decreases when the blood glucose concentration comes below 4.5 mmol/L in the model by Hovorka et al. [16]. Consequently, more insulin is required to decrease the concentration below this value. The second kink arises because of the soft lower bound, z_{\min} , in the penalty function. There are no kinks for person 4 because their blood glucose concentration increases very little after meals, i.e., there would be kinks for meals with more than 150 g carbohydrates. In conclusion, a piecewise linear function is a reasonable approximation of the optimal insulin bolus curve.

III. ALGORITHM

At time t_k [min], the AP receives a CGM measurement, y_k [mmol/L], and computes the basal and bolus insulin flow rates, $u_{ba,k}$ [mU/min] and $u_{bo,k}$ [mU/min]. These are clipped and collected in the vector of manipulated inputs,

$$u_k = \max \left\{ 0, \min \left\{ u_{\max}, \begin{bmatrix} u_{ba,k} \\ u_{bo,k} \end{bmatrix} \right\} \right\}, \quad (4)$$

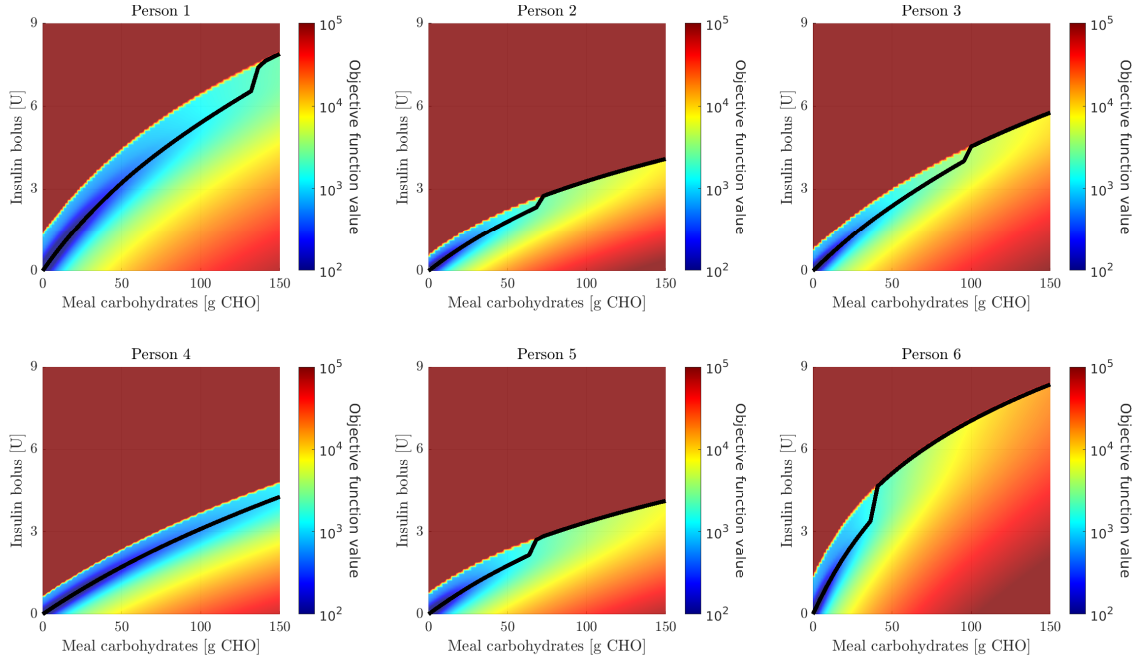


Fig. 1. Values of the objective function (1a) for different (absolute) meal carbohydrate contents and insulin boluses. The black lines indicate the optimal insulin boluses as functions of the meal carbohydrate content, i.e., the solutions to the dynamic optimization problem (1).

which is administered over the following control interval, $[t_k, t_{k+1}]$. The upper bounds on the insulin basal and bolus insulin flow rates (i.e., the elements of u_{\max}) are 55 mU/min and 8000 mU/min, respectively. Furthermore, the control and sampling intervals are identical, and their lengths are $T_s = t_{k+1} - t_k = 5$ min.

If the CGM measurement is above the target value of $\bar{y} = 6$ mmol/L, the basal insulin flow rate is the sum of an estimated nominal basal insulin flow rate, $\bar{u}_{ba,k}$ [mU/min], and a microadjustment term, $u_{ma,k}$ [mU/min]. If the measurement is between the target and the safety threshold $y_s = 3$ mmol/L, the microadjustments are clipped to be non-positive (for safety reasons). Finally, if the measurement is below the safety threshold, the basal rate is zero, i.e.,

$$u_{ba,k} = \begin{cases} \bar{u}_{ba,k} + u_{ma,k} & \text{if } \bar{y} \leq y_k, \\ \bar{u}_{ba,k} + [u_{ma,k}]^- & \text{if } \bar{y} > y_k > y_s, \\ 0 & \text{otherwise,} \end{cases} \quad (5)$$

where $[\cdot]^- = \min\{0, \cdot\}$. The nominal basal insulin flow rate is estimated using an extended integral (I) controller, and the microadjustments are computed using a proportional-derivative (PD) controller:

$$\bar{u}_{ba,k} = I_{ba,k}, \quad (6a)$$

$$u_{ma,k} = P_{ma,k} + D_{ma,k}. \quad (6b)$$

Here, $I_{ba,k}$ is an integral term (see Section III-A) and $P_{ma,k}$ and $D_{ma,k}$ are proportional and derivative terms (see Section III-B).

Based on the analysis in Section II, we compute the meal bolus insulin flow rate as a continuous piecewise linear function of the estimated normalized meal carbohydrate flow rate, \hat{d}_k [g CHO/(kg min)]. That is, \hat{d}_k is the amount of meal carbohydrates the user announces they will consume in the k 'th control interval, divided by the product of their bodyweight and the length of the control interval, T_s . Specifically, the meal bolus insulin flow rate is given by

$$u_{bo,k} = \begin{cases} \alpha_k d_{th} + \frac{\alpha_k}{\beta} (\hat{d}_k - d_{th}) & \text{if } \hat{d}_k > d_{th}, \\ \alpha_k \hat{d}_k & \text{otherwise.} \end{cases} \quad (7)$$

If the normalized meal carbohydrate flow rate is below the threshold $d_{th} = 0.1$ g CHO/(kg min), the insulin bolus flow rate is proportional to the meal carbohydrate flow rate and the slope, α_k [mU kg/(g CHO)], is essentially the inverse of the ICR. For higher normalized meal carbohydrate contents, the slope is divided by $\beta = 2$ (unitless). Both the threshold and β were identified by trial-and-error, and we estimate the meal bolus factor α_k using another extended I-controller, i.e.,

$$\alpha_k = I_{bo,k}, \quad (8)$$

where $I_{bo,k}$ is an integral term described in Section III-C.

A. Estimation of the basal rate

At time t_k , when a CGM measurement becomes available, we update the estimate of the basal rate and ensure that it is non-negative:

$$I_{ba,k} = \max\{0, I_{ba,k-1} + \Delta I_{ba,k}\}. \quad (9)$$

The increment is

$$\Delta I_{ba,k} = w_{ba,k} K_{I,ba} e_{ba,k} T_s, \quad (10)$$

where the unitless binary weight $w_{ba,k}$ is 1 if the last meal was announced more than $\Delta t_m = 9.5$ h ago and 0 otherwise. Furthermore, the integrator gain is $K_{I,ba} = 4 \cdot 10^{-4}$ mU L/(mmol min²), and the error is computed using the deadband $[y_{ba}^l, y_{ba}^u] = [3.9, 8.0]$ mmol/L and a (unitless) hypoglycemia amplification factor, $\gamma = 100$:

$$e_{ba,k} = \begin{cases} y_k - y_{ba}^u & \text{if } y_k > y_{ba}^u, \\ \gamma(y_k - y_{ba}^l) & \text{if } y_k < y_{ba}^l, \\ 0 & \text{otherwise.} \end{cases} \quad (11)$$

B. Microadjustments of the basal rate

The proportional term in the microadjustment of the basal insulin flow rate is

$$P_{ma,k} = w_{ma,k} K_{P,ma} e_k, \quad (12)$$

where the gain is $K_{P,ma} = 0.3$ mU L/(mmol min), and the error is

$$e_k = y_k - \bar{y}. \quad (13)$$

The unitless binary weight $w_{ma,k}$ is 1 if the CGM measurement is below the target or if $w_{ba,k} = 1$. Otherwise, it is zero:

$$w_{ma,k} = \begin{cases} 1 & \text{if } y_k < \bar{y} \text{ or } w_{ba,k} = 1, \\ 0 & \text{otherwise.} \end{cases} \quad (14)$$

The derivative term is

$$D_{ma,k} = w_{ma,k} K_{D,ma} \frac{y_k - y_{k-1}}{T_s}, \quad (15)$$

where the gain is $K_{D,ma} = 10$ mU L/(mmol min) and we disregard changes in the setpoint (which is also constant in this work).

C. Estimation of the meal bolus factor

As for the basal rate, we update the estimate of the meal bolus factor whenever a CGM measurement becomes available and ensure that it is non-negative, i.e.,

$$I_{bo,k} = \max\{0, I_{bo,k-1} + \Delta I_{bo,k}\}, \quad (16)$$

where the increment is

$$\Delta I_{bo,k} = w_{bo,k} K_{I,bo} e_{bo,k} T_s. \quad (17)$$

The unitless binary weight $w_{bo,k}$ is 1 for a time period of Δt_m after every announced meal, i.e., $w_{bo,k}$ and $w_{ba,k}$ never have the same value. Furthermore, the gain is $K_{I,bo} = 0.05$ mU kg L/(g CHO mmol min), and we use both a deadband of $[y_{bo}^l, y_{bo}^u] = [3.9, 10]$ mmol/L, the hypoglycemia amplification factor γ , and clipping to compute the error:

$$e_{bo,k} = \begin{cases} y_{bo}^{th} - y_{bo}^u & \text{if } y_k > y_{bo}^{th}, \\ y_k - y_{bo}^u & \text{if } y_k \in [y_{bo}^l, y_{bo}^{th}], \\ \gamma(y_k - y_{bo}^l) & \text{if } y_k < y_{bo}^l, \\ 0 & \text{otherwise.} \end{cases} \quad (18)$$

The clipping ensures that all CGM measurements above the threshold $y_{bo}^{th} = 13.9$ mmol/L result in the same error.

TABLE II

THE COMPOSITIONS OF THE SEASONS AND THE WEEKS AND THE MEAL CARBOHYDRATE CONTENTS IN THE PROTOCOL DESCRIBED IN [15].

Compositions of the seasons

Season	Standard weeks	Active weeks	Vacation weeks
Winter	6	4	3
Spring	6	6	1
Summer	7	3	3
Autumn	9	3	1

Compositions of the weeks

Week type	Standard days	Active days	Movie nights	Late nights
Standard	4	1	1	1
Active	3	3	1	0
Vacation	5	0	0	2

Bodyweight-dependent meal carbohydrate contents

Meal size	Amount of carbohydrates	For a 70 kg person
Large meal	1.29 g CHO/kg	90 g CHO
Medium meal	0.86 g CHO/kg	60 g CHO
Small meal	0.57 g CHO/kg	40 g CHO
Snack	0.29 g CHO/kg	20 g CHO

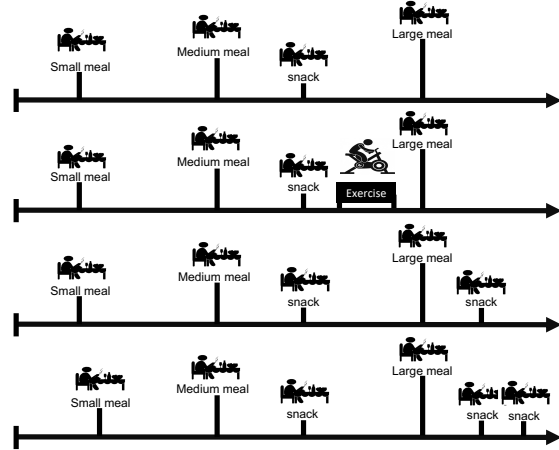


Fig. 2. The different types of days in the autumn and winter of the protocol proposed by Reenberg et al. [15]: standard (top), active (second from the top), day with a movie night (third from the top), and day with a late night (bottom). During spring and summer, the dinner is a medium meal and the afternoon snack is consumed between breakfast and lunch instead.

IV. VIRTUAL CLINICAL TRIAL

In this section, we test the AP algorithm described in Section III in a virtual clinical trial with 1,000,000 participants. The trial starts on January 1st, 2021 and lasts 52 weeks. We use 1) the virtual population and the protocol presented by Reenberg et al. [15] and 2) a previously developed Monte Carlo simulation framework [19], [20]. However, we replace participants for which any time constant is more than 1 order of magnitude smaller or larger than the mean (i.e., we generate new participants). The protocol mimics a Northern European lifestyle, and it consists of 4 seasons lasting 13 weeks each. Each week is categorized as *standard*, *active*, or *vacation*, and all weeks consist of *standard* days, *active* days, days with a *movie night*, and days with a *late night*.

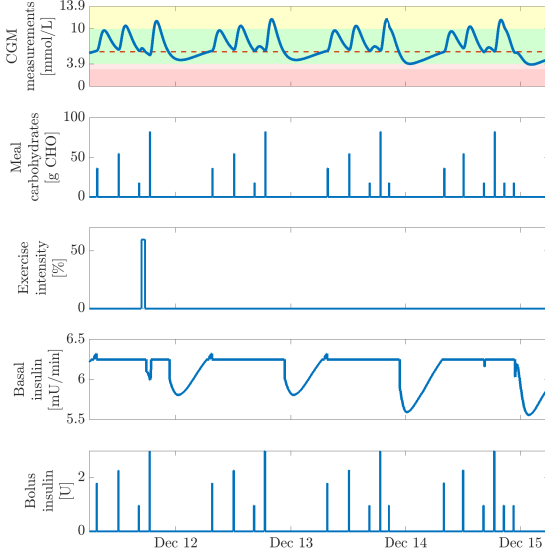


Fig. 3. A single participant's CGM values (top), meal carbohydrate contents (second from the top), exercise intensity (third from the top), basal insulin flow rate (fourth from the top), and insulin boluses (bottom) over 4 days (one of each type) starting at 6:00 AM on December 11th. The colored ranges are described in Table I.

(see Table II and Fig. 2). Each participant is represented using the mathematical model presented by Hovorka et al. [16] extended with a CGM model [18] and an exercise model [21]. The initial estimates of the basal rate and the meal bolus factor are zero, i.e., $I_{ba,0} = I_{bo,0} = 0$, and the initial state is the steady state without insulin administration.

Fig. 3 shows the results of the virtual clinical trial for one participant over four different types of days. The basal rate is constant for most parts of the day, and it is decreased when the CGM measurements are below the target of 6 mmol/L (which mostly happens at night). A bolus is administered for each meal, and for this participant, the majority of the CGM measurements are within the normoglycemic range. However, the estimated nominal basal rate is quite low. Therefore, the CGM measurements increase over night.

In the following, we discuss the efficacy of the AP based on the last 48 weeks of the trial as the estimates of the nominal basal insulin flow rate and the meal bolus factor vary significantly during the first 4 weeks. The participant who obtains the lowest CGM measurement during all 52 weeks (specifically, 1.05 mmol/L) is referred to as the worst-case participant, and Fig. 4 shows the mean and worst-case TIRs. The mean of 87.2% TIR exceeds the target of 70%, and the time in level 1 and 2 hypoglycemia is low, even for the worst-case participant. Fig. 5 shows the cumulative distribution of the CGM measurements. The left tail shows that all participants spend less than 1% of the time in level 2 hypoglycemia and less than 8% of the time in level 1 and 2 hypoglycemia. This can also be seen in Fig. 6 which shows box plots of the TIRs. It also shows that

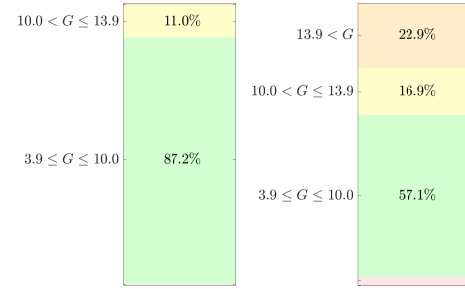


Fig. 4. The mean TIRs (left) and the TIRs for the worst-case participant (right) based on CGM measurements, G , and the ranges in Table I.

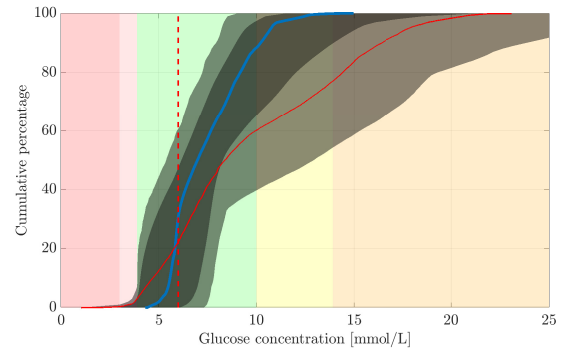


Fig. 5. The cumulative distribution of the CGM measurements for the mean (blue solid line), the worst-case participant (red solid line), the 95% central range (dark grey shaded area), and for all participants (light grey shaded area). The target is 6 mmol/L (red dashed line). The colored ranges are described in Table I.

most participants do not spend significant amounts of time in level 2 hyperglycemia. Table III shows the percentages of participants satisfying the glycemic targets described by Holt et al. [17]. Almost 82% satisfy all targets, and nearly 89% satisfy all average glucose, GMI, TAR, TIR, and TBR targets. Finally, Fig. 7 shows that most of the participants' average total daily doses (TDDs) of basal and bolus insulin are in the intervals [7.5, 25] U/day and [5, 20] U/day, respectively. However, the distributions have long tails towards the right indicating that a few participants require high insulin doses.

V. CONCLUSIONS

We propose a one-size-fits-all AP algorithm for people with T1D, which estimates both the basal insulin flow rate and the meal insulin bolus curve. It is based on physiological insight and concepts from PID control, and it only requires the bodyweight, CGM measurements, and meal carbohydrate estimates. We compute the meal insulin bolus as a piecewise linear function of the meal carbohydrate content normalized with bodyweight, and we test the AP algorithm in a 52 week virtual clinical trial with 1,000,000 participants. The mean TIR is 87.2%, and almost 89% of the participants satisfy targets on average glucose, GMI, TAR, TIR, and TBR.

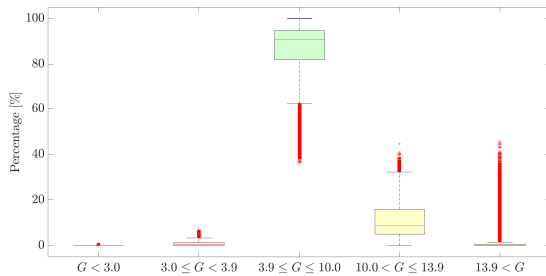


Fig. 6. Box plots of the TIRs with medians (red horizontal lines), boxes spanning the first to the third quartile, and whiskers (solid black horizontal lines). The whiskers are 1.5 times the interquartile ranges (the height of the boxes) above or below the medians, unless the most extreme values are closer to the medians. In that case, the whiskers are the most extreme values. The red pluses are values that are beyond the whiskers (i.e., outliers). The TIRs are based on CGM measurements, G , and the ranges in Table I.

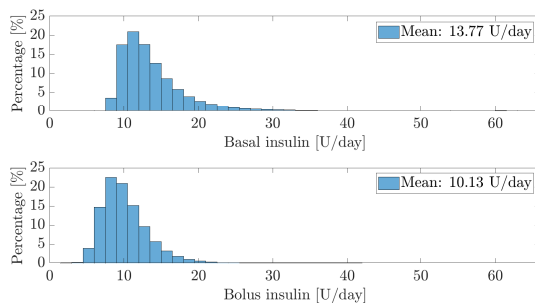


Fig. 7. The distributions of the average TDDs of basal and bolus insulin. Both distributions have long right tails which are hardly visible.

TABLE III

SATISFACTION OF THE GLYCEMIC TARGETS DESCRIBED IN [17].

Quantity	Target	Satisfied
Average glucose	< 154 mg/dL	97.69%
GMI	< 7%	97.77%
GV	≤ 36%	82.70%
TAR (level 2 hyperglycemia)	< 5%	93.97%
TAR (level 1 and 2 hyperglycemia)	< 25%	89.06%
TIR (normoglycemia)	> 70%	92.19%
TBR (level 1 and 2 hypoglycemia)	< 4%	98.85%
TBR (level 2 hypoglycemia)	< 1%	100.00%
All TAR, TIR, and TBR targets		88.92%
All targets except the GV target		88.87%
All targets		81.70%

and R. Nimri, "DREAM5: An open-label, randomized, cross-over study to evaluate the safety and efficacy of day and night closed-loop control by comparing the MD-Logic automated insulin delivery system to sensor augmented pump therapy in patients with type 1 diabetes at home," *Diabetes, Obesity and Metabolism*, vol. 21, no. 4, pp. 822–828, 2019.

- [10] K. J. Åström and R. M. Murray, *Feedback Systems: An Introduction for Scientists and Engineers*, 2nd ed. Princeton University Press, 2008.
- [11] G. Marchetti, M. Barolo, L. Jovanovic, H. Zisser, and D. E. Seborg, "An improved PID switching control strategy for type 1 diabetes," *IEEE Transactions on Biomedical Engineering*, vol. 55, no. 3, pp. 857–865, 2008.
- [12] L. M. Huyett, E. Dassau, H. C. Zisser, and F. J. Doyle III, "Design and evaluation of a robust PID controller for a fully implantable artificial pancreas," *Industrial & Engineering Chemistry Research*, vol. 54, pp. 10 311–10 321, 2015.
- [13] J. B. Jørgensen, D. Boiroux, and Z. Mahmoudi, "An artificial pancreas based on simple control algorithms and physiological insight," *IFAC PapersOnLine*, vol. 52, no. 1, pp. 1018–1023, 2019.
- [14] M. Sejersen, D. Boiroux, S. E. Engell, T. K. S. Ritschel, A. T. Reenberg, and J. B. Jørgensen, "Initial titration for people with type 1 diabetes using an artificial pancreas," *IFAC PapersOnLine*, vol. 54, no. 15, pp. 484–489, 2021.
- [15] A. T. Reenberg, T. K. S. Ritschel, B. Dammann, and J. B. Jørgensen, "High-performance uncertainty quantification in large-scale virtual clinical trials of closed-loop diabetes treatment," in *Proceedings of the 2022 American Control Conference (ACC)*, 2022, pp. 1367–1372.
- [16] R. Hovorka, V. Canonico, L. J. Chassin, U. Haueter, M. Massi-Benedetti, M. O. Federici, T. R. Pieber, H. C. Schaller, L. Schaupp, T. Vering, and M. E. Wilinska, "Nonlinear model predictive control of glucose concentration in subjects with type 1 diabetes," *Physiological Measurement*, vol. 25, no. 4, pp. 905–920, 2004.
- [17] R. I. G. Holt, J. H. DeVries, A. Hess-Fischl, I. B. Hirsch, M. S. Kirkman, T. Klupa, B. Ludwig, K. Nørgaard, J. Pettus, E. Renard, J. S. Skyler, F. J. Snoek, R. S. Weinstock, and A. L. Peters, "The management of type 1 diabetes in adults. A consensus report by the American Diabetes Association (ADA) and the European Association for the Study of Diabetes (EASD)," *Diabetologia*, vol. 64, pp. 2609–2652, 2021.
- [18] A. Facchinetti, S. D. Favero, G. Sparacino, J. R. Castle, W. K. Ward, and C. Cobelli, "Modeling the glucose sensor error," *IEEE Transactions on Biomedical Engineering*, vol. 61, no. 3, pp. 620–629, 2014.
- [19] M. R. Wahlgreen, A. T. Reenberg, M. K. Nielsen, A. Rydahl, T. K. S. Ritschel, B. Dammann, and J. B. Jørgensen, "A high-performance Monte Carlo simulation toolbox for uncertainty quantification of closed-loop systems," in *Proceedings of the 60th Conference on Decision and Control (CDC)*, 2021, pp. 6755–6761.
- [20] DTU Computing Center, "DTU Computing Center resources," 2021, Technical University of Denmark. [Online]. Available: <https://doi.org/10.48714/DTU.HPC.0001>
- [21] M. Rashid, S. Samadi, M. Sevil, I. Hajizadeh, P. Kolodziej, N. Hobbs, Z. Maloney, R. Brandt, J. Feng, M. Park, L. Quinn, and A. Cinar, "Simulation software for assessment of nonlinear and adaptive multivariable control algorithms: Glucose–insulin dynamics in type 1 diabetes," *Computers & Chemical Engineering*, vol. 130, p. 106565, 2019.

REFERENCES

- [1] International Diabetes Federation, "IDF diabetes atlas," 2021, ISBN: 978-2-930229-98-0.
- [2] R. A. Lal, L. Eklaspour, K. Hood, and B. Buckingham, "Realizing a closed-loop (artificial pancreas) system for the treatment of type 1 diabetes," *Endocrine Reviews*, vol. 40, no. 6, pp. 1521–1546, 2019.
- [3] D. Boiroux, A. K. Duun-Henriksen, S. Schmidt, K. Nørgaard, S. Madsbad, N. K. Poulsen, H. Madsen, and J. B. Jørgensen, "Overnight glucose control in people with type 1 diabetes," *Biomedical Signal Processing and Control*, vol. 39, pp. 503–512, 2018.
- [4] D. Boiroux and J. B. Jørgensen, "Nonlinear model predictive control and artificial pancreas technologies," in *2018 IEEE Conference on Decision and Control (CDC)*, 2018, pp. 284–290.
- [5] A. Chakrabarty, E. Healey, D. Shi, S. Zavitsanou, F. J. Doyle III, and E. Dassau, "Embedded model predictive control for a wearable artificial pancreas," *IEEE Transactions on Control Systems Technology*, vol. 28, no. 6, pp. 2600–2607, 2020.
- [6] M. Messori, G. P. Incremona, C. Cobelli, and L. Magni, "Individualized model predictive control for the artificial pancreas: In silico evaluation of closed-loop glucose control," *IEEE Control Systems Magazine*, vol. 38, no. 1, pp. 86–104, 2018.
- [7] M. G. Forbes, R. S. Patwardhan, H. Hamadah, and R. B. Gopaluni, "Model predictive control in industry: Challenges and opportunities," *IFAC-PapersOnLine*, vol. 48, no. 8, pp. 531–538, 2015.
- [8] I. Capel, M. Rigla, G. Garcia-Saez, A. Rodriguez-Herrero, B. Pons, D. Subias, F. Garcia-Garcia, M. Gallach, M. Aguilar, C. Perez-Gandia, E. J. Gomez, A. Caixas, and M. E. Hernandez, "Artificial pancreas using a personalized rule-based controller achieves overnight normoglycemia in patients with type 1 diabetes," *Diabetes Technology and Therapeutics*, vol. 16, no. 3, pp. 172–179, 2014.
- [9] T. Biester, J. Nir, K. Remus, A. Farfel, I. Muller, S. Biester, E. Atlas, K. Dovc, N. Bratina, O. Kordoukouri, T. Battelino, M. Philip, T. Danne,

APPENDIX N

Conference Paper - BMS 2021

Initial titration for people with type 1 diabetes using an artificial pancreas

Authors:

Maria Sejersen, Dimitri Boiroux, Sarah Ellinor Engell, Tobias Kasper Skovborg Ritschel, Asbjørn Thode Reenberg, John Bagterp Jørgensen

Published in:

IFAC-PapersOnLine, 54–15, 484–489, 2021.

Proceedings of the 11th IFAC Symposium on Biological and Medical Systems BMS 2021: Ghent, Belgium, 19–22 September, 2021.



Initial titration for people with type 1 diabetes using an artificial pancreas

Maria Sejersen* Dimitri Boiroux* Sarah Ellinor Engell*
 Tobias Kasper Skovborg Ritschel*
 Asbjørn Thode Reenberg* John Bagterp Jørgensen*

* *Department of Applied Mathematics and Computer Science,
 Technical University of Denmark, DK-2800 Kgs. Lyngby, Denmark*

Abstract: For people with type 1 diabetes and some with type 2 diabetes, the problem of insulin titration, i.e. finding an adequate basal rate of insulin, is a complex and time-consuming task. This paper proposes a simple model-free algorithm and a procedure for fast initial titration in people with type 1 diabetes (T1D). A modified proportional-integral-derivative (PID) controller (i) updates the estimated insulin basal rate, and (ii) administers micro-boli of insulin every 5 minutes using glucose measurements from a continuous glucose monitor (CGM). A bolus calculator mitigates the effect of meals and reduces postprandial peaks. We evaluate the performance of our system qualitatively and numerically using a virtual clinic of 1,000 T1D patients with a broad inter-patient variability representative of a real population of people with T1D. We let the titration phase run for three consecutive days, followed by a three-day test phase using the newly computed basal insulin infusion rate. The proposed algorithm is able to provide a safe titration and individualized treatment for people with T1D.

Copyright © 2021 The Authors. This is an open access article under the CC BY-NC-ND license (<https://creativecommons.org/licenses/by-nc-nd/4.0/>)

Keywords: Control algorithm, PID, Feed-forward control, Run-to-run control, Diabetes, Artificial pancreas.

1. INTRODUCTION

Type 1 diabetes (T1D) accounts for around 10% of the 463 million people living with diabetes worldwide. Due to autoimmune β -cell destruction, people with T1D are unable to produce insulin. Life-long treatment using daily insulin injections is vital to avoid an elevated blood glucose (BG) level (Riddle et al., 2018). Common ways to administer insulin are multiple daily injections (MDI) and continuous subcutaneous insulin infusion (CSII) therapy. MDI therapy uses pens to administer long-acting insulin once daily and rapid-acting insulin several times per day, usually before meals. CSII therapy uses a pump to continuously administer a rapid insulin analogue.

The artificial pancreas (AP) provides closed-loop insulin therapy for T1D, and has even been considered to treat some people with T2D (Bally et al., 2018; Taleb et al., 2019). The AP consists of (i) a continuous glucose monitor (CGM), (ii) a control algorithm and (iii) a CSII pump. The CGM provides frequent glucose measurements, typically every 5 minutes. The control algorithm resides on a smartphone for most prototypes (Cobelli et al., 2012; Kovatchev et al., 2013), but for commercial systems the control algorithm should preferably be embedded on the pump.

Several control technologies have been considered for the AP, such as linear model predictive control (MPC) (Eren-Oruklu et al., 2009; Schmidt et al., 2013; Boiroux et al.,

2018), nonlinear MPC (Hovorka et al., 2004; Boiroux and Jørgensen, 2018), fuzzy logic control (Biester et al., 2019), and proportional integral derivative (PID) control (Marchetti et al., 2006, 2008; Ly et al., 2016). Although MPC-based APs showed similar or slightly better performance in clinical studies than PID-based APs (Steil, 2013; Pinsker et al., 2016), PID technology has proven to be successful in currently available hybrid control systems (Laxminarayan et al., 2012; Ly et al., 2017). The PID-controller can easily be implemented using simple tuning rules, does not require any metabolic model of the insulin-glucose dynamics, and mimics the behavior of the pancreas for a healthy patient (Steil et al., 2004).

The initial use of CSII can be challenging considering the need of estimating the insulin basal rate that brings the BG level to a safe range (King et al., 2016). The basal rate needs to be high enough to lower the glucose level. However, too much insulin causes hypoglycemia and in worst case can be fatal. To estimate the initial basal rate for adult patients in today's CSII treatment, the healthcare professionals calculate the initial basal rate. Either based on the total daily dose (TDD) of MDI or on a combination of the TDD with a body-weight-based method (King, 2012; Chow et al., 2016; Bode et al., 2011). A recent study shows that the TDD method underestimated the patients basal rate with a median error of 10.06%, while the body weight-based method overestimates the patient's basal rate with a median error of 11.1% (Chow et al., 2016).

As an approach to find a safe basal rate for CSII treatment when the TDD is unknown, e.g. for insulin naive patients, we present an implementation of a model-free controller

* This project has partially been funded by the IFD Grand Solution project ADAPT-T2D: 9068-00056B. Corresponding author: J.B. Jørgensen (e-mail: jbjo@dtu.dk)

for initial titration of people with T1D. The proposed controller is a modified PID-controller in the sense that it uses a deadband and contains an anti-windup algorithm. A further modification is that at mealtimes, we suspend the PID-controller for 5.5 hours and give bolus insulin to compensate for the carbohydrates (CHO) intake. To find the estimated basal rate, the patients use an AP with the PID-controller in a three days titration phase. When the estimated basal rate is obtained, we let the study continue with a three days test phase, to test the suggested basal rate. We evaluate the performance of the method by simulating a cohort of 1,000 random generated virtual patients.

The rest of the paper is structured as follows. Section 2 describes the control algorithm. We define the scenario and the simulator used for in silico trials in Section 3. The results are presented in Section 4, the discussion in Section 5, and the conclusion in Section 6.

2. CONTROL ALGORITHM

People with T1D need basal insulin to compensate for the long-term endogenous glucose production, and bolus insulin to control the glucose level after intake of CHO. For each discrete time, t_k , the insulin pump administers the total amount of insulin, $u_{tot}(t_k)$, given by,

$$u_{tot}(t_k) = u_{micro-bolus}(t_k) + u_{bolus}(t_k). \quad (1)$$

$u_{micro-bolus}(t_k)$ is the amount of micro-bolus insulin required to manage the endogenous glucose production, and $u_{bolus}(t_k)$ is the bolus insulin estimated to compensate for the intake of CHO. The micro-bolus insulin basal rate is calculated as,

$$\bar{u}_{micro-bolus}(t_k) = \frac{u_{micro-bolus}(t_k)}{\Delta t_k} = \bar{u}_{basal}(t_k) + \bar{v}(t_k). \quad (2)$$

The nominal basal rate is described by $\bar{u}_{basal}(t_k)$ and $\bar{v}(t_k)$ is the adjustments in the basal rate. $\Delta t_k = T_s$ denotes the time interval the calculated basal rate will be applied for i.e. the sampling time (Jørgensen et al., 2019).

2.1 Filter

The derivative term of the PID-controller is highly sensitive to noise. Though modern CGM systems provide a filtered signal, a first order low-pass filter in discrete time is implemented before computing the basal rate. The filtered CGM-signal $y_F(t_k)$ is calculated as,

$$y_F(t_k) = \alpha y_{CGM}(t_k) + (1 - \alpha)y_F(t_{k-1}), \quad (3)$$

where the smoothing factor $\alpha = 0.2$, corresponding to a time constant of approximately 20 minutes, and $y_{CGM}(t_k)$ is the signal provided by the CGM.

2.2 Micro-bolus and basal rate

The basal insulin rate for controlling the glucose level is conducted by a PID-controller using the filtered CGM-signal $y_F(t_k)$. In continuous time, we consider a PID-controller defined by,

$$\bar{v}(t) = K_p(\bar{y}(t) - y_F(t)) + K_i \int_0^t e_i(\tau) d\tau - K_d \frac{dy_F(t)}{dt}, \quad (4)$$

where K_p, K_i , and K_d denote the proportional, integral, and derivative gains. $\bar{y}(t)$ is the glucose target and $e_i(\tau)$ is the error at the integral. The discrete-time PID-controller corresponding to the continuous-time PID-controller is

$$\bar{v}(t_k) = K_p(\bar{y}(t_k) - y_F(t_k)) + I(t_k) - \frac{K_d}{T_s}(y_F(t_k) - y_F(t_{k-1})). \quad (5)$$

The sampling time, T_s , equals the sampling rate of the CGM, commonly 5 minutes. $I(t_k)$ describes the changes in the basal rate and can be expressed as,

$$I(t_k) = I(t_{k-1}) + K_i T_s e_i(t_k). \quad (6)$$

The error term $e_i(t_k)$ has an integral deadband in the range from 4 to 8 mmol/L. The deadband prevents the integrator from integrating when the glucose level is inside the range of the deadband,

$$e_i(t_k) = \begin{cases} l_{low} - y_F(t_k), & y_F(t_k) \leq l_{low}, \\ 0, & l_{low} < y_F(t_k) \leq l_{up}, \\ l_{up} - y_F(t_k), & y_F(t_k) > l_{up}, \end{cases} \quad (7)$$

where l_{low} and l_{up} are the lower and upper limits of the target range. To avoid integrator windup and negative micro-bolus rate, $\bar{u}_{micro-bolus}(t_k)$ is limited to the interval $[0, U_{max}]$, where $U_{max} = 12$ mU/min for the first 12 hours of simulation while the virtual patients are fasting, and afterwards at the time $t = 12$ hours, the limit is set to $U_{max} = 2I(t_{k-1})$. The micro-bolus rate $\bar{u}_{micro-bolus}(t_k)$ is then,

$$\bar{u}_{micro-bolus}(t_k) = \min(\max(0, \bar{u}_{basal}(t_k) + \bar{v}(t_k)), U_{max}). \quad (8)$$

For patients with low insulin sensitivity the limit on 12 mU/min will in some cases be too insufficient to influence the BG. Therefore, before U_{max} is changed from 12 mU/min to $2I(t_{k-1})$, we measure the filtered CGM signal $y_F(t_k)$. If $y_F(t_k)$ is in the hyperglycaemic range above $y_{hyper} = 10$ mmol/L, and the basal rate after 12 hours is limited to U_{max} , then $I(t_{12hours})$ is set to U_{max} ,

$$I(t_{12hours}) = \begin{cases} U_{max}, & (y_F(t_k) > y_{hyper}) \wedge \\ & (u_{basal}(t_k) = U_{max}), \\ I(t_k), & otherwise. \end{cases} \quad (9)$$

The above definition of the micro-bolus rate consists of the estimated basal rate as well as corrections computed by the PD-controller. Hence, the estimated basal insulin rate is

$$\hat{u}_{basal}(t_k) = \bar{u}_{basal}(t_k) + I(t_k) \quad (10)$$

2.3 Bolus calculator

To balance the glucose level after intake of CHO, people with T1D need bolus insulin. The size of the bolus is calculated using a bolus calculator. Common equations for bolus calculation typically exist of three parts 1) meal insulin, 2) correction insulin, and 3) insulin on board (IOB) (Schmidt and Nørgaard, 2014). The equation is given as (Jørgensen et al., 2019)

$$u_{bolus}(t) = \frac{\hat{d}(t)}{carbF} + \alpha_{corr} \frac{y_F(t) - \bar{y}(t)}{corrF} - \alpha_{IOB} IOB(t). \quad (11)$$

For this paper we only use the meal insulin part of the bolus calculator, and assume that the PID-controller used for the basal rate will do the corrections of the error (Jørgensen et al., 2019). The equation for the bolus calculator is given by

$$u_{bolus}(t) = ICR \cdot \hat{d}(t), \quad (12)$$

where $ICR = 1/carbF$ and $\hat{d}(t)$ is the estimated amount of CHO in grams in the meal. ICR ($U/gCHO$) is the insulin to CHO ratio, i.e. ICR denotes the amount of CHO covered by 1 unit of insulin. Appendix A reports the procedure for computation of the ICR in this paper.

3. SCENARIO

To evaluate the control algorithm, we use a simulator based on the physiological model developed by Hovorka et al. (2004). The Hovorka model describes the metabolic system for people with T1D. It interprets the pharmacokinetic (PK) and pharmacodynamics (PD) response of subcutaneous insulin infusion, CHO absorption, and insulin action.

In the scenario, we simulate a population of 1,000 randomly generated virtual patients. The parameter distribution is stated in Hovorka et al. (2002); Wilinska et al. (2010) and Boiroux et al. (2018). The first three days of the scenario is the titration phase. In this phase, the virtual patients use an AP with the PID-controller to estimate the basal rate. The titration phase is followed by a three-day test phase where we test the estimated basal rate.

We start the study at 18:00 assuming that the patient has not taken any dinner to initiate the titration overnight. For the remaining time of simulation an intake of 60 g, CHO is simulated at 6:00 AM and at 12:00 PM, and an intake of 90 g CHO is simulated at 6:00 PM. The controller gets an announcement at mealtimes, and a bolus is calculated to correct the glucose level after CHO intake. In the titration phase, the PID-controller is suspended for 5.5 hours after a meal, and the basal rate is fixed to the last calculated rate before the meal announcement.

4. RESULTS

Fig. 1 illustrates the glucose concentration, the CHO intake, the bolus insulin administration, the micro-bolus insulin administration and the estimated basal insulin for 10 virtual patients. The first chart shows the glucose concentration, where the postprandial peaks are a response to the CHO intake shown in the second chart. The amplitude of the peaks depends on the amount of CHO and the ratio between the time constants for CHO absorption and subcutaneous (sc) insulin absorption (El Fathi et al., 2018; Boiroux and Jørgensen, 2018). The third chart shows the calculated bolus based on the estimated amount of CHO intake and the virtual patients ICR. After the first 12 hours of simulation, U_{max} is set to $2I(t_{k-1})$, which is reflected by the adjustments in the micro-bolus rate in the fourth

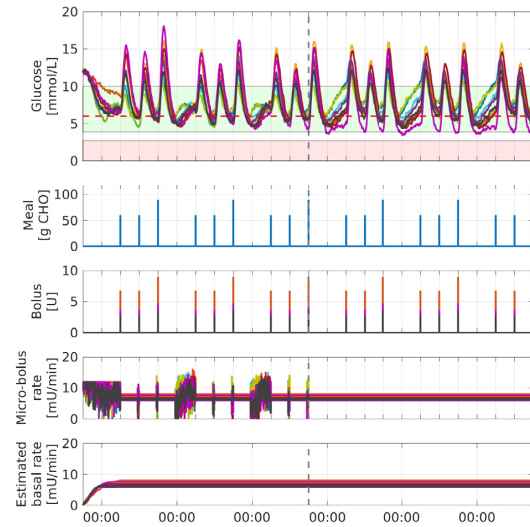


Fig. 1. Simulation of 10 virtual patients. The titration phase runs for three days, followed by a three-day test phase using the estimated basal rate.

Table 1. Distribution of time spend in different glucose concentration ranges during the titration phase for a population of 1,000 virtual patients.

Glucose(mmol/L)	Mean	Q_1	Q_2	Q_3
$0 \leq G < 3$	0.0%	0.0%	0.0%	0.0%
$3 \leq G < 3.9$	0.2%	0.0%	0.0%	0.0%
$3.9 \leq G \leq 10.0$	77.7%	71.9%	77.4%	84.6%
$10.0 < G \leq 13.9$	19.2%	15.0%	19.7%	23.3%
$13.9 < G \leq 26.1$	3.0%	0.0%	0.6%	3.8%

chart. The integrator value emulates the basal rate that we aim to find and is shown in the fifth chart of the figure.

We evaluate the performance of the controller based on the three-day test phase using the estimated basal rate. The mean of the estimated basal rate for the virtual clinic is 8.04 mU/min with a minimum of 5.06 mU/min and a maximum of 29.86 mU/min.

A cumulative distribution was performed on the glucose values of the 1,000 virtual patients in the test phase. Fig. 2 illustrates the result for the cumulative distribution with a mean time in range (TIR) of 78.5%.

Tables 1 and 2 report the population distribution of the time spent in different glucose concentration ranges. Figure 3 illustrates the glucose concentration trajectory for the patient having the worst hypoglycemic episodes (lowest and most time spent in hypo). From these results, it is clear that while the titration is not perfect, it improves current practice and leads to no severe situations.

Recommendations from the International Consensus on TIR (Battelino et al., 2019) states that people living with T1D should spend above 70% time in target range (3.9–10.0 mmol/L), less than 4% below 3.9 mmol/L, less than

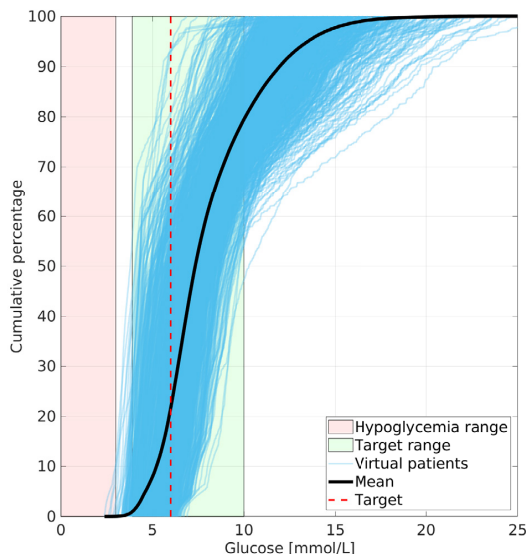


Fig. 2. Cumulative distribution of glucose values, for 1,000 virtual patients in the test phase.

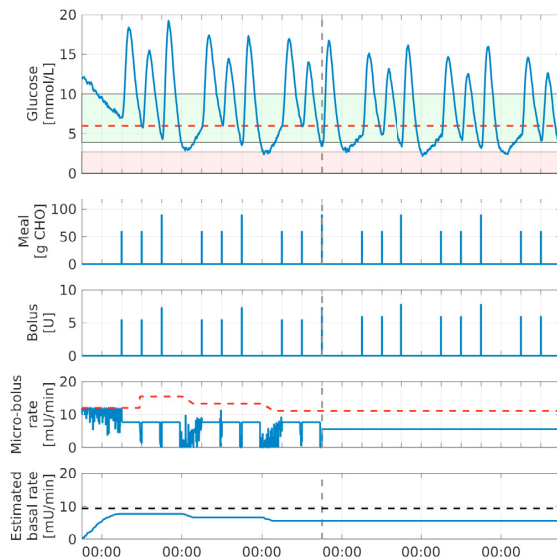


Fig. 3. Profiles for the patient with most time in the glucose concentration range $0 \leq G < 3$. Notice that the time in severe hypoglycemia is very limited and not due to the basal insulin rate being too high. Rather it is due to an overestimated insulin bolus to compensate for the meal.

1% below 3.0 mmol/L, less than 25% above 10.0 mmol/L and less than 5% above 13.9 mmol/L.

In respect to hypoglycemia in our scenario, 2 out of 1,000 virtual patients spend more than 1% below 3.0 mmol/L in the titration phase. In the test phase the number increases to 5 virtual patients, with a minimum of 2.4 mmol/L for both phases. 20 out of 1,000 virtual patients spend more

Table 2. Distribution of time spend in different glucose concentration ranges during the test phase for a population of 1,000 virtual patients.

Glucose (mmol/L)	Mean	Q_1	Q_2	Q_3
$0 \leq G < 3$	0.0%	0.0%	0.0%	0.0%
$3 \leq G < 3.9$	0.9%	0.0%	0.0%	0.0%
$3.9 \leq G \leq 10.0$	78.5%	72.1%	78.0%	84.6%
$10.0 < G \leq 13.9$	16.5%	13.3%	17.7%	20.8%
$13.9 < G \leq 25.9$	4.1%	0.0%	0.0%	6.8%

than 4% below 3.9 mmol/L in the titration phase. In test phase the number increases to 59 virtual patients.

200 out of 1,000 virtual patients did not achieve the goal of 70% TIR during the titration phase. In the test phase the number decreases to 183 virtual patients.

Regarding hyperglycemia 161 out of 1,000 virtual patients spend more than 25% above 10.0 mmol/L in the titration phase while the number decreases to 53 in the test phase. 204 out of 1,000 virtual patients spend more than 5% above 13.9 mmol/L in the titration phase, and in the test phase the number increases to 294.

By using the suggested method, we can get 61.9% of the virtual patient to achieve the recommendations within a 6 days study.

5. DISCUSSION

We evaluated the performance of our system on a virtual clinic of 1,000 T1D patients with a broad inter-patient variability representative of a real population of people with T1D.

It is important to note that the implemented model does neither account for patient intraday variability nor changes in ISF and ICR over time. The effect of exercising or inactivity, e.g. during sleep, is not considered in this paper. In real life, T1D patients in CSII treatment will schedule their basal rates throughout the day. In our test phase we do not tailor the basal rate to the time of the day, which will leave room for improvement of the study. Before the method can be implemented in a real life scenario, we need to obtain the ICR for the patient (King, 2012). In this paper, we use the approach described in Appendix A.

By analyzing our simulations, we can tell that the reason some of the virtual patients suffer from hypoglycemia is mainly due to the bolus insulin. Different bolus administration strategies have an impact on glucose regulation for people with T1D. A more sophisticated bolus calculator could therefore be considered as described in Boiroux et al. (2017), but that would require to identify a T1D model for every patient, and is beyond the scope of this paper.

When the patients start the titration phase, the basal rate is unknown. If we should have used an MPC instead of a PID-controller, we would have needed a good guess on the initial basal rate. Though the MPC might perform better in the long run, it is not suited for the goal of this paper. In addition, after the titration phase is over, and the estimated basal rate is found, it could be considered to

initialize a treatment using an AP with an MPC. Due to cost or individual preferences other patients might prefer to continue the treatment using CSII or MDI.

The goal we use for TIR is internationally recommended. However, goal-settings for glucose regulation should be individualized due to achievable goals for the single patient (Battelino et al., 2019). Large real-world data and studies shows that the average T1D patient's TIR usually lies between 50%-60% (Beck et al., 2019). Therefore, a goal at 70% TIR may not be achievable for all patients. In our results, we stated that it was not possible for all 1,000 virtual patients to reach the goals recommended by the International Consensus within the 6 days scenario; but the majority of patients are better off with the titration method suggested in this paper.

6. CONCLUSION

In this paper we propose a method for initial titration based on a modified PID-controller combined with a simple bolus calculator. We construct a 6 days scenario consisting of a three days titration phase followed by a three days test phase. In the titration phase, we use an AP with the PID-controller. At mealtimes, we calculate a bolus, suspend the controller for 5.5 hours, and set the basal rate to a fixed rate. When the titration phase ends, we switch off the controller and test the estimated basal rate in a three days test phase. The performance of our system is qualitatively and numerically evaluated using a virtual clinic of 1,000 T1D patients.

Goal-settings and treatment of people living with T1D should be individualized. While our method may not be suited for all, we can get 61.9% of the virtual patients to achieve the recommendations from the International Consensus on TIR within a 6 days study.

The results indicate the potential of the method compared to conventional titration. Further studies of the process and clinical studies are required before the titration method can be recommended for clinical practice.

Appendix A. BOLUS CALCULATOR AND INSULIN-TO-CARB RATIO

To estimate the ICR for the virtual patients in the model, we use the penalty function described below to find the bolus size for meals in the range 20 g to 120 g of CHO with an increment of 20 g CHO. When the bolus for the different meal sizes are obtained, linear regression is used to find the insulin to CHO ratio.

As described in Boiroux and Jørgensen (2018) and in Jørgensen et al. (2019), the quadratic glucose penalty function is given by

$$\bar{\rho}(z(t), \bar{z}) = \frac{1}{2}(z(t) - \bar{z})^2, \quad (\text{A.1a})$$

$$\rho_{\min}(z(t), \bar{z}_{\min}) = \frac{1}{2}(\min\{0, z(t) - \bar{z}_{\min}\})^2, \quad (\text{A.1b})$$

$$\rho_{\max}(z(t), \bar{z}_{\max}) = \frac{1}{2}(\max\{0, z(t) - \bar{z}_{\max}\})^2, \quad (\text{A.1c})$$

in which $z(t)$ denotes the predictive BG concentration, and the glucose setpoint \bar{z} is set to 6.0 mmol/L. The lower

threshold is $z_{\min} = 5.3$ mmol/L, and the upper threshold is $z_{\max} = 8.3$ mmol/L. The penalty function is defined as

$$\rho(z(t)) = \bar{\rho}(z(t), \bar{z}) + \kappa \rho_{\min}(z(t), \bar{z}_{\min}) + \lambda \rho_{\max}(z(t), \bar{z}_{\max}), \quad (\text{A.2})$$

where κ and λ are weights associated with hypoglycemia and hyperglycemia, respectively. Since we want the bolus calculator to safely mitigate the effects of CHO intake, i.e. to avoid postprandial hypoglycemia, we set $\kappa \gg \lambda$. The optimal bolus size, u_{bolus} , for a given estimated meal size, \hat{d} , from a steady state, x_{ss} , and with subsequent administration of the basal insulin rate, u_{basal} , is given by minimizing the area under the glucose penalty function curve, i.e. $u_{\text{bolus}} = u_{\text{bolus}}(\hat{d}; x_{ss}, u_{\text{basal}})$ is obtained by solution of the following univariate optimization problem:

$$\min_{u_{\text{bolus}}} \phi = \int_{t_0}^{t_N} \rho(z(t)) dt, \quad (\text{A.3a})$$

$$\text{s.t.} \quad x(t_0) = x_{ss} + \Gamma_u u_{\text{bolus}} + \Gamma_d \hat{d}, \quad (\text{A.3b})$$

$$\dot{x}(t) = f(x(t), u_{\text{basal}}, 0), \quad t \in [t_0, t_N], \quad (\text{A.3c})$$

$$z(t) = g(x(t)), \quad t \in [t_0, t_N], \quad (\text{A.3d})$$

$$0 \leq u_{\text{bolus}} \leq u_{\text{bolus}, \max}. \quad (\text{A.3e})$$

REFERENCES

- Bally, L., Thabit, H., Hartnell, S., Andereggen, E., Ruan, Y., Wilinska, M.E., Evans, M.L., Werth, M.M., Coll, A.P., Stettler, C., et al. (2018). Closed-loop insulin delivery for glycemic control in noncritical care. *New England Journal of Medicine*, 379(6), 547–556.
- Battelino, T., Danne, T., Bergenstal, R.M., Amiel, S.A., Beck, R., Biester, T., Bosi, E., Buckingham, B.A., Cefalu, W.T., Close, K.L., et al. (2019). Clinical targets for continuous glucose monitoring data interpretation: recommendations from the international consensus on time in range. *Diabetes Care*, 42(8), 1593–1603.
- Beck, R.W., Bergenstal, R.M., Riddlesworth, T.D., Kollman, C., Li, Z., Brown, A.S., and Close, K.L. (2019). Validation of time in range as an outcome measure for diabetes clinical trials. *Diabetes Care*, 42(3), 400–405.
- Biester, T., Nir, J., Remus, K., Farfel, A., Muller, I., Biester, S., Atlas, E., Dovc, K., Bratina, N., Kordonouri, O., Battelino, T., Philip, M., Danne, T., and Nimri, R. (2019). DREAM5: An open-label, randomized, cross-over study to evaluate the safety and efficacy of day and night closed-loop control by comparing the MD-logic automated insulin delivery system to sensor augmented pump therapy in patients with type 1 diabetes at home. *Diabetes, Obesity and Metabolism*, 21(4), 822–828.
- Bode, B., Kylo, J., and Kaufman, F. (2011). Medtronic pumping protocol: A guide to insulin pump therapy initiation. 2011. <https://docplayer.net/8616209-Pumping-protocol-a-guide-to-insulin-pump-therapy-initiation.html>.
- Boiroux, D., Aradóttir, T.B., Nørgaard, K., Poulsen, N.K., Madsen, H., and Jørgensen, J.B. (2017). An adaptive nonlinear basal-bolus calculator for patients with type 1 diabetes. *Journal of diabetes science and technology*, 11(1), 29–36.
- Boiroux, D., Duun-Henriksen, A.K., Schmidt, S., Nørgaard, K., Madsbad, S., Poulsen, N.K., Madsen, H., and Jørgensen, J.B. (2018). Overnight glucose control in people with type 1 diabetes. *Biomedical Signal Processing and Control*, 39, 503–512.

- Boiroux, D. and Jørgensen, J.B. (2018). Nonlinear model predictive control and artificial pancreas technologies. In *57th IEEE Conference on Decision and Control (CDC 2018)*, 284–290.
- Chow, N., Shearer, D., Tildesley, H.G., Plaa, J.A., Pottinger, B., Pawlowska, M., White, A., Priestman, A., Ross, S.A., and Tildesley, H.D. (2016). Determining starting basal rates of insulin infusion for insulin pump users: a comparison between methods. *BMJ Open Diabetes Research and Care*, 4(1), e000145.
- Cobelli, C., Renard, E., Kovatchev, B.P., Keith-Hynes, P., Brahim, N.B., Place, J., Del Favero, S., Breton, M., Farret, A., Bruttomesso, D., Dassau, E., Zisser, H., Doyle III, F.J., Patek, S.D., and Avogaro, A. (2012). Pilot studies of wearable outpatient artificial pancreas in type 1 diabetes. *Diabetes Care*, 35(9), e65.
- El Fathi, A., Smaoui, M.R., Gingras, V., Boulet, B., and Haidar, A. (2018). The artificial pancreas and meal control: an overview of postprandial glucose regulation in type 1 diabetes. *IEEE Control Systems Magazine*, 38(1), 67–85.
- Eren-Oruklu, M., Cinar, A., Quinn, L., and Smith, D. (2009). Adaptive control strategy for regulation of blood glucose levels in patients with type 1 diabetes. *Journal of Process Control*, 19, 1333–1346.
- Hovorka, R., Canonico, V., Chassin, L.J., Haueter, U., Massi-Benedetti, M., Federici, M.O., Pieber, T.R., Schaller, H.C., Schaupp, L., Vering, T., and Wilinska, M.E. (2004). Nonlinear model predictive control of glucose concentration in subjects with type 1 diabetes. *Physiological Measurement*, 25, 905–920.
- Hovorka, R., Shojaae-Moradie, F., Carroll, P.V., Chassin, L.J., Gowrie, I.J., Jackson, N.C., Tudor, R.S., Umpleby, A.M., and Jones, R.H. (2002). Partitioning glucose distribution/transport, disposal, and endogenous production during IVGTT. *American Journal of Physiology*, 282, 992–1007.
- Jørgensen, J.B., Boiroux, D., and Mahmoudi, Z. (2019). An artificial pancreas based on simple control algorithms and physiological insight. *IFAC-PapersOnLine*, 52(1), 1018–1023.
- King, A.B., Kuroda, A., Matsuhisa, M., and Hobbs, T. (2016). A review of insulin-dosing formulas for continuous subcutaneous insulin infusion (csii) for adults with type 1 diabetes. *Curr Diab Rep.* 2016,16(9):83. doi: :10.1007/s11892-016-0772-0.
- King, A.B. (2012). Continuous glucose monitoring-guided insulin dosing in pump-treated patients with type 1 diabetes: a clinical guide. *Journal of diabetes science and technology*, 6(1), 191–203.
- Kovatchev, B.P., Renard, E., Cobelli, C., Zisser, H.C., Keith-Hynes, P., Anderson, S.M., Brown, S.A., Chernavsky, D.R., Breton, M.D., Farret, A., Pelletier, M., Place, J., Bruttomesso, D., Del Favero, S., Visentin, R., Filippi, A., Scotton, R., Avogaro, A., and Doyle III, F.J. (2013). Feasibility of outpatient fully integrated closed-loop control: first studies of wearable artificial pancreas. *Diabetes Care*, 36(7), 1851–1858.
- Laxminarayan, S., Reifman, J., and Steil, G.M. (2012). Use of a food and drug administration-approved type 1 diabetes mellitus simulator to evaluate and optimize a proportional-integral-derivative controller. *Journal of Diabetes Science and Technology*, 6(6), 1401–1412.
- Ly, T.T., Keenan, D.B., Roy, A., Han, J., Grosman, B., Cantwell, M., Kurtz, N., von Eyben, R., Clinton, P., Wilson, D.M., et al. (2016). Automated overnight closed-loop control using a proportional-integral-derivative algorithm with insulin feedback in children and adolescents with type 1 diabetes at diabetes camp. *Diabetes Technology & Therapeutics*, 18(6), 377–384.
- Ly, T.T., Weinzimer, S.A., Maahs, D.M., Sherr, J.L., Roy, A., Grosman, B., Cantwell, M., Kurtz, N., Carria, L., Messer, L., von Eyben, R., and Buckingham, B.A. (2017). Automated hybrid closed-loop control with a proportional-integral-derivative based system in adolescents and adults with type 1 diabetes: individualizing settings for optimal performance. *Pediatric Diabetes*, 18(5), 348–355.
- Marchetti, G., Barolo, M., Jovanović, L., Zisser, H., and Seborg, D.E. (2008). A feedforward-feedback glucose control strategy for type 1 diabetes mellitus. *Journal of Process Control*, 18(2), 149–162.
- Marchetti, G., Barolo, M., Jovanović, L., Zisser, H., and Seborg, D.E. (2006). An improved PID switching control strategy for type 1 diabetes. In *2006 International Conference of the IEEE Engineering in Medicine and Biology Society*, 5041–5044. New York City, USA.
- Pinsker, J.E., Lee, J.B., Dassau, E., Seborg, D.E., Bradley, P.K., Gondhalekar, R., Bevier, W.C., Huyett, L., Zisser, H.C., and Doyle, F.J. (2016). Randomized crossover comparison of personalized mpc and pid control algorithms for the artificial pancreas. *Diabetes Care*, 39(7), 1135–1142.
- Riddle, M. et al. (2018). American diabetes association: standards of medical care in diabetes. *Diabetes Care*, 41(1).
- Schmidt, S., Boiroux, D., Duun-Henriksen, A.K., Frøssing, L., Skyggebjerg, O., Jørgensen, J.B., Poulsen, N.K., Madsen, H., Madsbad, S., and Nørgaard, K. (2013). Model-based closed-loop glucose control in type 1 diabetes: The DiaCon experience. *Journal of Diabetes Science and Technology*, 7(5), 1255–1264.
- Schmidt, S. and Nørgaard, K. (2014). Bolus calculators. *Journal of diabetes science and technology*, 8(5), 1035–1041.
- Steil, G.M. (2013). Algorithms for a closed-loop artificial pancreas: the case for proportional-integral-derivative control. *Journal of Diabetes Science and Technology*, 7(6), 1621–1631.
- Steil, G.M., Panteleon, A.E., and Rebrin, K. (2004). Closed-loop insulin delivery—the path to physiological glucose control. *Advanced Drug Delivery Reviews*, 56(2), 125–144.
- Taleb, N., Carpentier, A.C., Messier, V., Ladouceur, M., Haidar, A., and Rabasa-Lhoret, R. (2019). Efficacy of artificial pancreas use in patients with type 2 diabetes using intensive insulin therapy: A randomized crossover pilot trial. *Diabetes Care*, 42(7), e107–e109.
- Wilinska, M.E., Chassin, L.J., Acerini, C.L., Allen, J.M., Dunger, D.B., and Hovorka, R. (2010). Simulation environment to evaluate closed-loop insulin delivery systems in type 1 diabetes. *Journal of Diabetes Science and Technology*, 4(1), 132–144.

APPENDIX 

Conference Paper - CDC 2019

Model Predictive Control of the Blood Glucose
Concentration for Critically Ill Patients in Intensive Care
Units

Authors:

Asbjørn Thode Reenberg, Dimitri Boiroux, Tobias Kasper Skovborg Ritschel, John Bagterp Jørgensen

Published in:

Proceedings of the 2019 IEEE 58th Conference on Decision and Control (CDC), Palais des Congrès et des Expositions Nice Acropolis, Nice, France, December 11–13, 2019.

2019 IEEE 58th Conference on Decision and Control (CDC)
 Palais des Congrès et des Expositions Nice Acropolis
 Nice, France, December 11-13, 2019

Model Predictive Control of the Blood Glucose Concentration for Critically Ill Patients in Intensive Care Units

Asbjørn Thode Reenberg, Dimitri Boiroux, Tobias Kasper Skovborg Ritschel, John Bagterp Jørgensen

Abstract—In this paper we present a linear model predictive control (MPC) algorithm for control of the blood glucose concentration of critically ill patients in an intensive care unit (ICU). We present a version of the algorithm that is suitable for automatic control. The algorithm can administer insulin and glucose. The insulin and glucose are administered using a parenteral (intravenous) route. We use a hysteresis logic to switch between insulin and glucose administration to prevent simultaneous administration of insulin and glucose. We test our algorithm *in silico* using three different simulation models to demonstrate the closed-loop performance of the algorithm. The MPC algorithm is based on linear models in the form of parsimonious second-order transfer functions describing the effect of intravenously injected insulin and glucose on the blood glucose concentration and a first-order disturbance transfer function containing an integrator to ensure offset-free control. The numerical results show that even in the ideal case without any measurement delay, tight glycemic control (80-110 mg/dL) cannot be achieved. Moreover, parenteral glucose is a requirement to avoid hypoglycemia and ensure extended tight glycemic control (60-140 mg/dL).

I. INTRODUCTION

In a seminal paper, Van den Berghe et al. [1] demonstrated that tight glycemic control (TGC) in the fasting normal range, 80-110 mg/dL, reduces morbidities and mortalities of critically ill patients in a surgical intensive care unit (ICU). Another study, NICE-SUGAR [2], was not able to confirm the benefits of TGC compared to conventional glucose control; TGC resulted in increased mortality and a significantly increased occurrence of hypoglycemic episodes compared to the conventional glucose control. In the Leuven study by Van den Berghe et al. [1], normal glucose control is defined as intervention when the measured glucose concentration exceeds 215 mg/dL, while the NICE-SUGAR study [2] defines normal glucose control as intervention when the glucose concentration exceeds 180 mg/dL and with a target of 140 mg/dL. Overall, the results from these studies suggest that it is beneficial to avoid hypoglycemia (glucose concentrations less than 60 mg/dL), hyperglycemia (glucose concentrations above 180 mg/dL), and to stay in a glucose concentration zone between 80 to 110 mg/dL, there is however no clear consensus on the optimal range associated to TGC at the moment [3], [4].

To achieve TGC, it is crucial to get accurate and frequent measurements of the glucose concentration. Several continuous or semi-continuous glucose monitoring (CGM)

devices are available on the market, with different designs, measurement methods, sampling frequency and analysis time. Generally, there are three different ways of measuring glucose concentration. It can be measured from 1) venous blood or arterial blood, 2) dialysate from venous or arterial blood or 3) interstitial fluid. Measuring glucose concentration from interstitial fluid is common for people with type 1 diabetes, but appears to be inappropriate in the ICU as they provide delayed and inaccurate glucose measurements and are prone to technical failures [5]. The sensors using venous or arterial blood provide higher accuracy and less analysis time than sensors using interstitial fluid, which we show has a large impact on TGC in the ICU. The benefit of sensors using dialysis is that they provide accurate measurements and avoid any antibody reaction. However, sensors using dialysis have a delay varying between 5 and 45 minutes [6]. The GlucoScout directly measures glucose concentration from venous or arterial blood, has been FDA approved, and has an analysis time of 50 seconds. The GlucoSet is another sensor directly measuring glucose concentration from venous or arterial blood. It is still in development and also has an analysis time of seconds. Numerous sensors using venous or arterial blood have however failed going from development into production and being commercially available [7].

Feeding of critically ill patients can be done by enteral nutrition (EN), i.e. through a tube, by parenteral nutrition (PN), i.e. using an intravenous (iv.) route, or a combination thereof (EN+PN). As a general guideline, it is preferable to use EN [8]. However, using EN is not always possible, e.g. if the digestive system is damaged, or if fasting of the patient is required. In most cases, using EN alone may lead to underfeeding [9] and would require to use PN as a complementary source. From a control perspective, using PN to provide glucose gives a direct access to the bloodstream, and allows to immediately raise glucose concentration whenever needed, whereas EN has a delay [10]. In general, there is no clear consensus on the benefits of one way of nutrition over the other, and using EN+PN has no negative effect compared to EN alone [11].

Hyperglycemia and insulin resistance are common in critically ill patients, even for patients without diabetes. Conventionally, nurses use paper-based protocols for glucose regulation in the ICU. Nevertheless, these protocols lead to suboptimal glucose regulation [12]. To reduce the occurrence of hyperglycemia and achieve TGC, it is necessary to use a computer-based algorithm.

*A. T. Reenberg, D. Boiroux, T. K. S. Ritschel and J. B. Jørgensen are with the Department of Applied Mathematics and Computer Science, Technical University of Denmark, DK-2800 Kgs. Lyngby, Denmark. Corresponding author: J. B. Jørgensen (E-mail: jbj@dtu.dk)

Model predictive control (MPC) and proportional integral derivative (PID) algorithms are the most popular algorithms for glucose regulation in critically ill patients [13]–[16]. However, in clinical studies, using a control algorithm administering insulin alone led to recurrent hypoglycemia [17], [18], unless the glucose target is set to a value outside the fasting normal range [19]. To reduce the risk of hyper- and hypoglycemia, we consider an MPC-based algorithm administering iv. insulin and iv. glucose. A hysteresis switch ensures that insulin and glucose are not administered simultaneously.

This paper is structured as follows. Section II reviews the physiological models of critically ill patients used in our simulations. Section III describes our MPC algorithm and the hysteresis switch logic between iv. insulin and iv. glucose administration. In Section IV, we numerically evaluate the performance of our controller using three patients based on three different physiological models. We use the same controller tuning for the three patients. The key contributions of this paper consist of the design of an MPC algorithm able to almost achieve TGC in the idealized case without measurement- noise and delay for three different virtual patients using identical controller parameters. The key contributions will also be listed in more detail in Section V.

II. SIMULATION MODELS

Numerous models have been presented by multiple research groups and the most accurate model has yet to be found [20]–[22]. In this study we perform simulations using three different models representing three different patients, namely the Bergman's Minimal model [25] slightly modified in [23], the Hovorka ICU model [10] and the Chase ICU model [24]. We present each model with the added term $R_a(t) = d(t) + \frac{u_G(t)}{V_G}$, where $d(t)$ represents the disturbance in the glucose concentration caused by stress and $u_G(t)$ is the glucose infusion. We use the models with units according to the parameters used. We note that the units are different for each model and we change the inputs from the controller in the simulations accordingly.

A. Bergman's Minimal Model

We use the parameters presented in [26]. The model is

$$\dot{G}(t) = -X(t)G(t) + p_1(G_b - G(t)) + R_a(t), \quad (1a)$$

$$\dot{X}(t) = -p_2X(t) + p_3(I(t) - I_b), \quad (1b)$$

$$\dot{I}(t) = \alpha\gamma \max(G(t) - \theta_I, 0) - \gamma_I(I(t) - I_b) + \frac{F_i}{V_I}. \quad (1c)$$

$G(t)$ represents the glucose concentration, $X(t)$ represents the insulin action on glucose concentration, and $I(t)$ represents the insulin concentration.

B. Hovorka ICU Model

In this paper, the model will be described in broad terms and the equations describing the time-dependent parameters will not be listed. We refer to [10] for a detailed description.

The differential equations describing the Hovorka ICU model are

$$\begin{aligned} \dot{Q}_1(t) = & -F_{01}^c(t) - k_{21}(t)Q_1(t) + k_{12}Q_2(t) - U_R(t) \\ & + \frac{5.551}{W} \left[\frac{R_a(t)V_G}{60} + \frac{A_2(t)}{t_{max,G}} \right] + EGP(t) \end{aligned} \quad (2a)$$

$$\begin{aligned} \dot{Q}_2(t) = & k_{21}(t)Q_1(t) \\ & - [k_{12} + S_{I,MOD}(t)S_{ID}x_2(t)]Q_2(t) \end{aligned} \quad (2b)$$

$$\begin{aligned} \dot{I}(t) = & \frac{1000}{60W} \frac{U_{IX}(t) + U_{IE}(t)}{V_I} \\ & - k_e \frac{K_{M,I}}{I(t) + K_{M,I}} I(t) \end{aligned} \quad (2c)$$

$$\dot{x}_1(t) = -k_{a1}[x_1(t) - I(t)] \quad (2d)$$

$$\dot{x}_2(t) = -k_{a2}[x_2(t) - I(t)] \quad (2e)$$

$$\dot{x}_3(t) = -k_{a3}[x_3(t) - I(t)] \quad (2f)$$

$$\dot{A}_1(t) = \frac{F_{GE}U_{GE}(t)}{60} - \frac{A_1(t)}{t_{max,G}} \quad (2g)$$

$$\dot{A}_2(t) = \frac{A_1(t)}{t_{max,G}} - \frac{A_2(t)}{t_{max,G}} \quad (2h)$$

$Q_1(t)$ and $Q_2(t)$ represent the glucose amount per kg as a two-compartment model, $I(t)$ represents the plasma insulin concentration, $x_1(t)$, $x_2(t)$, and $x_3(t)$ represent the insulin action on glucose concentration. $A_1(t)$ and $A_2(t)$ model the enteral glucose absorption. We use the parameters from Patient 3 in [10]. $G(t)$ is the glucose concentration, U_{IE} is the endogenous insulin secretion, F_{01}^c is the total non-insulin-dependent glucose flux corrected for the current glucose concentration. $U_R(t)$ is the renal glucose clearance and depends on the glucose concentration. The endogenous glucose production, $EGP(t)$, depends on the action of insulin, $x_3(t)$. $k_{21}(t)$ is the fractional transfer rate of glucose from the accessible to the non-accessible compartment, and depends on $x_1(t)$. $S_{I,MOD}$ is the insulin sensitivity modifier and is time-invariant in this paper.

C. Chase Model

We use the parameters presented in [15], and based on the model in [25]. The model is

$$\dot{G}(t) = -P_G G(t) - \frac{S_I(G(t) + G_E)Q(t)}{1 + \alpha_G Q(t)} + R_a(t), \quad (3a)$$

$$\dot{Q}(t) = -kQ(t) + kI(t), \quad (3b)$$

$$\dot{I}(t) = \frac{-nI(t)}{1 + \alpha_I I(t)} + \frac{u_{ex}}{V_I}. \quad (3c)$$

$G(t)$ represents the glucose concentration as a deviation from the glucose concentration at steady state, G_E . $Q(t)$ represents the insulin action on the glucose concentration. $I(t)$ is the insulin concentration as a deviation variable from the insulin steady state.

III. MODEL PREDICTIVE CONTROL

In this section, we present a model predictive control algorithm based on a stochastic continuous-discrete state space model. The model is a multiple input single output (MISO) transfer model function consisting of: 1) A second-order transfer function describing the effect of iv. insulin on glucose concentration, 2) a second-order transfer function describing the effect of iv. glucose on glucose concentration, and 3) a first-order transfer function without or with an integrator for the stochastic part. The measurements are corrupted by additive white noise.

A. Model

For the filtering and prediction, in the model predictive controller, we use a continuous-time linear stochastic model:

$$Z(s) = Z_D(s) + Z_S(s) \quad (4a)$$

$$= G_I(s)U_I(s) + G_G(s)U_G(s) + H(s)W(s), \quad (4b)$$

in which $Z_D(s) = G_I(s)U_I(s) + G_G(s)U_G(s)$ describes the deterministic part of the model, and $Z_S(s) = H(s)W(s)$ describes the stochastic part of the model. The deterministic part of the model is modelled using two second-order transfer functions:

$$G_I(s) = \frac{K_I}{(\tau_I s + 1)^2}; \quad G_G(s) = \frac{K_G}{(\tau_G s + 1)^2}. \quad (5)$$

The stochastic part of the model is a first-order transfer function without or with an integrator, i.e.

$$H(s) = \frac{K_w}{\tau_w s + 1}, \quad (6)$$

or

$$H(s) = \frac{1}{s} \frac{K_w}{\tau_w s + 1}. \quad (7)$$

The transfer function model (4) may be realized as a system of linear stochastic differential equations (SDEs)

$$dx(t) = (A_c x(t) + B_c u(t)) dt + G_c d\omega(t), \quad (8a)$$

$$z(t) = Cx(t), \quad (8b)$$

with $x = [x^D; x^S]$. $d\omega(t)$ is a standard Wiener process, i.e. $d\omega(t) \sim N_{iid}(0, dt)$, and

$$A_c = \begin{bmatrix} A_{cD} & 0 \\ 0 & A_{cS} \end{bmatrix}, \quad B_c = \begin{bmatrix} B_{cD} \\ 0 \end{bmatrix}, \quad G_c = \begin{bmatrix} 0 \\ G_{cS} \end{bmatrix}, \quad (9a)$$

$$C = [C_D \quad C_S]. \quad (9b)$$

The transfer functions (5) are realized in observer canonical form by

$$A_{cD} = \begin{bmatrix} A_{cD;I} & 0 \\ 0 & A_{cD;G} \end{bmatrix} = \begin{bmatrix} -\frac{2}{\tau_I} & 1 & 0 & 0 \\ -\frac{1}{\tau_I^2} & 0 & 0 & 0 \\ 0 & 0 & -\frac{2}{\tau_G} & 1 \\ 0 & 0 & -\frac{1}{\tau_G^2} & 0 \end{bmatrix}, \quad (10a)$$

$$B_{cD} = \begin{bmatrix} B_{cD;I} & 0 \\ 0 & B_{cD;G} \end{bmatrix} = \begin{bmatrix} 0 & 0 \\ \frac{K_I}{\tau_I^2} & 0 \\ 0 & 0 \\ 0 & \frac{K_G}{\tau_G^2} \end{bmatrix}, \quad (10b)$$

$$C_D = [C_{D;I} \quad C_{D;G}] = [1 \quad 0 \quad 1 \quad 0]. \quad (10c)$$

Similarly, the transfer functions in (6)-(7) may be realized in observer canonical form by

$$A_{cS} = -\frac{1}{\tau_w}, \quad G_{cS} = \frac{K_w}{\tau_w}, \quad C_S = 1, \quad (11a)$$

$$A_{cS} = \begin{bmatrix} -\frac{1}{\tau_w} & 1 \\ 0 & 0 \end{bmatrix}, \quad G_{cS} = \begin{bmatrix} 0 \\ \frac{K_w}{\tau_w} \end{bmatrix}, \quad C_S = [1 \quad 0]. \quad (11b)$$

Using a zero-order-hold discretization for the manipulated variable, $u(t) = [u_{k;I} \quad u_{k;G}]'$ for $t_k \leq t < t_{k+1}$, (8) may be converted to the linear stochastic difference equation

$$x_{k+1} = Ax_k + Bu_k + w_k, \quad w_k \sim N_{iid}(0, Q), \quad (12a)$$

$$z_k = Cx_k, \quad (12b)$$

where

$$A = \exp(A_c T_s), \quad (13a)$$

$$B = \int_0^{T_s} \exp(A_c s) ds B_c, \quad (13b)$$

$$Q = \int_0^{T_s} \exp(A_c s) G_c G_c' \exp(A_c' s) ds. \quad (13c)$$

Using the matrix exponential, (A, B, Q) in (13) may be computed by the procedure [27]

$$\begin{bmatrix} A & B \\ 0 & I \end{bmatrix} = \exp \left(\begin{bmatrix} A_c & B_c \\ 0 & 0 \end{bmatrix} T_s \right), \quad (14a)$$

$$\begin{bmatrix} \Phi_{11} & \Phi_{12} \\ 0 & \Phi_{22} \end{bmatrix} = \exp \left(\begin{bmatrix} -A_c & G_c G_c' \\ 0 & A_c' \end{bmatrix} T_s \right), \quad (14b)$$

$$Q = \Phi_{22}' \Phi_{12}, \quad (14c)$$

where A , B , and Q have the structure:

$$A = \begin{bmatrix} A_D & 0 \\ 0 & A_S \end{bmatrix} = \begin{bmatrix} A_{D;I} & 0 & 0 \\ 0 & A_{D;G} & 0 \\ 0 & 0 & A_S \end{bmatrix}, \quad (15a)$$

$$B = \begin{bmatrix} B_D \\ 0 \end{bmatrix} = \begin{bmatrix} B_{D;I} & 0 \\ 0 & B_{D;G} \\ 0 & 0 \end{bmatrix}, \quad (15b)$$

$$Q = \begin{bmatrix} 0 & 0 \\ 0 & Q_S \end{bmatrix}. \quad (15c)$$

Consequently, we may use this structure as well as (4) to separate the output, z_k , into a deterministic part, z_k^D , and a stochastic part, z_k^S :

$$z_k = z_k^D + z_k^S. \quad (16)$$

The deterministic output, z_k^D , is given by

$$x_{k+1}^D = A_D x_k^D + B_D u_k, \quad (17a)$$

$$z_k^D = C_D x_k^D, \quad (17b)$$

where

$$\begin{bmatrix} A_D & B_D \\ 0 & I \end{bmatrix} = \exp \left(\begin{bmatrix} A_{cD} & B_{cD} \\ 0 & 0 \end{bmatrix} T_s \right). \quad (18)$$

Let $\beta_i = T_s/\tau_i$, where $i \in \{I, G\}$. Then the transfer functions (5) allow explicit expressions for $A_{D;i}$ and $B_{D;i}$:

$$A_{D;i} = \begin{bmatrix} (1 - \beta_i)e^{-\beta_i} & T_s e^{-\beta_i} \\ -\frac{\beta_i}{\tau_i} e^{-\beta_i} & (1 + \beta_i)e^{-\beta_i} \end{bmatrix}, \quad (19a)$$

$$B_{D;i} = \begin{bmatrix} K_i (1 - \beta_i e^{-\beta_i} - e^{-\beta_i}) \\ K_i \frac{2 - \beta_i e^{-\beta_i} - 2e^{-\beta_i}}{\tau_i} \end{bmatrix}. \quad (19b)$$

The stochastic part of the output, z_k^S , is given by

$$x_{k+1}^S = A_S x_k^S + B_S w_k^S, \quad w_k^S \sim N(0, Q_S), \quad (20a)$$

$$z_k^S = C_S x_k^S, \quad (20b)$$

where $B_S = I$ and

$$\begin{bmatrix} \Phi_{S,11} & \Phi_{S,12} \\ 0 & \Phi_{S,22} \end{bmatrix} = \exp \left(\begin{bmatrix} -A_{cS} & G_{cS} G'_{cS} \\ 0 & A'_{cS} \end{bmatrix} T_s \right), \quad (21a)$$

$$A_S = \Phi'_{S,22}, \quad (21b)$$

$$Q_S = A_S \Phi_{S,12}. \quad (21c)$$

The matrices (A_S, Q_S) for the stochastic state-space model may be computed explicitly for the transfer function in (6)-(7). Let $\beta_w = T_s/\tau_w$. In the case of a first-order filter without an integrator (6), we have [27]

$$A_S = e^{-\beta_w}, \quad (22a)$$

$$Q_S = \frac{K_w^2}{2\tau_w} (1 - e^{-2\beta_w}). \quad (22b)$$

In the case of a first-order filter with an integrator (7), we have [27]

$$A_S = \begin{bmatrix} e^{-\beta_w} & \tau_w (1 - e^{-\beta_w}) \\ 0 & 1 \end{bmatrix}, \quad (23a)$$

$$Q_S = K_w^2 \begin{bmatrix} \alpha & \beta_w - 1 + e^{-\beta_w} \\ \beta_w - 1 + e^{-\beta_w} & \frac{\beta_w}{\tau_w} \end{bmatrix}, \quad (23b)$$

where

$$\alpha = \tau_w \left(\beta_w - \frac{3}{2} + 2e^{-\beta_w} - \frac{1}{2}e^{-2\beta_w} \right). \quad (24)$$

B. Filtering and Prediction

1) *No measurement delay*: The measurement of the blood glucose concentration, y_k , is the output, z_k , corrupted by additive normally distributed noise, v_k , i.e.

$$y(t_k) = z(t_k) + v_k, \quad v_k \sim N_{iid}(0, R), \quad (25)$$

where $R = \sigma_{vv}^2$. The corresponding stochastic measurement defined as $y_k^S = y_k - z_k^D$ may be expressed as

$$y_k^S = y_k - z_k^D = z_k^S + v_k \quad (26)$$

such that we get the following model for filtering and prediction

$$x_{k+1}^S = A_S x_k^S + B_S w_k^S, \quad (27a)$$

$$z_k^S = C_S x_k^S, \quad (27b)$$

$$y_k^S = C_S x_k^S + v_k, \quad (27c)$$

where $C_{Sz} = C_{Sy} = C_S$ such that $y_k^S = z_k^S + v_k$. The corresponding Kalman filter for filtering is

$$\hat{x}_{k|k-1}^S = A_S \hat{x}_{k-1|k-1}^S, \quad (28a)$$

$$e_k = y_k^S - C_{Sy} \hat{x}_{k|k-1}^S, \quad (28b)$$

$$\hat{x}_{k|k}^S = \hat{x}_{k|k-1}^S + K_k e_k, \quad (28c)$$

where

$$P_{k|k-1} = A_S P_{k-1|k-1} A_S' + B_S Q_S B_S', \quad (29a)$$

$$R_{e,k} = C_{Sy} P_{k|k-1} C_{Sy}' + R, \quad (29b)$$

$$K_k = P_{k|k-1} C_{Sy}' R_{e,k}^{-1}, \quad (29c)$$

$$P_{k|k} = P_{k|k-1} - K_k R_{e,k} K_k'. \quad (29d)$$

Let $P = \lim_{k \rightarrow \infty} P_{k|k-1}$ and $K = \lim_{k \rightarrow \infty} K_k$. The limits exist if (A_S, C_{Sy}) is detectable and $(A_S, B_S Q_S^{1/2})$ is stabilizable. P may be computed by fixed-point iteration in (29) or by solution of the discrete algebraic Riccati equation

$$P = A_S P A_S' + B_S Q_S B_S' - (A_S P C_{Sy}') (C_{Sy} P C_{Sy}' + R)^{-1} (A_S P C_{Sy}')'. \quad (30)$$

Given P , the Kalman filter gain, K , may be computed by

$$K = P C_{Sy}' (C_{Sy} P C_{Sy}' + R)^{-1}. \quad (31)$$

The filtered states using the stationary Kalman filter gain can be expressed as

$$\hat{x}_{k|k}^S = (I - K C_{Sy}) A_S \hat{x}_{k-1|k-1}^S + K(y_k - z_k^D). \quad (32)$$

The corresponding predictions are

$$\hat{x}_{k+j+1|k}^S = A_S \hat{x}_{k+j|k}^S, \quad (33a)$$

$$\hat{z}_{k+j+1|k}^S = C_{Sz} \hat{x}_{k+j+1|k}^S. \quad (33b)$$

Then the deterministic target values, $\bar{z}_{k+j|k}^D$, corresponding to the overall target values, $\bar{z}_{k+j|k}$ ((45), (46)), can be computed as

$$\bar{z}_{k+j|k}^D = \bar{z}_{k+j|k} - \hat{z}_{k+j|k}^S, \quad j = 1, 2, \dots, N. \quad (34)$$

Similarly, the value for deterministic soft minimum output constraints,

$$z_{k+j|k, \min}^D = z_{k+j|k, \min} - \hat{z}_{k+j|k}^S, \quad j = 1, 2, \dots, N. \quad (35)$$

2) *Measurement delay*: We assume that the glucose measurements are delayed with a delay of τ_m minutes, i.e.

$$y(t_k) = \hat{z}(k - \tau_m) + v_k, \quad v_k \sim N_{iid}(0, R). \quad (36)$$

Furthermore, we assume that the measurement delay is a multiple of the sampling time, i.e. $\tau_m = mT_s$ min with m being an integer.

In that case, we model the measurement delay using augmented states to represent the delay, i.e.

$$x_{k+1}^{Dd} = A_d x_k^{Dd} + B_d z_k^D, \quad (37a)$$

$$x_{k+1}^{Sd} = A_d x_k^{Sd} + B_d z_k^S, \quad (37b)$$

$$y_k = C_d x_k^{Dd} + C_d x_k^{Sd} + v_k, \quad (37c)$$

with

$$A_d = \begin{bmatrix} 0 & I \\ 0 & 0 \end{bmatrix}, B_d = \begin{bmatrix} 0 \\ 1 \end{bmatrix}, C_d = \begin{bmatrix} 1 & 0 \end{bmatrix}, \quad (38)$$

where I is an $m \times m$ identity matrix. Consequently, the overall state model consisting of (17), (20), and (37) becomes

$$\begin{bmatrix} x_{k+1}^D \\ x_{k+1}^{Dd} \\ x_{k+1}^S \\ x_{k+1}^{Sd} \end{bmatrix} = \begin{bmatrix} A_D & 0 & 0 & 0 \\ B_d C_D & A_d & 0 & 0 \\ 0 & 0 & A_S & 0 \\ 0 & 0 & B_d C_S & A_d \end{bmatrix} \begin{bmatrix} x_k^D \\ x_k^{Dd} \\ x_k^S \\ x_k^{Sd} \end{bmatrix} + \begin{bmatrix} B_D \\ 0 \\ 0 \\ 0 \end{bmatrix} u_k + \begin{bmatrix} 0 \\ 0 \\ B_S \\ 0 \end{bmatrix} w_k^S, \quad (39a)$$

$$z_k = \begin{bmatrix} C_D & 0 & C_S & 0 \end{bmatrix} \begin{bmatrix} x_k^D \\ x_k^{Dd} \\ x_k^S \\ x_k^{Sd} \end{bmatrix}, \quad (39b)$$

$$y_k = \begin{bmatrix} 0 & C_d & 0 & C_d \end{bmatrix} \begin{bmatrix} x_k^D \\ x_k^{Dd} \\ x_k^S \\ x_k^{Sd} \end{bmatrix} + v_k. \quad (39c)$$

The delay model (37) is constructed such that the model (39) can be decomposed into a deterministic model and a stochastic model. The deterministic sub model of (39) is

$$\begin{bmatrix} x_{k+1}^D \\ x_{k+1}^{Dd} \end{bmatrix} = \begin{bmatrix} A_D & 0 \\ B_d C_D & A_d \end{bmatrix} \begin{bmatrix} x_k^D \\ x_k^{Dd} \end{bmatrix} + \begin{bmatrix} B_D \\ 0 \end{bmatrix} u_k, \quad (40a)$$

$$z_k = \begin{bmatrix} C_D & 0 \end{bmatrix} \begin{bmatrix} x_k^D \\ x_k^{Dd} \end{bmatrix}, \quad (40b)$$

$$y_k^D = \begin{bmatrix} 0 & C_d \end{bmatrix} \begin{bmatrix} x_k^D \\ x_k^{Dd} \end{bmatrix}. \quad (40c)$$

Define the stochastic observation as

$$y_k^S = y_k - y_k^D. \quad (41)$$

Then the stochastic sub-model of (39) may be expressed as

$$\begin{bmatrix} x_{k+1}^S \\ x_{k+1}^{Sd} \end{bmatrix} = \begin{bmatrix} A_S & 0 \\ B_d C_S & A_d \end{bmatrix} \begin{bmatrix} x_k^S \\ x_k^{Sd} \end{bmatrix} + \begin{bmatrix} B_S \\ 0 \end{bmatrix} w_k^S, \quad (42a)$$

$$z_k^S = \begin{bmatrix} C_S & 0 \end{bmatrix} \begin{bmatrix} x_k^S \\ x_k^{Sd} \end{bmatrix}, \quad (42b)$$

$$y_k^S = \begin{bmatrix} 0 & C_d \end{bmatrix} \begin{bmatrix} x_k^S \\ x_k^{Sd} \end{bmatrix} + v_k. \quad (42c)$$

The stochastic sub-model (42) can be expressed in the standard form

$$\bar{x}_{k+1}^S = \bar{A}_S \bar{x}_k^S + \bar{B}_S w_k^S, \quad (43a)$$

$$z_k^S = \bar{C}_{Sz} \bar{x}_k^S, \quad (43b)$$

$$y_k^S = \bar{C}_{Sy} \bar{x}_k^S + v_k, \quad (43c)$$

where $\bar{x}_k^S = [x_k^S; x_k^{Sd}]$ and

$$\bar{A}_S = \begin{bmatrix} A_S & 0 \\ B_d C_S & A_d \end{bmatrix}, \quad \bar{B}_S = \begin{bmatrix} B_S \\ 0 \end{bmatrix}, \quad (44a)$$

$$\bar{C}_{Sz} = \begin{bmatrix} C_S & 0 \end{bmatrix}, \quad \bar{C}_{Sy} = \begin{bmatrix} 0 & C_d \end{bmatrix}. \quad (44b)$$

The structure of (43) is identical to the structure of the stochastic state model for the situation without measurement delay (27). Consequently, the Kalman filter gain, \bar{K} , for (43) may be computed by solution, \bar{P} , of the discrete algebraic Riccati equation (30) and computation of \bar{K} in (31) using $(\bar{A}_S, \bar{B}_S, \bar{C}_{Sy}, Q_S, R)$. Similarly, the filtering and predictions are done using (32)-(35) with the matrices $(\bar{A}_S, \bar{C}_{Sy}, \bar{K}, \bar{C}_{Sz})$.

C. Regulation

Let $x_k, \{\bar{z}_{k+j|k}\}_{j=1}^N, \{z_{k+j|k, \min}\}_{j=1}^N$ and $\{z_{k+j|k, \max}\}_{j=1}^N$ be given along with u_{\min} and u_{\max} . The optimal control problem (OCP) solved to determine the optimal insulin or glucose infusion is the following convex quadratic program (QP):

$$\min \phi \quad (45a)$$

$$\text{s.t. } x_{k+j+1|k} = A x_{k+j|k} + B_i u_{k+j|k; i}, \quad j \in \mathcal{N}, \quad (45b)$$

$$z_{k+j+1|k} = C x_{k+j+1|k}, \quad j \in \mathcal{N}, \quad (45c)$$

$$u_{\min} \leq u_{k+j|k; i} \leq u_{\max}, \quad j \in \mathcal{N}, \quad (45d)$$

$$z_{k+j+1|k} + s_{k+j+1|k} \geq z_{k+j+1|k, \min}, \quad j \in \mathcal{N}, \quad (45e)$$

$$z_{k+j+1|k} - t_{k+j+1|k} \leq z_{k+j+1|k, \max}, \quad j \in \mathcal{N}, \quad (45f)$$

$$s_{k+j+1|k} \geq 0, \quad j \in \mathcal{N}, \quad (45g)$$

$$t_{k+j+1|k} \geq 0, \quad j \in \mathcal{N}, \quad (45h)$$

with $\mathcal{N} = \{0, 1, \dots, N-1\}$, $i \in \{I, G\}$. The objective function, ϕ , is defined as

$$\phi = \underbrace{\frac{1}{2} \sum_{j=1}^N \gamma_{z; i} (z_{k+j|k} - \bar{z}_{k+j|k})^2 + \gamma_{s; i} s_{k+j|k}^2 + \gamma_{t; i} t_{k+j|k}^2}_{\text{penalty function}} + \underbrace{\frac{1}{2} \sum_{j=0}^{N-1} \gamma_{\Delta u; i} \Delta u_{k+j|k; i}^2}_{\text{regularization}}, \quad i \in \{I, G\}. \quad (46)$$

To avoid the simultaneous administration of insulin and glucose, we use a hysteresis switch logic. The switch uses the following logic:

- If the glucose concentration falls under $z_{\min} + 5$ mg/dL, we switch off the insulin administration and switch on the glucose administration.
- If glucose concentration raises over $z_{\max} - 5$ mg/dL, we switch on the insulin administration and switch off the glucose administration.

Since patients in the ICU usually enter the clinic with elevated glucose concentrations, we always initialize our controller using insulin administration.

IV. SIMULATION RESULTS

In this section, we test our MPC algorithm presented in Section III using three virtual patients. To ensure offset-free control of the glucose concentration during stress periods, we use the first-order stochastic model with integrator (7).

TABLE I
PARAMETER VALUES FOR THE CONTROLLER WITHOUT AND WITH
MEASUREMENT DELAY.

Parameter	Value (w/o. delay)	Value (w. delay)	Unit
K_I	-0.0044	-0.0044	[(mg/dL)/(μU/min)]
τ_I	85	85	[min]
K_G	0.05	0.05	[(mg/dL)/(mg/min)]
τ_G	1	2	[min]
K_w	1	1	[mg/dL]
τ_w	10	1	[min]
T_s	5	5	[min]
R	1	2	[mg/dL] ²
m	0	2	[-]
N	144	144	[-]

TABLE II
PENALTY VALUES FOR THE CONTROLLER WITHOUT AND WITH
MEASUREMENT DELAY.

Penalty	Value (w/o. delay)	Value (w. delay)
γ_z	1	1
γ_s	$1 \cdot 10^6$	$1 \cdot 10^6$
γ_t	$1 \cdot 10^4$	$1 \cdot 10^4$
$\gamma_{\Delta u}^I$	$1 \cdot 10^{-9}$	$1 \cdot 10^{-10}$
$\gamma_{\Delta u}^G$	$1 \cdot 10^{-3}$	$1 \cdot 10^{-2}$

We simulate 1) cases where the glucose concentration is measured without any delay corresponding to a glucose sensor with direct access to venous or arterial blood and 2) cases where the glucose concentration is measured with a delay of 10 minutes (i.e. $m = 2$ time samples) corresponding to a sensor measuring glucose concentration from a dialysate. We assume that the three ICU patients have a body mass of 75 kg.

Table I shows the tuning parameters used in the MPC algorithm. These tuning parameters are identical for the three ICU patients. The gains associated with insulin and glucose injections, K_I and K_G , can be personalized depending on the body mass. The prediction and control horizon, N , is 144 samples, i.e. 12 hours. Having a long prediction and control horizon ensures that the solution of the OCP (45) converges back to the glucose setpoint. Therefore, the performance of the controller in this paper is similar to a controller with an infinite prediction and control horizon.

Table II shows the penalty values used for the controller with and without delay. Again, these parameters are identical for the three simulated patients. Since hypoglycemia should be avoided, we set the penalty weight associated to hypoglycemia, γ_s , to a much larger value than the penalty weight associated to hyperglycemia, γ_t . γ_z , γ_s and γ_t , are identical for the insulin and the glucose controllers.

Table III shows the glucose setpoint for each patient. This setpoint also corresponds to the basal glucose concentration. For the Hovorka model, it corresponds to the steady state solution of the Hovorka ICU model (2). For the Chase model (3) and the Bergman minimal model (1), we set these values to 90 mg/dL. The upper limits on insulin and glucose injections, $u_{\max;I}$ and $u_{\max;G}$, are set to high values and are never reached. The glucose thresholds, z_{\min} and z_{\max} , correspond to the tight glucose range (80-110 mg/dL).

TABLE III
SETPOINT (BASAL GLUCOSE CONCENTRATION) FOR EACH PATIENT.

Patient:	Basal glucose conc	Unit
Hovorka ICU Model (Patient 1)	97.16	[mg/dL]
Chase Model (Patient 2)	90.00	[mg/dL]
Bergman minimal Model (Patient 3)	90.00	[mg/dL]

Fig. 1 shows the glucose concentration, iv. insulin infusion and iv. glucose infusion for the three considered patients. We consider a 12-hour scenario with a stress period (highlighted in yellow) corresponding to a steady state at around 200 mg/dL in the cases without any glucose control (black curves).

In the cases without measurement delay (Figs. 1(a), 1(c), and 1(e)), TGC with glucose concentrations between 80 and 110 mg/dL can almost be achieved. No glucose concentration below 80 mg/dL has been reported for Patient 1 and Patient 3, and Patient 2 spent 1.39% of the time with a glucose concentration below 80 mg/dL. Moreover, no severe hypoglycemia (i.e. $G < 60$ mg/dL) has been observed. For all three patients, we can achieve offset-free control of glucose concentration during and after the stress period. Due to the slow dynamics, Patient 1 still requires an infusion of iv. glucose at the end of the simulation. The iv. insulin infusions for patients 1 and 3 are slightly oscillating during the stress period. However, the sequence of insulin infusions and the glucose concentration stabilize during the stress period. These oscillations are due to the fact that the tuning of the controller is common to the three patients. For all three patients, insulin is administered only during the stress period, and glucose is administered only after the stress period. Patient 2 required the highest amount of iv. glucose (30.4 g), which corresponds to a calorie intake of approximately 121.6 kcal.

The performance of the controller deteriorates in the cases with a 10-minute measurement delay (Figs. 1(b), 1(d), and 1(f)), particularly when the glucose dynamics are rapidly changing, i.e. right after the onset of stress and right after the end of the period of stress. After the end of the stress period, all three patients experience a prolonged period of mild hypoglycemia (i.e. $G < 80$ mg/dL). No severe hypoglycemia (i.e. $G < 60$ mg/dL) has been observed for any of the three patients. Similarly to the case without any measurement delay, the controller is able to bring all three patients into TGC during the period of stress by administering iv. insulin and after the end of the stress period by administering iv. glucose. Unlike the cases without measurement delay, iv. insulin is injected for a short while after the end of the stress period due to the glucose measurement delay. Iv. glucose is administered only after the stress period.

These results demonstrate 1) the necessity of being able to inject glucose in addition to insulin for critically ill patients, 2) the necessity of continuously monitoring glucose and 3) the necessity of frequent adjustments in iv. insulin and iv. glucose doses. Also, due to sudden and unpredictable metabolic variations in glucose concentrations, minimizing the lags and delays associated to glucose sensing, administration of insulin and glucose is crucial to achieve TGC.

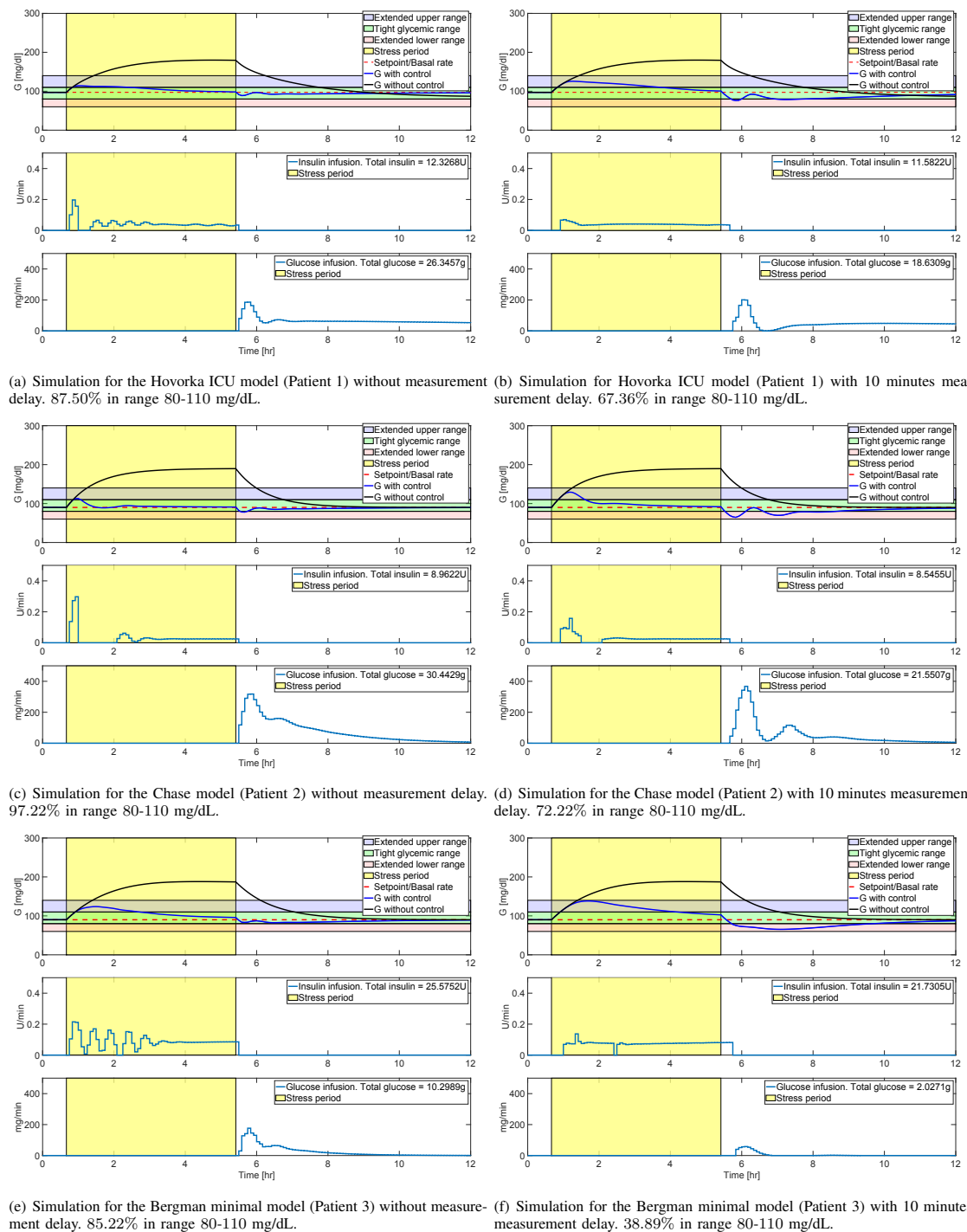


Fig. 1. Closed-loop simulation results for the different models with and without measurement delay. In each subfigure, Top: Glucose concentration with (blue) and without (black) closed-loop control. Middle: Iv. insulin infusion rate. Bottom: Iv. glucose administration.

In a real clinical study, the iv. glucose injections would also be complemented with further nutrition in carbohydrates, fats and proteins to ensure an adequate supply of calories. The problem of TGC in the ICU combined with nutrition leads to further challenges that can also be solved using model-based control algorithms, see e.g. [28], [29].

V. CONCLUSION

In this paper we applied MPC to regulate blood glucose concentration in critically ill patients. The model used in the MPC-based algorithm contains a deterministic part representing the dynamics of iv. insulin and iv. glucose, and a stochastic part capturing the uncertainties arising from the mismatch between the model and the patient, and the effect of unpredicted disturbances such as increased insulin resistance during stress periods. Using iv. insulin in combination with iv. glucose is a requirement to get blood glucose concentrations near TGC. In the idealized case without any measurement noise and delay, it is possible to almost achieve TGC without any overfeeding. Additional measurement lags and delays associated to glucose sensing or EN make TGC more difficult to achieve. The stringent range required for TGC increases the risk of hypoglycemia.

REFERENCES

- [1] G. Van den Berghe, P. Wouters, F. Weekers, C. Verwaest, F. Bruyninckx, M. Schetz, D. Vlasselaers, P. Ferdinande, P. Lauwers, and R. Bouillon, "Intensive insulin therapy in critically ill patients," *New England Journal of Medicine*, vol. 345, no. 19, pp. 1359–1367, 2001.
- [2] S. Finfer and NICE-SUGAR Study Investigators, "Intensive versus conventional glucose control in critically ill patients," *New England Journal of Medicine*, vol. 360, no. 13, pp. 1283–1297, 2009.
- [3] G. Van den Berghe, M. Schetz, D. Vlasselaers, G. Hermans, A. Wilmer, R. Bouillon, and D. Mesotten, "Intensive insulin therapy in critically ill patients: NICE-SUGAR or Leuven glucose target?" *The Journal of Clinical Endocrinology & Metabolism*, vol. 94, no. 9, pp. 3163–3170, 2009.
- [4] J. Gunst and G. Van den Berghe, "Blood glucose control in the intensive care unit: Benefits and risks," *Seminars in Dialysis*, vol. 23, no. 2, pp. 157–162, 2010.
- [5] R. T. van Hooijdonk, J. H. Leopold, T. Winters, J. M. Binnekade, N. P. Juffermans, J. Horn, J. C. Fischer, E. C. van Dongen-Lases, and M. J. Schultz, "Point accuracy and reliability of an interstitial continuous glucose-monitoring device in critically ill patients: a prospective study," *Critical Care*, vol. 19, no. 1, p. 34, 2015.
- [6] T. Koschinsky and L. Heinemann, "Sensors for glucose monitoring: technical and clinical aspects," *Diabetes/Metabolism Research and Reviews*, vol. 17, no. 2, pp. 113–123, 2001.
- [7] J. L. Smith and M. J. Rice, "Why have so many intravascular glucose monitoring devices failed?" *Journal of Diabetes Science and Technology*, vol. 9, no. 4, pp. 782–791, 2015.
- [8] K. Kreymann, M. Berger, N. e. Deutz, M. Hiesmayr, P. Jolliet, G. Kazandjiev, G. Nitenberg, G. Van den Berghe, J. Wernerman, DGEM, C. Ebner, W. Hartl, C. Heymann, and C. Spies, "ESPEN guidelines on enteral nutrition: intensive care," *Clinical Nutrition*, vol. 25, no. 2, pp. 210–223, 2006.
- [9] M. Kuslapuu, K. Jögelä, J. Starkopf, and A. R. Blaser, "The reasons for insufficient enteral feeding in an intensive care unit: A prospective observational study," *Intensive and Critical Care Nursing*, vol. 31, no. 5, pp. 309–314, 2015.
- [10] R. Hovorka, L. J. Chassin, M. Ellmerer, J. Plank, and M. E. Wilinska, "A simulation model of glucose regulation in the critically ill," *Physiological Measurement*, vol. 29, pp. 959–978, 2008.
- [11] R. Dhaliwal, B. Jurewitsch, D. Harrietha, and D. K. Heyland, "Combination enteral and parenteral nutrition in critically ill patients: harmful or beneficial? a systematic review of the evidence," *Intensive Care Medicine*, vol. 30, no. 8, pp. 1666–1671, 2004.
- [12] M. Hoekstra, M. Vogelzang, E. Verbitskiy, and M. W. Nijsten, "Health technology assessment review: Computerized glucose regulation in the intensive care unit-how to create artificial control," *Critical Care*, vol. 13, no. 5, p. 223, 2009.
- [13] T. Van Herpe, N. Haverbeke, B. Pluymers, G. Van den Berghe, and B. De Moor, "The application of model predictive control to normalize glycemia of critically ill patients," in *Proceedings of the European Control Conference 2007*, Kos, Greece, July 2-5 2007, pp. 3116–3123.
- [14] T. Van Herpe, B. De Moor, and G. Van den Berghe, "Towards closed-loop glycaemic control," *Best Practice & Research Clinical Anaesthesiology*, vol. 23, pp. 69–80, 2009.
- [15] J. Sun, F. Cameron, and B. W. Bequette, "A habituating glucose control strategy for the critical ill," *Journal of Process Control*, vol. 22, pp. 1411–1421, 2012.
- [16] M. Ottaviano, M. Barolo, H. Zisser, E. Dassau, and D. E. Seborg, "Adaptive blood glucose control for intensive care applications," *Computer Methods and Programs in Biomedicine*, vol. 109, pp. 144–156, 2013.
- [17] G. Van den Berghe, A. Wilmer, I. Milants, P. J. Wouters, B. Bouckaert, F. Bruyninckx, R. Bouillon, and M. Schetz, "Intensive insulin therapy in mixed medical/surgical intensive care units: benefit versus harm," *Diabetes*, vol. 55, no. 11, pp. 3151–3159, 2006.
- [18] J.-C. Preiser, P. Devos, S. Ruiz-Santana, C. Mélot, D. Annane, J. Groeneveld, G. Iapichino, X. Leverve, G. Nitenberg, P. Singer, J. Wernerman, M. Joannidis, A. Stecher, and R. Chioléro, "A prospective randomised multi-centre controlled trial on tight glucose control by intensive insulin therapy in adult intensive care units: the glucontrol study," *Intensive Care Medicine*, vol. 35, no. 10, p. 1738, 2009.
- [19] J.-C. Preiser, J. G. Chase, R. Hovorka, J. I. Joseph, J. S. Krinsley, C. De Block, T. Desai, L. Foubert, P. Kalfon, U. Pielmeier, T. V. Herpe, and J. Wernerman, "Glucose control in the ICU: a continuing story," *Journal of Diabetes Science and Technology*, vol. 10, no. 6, pp. 1372–1381, 2016.
- [20] T. D. Knab, G. Clermont, and R. S. Parker, "Zone model predictive control and moving horizon estimation for the regulation of blood glucose in critical care patients," *IFAC-PapersOnLine*, vol. 48, no. 8, pp. 1002–1007, 2015.
- [21] —, "A "virtual patient" cohort and mathematical model of glucose dynamics in critical care," *IFAC-PapersOnLine*, vol. 49, no. 26, pp. 001–007, 2016.
- [22] A. Pritchard-Bell, G. Clermont, T. D. Knab, J. Maalouf, M. Vilkhovoy, and R. S. Parker, "Modeling glucose and subcutaneous insulin dynamics in critical care," *Control Engineering Practice*, vol. 58, pp. 268–275, 2017.
- [23] T. Van Herpe, B. Pluymers, M. Espinoza, G. Van den Berghe, and B. De Moor, "A minimal model for glycemia control in critically ill patients," in *Proceedings of the 28th IEEE EMBS Annual International Conference*, New York City, USA, Aug 30-Sept 3 2006, pp. 5432–5435.
- [24] J. G. Chase, G. M. Shaw, X. W. Wong, T. Lotz, J. Lin, and C. E. Han, "Model-based glycemic control in critical care," *Biomedical Signal Processing and Control*, vol. 1, no. 1, pp. 3–27, 2006.
- [25] R. N. Bergman, L. S. Phillips, and C. Cobelli, "Physiologic evaluation of factors controlling glucose tolerance in man," *The American Society for Clinical Investigation*, vol. 68, pp. 1456–1467, December 1981.
- [26] T. Van Herpe, N. Haverbeke, M. Espinoza, G. Van den Berghe, and B. De Moor, "Adaptive modeling for control of glycemia in critically ill patients," *10th International IFAC Symposium on Computer Applications in Biotechnology*, vol. 1, June 4-6 2007.
- [27] M. Hagdrup, D. Boiroux, Z. Mahmoudi, H. Madsen, N. K. Poulsen, B. Poulsen, and J. B. Jørgensen, "On the significance of the noise model for the performance of a linear MPC in closed-loop operation," *IFAC-PapersOnLine*, vol. 49, no. 7, pp. 171–176, 2016.
- [28] X. W. Wong, J. G. Chase, G. M. Shaw, C. E. Hann, T. Lotz, J. Lin, I. Singh-Levett, L. J. Hollingsworth, O. S. W. Wong, and S. Andreassen, "Model predictive glycaemic regulation in critical illness using insulin and nutrition input: a pilot study," *Medical Engineering & Physics*, vol. 28, no. 7, pp. 665–681, 2006.
- [29] U. Pielmeier, M. L. Rousing, S. Andreassen, B. S. Nielsen, and P. Haure, "Decision support for optimized blood glucose control and nutrition in a neurotrauma intensive care unit: preliminary results of clinical advice and prediction accuracy of the glucosafe system," *Journal of Clinical Monitoring and Computing*, vol. 26, no. 4, pp. 319–328, 2012.

APPENDIX P

Technical Report

User interfaces for diabetes applications

Authors:

Asbjørn Thode Reenberg, Tobias K. S. Ritschel, John Bagterp Jørgensen

Submitted to:

arXiv 2023.



User interfaces for diabetes applications

Technical report

Asbjørn Thode Reenberg
Tobias K. S. Ritschel
John Bagterp Jørgensen

Department of Applied Mathematics and Computer Science,
Technical University of Denmark, DK-2800 Kgs. Lyngby, Denmark

DTU Compute
Department of Applied Mathematics and Computer Science
Technical University of Denmark

Matematiktorvet
Building 303B
2800 Kongens Lyngby, Denmark
Phone +45 4525 3031
compute@compute.dtu.dk
www.compute.dtu.dk

Summary

In this technical report, we describe and demonstrate a user interface for diabetes management. Specifically, we show a full-stack web application to visualize diabetes data and describe the software tools used to build it. Furthermore, we briefly discuss and compare with a user interface for an artificial pancreas mobile application. The web application consists of a database, a backend to read and process data from the database, a frontend to visualize and filter the data, and an application programming interface (API) to communicate between the backend and frontend. The database is a PostgreSQL database, the backend is a Spring Boot Java application, and the frontend is a Vue.js application. The visualized data in the web application is simulated from 1000 virtual people over 1 month. The web application allows people with diabetes to view different representations of their own data, but also, e.g., medical personnel to log in and view the data from all their patients.

Contents

Summary	i
Contents	iii
1 Introduction	1
2 Dependencies	7
2.1 IDEs	7
2.2 Coding languages	8
2.3 Dependencies	8
3 Rest API	11
3.1 Models	11
3.2 Endpoints	13
4 Database	15
4.1 Tables	15
4.2 Sample data	16
5 Backend	17
5.1 Model	17
5.2 Repository	19
5.3 Controller	20
6 Frontend	23
6.1 Backend and API	23
6.2 Pages	24
6.3 Components	25
6.4 Demonstration	27
7 Conclusions	33
Bibliography	35

CHAPTER 1

Introduction

In this technical report, we describe and demonstrate a web application for visualizing diabetes data. The web application allows people with diabetes to get both quick overview of the targets specified by Battelino et al. [1], but also to view more detailed representations of the data and see statistics. Furthermore, it allows medical personnel to log in and inspect data from all the patients. We briefly discuss differences between the web application and a mobile application for an artificial pancreas and we describe the software tools used to build the web application. Finally, we show a demonstration of the web application. In this section we describe the motivation, the key details of the web application, and provide an outline of the report.

Motivation More and more people with diabetes use devices that collect data such as continuous glucose monitors (CGMs), pumps, and automatic dosing systems (e.g. an artificial pancreas) [2]. Furthermore, various simulators that can be used for both virtual clinical trials and education have become available [3, 4]. Therefore, there is a need for tools to both visualize and analyze the large amounts of collected data. Applications that allow people to see their data in real time can be on, e.g., a smartphone. The DiaCon dual-hormone artificial pancreas is an example of an application with a real time user interface implemented on a smartphone. However, a smartphone is not suitable for viewing large amounts of data and performing large computations (e.g. simulations). Therefore, we build a modern full stack web application in addition to the DiaCon smartphone application. Figure 1.1 shows the concept, where the web application, the artificial pancreas, and one or multiple simulators is connected through a database. The web application serves multiple purposes, 1) it allows the user to see more detailed representations of data that are not available on a smartphone, 2) it allows, e.g., doctors or parents to remotely access data from the artificial pancreas, and 3) it allows the user to perform simulations for educational purposes or researchers to test new treatment strategies. In this technical report, we only describe the web application and assume that the data from the artificial pancreas or simulator already exists in the database.

Architecture The web application consists of a PostgreSQL database, a Java Spring Boot backend application, an application programming interface (API), and a Vue.js frontend application. Figure 1.2 shows the architecture and tools used to build each element. The architecture provides a flexible design where, e.g., multiple backend servers can serve one or more frontends. Furthermore, the API provides a generic interface and

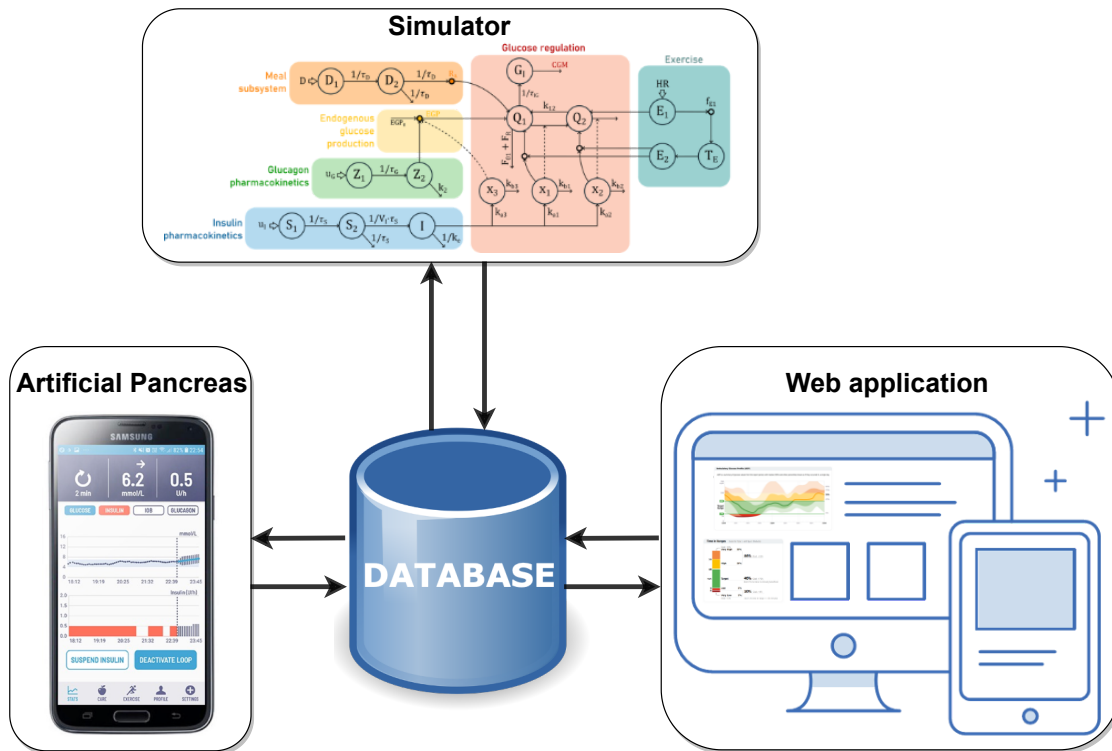


Figure 1.1: The vision of an artificial pancreas, a web application, and a simulator connected through a database.

ensures that the frontend can send requests to the backend without having information about e.g. the database.

Database We use a PostgreSQL database. PostgreSQL is a free and open source relational database management system with SQL compliance. The web application works with any database system, but PostgreSQL was chosen here, as it was already used by other members in John Bagterp Jørgensens' research group and excels when working with huge datasets.

Backend We use Spring Boot to create the backend application. Spring Boot is an open source Java-based framework used to build stand alone applications without relying on an external web server. The backend answers requests from the frontend application through the API that we document with Swagger.

Frontend The frontend is a Vue.js application and provides a graphical user interface (GUI). Vue.js is an open source model-view-viewmodel (Figure 1.4) frontend JavaScript framework for building user interfaces. Vue.js builds on top of standard HTML, CSS, and JavaScript and provides a declarative and component-based programming model

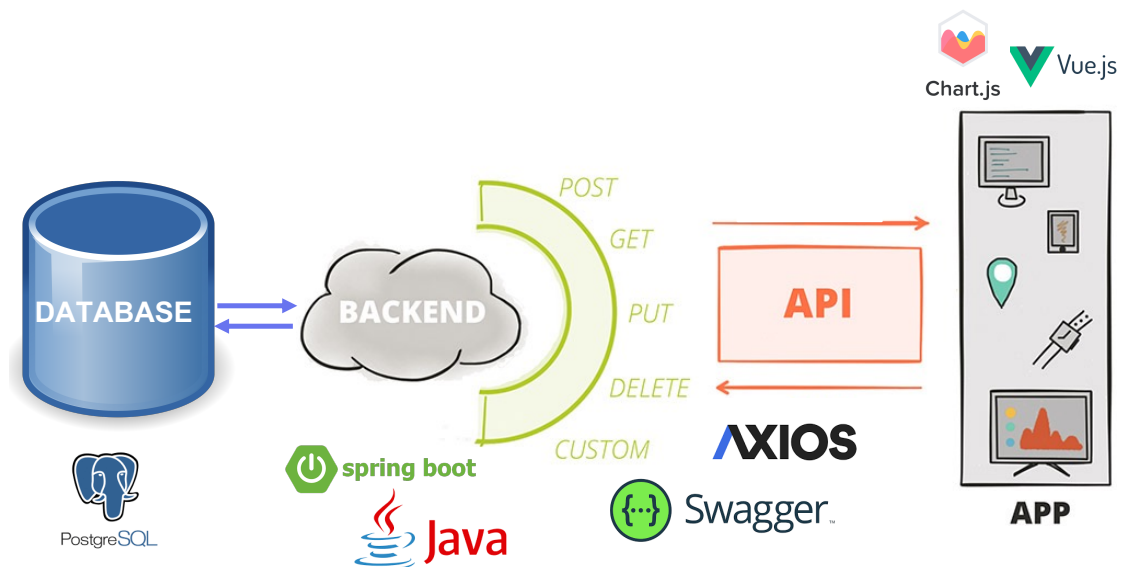


Figure 1.2: Architecture of the web application that consists of a PostgreSQL database, a Java Spring Boot backend application, an API, and a Vue.js frontend application. The charts in the frontend are build with Chart.js.

that helps to efficiently develop user interfaces. In contrast, the frontend in the DiaCon artificial pancreas, is an android application using the model-view-presenter framework (Figure 1.3).

Structure of the report In Chapter 2, we list the dependencies and tools used to build the web application. We describe the API in Chapter 3 and the database in Chapter 4. In Chapter 5, we describe the backend and in Chapter 6 we show a demonstration of the frontend and describe how it is build. Finally, in Chapter 7, we provide conclusions and discuss future work and possible improvements.

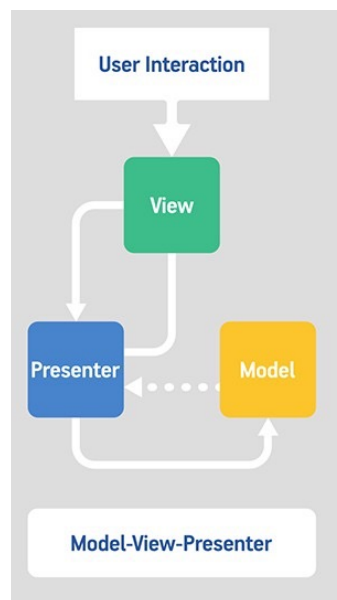


Figure 1.3: Model-view-presenter framework in the DiaCon Android application.

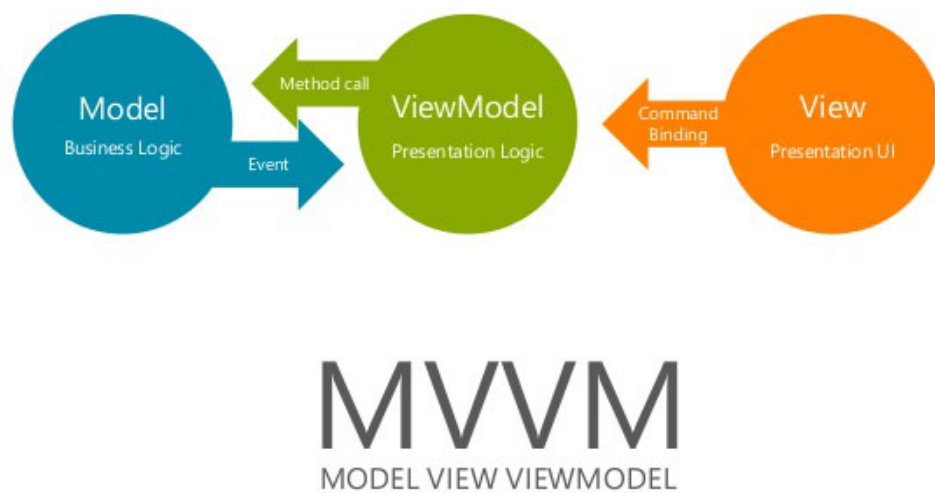


Figure 1.4: Model-view-viewmodel framework used in Vue.js.

CHAPTER 2

Dependencies

This chapter lists the tools and dependencies used to build the full-stack web application.

2.1 IDEs

We use integrated development environments (IDEs) to write and build the code. We use Eclipse for the backend code and Visual Studio Code for the frontend code. Furthermore, we use the Vue UI to manage dependencies and run the frontend application. These tools are not mandatory and it is both possible to use other IDEs or run everything directly in the terminal. Fig. 2.1 shows the Vue UI with the current status and where the frontend application can be started.

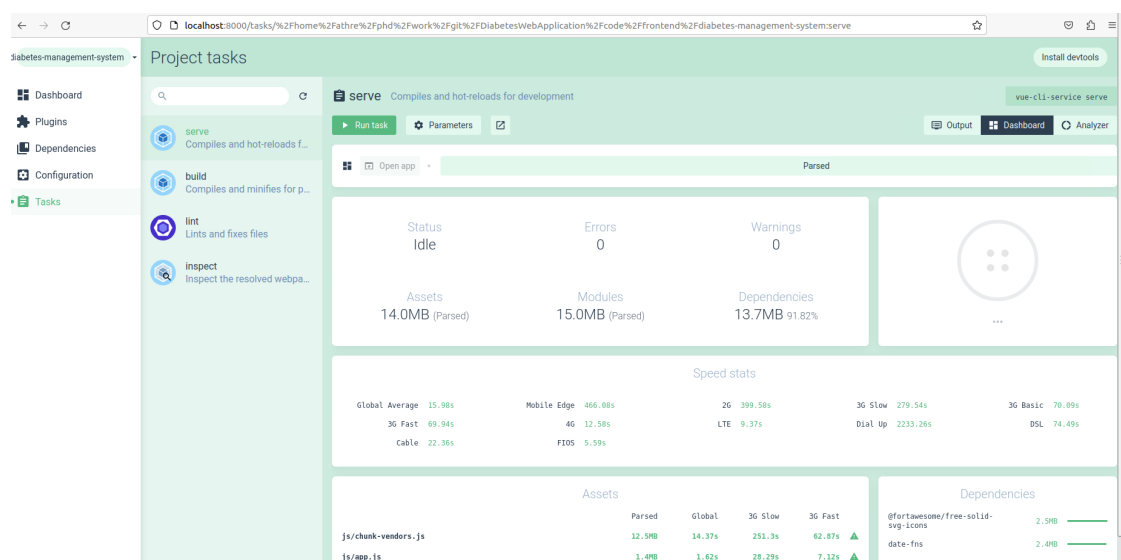


Figure 2.1: A screenshot of the Vue UI that can run and manage the frontend application.

2.2 Coding languages

The web application is build using the following coding languages

- SQL (used for the database)
- Java (used for the backend)
- JavaScript (scripting language for the frontend)
- CSS (used to style the frontend)
- HTML (markup language for the frontend)

2.3 Dependencies

Here we list all the dependencies. Eclipse help with managing the dependencies in the backend, e.g., Spring Boot and the Vue UI lets the user install and manage dependencies directly from the interface as shown in Fig. 2.2.

- npm
- Node.js
- Vue.js
- Yarn
- PostgreSQL
- Spring Boot
- Popper.js
- Vue Router
- fontawesome
- Axios
- Bootstrap
- Chart.js
- chartjs-adapter-date-fns
- chartjs-plugin-datalabes
- cors

2.3 Dependencies

9

- core-js
- date-fns
- Moment

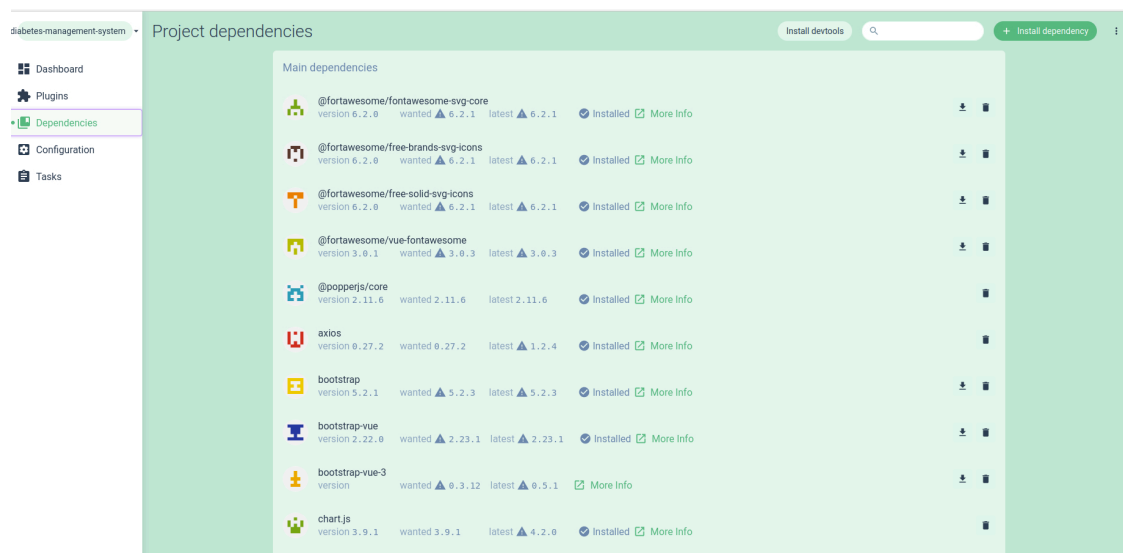


Figure 2.2: Dependency manager in the Vue UI that gives an overview of the installed dependencies and makes it straightforward to install new dependencies.

CHAPTER 3

Rest API

In this chapter, we describe the API used to communicate between the backend and the frontend. An API is a collection of HTTP endpoints known to both the server (or more servers) and the client to manipulate resources. The communication happens via the HTTP verbs; GET (retrieve a specific resource), POST (create a new resource), PUT (update a specific resource), and DELETE (remove a specific resource). The API should be identified and designed based on the purpose of the application. We use Swagger <https://swagger.io/> (Accessed: December 22nd, 2022) to document the API. Swagger is an online tool for interactive documentation of APIs and allows the user to test the endpoints without implementing a frontend. Figure 3.1 shows the frontpage of the swagger documentation. In swagger, the keyword 'model' is used for resources. The following sections describe the models and endpoints.

3.1 Models

We define a model for patients, glucose measurements, basal insulin, bolus insulin, carbohydrates, and physical activity. Figure 3.2 shows a list of the models and their properties. The patient model contains basic information about each patient and the remaining models describe glucose, insulin, meal and physical activity values for all patients. The patient id is used to select the values for a specific patient. The 'deviceID' property is used to distinguish between the device that was used for the measurement to allow for, e.g., selecting only the glucose measurements that were received from a CGM.

Diabetes management system 1.0.0

[Base URL: localhost:8080/api/v1/]

This is a description of the API for the diabetes management system

Schemes

HTTP

Figure 3.1: Swagger frontpage for documentation of the models and endpoints in the API.

```
patient ∨ {  
  id                integer  
                    items: OrderedMap { "$ref": "#/definitions/patient" }  
  name              string  
  dateofbirth       string($date)  
  email             string  
}  
  
glucosemeasurement ∨ {  
  userId            integer  
                    items: OrderedMap { "$ref": "#/definitions/glucosemeasurement" }  
  time              string($date-time)  
  deviceId          string  
  measurement       number  
}  
  
basalinsulin ∨ {  
  userId            integer  
                    items: OrderedMap { "$ref": "#/definitions/basalinsulin" }  
  time              string($date-time)  
  deviceId          string  
  basalinsulin      number  
}  
  
bolusinsulin ∨ {  
  userId            integer  
                    items: OrderedMap { "$ref": "#/definitions/bolusinsulin" }  
  time              string($date-time)  
  deviceId          string  
  bolusinsulin      number  
}  
  
carbohydrates ∨ {  
  userId            integer  
                    items: OrderedMap { "$ref": "#/definitions/carbohydrates" }  
  time              string($date-time)  
  deviceId          string  
  carbohydrates     number  
}  
  
physicalactivity ∨ {  
  userId            integer  
                    items: OrderedMap { "$ref": "#/definitions/physicalactivity" }  
  time              string($date-time)  
  deviceId          string  
  exercise          number  
}
```

Figure 3.2: List and descriptions of the models and their properties in the API.

3.2 Endpoints

We also use Swagger to document the endpoints that trigger a reply from the controller in the backend. Figure 3.3 shows an example of the endpoint that *gets* the bolus insulin values for a specific patient, delivered with a specific device (e.g. a pump) between the start and end date. The Swagger documentation provides a description of each endpoint, but also allows the developer to test if the backend responds the request without implementing a frontend. We define a number of endpoints for each model, but these are left out of this technical report for brevity. Each additional endpoint follow the same structure as the one shown Figure 3.3.

GET

/bolusinsulin/{userId}/{deviceId}/{startDate}/{endDate}

Returns bolus insulin for patientId between start and end date

^

Parameters

Cancel

Name	Description
userId * required integer (path)	The id of the user
deviceId * required string (path)	Type of insulin administration device
startDate * required string(\$date-time) (path)	Start date of bolus insulin values to get
endDate * required string(\$date-time) (path)	End date of bolus insulin values to get

Execute

Responses

Response content type application/json

Code	Description
200	the list of bolus insulin values

Example Value | Model

```
[
  {
    "userId": 0,
    "time": "2022-12-21T15:15:32.797Z",
    "deviceId": "string",
    "bolusinsulin": 0
  }
]
```

Figure 3.3: Example of the bolus insulin endpoint in the Swagger documentation.

CHAPTER 4

Database

In this chapter, we describe the database. We describe how each table is defined and how we generate the sample data that is inserted in the database. Here, we use a PostgreSQL database, but any database system can be used. We use a Java Spring Boot application in the backend where the `pom.xml` file defines the database type and we add a PostgreSQL dependency, as shown in Listing 4.1. Listing 4.2 shows how the properties of the database are defined in the `application.properties` file. Here, we host the database on the localhost with port 5432 (this is the default port for a PostgreSQL database) where the name of the database is *diabeteswebapplication* and we grant privileges to the user *dbuser* with the password *thepassword*.

```
1 <dependency>
2   <groupId>org.postgresql</groupId>
3   <artifactId>postgresql</artifactId>
4   <scope>runtime</scope>
5 </dependency>
```

Listing 4.1: Define database system in `pom.xml`.

```
1 spring.datasource.initialization -mode=always
2 spring.datasource.platform=postgres
3 spring.datasource.url=jdbc:postgresql://localhost:5432/
   diabeteswebapplication
4 spring.datasource.username=dbuser
5 spring.datasource.password=thepassword
```

Listing 4.2: Definition of the database properties in `application.properties`.

4.1 Tables

Each table in the database represents a model described in Figure 3.1. Listing 4.3 shows an example of how to create a table in the database with SQL code. The table shows how the table for the bolus insulin model is created and we create tables for the remaining models in a similar way. The tables are created with a primary key for the user id and the time stamp. The primary key ensures that each entry for a given user at a specific time is unique, i.e., there cannot be two bolus insulin values for the same user at the same time.

```
1 drop table if exists bolusinsulin;  
2 create table bolusinsulin (  
3     user_id integer ,  
4     timestam timestamp ,  
5     device_Id varchar(25) ,  
6     bolusinsulin float ,  
7     primary key (user_id , timestam)  
8 );
```

Listing 4.3: Create table for the bolus insulin model in the database.

4.2 Sample data

The database should be able to handle data from real people, but since we do not have data available, we generate data to represent real people. The personal data is generated with Mockaroo <https://www.mockaroo.com> (Accessed: December 22nd, 2022). Mockaroo allows for generation of random data of anything from names, emails to cars or IP addresses. We use Mockaroo to generate names, date of birth, emails, and an ID. The diabetes data is generated from a Monte Carlo simulation using an extension of Hovorka's model [5] for 1000 virtual people over 1 month similar to the procedure described in [6].

CHAPTER 5

Backend

In this chapter, we describe the backend. The backend is the server-side software and handles everything that is not visible in the frontend. The backend communicates with the database, can do computations, and replies the requests from the client (frontend). Here, the backend is a Java Spring Boot application. Figure 5.1 shows the architecture of a Spring Boot application. Spring Boot applications use multiple annotations that automatically handle certain functions. The Spring Boot application consists of three components: 1) Model, 2) Repository, and 3) Controller that each are a Java package.

5.1 Model

The model defines each entity as a Java class and match both the tables in the database and models described in the API (Figure 3.2). The properties of each model should have corresponding getters and setters. The properties must be same as each column in the database tables. Listing 5.1 shows selected code from an example of how we define the model for bolus insulin (dots represent missing lines of code). Similar classes should be defined for the remaining models as well. Here, we define the name of the table in the database, where the annotation `@Column` indicates that the class member is a column in the database. The `@Id` annotation indicates that it is a primary key in the database and Listing 5.2 shows the class that ensures that new entries in the database are unique w.r.t. user ID and timestamp.

```
1 package dtu.model;
2
3 ... // imports
4
5 @Entity
6 @Table(name = "bolusinsulin") // name of table in database
7 @IdClass(BolusInsulinId.class) // ensure unique id + time
8 public class BolusInsulin {
9     @Id
10    @Column
11    private long userId;
12    @Id
13    @Column
14    private Timestamp timestamp;
15
16    @Column
```

Spring Boot Flow Architecture

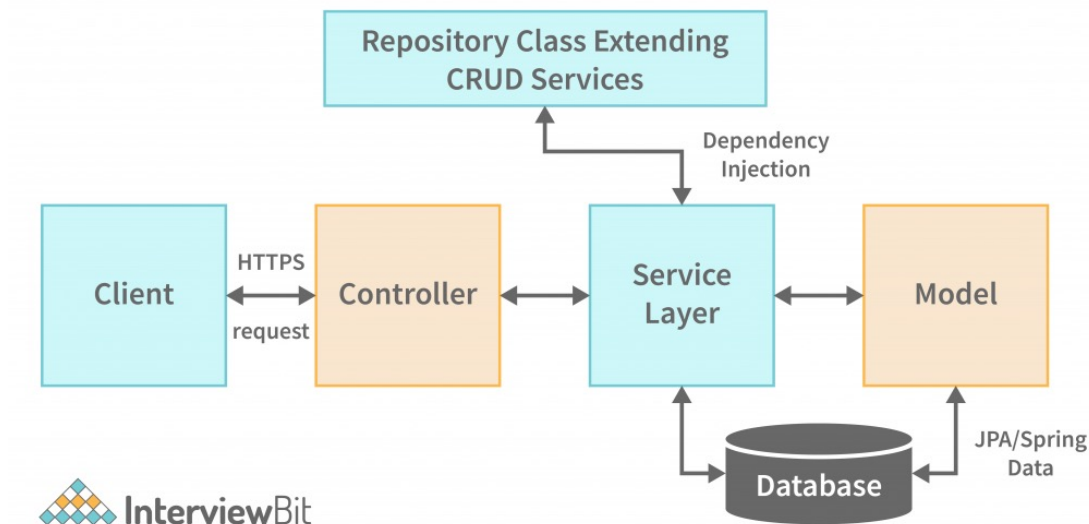


Figure 5.1: Architecture of a Java Spring Boot application consisting of 1) Model, 2) Repository (service layer), and 3) Controller. The Spring Boot application depends on a database and can answer requests from clients.

```

17 private String device_Id;
18
19 @Column
20 private double bolusinsulin;
21
22 ... // getters and setters
23
24 }

```

Listing 5.1: The bolus insulin model.

```

1 package dtu.model;
2
3 ... // imports
4
5 public class BolusInsulinId implements Serializable {
6
7     private Long userId;
8     private Timestamp timestam;
9
10    public BolusInsulinId() {
11    }

```

```
12
13     public BolusInsulinId(Long UId, Timestamp time) {
14         this.userId = UId;
15         this.timestam = time;
16     }
17
18     @Override
19     public boolean equals(Object o) { // Ensure that id and timestamp is
20         unique
21         if (this == o) return true;
22         if (o == null || getClass() != o.getClass()) return false;
23         BolusInsulinId measurementId = (BolusInsulinId) o;
24         return this.userId == measurementId.userId &&
25             timestam.equals(measurementId.timestam);
26     }
27
28     @Override
29     public int hashCode() {
30         return Objects.hash(userId, timestam);
31     }
}
```

Listing 5.2: The bolus insulin id class.

5.2 Repository

The repositories provide an interface to the Spring Boot CRUD (create, read, update and delete) repository that contains methods for CRUD operations and functions as a service layer. Spring Boot automatically constructs classes that contains CRUD methods for the specified interface for the given model. Spring Boot can automatically write the query to the database for standard methods such as, e.g., *findAll*. Advanced queries can not be automatically generated and need to be specified in the repository. Listing 5.3 shows selected code from the bolus insulin repository that works as an interface for the bolus insulin model described in listing 5.1. Again, dots represent lines of code that are left out for brevity. The `@Query` annotation is used to write queries to the database. The queries should be defined above the interface. The query shown in Listing 5.3 selects all non-zero bolus insulin values for a specific user between two timestamps and orders the output based on the timestamps.

```
1 package dtu.repositories;
2
3 ... // imports
4
5 import dtu.model.BolusInsulin;
6
7 @Repository
```

```

8 public interface BolusInsulinRepository extends CrudRepository<
    BolusInsulin, Long>{
9
10     ... // more interfaces
11
12     // query to database - only select non-zero values
13     @Query(value = "select t.* from ( select *, row_number() OVER(order by
        timestamp) as row from bolusinsulin where user_id=?1 "
14         + "And timestamp BETWEEN TO_TIMESTAMP(?2,'YYYY-MM-DD HH24:MI ')
        AND TO_TIMESTAMP(?3,'YYYY-MM-DD HH24:MI:SS ')) "+
15         "t where bolusinsulin>0", nativeQuery=true)
16     List<BolusInsulin> findByUserIdByTimeBetween(Long userId, String
        startDate, String endDate);
17
18 }

```

Listing 5.3: Bolus insulin repository with a query to select non-zero values for a specific user between two dates.

5.3 Controller

The controllers are the final layers in the backend and receive the HTTPS requests from the clients, i.e., this is where the users request to receive or insert data enter the backend. The controllers can manipulate the data before it is delivered to the user or inserted in the database. The controllers can also perform computations to reduce the load on the frontend. Listing 5.4 shows selected code from the controller that answers requests for bolus insulin data. The API endpoint is defined with the `@GetMapping` annotation and corresponds to the endpoint shown in Figure 3.3. This method calls the `findByUserIdByTimeBetween` from the repository and checks the result. If the result is not empty, the controller responds the request from the frontend.

```

1 package dtu.controllers;
2
3 ... // imports
4
5 import dtu.model.BolusInsulin;
6 import dtu.repositories.BolusInsulinRepository;
7
8 @Controller
9 @CrossOrigin
10 public class BolusInsulinControllers {
11
12     @Autowired
13     private BolusInsulinRepository repository;
14
15     ... // more methods
16

```

```
17 // return all bolus insulin values for user between start and end date
18 @GetMapping("/api/v1/bolusinsulin/{userId}/{deviceId}/{startDate}/{
    endDate}") // API
19 public ResponseEntity<List<BolusInsulin>> getAll(@PathVariable long
    userId, @PathVariable String startDate,
20     @PathVariable String endDate) {
21     List<BolusInsulin> result = repository.findByUserIdByTimeBetween(
        userId, startDate, endDate);
22     if (result.isEmpty()) { // check result
23         return ResponseEntity.notFound().build();
24     }
25     return ResponseEntity.ok(result);
26 }
27
28 ... // more methods
29
30 }
```

Listing 5.4: The bolus insulin controller.

CHAPTER 6

Frontend

In this chapter, we describe the frontend. The frontend lets the user interact with the application and shows the GUI. The frontend receives inputs from the user and sends requests to the backend through the API. Figure 6.1 shows the structure of the frontend application. The frontend application consists of multiple pages that each consist of components. In the following sections, we describe the pages and components (e.g. charts) used in the frontend and we describe how the frontend sends requests to the backend. Finally, we show a demonstration of the GUI with selected screenshots. The frontend is built using Vue.js and is a Vue.js application.

6.1 Backend and API

The frontend communicates with the backend through the API as described in Chapter 3. Listing 6.1 shows an example of how the endpoint to receive bolus insulin data is defined in the frontend. All the endpoints that are used in the frontend should be defined here.

```
1 export default class Backend{  
2   constructor() {  
3     this.url = "http://localhost:8080/api/v1"
```

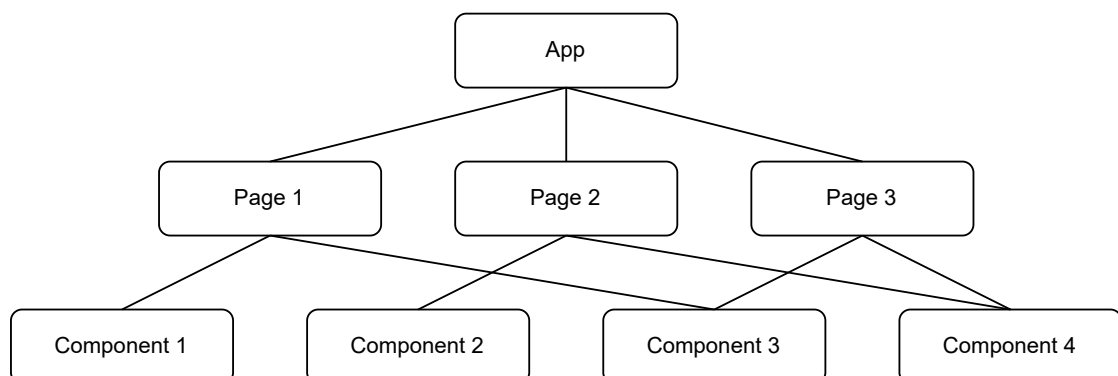


Figure 6.1: Structure of the frontend that consists of different pages that each consists of a number of components.

```

4     }
5
6     getUrlBolusInsulinBetweenDates(id, deviceId, startDate, endDate){
7         return this.url + "/bolusinsulin/" + id + "/" + deviceId + "/" +
            startDate + "/" + endDate
8     }
9 }

```

Listing 6.1: API endpoints in the frontend.

6.2 Pages

The GUI can display different pages where each page consists of components. The same components can be used in multiple pages. We use the Vue router to navigate between the pages. The different pages allow the users to switch between different views. In this web application, we use a login page and depending on the users' permissions, they see different pages. We distinguish between *patients* and *doctors*. The *patients* can only view their own data whereas the *doctors* can view the data from all their *patients*. Additionally, the *administrator* login has similar permissions as the *doctors*, but should also be able to compute statistics on all the data to see if there are specific trends in the *patient* population, but this is currently work in progress.

```

1 import {createRouter, createWebHistory} from 'vue-router'
2
3 ...
4
5 const routes = [
6     {
7         path: '/pages/patientAllPatientDataPage/:id/:PatientName/:
            PatientEmail',
8         component: patientAllPatientDataPage,
9         name: 'patientAllPatientDataPage',
10        meta: { showAllPatientData: true }
11    },
12 ]
13
14 const router = createRouter({
15     history: createWebHistory(),
16
17     routes: routes,
18     linkActiveClass: 'active'
19 });
20
21 export default router

```

Listing 6.2: Vue Router to navigate between pages.

```
1 <template>
2   ...
3   <BolusInsulinChart @dailyBolusEmit="receiveDailyBolus" :
4     startTime="this.startTime" :endTime="this.endTime" :userId="
5     this.PatientId"/>
6
7 </template>
8
9 <script>
10  ...
11  export default {
12    components: { ... },
13    methods: {
14      ...
15
16      handleStartTimeEmit(value){
17        this.startTime = value;
18      },
19
20      ...
21
22    },
23    watch: {
24      startTime() {
25        this.refresh()
26      },
27
28      ...
29
30    },
31
32    ...
33  }
34 </script>
```

Listing 6.3: Bolus insulin page build from components.

6.3 Components

The components allow us to split up the GUI into independent and reusable pieces. Therefore, e.g., the charts are components that can be reused in different pages. The charts are build using Vue Charts.js. Chart.js is a free and open source chart library that works with multiple JavaScript frameworks (including Vue.js). Listing 6.4 shows selected code from the bolus insulin chart. In general, the charts consist some properties, options, methods (e.g. to update data), watches (do something when a variable changes), and

computed values (define non-static variables, e.g., the chart data that is updated). We also define the styling of the visualized data under `chartData`, where, e.g., the linestyle and color is defined. Listing 6.4 also shows how we use `Axios` (`Axios` is a promise based HTTP client for the browser and `node.js`) to handle HTTP request to get data from the backend (line 21-22).

```

1  <script>
2  import { Scatter } from 'vue-chartjs'
3  ...
4
5  export default {
6    name: 'BolusInsulinChart',
7    components: { Scatter },
8    props: {
9      ...
10   },
11   emits: [ 'dailyBolusEmit' ],
12   options: {
13     ...
14   }
15 }
16 async mounted() {
17   this.updateData(this.userId, 'cgm', this.startTime, this.endTime)
18 },
19 methods: {
20   async updateData(id, deviceId, startDate, endDate) {
21     this.axios
22       .get(this.$backend.getUrlBolusInsulinBetweenDates(id, deviceId,
23         startDate, endDate))
24       .then(res => {
25         ...
26       })
27   },
28   watch: {
29     startTime() {
30       this.updateData(this.userId, 'cgm', this.startTime, this.endTime);
31     },
32     ...
33   },
34   computed: {
35     chartData() {
36       return {
37         datasets: [
38           {
39             ...
40           }
41         ]
42       }
43     }
44   }

```

```
45 </script>
```

Listing 6.4: Bolus insulin chart component.

6.4 Demonstration

In this section, we show and discuss a selection of the pages from the GUI. The GUI is designed to have different views depending on the permissions of the user. The user privileges are granted through the login page. Currently, you can either login as a *patient* and view your own data or you can login as a *doctor* and view the data from all the *patients*. The *doctors* have the same view and can see the same data as the *patients*, but are also allowed to switch between all their *patients*. It is also possible to login as an administrator that can, e.g., compute statistics based on the *patient* population, but the GUI for the administrator is work in progress and will not be described here.

6.4.1 Login page

Figure 6.2 shows the login page where you can login as either a *patient* or a *doctor*. In this example, the users are predefined and it is not possible to create new users. The icons are imported from the fontawesome library.

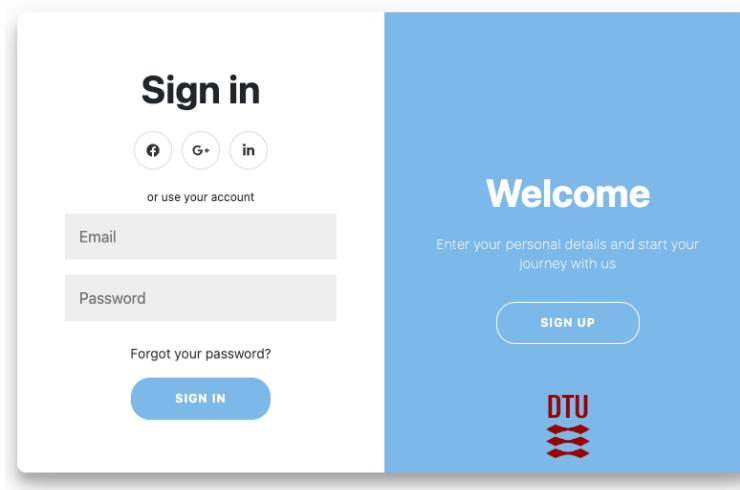


Figure 6.2: Login page that allows the user to log in as either a *patient* to view your personal data or as a *doctor* to view the data from all their *patients*.

6.4.2 Personal login

The GUI lets the user view data in three different ways by switching between three pages. All pages allow the user to select different time periods, change the unit and switch between the pages. The person's name is also shown (this virtual person is called Penrod Tetley). Figure 6.3 shows the first page that shows an overview of glucose data. The top bar shows selected key performance indicators (KPIs) such as average glucose and variability. The side bar shows the time in the different ranges during the selected time period. Finally, the page shows a time series chart with the glucose data for the selected time period. The user can then choose to add meals, insulin, and exercise data beneath the glucose data as shown in Figure 6.4 by clicking on *All timeseries*. Here, both the time series data and daily amounts are shown (we show session per week for exercise data). Finally, the user can choose to view statistics by clicking on *Glucose statistics*. Figure 6.5 shows the mean and 95% confidence intervals for an overlay of the days in the selected period. This allows the user to see if, e.g., there are certain times of the day where the user has a tendency to reach hypoglycemia. The 95% confidence intervals are relatively narrow for this simulated data as the variability in the size and time of the meals is limited. Figure 6.6 shows the time in the different ranges for each day in the selected time period which allows the user to see trends in the time in range. Here, the user improved the time in range during the month, but the chart would also show if, e.g., the user is not in range during the weekends or maybe every Thursday the user is exercising and reaches hypoglycemia.

Diabetes Management System

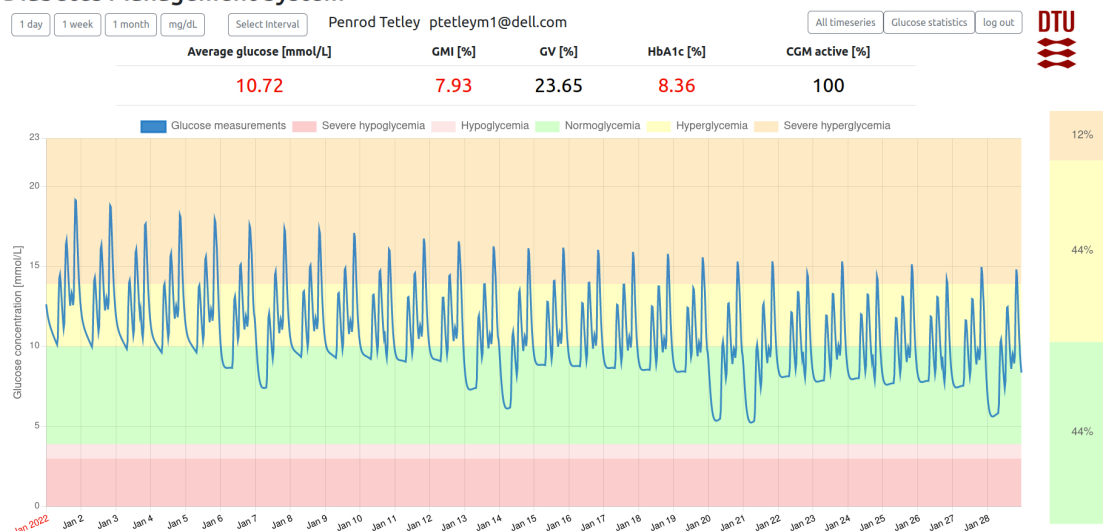


Figure 6.3: An overview of personal glucose data with a chart of the glucose data in the selected period. Top bar: select between different time periods, change unit, and change to a different page. Second top bar: KPIs. Right bar: time in the different ranges in the selected period.

6.4 Demonstration

29

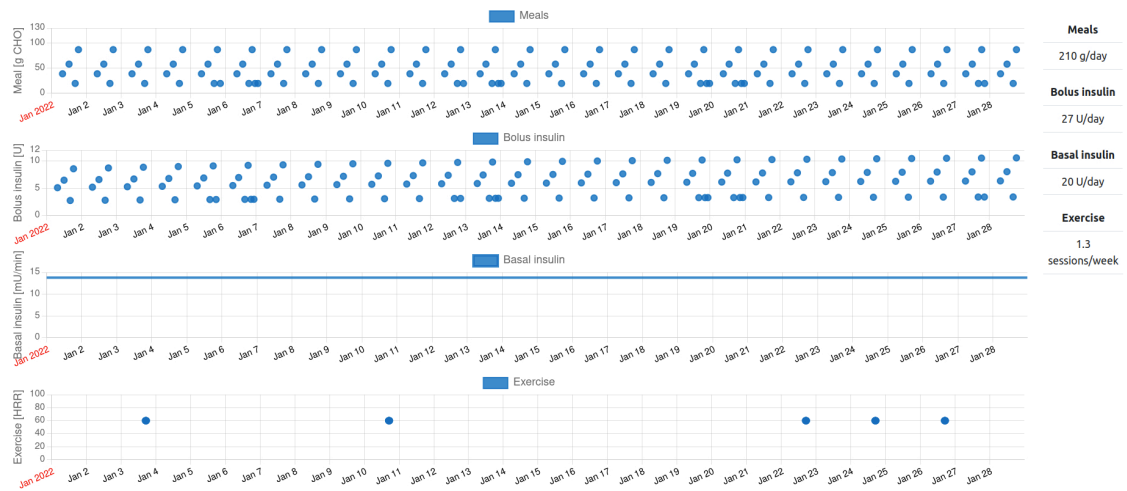


Figure 6.4: Time series for meals, bolus insulin, basal insulin, and exercise data. Right bar: average daily amounts for meals and insulin and average weekly exercise sessions.

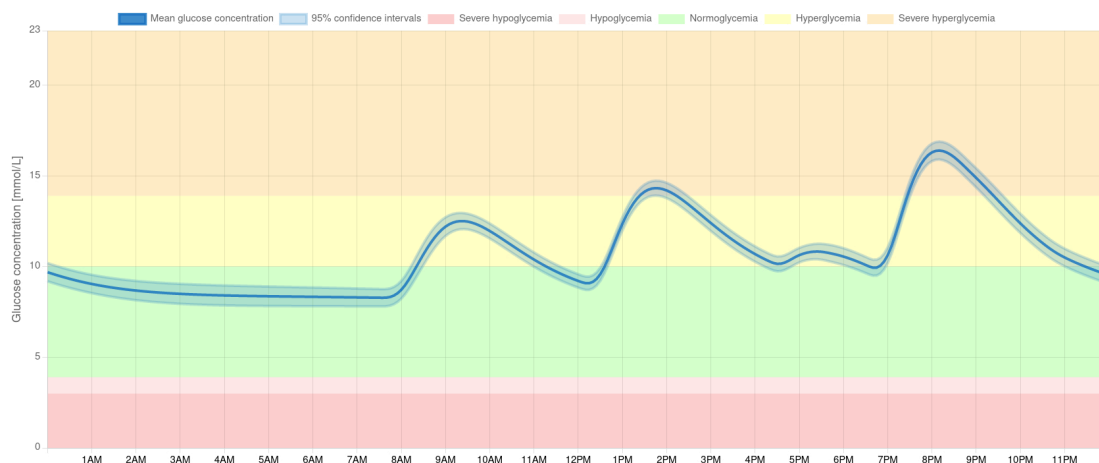


Figure 6.5: Mean and 95% confidence intervals of the glucose data for each time stamp in the selected period.

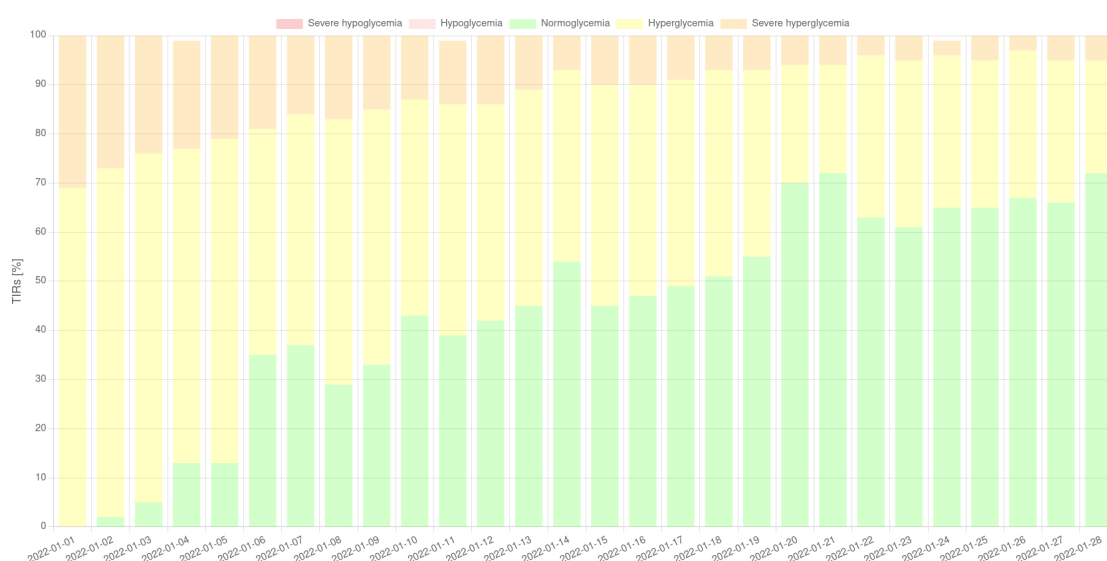


Figure 6.6: Time in the different ranges for each day in the selected period.

6.4.3 Doctor login

The *doctors* can see the exact same pages as the *patients*, but are able to view the data from all the *patients*. Figure 6.7 shows the glucose overview page with the *doctor* login. The components are the same as the individual *patients* can see, but in the left panel, the *doctors* can see all the *patients*, search for them, and click on the one they would like to inspect. In Figure 6.7, the *doctor* is viewing the virtual *patient* Hirsch Vell. Currently, it is only possible to filter the *patients* based on their name or date of birth, but in the next version it should also be possible to sort the *patients* based on their treatment, such that the *doctors* can, e.g., identify the *patients* that have poor treatment and need care.

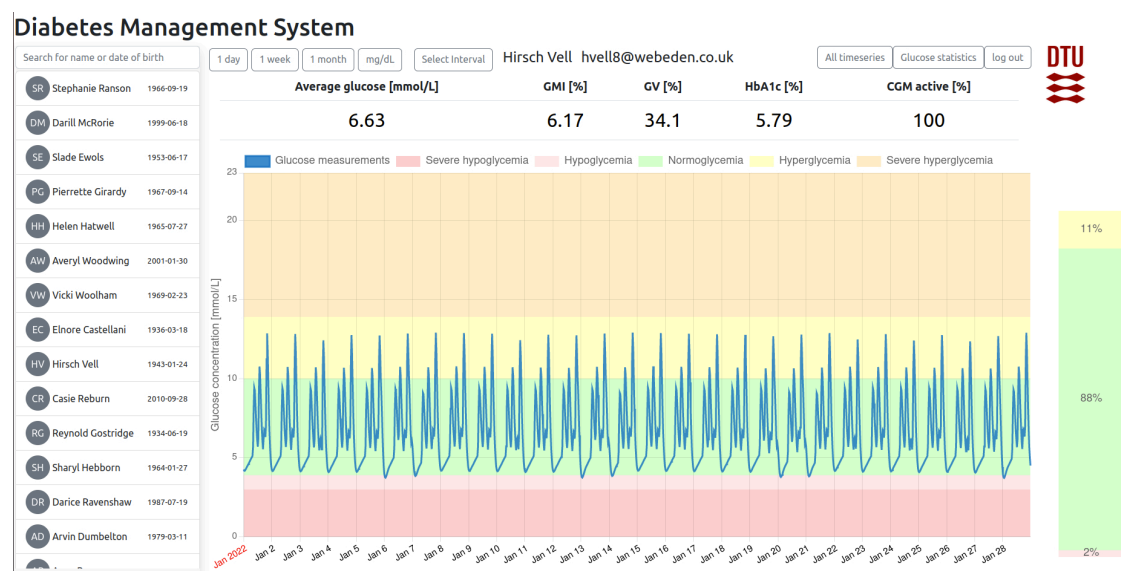


Figure 6.7: Front page with the *doctor* login. Left bar: list of all the *patients* that the doctor can view. Top bars and charts are the same as for the *patient*.

CHAPTER 7

Conclusions

In this technical report, we introduced and demonstrated a web application for visualizing and interacting with diabetes data. The web application is build using a PostgreSQL database, a Spring Boot Java application (the backend), a rest API, and a Vue.js application (the frontend). The web application allows the user to login and get different views based on the permissions of the user. Currently, it is possible to login as a *patient* to view your personal data or as a *doctor* to view data from all their *patients*. The architecture allows for a flexible design, where the backend or frontend application can be replaced as long as the same API interface is used. The GUI is designed to show the targets specified by Battelino et al. [1] and let the user choose between different time periods and visualizations. In future versions, a number of improvements and extensions can be made 1) the administrator user should be able to compute statistics based on the population of the *patients*, 2) it should be possible for the users to perform simulations directly from the frontend, 3) the web application should updated to make it possible to upload data from, e.g., an AP or the DiaCon AP should be able to upload data directly to the database, and 4) it should be possible for the *doctors* to sort and filter their *patients* based on treatment represented by, e.g., TIR.

Bibliography

- [1] Tadej Battelino, Thomas Danne, Richard Bergenstal, Stephanie Amiel, Roy Beck, Torben Biester, Emanuele Bosi, Bruce Buckingham, William Cefalu, Kelly Close, Claudio Cobelli, Eyal Dassau, J DeVries, Kim Donaghue, Klemen Dovc, Francis Doyle, Shefally Garg, George Grunberger, Simon Heller, and Moshe Phillip. “Clinical Targets for Continuous Glucose Monitoring Data Interpretation: Recommendations From the International Consensus on Time in Range”. In: *Diabetes Care* 42.8 (2019), pages 1593–1603. DOI: <https://doi.org/10.2337/dci19-0028>.
- [2] Moshe Phillip, Revital Nimri, Richard M. Bergenstal, Katharine Barnard-Kelly, Thomas Danne, Roman Hovorka, Boris P. Kovatchev, Laurel H. Messer, Christopher G Parkin, Louise Ambler-Osborn, Stephanie A. Amiel, Lia Bally, Roy W Beck, Sarah Biester, Torben Biester, Julia E. Blanchette, Emanuele Bosi, Charlotte K. Boughton, Marc D. Breton, Sue A. Brown, Bruce A. Buckingham, Albert Cai, Anders L. Carlson, Jessica R. Castle, Pratik Choudhary, Kelly L. Close, Claudio Cobelli, Amy B. Criego, Elizabeth Davis, Carine de Beaufort, Martin I. de Bock, Daniel J. DeSalvo, J. Hans DeVries, Klemen Dovc, Francis J Doyle III, Laya Ekhlaspour, Naama Fisch Shvalb, Gregory P. Forlenza, Geraldine Gallen, Satish K. Garg, Dana C. Gershenoff, Linda A. Gonder-Frederick, Ahmad Haidar, Sara Hartnell, Lutz Heinemann, Simon Heller, Irl B. Hirsch, Korey K. Hood, Diana Isaacs, David C. Klonoff, Olga Kordonouri, Aaron Kowalski, Lori Laffel, Julia Lawton, Rayhan A. Lal, Lalantha Leelarathna, David M. Maahs, Helen R. Murphy, Kirsten Nørgaard, David O’Neal, Sean Oser, Tamara Oser, Eric Renard, Michael C. Riddell, David Rodbard, Steven J. Russell, Desmond A. Schatz, Viral N. Shah, Jennifer L. Sherr, Gregg D. Simonson, R. Paul Wadwa, Candice Ward, Stuart A. Weinzier, Emma G. Wilmot, and Tadej Battelino. “Consensus Recommendations for the Use of Automated Insulin Delivery Technologies in Clinical Practice”. In: *Endocrine Reviews* (2022), pages 1630–1640. DOI: [10.1210/endrev/bnac022](https://doi.org/10.1210/endrev/bnac022).
- [3] Claudio Cobelli, Chiara Dalla Man, Giovanni Sparacino, Lalo Magni, Giuseppe De Nicolao, and Boris P. Kovatchev. “Diabetes: Models, Signals, and Control”. In: *IEEE reviews in biomedical engineering* 2 (2009), pages 54–96. DOI: [10.1109/RBME.2009.2036073](https://doi.org/10.1109/RBME.2009.2036073).
- [4] Malgorzata E. Wilinska, Ludovic J. Chassin, Carlo L. Acerini, Janet M. Allen, David B. Dunger, and Roman Hovorka. “Simulation Environment to Evaluate Closed-Loop Insulin Delivery Systems in Type 1 Diabetes”. In: *Journal of Diabetes Science and Technology* 4.1 (2010), pages 132–144. DOI: [10.1177/193229681000400117](https://doi.org/10.1177/193229681000400117).

- [5] Roman Hovorka, Fariba Shojaee-Moradie, Paul V. Carroll, Ludovic J. Chassin, Ian J. Gowrie, Nicola C. Jackson, Romulus S. Tudor, A. Margot Umpleby, and Richard H. Jones. “Partitioning glucose distribution/transport, disposal, and endogenous production during IVGTT”. In: *American Journal of Physiology-Endocrinology and Metabolism* 282 (2002), E992–E1007. DOI: 10.1152/ajpendo.00304.2001.
- [6] Asbjørn Thode Reenberg, Tobias K. S. Ritschel, Bernd Dammann, and John Bagterp Jørgensen. “High-performance uncertainty quantification in large-scale virtual clinical trials of closed-loop diabetes treatment”. In: *Proceedings of the 2022 American Control Conference (ACC)*. 2022, pages 1367–1372. DOI: 10.23919/ACC53348.2022.9867234.

